

Decision Support System in the Design, Production and Quality Control of Glass Containers

Programa Doutoral em Engenharia Mecânica (PRODEM)
Departamento de Engenharia Mecânica (DEMec)
Faculdade de Engenharia (FEUP)
Universidade do Porto (UP)
PORTUGAL 

Bruno Miguel Rodrigues Martins
Orientador: Prof. Dr. José César de Sá
Co-orientador: Prof. Dr. Ana Reis
July 2017

“They are wild, they are free, they are not different from us...”

Jeremy Wade

À minha família e amigos.

Acknowledgements

O trabalho apresentado apenas foi possível fruto da colaboração e apoio de algumas pessoas, pelas quais não posso deixar de prestar o meu reconhecimento e agradecimento.

Ao Professor Doutor José Manuel de Almeida César de Sá um profundo agradecimento por ter-me acolhido como seu orientando, pelo apoio prestado durante o decorrer deste trabalho. O conteúdo das discussões científicas foram sempre muito produtivas e esclarecedoras. Agradeço ainda pela paciência, disponibilidade e amizade demonstrada.

À Professora Doutora Ana Reis um agradecimento pelo apoio, empenho e aconselhamento dado durante o desenvolvimento do trabalho. Ainda um agradecimento pelo acolhimento e confiança em acreditar na finalização do projecto com sucesso.

Ao Doutor Pedro Teixeira pelo suporte dado durante o projecto. Sem a sua colaboração grande parte deste trabalho não teria sido possível. Adicionalmente, um enorme agradecimento pela incessante partilha de conhecimentos, paciência e amizade demonstrados.

A Doutora Margarida Machado pelo apoio dado, as discussões científicas foram sem dúvida enriquecedoras e ainda pela ajuda em determinar as linhas de rumo para levar este trabalho a bom porto.

Ao Doutor Jaime Rodrigues pelo precioso auxílio dado em áreas estratégicas que sem a sua ajuda seriam muito mais complicadas em realizar. Um enorme gosto em trabalhar com uma pessoa com um enorme conhecimento científico.

À Empackglass por todo o apoio técnico para a execução do trabalho e pelo fornecimento de resultados experimentais. Quero agradecer também pelas orientações e sugestões práticas.

Ao Professor Doutor Abel Dias dos Santos um especial agradecimento pelo acolhimento inicial, por ter concedido a oportunidade de trabalhar num ambiente científico e por ter despertado em mim o gosto pela investigação científica. Por toda a paciência demonstrada e também por todo o conhecimento científico ensinado. Não tenho dúvidas que o seu apoio prévio foi sem dúvida essencial para concretizar este trabalho até ao fim.

Ao INEGI - instituto de ciência e inovação em engenharia mecânica e engenharia industrial desejo agradecer à unidade CETECOP/UTAF - Unidade das Tecnologias de Conformação Plástica/ Unidade de Tecnologias Avançadas de Fabrico. Pelo todo apoio técnico e humano dado durante e execução do trabalho.

Ainda a toda a minha família e amigos.

Finalmente, a todos os que diretamente ou indiretamente contribuíram para que este trabalho chegasse a bom porto.

Abstrat

In this work a numerical model, based on the finite element method, for all processes of glass forming of glass containers is presented. Glass forming processes involve coupled thermomechanical phenomena which heat transfer and viscous flow are dependent, as glass viscosity is highly dependent on temperature and the significant shape changes and contact conditions affect the temperature distribution. During the overall process glass changes from a molten state to a solid state. Therefore, adequate cooling conditions must be set appropriately. The ultimate aim is to set the better process parameters so that the final products will have the required geometrical shape and thickness distribution.

From the numerical point of view geometrical modelling must be robust so as to adjust to the different sequenced stages. Remeshing techniques requiring adequate transfer the data correctly. Different thermal and mechanical contact conditions between glass and moulds must be taken into account adequately. Also effective treatment of the incompressible conditions associated with glass flow must be dealt appropriately. The numerical model developed, addressing all these issues is validated with real industrial products. Numerical aspects associated with the model implementation and its validation with real formed products are discussed.

Keywords: Glass container forming, Finite element method, Thermomechanical model

Resumo

Neste trabalho é apresentado um modelo numérico baseado no método dos elementos finitos para todas as etapas da produção de garrafas de vidro. O modelo trata o processo de prensado/soprado e soprado/soprado. O processo de produção de garrafas de vidro envolve um modelo termomecânico tendo a viscosidade do material grande influência no fenômeno térmico e mecânico. Uma vez que a viscosidade é altamente dependente da temperatura influenciando significativamente a forma e as condições de contacto afetando desse modo a distribuição de temperatura. Durante o processo tecnológico o vidro muda o seu estado de líquido para sólido num período de tempo curto. Assim, as condições de arrefecimento entre o vidro e os moldes têm de ser conhecidas com rigor. O objetivo deste trabalho é simular o processo de produção de garrafas de vidro de modo que os parâmetros do processo possam ser alterados de forma a obter a forma da garrafa e a distribuição de espessura.

O modelo deve ser robusto do ponto de vista numérico para que durante todas as etapas desde a queda da gota, a formação da primeira forma até à forma final durante o prensado ou o primeiro soprado. A transferência da informação entre malhas deve ser realizada adequadamente. As condições de incompressibilidade associadas ao vidro devem ser também alvo de atenção. O modelo desenvolvido tendo em conta todos estes aspetos foi validado com resultados reais resultantes da produção de garrafas de vidro. Os aspetos numéricos associados ao modelo implementado e a sua validação são discutidos neste trabalho.

Keywords: Produção de garrafas de vidro, Método dos elementos finitos, Modelo termomecânico

Index

ACKNOWLEDGEMENTS	IV
ABSTRAT	V
RESUMO	VI
INDEX	VII
LIST OF FIGURES	X
LIST OF TABLES	XIX
NOMENCLATURE	XX
<i>CHAPTER 1</i>	<i>1</i>
1 INTRODUCTION	1
1.1 HISTORIC REVIEW OF GLASS MAKING.....	1
1.2 HISTORY OF GLASS MOULDING	2
1.3 GLASS CONTAINERS INDUSTRY	3
1.4 GLASS CONTAINER QUALITY.....	4
1.5 GLASS CONTAINERS TERMINOLOGY	ERRO! MARCADOR NÃO DEFINIDO.
1.6 GLASS CONTAINER SIMULATION	5
1.7 OBJECTIVES	7
1.8 THESIS SYNOPSIS	7
2 GLASS MATERIAL PROPERTIES	9
2.1 BRITTLENESS	9
2.2 DENSITY	9
2.3 THERMAL EXPANSION	10
2.3.1 <i>Glass Cord</i>	10
2.4 TEMPERATURE DEPENDENCE OF VISCOSITY	11
2.5 CHEMICAL DURABILITY	14
2.5.1 <i>Dealkalization</i>	15
2.6 LIQUIDUS TEMPERATURE	15
2.6.1 <i>Devitrification</i>	15
2.7 LIGHT TRANSMISSION – COLOUR	15
2.8 CULLET.....	16
2.9 STRENGTH OF THE GLASS	17
2.10 THERMAL SHOCKS	17
2.11 GLASS COMPOSITION.....	18
3 GLASS CONTAINER PRODUCTION	21

3.1	BATCH	22
3.1.1	Batch – Storing	22
3.1.2	Batch – Weighting.....	23
3.1.3	Batch – Mixing.....	23
3.2	MELTING	24
3.2.1	Regenerative Furnace	25
3.2.2	Recuperative Furnace.....	28
3.2.3	Boosting	30
3.2.4	Bubbler.....	32
3.2.5	Barrier Wall.....	33
3.2.6	Refining Bank.....	33
3.2.7	Drain.....	34
3.2.8	Cullet Preheating.....	34
3.2.9	Melting Process and glass formation.....	35
3.3	GLASS CONDITIONING	36
3.3.1	Forehearth	37
3.4	FORMING	42
3.4.1	Feeder	42
3.4.2	Blow and Blow	52
3.4.3	Press and Blow	54
3.5	HOT END COATING.....	56
3.6	ANNEALING	58
3.6.1	Internal Stress	59
3.6.2	Cycle	60
3.6.3	Quality control.....	61
3.7	COLD END COATING.....	62
3.8	INSPECTION AND QUALITY CONTROL	63
3.8.1	Defects	68
3.8.2	Quality Control Laboratory.....	78
3.9	PALLETIZING	79
3.10	SHRINK-WRAPPING	81
4	MATHEMATICAL MODELLING OF GLASS FORMING PROCESSES	83
4.1	FINITE ELEMENT FORMULATION FOR THERMOMECHANICAL BEHAVIOUR.....	83
4.1.1	Constitutive Model.....	83
4.1.2	Finite Element Method Formulation.....	85
4.2	FINITE ELEMENT FORMULATION FOR HEAT TRANSFER	88
4.2.1	Transient Analysis.....	88
4.2.2	Time Integration.....	91
5	SIMULATING MODEL FOR GLASS CONTAINERS.....	95
5.1	ELEMENT TECHNOLOGY	96
5.1.1	Library of Elements.....	96
5.1.2	Spurious Oscillations Due to Smaller Time Increments	96
5.1.3	Hourglass and Locking.....	96
5.2	CONTACT.....	97
5.2.1	Contact Algorithm.....	98
5.2.2	Sticking Condition.....	100
5.2.3	Sliding Conditions.....	102
5.2.4	Updating Boundary Conditions	102
5.3	MESH UPDATING AND REMESHING.....	106
5.3.1	Mesh Updating.....	107

5.3.2	<i>Remeshing</i>	108
6	ELEMENTS VALIDATION AND TESTING	115
6.1	HEAT TRANSFER VALIDATION.....	115
6.2	MECHANICAL VALIDATION	129
7	COMPUTER PROGRAM	156
7.1	SOFTWARE ENVIRONMENT.....	156
7.1.1	<i>Graphic Engine</i>	156
7.1.2	<i>Preprocessor</i>	156
7.1.3	<i>Postprocessor</i>	158
7.2	SOFTWARE CORE.....	160
7.3	COMPUTER PROGRAM FILES	161
7.3.1	<i>Input File</i>	162
7.3.2	<i>Result File</i>	163
7.3.3	<i>Warning File</i>	164
7.3.4	<i>Error File</i>	164
7.3.5	<i>Restart File</i>	164
7.3.6	<i>Remeshing Files</i>	164
7.3.7	<i>Update File</i>	164
7.3.8	<i>List File</i>	164
8	GLASS CONTAINERS SIMULATION CASES	166
8.1	BLOW AND BLOW PROCESS	173
8.1.1	<i>Gob Loading</i>	173
8.1.2	<i>Settle Blow</i>	182
8.1.3	<i>Corkage Reheat</i>	189
8.1.4	<i>Counter Blow</i>	190
8.1.5	<i>Reheat</i>	205
8.1.6	<i>Invert</i>	206
8.1.7	<i>Rundown</i>	209
8.1.8	<i>Final Blow</i>	216
8.1.9	<i>Mould Open</i>	223
8.1.10	<i>Bottle Thickness</i>	225
8.2	PRESS AND BLOW PROCESS	230
8.2.1	<i>Gob Loading</i>	230
8.2.2	<i>Baffle On</i>	240
8.2.3	<i>Plunger Up</i>	241
8.2.4	<i>Reheat</i>	262
8.2.5	<i>Invert</i>	263
8.2.6	<i>Rundown</i>	267
8.2.7	<i>Final Blow</i>	278
8.2.8	<i>Mould Open</i>	288
8.2.9	<i>Bottle Thickness</i>	293
8.3	EVALUATION OF SOME NUMERICAL ASPECTS.....	299
8.3.1	<i>Volume Evolution</i>	299
8.3.2	<i>Evolution of the Number of Nodes</i>	303
8.3.3	<i>Plunger Displacement</i>	306
8.3.4	<i>Time Evolution</i>	307
9	CONCLUSIONS AND FUTURE WORK	312
10	REFERENCES	315

List of Figures

<i>Figure 2.1: a) Examples of a cord defects after cooling. b) Glass cord observed by viewing in polarized light</i>	11
<i>Figure 2.2: Viscosity evolution in working zone temperature [12].</i>	12
<i>Figure 2.3: Chemical durability of a container.</i>	14
<i>Figure 2.4: Glass colours presented in some container.</i>	16
<i>Figure 2.5: Effects of some oxides in glass properties.</i>	19
<i>Figure 3.1: Production line of glass containers.</i>	22
<i>Figure 3.2: a) Glass plant batch house.</i>	23
<i>Figure 3.3: Weighting the raw material.</i>	23
<i>Figure 3.4: Mixing the raw material operation.</i>	24
<i>Figure 3.5: Melting plant scheme with the temperature gradient.</i>	25
<i>Figure 3.6: Regenerative furnace layout.</i>	26
<i>Figure 3.7: Regenerative end fired furnace [18].</i>	27
<i>Figure 3.8: Regenerative furnace heat exchange [18].</i>	28
<i>Figure 3.9: Recuperative furnace [18].</i>	29
<i>Figure 3.10: Side fired recuperative furnaces [18].</i>	30
<i>Figure 3.11: Comparison of energy consumption of a regenerative and a recuperative furnace at part load [18].</i>	30
<i>Figure 3.12: Boosting system in an end fired furnace.</i>	31
<i>Figure 3.13: a) Melting booster b) Barrier booster c) Local booster [18].</i>	31
<i>Figure 3.14: Bubbling principle [18].</i>	33
<i>Figure 3.15: Barrier wall.</i>	33
<i>Figure 3.16: Drain cross section [18].</i>	34
<i>Figure 3.17: Furnace temperature evolution and the respective convection.</i>	35
<i>Figure 3.18: Flux of glass inside a furnace.</i>	36
<i>Figure 3.19: Working end furnace.</i>	36
<i>Figure 3.20: Glass conditioning general view.</i>	37
<i>Figure 3.21: Glass Conditioning heat transfer.</i>	38
<i>Figure 3.22: Forehearth Type K.</i>	38
<i>Figure 3.23: Forehearth Type K.</i>	39
<i>Figure 3.24: Forehearth longitudinally cooled.</i>	39
<i>Figure 3.25: Radiation cooled forehearths.</i>	40
<i>Figure 3.26: Muffle cooled forehearths.</i>	40
<i>Figure 3.27: System 500 forehearths.</i>	41
<i>Figure 3.28: System 500 forehearths a) cooling cycle b) Heating cycle c) Normal operation.</i>	41
<i>Figure 3.29: System 500 forehearths cooling zones.</i>	42
<i>Figure 3.30: System 500 forehearths cooling zones.</i>	42
<i>Figure 3.31: Forming feed machine.</i>	43
<i>Figure 3.32: a) Tube height raised.</i>	44
<i>Figure 3.33: Examples of a) Spout bowl b) Feeder tubes c) Orifice ring.</i>	44

Figure 3.34: a) Small Orifice Ring	45
Figure 3.35: Glass feeder plungers.	45
Figure 3.36: Representation of plunger motion and gob shear cutting [1].	46
Figure 3.37: Effect on gob with different plungers [20].	46
Figure 3.38: a) Plunger height lowered.	47
Figure 3.39: Gob cutting shears.	47
Figure 3.40: Shear tension effect on gob shearing [20].	48
Figure 3.41: Shear overlap effect on gob shearing [20].	48
Figure 3.42: Plunger/shear differential adjustments a) Differential 0° setting b) Differential 10° setting c) Differential 30° setting. [20].	49
Figure 3.43: Different types of tuning a feeder a) Glass temperature increased. b) Glass temperature decreased. c) Machine speed increased. d) Machine speed decreased. [20]	49
Figure 3.44: Gob shape parts affected by feeder controls [20].	50
Figure 3.45: Gob distributor scheme.	51
Figure 3.46: Gob distributor.	51
Figure 3.47: a) Gob loading b) Settle blow c) Counter blow d) Invert e) Final blow f) Take out	53
Figure 3.48: a) Gob loading b) Baffle on c) Plunger up d) Invert e) Rundown f) Final Blow g) Take out	56
Figure 3.49: Hot end coating.	57
Figure 3.50: Application of hot end coating.	57
Figure 3.51: Application of hot end coating.	58
Figure 3.52: Rapid cooling from forming to annealing Lehr.	59
Figure 3.53: Stress after coating process.	59
Figure 3.54: Tension inside the container thickness.	60
Figure 3.55: Tension inside the container thickness.	61
Figure 3.56: Measurement of glass stress with a polariscope.	62
Figure 3.57: Different surface treatments through a convey belt.	62
Figure 3.58: Application of cold end coating.	63
Figure 3.59: The packaging materials include pallets, cartons, trays, and shrink wrap and stretch wrap materials.	64
Figure 3.60: Furnace control.	65
Figure 3.61: Hot end coating quality control.	66
Figure 3.62: Cond end coating quality control.	67
Figure 3.63: Defects can be presented in a glass container [Emhart].	70
Figure 3.64: Vertical palletizing.	81
Figure 3.65: Shrink-wrapping a pallet.	81
Figure 5.1: Model domain contact problem.	97
Figure 5.2: Target for glass node contact the mould.	98
Figure 5.3: Contact algorithm flowchart for each node.	99
Figure 5.4: Contact representation for sticking condition.	100
Figure 5.5: Contact flowchart for candidate segment selection.	101
Figure 5.6: Contact velocity components a) Nodes in contact to the mould with the velocity components.	102
Figure 5.7: Local coordinates at each contact node between the plunger and the glass.	103
Figure 5.8: Contact between two bodies at different temperatures considering the different boundaries for each physical field.	105
Figure 5.9: Contact between two bodies at different temperatures considering the different boundaries for each physical field.	106
Figure 5.10: a) Example of a triangular linear mesh.	106
Figure 5.11: Example of an element with negative Jacobian.	107
Figure 5.12: Meshing a curve with different mesh size.	108
Figure 5.13: Flowchart of remeshing technique.	109

Figure 5.14: Correction of the new boundary nodes.....	110
Figure 5.15: Example of a boundary segments.	110
Figure 5.16: Cross product between a node that belong to a new mesh and the older element.....	112
Figure 6.1: Mesh used to simulation for heat transfer validation a) linear triangle b) quadratic triangle c) linear quadrilateral d) quadratic quadrilateral.....	116
Figure 6.2: Scheme to validate the prescribed temperature at the boundary of a cylinder.....	116
Figure 6.3: Results for the analytical equation for the prescribed boundary temperature a) Temperature/Radius b) Temperature/Time evolution.....	117
Figure 6.4: Results for Abaqus simulation for the prescribed boundary temperature a) Linear triangular elements b) Linear quadrilateral elements c) Quadratic triangular elements d) Quadratic quadrilateral elements.....	118
Figure 6.5: Results for Empaktor software for the prescribed boundary a) Linear triangular elements b) Linear quadrilateral elements c) Quadratic triangular elements d) Quadratic quadrilateral elements.	119
Figure 6.6: Results for Empaktor software for the prescribed boundary temperature using only the diagonal values for the capacity matrix a) Linear triangular elements b) Linear quadrilateral elements c) Quadratic triangular elements d) Quadratic quadrilateral elements.....	120
Figure 6.7: Results for Empaktor software for the prescribed boundary temperature using a pondered capacity matrix a) Linear triangular elements b) Linear quadrilateral elements c) Quadratic triangular elements d) Quadratic quadrilateral elements.....	121
Figure 6.8: Scheme to validate the prescribed flux at the boundary cylinder.....	121
Figure 6.9: Results for the analytical equation for the prescribed boundary flux a) Temperature/Time b) Temperature/Radius evolution.....	122
Figure 6.10: Results for Abaqus simulation for the prescribed flux a) Linear triangular elements b) Linear quadrilateral elements c) Quadratic triangular elements d) Quadratic quadrilateral elements.	123
Figure 6.11: Results for Empaktor software for the prescribed Flux a) Linear triangular elements b) Linear quadrilateral elements c) Quadratic triangular elements d) Quadratic quadrilateral elements.	124
Figure 6.12: Results for Empaktor software for the prescribed flux using only the diagonal values for the capacity matrix a) Linear triangular elements b) Linear quadrilateral elements c) Quadratic triangular elements d) Quadratic quadrilateral elements.....	125
Figure 6.13: Results for Empaktor software for the prescribed flux using a pondered capacity matrix a) Linear triangular elements b) Linear quadrilateral elements c) Quadratic triangular elements d) Quadratic triangular elements.....	126
Figure 6.14: Mesh used for heat transfer validation for quadratic triangular and quadratic quadrilateral.....	127
Figure 6.15: Results for prescribed temperatures a) Quadratic triangular elements in Abaqus b) Quadratic triangular elements Empaktor software c) Quadratic quadrilateral elements in Abaqus d) Quadratic quadrilateral elements Empaktor software.....	128
Figure 6.16: Results for prescribed flux temperatures a) Quadratic triangular elements in Abaqus b) Quadratic triangular elements Empaktor software c) Quadratic quadrilateral elements in Abaqus d) Quadratic quadrilateral elements Empaktor software.....	129
Figure 6.17: Axisymmetric deformation modes for the linear triangular element using 1 Gauss point.	131
Figure 6.18: Orthogonalizing deformation modes for the linear triangular element using 1 Gauss point.	131
Figure 6.19: Axisymmetric deformation modes for the linear triangular element using 1 Gauss point.	132
Figure 6.20: Axisymmetric deformation modes for the linear triangular element using 3 Gauss point.	132
Figure 6.21: Axisymmetric deformation modes for the linear triangular element using 7 Gauss point.	132

Figure 6.22: Axisymmetric deformation modes for the MINI linear triangular element using one Gauss point.....	133
Figure 6.23: Orthogonalizing deformation modes for the MINI linear triangular element using 1 Gauss point.....	133
Figure 6.24: Axisymmetric deformation modes for the MINI linear triangular element using one Gauss point.....	134
Figure 6.25: Axisymmetric deformation modes for the MINI linear triangular element using three Gauss point.....	134
Figure 6.26: Axisymmetric deformation modes for the MINI linear triangular element using three Gauss point.....	135
Figure 6.27: Axisymmetric deformation modes for the MINI linear triangular element using seven Gauss point.....	135
Figure 6.28: Axisymmetric deformation modes for the quadratic triangular element using one Gauss point.....	136
Figure 6.29: Orthogonalizing deformation modes for the quadratic triangular element using one Gauss point.....	136
Figure 6.30: Axisymmetric deformation modes for the quadratic triangular element using one Gauss point.....	137
Figure 6.31: Axisymmetric deformation modes for the quadratic triangular element using three Gauss point.....	138
Figure 6.32: Axisymmetric deformation modes for the quadratic triangular element using three Gauss point.....	139
Figure 6.33: Axisymmetric deformation modes for the quadratic triangular element using seven Gauss point.....	139
Figure 6.34: Axisymmetric deformation modes for the quadratic triangular element using seven Gauss point.....	140
Figure 6.35: Axisymmetric displacement modes for the linear quadrilateral element using one Gauss point.....	141
Figure 6.36: Orthogonalizing deformation modes for the linear quadrilateral element using one Gauss point.....	142
Figure 6.37: Axisymmetric deformation modes for the linear quadrilateral element using one Gauss point.....	142
Figure 6.38: Axisymmetric deformation modes for the linear quadrilateral element using 2x2 Gauss point.....	143
Figure 6.39: Axisymmetric deformation modes for the linear quadrilateral element using 2x2 Gauss point.....	143
Figure 6.40: Axisymmetric deformation modes for the linear quadrilateral element using 3x3 Gauss point.....	143
Figure 6.41: Axisymmetric deformation modes for the linear quadrilateral element using 3x3 Gauss point.....	144
Figure 6.42: Axisymmetric deformation modes for the quadratic quadrilateral element for one Gauss point.....	145
Figure 6.43: Orthogonalizing deformation modes for the quadratic quadrilateral element using one Gauss point.....	145
Figure 6.44: Axisymmetric deformation modes for the quadratic quadrilateral element using one Gauss point.....	147
Figure 6.45: Axisymmetric deformation modes for the quadratic quadrilateral element for 2x2 Gauss point.....	148
Figure 6.46: Axisymmetric deformation modes for the quadratic quadrilateral element for 2x2 Gauss point.....	149
Figure 6.47: Axisymmetric deformation modes for the quadratic quadrilateral element for 3x3 Gauss point.....	150

Figure 6.48: Axisymmetric deformation modes for the quadratic quadrilateral element for 3x3 Gauss point.....	151
Figure 6.49: Axisymmetric deformation modes for the quadratic quadrilateral element for 4x4 Gauss point.....	152
Figure 6.50: Scheme for the compression test.....	153
Figure 6.51: Mesh used for compression test a) Linear triangular elements b) Quadratic triangular elements c) linear quadrilateral elements d) Quadratic quadrilateral elements.....	153
Figure 6.52: Displacement results for the compression test for the different elements type.....	154
Figure 6.53: Scheme to validate the prescribed temperature at the boundary cylinder.....	155
Figure 6.54: a) Pressure teste for one linear quadrilateral element using two Gauss points to integrate the force b) using one Gauss point to integrate the force.....	155
Figure 7.1: Layout of the preprocessor.....	157
Figure 7.2: Option to model the simulation.....	158
Figure 7.3: Software postprocessor overview.....	159
Figure 7.4: Software postprocessor.....	159
Figure 7.5: Software postprocessor thickness distribution.....	160
Figure 7.6: Software core diagram.....	161
Figure 7.7: Input file example.....	163
Figure 7.8: Example of the results file.....	163
Figure 7.9: Example of the update file.....	164
Figure 7.10: Example of the list file.....	165
Figure 8.1: Process selection for container height (cm).....	167
Figure 8.2: Gob shape calculation.....	167
Figure 8.3: Temperature distribution in gob loading for the case 1 for 0.334s, 0.342s, 0.427s and 0.763s.....	175
Figure 8.4: Boundary temperature for gob loading stage for case 1.....	175
Figure 8.5: Temperature distribution in gob loading for case 2 for 0.365s, 0.382s, 0.429s and 0.555s.....	176
Figure 8.6: Boundary temperature for gob loading stage for case 2.....	176
Figure 8.7: Displacement module in gob loading for case 2 for 0.368s, 0.375s and 0.381s.....	177
Figure 8.8: Displacement module with the neckring detail in gob loading for case 2 for 0.3877s, 0.3973s 0.4165s.....	178
Figure 8.9: Displacement vector with neck ring detail in gob loading for case 2 for 0.3877s, 0.3973s 0.4165s.....	178
Figure 8.10: Temperature distribution in gob loading for case 3 0.326s, 0.335s, 0.369s and 0.490s.....	179
Figure 8.11: Boundary temperature for gob loading stage for case 3.....	179
Figure 8.12: Temperature distribution in gob loading for case 4 for 0.255s, 0.310s, 0.373s and 0.772s.....	180
Figure 8.13: Boundary temperature for gob loading stage for case 4.....	180
Figure 8.14: Temperature distribution in gob loading for case 5 for 0.731s, 0.745s, 0.819s and 1.129s.....	181
Figure 8.15: Boundary temperature for gob loading stage for case 5.....	181
Figure 8.16: Temperature distribution in settle blow for the case 1 for 0.796s, 0.934s and 1.083s.....	183
Figure 8.17: Boundary temperature for settle blow stage for case 1.....	183
Figure 8.18: Temperature distribution in settle blow for the case 2 for 0.555s, 0.666s and 1.333s.....	184
Figure 8.19: Boundary temperature for settle blow stage for case 2.....	184
Figure 8.20: Displacement module with the neckring detail in gob loading for case 2 for 0.555s, 0.744s 0.850s.....	185
Figure 8.21: Displacement vector with the neckring detail in gob loading for case 2 for 0.555s, 0.744s 0.850s.....	185
Figure 8.22: Temperature distribution in settle blow for the case 3 for 0.500s, 0.543s and 0.784s.....	186
Figure 8.23: Boundary temperature for settle blow stage for case 3.....	186

Figure 8.24: Temperature distribution in settle blow for the case 4 for 0.772s, 0.951s and 2.272s.	187
Figure 8.25: Boundary temperature for settle blow stage for case 4.	187
Figure 8.26: Temperature distribution in settle blow for the case 5 for 1.129s, 1.424s and 1.835s.	188
Figure 8.27: Boundary temperature for settle blow stage for case 5.	188
Figure 8.28: Temperature distribution in corkage reheat for the case 1 in 1.500s, for the case 2 in 2.044s, for the case 3 in 1.863s, for the case 4 in 4.090s and for the case 5 in 2.682s.....	189
Figure 8.29: Temperature distribution in counter blow for the case 1 for 1.500s, 1.538s, 1.570s, 1.622s,	192
Figure 8.30: Simulation temperature of the boundary for counter blow stage for case 1.	192
Figure 8.31: Displacement module in counter blow for the case 1 for 1.500s, 1.538s, 1.570s, 1.622s,	194
Figure 8.32: Temperature distribution in counter blow for the case 2 for 2.044s, 2.161s, 2.376s, 2.571s,	196
Figure 8.33: Boundary temperature for counter blow stage for case 2.....	196
Figure 8.34: Displacement module in counter blow for the case 2 for 2.044s, 2.161s, 2.376s, 2.571s,	198
Figure 8.35: Displacement vectors with the baffle detail in counter blow for the case 2 for 2.939s, 2.962s, 2.974s and 2.991s.....	198
Figure 8.36: Temperature distribution in counter blow for the case 3 for 1.863s, 1.891s, 1.938s, 1.994s,	200
Figure 8.37: Boundary temperature for counter blow stage for case 3.....	200
Figure 8.38: Temperature distribution in counter blow for the case 4 for 4.090s, 4.126s, 4.190s, 4.218s,	202
Figure 8.39: Boundary temperature for counter blow stage for case 4.....	202
Figure 8.40: Temperature distribution in counter blow for the case 5 for 2.682s, 2.723s, 2.758s, 2.822s,	204
Figure 8.41: Boundary temperature for counter blow stage for case 5.....	204
Figure 8.42: Temperature distribution in reheat for the case 1 in 3.958s, for the case 2 in 5.622s, for the case 3 in 4.705s, for the case 4 in 10.227s and for the case 5 in 6.117s.....	205
Figure 8.43: Temperature distribution in invert for the case 1 in 4.514s , for the case 2 in 6.666s, for the case 3 in 5.490s, for the case 4 in 11.590s and for the case 5 in 6.823s.....	207
Figure 8.44: Boundary temperature for invert stage for case 1, case 2, case 3, case 4 and case 5.	209
Figure 8.45: Temperature distribution in rundown for the case 1 in 4.514s, 5.201s, 5.833s.	210
Figure 8.46: Boundary temperature in rundown for case 1.	210
Figure 8.47: Temperature distribution in rundown for the case 2 in 6.666s, 7.222s and 9.111s.	211
Figure 8.48: Boundary temperature in rundown for case 2.	211
Figure 8.49: Displacement module in rundown for the case 2 in 6.666s, 7.222s and 9.111s.	212
Figure 8.50: Temperature distribution in rundown for the case 3 in 5.490s, 6.590s and 7.843s.	213
Figure 8.51: Boundary temperature in rundown for case 3.	213
Figure 8.52: Temperature distribution in rundown for the case 4 in 11.590s, 12.898s, 14.545s.	214
Figure 8.53: Boundary temperature in rundown for case 4.	214
Figure 8.54: Temperature distribution in rundown for the case 5 in 6.823s, 8.527s and 9.882s.	215
Figure 8.55: Boundary temperature in rundown for case 5.	215
Figure 8.56: Temperature distribution in final blow for the case 1 in 5.555s, 5.556s, 5.558s,	217
Figure 8.57: Temperature distribution in final blow for the case 2 in 9.111s, 9.125s, 9.133s,	218
Figure 8.58: Displacement module in final blow for the case 2 in 9.111s, 9.125s, 9.133s,.....	219
Figure 8.59: Temperature distribution in final blow for the case 3 in 7.843s, 7.846s, 7.848s,	220
Figure 8.60: Temperature distribution in final blow for the case 4 in 14.545s, 14.552s, 14.563s,	221
Figure 8.61: Temperature distribution in rundown for the case 5 in 9.882s, 9.884s, 9.892s,	222
Figure 8.62: Temperature distribution in mould open for the case 1 in 7.292s, for the case 2 in 12.555s, for the case 3 in 10.294s, for the case 4 in 22.500s and for the case 5 in 14.282s.	223
Figure 8.63: Final boundary temperature for case 1, case 2, case 3, case 4 and case 5.	225
Figure 8.64: Bottle thickness (mm) distribution in case 1.	226
Figure 8.65: Bottle thickness (mm) distribution in case 2.	227

Figure 8.66 Bottle thickness (mm) distribution in case 3.	228
Figure 8.67: Final bottle shape for the case 4.	228
Figure 8.68: Bottle thickness (mm) distribution in case 4.	229
Figure 8.69: Bottle thickness (mm) distribution in case 5.	229
Figure 8.70: Temperature distribution in gob loading for the case 1 in 0.175s, 0.199s, 0.252s and 0.466s.	231
Figure 8.71: Boundary temperature for gob loading stage for case 1.	231
Figure 8.72: Temperature distribution in gob loading for the case 2 in 0.096s, 0.140s, 0.238s, 0.383s.	232
Figure 8.73: Boundary temperature for gob loading stage for case 2.	232
Figure 8.74: Temperature distribution in gob loading for the case 3 in 0.078s, 0.115s, 0.275s, 0.800s.	233
Figure 8.75: Boundary temperature for gob loading stage for case 3.	233
Figure 8.76: Temperature distribution in gob loading for the case 4 in 0.251s, 0.266s, 0.355s, 0.555s.	234
Figure 8.77: Boundary temperature for gob loading stage for case 4.	234
Figure 8.78: Displacement module in gob loading for the case 4 in 0.2513s, 0.2667s, 0.3213s.	235
Figure 8.79: Displacement vector in gob loading for the case 4 in 0.2513s, 0.2667s, 0.3213s.	235
Figure 8.80: Temperature distribution in gob loading for the case 5 in 0.088s, 0.107s, 0.421s, 0.625s.	236
Figure 8.81: Boundary temperature for gob loading stage for case 5.	236
Figure 8.82: Temperature distribution in gob loading for the case 6 in 0.076s, 0.128s, 0.303s and 0.460s.	237
Figure 8.83 Boundary temperature for gob loading stage for case 6.	237
Figure 8.84: Temperature distribution in gob loading for the case 7 in 0.497s, 0.531s, 0.635s, 0.820s.	238
Figure 8.85: Boundary temperature for gob loading stage for case 7.	238
Figure 8.86: Temperature distribution in gob loading for the case 8 in 0.095s, 0.548s, 0.609s, 0.676s.	239
Figure 8.87: Boundary temperature for gob loading stage for case 8.	239
Figure 8.88: Temperature distribution in baffle on for the case 1 in 0.800s, for the case 2 in 0.859s, for the case 3 in 1.147s, for the case 4 in 0.889s, for the case 5 in 0.972s, for the case 6 in 0.801s, for the case 7 in 0.957s and for the case 8 in 1.126s.	241
Figure 8.89: Temperature distribution in plunger up for the case 1 in 0.8000s, 0.8002s, 0.8003s.	243
Figure 8.90: Boundary temperature in plunger up for case 1.	243
Figure 8.91: Temperature distribution in plunger up for the case 2 in 0.8588s, 0.8590s, 0.8592s.	245
Figure 8.92 Boundary temperature for plunger up stage for case 2.	245
Figure 8.93: Temperature distribution in plunger up for the case 3 in 1.1466s, 1.1468s, 1.1469s.	247
Figure 8.94 Boundary temperature for plunger up stage for case 3.	247
Figure 8.95: Temperature distribution in plunger up for the case 4 in 0.8888s, 0.8890s, 0.8891s.	249
Figure 8.96 Boundary temperature for gob loading stage for case 4.	249
Figure 8.97: Displacement module in plunger up for the case 4 in 0.8888s, 0.8890s, 0.8891s.	251
Figure 8.98: Displacement vectors in plunger up for the case 4 in 0.8888s, 0.8890s, 0.8891s.	252
Figure 8.99: Temperature distribution in plunger up for the case 5 in 0.9722s, 0.9727s, 0.9729s.	254
Figure 8.100 Boundary temperature for plunger up stage for case 5.	254
Figure 8.101: Temperature distribution in plunger up for the case 6 in 0.8013s, 0.8014s.	256
Figure 8.102: Boundary temperature in plunger up for case 6 and the thickness (mm) in plunger up stage for case 6.	257
Figure 8.103: Temperature distribution in plunger up for the case 7 in 0.9572s, 0.9575s, 0.9580s.	259
Figure 8.104 Boundary temperature for plunger up stage for case 7.	259
Figure 8.105: Temperature distribution in plunger up for the case 8 in 1.1267s, 1.1272s, 1.1277s.	261
Figure 8.106 Boundary temperature for plunger up stage for case 8.	261

Figure 8.107: Temperature distribution in reheat for the case 1 in 2.733s, for the case 2 in 2.837s, for the case 3 in 3.160s, for the case 4 in 2.777s, for the case 5 in 2.847s, for the case 6 in 3.178s, for the case 7 in 2.871s and for the case 8 in 3.943s.....	263
Figure 8.108: Temperature distribution in invert for the case 1 in 3.760s, for the case 2 in 3.910s, for the case 3 in 3.733s, for the case 4 in 4.194s, for the case 5 in 3.819s and for the case 6 in 3.561s, for the case 7 in 3.487s and for the case 8 in 4.788s.....	265
Figure 8.109: Boundary temperature for invert stage for case 1, case 2, case 3, case 4, case 5, case 6, case 7 and case 8.....	267
Figure 8.110: Temperature distribution in rundown for the case 1 in 3.760s, 5.026s and 5.800s.....	268
Figure 8.111 Boundary temperature for run down stage for case 1.....	268
Figure 8.112: Temperature distribution in rundown for the case 2 in 3.910s, 4.627s and 4.907s.....	269
Figure 8.113: Boundary temperature in rundown for case 2.....	269
Figure 8.114: Temperature distribution in rundown for the case 3 in 3.733s, 4.543s and 5.467s.....	270
Figure 8.115: Boundary temperature in rundown for case 3.....	270
Figure 8.116: Temperature distribution in rundown for the case 4 in 4.194s, 4.974s and 5.972s.....	271
Figure 8.117: Boundary temperature in rundown for case 4.....	271
Figure 8.118: Displacement module in rundown for the case 4 in 4.194s, 4.974s and 5.972s.....	272
Figure 8.119: Temperature distribution in rundown for the case 5 in 3.819s, 5.131s and 5.694s.....	273
Figure 8.120: Boundary temperature in rundown for case 5.....	273
Figure 8.121: Temperature distribution in rundown for the case 6 in 3.561s, 4.298s.....	274
Figure 8.122: Boundary temperature in rundown for case 6 and the thickness (mm) in run down stage for case 6.....	275
Figure 8.123: Temperature distribution in rundown for the case 7 in 3.487s, 4.664s and 5.059s.....	276
Figure 8.124: Boundary temperature in rundown for case 7.....	276
Figure 8.125: Temperature distribution in rundown for the case 8 in 4.788s, 6.459s and 6.854s.....	277
Figure 8.126: Boundary temperature in rundown for case 8.....	277
Figure 8.127: Temperature distribution in final blow for the case 1 in 5.800s, 5.803s, 5.804s.....	279
Figure 8.128: Temperature distribution in final blow for the case 2 in 4.907s, 4.909s, 4.910s.....	280
Figure 8.129: Temperature distribution in final blow for the case 3 in 5.467s, 5.469s, 5.471s.....	281
Figure 8.130: Temperature distribution in final blow for the case 4 in 5.972s, 5.418s, 5.419s.....	282
Figure 8.131: Displacement module in final blow for the case 4 in 5.972s, 5.418s, 5.419s.....	283
Figure 8.132: Temperature distribution in final blow for the case 5 in 5.694s, 5.700s, 5.705s.....	284
Figure 8.133: Temperature distribution in final blow for the case 6 in 5.584s 5.583s.....	286
Figure 8.134: Temperature distribution in final blow for the case 7 in 5.059s, 5.065s, 5.067s.....	287
Figure 8.135: Temperature distribution in final blow for the case 8 in 6.854s, 6.860s, 6.862s.....	288
Figure 8.136: Temperature distribution in mould open for the case 1 in 7.399s, for the case 2 in 8.205s, for the case 3 in 7.600s, for the case 4 in 7.750s, for the case 5 in 7.847s, for the case 6 in for the case 7 in 7.653s and for the case 8 in 10.516s.....	290
Figure 8.137: Final boundary temperature for case 1, case 2, case 3, case 4, case 5, case 6, case 7 and case 8.....	292
Figure 8.138: Bottle thickness (mm) distribution in case 1.....	293
Figure 8.139: Bottle thickness (mm) distribution in case 2.....	294
Figure 8.140: Bottle thickness (mm) distribution in case 3.....	295
Figure 8.141: Bottle thickness (mm) distribution in case 4.....	295
Figure 8.142: Real thickness (mm) distribution in case 4.....	296
Figure 8.143: Thickness (mm) distribution in case 5.....	296
Figure 8.144: Thickness (mm) distribution in case 6.....	297
Figure 8.145: Thickness (mm) distribution in case 7.....	298
Figure 8.146: Thickness (mm) distribution in case 8.....	299
Figure 8.147: Volume evolution for blow and blow process for the case 1, case 2, case 3, case 4 and case 5.....	301

<i>Figure 8.148: Volume evolution for press and blow process for the case 1, case 2, case 3, case 4, case 5, case 6, case 7 and case 8.</i>	<i>303</i>
<i>Figure 8.149: Number of nodes for the case 1, case 2, case 3 case 4 and case 5.</i>	<i>304</i>
<i>Figure 8.150: Number of nodes for the case 1, case 2, case 3 case 4, case 5, case 6, case 7 and case 8.</i>	<i>305</i>
<i>Figure 8.151: Plunger displacement for case 1, case 2, case 3, case 4, case 5, case 6, case 7 and case 8 for a slip penalty value of 1.0e04.</i>	<i>307</i>
<i>Figure 8.152: Time increment for blow and blow process for case 1, case 2, case 3, case 4 and case 5.</i>	<i>309</i>
<i>Figure 8.153: Time increment for blow and blow process for case 1, case 2, case 3, case 4, case 5, case 6, case 7 and case 8.</i>	<i>311</i>

List of Tables

<i>Table 2.1: Viscosity reference temperatures.....</i>	<i>11</i>
<i>Table 2.2: Composition of typical glass containers.....</i>	<i>18</i>
<i>Table 2.3: Oxides functions in glass containers.</i>	<i>19</i>
<i>Table 7.1: Files created during the simulation.....</i>	<i>161</i>
<i>Table 8.1: Simulation cases for the blow and blow and press and blow process.</i>	<i>166</i>
<i>Table 8.2: Simulation variables for blow and blow (left) and press and blow (right) processes.</i>	<i>168</i>
<i>Table 8.3: Machining timing for the blow and blow cases being respectively the case 1, case 2, case 3, case 4 and case 5.</i>	<i>169</i>
<i>Table 8.4: Machining timing for the press and blow cases being respectively the case 1, case 2, case 3, case 4, case 5, case 6, case 7 and case 8.</i>	<i>171</i>
<i>Table 8.5: Air temperature considered in the different stages.....</i>	<i>171</i>
<i>Table 8.6: Material chemical composition for different simulations cases in blow and blow and press and blow processes.</i>	<i>172</i>
<i>Table 8.7: Material behaviour for different simulations cases in blow and blow process.</i>	<i>172</i>
<i>Table 8.8: Material behaviour for different simulations cases in press and blow process.....</i>	<i>173</i>

Nomenclature

Physical Quantities

Symbol	Description	Unity [SI]
Scalar		
A	Area	[m ²]
A, B, C, D, T_0	Empirical constants	
B_i	Biot number	
c	Specific heat	[JKg ⁻¹ K ⁻¹]
c^*	Critical crack length	[m]
E	Young's modulus	[Pa]
Fo	Fourier number	
G	Shear modulus	
h	Heat transfer coefficient	[Wm ⁻² K ⁻¹]
k, k_x, k_y, k_z	Thermal conductivity	[Wm ⁻¹ K ⁻¹]
L	Length	[m]
m	Mass	[Kg]
P	Pressure	[Pa]
Q	Heat Energy	[J]
R	Molar gas constant	[m ² Kgs ⁻² K ⁻¹ mol ⁻¹]
r	Radius	[m]
t	Time unity	[s]
t_0	Initial time	[s]
T	Temperature	[K]
$T_{1,m}, T_{2,m}$	Temperature mould node	[K]
T_i	Initial temperature	[K]
T_a, T_∞	Ambient temperature	[K]
u	Displacement	[m]
V	Volume	[m ³]
V_c	Characteristic volume	[m ³]
α	Heat transfer coefficient	[Wm ⁻² K ⁻¹]
α	Penalty value	
α_c	Heat transfer coefficient convection	[Wm ⁻² K ⁻¹]
α_{cr}	heat transfer coefficient convection/radiation	[Wm ⁻² K ⁻¹]
β	Stefan–Boltzmann constant	[Wm ⁻² K ⁻⁴]
ε	Emissivity	

$\dot{\epsilon}$	Strain Rate	[s ⁻¹]
$\dot{\epsilon}_e$	Elastic strain rate	[s ⁻¹]
$\dot{\epsilon}_p$	Plastic strain rate	[s ⁻¹]
η	Viscosity	[Pa.s]
η_0	pre-exponential factor	
η_k	shear viscosity	[Pa.s]
λ	Penalty number	
ρ	Density	[Kgm ⁻³]
σ_f	failure stress	[Pa]
$\dot{\sigma}_e$	Stress rate	[Pa.s ⁻¹]
ΔG	Activation energy	[J]
ΔL	Element size	[m]
ΔT	Temperature difference	[K]
ΔV	Volume difference	[m ³]

Symbol	Description
Vector	
\mathbf{b}	Volume forces
f_i, \mathbf{f}	applied forces
N_i, \mathbf{N}	Shape functions
\mathbf{R}	Rotation matrix
Q_i, \mathbf{Q}	Thermal loads
T_i	Nodal temperature
v_i, \mathbf{v}	Velocity

Symbol	Description
Matrix	

\mathbf{B}	Derivative matrix
C_{ij}, \mathbf{C}	Capacity matrix
$\dot{\epsilon}_{ii}$	Dilatational strain rate
$\dot{\epsilon}_{ij}$	Deviatoric strain rate
K_{ij}, \mathbf{K}	Stiffness matrix
S_{ij}	Deviatoric stress tensor
α_{ij}	Thermal expansion tensor
ϵ_{ij}	Strain tensor
\mathcal{E}_{ii}	Dilatational strain tensor
$\dot{\mathcal{E}}_{ij}$	Strain rate tensor
σ_{ij}	Stress tensor
σ_m	Dilatational stress

Symbol	Description
Number	
i, m, n	Matrix index

Symbol	Description
Abbreviations	
VFT	Vogel–Fulcher–Tammann equation
AG	Adam–Gibbs Equation
WLF	Williams-Landel-Ferry Law
CPU	Central Processing Unit
FEM	Finite Element Method
RAM	Random Access Memory
PLC	Programmable Logic Controller
HEC	Hot End Coating
CVD	Chemical Vapour Deposition
CEC	Cold End Coating
HTC	Heat Transfer Coefficient
RI	Reduced Integration
IS machine	Individual Section Machine
SPC	Statistical Process Control

CHAPTER 1

1 Introduction

A brief introduction about the glass manufacturing is done in this chapter and, in addition, a thesis synopsis and the objectives are presented.

1.1 Historic Review of Glass Making

Created millions of years ago, glass is an abundant and easily accessible material that has been present since the formation of our planet. It is formed by high temperature phenomena such as volcanic eruptions, lightning strikes or by the impact of meteorites that melt the rock then, rapidly enough, solidifies it, making the liquid-like structure stay in a glassy state [1].

Lava spewed by volcanos gets cooled to form glass. Meteor impacts are also known to melt the earth's crust and with the occurrence of subsequent impacts form smaller bits of glass [2]. Impactites are a natural occurring type of glass formed by amorphous crystalline material after the impact of a meteorite shockwave [2]. When glass was invented it was quickly noticed how resistant it was, how it didn't suffer from devitrification as well as water corrosion. Our stone-age ancestors noticed the strength and sharpness of this material when they used obsidian to produce tools and arrowheads[1].

The melting of raw materials to create glass is a process that was discovered thousands of years ago. The Egyptians, no earlier than 7000 B.C., manufactured jewellery and glass beads [3]. In Mesopotamia, objects with coloured glazes containing copper compounds have been found dating to 4000 B.C. [2]. Feathery or zigzag patterns of coloured threads on the surface of some objects have also been found [4]. Glass was produced by the Egyptians until 1500 B.C. [3]. The recovered glass vessels from Egypt were manufactured between 14th and 16th century B.C. [2]. The adopted method is believed to have been to melt the glass, draw the threads out, turn them around a clay or sand object and then remelt the glass threads, using chemicals to give colour to the glass. Patterns were made by remelting pieces of coloured glass. The manufacture of Egyptian glass declined around the 11th century B.C. and in the meantime, it spread to other eastern Mediterranean regions such as Syria, Cyprus and Palestine. The major glass making centres became Syria and Palestine using the same techniques and colours that the Egyptians used, after 1000 B.C. they made core-formed vessels with different shapes [2]. Around 200 B.C. the Syrian craftsmen revolutionized the making of glass by discovering the blowing pipe [3]. With the development of the glass

blowing technique the possibilities of shaping glass became endless [4]. Generating an amazing range of glass applications as well as improving the quality of glass jars and bottles making the glass drinking vessels popular [3]. The next step was to use clay moulds for contours while blowing the glass to create flasks and other shapes, they also realized that glass could be shaped freehand to any form they desired. This created decorative elements, handles, feet that could be added as one desired [4]. Around 400 B.C. Macedonia and Greece emerged also as centres of glass manufacture [2]. Techniques for making glass tableware such as bowls, the use of brilliant colours, also the use of lathes and grinding wheels to manufacture decorations had already been developed. Greeks developed a technique to sandwich gold layers between clear glass parts and the mosaic forming, this technique was developed in order to impart special colour effects. The Roman Empire, between 3rd and 2nd century B.C., spread the making of glass through Rome and Italy with the methods of imparting different colours and glass blowing becoming widely popular. The making of cameo glass became one of the most sought techniques of this era [2]. Romans became the first civilization to experiment blowing glass inside moulds leading to improve the glass jars and bottles and the production of drinking vessels thereafter [5]. After the Roman Empire, the Byzantine regions (Greek Empire), under Islam, came with new developments. In the 7th century A.C. glass manufacture thrived in Syria and Palestine. The hedwig glass belongs to this era and it was created using diamond cutting. Baghdad emerged as the glass making centre of the 9th A.D. century after the Arab invasion that spread through most part of Asia and the closest Mediterranean parts of Europe. In the 13th century A.C. and through the next two centuries Persia became the major manufacturer of fine glassware and developed the technique of grinding glass surfaces. In the 14th century the independent republic of Venice became the centre for glass manufacture of Europe. Two significant developments occurred at this time: the discovery that the addition of calcia gave bright, shiny glass and the glass could also be worked to be incredibly thin, crystal-like clear with feather-light weight; the second was the creation of ice glass by plunging molten hot glass into ice cold water with an iron pipe for just a few moments and then blown, creating what appeared to be a tiny cracks within its surface. Glass making only flourished to the other parts of Europe by the end of the 16th century, it was at this time that English workers develop the waldglass (green or amber tinted glass). Development in Europe came in the form of techniques and popular designs that made glass articles affordable by the middle classes. With the 19th century came the birth of the mechanized glasswork not only in Europe but the United States as well. Opaline, a translucent milky-white glass, was created in France around 1810 by adding metallic oxides to the glass mixture. The modern method of glass making grew roots in most countries in Europe, America, Japan, India and China in the end of the 19th century. It was in the 20th century that glass became part of the human life with an evolution of manufacturing techniques and a deeper scientific understanding of it. This scientific understanding of glass was proportionally connected to the growth of chemistry and physics understanding, mainly in the field of inorganic materials. This growth was born from the observation of the effects of the addition of oxides and other chemicals produced in silica glass [2]. The invention of glass vacuum tubes paved the path to create most modern electronics today. The development of glass fibre optics is revolutionizing the telecommunications industry by replacing copper wires enhancing our ability to transmit data around the world [3]. Since its discovery glass became a stalwart material for our society, from its commonly day uses to architecture, to science and many other fields.

1.2 History of Glass Moulding

Blow moulding is believed to have been created around 1821 in Bristol, England. In 1859 Mein of Glasgow designed the first vertically spilt iron mould which had a movable base plate to make bottles by blowing compressed air. The biggest change to the manual process was to make the mouth or finish first so that the glass could be held in place while the rest of the manufacture operations were performed [6]. In 1866, H.M. Ashley and Josiah Arnall changed the way to fabricate containers. To answer the demands for sterile and refrigeration containers they created a new way to produce bottles, with semi-automatic machines, using an inverted mould with a plug at the bottom to create the mouth. [6]. While in hand blowing, the bottle neck was finished last (after blowing operations), a major change happened when this operation was made first by the machine [1]. In 1887, Ashley made some improvements, a separate parison¹ mould gave a better

¹ Mass of glass that has been partially shaped or molded.

distribution of wall thickness and a separate neckring mould to hold glass while being manipulated. This was done with a simple machine that needed to be fed gobs of glass by hand, reducing the labour cost or so it was claimed. This achieved an almost consistent weight of glass and internal capacity [6].

In the 1900 the progressive use of soda-lime-silica glass was started in the glass containers production. Mechanization in the production of glass containers was also in development.

An American engineer called Michael Owens (1859–1923) invented an automatic bottle blowing machine. This innovation was a successful process, which arrived in Europe after the turn of the century and considerably transformed the containers industry. A further improvement of the process is given by Hartford Company which invented the feeder in 1922 to provide the forming machines with a thermally conditioned glass gob². The feeder mechanism worked constantly as an extrusion machine which create a uniformly gob with a specified rate.

The feeders are still employed today and with the invention of individual section (IS) machines by 1925, they deliver several forming machines. A great advantage of the machine was that one section could be shut down to change moulds without stopping the production in the other sections. These inventions answered the growing demand for glass containers.

Along time glass as become a common material used in diverse applications. Firstly, empirical knowledge had a principal importance in developing glass industry. Nowadays trial and error is still a manner to improve quality in glass industry, however this type of production is highly time consuming and expensive. We live in a world in which glasses play a very important role in all aspects of our daily life and this is enough reason for us to study its forming processes.

1.3 Glass Containers Industry

Glass forming processes take place at high production rates. At the same time, glass manufacturers desire to optimize glass products to their customer's satisfaction. Glass containers process is a very complex procedure which must be thoroughly controlled in order to be able to satisfy the even more exigent costumers. Unfortunately, practical experiments are in general quite expensive, whereas the majority has to be performed under complicated circumstances. In addition, each glass manufacturing company keeps secret about its own experimental data. Therefore, it is no surprise that in the recent past glass process techniques were based on experience, rather than on scientific research. Nowadays computer simulation models are necessary to gain improvement and a better understanding of glass forming processes.

The glass containers manufacturers have to deal with challenges to improve the productivity of the plant or reduce the productions costs without the decrement of the quality levels imposed by the customer. Glass industry needs to work 24h per day and 7 days a week in order to keep the furnace working. Combine high productivities and low production costs are the main goals that the glass industry tries to achieve. Glass industries require sustainable profitability, quality and increase market share in the packaging industry. To maintain the glass containers quality the forming process needs stability. Glass industry tends to approve the new technologies slowly preferring to use the empirical knowledge of their workers. The competitiveness in glass industry brings the necessity to improve the design and the quality of their products. Different shapes, glass composition, colours may needs different changes in the processing parameters which can have very expensive costs.

Nowadays, glass industry has achieved considerable goals in efficiency and production rate without loss of product quality. They have been doing progresses in developing raw materials and processes using the knowledge created along the years. Utilizing the knowledge existent in materials properties and tools and R&D progress and opportunities, the glass industry is improving the production. Glass researchers are

² A small mass of glass with shape of a cylinder

making progress in manufacturing new functional glasses, upgrading existent technology continuously and also the simulation of the process can play an important role in this field.

1.4 Glass Container Quality

Glass has a wide range of uses. The main characteristics of glass are including shock-resistance, soundproofing, transparency and reflecting properties, which makes it particularly suitable for a wide range of applications, such as windows, television screens, bottles, drinking glasses, lenses, fibre optic cables, sound barriers and many other applications.

Glass products are engineered to fit the needs of customers, the major qualities their claim are resistance, durability, and ability to support rigorous condition. Special customers may need especial glass with special chemical composition and the glass industry should be prepared for the melting point and especial production processes needed to meet these requirements.

A key issue in glass containers is the wall thickness distribution. The thicker the container, the stronger it is and the less easily it breaks. The thinner the container, the lighter it is and less costs are spent on material. The optimal wall thickness distribution have to be optimize between these aspects. The ideal thickness distribution is not necessarily uniform, as some parts of the container are more vital than others, e.g. corners, and should be thicker for optimal strength. The difficulty in blow moulding a container with a prescribed wall thickness distribution is that the corresponding initial operating settings are not known beforehand. There are essentially two ways to deal with this. The first approach is the use of numerical simulation. If the initial operating conditions can be estimated, for example by empirical expertise of the process, a mathematical model can be developed that can directly compute the corresponding container production. Then, the initial operating settings of the blow moulding process can be adjusted to improve the wall thickness of the computed container. The first approach to attempt the desired wall thickness distribution is commonly a trial and error procedure, which is often based on the manufacturer's knowledge of the process. However, empirical expertise is often insufficient to find the initial operating settings, particularly when innovative processes are involved. A second approach is to solve an inverse mathematical problem to find the initial operating settings corresponding to the container with the desired wall thickness distribution. This class of inverse problems is quite challenging, as in general couple, highly nonlinear physical systems and complicated geometries are involved [7]. Usually, numerical optimization methods are employed to find a solution to the inverse problem [8]. Some advantages of lighter weight containers are, less cost to manufacture, higher forming machine production rates possible, shipping load and space requirements reduced, more competitive with plastic, cans, and paper containers.

The design of a container must be suitable for weight reduction without a reduction in strength. This is extremely important because a bottle can usually be effectively made lighter in weight only if can be designed with a stronger structural shape taking into consideration the particular forming process used to produce the containers.

Light weighting is important to improve productivity, when the glass containers are thinner and lighter some contribution for productivity are made and are the following,

- Lighter weight containers means that more containers per ton of glass can be produced.
- Lighter weight means less glass and therefore, less heat to be removed and the result is an increase in production speed.
- Saving weight also reduces glass cost per container which is a contribution of financial productivity.

Glass is basically made from sand and sand is largely spread throughout the earth's crust with very high purity of silica and uniform grain size. Uniform grain size is a very desirable quality because it can correspond to a consistent chemical composition. Sand before being used as a raw material needs some treatments to remove impurities like iron and ferric oxide, chromic oxide and heavy minerals. In the glass

the control of chemical composition of raw materials used in the processes is necessary in order to guarantee a high and constant level of quality of the product.

Glass is chemically inert, and environmentally friendly. Glass material is a preferred material of choice for the packaging industry worldwide for many years. The knowledge of the temperature is important in almost all stages of the glass production and glass processing. During the melting process in the glass tank the temperature influences the homogeneity of the glass melt. Undesired cracks could be the result of a wrong cooling of the glass [9]. Thus, the knowledge of the right temperature is important to guarantee the quality of the final products.

Heat conduction, heat convection and radiation plays an important role in the production of glass containers. Other properties, such as viscosity, thermal expansion, and electrical conductivity, are strongly dependent on glass composition. Glass is a very versatile material, it is quick to form in shape, cheap to produce and, depending on the recipe used it can be extremely durable. It can be transparent, opaque and take a greater range of colour and decorative effects than any other man made material.

Viscosity is the most important mechanical property in glass material and varies enormously with chemical composition. Since viscosity varies with chemical composition and is highly dependent of temperature, different glass types have very different behaviours while are worked at high temperatures.

Customers usually take no particular interest in the chemical composition of glass. Most catalogues by glass producers, therefore, do not indicate the chemical composition of the products. For glass producers, however, the chemical composition of the products and its control are highly important. To know the temperature dependence on viscosity is of fundamental importance for glass science and technology [10].

1.5 Glass Container Simulation

Modelling has become an important tool to accelerate the innovation while reducing the trial and error methods commonly used in production environments. Numerical simulation provides detailed information about forming process and thereby helps in determining the effects of different parameters on the final form of the item. Simulation can be done in shorter times and their costs are much lower than that of making trial moulds. Therefore, numerical simulation technique has the potential capacity to largely replace the other design techniques.

Glass forming techniques are still mostly based on empirical knowledge and hands on experience. Experimental trial using glass forming machines are in general very expensive and time consuming. Simulations give an alternative to an empirical knowledge avoiding the trial error procedures used in factories. Also help to reduce waste as well as the wall thickness reducing weight and maximizing strength.

In the last years, simulations software based on the finite element method has become an important tool to improve understanding, controlling and optimized the process. It is expected that this can give the final shape, thickness distribution, temperature distribution, etc.

The production of glass container takes place at high production rates. Time quality factors of the products, such as smoothness, strength, weight and cooling conditions, are optimized in order to pass the quality control process. To optimize and control the process is required knowledge. Unfortunately, measurements are often complicated, considering that blow moulding processes take place at high rates in closed constructions under complicated circumstances at high temperatures. Simulation models may offer a good alternative for complicated experimental measurements.

Glass-packaged products face a significant competitive pressure from products made of alternative materials. Nowadays, plastic, paper and related material and metallic (Aluminium and steel) containers share a large part of the container market. This has forced the glass industry to produce lighter containers (this has pushed the tools toward and the glass containers have more uniform glass distribution all over the article) for short-term conservation purposes while offering new attractive designs and promoting glass recycling. The growth of competitiveness on the industries that use glass containers puts demands on the

glass industry to develop new designs. In this context, simulation models are essential as virtual prototyping tools, reducing time and costs. To be effective, the model must give some information for the optimization of the process, namely thickness distribution, residual stresses and mould temperature distributions.

Glass container production can be simulated by means of a mathematical model, which is solved numerically to visualize the process at discrete times. A representative numerical simulation should give as output the container's final shape and wall thickness. In addition, numerical tools to simulate the glass forming process can be used to optimize an existing process. Process simulations can help minimize undesired variations in the wall thickness and reduce the weight while maintaining the strength. They can also help optimize cooling conditions and increase the production speed. The goal of all modelling software is to reduce the risk of new designs, reduce development time and find more optimal solutions in a virtual environment before physical creation.

The forming of hollow ware glass articles is a complex coupled thermal/mechanical problem with interaction between the heat transfer analysis and the viscous flow of molten glass. The glass viscosity, which governs the glass flow during the forming process, is strongly dependent on the temperature [11] and the contact with the moulds along with the constant geometry changes alters significantly the heat transfer process. The final product thickness distribution is one of the aspects which is more affected by changing process conditions. Simulating glass forming with FEM is a particularly difficult task since the material behaviour lies somewhere between a fluid and a solid. One of the first models was developed by Cesar de Sa [11]. In his approach, the thermal problem is coupled to the mechanical one at every time step, in order to handle the strong coupled phenomena. The model has provided good predictions of glass flow, resulting from gravity and blow pressure. The model was the basis for the development of a commercial 2D code [9]. But, nowadays, manufacturers are facing an evolving and increasing competition in the development of new complex 3D products. Tools are available which are capable of dealing with the most important aspects of these forming processes [10-11]. Nevertheless, some particular aspects require a dedicated software or some user intervention in order to adapt commercial codes to this particular field (which may not be an easy task). Besides the referred commercial code, a new approach has been recently released, [12], based on meshless methods, with 3D modelling. Nevertheless, in those software some important features in terms of process knowledge still lack or are simplified like, for example, the plunger movement defined by a prescribed velocity, which does not represent the real case, where a pressure must be set. A software suite for glass forming should include the calculation of the gob initial geometry and temperature distribution, as well as moulds heat transfer with the glass and with external ambient temperature, in order to optimize the final geometry and process efficiency. This last feature is not available in the mentioned software. Besides the paramount importance in the final container thickness distribution, it can be also extremely useful for machine developers since it allows to design dedicated cooling systems that could push the process further to its limits. Therefore, the main objective is to build a robust and reliable suite of numerical modelling programs designed to provide glassmakers with decision support system tools to aid in the design, production and quality control of all types of glass containers. The programs should combine the latest numerical technology to provide practical, representative simulation tools that glassmakers can use and benefit from. They should be rooted in sound theoretical formulations to deal with the complex coupled thermal and mechanical phenomena, as glass viscosity is dramatically influenced by temperature distribution that itself is highly influenced by shape modification and contact with the tools and moulds. The suite of programs should also comprise pre and post processors and analysis modules for the complete definition of the problem, analysis and viewing of the results. It should be used to simulate the forming process of round and non-round glass containers on an IS (individual section) forming machine from gob delivery through parison formation, invert and final blow until mould opens. The types of forming process modelled should include BB (Blow and Blow), PB (Wide Mouth Press/Blow) and NNPB (Narrow Neck Press/Blow) processes. As final result it should be possible to: predict the glass thickness distribution in the final product under a variety of conditions; analyse the thermal behaviour of the blank and blow moulds; investigate the influence of process conditions like glass composition, IS Machine timing, gob temperature, mould temperatures upon final container wall thickness results; evaluate the effects of mould cooling on the forming process and container wall thickness results. The final program should be not only

a design tool for improvement and optimization of existing products but also a means of understanding the main process parameters role to provide the assessment of new ideas for new products and innovation.

1.6 Objectives

The main objective is to perform a numerical tool to simulate the glass container forming. The program results are the wall thickness distribution, final shape and temperature distribution. Also the program has to be a robust and reliable suite of numerical modelling program. In general the program should provide glassmakers with decision support system tools to aid in the design, production and quality control of all types of glass containers.

1.7 Thesis Synopsis

Chapter 1 is dedicated to present the current of state glass industry. Then, chapter 2 focusses on the glass material properties. On chapter 3 an exhaustive description of the glass container production is done, since the raw material until the packaging. Chapter 4 explains the mathematical modelling of the glass forming process. The constitutive model for the thermomechanical behaviour and a subsequently the finite element solution method implementation is discussed. Chapter 5 goes into further detail on the numerical model of the glass container simulation. In this chapter, numerical aspects are addressed, such as the elements definition, the contact algorithm, mesh updating and the solution of the resulting system of equations. Chapter 6 discusses the validation of the thermal and the thermomechanical formulation. Some particular attention is paid in comparing the analytical heat transfer equation to the formulation proposed. Also, the thermomechanical formulation is verified. Subsequently, in chapter 7 the software layout is explained, in particular its environment and the program files. In chapter 8 a description of a set of the simulation cases is performed. It includes a reference to the material properties, machining timings, as well as the process parameters. All the process stages results for the blow-blow process and press-blow process respectively are presented. Finally, in chapter 9 states some conclusions are drawn and some future tasks are proposed.

This page intentionally left blank

CHAPTER 2

2 Glass Material Properties

A description of the glass material properties is presented in this chapter.

2.1 Brittleness

Glass is a brittle material at room temperature, this means that when is subjected to loads it can break without significant deformations. Brittle materials cannot absorb plastic deformation, failing in a sudden and catastrophic manner. Glass fracture once a critical stress is reached from a defect present in the glass. Brittleness is affected by glass composition through hardness and toughness. These type of materials fail when there is little or no evidence of plastic deformation before failure. However they have usually high strength.

2.2 Density

Density of a material is defined as the mass divided per unit of volume:

$$\rho = \frac{m}{V} \quad 2.1$$

Density calculated is true density of the material considering that the sample is free of bubbles, voids, or other defects. However, if the samples contain defects, as referred before, the density will be less than the true density. Glass containing unknown material, such as, impurities from raw material, unmelted batch or crystals formed during cooling, will cause an imprecise glass density. Viscosity can change the density. Also, glass structure will vary the density depending on the cooling rate. Varying the cooling rate will influence the atomic rearrangement of atoms which will change the final volume. This uncertain density can make difficult to predict the stress.

2.3 Thermal Expansion

When the material is subjected to a temperature change, i.e. is heated from room temperature to a temperature that promotes softening and dilatation. The thermal expansion coefficient has a relation between the volume of a glass and its temperature being strongly influenced by the chemical composition of the glass.

The deformation caused by the thermal expansion is given by:

$$\varepsilon_{ij} = \alpha_{ij} \Delta T \quad 2.2$$

which α_{ij} is the thermal expansion coefficient.

Glass material is characterized to have low thermal expansion. This mean that material will not expand or contract very significant. However, the thermal expansion of glass can lead to residual stresses when it cools to fast or is subjected to thermal shock. Theses stresses can be high enough to damage or fracture the container. When the glass is being formed some concerns should be taken due to temperature gradients inside the container. For example, if the surface of a material is cooling faster than the interior, the surface will attempt to contract but it will be constrained by the internal material resulting in tension and the interior in compression. For glass materials this can be sufficient to extend cracks, causing damage or fracture.

Residual stresses can be inside a container during the coating processes or in the thermal tempering. Thermal expansion can lead to compression or tension stress. If the stresses are tensile, this can lead to crack formation but if compressive, they can be used for strengthening.

2.3.1 Glass Cord

Different glass compositions can lead to different thermal expansion coefficients. When glass is produced with the same chemistry composition, the properties will be consistent. When a nonstandard glass is made from one batch or a series of batches, that glass will be a separate streak in the glass flow. If there is a difference in the coefficient of expansion between the two glasses, a permanent stress will result as the glass cools bellow the strain point ($\approx 500^\circ\text{C}$). The stress occurs because the entire piece begins to contract as it cools. The nonstandard glass might want to contract at different amount than the base glass. Since it must contract to the actual amount determined by the base glass, that glass will have a stress induced proportional to the difference in expansion coefficients. All these factors will influence the capacity of container to withstand different types of stresses (pressure, thermal shock, impact, etc) before it breaks.

Glass cord is defined as a chemical inhomogeneity of the glass resulting in permanent stress due to different coefficients of expansion between the layers of inhomogeneity. Cord usually is the result of the normal glass having a streak of nonstandard glass due to batching problems, Figure 2.1a). Cord can also occur when all batch ingredients are properly weighted but not well mixed. Each batch should be of relatively uniform consistency to avoid cord. Segregation of materials in mixed batch storage can result in chronic cord in the average glass density. Glass cord is observed by viewing in polarized light, Figure 2.1b). The amount of stress will shift the light as passes through it and a corresponding colour shift (birefringence) occurs.



Figure 2.1: a) Examples of a cord defects after cooling. b) Glass cord observed by viewing in polarized light [12].

2.4 Temperature dependence of viscosity

Viscosity is considered to be the most important criteria in glass making and the way the viscosity of a melt varies with temperature forms the only determining step for shaping of glass articles since it depends of capacity to formability at certain temperature. Viscosity also controls the stresses and strains to be applied to form the glass. It determines the melting conditions, the temperature regimes for forming, annealing and tempering, and the maximum temperature to avoid devitrification, Table 2.1. Consequently, numerous ways to relate the glass viscosity as a function of temperature and composition have been made. The relationship between viscosity and other physical properties can also lead to a better understanding of the glass structure. For the forming machines used in the container glass making industry, it is essential that a constant viscosity regime is maintained throughout in order to avoid or minimize any dimensional variation and also to avoid defect formation.

	Log	Viscosity (Poise)	Approx. Temperature (°C)
<i>Melt Viscosity</i>	2	100	1449
<i>Gob Viscosity</i>	3	1 000	1185
<i>Softening Point</i>	7.65	44 668 000	724
<i>Conveyor Viscosity</i>	10	10 000 000 000	632
<i>Annealing Point</i>	13.37	23 442 000 000 000	546
<i>Strain Point</i>	14.6	398 110 000 000 000	499

Table 2.1: Viscosity reference temperatures.

Viscosity is highly dependent on temperature, as glass is heated the material resistance to deformation gradually gets less important. Viscosity measures the resistance to shear deformation, therefore, measures the resistance to flow.

At certain temperatures, known as the glass transition temperature T_g , some materials are no longer considered to be liquids but rather amorphous solids or glasses.

Viscosity values should be considered with great care. The curve suggests that the rate of increase of viscosity with decreasing temperature becomes greatly reduced, Figure 2.2.

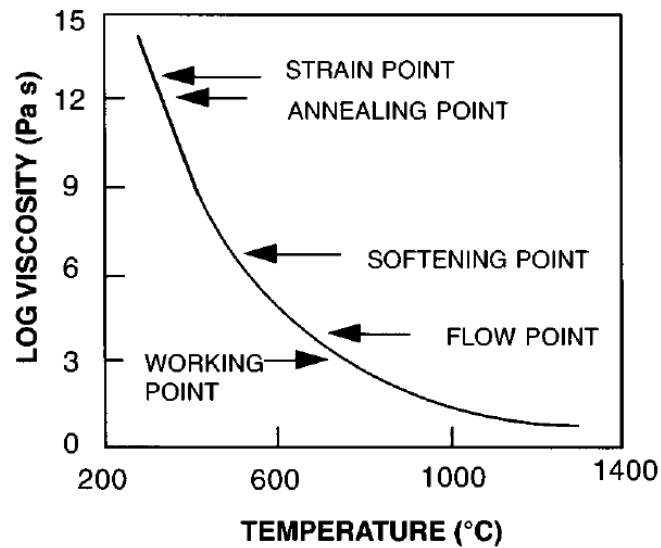


Figure 2.2: Viscosity evolution in working zone temperature [13].

Arrhenius equation was one of the first equations that could describe the viscosity-temperature evolution. The relationship between the viscosity-temperature of a glass is based on commonly employed conceptions in order to describe the transport phenomena in solids and liquids where ionic species have, under the influence of an electrical field, to overcome a potential barrier to affect conduction or diffusion. In this case however, using the thermal energy available at a certain temperature, the viscous flow of atoms and/or molecules needs to overcome the energy barrier [14]. The Arrhenius behaviour equation is given by,

$$\eta(T) = \eta_0 \exp\left(\frac{\Delta G}{RT}\right) \quad 2.3$$

where ΔG and η_0 are temperature-independent coefficients called the activation energy (for viscous flow) and the pre-exponential factor, respectively. An Arrhenius temperature dependence of viscosity is quite easily used and allows for rapid prediction of viscosity at a given temperature. This exponential expression, however, doesn't adequately describe viscosity variation over a wide temperature range since, with glass forming melts, the activation energy isn't a constant over the entire viscosity range [14].

Due to the limitations described above, various empirical equations have been put forward to deal with practical production situations. Notably, Vogel, Fulcher and Tamman and Hesse found independently that the following general equation provides a very good representation of the viscosity-temperature relationship which is satisfactory, for most practical purpose, for a wide temperature interval [14]. For silicate glasses, the VFT (Vogel–Fulcher–Tammann) equation often fits the temperature dependence over ten orders of magnitude in viscosity [13]. The behaviour of the super cooled liquid ($T > T_g$) can be fitted empirically by the Vogel–Fulcher–Tammann. The VFT equation involving three empirical constants (T_0 , A and B) and is given by:

$$\log_{10} \eta = A + \frac{B}{T - T_0} \quad 2.4$$

This equation can capture relatively well the non-Arrhenius temperature dependence over the melt-forming region. This law can be considered as a correction of the Arrhenius law adding a T_0 term. The VFT approximation is still easy to use and allows for close prediction of the actual viscosity.

Such models however, can be used only within limited temperature ranges. However they don't permit a clear understanding of the changes that occur with temperature or composition [15]. Doremus provided a further theoretical explanation of the Fulcher equation based on either free volume or temperature dependence of the size of the structural units that actively participate in the viscous flow [14];

$$\eta(T) = A \exp\left(\frac{B}{RT}\right) \left[1 + C \exp\left(\frac{D}{RT}\right)\right] \quad 2.5$$

where T is temperature, R is molar gas constant, A , B , C , and D are constants. This formula can be fitted to the experimental data so it can give us the correct Arrhenius-type asymptotes of viscosity at high and low temperatures [15].

An empirical formula proposed by Richert and Bassler in 1990, of some merit, fits the viscosity data, particularly in the high viscosity regime ($\eta > 10^6$ poises) [2].

$$\eta = \eta^0 \exp\left(\frac{T_0'}{T}\right)^2 \quad 2.6$$

where T_0' is a constant. This formulation is attractive, it avoids having to invoke any other temperature of divergence as in the VTF equation [2].

Dyre et al. (1996) had a different approach to account for the experimental viscosity variations with temperature as an alternative to VTF and AG models. They considered the flow in viscous liquids to arise from unpredictable events involving motion and molecular reorganization. With the mechanism in mind, the energy needed for such flow is decreased if the surrounding liquid is shoved aside to create the necessary volume for rearrangement. This volume is completely different from the volume of the free volume theory and is, in general, an activation volume. The free energy involved has five important thermal parameters, namely the melting point, crystallization temperatures, glass transition temperature, softening temperature and thermal expansion coefficient [2];

$$\eta = \eta_0 \exp\left(\frac{\Delta F(T)}{kT}\right)^2 \quad 2.7$$

where $\Delta F(T)$

$$\Delta F(T) = G_\infty(T) \cdot V_c \quad 2.8$$

where G_∞ is the shear modulus, V_c is some characteristic volume, which is related to the activation volume, and ΔV the volume of the liquid before shoving. It is given by [2].

$$V_c = \frac{2(\Delta V)^2}{3V} \quad 2.9$$

The non-linearity of the log viscosity as a function of inverse temperature arises due to the fact that $G_\infty(T)$ itself is temperature-dependent [2].

$$\eta = \eta_0 \exp\left(\frac{D}{f_g + (\beta_L - \beta_C)(T - T_g)}\right) \quad 2.10$$

The previous relation is known as the Williams-Landel-Ferry (WLF) law.

The approach in the Adams-Gibbs model is to consider the configurational entropy S_c of the liquid. Viscous flow is viewed as a cooperative rearrangement of the molecules [16]. As temperature decreases, less configurations will be available and rearrangement will need an increasing number of molecules. This leads to a decrease in configurational entropy and a decrease in mobility. The theory can be conveyed as [13];

$$\eta = \eta_0 \exp\left(\frac{E}{TS_c}\right) \quad 2.11$$

where E and η_0 are constants. The configurational entropy can be approximated by,

$$S_c = \alpha \left(\frac{1}{T_k} - \frac{1}{T}\right) \quad 2.12$$

where α is a constant and T_k is the temperature at which S_c goes to zero.

2.5 Chemical Durability

Chemical durability refers to glass resistance from exposure to warm, humid conditions, etc. Non-silicate glasses are very susceptible to dissolution in water, which limits their utility for applications involving contact with aqueous liquids or water vapour, Figure 2.3. Routine tests for surface dealkalization in the glass container industry generally evaluate the amount of alkali extracted from the glass when it is rinsed with or exposed to purified water.



Figure 2.3: Chemical durability of a container [12].

2.5.1 Dealkalization

Dealkalization is a process of surface modification applicable to glasses containing alkali ions, wherein a thin surface layer is created that has a lower concentration of alkali ions than is present in the underlying, bulk glass. Commercial glass containers are made of soda-lime glass, therefore, have a substantial percentage of sodium ions in their internal structure. Since sodium is an alkali element, its selective removal from the surface results in a dealkalized surface. Dealkalization treatment hinders this process by removing alkali from the inside surface. Not only does this mean less extractable alkali in the glass surface directly contacting the product, but it also creates a barrier for the diffusion of alkali from the underlying bulk glass into the product. The process of dealkalization should take in account the final product which will be introduced inside the container.

2.6 Liquidus Temperature

The liquidus temperature is designated as the maximum temperature at which crystals can co-exist with the melt in thermodynamic equilibrium. Above the liquidus temperature the material is homogeneous and liquid at equilibrium. In the other hand, below the liquidus temperature more crystals may form in the melt. The liquidus temperature for glass container is approximately 1024°C. This means that if we hold the temperature slightly below this temperature for a long period of time (hours to days) there will be crystals which form in glass. This only occurs where abnormal cooling of the glass occurs in the refiner, foreheart or spout areas.

2.6.1 Devitrification

Devitrification is the process of crystallization in a formerly crystal-free (amorphous) glass. The causes of devitrification, can include to holding a temperature slightly below liquidus temperature for too long, which causes the nucleation of crystals. In addition, the chemical compositions of some types of glass can make them more vulnerable to devitrification than others.

2.7 Light Transmission – Colour

Glass colouring can be obtained by adding of colouring ions. Metals and metal oxides can be added to glass during its manufacture to change its colour which can vary its aesthetic appeal. These oxides can be added to give or hide colour from glass, Figure 2.4. Brightness is the average amount of visible light transmitted by the glass.

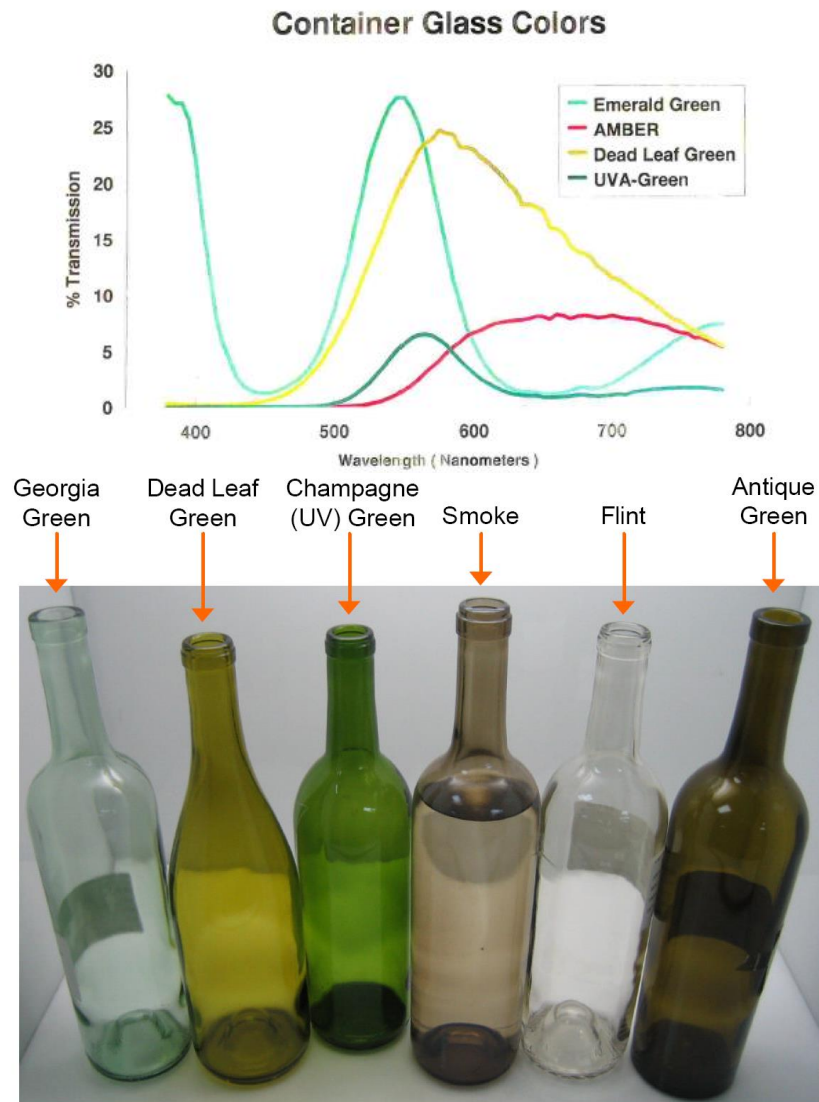


Figure 2.4: Glass colours presented in some container [12].

2.8 Cullet

Cullet from various melting units usually can be added to the respective glass batch. Cullet (recycled glass) can be used in the glass manufacturing process in variable percentages. The proportion depends on: availability, type of glass and quality (colour). The use of cullet, or scrap glass, not only reduces waste, but also aids in reducing batch-free time by both reducing the amount of refractory material in the batch, and by providing additional liquid throughout the melting process.

Glass cullet is a high-value material since its usage results in:

- Reduction of consumption of raw materials (silica sand, soda, dolomite, etc.);
- Reduction of CO₂ emission that is generated while melting the raw materials;
- Prolongation of the service-life of the glass furnace even up to 30%, because of the lower melting temperature of glass cullet than of the raw materials;
- reduction in the consumption of energy sources for melting the raw materials, which means also fewer emissions of NO_x, SO₂ and particles into the environment;

- cullet is 100% recyclable, out of 100 Kg of glass cullet 100 Kg of glass containers can be produced;

Impurities have to be removed from cullet, such as: ceramics, stones, iron and non-ferrous metals (Aluminium, lead), quartz, glass ceramics, opal, and organic waste (paper, plastic, food rests).

The impact of these impurities in the recycled glass is the following:

- Ceramic materials like stones and chinaware, being hardly fusible or which hardly dissolve in the molten glass, and non-ferrous metals;
- Alumina particles (Al_2O_3) not completely dissolve in the glass melt in the glass melting furnace;
- Metallic Aluminium in the glass melt reduces SiO_2 into Si – globules (Si – spherically shaped due to high interface tension) which have a different expansion coefficient;
- Other glass types like vitreous silica and glass ceramics, generally occur less often as impurity, but if present will also create stress concentrations within the glass product;
- The organic components in the recycling glass can only be separated to a certain extent. These impurities have a strong reducing effect on the glass melt (addition of C). Consequently the redox state of the melt is decreased which may cause fining problems and colour variations in the glass.

2.9 Strength of the Glass

Strength of the glass is defined as the stress at failure and is measured of the resistance of glass fracture. Inherently, glass is a strong material, however, it is sensitive do surface flaws. The reduction in strength is due to surface flaws that severely weaken the glass. These flaws act as stress concentration points, increasing the local stress to levels that exceed the theoretical strength and causes the fracture of glass. Griffith handled this problem in detail and derived the expression [13]:

$$\sigma_f = \sqrt{\frac{2E\gamma}{\pi c^*}} \quad 2.13$$

where σ_f is the failure stress and c^* is the critical crack length.

The critical crack length attainment is only a necessary condition for crack to grow. It is also crucial for the stress at the cracks tip to exceed the theoretical strength of the glass before the crack starts to grow spontaneously [13].

There are two methods to increase glass strength. Removal of flaws is only effective in short periods of time since new flaws are easily formed, while preventing their formation. We must concentrate on the prevention of crack growth and accept the fact that there will be flaws. Since crack growth needs the presence of a tensile stress at the flaw tip, creating compression on a near-surface region may prevent the cracks to growth. Crack growth won't occur until the stress applied is large enough to overcome the compressive stress and produce a tensile stress at the crack tip. Compressive surfaces can be manufactured by ion exchange, thermal tempering, by application or formation of a compressive coating [13].

2.10 Thermal Shocks

Some manufacturers have tried to create tempered containers. Thermal shock is a genuine problem wherever glass is rapidly cooled over lengthy temperature ranges. A cooling rate gradient can lead to thermal tempering of glass by producing distinct fictive temperatures in the surface and bulk of the glass. Unfortunately, cooling with a temperature gradient in a glass creates temporary stresses that counteract the permanent stresses because of the differences in fictive temperature [13].

Even though the stresses formed during cooling are not permanent, failure can happen due to the high stress that occurs when the surface temperature and bulk temperature vary. The maximum amount of stress will

be generated if the surface is instantaneously cooled, while the bulk remains at the original temperature. In these conditions, the stress is given by this equation [13]:

$$\sigma = \frac{E\alpha\Delta T}{(1-\nu)} \quad 2.14$$

where the difference between the surface and bulk temperatures is represented by ΔT and α is the materials thermal expansion coefficient.

The best thermal shock resistance is for low expansion and low modulus glass. The maximum temperature differential that can be used, without sample failure, will be very high for a very low thermal expansion glass. [13].

2.11 Glass Composition

Throughout the years the knowledge developed on how any change in glass chemistry has a correspondent change in each physical property. This has allowed to calculate an expected (or theoretical) property from glass composition. Maintaining consistent glass chemistry will lead to maintaining consistent glass properties. As each component oxide percentage changes in a glass composition, every physical properties will be affected. Some components have large influence on some properties more than others. Container glass is usually made with eight major oxide groups. Below is listed a container glass oxide composition.

Composition	Oxide Term	Raw Material Source(s)
<i>72,4% SiO₂</i>	Silica	Sand (Nepheline Syenite, Calumite)
<i>1,8% Al₂O₃</i>	Alumina	Nepheline Syenite (Calumite, Feldspar)
<i>0,05% Fe₂O₃</i>	Iron	(Calumite, Sand, Limestone)
<i>14,3% Na₂O</i>	Soda	Soda Ash (Nepheline Syenite)
<i>0,3% K₂O</i>	Potassia	Nepheline Syenite (Feldspar)
<i>10,7% CaO</i>	Calcia	Limestone (Calumite)
<i>0,3% MgO</i>	Magnesia	Limestone (Calumite, Dolomite)
<i>0,18% SO₃</i>	SulphurTrioxide	Salt Cake (sodium sulphate)

Table 2.2: Composition of typical glass containers

Oxide Type	Function	Example (container glass)
<i>Network-Forming</i>	Build the glass structure. Form glasses when melted and cooled	SiO ₂
<i>Intermediate</i>	Not capable of forming a glass, but it can take part in the glass network. In conjunction with the glass former oxide builds the glass structure	Al ₂ O ₃ , ... ,
<i>Network Modifier</i>	Not able to build up the glass network and instead weakens the glass structure. Lower the melting temperature.	Na ₂ O
<i>Fining Agent</i>	Remove bubbles from glass melts.	Na ₂ SO ₄
<i>Accessories</i>	Colouring	FeO (green-blue), Fe ₂ O ₃ (green-yellow), Co ₂ O ₃ (blue), Cr ₂ O ₃ (green)

Table 2.3: Oxides functions in glass containers.

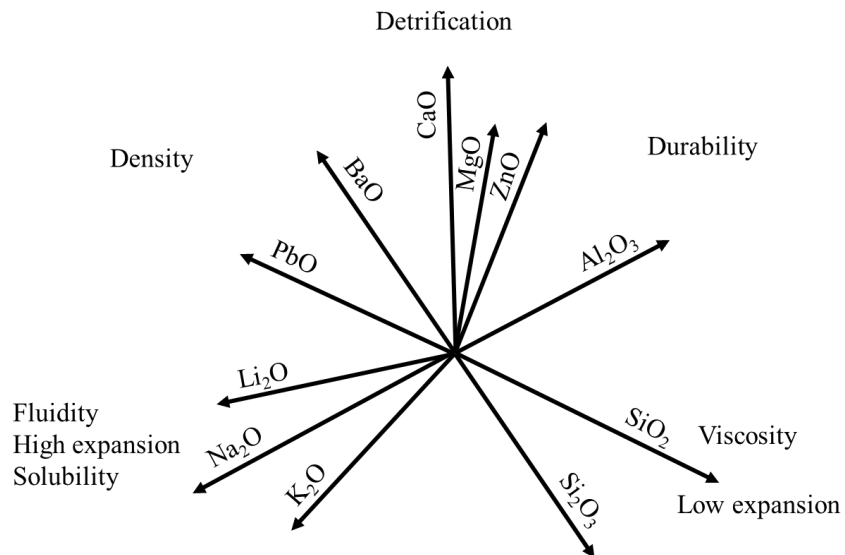


Figure 2.5: Effects of some oxides in glass properties.

This page intentionally left blank

CHAPTER 3

3 Glass Container Production

On a larger scale glass containers are formed using different processes, we shall focus on blow/blow and the press/blow processes. All processes start with batching and melting, after conditioning the materials to the desired temperature, subsequently the hot gob is transferred from the furnace to the forming operations through the gob feeders. The gob feeder controls the weight, temperature and shape of the gob, which are critical to the container quality. Many forming sections are distributed by only one gob feeder. The gob feeder comprises a plunger that drives the glass melt to the aperture and shears that cuts the gob for the desired volume. The cutting of the gob is helped by the cooling of the glass melt resulting from the shear contact, increasing the viscosity, while the backward movement of the plunger induces the upward rearrangement of the glass melt. The formed gob then enters the forming operations. After the forming operation, the containers go to a convey, annealing, coating, inspection and palletizing operations [1], Figure 3.1.

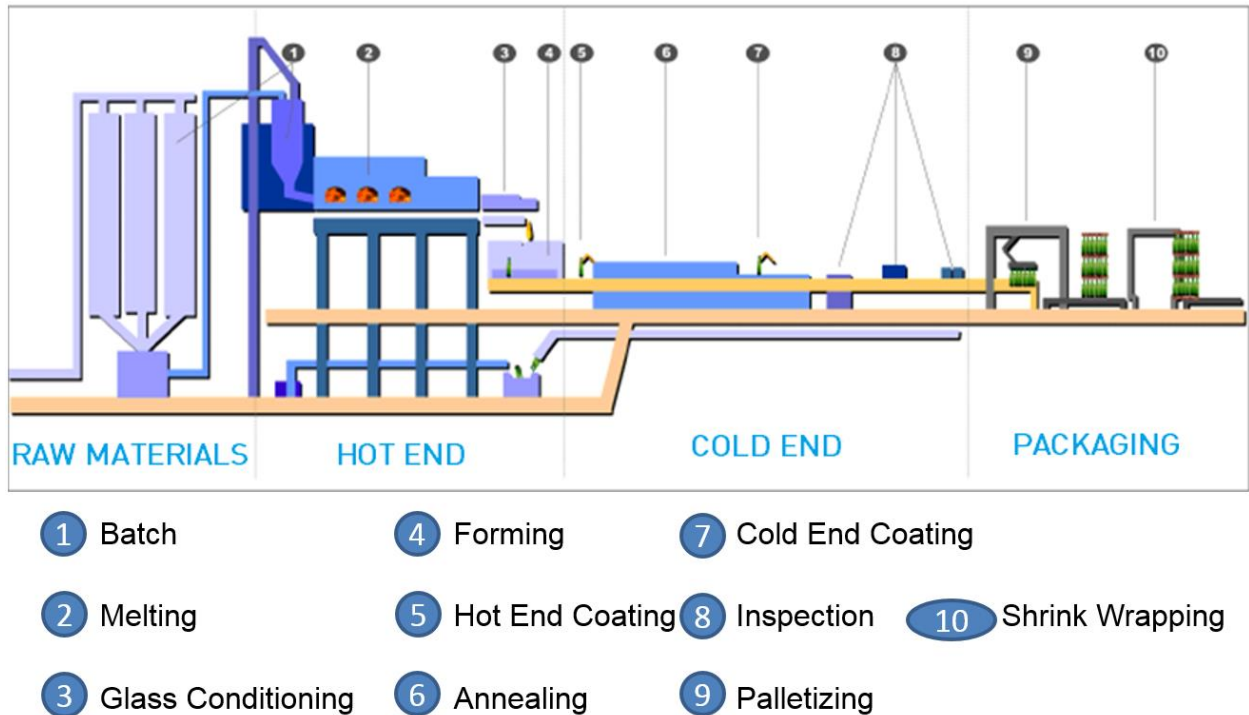


Figure 3.1: Production line of glass containers [12].

3.1 Batch

The batch is a key element in the glass melting process. The quality of glass is very much affected by non-homogeneous mixtures and inaccurate administration systems. A glass batch plant needs the capacity to fulfil the three main functions, as raw material storage, batch, preparation and batch transport [17]. Some concerns can influence the quality of the batch such as:

- Unclean trucks with foreign residues can introduce contamination;
- Variations in the chemical composition of raw materials: high iron content in sand (and other raw materials) imparts an undesired green tint to glass;
- Contamination such as metal and ceramic in cullet will cause defects such as “stones” in finished glass bottle;
- Weighting errors;
- Overmixing of the batch can lead to segregation of the batch materials;

3.1.1 Batch – Storing

Raw materials reach the glass plant batch house by rail or truck, they are visually inspected and sampled to ensure they fulfil the specifications, Figure 3.2a). Depending on the needed quantity, raw materials can be supplied in bulk, sacks or drums. The silos are filled pneumatically or mechanically, Figure 3.2b) [17].

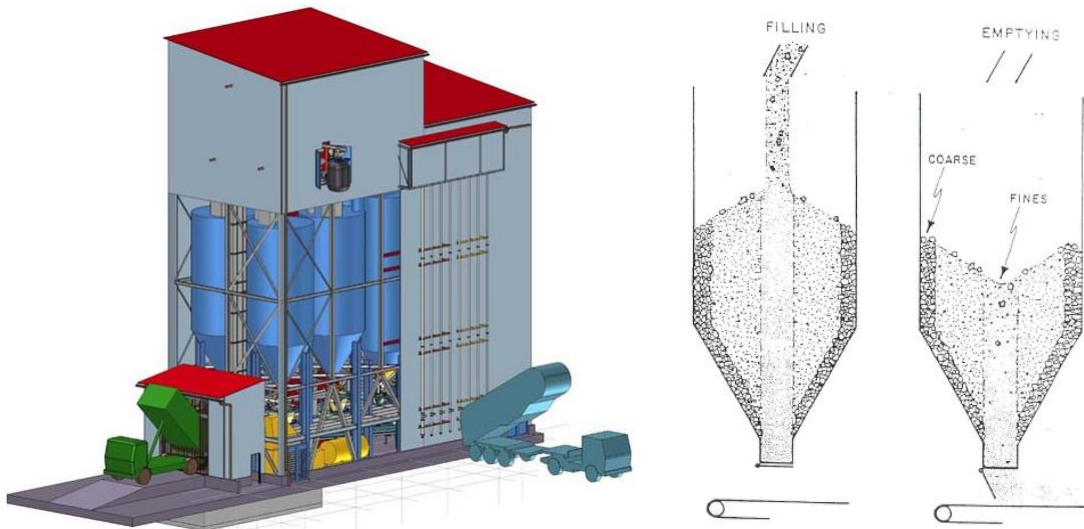


Figure 3.2: a) Glass plant batch house [12].

b) Batch house of a glass container line [12].

3.1.2 Batch – Weighting

Before going into the furnace, materials are proportioned into batches and weighed on scales located under the storage silos, Figure 3.3. There is usually one scale for each raw material and each batch must be accurate. Scales can be electronic or hybrid. In both systems, loading cells measure the weight of the raw material. To ensure its accuracy the scales should be checked periodically for sensitivity and calibration.



Figure 3.3: Weighting the raw material [12].

3.1.3 Batch – Mixing

After being weighed, materials are sent to the mixer, Figure 3.4. When all raw materials are inside the mixer the dry mixing begins. After dry mixing, water can be added and the wet mixing starts [17]. This is done to decrease the possibility of dusting and segregation as well as to suppress demixing during transport. A wet batch enhances the batch control pattern in the furnace, which is important for an efficient melting. Normally, after mixing, cullet is added on the top of the batch [17]. This is done to minimize wear and tear

of the mixer. The cullet may be added continuously or discontinuously to the mixture [17]. The mixed batch is then carried to the furnace by a conveyor.



Figure 3.4: Mixing the raw material operation [12].

3.2 Melting

In an industry of glass containers, the products are produced from melting raw materials and recycled glass in tank furnaces at high temperatures. Furnaces are made of three main parts, the melter, refiner and regenerators or checkers. Most furnaces are designed to use natural gas, they are capable of using alternate fuels like oil, propane and electricity, if necessary [18].

The melter is a rectangular basin in which the actual melting and fining (seed removal) takes place, Figure 3.5. In a side fired furnace, the batch is fed into the furnace through the doghouse, an extension of the melter, protruding from the back wall. Along the sides of the melter, above glass level, are three to seven ports, containing natural gas burners that direct the combustion air and exhaust gases [18]. A combination of electrical heating and fuel is used to improve heating uniformity and melt efficiency, it also reduces gas consumption and emission. The melter basin is connected with the refiner by the bridge wall (throat end wall). Glass passes from the melter to the refiner through the throat, a water or air-cooled tunnel that extends through the bridge wall [18].

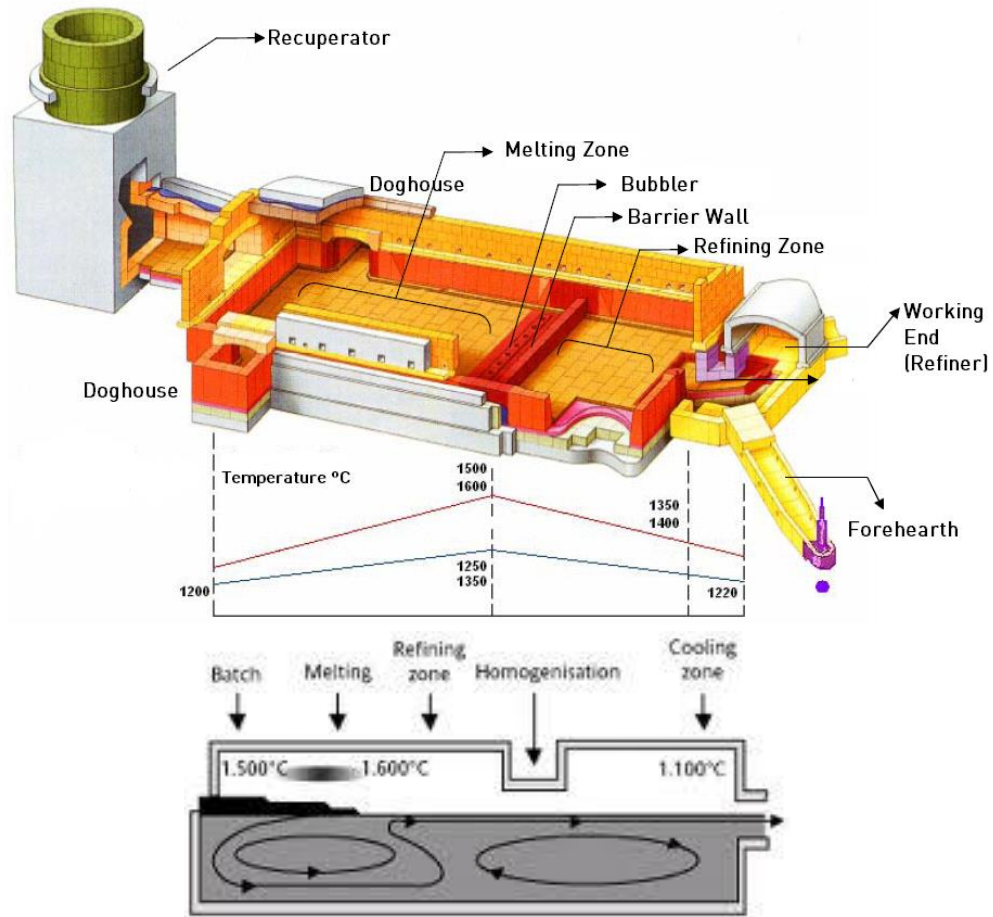


Figure 3.5: Melting plant scheme with the temperature gradient [12].

3.2.1 Regenerative Furnace

There are some different types of modern fossil fired furnaces, the heat contained in the released waste gases leaving the furnace is used to preheat the combustion air to produce higher flame temperatures and improve efficiency [19].

Regenerators form an intermediate storage medium, consisting of two chambers, each one is filled with a network of refractories, named the packing [19]. The waste gases from the furnace go through one of the chambers, heating up the refractories in the chamber. The combustion air goes through the other chamber into the furnace, Figure 3.6 [19]. Sometime after, both flows of air and waste gases are reversed. The combustion air now flows through the hot chamber and heats up by heat transfer from the refractories, whilst the waste gases pass through the other chamber and heat the refractories in this chamber again. Regenerator chambers are normally constructed vertically making the waste gases pass downwards, while the combustion air travels upwards [19].

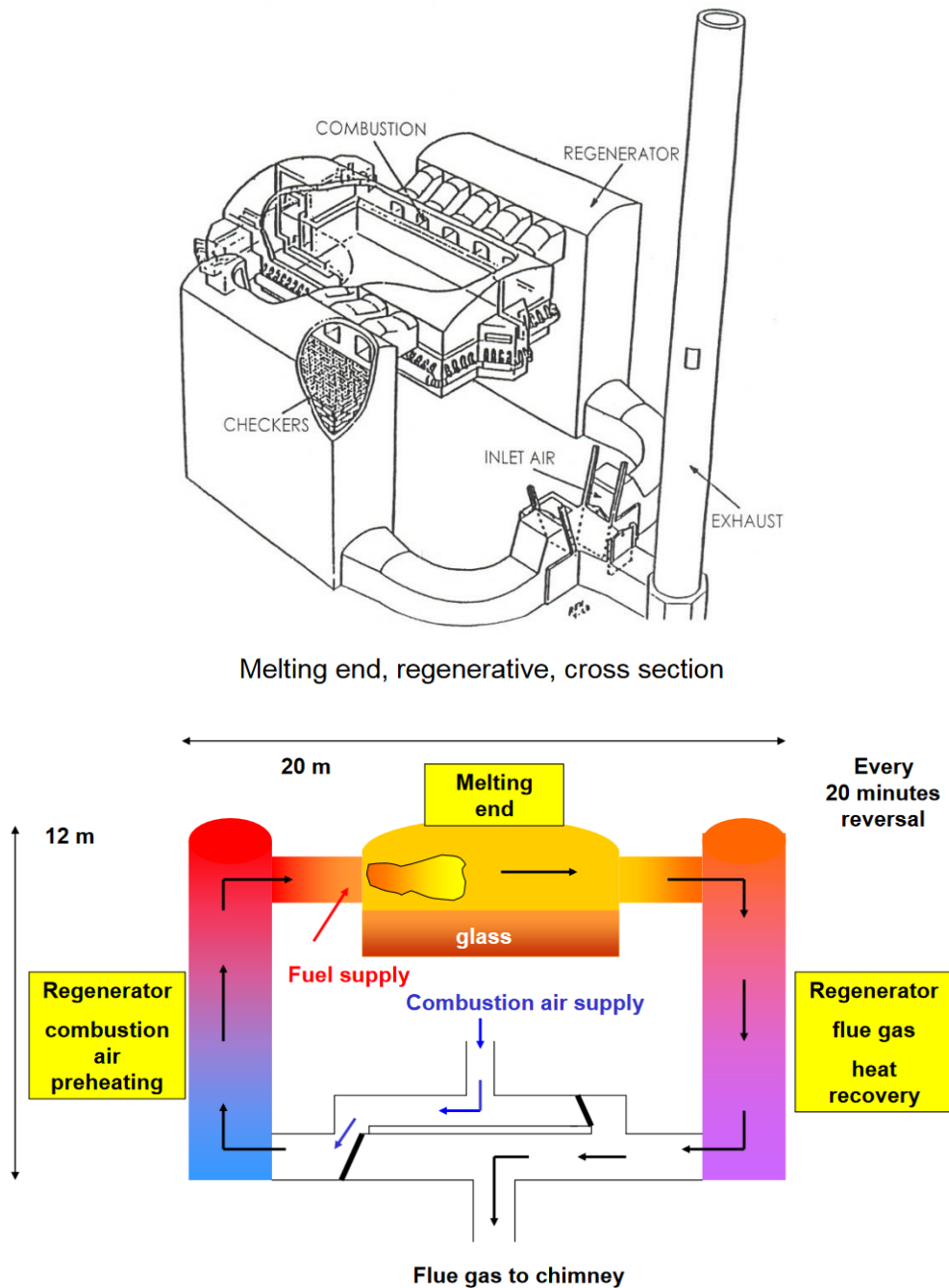


Figure 3.6: Regenerative furnace layout [12].

Regenerator chambers are normally constructed vertically making the waste gases pass downwards, while the combustion air travels upwards. Regenerative furnaces can be divided into two basic types based on the location of the burner and the flame path which is regenerative furnaces side port (cross fired) and end port (end fired) [19].

- End fired furnaces;

End fired regenerative furnaces has two burner ports, side by side in the rear wall furnace, and the regenerators are located behind the furnace. The flame travels forward from the burner port, does a 180° turn and exits through the second burner port. Making the flame and waste gas path take the shape of a horizontal “U”. Results is that the combustion gases, in the furnace, have a relatively long residence time,

achieving a good energy utilization. The raw materials go through one or two doghouses by the sides of the furnace, located next to the rear wall [19], Figure 3.7. This type of furnaces have the following advantages:

- Very flexible furnace type;
- Lower construction costs than with cross fired furnaces;
- Lower energy consumption than a cross fired furnace,

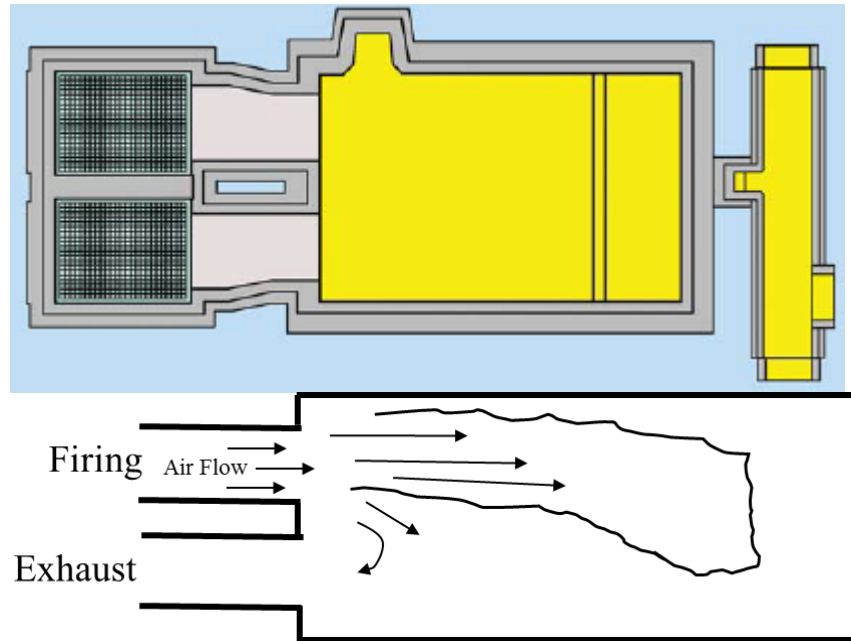


Figure 3.7: Regenerative end fired furnace [19].

• Cross fired furnaces;

Cross fired regenerative furnaces have burner ports located along the furnace side walls, normally covering most of its length. The amount of ports depends on the size of the furnace and usually within the range of three to five. Each port has from two to four burners, depending on the size of the furnace. The flame travels in one side to the other of the furnace and the waste gases are exhausted in the opposing entry burner port. The maximum flame size available is determined by the furnace width. With this type of furnace the regenerator chamber supplies many burner ports [19], Figure 3.8.

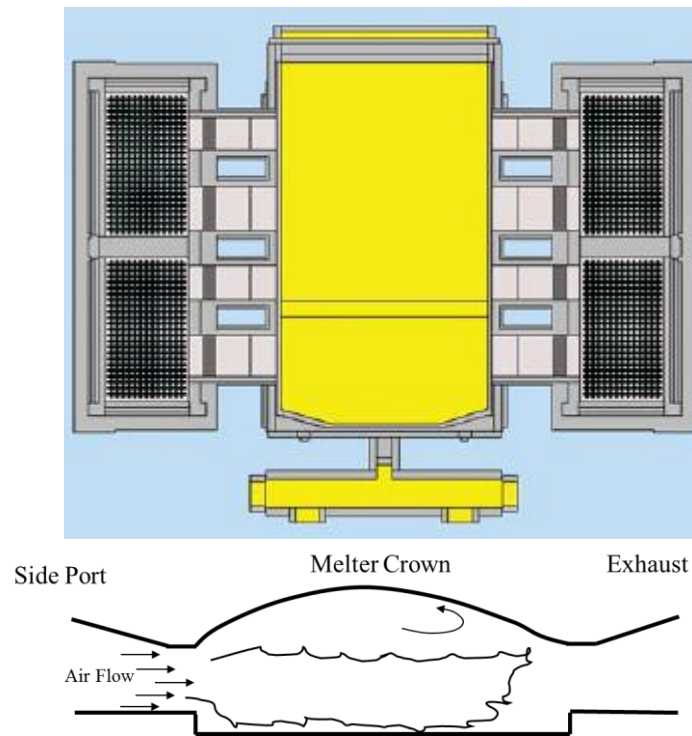


Figure 3.8: Regenerative furnace heat exchange [19].

The single doghouse is situated on the furnaces rear wall and the batch usually covers almost the complete tank width. As a result of the bigger number of ports and larger regenerator chambers, the heat loss area is greater than with comparable end fired furnaces [19].

3.2.2 Recuperative Furnace

In recuperative furnace the hot waste gases as well as the cold combustion air pass through parallel but separate channels and heat transfer takes place through the intermediate wall, Figure 3.9. Recuperatively preheated combustion air provides continuous heating without the flame/waste gas path reversal that is necessary with the regenerative systems. Lower investment than regenerators. Load energy usage increases more slowly than with regenerative furnaces. However, the air preheat temperatures are lower than with regenerators [19].

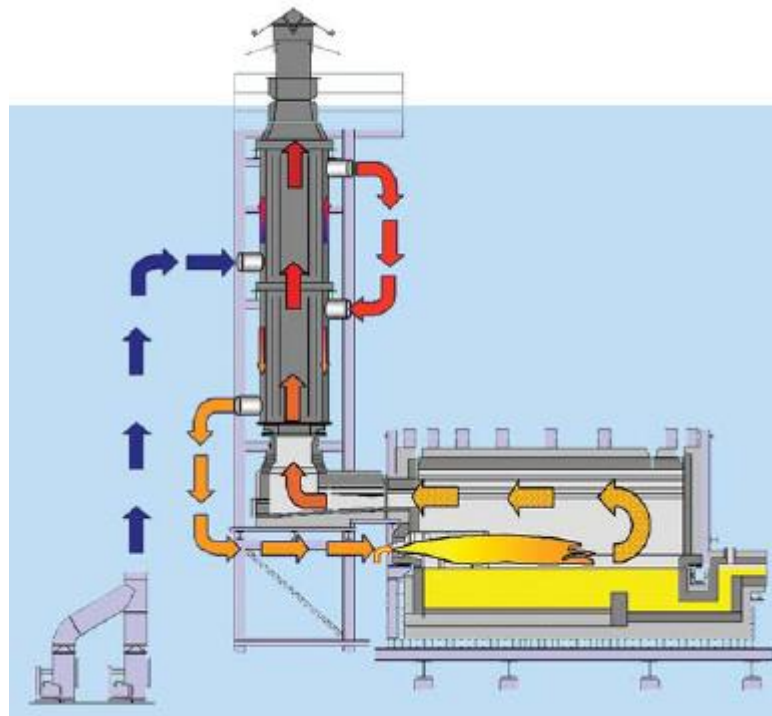


Figure 3.9: Recuperative furnace [19].

Most recuperative furnaces use steel recuperators to melt glass. They are always installed vertically, where the waste gas flows either upwards or downwards. The basic types of steel recuperator used are [19]:

- Double shell recuperator;
- Tube cage recuperator;

Double shell recuperator is made of two concentric high temperature resistant steel tubes of similar diameter, so that a narrow annular slit is formed in the centre of the two tubes. The hot waste gases pass through the inner tube, while the combustion air goes through the annular slit. The air may pass in the same basic direction as the waste gases (parallel flow) or go in the opposite direction (counter flow). Double shell recuperators can give a typical air preheat temperature with the range of 450 – 650 °C. The bulk of these units are used for small furnaces up to a melting capacity of approximately 50 t/24 h [19].

In a tube cage recuperator the combustion air is driven through a large number of individual small diameter steel tubes arranged in a ring around the inner circumference of a large diameter outer tube, through where the waste gases flow. The outer tube is made of steel, coated with refractory material [19].

Conventional recuperative furnaces can be branched into two types based on the location of the burner and the flame path [19]:

- End fired furnaces;
- Side fired furnaces;

There are many installation arrangements for burners and the recuperator in end fired recuperative furnaces. Similar to regenerative furnace, the burners are on the furnace rear wall, with the waste gas port immediately above, in the same wall. The flame leaves the burner and rides along the furnace, turns upwards and back to exhaust right above the burners. The flame path creates the shape of a vertical “U”. The single doghouse is on a side wall, next to the rear wall. This furnace concept is mainly used for small installations, with melting capacities of up to approximately 35 t/24 h [19].

The side fired burners of the recuperative furnaces are equipped along both side walls. The waste gases are exhausted towards the rear. Either one or two exhaust ports are outfitted in the furnace rear wall or a side wall. The furnace can be designed with a single or a double doghouse, either on the rear wall of the tank or immediately adjacent to the rear wall. Controlling the temperature of larger furnaces requires the use of control zones along the length of the furnace, Figure 3.10 [19].

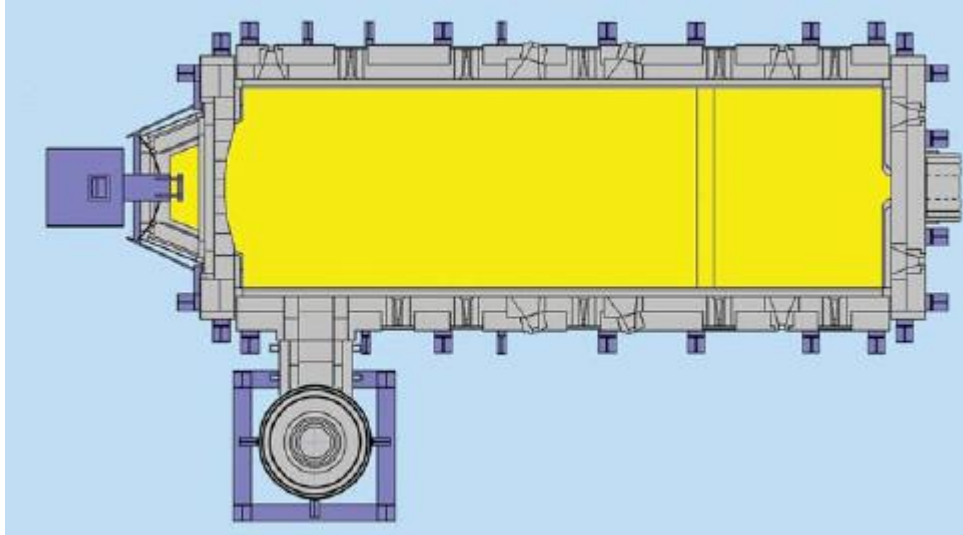


Figure 3.10: Side fired recuperative furnaces [19].

The needed energy consumption of side fired recuperative furnaces at full load is higher than that of comparable regenerative furnaces, yet is lower with partial load, Figure 3.11 [19].

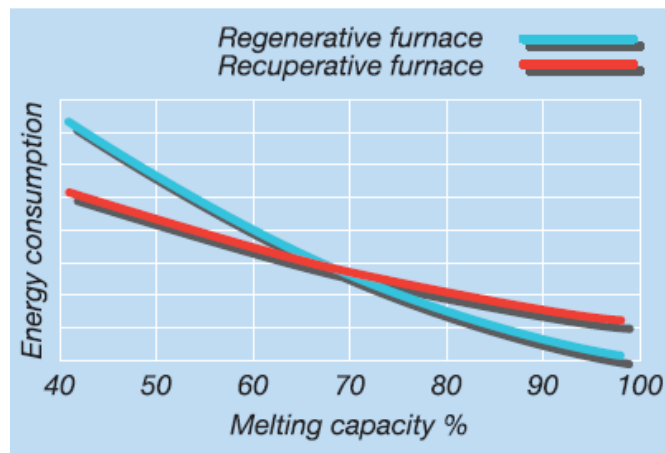


Figure 3.11: Comparison of energy consumption of a regenerative and a recuperative furnace at part load [19].

3.2.3 Boosting

The use of electrical energy as an additional energy source in conventional fossil-fuel fired furnaces is named as electric boosting [19]. Molybdenum electrodes can be equipped horizontally through the tank side walls, or vertically through the furnace bottom, Figure 3.12. A mixture of these methods is also possible. Under some circumstances an electric booster can be equipped in an operating furnace: in some furnaces, they make arrangements for a later installation during construction. Boosting systems can be branched into three groups according to their usage [19].

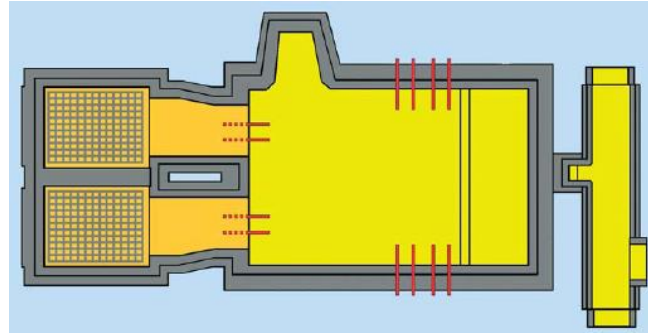


Figure 3.12: Boosting system in an end fired furnace [19].

Melting booster - a boosting system in the melting area gives additional energy directly to the glass bath and this leads to a higher melting capacity, Figure 3.13. a) [19].

Barrier booster - The installation of an electric booster around the hot spot boosts the convection currents and this increases the bottom temperature of the glass bath. This has a positive effect on the glass quality [19]. Furthermore, additional energy is given to the glass bath and the temperature of the glass flowing from the hot spot to the melting area is boosted. This may lead to a small increase in the melting capacity, Figure 3.13. b) [19].

Local booster - Here the electrodes are equipped in order to heat a precise area of the glass bath. The majority of these boosters are equipped in the throat and riser, where the glass can cool down more when the melting rate is low, Figure 3.13. c) [19].

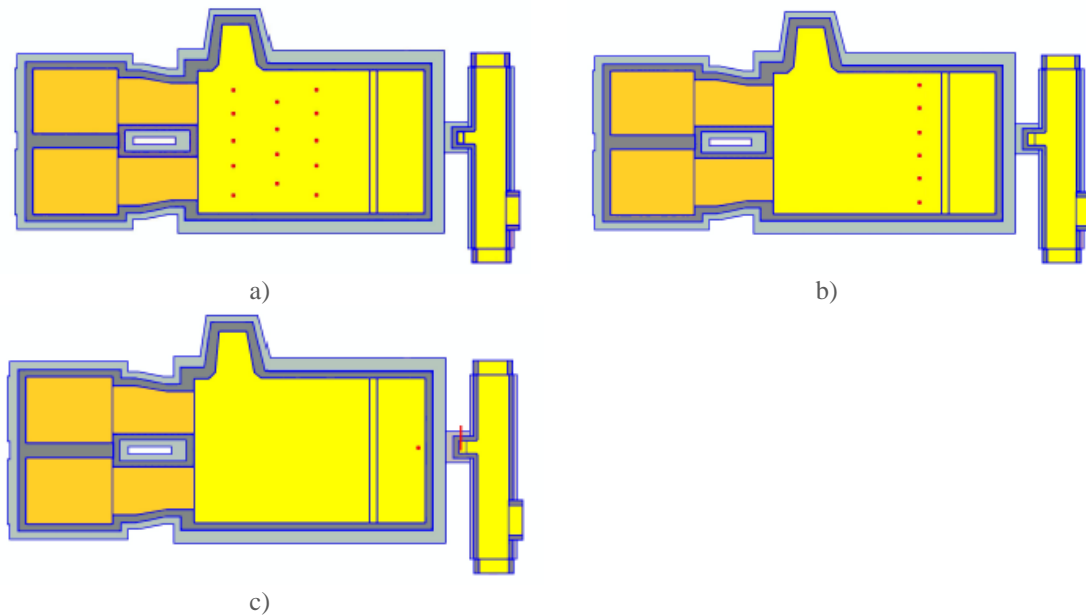


Figure 3.13: a) Melting booster b) Barrier booster c) Local booster [19].

3.2.4 Bubbler

Air or other gases are blown through special bubbler nozzles equipped in the furnace bottom. This makes bubbles in the glass, bubbles then rise to the surface and the gas is exhausted into the furnace atmosphere. The upward movement of the bubbles makes strong localized convection currents around their path, and these currents move the bottom glass upwards with an increase glass temperature at the bottom of the tank. The bursting bubbles on the glass surface also creates an effective barrier that prevents the unmelting batch from moving forwards on the glass bath surface. Generally the bubbler tubes are equipped in a row over the complete furnace at the location of the hot spot to reinforce the convection currents at this place [19]. The creation of this amount of gas, however, also leads to the formation of an extremely large number of bubbles, which must be removed from the melt before processing is finished because bubbles in commercial products are almost always considered flaws and result in rejection of the product [3].

Bubbles can be eliminated from melts either by physically rising to the surface, or by chemical dissolution of the gas into the surrounding melt. Since the density of a bubble is less than that of the surrounding liquid, a bubble will automatically surface and burst unless prevented from doing so by some external agent. If bubbles do not rise fast enough in a quiescent melt, the fluid itself can sometimes be moved by convection or stirred in such a manner that the bubbles are carried to the surface. Upward fluid motion can be done by mechanical stirring, by design of a glass tank floor to produce upward currents, by localized heating to make a locally hotter and thus less dense region in the melt, or by bubbling with a gas introduced near the bottom of the melt. In practice, all of these techniques were used to varying degrees in either tank or crucible melting [3].

Bubbles can be built by physically trapping atmospheric gases during the initial phase of batch melting, or by the decomposition of batch components. The gases in the apertures between batch particles may be cornered as the particles begin to soften and form a viscous liquid. As the viscosity decreases with increasing temperature, these apertures become fully surrounded by liquid. Surface forces then cause these apertures to assume the spherical shape of bubbles. These bubbles contain gases characteristic of the melting atmosphere, which can be air, combustion gases or some gas deliberately introduced to control chemical reactions with the batch. Prevention the formation of these bubbles involves eradication of gas from the apertures of the batch, i.e., melting under vacuum [3].

Bubbles can be created by the following causes;

- Trapping of atmospheric gases is enhanced by the use of very fine sand in the batch or by the use of batch components of broadly differing particle sizes. Both factors create a large concentration of very fine apertures within the unmelted batch. Agglomeration of particles is particularly effective in trapping atmospheric gases inside the agglomerate, becoming effectively surrounded by the viscous melt. Stirring mechanically a melt can introduce bubbles by trapping air and forcing it into the melt [3].

- Decomposition of batch materials can produce awfully large quantities of gases like CO, SO₃, NO_x, H₂O, etc. Reactions with metals making contact with the melt can generate oxygen, carbon dioxide, or hydrogen by electrolytic reactions. Erosion of refractories can open previously closed pores to the melt, releasing the gas contained in those pores into the melt. Residual carbon in refractories, or carbide refractories such as SiC, can react with oxide melts to create CO, or CO₂. The products of these reactions can agglomerate to form bubbles [3].

- Bubbles can also be created by precipitation from the melt whenever super saturation occurs for a specific gas. Since many gases have a large enthalpy of solution in glass forming melts, their solubility is a strong function of temperature. Species which alter their chemical form with temperature or changes in melt composition are particularly affected by precipitation from melts where they were previously soluble. Carbon dioxide, for example, is present in silica-rich melts as CO₂ molecules, where it chemically reacts with alkali-rich melts to form carbonate species, which are far more soluble than the molecular species. The solubility of carbon dioxide in the alkali-rich regions neighbouring silica grains during the early stages of batch melting is quite high. As the silica grains dissolve, the melt becomes locally enhanced in silica, which converts the dissolved species to CO, molecules, which have a much lower solubility. The melt

becomes supersaturated locally and CO₂ bubbles are created. As a result, CO₂ bubble generation will keep happening long after the initial decomposition of the carbonate batch components [3].

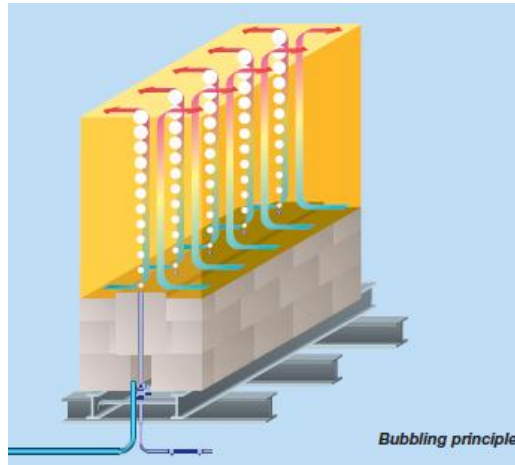


Figure 3.14: Bubbling principle [19].

3.2.5 Barrier Wall

In conventional glass furnaces the convection currents in the furnace have a compelling influence on the melting capacity and glass quality. An upward current is created at the hot spot as a result of the temperature distribution in the furnace. This current stops the forward flow of the colder bottom current and diverts it upwards to areas of higher temperatures. This avoids lower quality bottom glass from flowing directly into the throat. Nowadays this effect is aggravated by a barrier that is anchored in the bottom and projects upwards. This barrier wall is put up from one side of the furnace to the other at the location of the hot spot. The height of the barrier banks depends on the glass bath depth, Figure 3.15 [19].

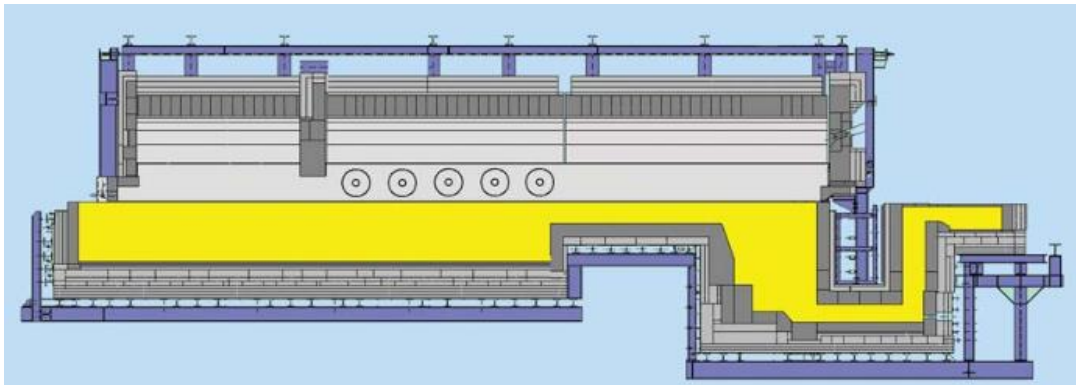


Figure 3.15: Barrier wall [19].

3.2.6 Refining Bank

The Refiner performs as a holding basin where the glass is allowed to cool to a uniform temperature before entering the forehearth. The melter and refiner are enclosed by crowns to contain the heat [18].

Successfully refining glass is largely dependent on two factors: time and temperature, where temperature has the most influence. The refining bank is an additional device in the tank, devised to raise the glass temperature in the refining zone, without increasing the superstructure temperature [19].

The bottom of the tank is raised over a precise distance, to give a shallower glass depth. The glass going to the throat is forced upwards into the hotter area near the glass bath surface. This fulfils one of the prerequisites for enhanced refining at higher temperatures. Higher glass temperatures in the refining zone gives lower glass viscosity. Thus, the refining gases reach the glass bath surface more easily. The shallower glass bath means that the current distance to the surface is shorter [19].

Glass fining produces a melt that is homogeneous in terms of composition, temperature and bubble free. In fact, the temperature of the glass delivered from the melting furnace, and its composition, has to be regulated very carefully. This requirement affects the next operation, that is, glass forming, the latter operation is reliant on viscosity, that is, on the way the glass has been prepared [1].

3.2.7 Drain

Zircon cords in finished articles are the result of deterioration of the refractory material that is used in large quantities in modern glass furnaces. Zircon has a somewhat higher density than normal soda-lime glass. Consequently, zircon-rich material created because of refractory corrosion tends to gather on the furnace bottom. The drain is designed to allow the continuous draining of very small quantities of material from the furnace, working end or forehearth bottom. The low draining velocity prevents glass from higher regions to be pulled down as a result of the funnel effect and helps to ensure that that contaminated material is taken out effectively from the furnace bottom level, Figure 3.16 [19].

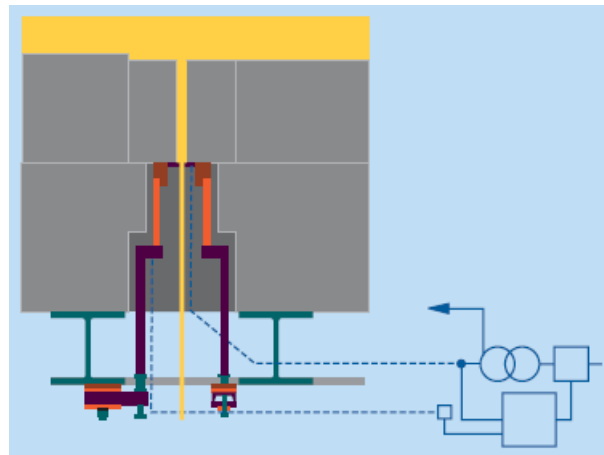


Figure 3.16: Drain cross section [19].

3.2.8 Cullet Preheating

When the cullet composition in the batch amounts to more than 60%, the use of cullet preheating to recover additional heat from the furnace waste gases is an economically feasible proposition. Cullet enters the tower structure at the top and slowly makes its way downwards to the exit. The waste gases arrive at the bottom on one side and are exhausted at the top on the other side, and so the cullet and the gases are in cross counter flow. The waste gases enter the preheater at a temperature of approximately 500°C and leave with approximately 200 °C. The cullet preheat temperature is normally approximately 400°C [19].

3.2.9 Melting Process and glass formation

Most commercial glasses are based upon chemical modifications made to melt and modify the structure of silica. Crystalline silica melts above 1700°C. By adding fluxing ingredients such as alkali (Na₂O, K₂O), the melting point drops significantly. To improve chemical durability and to obtain other physical properties other Alkaline Earth's (CaO, MgO) and other modifiers (Al₂O₃) are added. The resultant material is converted from a crystalline structure to a glass.

Glass formation involves a number of key steps – starting by properly formulating specific raw materials to contribute required oxides. The properly prepared batch ingredients must be kept in close proximity as they are heated. A serial of chemical reactions initiate some components melting and performing conversions of others into new, intermediate compounds. Large volumes of gases are evolved during the thermal decomposition of carbonates, hydrates and sulphates. Eventually, the final glass chemistry is reached when all raw materials have reacted and intermediate compounds combined into final product.

Chemical finning agents are materials intentionally added to the batch which promote the evolution of gases generated during the fusion process at elevated temperatures. Some processes make the bubbles larger in size, which can rise more quickly out of the melt. Others promote more physical agitation of the less soluble types of gases.

Thermal heat transfer for melting begins with a combusting process generating a flame. Radiation from the flame is directed to the melting batch and molten glass bath. It can also go to the refractory structure for reradiation into the melting system.

The heat transfer to the melting batch and freshly formed glass requiring thermal refining is controlled by flame place location and combustion control. It is difficult to measure temperatures within the melting batch for controlling that aspect of the process. Most operations establish temperature profiles within the furnace by a variety of sensors in the crown, bottom, molten glass or melter superstructure surface readings by portable optical pyrometers. By controlling these reference readings, the resultant glass quality helps establish control parameters for consistent melting and refining results.

Most furnace operations rely upon establishing and maintaining a hot spot. In this system of furnace the temperature gradient (or profile) relies upon the principle that hotter glass expands and flows on the surface towards colder areas. The surface flow can help contain the batch piles behind the hot spot and prevent partially melted glass of leaving the melting zone, Figure 3.17.

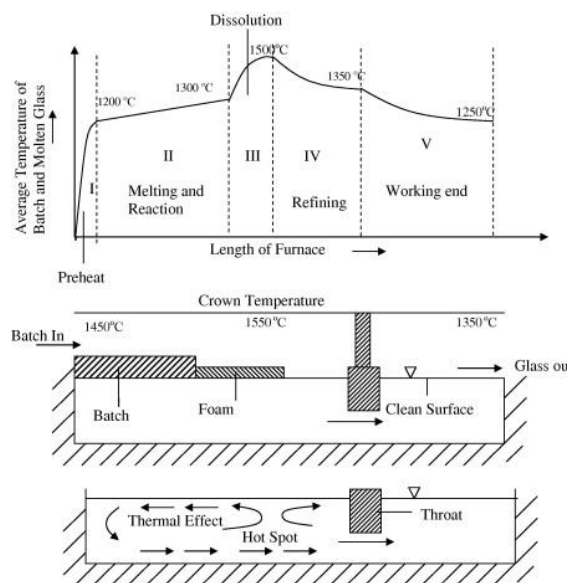


Figure 3.17: Furnace temperature evolution and the respective convection.

A convection pattern is established when glass lower in the melt is drawn upward to replace the glass flowing on the surface away from the hot spot, Figure 3.18. The batch charging establishes the pile shape and initial direction of flow into the melter. From that point on the operating temperatures and glass surface convection flow will determine the path the batch follows until is converted to bottles, Figure 3.19.

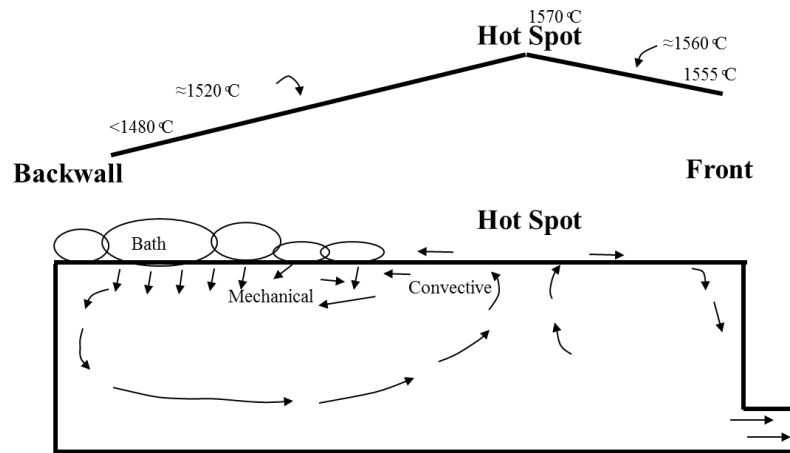


Figure 3.18: Flux of glass inside a furnace.

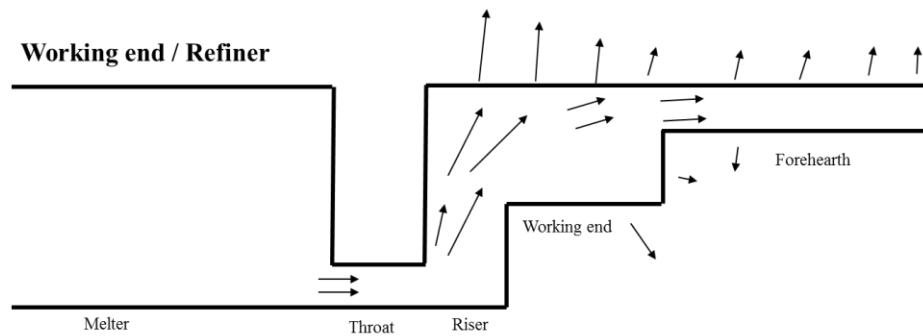


Figure 3.19: Working end furnace.

3.3 Glass Conditioning

Glass conditioning is a thermal process that can be defined as the achievement of a stable, desired glass temperature, distributed throughout the vertical and horizontal planes of the glass at the entrance of the spout, Figure 3.20.

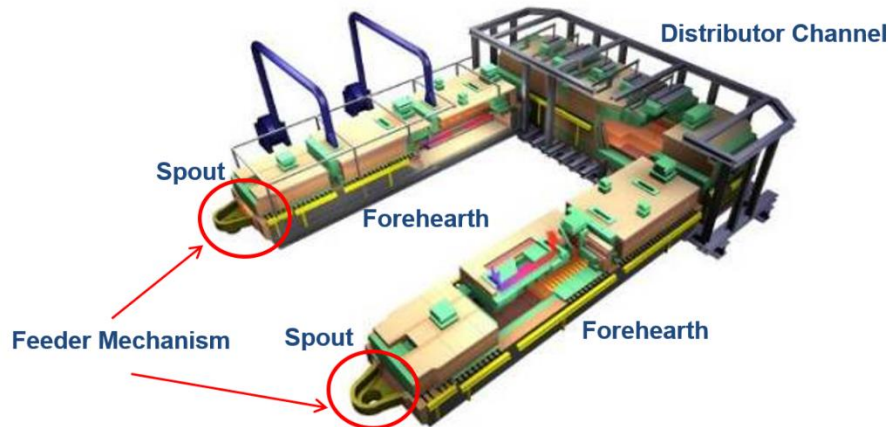


Figure 3.20: Glass conditioning general view.

3.3.1 Forehearth

The forehearth plays no role in chemical conditioning or refining of the glass nor does it lead to the removal of bubble or seeds from the glass. These functions are carried out only in the furnace [20]. Forehearths simply don't have the subsystems to fix furnace faults. Consequently, furnace-derived problems will be given by the forehearth to all subsequent stages in the manufacturing process [20].

However, it is expected that it can mitigate the effects of:

- Upsets in the melter or distributor;
- Fluctuations in air temperature between day & night;
- Fluctuations in humidity;
- Fluctuations in pull rate;
- Fluctuations in glass level either from the melter or from head loss on adjacent forehearths.

Forehearth requirements:

- Temperature stability;
- Temperature homogeneity;
- Glass flow (along the forehearth and trough bends – the forehearth is slightly tilted downward);
- Fast response time (at job change and in response to external disturbances);
- Low energy consumption.

If the forehearth fails to produce its conditioning objectives, the ensuing problems will be fed to the subsequent forming process. Approximately 100 types of errors have been identified, around 50% may be related to the temperature and thermal homogeneity of the glass, and by implication, to the effectiveness of the thermal conditioning properties of the forehearth design [20].

The ability of the forehearth to get thermal stability rapidly after a job change is another key element in the efficiency of the overall forming process. The time needed to stabilize the glass after a job change is a part of the response time of the forehearth and is determined by the efficiency of both combusting and cooling systems, as well as the effectiveness of the superstructure geometry [20].

The homogeneity of the melted glass in the forehearth needs to be monitored by measuring the temperature in three different points at three different levels in each forehearth zone (typically: rear, middle, front) – 9 points grid, Figure 3.21.

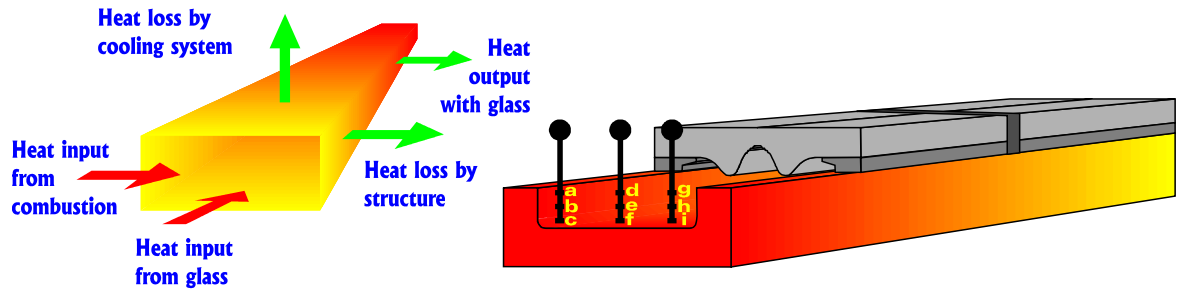


Figure 3.21: Glass Conditioning heat transfer [12].

There are some types of different forehearth which include forehearth type K, forehearth longitudinally cooled, radiation cooled forehearths, muffle cooled forehearths and system 500 forehearths. Each forehearths will be described as follows:

- Forehearth type K

Cooling is applied through passages in the side of the superstructure, passing under the forehearth roof and exiting through the central flue with the combustion gases, Figure 3.22.

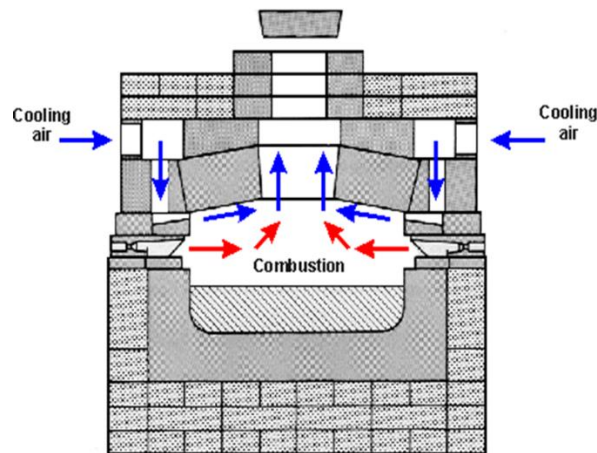


Figure 3.22: Forehearth Type K [12].

Three problem can be founded in forehearth type K which are;

1st problem: Heat is taken out of the sides of the glass flow by radiation to the colder surface of the roof block. Effect: This causes the sides of the glass flow to be cooler than the centre, Figure 3.23 a)

2nd problem: The cooling air and combustion gases exhaust through the same single flue. Effect: It is not possible to separate the cooling functions from the heating functions within the forehearth, Figure 3.23b)

3rd problem: There is insufficient insulation applied to the substructure. Effect: There are substantial uncontrolled heat losses through the forehearth sides and base, Figure 3.23 c).

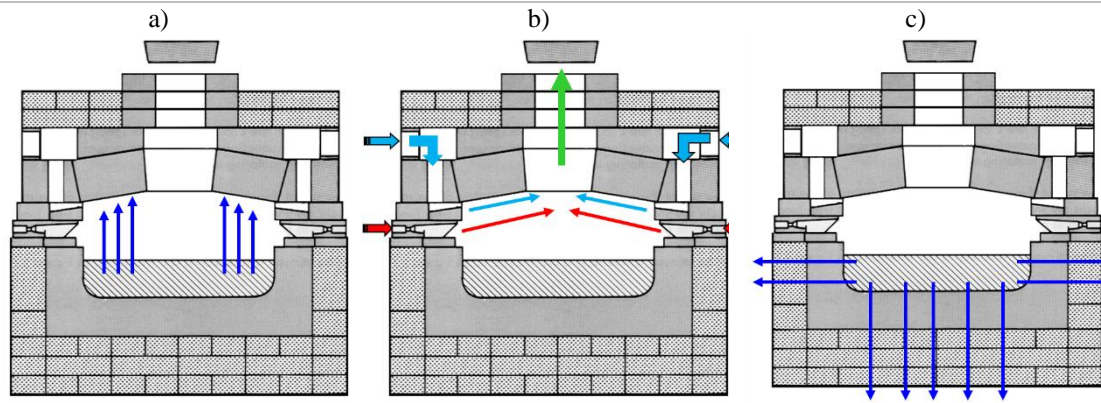


Figure 3.23: Forehearth Type K [12].

o Forehearth longitudinally cooled

Cooling is applied longitudinally under the forehearth roof, cooling the underside of the roof block. Heat is taken out of the glass by radiation to the colder refractory surface, Figure 3.24. Three problem can be founded in Forehearth longitudinally cooled which are:

1st problem: With only a single flue for both the combustion and cooling, the cooling air and combustion gases mix together. This effect prevents separate control of the heating and cooling functions within the forehearth.

2nd problem: The cooling air is quickly spread across the entire forehearth width causing the cooling effect is insufficiently concentrated on the central flow of glass.

3rd problem: The cooling zones are too long and the cooling effect is spent soon after entering the forehearth. The effect for a significant part of each zone the cooling air is ineffective, limiting forehearth response time and flexibility.

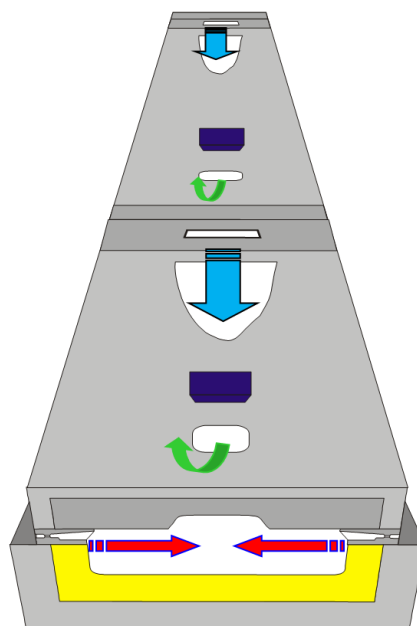


Figure 3.24: Forehearth longitudinally cooled [12].

- Radiation Cooled forehearths

The method of operation contain large flues are left in the forehearth superstructure enabling heat from the glass to radiate to the colder atmosphere as it flows beneath a flue, Figure 3.25. Three problem can be founded in radiation cooled forehearths which are;

1st problem: Allowing heat from the glass to radiate to atmosphere causes massive heat loss beneath the flues. Effect: As the glass flows beneath a closed section of superstructure the glass reheats, causing cycling in the glass temperature.

2nd problem: Radiation cooling is extremely severe. Effect: Close control of the glass temperature is difficult to achieve and often results in overcooling, chilling of the glass surface, and prevention of further heat removal.

3rd problem: The presence of large open flues prevents control of the internal forehearth pressure. Effect: Fuel efficiency is very poor.

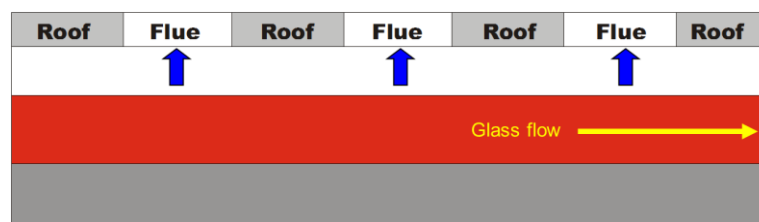


Figure 3.25: Radiation cooled forehearths [12].

- Muffle cooled forehearths

Cooling wind is passed along a muffle in the forehearth superstructure, cooling conductive tiles set in the forehearth roof, enabling the glass to cool by radiation to the tile's cooler surface, Figure 3.26.

The problem associated to this type of forehearth is the heat from the glass has to be conducted through the muffle tile. Effect: Cooling capacity is restricted and response time is slow. Forehearths need to be longer to compensate for the lack of cooling.

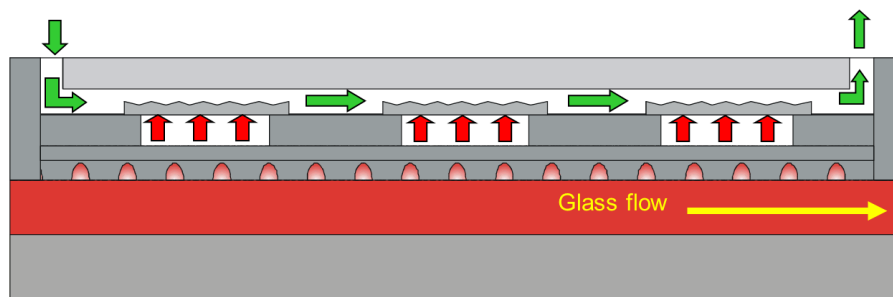


Figure 3.26: Muffle cooled forehearths [12].

- System 500 forehearths

The main features of this type of forehearth include separate combustion and cooling dampers, fully automatically controlled, cooling subzones for greater cooling capacity, hot face longitudinal cooling, a single piece roof block profiled to separate the combustion from the cooling, Figure 3.27.

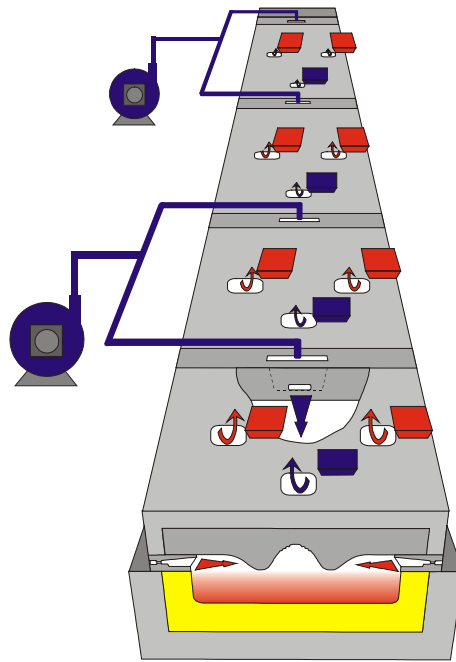


Figure 3.27: System 500 forehearths [12].

Combustion takes place at the sides of the glass flow and exhausts through dedicated side exhaust dampers. Cooling air passes longitudinally down the forehearth under the roof blocks exhausting through dedicated central exhaust dampers, Figure 3.28a).

The cooling air is automatically terminated, the side dampers closed, and all the products of combustion exhaust through the central flue, heating up the entire forehearth width, Figure 3.28b).

In normal operation the forehearth operates automatically between the heating and cooling modes, adjusting the firing rate and the flow of cooling air to obtain the required glass temperature and optimum thermal homogeneity, Figure 3.28 c).

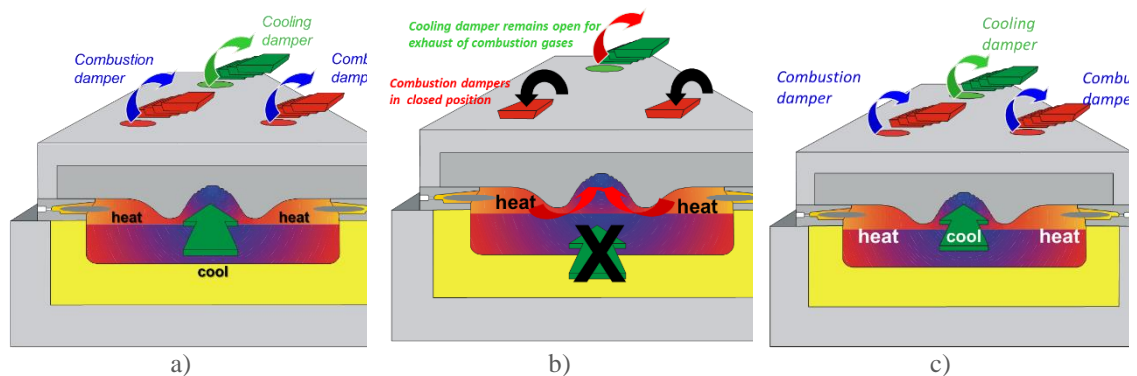


Figure 3.28: System 500 forehearths a) cooling cycle b) Heating cycle c) Normal operation [12].

In conventional longitudinally cooled forehearths the cooling zones are the same length as the combustion zones approximately 2500-3000mm long. However, with such long cooling zones the cooling effect from the cooling air is dissipated after travelling 50% of the zone length, Figure 3.29 and Figure 3.30.

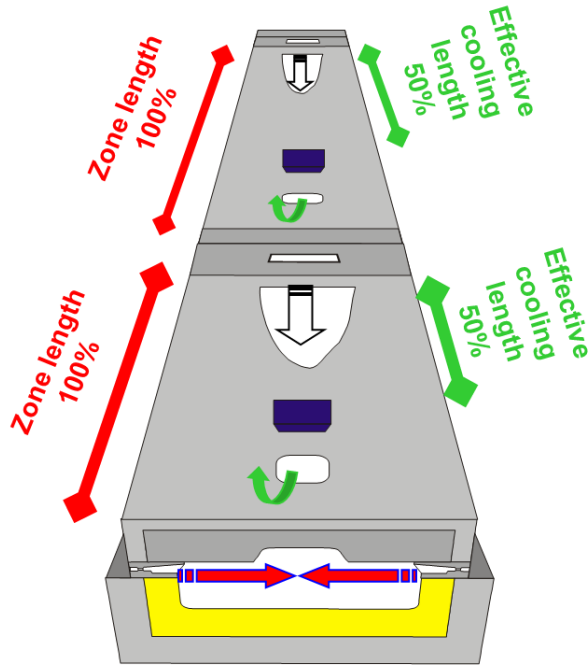


Figure 3.29: System 500 forehearths cooling zones [12].

Control zones are subzoned into multiple cooling ‘subzones’, significantly increasing the cooling capacity and flexibility of the forehearth and quicken the response time.

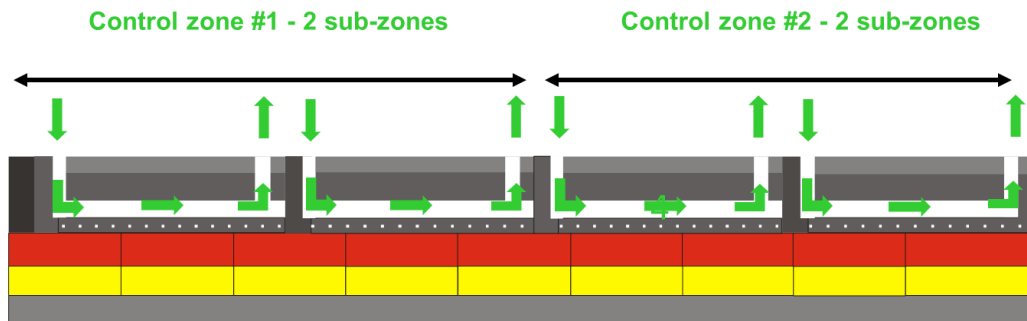


Figure 3.30: System 500 forehearths cooling zones [12].

3.4 Forming

In this subsection the process of the forming of glass containers will be described.

3.4.1 Feeder

The molten glass goes from the melting furnace into the thermal conditioning forehearth. Once the right thermal homogeneity and viscosity are achieved, the feeding mechanism cuts the string of liquid glass into gobs of required size, shape and weight, Figure 3.31. The red hot gobs of glass (1.200° C approximately) vertically drop into the delivery system and then distributes them to the various sections of the I.S. Machine.

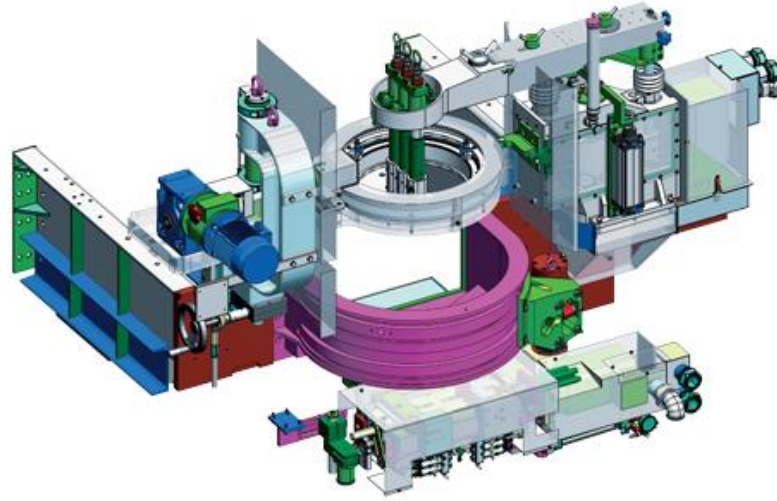


Figure 3.31: Forming feed machine [12].

The spout bowl is a refractory part in the end of the forehearth channel. It has a circular hole at the bottom where fits the orifice ring. A cylindrical tube overlies the spout bowl and a selected clearance can be established between the bottom of the tube and the surface of the spout bowl around the opening to control glass flow from the spout bowl, Figure 3.33.

Feeder tubes are used in the spout section to homogenize the glass by rotation, and to allow heating or cooling through the vent holes if present. The tube is mainly used to control the flow of glass through to the orifice ring below. The feeder tube is also used to shut off the flow of glass if necessary by lowering onto the surface of the spout. These tubes have a collar on the top to fit the mechanism used for rotation.

There is a scale which gives us the height of the tube – 0 position being at the bottom, with the tube shutting off the glass flow. The tube is often viewed mostly as a tool for controlling gob weight, but the height of the tube, in conjunction with the plunger, is also an important factor in gob shaping. There is an optimal tube height for every orifice ring size. For instance, with a small gob of 14 to 28 grams in weight, the area of the orifice is very small making the tube height very low and critical. If the tube is too high, that will make the gob to lose action and gain very little weight. Glass runs from the orifice unencumbered. If the tube is too low it will cause the orifice to run empty, resulting in loss of action and weight, plus a long and stringy gob shape [21].

As the tube height is raised, more glass is permitted to flow under it. Also the height of glass below the tube is increased. This in turn increases the effectiveness of the plunger action within the glass due to more glass adhering to the plunger, which consequently is pushed out of the orifice. Resulting the gob becomes heavier, longer and begins to have a ‘waist’ in the middle, Figure 3.32a). As the tube is lowered, the amount of glass beneath the tube is reduced as is the height of glass below the tube. This also decreases the effectiveness of the plunger action and less glass is pushed through the orifice. Resulting the gob be lighter, shorter and more compact in shape, Figure 3.32b).

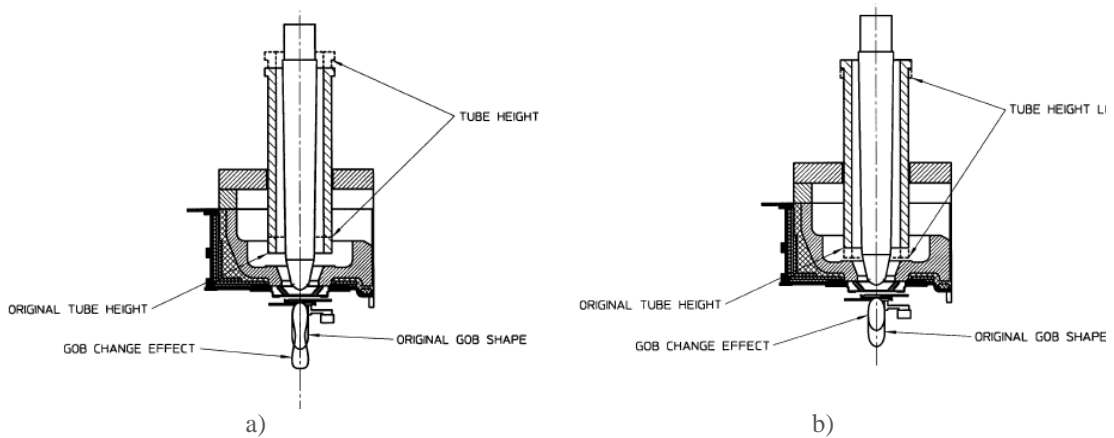


Figure 3.32: a) Tube height raised.

b) Tube height lowered [21].

The function of the orifice ring is to control the diameter of the molten glass gob, and the number of gobs required for the particular glass operations. The orifice ring is typically round and contains the appropriate number of gob holes, normally from one to four holes centrally located in the orifice ring. The orifice rings are installed in the bottom of the spout. The molten glass is forced through the holes in the orifice ring by means of mechanical force from the plunger(s) located above the orifice ring, Figure 3.33c).



a)



b)



c)

Figure 3.33: Examples of a) Spout bowl b) Feeder tubes c) Orifice ring [12].

The orifice diameter is usually determined by feeder manual charts and previous experience and operation of similar situations (same weight and gob shape). When making a gob, if unable to get enough weight and the gob is short and stubby, this usually indicates that the orifice is too small, Figure 3.34 a). If the weight cannot be reduced to what is required with the tube and plunger on their lowest point, this indicates that the orifice is too large, Figure 3.34b) [21]. If unable to get a low weighted gob and the tube and plunger are low, the change to a smaller orifice ring is the most indicated action. In each case the requirement is to change the orifice ring (assuming that the glass temperature and machine speed are correct and appropriate for the situation).

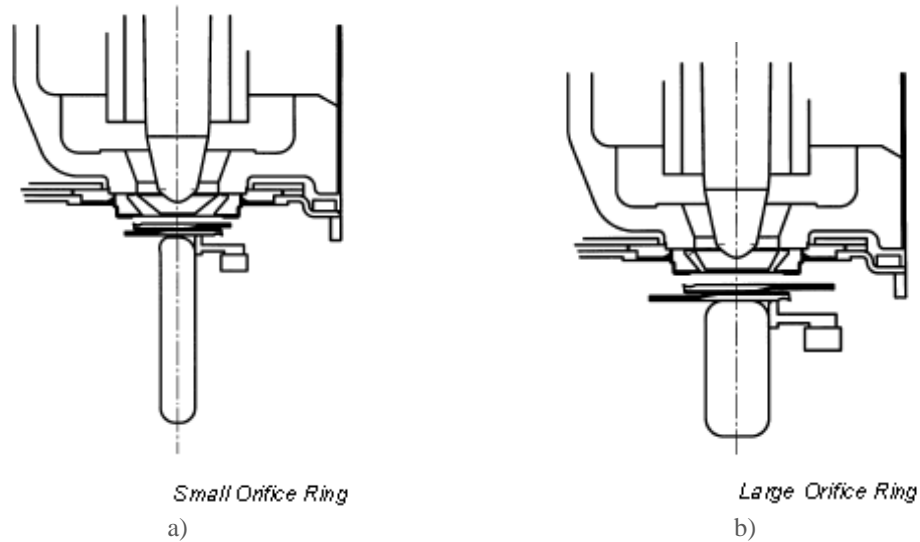


Figure 3.34: a) Small Orifice Ring.

b) Large Orifice Ring [21].

Plungers are available in different shapes, diameter and lengths, depending on the type of feeders and process being used, i.e. size of refractory tube, single, double or triple gob. Plunger tip profile and diameter are very important to the gob weight and shape control. Taper point (standard, long and offset) and ball point plungers are the ones often used. The tapered plunger will form a tapered gob while the ball point will make a straight cylinder type gob, Figure 3.35 [21].

Glass feeder plungers operate in coordination with shears and other components in order to control the manner in which molten glass is delivered to glassware forming equipment downstream of the feeder. A glass feeder may have one or more plungers, each axially lined up above an associated orifice in the bottom of the feeder spout bowl through which emanates a stream of molten glass. Each plunger (and orifice) has implemented with it a pair of shears, and all plungers and shears are synchronized with the glassware forming machine and operate in cycles in order to cut the respective stream into predetermined gobs of molten glass [22].



Figure 3.35: Glass feeder plungers [12].

Each plunger controls the speed with which the glass emanates from its associated orifice. Therefore, the cyclical motion of each plunger has to be controlled in a predetermined manner in order to achieve desired gob shapes and weights [22]

Plunger motion profiles are dependent of a lot of variables including glass temperature and type, machine speed, the type and size of glassware to be produced, etc. As a result, even with job changes, minimal changes of plunger movement are desirable to keep an optimum machine operation and speed. Furthermore

the motion profile of each plunger, adjustments of the plunger differential (i.e. phase relationship of plunger cam to shear cut), stroke length and height (i.e. defined as the lowest point of the plunger tip above orifice) also affect gob formation [22], Figure 3.36.

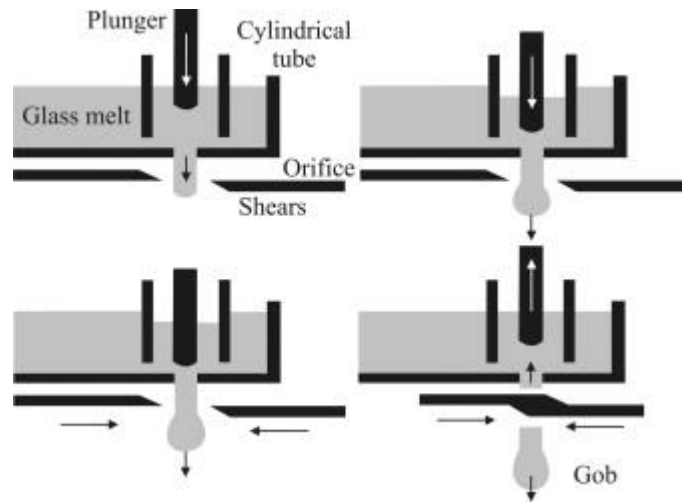


Figure 3.36: Representation of plunger motion and gob shear cutting [1].

The plunger extent is important. It not only controls, in alliance with the tube, the gob weight, but also is key in determining the ultimate gob shape. When the plunger is lowered, there is a reduction in gob weight, but it also increases the action inside the gob. When raised the gob weight increases, but reduces the action in the gob, less control over the glass flow. There is also an optimal plunger height in relation to tube height. There is a scale that shows the position of plunger height above the orifice ring, Figure 3.37 [21].

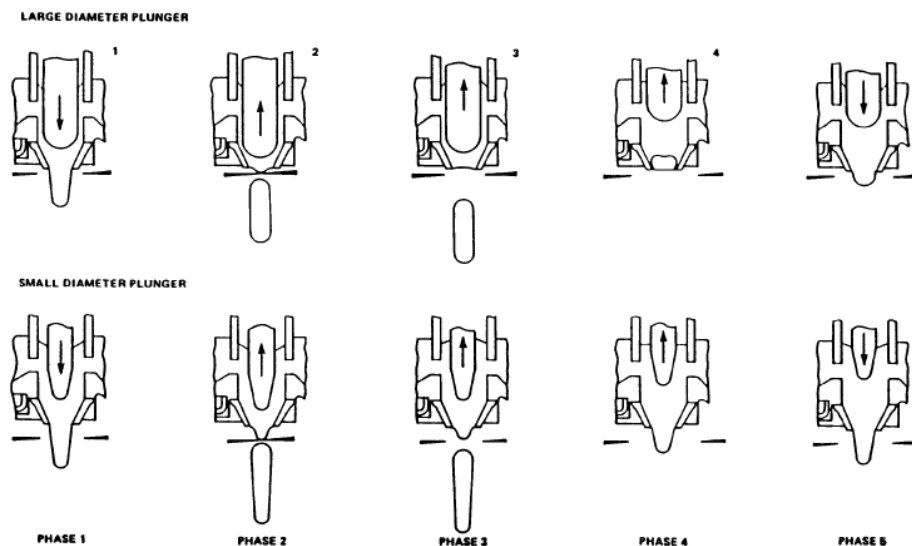


Figure 3.37: Effect on gob with different plungers [21].

As the plunger height is lowered, the low point of the plunger is adjacent to the orifice. The plunger is also farther into the glass inside the tube giving more grip to the glass and restricting the flow, Figure 3.38a). As the plunger is raised, the low point of the plunger rises farther above the orifice ring and out of the height of glass inside the tube, Figure 3.38b). This reduces the effect of the plunger action within the glass and

consequently control over the glass flow through the orifice ring is moderately lost allowing the glass to flow more freely [21].

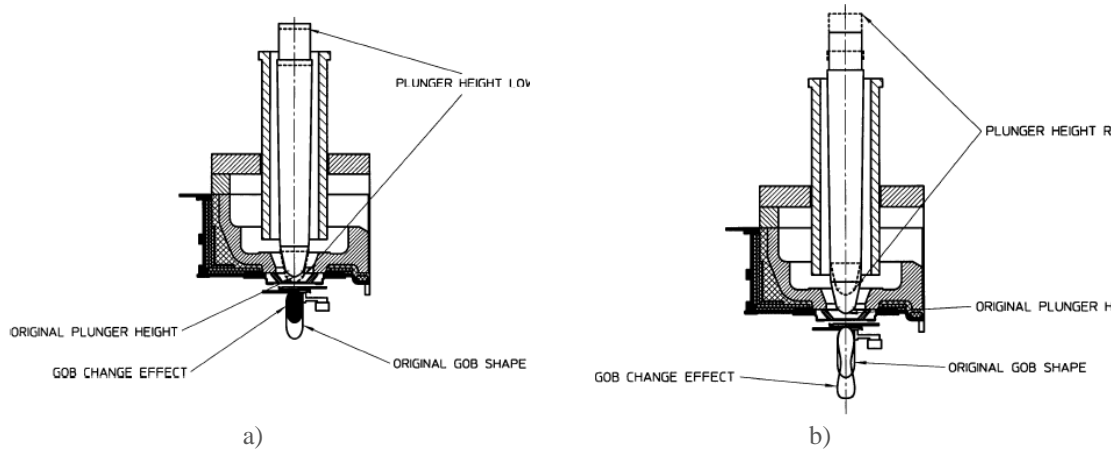


Figure 3.38: a) Plunger height lowered.

b) Plunger height raised [21].

Gob cutting shears are employed to systematically sever the lower most portion of the vertical glass flow that comes out of each orifice ring, into a discrete glass gob of fixed volume, Figure 3.39. After the gob has been severed it then falls or slides down a suitable feed chute into a glass forming mould. The cutting of gobs of glass is a crucial operation since minor defects or irregularities caused as the gob is cut may result in a defectively formed glass article [22].



Figure 3.39: Gob cutting shears [12].

The shear height is changeable. The integral shear mechanism is either moved up or down, close to the orifice or further away from the orifice. Shear height is very useful to get the final frame of the gob. Weight, temperature differential may be correct but shears height too high or too low can blemish the gobs shape. Raising the shears closer to the orifice will shorten the gob, lowering the shears farther from the orifice will lengthen the gob. Both adjustments control shape of the gob at its lower end. Shear tension is very important. Tension is adjusted by the raising or lowering of one shear arm where the blades are tensioned one against the other. Care should be taken when this operation is carried out as too much tension creates excessive abrasion on the blades and the shearing edge is lost very quickly, resulting in heavy shear marks. Too little tension on the other hand can create feathering of the cut, again creating a bad shear mark or occasional stringing of the gob, Figure 3.40 [21].

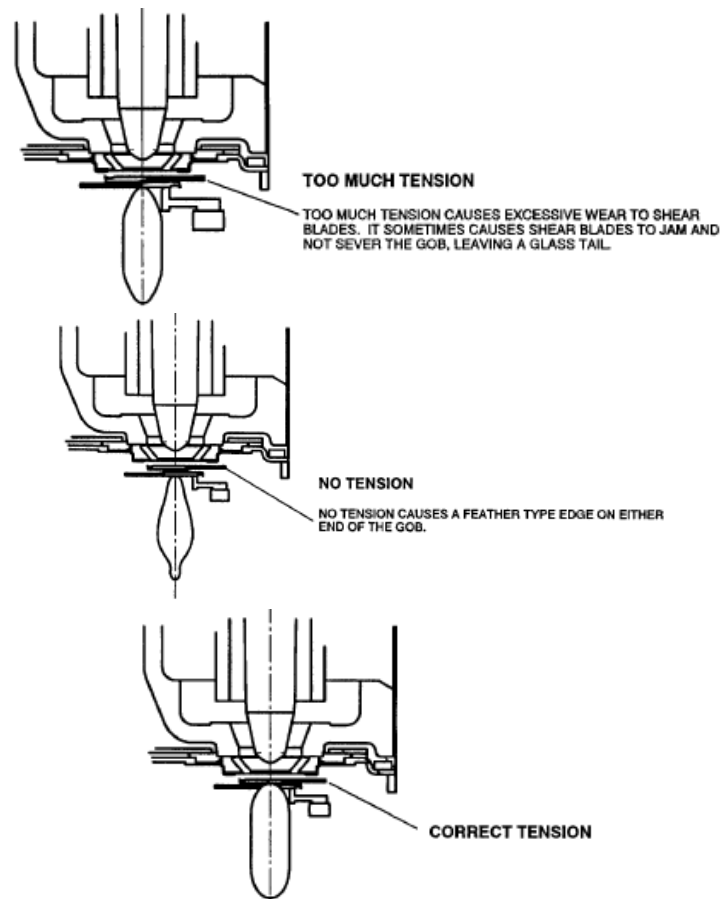


Figure 3.40: Shear tension effect on gob shearing [21].

Shear overlapping is controlled by adjusting one shear arm stop. This, through gear sections on each shear arm, can be used to alter the amount of crossover of each blade with the other. At this point the gob has been sheared. Excessive overlap can interfere with gob loading and unnecessary adjustments have to be made to overcome this. It is important that after shearing, the gobs leave the blades clearly vertical without inclination. Drop guides are generally positioned and fixed on the right hand shear arm and are used to adjust the gob angle at the shear cut. The adjustment is made side to side and front to rear directions, Figure 3.41.

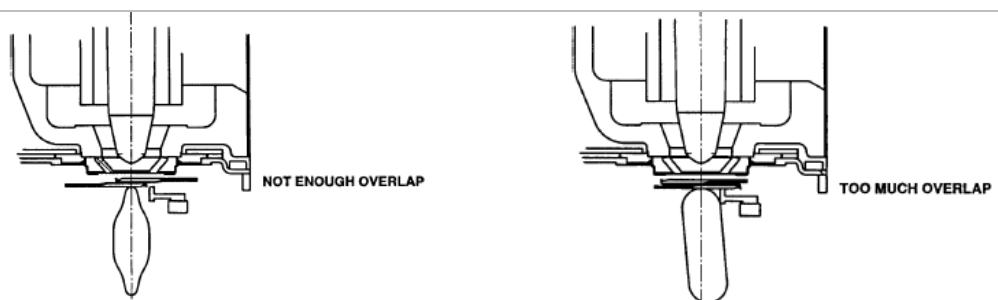


Figure 3.41: Shear overlap effect on gob shearing [21].

The difference in timing action of Plunger Action/Shear Cut is applied to gob shaping. This is done via the PLC timing system, accelerating or decelerating the plunger action. If the plunger is at its lowest point at the same time the shears cut off, glass will lay on the shears, withdraw a large heavy shear mark and flatten the gob. If the plunger action is advanced starting the upstroke lifting the glass before the shears cut off this

gives a small shear scar and leaves a point on the gob that will elongate into a good shaped gob, Figure 3.42 [21].

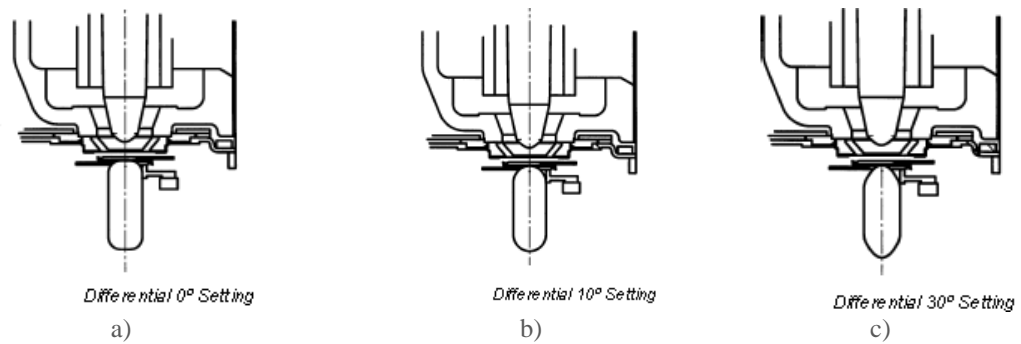


Figure 3.42: Plunger/shear differential adjustments a) Differential 0° setting b) Differential 10° setting c) Differential 30° setting. [21].

As the glass temperature rises, the glass becomes more fluid. More glass will flow under the tube and the plunger action will be less effective on holding the gob together. The glass will move more freely through the orifice, Figure 3.43a). As the glass temperature declines, the glass becomes less fluid. Less glass will move under the tube and consequently the gob will lose weight. Since it is colder, the plunger will have more grip on the glass during its upstroke, restraining the flow from the orifice, Figure 3.43b) [21].

As the machine speed is increased, the action of the plunger and shears also increases. Due to the increased motion of the feeder assuming that the glass temperature and all other things are the same, less glass will be out of the orifices for each gob, Figure 3.43c). As the machine speed is decreased, the action of the plunger and shears is lesser due to the decrease in feeder motion. All other things being equal, more glass will come out for each gob, Figure 3.43d) [21].

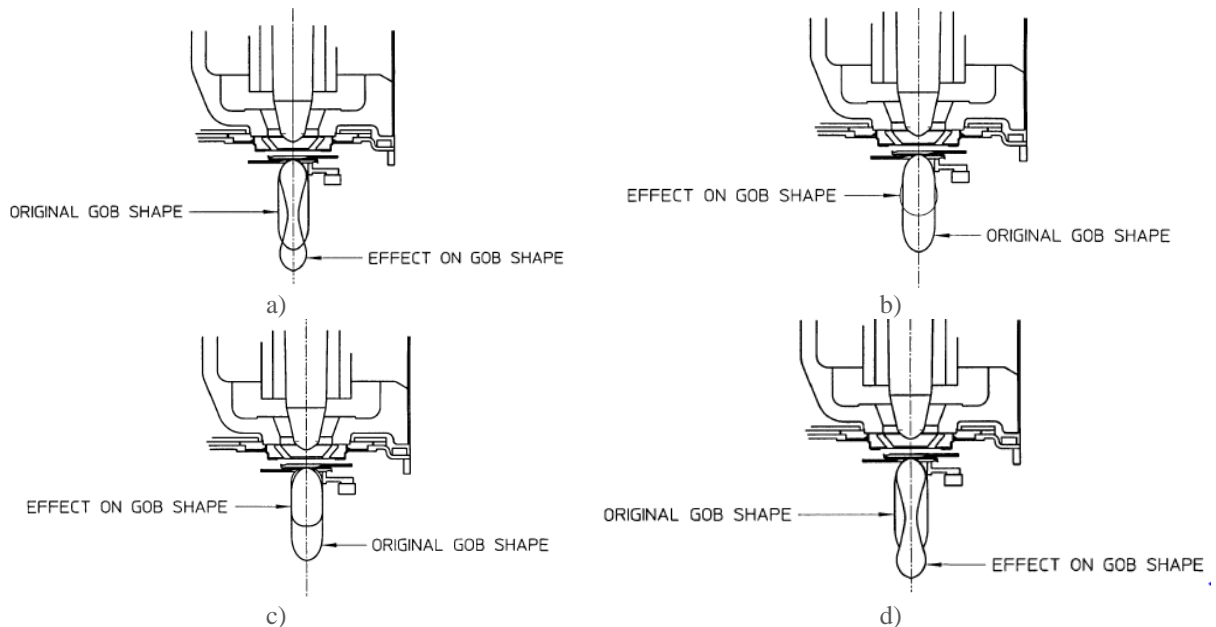


Figure 3.43: Different types of tuning a feeder a) Glass temperature increased. b) Glass temperature decreased. c) Machine speed increased. d) Machine speed decreased. [20]

The objective when shaping a glass gob is to deliver a gob of ideal shape and. This shape must be consistent and reproducible. This is one aspect which, in the past, empirical experience and practice were the best teachers. This still applies, in part, today. But with increasing machine speeds, a much broader understanding relating to controlling more precisely, gob shaping and loading techniques has come about. It is true to say that the best gob to use for the majority of the jobs, is the shortest most compact gob it is possible to load consistently into the blank mould, Figure 3.44

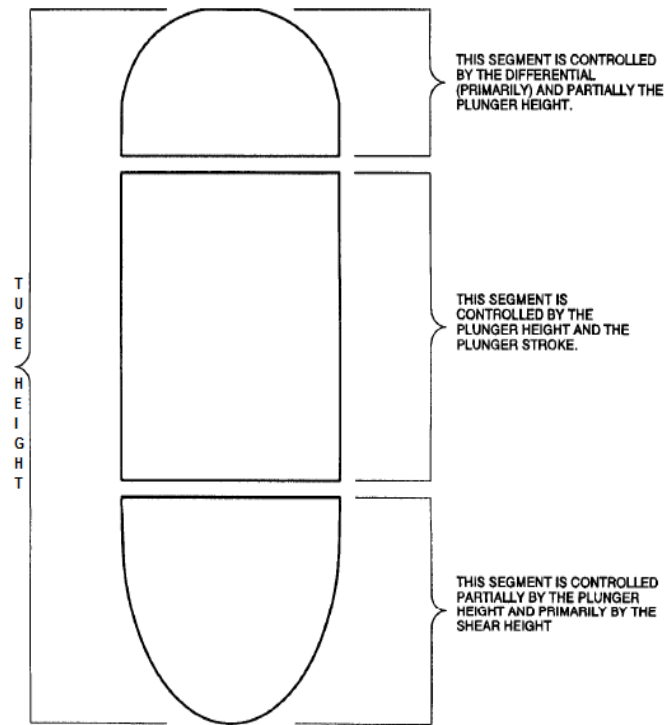


Figure 3.44: Gob shape parts affected by feeder controls [21].

The gob distributor and delivery system on an IS machine gets the gobs after the shear cut, for delivery to the individual sections of the machine. The gob distributor moves the scoop with a high speed and accuracy to the entryway of the troughs in accordance with the firing order (the order in which each section receives gobs from the gob distributor). The firing order is calculated to reduce the scoop travelling distance keeping the timings and movements synchronized.

In the delivery of various gobs of molten glass, simultaneously, to one of a plurality of stationary glass moulding machine sections positioned beneath the gob former, it has been a constant goal that the various gobs arrive at the mould of a section at the same precise time so that the gobs will all undergo the same degree of cooling while being transformed into a parison. This goal is an obviously difficult one to attain because the gobs may be travelling slightly different distances and due to manufacturing differences between delivery system geometry, Figure 3.45.

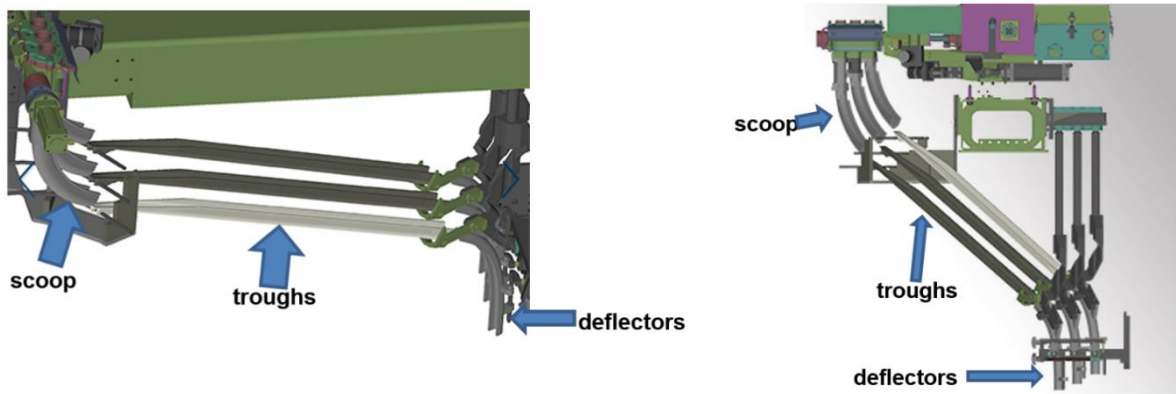


Figure 3.45: Gob distributor scheme [12].

When considering the problem of achieving consistent and predictable loading characteristics between as many as 10 or 12 sections which will each get the various gobs at timed intervals from a feeder that is cutting gobs at a preset rate, it can be seen that there are huge timing problems involved. In order to avoid inconsistent loading of gobs, various systems have evolved, but most have culminated in what would best be termed an accommodation between the practical and the expensive systems [23], Figure 3.46.

Studies of gob delivery systems in operation with high speed cameras expose many unforeseen situations that can affect the actual time of travel of an individual gob from the point of detachment from the stream at the feeder to the actual channel of the gob into the upper end of the parison mould cavity [23].

The fact remains that gob delivery to each cavity on a machine is occasionally very inconsistent and that the inconsistency is random in nature. A given cavity may be satisfactory, and then for no foreseen reason, it becomes bad. One factor that will contribute to an inconsistent delivery is mediocre maintenance of the equipment [23].

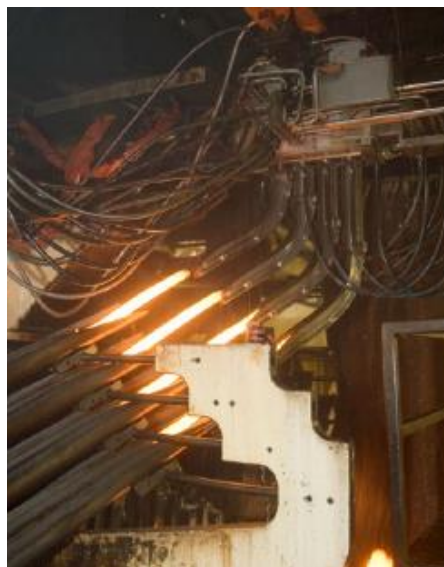


Figure 3.46: Gob distributor [12].

3.4.2 Blow/Blow

In this section the stages for the blow/blow process will be explained in detail.

- Gob Loading

The gob should be guided through the funnel into the blank mould with the minimum rubbing and with approximately 0.8mm clearance on the diameter. This will give accurate loading with a minimum marking of the gob and give sufficient vent to the blank mould to keep the undesirable formation of an air pocket to a minimum, which would prevent solid loading. With good loading the gob settles uniformly and almost entirely into the shape of the finish before settle blow air is applied. To ensure good loading, the clearance between the plunger and thimble or plunger and finish guide plate should be as specified in the I.S Machine mould, Figure 3.47a). Equipment must be kept clean to prevent dirt from building up in the vents.

- Settle Blow

First, in the settle blow the glass gob is blown from above to form the bottle neck. Settle blow should be applied as soon as possible after loading to obtain uniform glass/metal contact at the earliest possible moment. The settle blow time should be kept to a minimum, using only sufficient time to set up the bore of the finish to withstand the counterblow. Large or heavy finishes require more time to set up the finish than the smaller finishes. The minimum settle blow time will also give the minimum settle wave in the finished bottle, Figure 3.47b).

- Corkage Reheat

As soon as the settle blow action is completed, the plunger should be withdrawn to allow corkage reheat, or softening of the glass immediately above the plunger, to permit counterblow to form a symmetrical bubble in the parison without distorting the neck of the bottle.

- Counter Blow

The earlier counterblow is applied, the less settle wave will be apparent in the final bottle. The longer the counterblow is left on, the better the balance of heat removal between the blank and blow mould, permitting maximum machine speed and hot mould practice, i.e. operating the blank mould at a maximum temperature consistent with the production of a firm parison. The pressure used must be suited to the particular size of the bottle, that is, the larger quantity of glass the greater pressure. In general, more stable operation, better glass distribution and higher speed can be obtained by using maximum blank contact time, Figure 3.47c).

- Parison Reheat

After the counterblow the blank mould is opened and the parison is allowed to reheat before inverting into the blow mould. This reduces the cold skin produced by the glass contact with the blank mould.

- Invert

During the time the parison is transferred from the blank to the blow mould, the parison is reheating. The speed of invert affects the distribution of the finished bottle, if it is too slow, the parison will sag backward due to gravity; if too fast, the parison is thrown forward by centrifugal force. The speed must be varied to suit the weight, viscosity and shape of parison, Figure 3.47d).

- Rundown

The only force acting in the rundown stage is gravity. A cooling effect will appear when the glass contacts the baffle. During this time, the parison continues its reheat or temperature equalization. Too much reheating on the blank side allows the parison to sag and on the blow mould side to run, and the two effects have to be counterbalanced.

- Final Blow and Vacuum

Vacuum is applied to the blow mould cavity to form the finished bottle, and the final blow air is also used in helping to form the shape of the bottle. By circulating the air through the internal cooling blowhead arm when the blowhead is on top of the mould, the internal temperature of the bottle is reduced. In general terms, the vacuum and final blow time should be the maximum to form the bottle before it is removed from the blow mould, Figure 3.47e). Blowing is an important stage in production of glass containers. In this stage the shape of a bottle is reached.

- Mould open and takeout

After the blow mould opens, the takeout tongs pick up the finished bottle and place it on the conveyor dead plate. Takeout tongs should be aligned correctly and have sufficient clearance so that the bottle hangs freely, and the takeout mechanism should move smoothly to avoid distorting or chipping the glass, Figure 3.47f). An important concern in blowing is the distribution of wall thickness at the end of final blow stage.

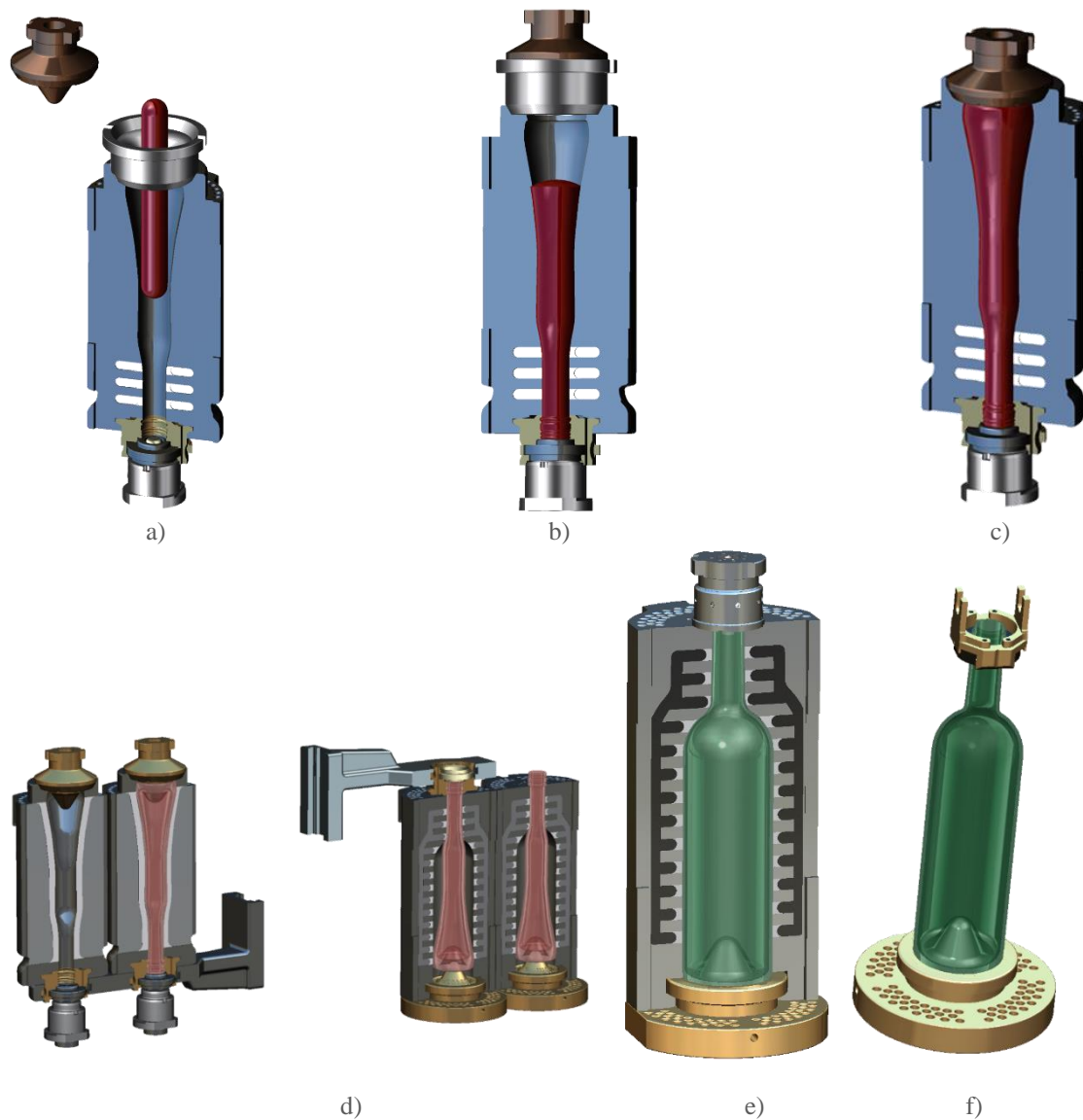


Figure 3.47: a) Gob loading b) Settle blow c) Counter blow d) Invert e) Final blow f) Take out [12]

3.4.3 Press/Blow

The narrow neck press/blow (NNPB) process has been introduced to gain improved control over glass distribution in the bottle. The better control over glass distribution has enabled a significant reduction in glass weight of up to 33% without negatively affecting the mechanical performance of the container. A key component in the above process is the plunger, used to form the cavity in the parison in the forming stage. The function of the plunger is to uniformly distribute the glass within the blank mould cavity and to aid the elimination of thermal energy from the internal surface of the parison [24].

- Gob loading

With the plunger in loading position, the gob goes through the funnel of the blank and loads on top of the plunger. The gobs shape and the loading depth are the most important factors [6].

- Baffle on

After gob loading and with the plunger in the loading position, baffle is then positioned on top of the blank mould.

- Plunger Up

The plunger starts the upward movement as quickly as possible, in order to press the glass while it still retains the maximum amount of heat and before it sets too hard. During the plunger up stage the plunger travels in an upward direction forcing the glass going up against the baffle and then, when the baffle is completely fill of glass, the glass travels to the neckring to complexly fill it. This action forms the finish in the neck ring and the parison is completely formed. The pressure applied to the plunger up movement must be regulated to a minimum to avoid splits and marks in the finish and parison, Figure 3.48c). Then, after the plunger up stage the plunger has to be removed. So, the plunger retracts to its full down position.

- Parison Reheat

After the pressing operation the plunger is withdrawn, the baffle is removed and the blank mould opened to allow the parison to reheat and equalize the temperatures to eliminate skin conditions before inverting to the blow mould. Parison reheat will then begin on the inside of the parison. At this point the colder inner skin of the parison will be heated up by the hotter glass in the middle of the parison [6]. Complete parison reheat is started when the baffle is up, the blank open, and the plunger is in the down position. This process will continue until the final blow is applied [6]. Reheat is important in order to equalize the temperature in the parison and to melt the solidified outside layer to make the blowing possible.

- Invert

During the time the parison is transferred from the blank to the blow mould, the parison is still reheating. The speed of the invert must be regulated to suit the size of the parison, as the centrifugal force will allow swing of the parison heel, which will affect distribution in the base of the finished bottle, Figure 3.48d).

- Rundown

As soon as the parison is transported to the mould side, it starts running towards the bottom of the blow mould. The amount of run time is set by the job being made. The longer the parison is allowed to run, the thicker the glass will become in the wall area, Figure 3.48e) [6].

- Final Blow and Vacuum

Vacuum is applied to the blow mould cavity to form the finished container. The final blow air is also used to help form the shape of the container, but also by circulating the air through the internal cooling blowhead arm and also the internal temperature of the jar is reduced. In general terms, the vacuum and final blow time should be the maximum to form the jar before it is removed from the blow mould, Figure 3.48f).

- Mould open and take out

The mould opens after the blow head is absolutely up and the takeout closes around the finish before the mould opens. The takeout action is as smooth as possible to decrease the change of defects, Figure 3.48g) [6].

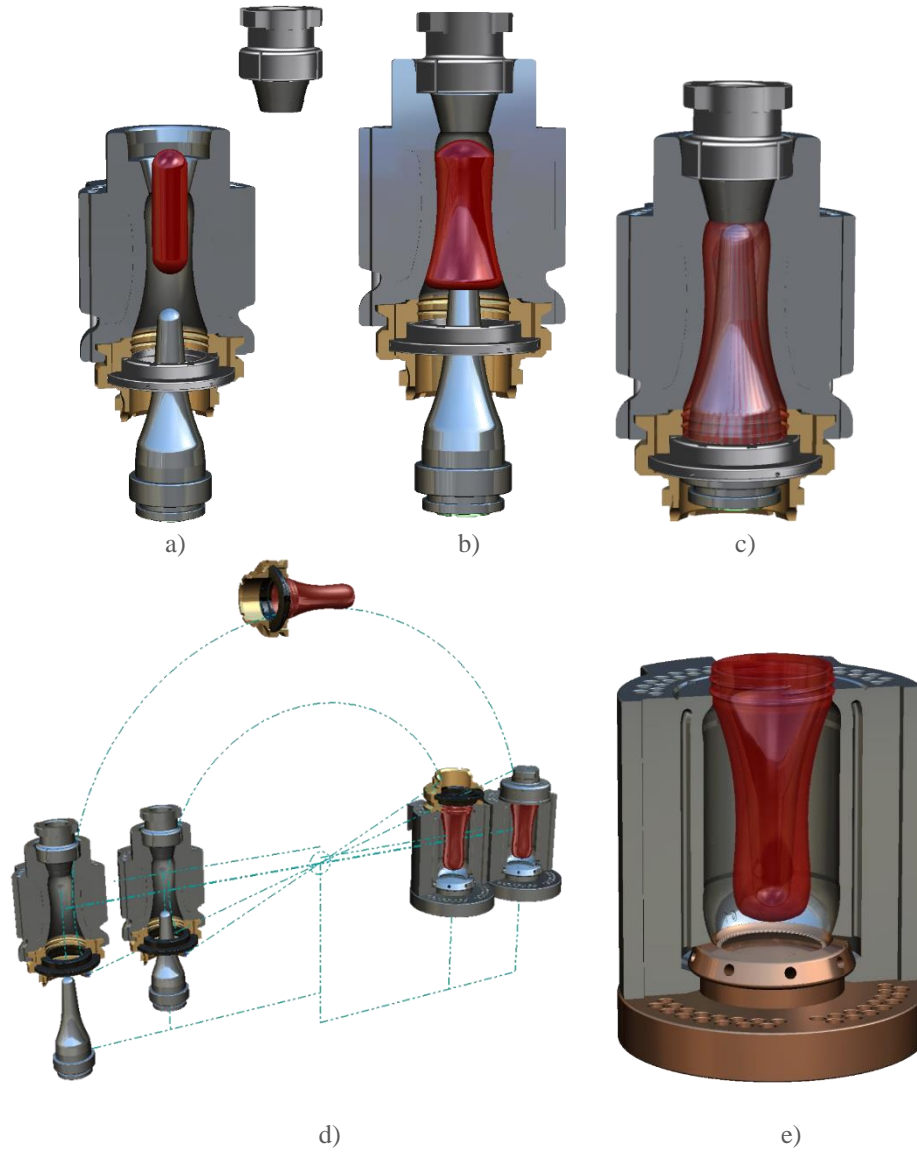




Figure 3.48: a) Gob loading b) Baffle on c) Plunger up d) Invert e) Rundown f) Final Blow g) Take out [12].

3.5 Hot End Coating

The container surface is regularly protected from abrasion damage with double coating. The hot end coating is enforced between forming and annealing. Glass containers are coated with two substances: one coating occurs at the hot end of the lehr³ immediately after creating (called a hot end coating), and the other occurs as the bottles go out of the annealing lehr (called a cold-end coating) [25].

The role of hot end coating is to increase strength and abrasion resistance, and also provides sufficient lubrication to ensure a smooth flow in the high speed procedures of inspection, automatic filling and packing. The hot end coating is applied by chemical vapour deposition (CVD), directly after forming the bottle and before they enter the annealing lehr. A thin layer of tin oxide is formed on the glass surface in seconds [26]. These materials are applied immediately after forming when the container surface temperature is between 450–600 °C. A range of precursors can be used, including monobutyltin trichloride, tin tetrachloride, dimethyltin dichloride, and titanium tetrachloride, Figure 3.49.

³ A furnace used for the annealing of glass

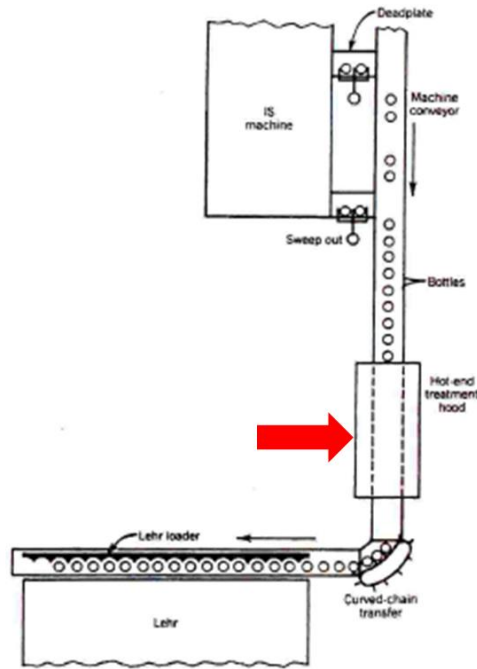


Figure 3.49: Hot end coating [12].

Other coating processes have been attempted but failed in the marketplace. None of these is used by manufacturers currently, primarily because of their higher cost and because they only increased the burst pressure without also improving the impact resistance. One step coatings were applied at the cold end and found to be inferior to the dual HEC/CEC coatings. On the positive side, however, there appear to be no technical barriers to achieving significant improvements to the properties of glass containers. Much of the technology already exists, Figure 3.50.

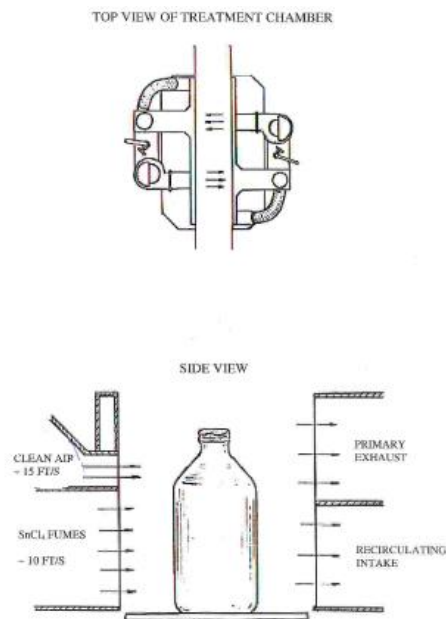


Figure 3.50: Application of hot end coating [12].

The tin compound is evaporated in air and comes into contact with the hot glass surface (600°C) during the vapour phase. In bottle coating, the mole concentration of product in air is approximately 0.02 per cent, leading to a very high excess of oxygen. As a result, the alkyl group is absolutely oxidized. The deposition rate of the film is mainly dependent on the tin concentration in the coating hood. Other causes are gas velocity and glass temperature. The gas temperature may range from 70 to 200°C and has nearly no effect on the deposition rate, as long as it is high enough to contain the tin compound in the vapour phase and low enough to bypass premature formation of tin oxide in the gas phase [26].

The coating air must contain water vapour; the water is supplied to the hood by exchange of ambient air. This usually leads to a large excess of water vapour. Under practical conditions, a residence time of 2 to 3 seconds is sufficient to deposit the 10nm thick film of tin oxide [26]. It is known that the structure of hot end film can be strongly affected by temperature; at relative low temperature the grain size is relative small while at relative high temperature a more column-like structure is obtained.

The inner loop receives and circulates a highly concentrated stream of vaporized hot end coating material. The outer loop captures any coating material vapour escaping from the inner loop and recirculates it in a low concentration. Coating vapour that escapes the outer loop is captured through exhaust slits located at each corner of the hood. The flow of fresh air through the centre section of the hood assures finish protection, Figure 3.51.

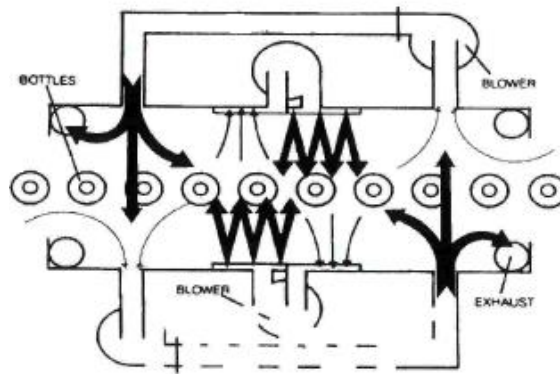


Figure 3.51: Application of hot end coating [12].

When a "hot end" coating is applied to glass containers, it is normally necessary to avoid depositing metal oxide coating on the finish of the container. The metal oxide coating on the finish can interact with the dissimilar metal of the cap, lid, crown, and can produce an unsightly corrosion issue [27]. Such corrosion issue, with its visual blemishes, is particularly acute since the coated glass containers are normally employed for beers, wines, soft drinks and foodstuffs, and the ultimate consumers won't buy products even appearing to be tainted [27].

3.6 Annealing

Development of stresses during the creation of glass may lead to fatigue of the product, or even to dimensional changes due to relaxation or optical refraction. The process of removing and reducing the stresses due to relaxation is called annealing [3]. In an annealing process the glass objects are arranged in a so called annealing lehr, where they are reheated and then again gradually cooled down. The rate of cooling is determined by the allowable stresses and property variations throughout the glass [3]. The annealing has to be overseed carefully in order to avoid excessive temperature differences that may affect the quality of the product or even lead to cracks in the material [28]

3.6.1 Internal Stress

The development of internal stresses in a glass container during the forming process is explained because, there is a very rapid cooling of the glass in a short period of time. Approximately 850°C in just 20 seconds, from cutting the gob until the finished glass container enters the annealing lehr, Figure 3.52.

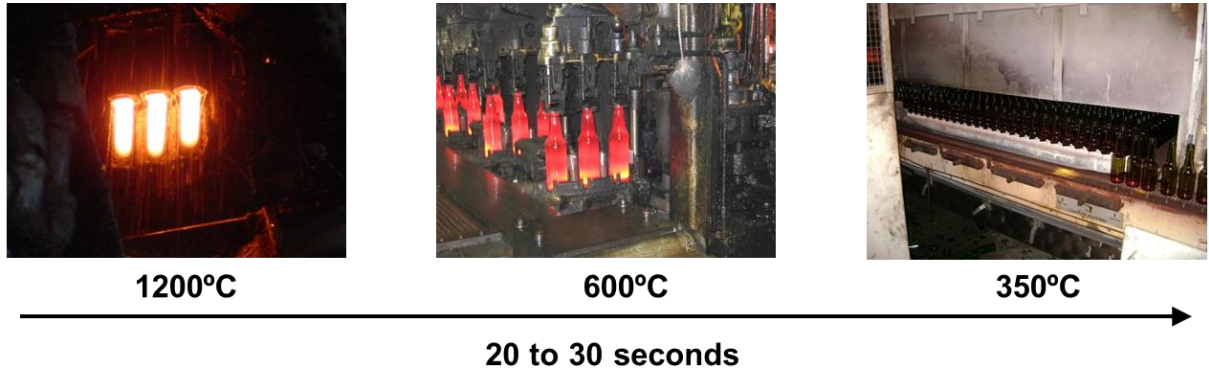


Figure 3.52: Rapid cooling from forming to annealing lehr [12].

Glass has a low thermal conductivity, therefore, the thermal dissipation does not process at the same velocity in all of its mass. It is established a thermal gradient from the centre of the glass mass, up to the external surface, Figure 3.53.

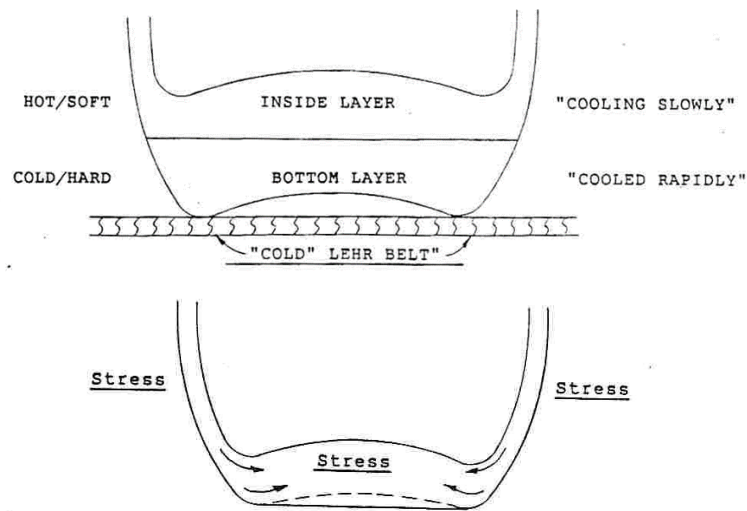


Figure 3.53: Stress after coating process [12].

Temperature gradients across glass wall thickness produces different cooling rates. Different cooling rates produce different times at which the glass undergoes the glass transition. This in turn produces thermal stress across sample. Surfaces cool more quickly, bulk cools more slowly. Surface gets put into compression, bulk in tension. The combination of tensile stresses and surface discontinuities at sufficient magnitude or severity occurring at same place and time result in a fracture, Figure 3.54.

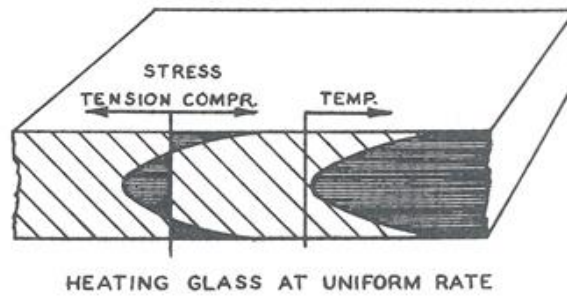


Figure 3.54: Tension inside the container thickness [12].

Containers must be free of internal stresses so that they don't spontaneously fail under pressure. Annealing has the objective of reducing the internal residual tensions to minimum values, enhancing its mechanical properties. This is achieved by the rearrangement of the molecular structure. Annealing is used to heat treat the glass near the softening point to relieve stresses. Glass has to cool more slowly through the transition region so as to not reintroduce thermal stresses. Glass which has not been annealed is liable to crack or shatter when subjected to a relatively small temperature change or mechanical shock. Annealing glass is critical to its durability. If glass is not annealed, it will retain many of the thermal stresses caused by quenching and significantly decrease the overall strength of the glass.

3.6.2 Cycle

Each different type of glass containers should have a determined annealing cycle. The duration and thermal condition of that cycle depends on the: glass characteristics (chemical composition), container geometry (non-cylindrical containers have intrinsically, because of its shape, more stress concentrators in the bottom and shoulder areas, therefore, need to spend more time to stabilize and to slow cool down) and container glass thickness.

Some issues should be taken into account in annealing:

- Thicker glass containers anneal more slowly, has larger stresses;
- Thinner glass containers anneal more quickly, has smaller stresses;
- Glass containers with large thermal expansion requires more annealing;
- Glass containers with smaller thermal expansion requires less annealing;

In the annealing process, the following 4 phases should be considered (that is 4 thermal gradients to reduce the internal stress in a glass container):

1. Preheating the container until the annealing point temperature. The preheating time depends on the temperature of the container when it enters the lehr, glass thickness and the value of the annealing point temperature. At this temperature the glass is still too hard to deform, but is soft enough for the stresses to relax, Figure 3.55;
2. Stabilization or homogenization at the annealing point temperature. At this temperature the internal stresses are reduced dramatically in a short period of time (a few minutes) through the homogenization of the molecular structure by internal viscous flow. The piece is allowed to heat-soak until its temperature is even throughout. At a glass container corresponds to a temperature of 540 to 565°C and a viscosity of $\log(13,4)$ (1013, 4 poises). At this temperature glass has the characteristics of a viscoelastic material. The stabilization time depends on the glass thickness and glass geometry, Figure 3.55.
3. Slow cooling from the annealing point temperature to the strain point temperature at a relatively slow and uniform velocity in order to assure that no new internal stress appears or is recovered. At this temperature the internal stresses are reduced in a period of hours and this is the highest temperature from which strain free glass can be cooled quickly without introducing permanent strains. At this temperature glass is predominantly in a solid state. At a glass container corresponds to a temperature of 495 to 520°C

and a viscosity of $\log(14,6)$ (1014,6 poises). The slow cooling time increases with the glass thickness and container geometry (increases for non-cylindrical type of containers), Figure 3.55.

In order to assured that all parts of the glass container are at a higher temperature than the strain point temperature this phase should be extended to a temperature of approximately 475°C. For typical soda-lime container type of glass the difference between the annealing point and the strain point should be around 35 to 45°C (viscous transition zone or annealing zone).

4. Rapid cooling from the strain point temperature until room temperature. The cooling speed should be limited in order to avoid breakages due to thermal shock, Figure 3.55.

The thermal gradients (cooling velocities) and permanency times at a certain temperature depend essentially of the glass thickness of a container and the glass expansion coefficient, which is to say the glass chemical composition.

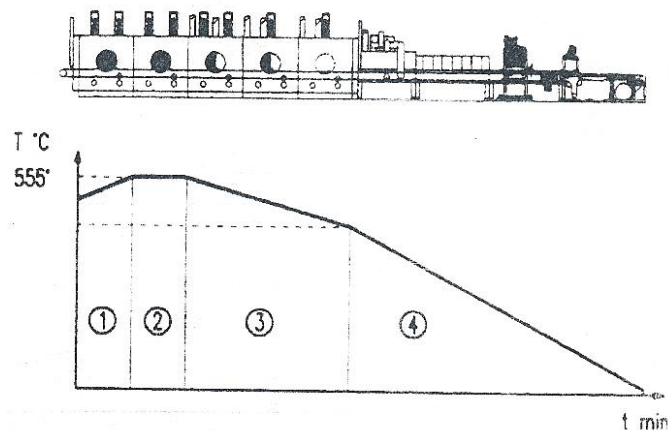


Figure 3.55: Tension inside the container thickness [12].

The annealing process is carried out in a temperature controlled kiln known as a lehr. A temperature controlled curve is inputted on the lehr, depending on the container characteristics. The tunnel is comprised of individual modules or zones of equal length. Width varies widely based on capacity but remains uniform from zone to zone. These zones are designed to produce a gradually decreasing temperature curve, which typically starts slightly above the calculated annealing point of the glass and decreases zone by zone until the desired glass exit temperature is achieved.

For the most efficient heat transfer method most modern lehrs use convection fans and can be heated with gas burners or electric elements. The annealing lehr continuously receives glassware directly from the forming process. Ware is conveyed through the tunnel via a metal mesh lehr belt that provides a stable surface for conveyance as well as allowing recirculated air to pass through and around the glass products.

3.6.3 Quality control

Transparent materials having internal mechanical stress are found to be birefringent, due to their anisotropic nature difference, when measured along different axes, in a material's physical or mechanical properties. That is, they demonstrate double refraction (having two indices of refraction). Transparent materials having internal mechanical stress can be analysed by a Polariscopes⁴. The Polariscopes incorporates a polarizing filter to convert white coloured into a polarized light source that is then directed through a glass sample. If the glass is free from stress, the light simply passes through unaffected. Stresses in the glass, however, retard the transmission of light, and produce various spectral colours when viewed through the

⁴ An instrument for measuring or exhibiting the polarization of light or for examining substances in polarized light, often to determine stress and strain in glass.

Polariscope, Figure 3.56. The level of stress present on the glass affect the amount that the light waves are retarded. Actual levels of stress (temper grade) can easily be determined by comparing colours exhibited during the test with those produced by calibrated standards (Standard Strain Disks), taking into account the thickness of the glass.

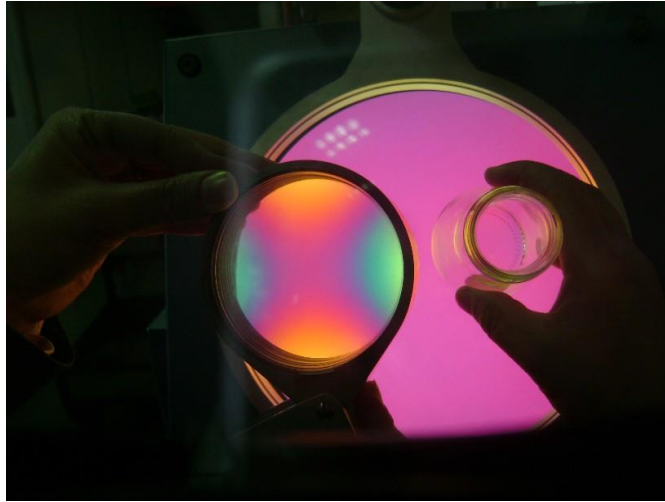


Figure 3.56: Measurement of glass stress with a polariscope [12].

3.7 Cold End Coating

In the past, when glass containers were heavy and line speeds slow, there was little need for surface treatment. In result the ware was incredibly heavy, the speed was awfully slow, and the lehr was covered with broken glass. However, in almost all modern manufacturing, bottles have become increasingly lighter in weight and speeds have accelerated extraordinarily, both in the glass plant and on the customers filling line. Because of these changes, the need for surface treatment is crucial, Figure 3.57 [25].

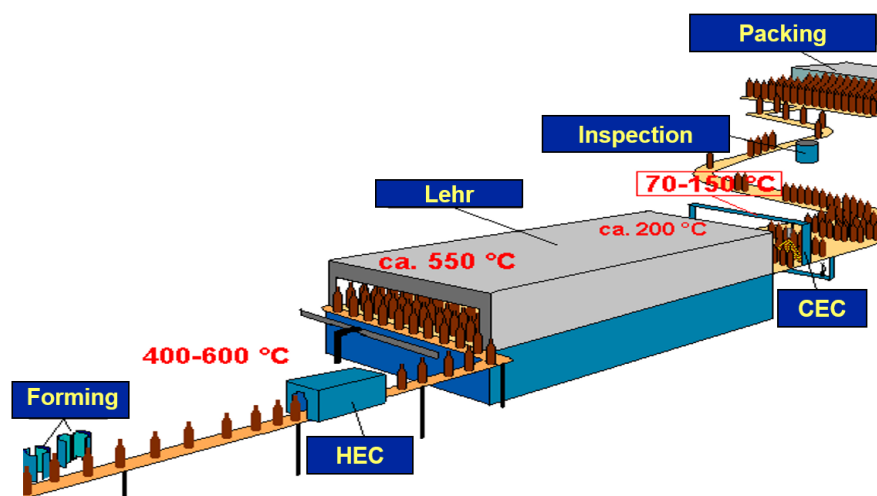


Figure 3.57: Different surface treatments though a convey belt [12].

Although glass is in theory a very strong material, conditions exist throughout the entire manufacturing process which can damage the ware to the extent that, unless the surface is protected, damage can occur. Resistance to scratching is paramount to keep the inherent bottle strength high [25].

Water based polyethylene emulsions are normally applied by some variation of the traverse spray system. This machine delivers the diluted material, that is mixed with approximately 100 to 200 parts of water, over at the cold end of the annealinglehr, from the shoulder of the bottle on down [25]. Care should be taken that the suggested amount of concentrate coating be mixed with water. Overuse of the concentrate won't enhance its performance values. If the mixture is too heavily concentrated, appearance of the ware can be debilitated. The glass containers will come out there streaked and can also be too slippery, resulting in filling-line pop-out. Too heavy concentration will also affect the labelling ability and can lead to failures in labelling. Conversely, too little concentrate will result in bottles without sufficient coverage to avoid surface abrasion, Figure 3.58 [25].

Temperature of application is also an aspect involved in successful cold end coating. The "cold end" isn't cold at all, with the bottle temperature ranging from 66° C to 177°C. It is important that the polyethylene coatings be applied in the range of 82°C to 113°C for the best labelling ability. If the coating is applied at a too low temperature, it will inadequately cure; if the temperature is too high, the danger of thermal shock is present. Another problem of high temperature application is that labelling failures may happen [25].

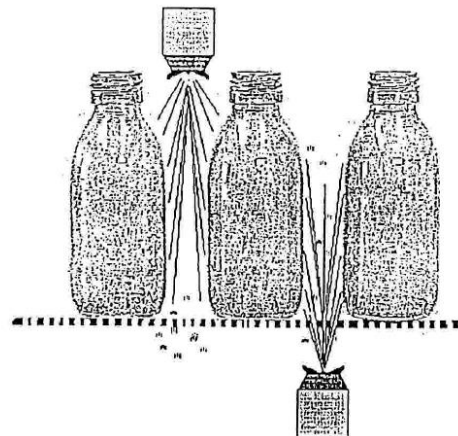


Figure 3.58: Application of cold end coating [12].

3.8 Inspection and quality control

It is essential to have good raw material specifications. A technical specification sometimes defining ideal or optimum limits in addition to the normal reject limits is necessary and is often part of the commercial contract against which raw material deliveries are made. Physical and chemical checking of incoming raw materials on receipt has now largely been replaced by either the provision of supplier certificates of conformance, or by the availability of a system whereby the glass manufacturer is given access to the raw material supplier's process control information when necessary. The latter facility may also be supplemented by audits of the raw material supply locations. The purpose of such audits is to ensure familiarity with the process control methods and standards used by the supplier and to conform their ability to adequately control the raw material within the specification.

When raw materials are received in the glass factory, the incoming check can simply confirm the nature of the material and the quantity being delivered if a certificate of conformance system is in operation. For certain materials or where there is a specified need, small samples can be taken and retained for laboratory examination. This may be done either on a random basis or regularly if required. An important part of the

raw material control system is ensuring the right material goes into the right raw material storage silo and this is usually done by means of an electrical interlock system or a manual padlock system on the silo input pipes. Certain checks on the raw materials are done on a regular basis as specified by the glass manufacturer.

Cullet is a very important raw material. Cullet is inspected at various stages in the cullet processing operation as it is converted from raw cullet e.g. as received from bottle banks, into a form which can be incorporated into the batch mix. Any large contaminating objects such as refractory bricks, are eliminated by hand packers as the cullet enters the processing plant on the input conveyor. Magnetic separators remove magnetic materials and light sources of contamination such as aluminium retaining rings are blown away from the crushed cullet. Control tests are regularly carried out on the processed cullet to ensure it is within the glass manufacturer's cullet specification. When processed cullet is received from an external cullet producer the manufacturer either carries out control checks similar to the above when deliveries are received or operates a formal compliance certificate system.

As with the conventional raw materials there is a close connection between the glass manufacturer and the mould suppliers, usually through the design and mould ordering departments of the glass manufacturer. In addition to any formal compliance certificate in the case of moulds, the supplier often forwards a summary of the final inspection data from checks carried out on the mould equipment at the time of manufacture. If the sampling raises a concern, this is either investigated in conjunction with the supplier, or if necessary, further samples of mould equipment are checked.

The packaging materials include pallets, cartons, trays, and shrink wrap and stretch wrap materials. Again, as with the raw materials, the main control is exercised by the packaging supplier who is monitored through certificates of conformance systems and supplier audits as appropriate, Figure 3.59.

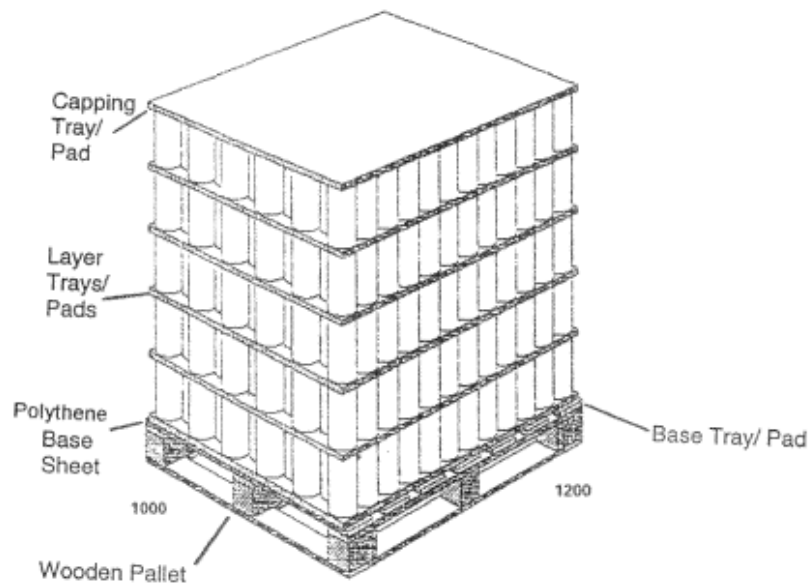


Figure 3.59: The packaging materials include pallets, cartons, trays, and shrink wrap and stretch wrap materials [12].

There are four main aspects of furnace control:

- To ensure the effective melting of the raw materials and to provide good quality glass to the forming machines. Samples of the glass being produced are retained for specified periods so that any change in appearance can be quickly detected.
- To ensure the most economic operation of the furnace and to minimize emissions, which might cause atmospheric pollution.

- To ensure the furnace fabric is maintained, e.g. to check that no hot spots or thin spots are developing and that the cooling systems are working effectively.
- To provide early warning of any aspect of furnace control or equipment which may require attention.

The controls carried out at furnace process control could typically include measurement of:

- Furnace temperatures.
- Regenerator temperatures.
- Glass melt temperatures.
- Furnace pressures – measurements of differential pressure relative to the atmosphere. The ideal melter pressure is the lowest amount which prevents any inspiration of the cold outside atmosphere;
- Glass level depth in the furnace – typical measuring location is in the refiner/distributor or the rear zone of forehearth. The glass position is referenced relative to a defined “zero”. Measuring precision must be to the nearest one hundredth of an inch. The reading must be accurate and reliable.
- Bubbler rates (when bubblers are used to assist melting);

Such items are regularly monitored and the results of checks carried out are either recorded in furnace log books or are available as a computer record, especially if the furnace is fully computer controlled as is often the case with modern glass melting units, Figure 3.60.



Figure 3.60: Furnace control [12].

The main test to assess melting / glass quality are:

- Glass density (dif < 0,0040 g/cm³).
- Homogeneity (this test indicates the presence of any inhomogeneous glass which shows up as coloured streaks under polarized light. The degree of inhomogeneity can be quantified if necessary by examination under a petrological microscope).
- Bubble (seed) count.
- Stone count (and determine origin).
- Colour (purity, brightness, dominant wave length).

The density test is carried out using a density bath which consists of several boiling tubes partially immersed in water within a water bath. The boiling tubes contain a special mixture, e.g. tetrabromoethane and bromonaphthaline or bromobenzene, the density of which approximates to the density of the glass. Small fragments of glass are then introduced into the boiling tubes together with control samples of the known density. As the temperature of the water bath is then increased at a controlled rate, the density of the liquid mixture changes slightly and the samples floating on the top gradually sink to the bottom. The temperature at which the samples (known density and unknown density) sink past a mark on the boiling tube is noted, and from this the density of the unknown glass can be determined.

Samples from each individual mould cavity on the forming machine are taken off at regular predetermined intervals and allowed to cool for inspection in a light box. Glass weight is another parameter which is regularly monitored. All checks are carried out having regard to the container specification and any other important control information made available by the quality assurance department. Such additional information could typically relate to previous customer complaints or concerns, or to special customer requirements for the job being manufactured. All bottles checked at the forming machine are rejected for cullet as they cannot be subsequently annealed. Another part of the manufacturing control system involves the regular monitoring of the mould numbers which are working on which forming sections of the machine and precisely when mould equipment is changed and for what reason.

One key aspect in the quality control system in a glass plant is the communication between the operators of hot end coating and cold end coating in the same production line. This communication should be bidirectional:

- Hot end operator should inform the cold end whenever a defect is detected in his normal sampling. This way cold end can react and eliminate the defect.
- Cold end operator should inform the hot end whenever a defect is detected in his normal sampling. This way hot end can react and correct (and eliminate) the defect.

Two test machines both supplied by A.G.R. are in common use. One is used for checking the surface coating on the body of the container as it is rotated in a vertical position against a sensing head. The other checks the surface coating on the finish of the container. In both cases as the coating is very thin (only angstrom units thick) the test machines assess the reflection from the depth of the coating rather than measuring the actual amount of material present, Figure 3.61.



Figure 3.61: Hot end coating quality control [12].

Associated with the annealing lehr it will have a process control variable the temperatures of each of the zones in the annealing lehr, against the temperature specified as necessary to give the correct annealing profile in the lehr usually in the form of preset controls. Unlike the other tests carried out on the finished container which are all performed on “rounds” or one container from each forming cavity taken at regular

intervals from the cold end, the annealing test is carried out on samples taken from designated positions across thelehr, e.g. either from the centre or from each side of the lehr, or from all three positions. The test samples are examined in a polariscope (or strain viewer) equipped with a tin plate. When looking through the eye piece of the polariscope, the amount of strain in the glass is proportional to the degree of colour observed in the field of view of the polariscope. A quantitative assessment of the strain can be made by comparing the observed colour against standard strain discs or against reference samples with the same design characteristics which themselves have been assessed against standard strain discs. This test is usually performed in the quality control laboratory of the plant, although for quick assessments it is possible to see polariscopes near production lines.

For process control cold end coating should be monitored for the correct operation of the application systems and also the temperatures of application. Simply rubbing the containers together as they leave the lehr normally provides sufficient confirmation that the surface treatment has been satisfactory. This test is usually performed by the cold end operators. A further confirmation is obtained by means of quantitative surface treatment checks done in the quality control laboratory. In this test two containers are placed side by side in a horizontal position on the stage of the machine and a third container is placed on the top. The stage is then raised at one end until the top container starts to slide. The angle at which this occurs is known as the slip angle and provides an assessment of the level of the cold end treatment, Figure 3.62.



Figure 3.62: Cond end coating quality control [12].

The cold end process controls are carried out after the containers emerge from the annealing lehr. Some controls are based on the examination of representative samples from each mould cavity at regular intervals (attributes inspection for stratified sampling). Such controls could include the gauging or measurement of specification dimensional features (qualitative assessment with go-no go gauges) and general assessments of the visual quality of the containers being produced from particular moulds.

If defects are found the cold end operator must reject the concerned cavity numbers and inform his hot end counterpart of all nonconformities detected. The effectiveness of the inspection machines, if present, in rejection that defect, must be assessed. If the production line is equipped with automatic inspection machines the cavity rejection is performed automatically. For that, the container has the mould number code engraved either as a dot code (digital body or bottom of the container) or with characters (alphanumeric bottom of the container).

One group of machines sidewall visual inspection check for features which may result in internal contamination of the container. The contamination may be caused during manufacture, e.g. a birdcage, or may be introduced subsequent to manufacture, e.g. a piece of broken glass. Basically these machines compare the image of the container against the expected image and deviations such as dark areas due to extraneous features cause the container to be rejected. Similarly, these machines can reject excessive visual

deviations which might be objectionable cosmetically. This machine is able to detect all stress defects generating tensions in the sidewall.

Another group of multi inspection machines uses light reflection principles to detect and automatically reject features such as splits. If a split is present, this reflects light from a lamp source as the container is rotated in front of it. The reflected light is picked up by a sensor and the container is rejected. These machines have several inspection stations, containers indexed by a star wheel check selected dimensions such as the bore of a bottle or the undulation of the sealing surface of a jar and glass thickness. If the container has the dot mould number code engraved on the body, the systematic mould rejection is made on this machine.

Using cameras to perform the automatic inspection, there is another group of machines that performs inspection to the base and finish of the containers and finish inspection machines. These machines are able to inspect a number of different visual defects on the base and finish and stress inspection on the base of the container. If the mould number code is engraved on the base of the container, it is on this machine that it is possible to reject systematically a specific mould number. The automatic inspection machines are regularly checked with control samples to ensure they are performing satisfactorily. The results of such control checks are recorded as are also the checks on the representative samples referred to in above. These results are useful should there be a need for subsequent investigation and they provide a valuable input for the preventative control measures employed at the hot end during forming.

These samples – must follow certain rules or good practices:

- The sample must present only one defect for a specific detector or camera.
- The defect on the sample must be of low magnitude constituting a real challenge to the inspection machine.
- The sample must be clean in order to avoid false rejections because of the dirtiness rather than the defect itself.

This procedure is key to assess the effectiveness of the inspection machines. Also at regular intervals the rejections of the inspection machines should be assessed by the cold end operator. This is to provide to the hot end valuable information for correction and at the same time assessing the machine functioning. After the inspection machines in the cold end usually have a manual visual inspection as the containers pass in front of an on line light box. Here the cold end operator inspects at regular intervals during a short period of time the containers that are passing in the line. The objective of this inspection is only to assess the visual quality of the containers, therefore, check the effectiveness of the inspection machines regarding this particular aspect.

Some containers, e.g. carbonated beverages, require a mechanical stress control to be applied to each individual bottle and this is achieved by passing the bottles through an on line impact simulator, or squeeze tester. In this device, the bottle is squeezed between two vertical rollers or pads which place a stress on the bottle so that weak containers are broken and eliminated.

After the inspection machines and just before the containers are packed on pallets, in the cold end of a glass plant, there can be another equipment: bottle (jar) inverter. This equipment turns the containers upside down and a clean air flow is blown inside the container. The aim is to remove any physical contamination from inside the container. Together with the inspection machines this is a typical Critical Control Point (CCP) for food safety in a glass plant. This is a critical equipment for the production of wide mouth jars. In some production lines that only produce bottles narrow mouth. A good practice to follow is to investigate any occurrences of loose glass found in the inverter trays. Additional statistical checks, or audits, are done as the containers are being, or when they have been, assembled on pallets for shrink-wrapping.

3.8.1 Defects

For the purpose of these checks, imperfections are often classified into three main groups. The first group concern critical defects, defects that could or are likely to result in hazardous or unsafe conditions for individuals using the glass container or be injurious to their health, under normal conditions of use as defined between the glass manufacturer and the filler. The second group concerns major defects, i.e. those

Chapter 3 Glass Container Production

which may affect the functionality of the container in some way. We can subdivide this group in two subgroups: Major A defects: any non-critical defect which the consumer could perceive as being harmful and/or which damages the bottler's or trademark owner's legal image and/or which can result in legal action against the Company; and Major B Defects: any defect which is likely to reduce the usability of the product for its intended purpose. The third group concerns minor defects any departure from established standards having little bearing on the effective use of the product (usually a defect that materially affects the appearance but not the performance of the product aesthetic or dimensional slight defects). Some defects are presented in the Figure 3.63.

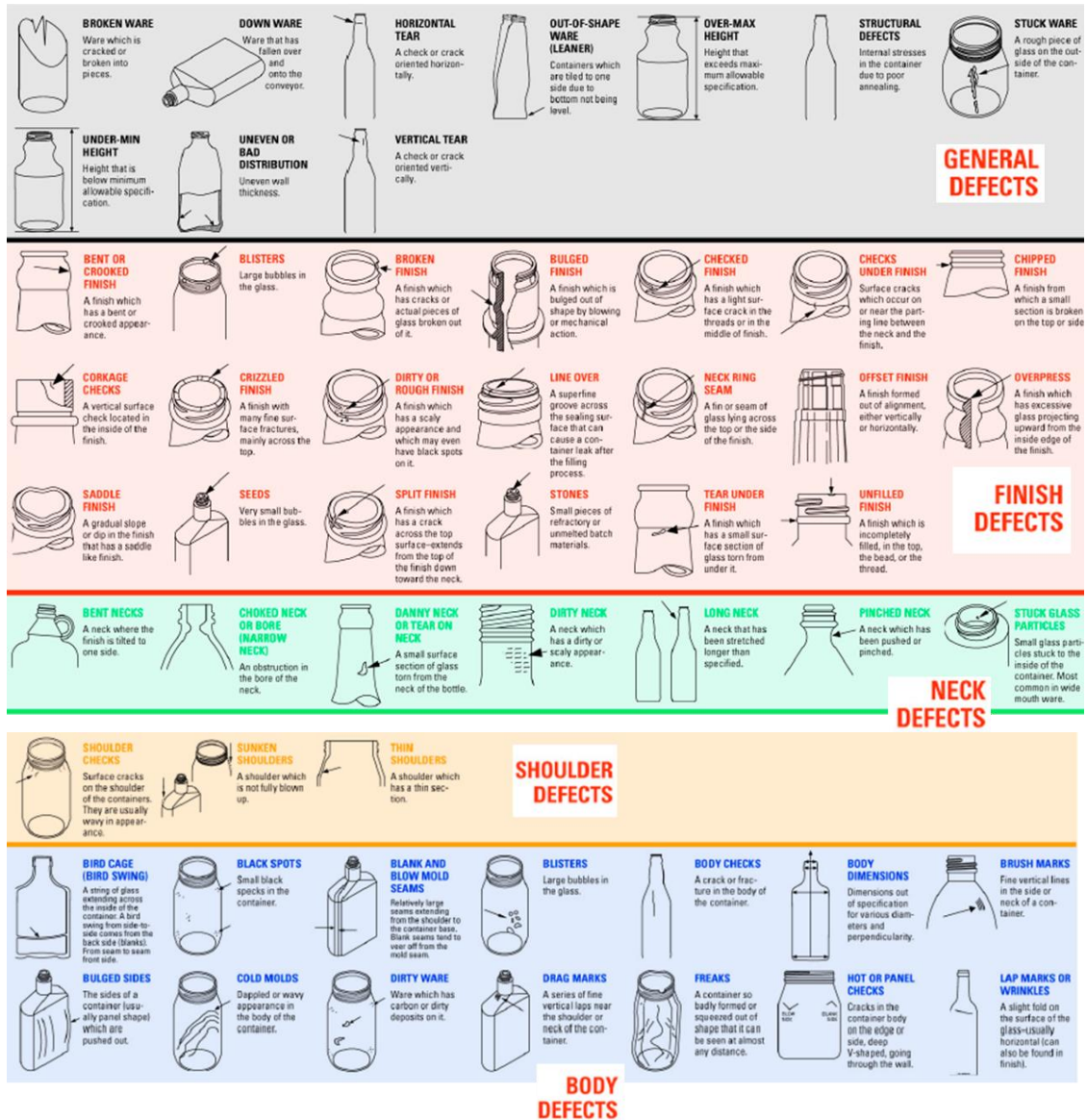
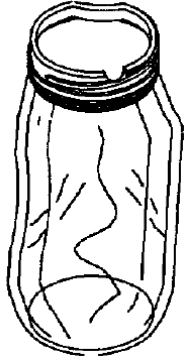
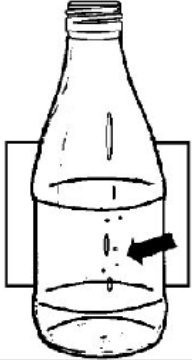
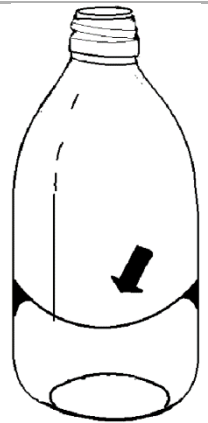
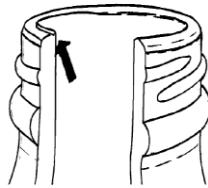
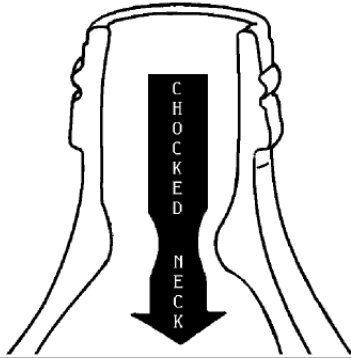
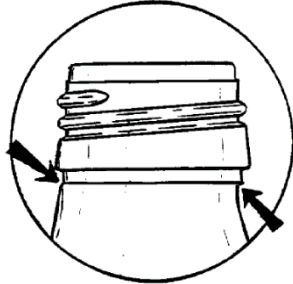
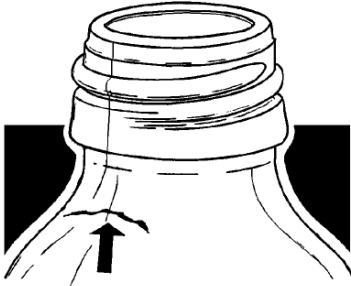
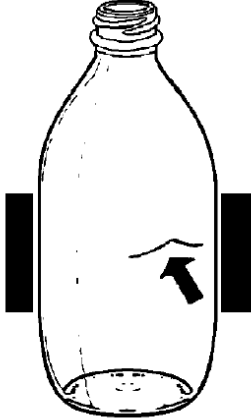
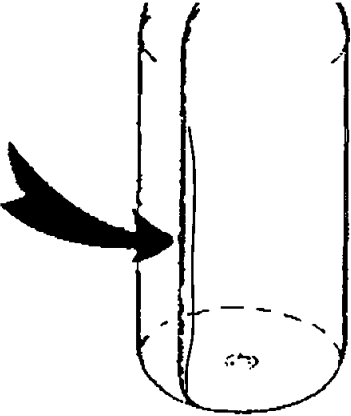


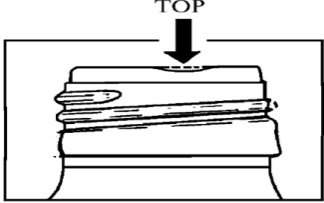
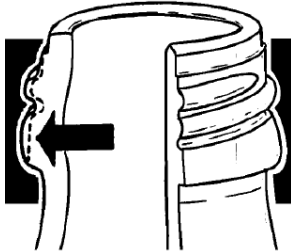
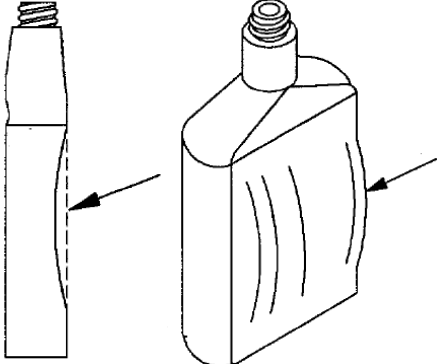
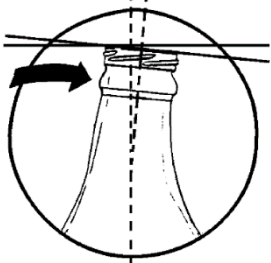


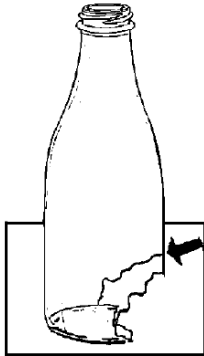
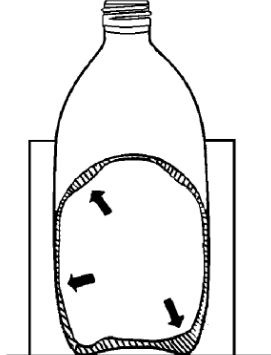
Figure 3.63: Defects can be presented in a glass container [12].

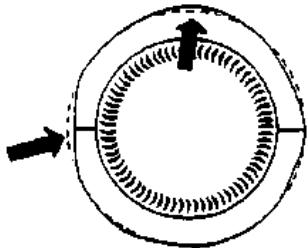
Critical	Type	Description	
	Freaks	Any container which is so badly deformed that it will not pass through a normal filling line and it can be seen at almost any distance	
	Spike (bottom)	Small projection of glass in the internal surface of the container (bottom). For Press/Blow and NNPB processes	
	Internal surface blisters	Air bubbles near the inside surface. These bubbles can easily break loosing glass particles inside the container. Usually associated with thin glass thickness.	

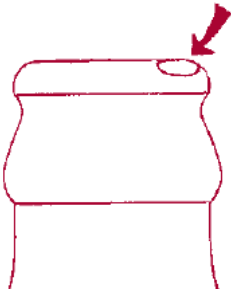
<p>Birdswing</p>	<p>Thin strand of glass across the inside of a container either between the walls or between the wall and the bottom. Contact of the parison internal walls before final blow</p>	
<p>Overpress</p>	<p>A finish which has excessive glass projecting upward from the inside edge of the finish.</p>	
<p>Stuck or loose glass inside</p>	<p>Excess of glass in the neck which partially or completely obstructs the bore (thermal or mechanical origin).</p>	
<p>Stuck ware</p>	<p>Rough or sharp glass on the outside surface of the container due to hot contact between two containers</p>	
<p>Offset finish</p>	<p>Offset of the finish (out of the correct position). If the finish rim is protruded there is a danger of breakage (mechanical origin).</p>	

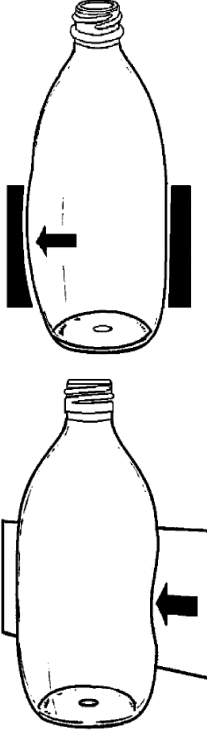
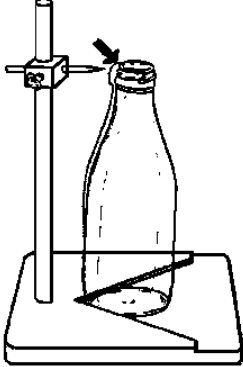
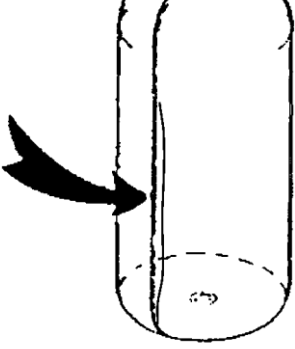
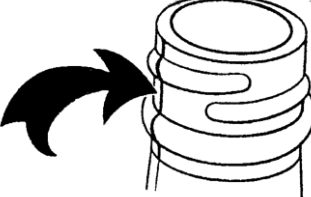
Major A	Type	Description	
	Check on the neck	Surface crack in the base of the neck. Usually occurs near the seam but it can occur anywhere along the neck diameter (thermal or mechanical origin).	
	Check on the body	Thin but deep crack – V shaped – on the body of the container. Two types of check: pressure – mechanical - check and hot panel – thermal - check.	
	Check on the seam	Thin and vertical cracks that occur near or on the blow mould seam	
	Check on the bottom	Crack on the bottom part of the container (near or on the bottom parting line).	
	Checks on the engravings, orientation marks	Small cracks on the engravings or other moulded container features.	

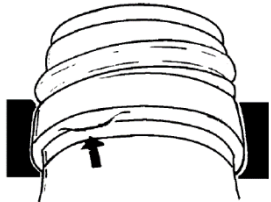
<p>Check on the finish</p>	<p>Crack on the finish of the container. Probably one of the most common type of defects (thermal or mechanical origin). Temporally corrected with swabbing.</p>	
<p>Chipped finish</p>	<p>A finish from which a small section is broken on the top or side.</p>	
<p>Unfilled finish</p>	<p>A finish which is incompletely filled, in the top, the bead or the thread</p>	
<p>Bulged finish</p>	<p>A finish which is bulged out of shape, either by blowing (thermal) or mechanical action. It may prevent the good capping of the container, which will spoil the filled product or lead to breakage</p>	
<p>Sunken / bulged sides</p>	<p>The sides of a container (usually panel shape) is sunken or pushed out.</p>	
<p>Bent neck</p>	<p>A neck which is tilted to one side or that has another type of deformation (mechanical or thermal origin).</p>	

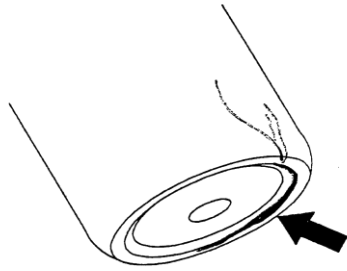
	Broken ware	Typically the containers crack/break inside the annealing lehr	
	Thin ware	Non-uniform glass distribution. Thin spots on the container, which are below the minimum acceptable level (thermal origin).	

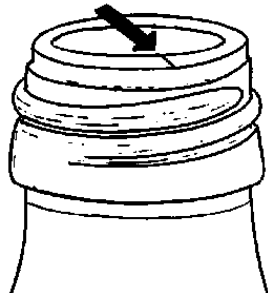
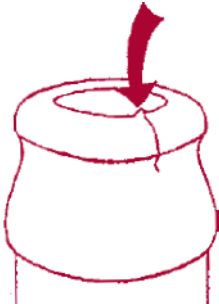
<i>Major B</i>	Type	Description	
	Out of round	The body of the container has a non-cylindrical / oval shape (thermal origin).	
	Rocker bottom	A bottom which has sagged, so that the container is unstable when placed on a flat surface.	

<i>Critical or major A</i>	Type	Description	
	Blister on the top of finish	Broken or very fragile bubbles on the top of the finish (risk of glass particles inside the container).	

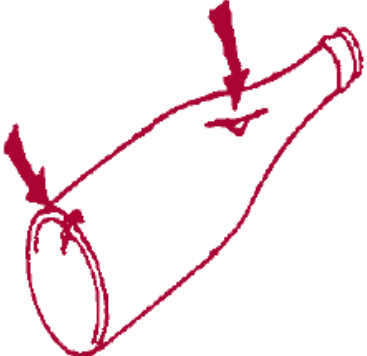
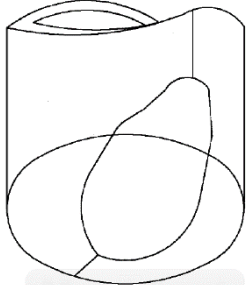
<i>Major A or Major B</i>	Type	Description	
	Out of shape container	Unfilled body shape or deformed after the opening of the blow mould.	
	Leaner	The body of the container is tilted from the vertical axis (not perpendicular to the base – thermal origin).	
	Blank and blow mould seam	Seams which are relatively large, extending from the shoulder to the bottom of the container. Blank seams tend to veer off from the blow mould seam.	
	Neck ring seam	A fin or seam of glass lying across the top or the side of the finish (mechanical origin).	

	Check under finish	Surface crack under or in the lower part of the finish, near or on the neck ring parting line.	
--	--------------------	------------------------------------------------------------------------------------------------	-------------------------------------------------------------------------------------

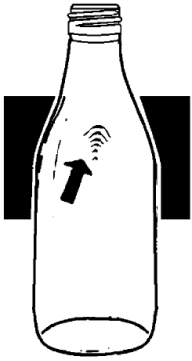
<i>Major A or Major B or minor</i>	Type	Description	
	Baffle mark	A seam occurring between the baffle and the blank mould (mechanical or thermal origin). It can show a crack or a tear which extends until the body of the container.	

<i>Critical or Major or minor</i>	Type	Description	
	Line over finish	Small crack in the outer top surface of the finish. It does not reflect light.	
	Crizzled finish	A finish with many fine surface fractures, mainly across the top.	

<i>Major or minor</i>	Type	Description	
	Wedge bottom, heel tap, slug bottom	A bottom thicker than specified in one of the sides. Mainly a cosmetic defect but it can cause thin spots in other parts of the container.	

<i>Major B or minor</i>	Type	Description	
	Tear	A small surface section torn from under it.	
	Open mark	Superficial and external mark with two separated, irregular rims.	
	Swung baffle	The baffle mark has swung to one side and is not central in the bottom of the container. The container can have low glass thickness in the opposite side of the swung baffle.	

<i>Minor</i>	Type	Description	
	Orange peel / toad skin marks	Rough, grainy and dirty aspect similar to the texture of an orange peel or toad skin.	

	Wash boards	A series of horizontal waves or folds on the side of the container	
	Cold moulds	Wavy appearance in the body of the container (thermal origin).	

3.8.2 Quality Control Laboratory

A failure during a routine process control test initiates an immediate retest of a larger sample to establish whether or not there is a downward quality trend. When substandard ware is detected, all the containers from the suspect mould cavities are rejected until there is a successful test. In addition, all the ware packed as good from the suspect mould cavities since the last successful test is regarded as suspect and reinvestigated so that all substandard ware can be rejected.

Any containers which have to withstand thermal shock in use, e.g. refillable bottles, or bottles subject to pasteurization, are subjected to a specified hot to cold thermal shock. The test samples are placed in a basket and then immersed in a hot water tank so that they are completely filled with water. They are then allowed to soak, after some time they are transferred to a cold water bath where they are immersed before removal and examination for signs of breakage.

In the internal pressure test the bottles are filled with water and then placed. In the tester where the pressure is applied hydro dynamically once the test head is sealed on top of the bottle. There are two types of testers in use. These are known respectively as “increment,” or “continuous” (or Ramp) testers.

The impact test is normally carried out as a design evaluation test rather than as a routine process control test. The test container is placed on the stage of the tester against either a V-shaped back stop, or in some cases a horizontal cylindrical back stop. The stage is then adjusted vertically so that a swinging impact bob will impact at the desired position when the arm supporting the bob is raised to a predetermined level and released. The test level is progressively increased until the container breaks or alternatively, the test can be terminated once the container has survived a particular test level.

In vertical load test, the test is carried out during design evaluation rather than as a routine process control test. The container is placed upright on the stage of the testing machine and the load is transmitted along the vertical axis of the container via a ball swivel head piece as the stage is gradually raised. The vertical load can be applied through an attachment to a standard internal pressure machine, or by means of any other machine which simulates this operation.

In the capacity (volume) test containers are weighed empty and then weighed again when filled with water either brim-full in the case of jars or to the designated fill point in the case of bottles. The difference between

the weight of the container when empty and when filled with water represents the capacity of the container. Capacity, dimensions and glass mass are, of course, interrelated.

The moulds in which glass containers are formed are usually made of cast iron and, when producing glass containers, operate at a temperature of approximately 750°C. The moulds have to be cleaned frequently of scale deposits caused by oxidation and carbon residues produced by mould lubrication. Thus, allowances have to be made for mould wear. As the external dimensions increase, the mass of the glass may have to be increased to keep the capacity within tolerance.

There are several ways in which the glass thickness is checked. Some require the container to be cut into segments or halves while others can be carried out on the whole container. The most common thickness measuring instruments in some cases are mounted on stands or incorporated into other support devices. Another instrument uses a magnetic ball which is introduced inside the container to be held directly opposite to the sensing head of the instrument. The instrument is moved over the external glass surfaces simultaneously moving the ball on the inner surface and the distance between the ball and the instrument head is the thickness of the glass.

Some measuring instruments are purpose built, e.g. to measure container height. Others are incorporated into special support devices, e.g. to measure verticality and ovality. Results are either logged on separate control sheets or automatically submitted for S.P.C. analysis, when this method of control is appropriate. The data collated from this activity serves to form part of the continuous improvement programme of operational control to achieve greater consistency of the glass manufacturing process. When dimensions are extremely difficult to gauge, or cannot be accurately gauged, profile projectors are normally used for control. These instruments project a profile of the glass onto a screen. The glass dimensions are then checked against graduations marked on the screen, or against profile transparencies placed in front of the screen, or by means of micrometres attached to the projector's stage. Finish dimensions are usually checked on some form of profile projector where the finish outline can be precisely measured or compared against a profile of the finish specification.

The type and number of gauges which are necessary to maintain good dimensional control will vary from one type of container to another. Most container specification drawings give tolerances for the ring finish, overall height, and the leading body dimensions, and so these dimensions will be subject to a gauging check, usually in the production line, both at hot end and cold end. Untoleranced dimensions are not subjected to a routine gauging check. Other gauges are used as required to control features such as sunken or bulged body, out of vertical, undulating finish on wide mouth containers, etc., where these features have an adverse effect on the performance of the container. Certain types of gauge, e.g. ring gauges, are constructed from metal blanks to predetermined sizes. Other gauges, e.g. height gauges, are often constructed so that they can be adjusted and preset for different types of containers. The sizes used when manufacturing fixed gauges or setting adjustable gauges are taken from the bottle or ring finish specification.

In the case of bottles, the internal bore and in some cases the profile is usually specified, particularly where the bottles are to be filled automatically or where they have closures which seal against the inside of the ring, e.g. cork closures. In such cases bore gauges would be used. On the other hand, bore gauges are rarely necessary for jars. There is equipment's who is able to measure automatically the inner profile of a bottle, giving a quick and visual indication of the profile.

3.9 Palletizing

When glass containers leave the production line they have to be packaged in some way. This packaging has to satisfy the requirements of both manufacturer and the customer. It has to provide for easy transportation and to protect against the ingress of foreign bodies and general atmospheric contamination. This is typically, nowadays, done using some form of automatic palletizer. Dependent on the container application and/or destination, the glass will be packed in either bulk or modular form. Bulk palletization consists of pallet sized layers of containers stacked to the required height and covered with suitable protection [29].

Modular packages are smaller groups of containers packed into small packages such as cartons, trays, brick-packs or crates. Each of these styles of pack are then loaded onto a pallet and again stacked to the required height. The palletized containers are then either shrink-wrapped or stretch wrapped and strapped (bottles) to aid stability and offer a barrier to the environment before being transferred to the warehouse usually by fork lift truck or a conveyor system. Each one of the pallets is labelled either manually or automatically to assure product traceability [29].

Before any glass containers are placed onto a pallet it is necessary to consider the interlayer between the pallet and the containers. When completed pallets are to be shrink-wrapped it is usual to have a polythene base sheet installed prior to any packing in order to create a barrier to upward contamination and to provide a base to seal the shrink-wrap bag. The base sheet will normally extend beyond each pallet side prior to shrinking. This fuses to the shrink-wrap to act as a damp proof membrane, provides an aid to pack integrity and aids stability. A pad or tray can be placed over the base sheet dependent on customer requirements.

In order to prevent damage to the glass containers and to help the stability of the bulk pallet, each layer of containers is separated from its neighbours by a sheet of corrugated or solid material, which is made from either plastic or cardboard. Alternatively, a cardboard tray may be used. This can be upright or inverted to provide additional stability. These trays can be either manual or automatically erected. The choice of layer dividers is often governed by the method of depalletization to be used at the filler premises. A capping tray or pad is used to complete the pallet.

To assemble the glass containers into modularized pallets nowadays are used palletizer systems from semi-automatic ones to fully automatic systems. Usually these equipment's only require human intervention for loading the bulk packaging materials into the palletizer. These equipment's transfer the layers of containers to the pallet either by dragging them or by vacuum operated or special designed heads. Even the most exotic products with demanding shapes can be arranged into one layer and can be taken over by the swivel arm stacker exactly as it is. These type of equipment's can also be used for cardboard box palletizing (modular packaging).

The shuttle car makes the transfer of completely formed pallets from the palletizers of each production line to the centralized units of shrink (stretch) wrapping (and sometimes strapping) units. These units make the traffic of forklift truck traffic between palletizer, shrink wrapping and empty pallet lines unnecessary. In this way shuttle cars produce a significant reduction in hazards for man and machine and provides transparent materials-flows.

In some circumstances it may be desirable to use strapping to hold the unit together and to provide additional support to the pack (e.g. bottles). Strapping can be applied horizontally around a layer of containers and/or vertically over the finished pack. Horizontal strapping, sometimes known as "banding", can be applied to the layer of containers at the bulk palletizer. It is used to minimise the movement of the layer during transportation but may increase the handling difficulties at the depalletizing stage.

Vertical or compression strapping can be used in conjunction with plastic layer pads. This requires the application of a returnable (reusable) top frame to distribute the load applied by strapping. The strapping units can be either integrated in the palletizers of each production line or be centralized units just before the wrapping operation, Figure 3.64.

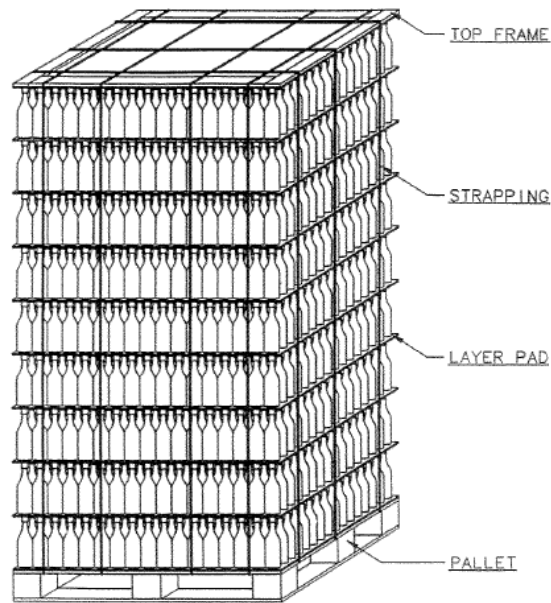


Figure 3.64: Vertical palletizing [12].

3.10 Shrink-wrapping

The assembled containers on the pallet are either covered with shrink wrap applied at a shrink oven station, or with stretch wrap applied by an automatic stretch wrap machine. Stretch wrap saves cost and space, while shrink wrap provides additional product retention, full weatherproofing and higher speed. In either case the processes are regularly checked against specified standards, and in the case of the shrink wrap machine, items such as the shrinking time/oven temperature, are additionally monitored and recorded.

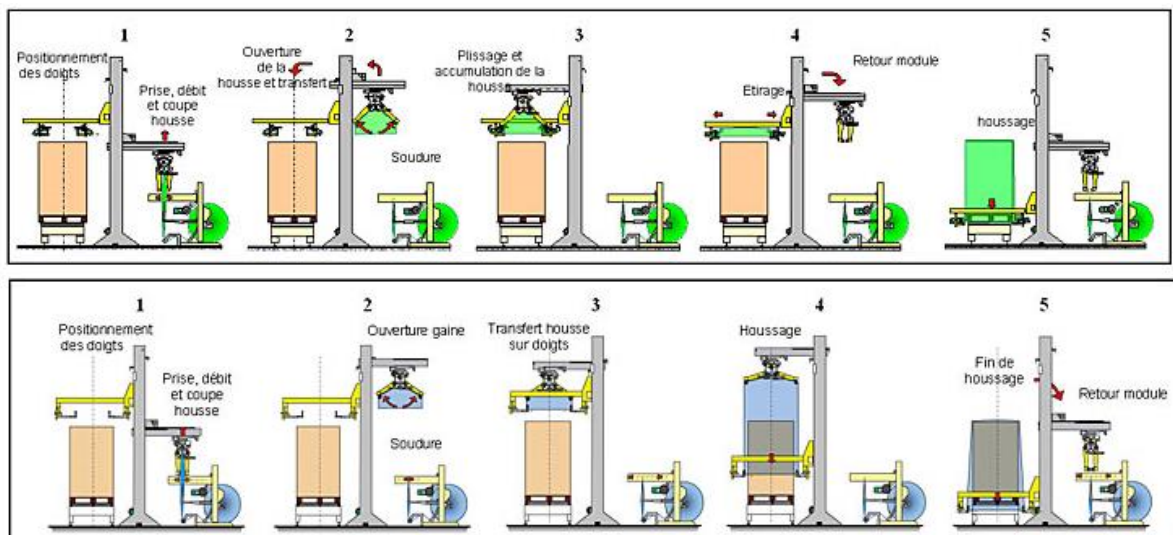


Figure 3.65: Shrink-wrapping a pallet [12].

Pallets are usually conveyed to the glass manufacturer's warehouse by forklift truck. They are then stacked and stored in designated bays, each of which has a separate code to enable easy stock location and to permit the greatest degree of regular stock rotation. Other important warehouse controls concern protection against infestation and contamination of the shrink or stretch wrap covers. Additionally, if there is any deterioration of the pack, or loss of pack integrity, then the pallets concerned are rejected for reprocessing or repack before they are loaded for dispatch. The main loading controls are checks to confirm the vehicle bed is clean, to see that the pallets are loaded correctly, and to see that the load is securely held and that all outer covers are in place before dispatch.

Perhaps the major quality concern at this stage of the process is the physical contamination of the product and/or pallet load. This is of special importance just before the pallet load is shrink or stretch wrapped. During the palletization process and the transfer of the unit load to the shrinking unit, the unit load is unprotected and subjected to possible sources of contamination. A possible and very probable source of contamination is the contamination by pieces of broken glass originated during the container manipulation either on the palletizer or during transport. At this stage of the process there are no additional equipment's that can detect and eliminate this contamination (either inspection machine or container inverter). This fact calls for a human control/supervision at this stage and the enforcement of "broken glass" procedures by the glass manufacturer. In order to avoid contamination the integrity of the shrink wrap must be assured during this operation and downstream the process until the pallet load reaches the filler. The shrinking time/oven temperature is a process parameter that should be monitored in order to achieve optimum performance. The pallets when stored in the warehouse should be inspected for integrity. If found with any hole in the plastic the pallet loaded should be rejected and returned to the production area for reinspection and reprocessing. The same inspection should take place just before the pallet is load into the truck or container.

Loading the pallet verticality is another key aspect to take into account. The deviation from vertical position of the pallet load can hamper the storing, transportation, depalletization and container integrity downstream the process. The causes of this phenomena are variable and can be related either with the operation: palletization, transfer of the pallet load from palletizer to shrink wrapping, incorrect shrink wrapping or the packaging material (not enough stiffness). Some of the shrink wrapping equipment's are able to re-centre the pallet load and correct any deviations to the vertical position just before this operations takes place through a centring device. However, this should be one of the controls to perform when storing the pallet loads in the warehouse. If the pallet load is strapped another aspect that should be object of control is the strapping tension. This parameter is of key importance to monitor the integrity of the strapped layers. This parameter should be monitored in all of the strapped layers and just before the shrink wrap takes place. A loose layer will definitely cause handling difficulties at the depalletizing stage.

CHAPTER 4

4 Mathematical Modelling of Glass Forming Processes

In this chapter the modelling techniques of glass container forming processes are presented. Modelling glass forming consists in the reproduction of the physics processes by means of mathematics and numerical models. The finite element method was here the choice to the development of a methodology for simulating this technology process. The physical process is a coupled thermomechanical problem evolving on the glass and its interaction with the air and equipment. In this chapter, the partial differential equations that describe the temperature field and mechanical behaviour are presented.

4.1 Finite Element Formulation for Thermomechanical Behaviour

4.1.1 Constitutive Model

Glass material can be mechanically characterized as an isotropic Maxwell viscoelastic material. When deforming the total strain rate $\dot{\epsilon}$ may be considered to be obtained as the sum of the elastic strain rate $\dot{\epsilon}_e$ and the viscous strain rate $\dot{\epsilon}_p$:

$$\dot{\epsilon} = \dot{\epsilon}_e + \dot{\epsilon}_p \quad 4.1$$

where:

$$\begin{aligned} \dot{\epsilon}_e &= \frac{\dot{\sigma}}{E} \\ \dot{\epsilon}_p &= \frac{\dot{\sigma}}{\eta} \end{aligned} \quad 4.2$$

where E is the Young's modulus and η is the viscosity. Therefore;

$$\dot{\epsilon} = \frac{\dot{\sigma}}{E} + \frac{\dot{\sigma}}{\eta} \quad 4.3$$

Nevertheless, experiments on stress relaxation show that for lower viscosities, i.e., for high temperatures, the relation between viscosity and the rate of stress release becomes linear indicating that the viscous flow is the main mechanism and hence permitting the neglect of elastic effects, which means that it can be assumed that $\dot{\epsilon}_e = 0$ [11].

By separating the stress-strain relation into its deviatoric (s_{ij} , $\dot{\epsilon}_{ij}$) and dilatational (σ_m , $\dot{\epsilon}_{ii}$) components we may write:

$$\sigma_{ij} = \sigma_m \delta_{ij} + s_{ij} \quad 4.4$$

where the deviatoric stress tensor is given by,

$$s_{ij} = 2\eta_\mu \dot{\epsilon}_{ij} \quad 4.5$$

and the hydrostatic stress is given by,

$$\sigma_m = \eta_k \dot{\epsilon}_{ii} \quad 4.6$$

being η_μ and η_k the shear and bulk viscosities, respectively.

At high temperatures glass deformation can be considered incompressible, i.e.

$$\dot{\epsilon}_{ii} = 0 \quad 4.7$$

and consequently the solution is driven by the deviatoric response and the constitutive equations take the more general form:

$$\begin{aligned} s_{ij} &= 2\eta_\mu \dot{\epsilon}_{ij} \\ \sigma_{ij} &= s_{ij} - p\delta_{ij} \end{aligned} \quad 4.8$$

being $\dot{\epsilon}_{ij}$ the strain rate tensor and p is the hydrostatic pressure:

$$p = -\frac{\sigma_{ii}}{3} \quad 4.9$$

4.1.2 Finite Element Method Formulation

The finite element model is established from the equilibrium equations for the thermoviscoelastic problem. Following the standard finite element method implementation and notation taking nodal velocities $\bar{\mathbf{v}}$ as the primal variables within any element the velocity field \mathbf{v} is defined, by means of the standard shape functions \mathbf{N} as:

$$\mathbf{v} = \mathbf{N}\bar{\mathbf{v}} \quad 4.10$$

The strain rate tensor,

$$\dot{\epsilon}_{ij} = \frac{1}{2}(v_{i,j} + v_{j,i}) \quad 4.11$$

can then be related with the nodal velocities by the \mathbf{B} Matrix⁵.

$$\dot{\boldsymbol{\epsilon}} = \mathbf{B}\bar{\mathbf{v}} \quad 4.12$$

The deviatoric stress (Equation 4.8) can be expressed in the matrix form:

$$\mathbf{s} = \mathbf{D}\dot{\boldsymbol{\epsilon}} = \mathbf{D}\mathbf{B}\bar{\mathbf{v}} \quad 4.13$$

being \mathbf{D} the shear stress viscosity matrix.

The penalty method is used to impose the incompressibility constraint by defining:

$$\dot{\epsilon}_{ii} = -\frac{p}{\alpha} \quad 4.14$$

where α is the penalty value, that can be related with the bulk viscosity. This penalty value is weighted locally with the bulk viscosity as

$$\alpha = \lambda \eta_{\mu} \quad 4.15$$

being λ a 'large' number.

Then, the hydrostatic stress can be related with the dilatational stress as:

⁵ \mathbf{B} matrix is composed of the space derivatives of the shapes function

$$\sigma_m = \frac{\sigma_{ii}}{3} = -p = \alpha \dot{\varepsilon}_{ii} \quad 4.16$$

or, in the matrix form,

$$\sigma_m = \alpha \mathbf{m}^T \dot{\boldsymbol{\varepsilon}} = \alpha \mathbf{m}^T \mathbf{B} \bar{\mathbf{v}} \quad 4.17$$

for the axisymmetric case \mathbf{m}^T is a vector given by,

$$\mathbf{m}^T = [1 \quad 1 \quad 1 \quad 0] \quad 4.18$$

Neglecting inertia forces the mechanical equilibrium equations are:

$$\frac{\partial \sigma_{ij}}{\partial x_j} + b_i = 0 \quad 4.19$$

where b_i are body forces components per unit volume.

Following the Galerkin method the final system of equations, obtained by performing integration over the full domain Ω and its boundary Γ , is then obtained in the standard form as:

$$\mathbf{K} \bar{\mathbf{v}} = \mathbf{f} \quad 4.20$$

The global stiffness matrix \mathbf{K} includes the deviatoric, \mathbf{K}_d , and dilatational, \mathbf{K}_h , as:

$$\mathbf{K} = \mathbf{K}_d + \mathbf{K}_h \quad 4.21$$

where

$$\mathbf{K}_d = \int_{\Omega} [\mathbf{B}]^T \mathbf{D} \mathbf{B} d\Omega \quad 4.22$$

and

$$\mathbf{K}_h = \int_{\Omega} \alpha \mathbf{B}^T \mathbf{m} \mathbf{m}^T \mathbf{B} d\Omega \quad 4.23$$

The load vector is,

$$\mathbf{f} = \mathbf{f}_p + \mathbf{f}_G \quad 4.24$$

where \mathbf{f}_p and \mathbf{f}_G represent the vectors of nodal applied ($P_{applied}$) and body (b) forces, respectively

$$\mathbf{f} = \int_{\Gamma} \mathbf{N}^T p_{applied} d\Gamma + \int_{\Omega} \mathbf{N}^T b d\Omega \quad 4.25$$

It is interesting to notice that if a mixed formulation is adopted, utilizing velocities and pressure as primal variables the final system of equation would take the form:

$$\begin{cases} \mathbf{K}_v \bar{\mathbf{v}} + \mathbf{Q}\mathbf{p} = \mathbf{f} \\ \mathbf{Q}^T \bar{\mathbf{v}} = \mathbf{0} \end{cases} \quad 4.26$$

or in a matrix form:

$$\begin{bmatrix} \mathbf{K}_v & \mathbf{Q} \\ \mathbf{Q}^T & \mathbf{0} \end{bmatrix} \begin{bmatrix} \bar{\mathbf{v}} \\ \mathbf{p} \end{bmatrix} = \begin{bmatrix} \mathbf{f} \\ \mathbf{0} \end{bmatrix} \quad 4.27$$

where the second set of equations relate to the incompressibility constraint.

Relaxing that constraint by means of a penalty parameter α such as

$$\mathbf{Q}^T \bar{\mathbf{v}} - \frac{1}{\alpha} \mathbf{I}\mathbf{p} \approx \mathbf{0} \quad 4.28$$

then

$$\begin{bmatrix} \mathbf{K}_v & \mathbf{Q} \\ \mathbf{Q}^T & -\frac{1}{\alpha} \mathbf{I} \end{bmatrix} \begin{bmatrix} \bar{\mathbf{v}} \\ \mathbf{p} \end{bmatrix} = \begin{bmatrix} \mathbf{f} \\ \mathbf{0} \end{bmatrix} \quad 4.29$$

Solving for pressure in the second set of equations,

$$\mathbf{Q}^T \bar{\mathbf{v}} - \frac{1}{\alpha} \mathbf{I}\mathbf{p} = \mathbf{0} \Leftrightarrow \mathbf{p} = \alpha \mathbf{Q}^T \bar{\mathbf{v}} \quad 4.30$$

and substituting in the first set of equations we obtain a system only dependent on the nodal velocities

$$\mathbf{K}_v \bar{\mathbf{v}} + \alpha \mathbf{Q}\mathbf{Q}^T \bar{\mathbf{v}} = \mathbf{f} \quad 4.31$$

where \mathbf{K}_v may be identified with \mathbf{K}_d , and $\alpha\mathbf{Q}\mathbf{Q}^T$ may be identified with \mathbf{K}_h .

It is well known that, to avoid “locking” effects, the number of variables associated with the constrain condition (incompressibility here) in the second set of equations must be smaller than the number of variables associated with the other primal field (velocities here) and that is related with the need of using reduced integration techniques when evaluating the \mathbf{K}_h .

In general, a nonlinear static finite element is most effectively performed using an incremental formulation, in which the static variables are updated incrementally corresponding to successive time steps in order to trace out the complete solution path. In this solution it is important that the governing finite element equations are satisfied at each time step to obtain sufficient accuracy, because otherwise, solution errors can be significantly accumulated that can lead even to solution instabilities [30].

The glass viscosity is dependent on the glass composition and also is highly dependent on the temperature, influencing greatly the flow of the material as discussed in the section 2.4. Therefore, it is essential to constantly model heat transfer within the glass and to the air and moulds and to couple it with the mechanical formulation that describes glass deformation.

4.2 Finite Element Formulation for Heat Transfer

In this section, it was consider the finite element formulation for the thermal problem. The main goal is to introduce the finite element formulation necessary for the solution of nonlinear transient heat transfer behaviour of glass containers production. Heat transfer and mechanical flow will be treated in an uncoupled but staggered manner, because glass viscosity and other material parameters are assumed to be temperature dependent.

4.2.1 Transient Analysis

The temperature is the most important parameter in almost all stages of glass making and glass processing. During the glass melting, the temperature influences the homogeneity of the glass melt, the drop in temperature influences the following forming process and finally the cooling of the hot glass influences possible thermal residual stresses inside the glass product [31].

The classical partial differential equation governing the transient heat transfer in a solid is:

$$\left[\frac{\partial}{\partial x} \left(k_x \frac{\partial T}{\partial x} \right) + \frac{\partial}{\partial y} \left(k_y \frac{\partial T}{\partial y} \right) + \frac{\partial}{\partial z} \left(k_z \frac{\partial T}{\partial z} \right) \right] + Q = \rho c \frac{\partial T}{\partial t} \quad 4.32$$

where T is the temperature, k_x, k_y, k_z are the thermal conductivity coefficients in x, y, z directions (if the material is isotropic then the thermal conductivity can be simplified as $k_x = k_y = k_z = k$), ρ is the density, C is the specific heat and Q is a heat source per unit of volume.

To solve it an initial temperature condition for the entire body, at an initial time t_0 must be known

$$T = T_i \quad \text{on } \Omega \quad \text{at } t = t_0 \quad 4.33$$

Thermal boundary conditions may be of different kind and can be classified into two types:

- Essential boundary conditions (Dirichlet boundary conditions):

where temperatures are imposed in part of the domain boundary, Γ_1 , are known

$$T = T_{\Gamma_1} \quad \text{in } \Gamma_1 \quad 4.34$$

- Natural boundary conditions (Neumann boundary conditions):

where heat flux can be imposed in part of the domain boundary, Γ_2 .

$$q_c = k \frac{\partial T}{\partial n} = -\alpha_c (T - T_a) \quad 4.35$$

where α_c is the heat transfer coefficient, T_a the temperature of surrounding fluid (air) and n is the outward direction normal to the boundary surface.

Also, a radiation flux can be imposed at the boundary surface;

$$q_r = -\beta \varepsilon (T^4 - T_\infty^4) \quad 4.36$$

where β is the Stefan–Boltzmann constant, ε the emissivity and the T_∞ the surround temperature. Along the free surface in contact with air, a condensed formulation can take into account both convective and radiative heat flux, the sum of which being written as q_{cr} .

$$q_{cr} = q_c + q_r \quad 4.37$$

The heat flux considering the convection and radiation, may be given by,

$$q_{cr} = \alpha_c (T - T_a) + \beta \varepsilon (T^4 - T_\infty^4) \quad 4.38$$

or,

$$q_{cr} = \alpha_c (T - T_{amb}) + \beta \varepsilon (T^2 - T_\infty^2)(T^2 + T_\infty^2) \quad 4.39$$

and,

$$q_{cr} = \alpha_c (T - T_{amb}) + \beta \varepsilon (T^2 + T_\infty^2)(T + T_\infty)(T - T_\infty) \quad 4.40$$

Therefore, a temperature dependent “equivalent heat transfer parameter” can be defined for radiation as,

$$\alpha_r = -\beta\varepsilon(T^2 + T_\infty^2)(T - T_\infty) \quad 4.41$$

Assuming that T_a and T_∞ are the same in a condensed approach may be written as

$$q_{cr} = \alpha_{cr}(T - T_a) \quad 4.42$$

where α_{cr} is an effective temperature dependent parameter or heat transfer “coefficient” (HTC). The heat transfer coefficient (HTC) depends also on the velocity and on the material. Therefore, in hollow glass production the heat transfer coefficient can be different in different regions of the mould, the ring, the baffle or the plunger.

To solve equation 4.32 a finite element solution based on the Galerkin weighted residual method was used. The temperature T is interpolated from the nodal values \bar{T}_i using the approximating functions N_i

$$T = \sum_{i=1}^n N_i \bar{T}_i \quad 4.43$$

where Γ represent the whole boundary and n is the total number of nodes.

Applying the Galerkin weight residual method to the transient analysis gives:

$$\int_{\Omega} N_i \left[\left[\frac{\partial}{\partial x} \left(k_x \frac{\partial T}{\partial x} \right) + \frac{\partial}{\partial y} \left(k_y \frac{\partial T}{\partial y} \right) + \frac{\partial}{\partial z} \left(k_z \frac{\partial T}{\partial z} \right) \right] + Q - \rho c \frac{\partial T}{\partial t} \right] d\Omega = 0 \quad 4.44$$

for $i=1, n$.

Integrating by parts we obtain for each equation,

$$\begin{aligned} & \int_{\Omega} \left[-\frac{\partial N_i}{\partial x} \left(k_x \frac{\partial T}{\partial x} \right) - \frac{\partial N_i}{\partial y} \left(k_y \frac{\partial T}{\partial y} \right) - \frac{\partial N_i}{\partial z} \left(k_z \frac{\partial T}{\partial z} \right) + N_i Q - N_i \left(\rho c \frac{\partial T}{\partial t} \right) \right] d\Omega \\ & + \int_{\Gamma} N_i \left(k_x \frac{\partial T}{\partial x} \right) d\Gamma + \int_{\Gamma} N_i \left(k \frac{\partial T}{\partial y} \right) d\Gamma + \int_{\Gamma} N_i \left(k \frac{\partial T}{\partial z} \right) d\Gamma = 0 \end{aligned} \quad 4.45$$

with the boundary conditions are:

$$\int_{\Gamma} N_i \left(k_x \frac{\partial T}{\partial x} \right) d\Gamma + \int_{\Gamma} N_i \left(k \frac{\partial T}{\partial y} \right) d\Gamma + \int_{\Gamma} N_i \left(k \frac{\partial T}{\partial z} \right) d\Gamma = -\int_{\Gamma} N_i q d\Gamma - \int_{\Gamma} h(T - T_a) d\Gamma \quad 4.46$$

where h is the heat transfer coefficient

The final finite element formulation for the thermal behaviour in matrix form is generally given by,

$$\underline{\mathbf{K}}\underline{\mathbf{T}} + \underline{\mathbf{C}}\dot{\underline{\mathbf{T}}} = \underline{\mathbf{Q}} \quad 4.47$$

being,

$$\dot{\underline{\mathbf{T}}} = \frac{\partial \underline{\mathbf{T}}}{\partial t} \quad 4.48$$

the time derivative of the nodal temperatures $\underline{\mathbf{T}}$,

$\underline{\mathbf{K}}$ is the of the “conductivity” matrix, with K_{ij} terms for $i,j=1,n$

$$K_{ij} = \int_{\Omega} \left(\frac{\partial N_i}{\partial x} \frac{\partial N_j}{\partial x} k_x \bar{T}_j + \frac{\partial N_i}{\partial y} \frac{\partial N_j}{\partial y} k_y \bar{T}_j + \frac{\partial N_i}{\partial z} \frac{\partial N_j}{\partial z} k_z \bar{T}_j \right) d\Omega + \int_{\Gamma} (h N_i N_j) d\Gamma = 0 \quad 4.49$$

and $\underline{\mathbf{C}}$ is the heat source term with Q_i terms defined as,

$$C_{ij} = \int_{\Omega} \rho c N_i N_j d\Omega \quad 4.50$$

and Q_i the terms of the “thermal load” vector,

$$Q_i = \int_{\Omega} N_i Q d\Omega - \int_{\Gamma} N_i q d\Gamma - \int_{\Gamma} N_i h T_a d\Gamma \quad 4.51$$

4.2.2 Time Integration

For the integration in time we introduce a set of approximations to the time derivative by linear interpolation of two consecutive time values

$$t_{n+1} = t_n + \Delta t_n \quad 4.52$$

by

$$\underline{\mathbf{T}}_{n+1} = \underline{\mathbf{T}}_n + \Delta t \left[(1-\gamma) \dot{\underline{\mathbf{T}}}_n + \gamma \dot{\underline{\mathbf{T}}}_{n+1} \right] \quad 4.53$$

where $0 \leq \gamma \leq 1$.

Writing the previous equation at time t_n

$$\mathbf{K}\underline{\mathbf{T}}_n + \mathbf{C}\dot{\underline{\mathbf{T}}}_n = \mathbf{Q}_n \quad 4.54$$

using that linear interpolation, assuming that \mathbf{K} and \mathbf{C} are kept constant in the time interval Δt_n and obtaining $\dot{\underline{\mathbf{T}}}_{n+1}$ from equation:

$$\mathbf{K}\underline{\mathbf{T}}_{n+1} + \mathbf{C}\dot{\underline{\mathbf{T}}}_{n+1} = \mathbf{Q}_{n+1} \quad 4.55$$

we may write

$$\left[\gamma \mathbf{K} + \frac{1}{\Delta t} \mathbf{C} \right] \underline{\mathbf{T}}_{n+1} = (1-\gamma) \mathbf{Q}_n + \gamma \mathbf{Q}_{n+1} - \left[(1-\gamma) \mathbf{K} - \frac{1}{\Delta t} \mathbf{C} \right] \underline{\mathbf{T}}_n \quad 4.56$$

where

$$\hat{\mathbf{C}} = \left[\gamma \mathbf{K} + \frac{1}{\Delta t} \mathbf{C} \right] \quad 4.57$$

$$\hat{\mathbf{K}} = \left[\frac{1}{\Delta t} \mathbf{C} - (1-\gamma) \mathbf{K} \right] \quad 4.58$$

Different values for γ may be used that lead to different type of solutions:

$\gamma = 0$ - Forward difference or Euler scheme (conditionally stable)

$\gamma = \frac{1}{2}$ - Crank-Nicolson or trapezoidal rule scheme

$\gamma = \frac{2}{3}$ - Galerkin scheme

$\gamma = 1$ - Backward difference scheme (unconditionally stable)

When $\gamma = 0$ the scheme is termed explicit. The others schemes are termed implicit.

Implicit schemes are unconditionally stable in linear problems. This means that the numerical process will not diverge even if Δt is large, but the solution may be coarse because important changes may take place on a small time scale. Implicit schemes are second order accurate, which means that numerical errors in T produced by the algorithm is approximately quartered when Δt is halved.

Among the implicit methods, the choice of $\gamma = \frac{1}{2}$ is popular, but sharp transient conditions may provoke annoying oscillations in the solution. Oscillations can be reduced using smaller values of Δt or numerically damp the solution by using a value of γ somewhat greater than $\frac{1}{2}$.

If \mathbf{Q} represents a thermal shock the solution may display some spurious oscillation, which can be reduced by using a value of γ greater than $\frac{1}{2}$ so as to introduce algorithmic damping.

The explicit scheme may be unstable unless we adopt a time step smaller than

$$\Delta t_{cr} = \frac{2}{(1-2\gamma)\lambda_{max}} \quad 4.59$$

where λ_{max} is maximum eigenvalue of the eigenvalue problem $\hat{\mathbf{K}} \mathbf{T} = \lambda \hat{\mathbf{C}} \mathbf{T}$.

This page intentionally left blank

CHAPTER 5

5 Simulating Model for Glass Containers

Some of the main features of the general computational model for glass forming derived, namely for press/blow and blow/blow processes are described here. Various modelling aspects are discussed for each process, while several key issues, such as the movement of the plunger, contact, and remeshing technique are examined thoroughly.

Certain steps in formulating a finite element analysis of a physical problem should be embodied in the finite element software. Before running a simulation a model has to be created. So as a first step a preprocessor tool is needed to create a model. The preprocessing step is, basically, used to define the model and it includes

- Definition of the geometric domain of the problem.
- Definition of the element type(s) to be used.
- Definition of the material properties associated to the elements.
- Definition of the physical constraints (boundary conditions).
- Definition of the loads.
- Generation of the mesh.

The preprocessing is an important step to obtain a “good” result. Then, to run a simulation some few steps are needed. The main procedures in the finite element analysis are:

- Input reading.
The input needed for the finite element analysis comprise:
 - Geometry definition,
 - Finite element mesh information (number of nodes, number of elements, nodal connectivity,
 - Finite element parameters,
 - Material properties,
 - Node temperatures,
 - Load information;

- Process parameters.
- Obtain the element associated matrices and vectors.
- Assembling element matrices.
- Apply constrains to the matrix and vector according to the imposed boundary conditions.
- Solve the equation system of resulting non-linear equations, with an iterative process to compute the unknown values of the primary field variables.
- Compute secondary variables, such as, from the known nodal temperatures/velocities, if required, strains and stresses can be computed.
- Post Processing, plot results.

The visualization of the results is performed through a postprocessor. The customised post processor is used to allow the user to rotate, translate and zoom into and out from the objects. The postprocessor software contains sophisticated routines used for sorting, printing, and plotting selected results from the finite element solution. Animations and movies can also be produced to simulate the dynamic aspects of a problem. Outputs in form of text files and x–y plots are also available. The output data are processes in a desired format for plotting. While solution data can be manipulated in many ways in the postprocessing, the most important objective is to apply sound engineering judgment in determining whether the solution results are physically reasonable [32].

5.1 Element Technology

The software is able to perform a simulation with several elements type such as triangular and quadrangular elements with linear and quadratic integration. Next these different elements and the problems associated to them will be described.

5.1.1 Library of Elements

The most used 2D shapes the triangle with 3 nodes, 3 nodes with bubble function and the quadrilateral with 4 nodes or 8 nodes are included.

5.1.2 Spurious Oscillations Due to Smaller Time Increments

Some oscillation in the solution of the temperatures that can occur in the time domain. Such behaviour is directly associated with the numerical characteristics of the time integration scheme involved and the time increment being employed in the solution.

In particular, the solution of time dependent field problems using quadrilateral or triangular elements is often accompanied by increase or decrease in temperature that violate the physical aspects of the problem. In transient heat transfer analysis with second-order elements there is a relationship between the minimum usable time increment and the element size that should be taken into account [33]. A simple guideline is:

$$\Delta t > \frac{\rho c}{6K} \Delta L^2 \quad 5.1$$

where ρ is the density, c the specific heat, K the conductivity and ΔL the element size.

5.1.3 Hourglass and Locking

One of the important issues that have been discussed in the literature is the locking problem. Some finite elements exhibit in some applications overly stiff behaviour characterised by the fact that important modes of deformation cannot be effectively reproduced. This is the case when using elements with low order interpolating polynomials in problems involving the incompressible constraint in the deformation of a medium, as is the case in glass forming. Typical solutions may involve the use of high order elements, mixed formulations or selective reduced integration techniques. However these solutions may, in certain cases, introduce some spurious energy deformation modes, commonly known as hourglass effects, and

some stabilization techniques may be needed. In the next chapter an analysis of the underlying deformation modes associated with different types of elements used here will be analysed.

5.2 Contact

Most of the problems in the simulation of manufacturing processes involve contact between two or more bodies, sometimes involving complex geometries and undergoing large deformations. From a mechanical point of view, at macroscopic scale, contact is the notion of the interaction between bodies coming in to touch and exchanging load and energy [34]. The key condition on these processes is the condition of impenetrability, namely, the condition that two bodies cannot interpenetrate. Nonetheless, all physical processes involved in contact such as friction, heat transfer, must be considered.

To model the contact in glass container forming we may consider two states. The first is the so called 'sticking' state in which a point of the glass mesh is in contact and it is impossible to move in the tangential direction, i.e, against the mould. The second case is 'sliding', which means that a node can move freely in tangential direction through the contact interface. In between these two states a sliding with friction state can occur. The contact between two bodies is described by a choice of both behaviours, such as, normal and tangential conditions. Contact with sticking friction is a good macroscopic description of perfect adherence whilst sliding contact can be considered as a perfectly lubricated contact.

In the case of thermomechanical contact problems two fields - deformation and temperature - interact, and thus have to be considered within the formulation. In the general settings, these fields are coupled, since the constitutive parameters depend upon the temperature. Furthermore, the evolution of the thermal field is related to the deformation.

In the contact of two bodies, two different areas can be distinguished. The area where there is contact and the area where there is no contact, Figure 5.1.

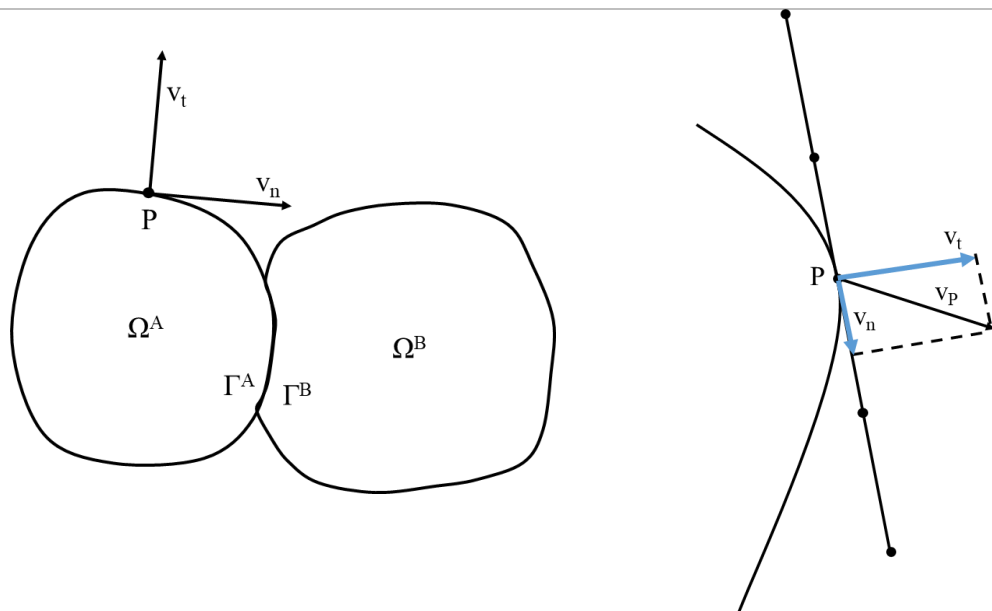


Figure 5.1: Model domain contact problem.

The velocity vector at each point in contact can be expressed in the rotated axis in relation to the contact surface.

$$v_p = v_n + v_t \quad 5.2$$

where v_p are the velocity of the node and v_n and v_t are the normal and tangential components of velocity. The position of a point at time $t + \Delta t$ is obtained as:

$$\mathbf{x}^{t+\Delta t} = \mathbf{x}^t + \mathbf{u}^t \tag{5.3}$$

with \mathbf{u}^t being the displacement measured at time t and

$$\mathbf{u}^t = \Delta t \mathbf{v}^t \tag{5.4}$$

In order to prevent node penetration of the glass through the mould a correction of current increment time can have to be performed, Figure 5.2. This will be clarified in the next sections

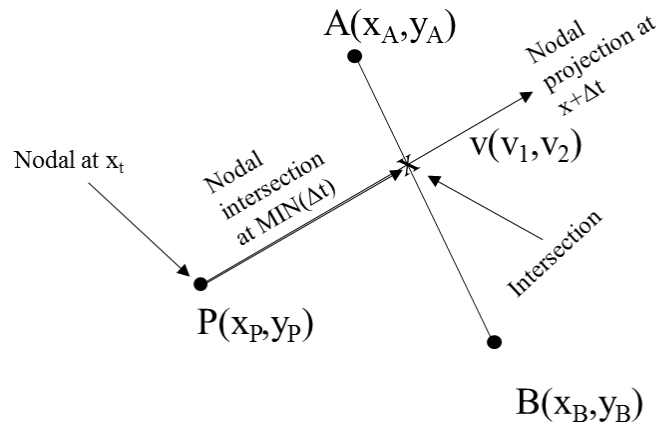


Figure 5.2: Target for glass node contact the mould.

5.2.1 Contact Algorithm

The initial assumption of the algorithm is that only one node of the FEM mesh representing the glass can touch the mould at each time interval. This may redefine the initial assumed time increment as it will be explained for either sliding or sticking conditions.

The contact detection is a search of closest glass node that can come into contact with the mould during the current solution step. Large contact problems may imply a large number of contacting nodes. This simple detection technique, based on a comparison of distances from each 'slave' node to all components of the 'master' surface, may lead to an excessive time consumption, especially, if contact elements must be frequently updated. The flowchart of the general contact algorithm is presented in Figure 5.3.

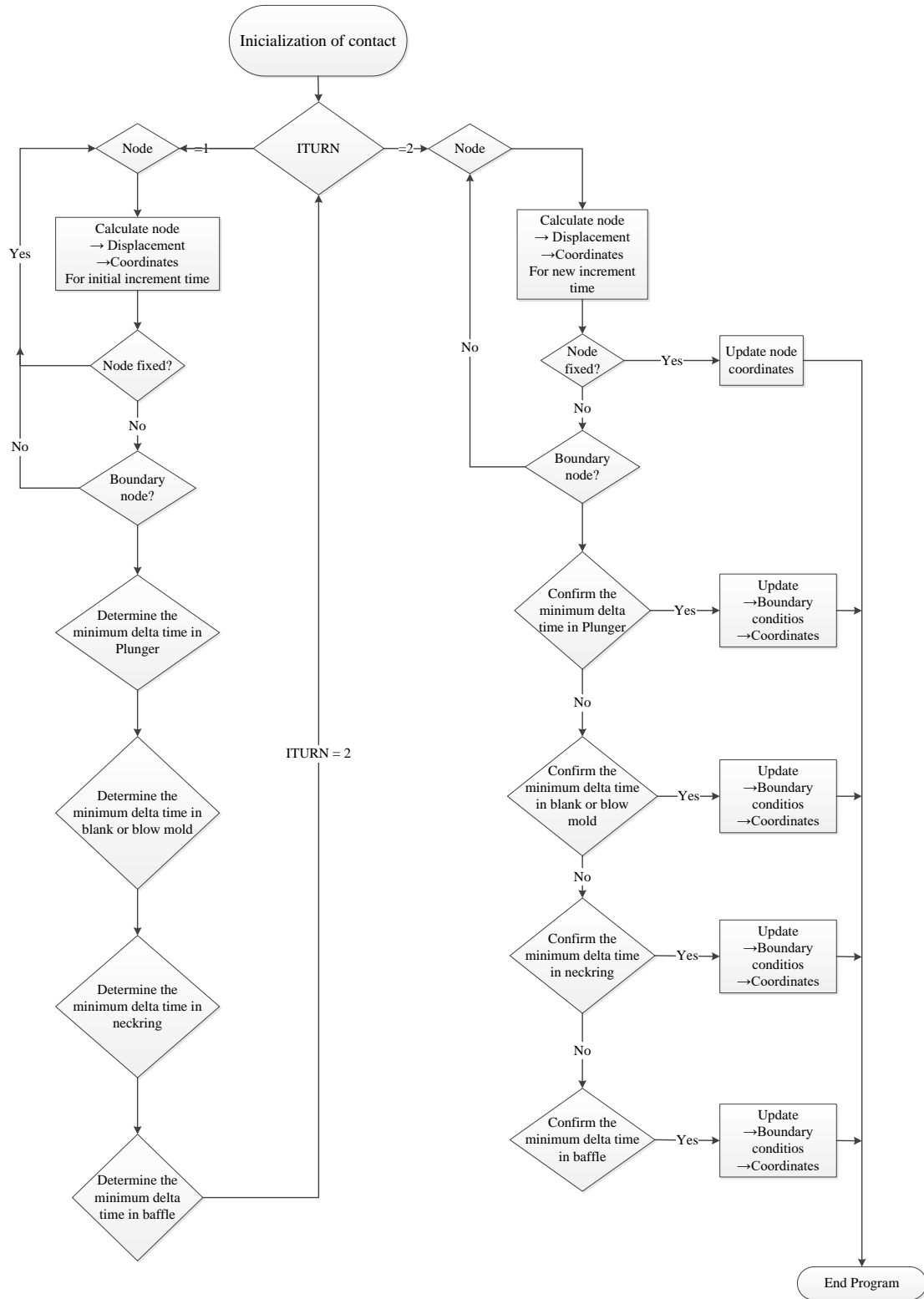


Figure 5.3: Contact algorithm flowchart for each node.

5.2.2 Sticking Condition

A point which sticks to the mould does not move in a tangential direction. This is a valid assumption for certain stages of the process.

Firstly all boundary nodes are candidate to contact the mould. The algorithm tracks all the surface nodes, excluding the nodes that have already touched the mould. The next step is to calculate which mould element can be reached, according to the calculated velocity, and the time needed to reach the mould.

A mathematical condition can be built to satisfy the node positioning over the mould and the time needed to reach it, as represented in Figure 5.4.

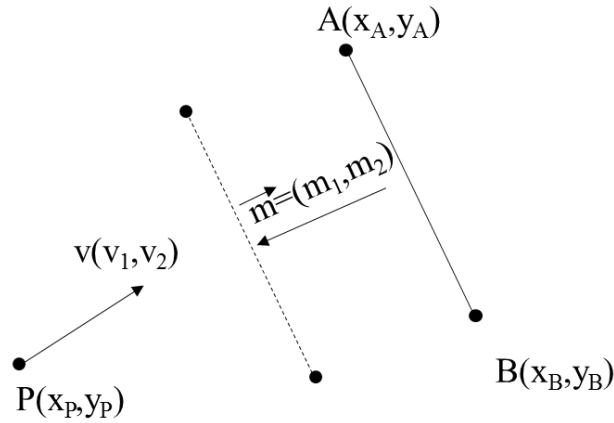


Figure 5.4: Contact representation for sticking condition.

The two conditions must be satisfied:

$$\begin{aligned} \mathbf{x} &= (\mathbf{A} + \Delta t \mathbf{m}) + u(\mathbf{B} - \mathbf{A}) \\ \mathbf{x} &= \mathbf{P} + \Delta t \mathbf{v} \end{aligned} \tag{5.5}$$

where \mathbf{A} and \mathbf{B} are two points of the mould segment, \mathbf{P} and \mathbf{v} the position of the candidate node to contact and its velocity, u is the position of the mould element where the node will stick, Δt is the time needed to reach the mould element and \mathbf{m} is the mould velocity.

The intersection is given by;

$$\begin{cases} x_A + \Delta t m_1 + u(x_B - x_A) = x_P + \Delta t v_1 \\ y_A + \Delta t m_2 + u(y_B - y_A) = y_P + \Delta t v_2 \end{cases} \tag{5.6}$$

or, in matrix form,

$$\begin{bmatrix} (m_1 - v_1) & (x_B - x_A) \\ (m_2 - v_2) & (y_B - y_A) \end{bmatrix} \begin{bmatrix} \Delta t \\ u \end{bmatrix} = \begin{bmatrix} (x_P - x_A) \\ (y_P - y_A) \end{bmatrix} \tag{5.7}$$

Taking:

$$\Delta = \begin{vmatrix} (m_1 - v_1) & (x_B - x_A) \\ (m_2 - v_2) & (y_B - y_A) \end{vmatrix} \quad 5.8$$

and using the Cramer's rule we obtain,

$$\Delta t = \frac{\begin{vmatrix} (x_P - x_A) & (x_B - x_A) \\ (y_P - y_A) & (y_B - y_A) \end{vmatrix}}{\Delta} \quad 5.9$$

and,

$$u = \frac{\begin{vmatrix} (m_1 - v_1) & (x_P - x_A) \\ (m_2 - v_2) & (y_P - y_A) \end{vmatrix}}{\Delta} \quad 5.10$$

For each node then is checked in which mould segments u lies between $[0,1]$ and the smaller time increment (Δt) the touching segment is selected and the time step redefined. The coordinates of all nodes and boundary conditions are then updated.

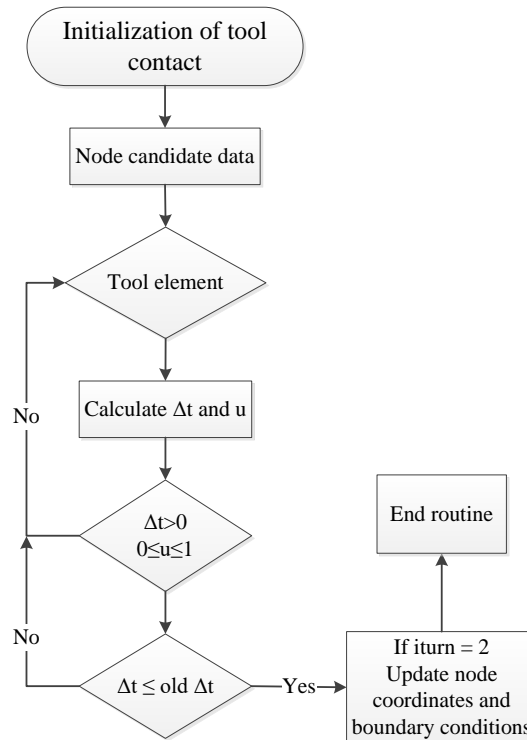


Figure 5.5: Contact flowchart for candidate segment selection.

5.2.3 Sliding Conditions

In the sliding case, some differences have to be implemented in the previous algorithm. The first obvious difference is when the node is in contact with the mould. This means that the node can slide along the mould segment. Slipping may result in two parallel vectors, Figure 5.6b). The tangential velocity and the tool element vector are parallel, therefore, Δ is equal zero in equation 5.8. So, for this case the algorithm has to be changed. In that scenario Δt is calculated so that the distance between the contact node and the mould node in the velocity direction is calculated using:

$$\Delta t = \frac{\sqrt{(x_A - x_P)^2 + (y_A - y_P)^2}}{\sqrt{v_1^2 + v_2^2}} \quad 5.11$$

For the moulds and the plunger, we may allow both slip and no slip boundary conditions.

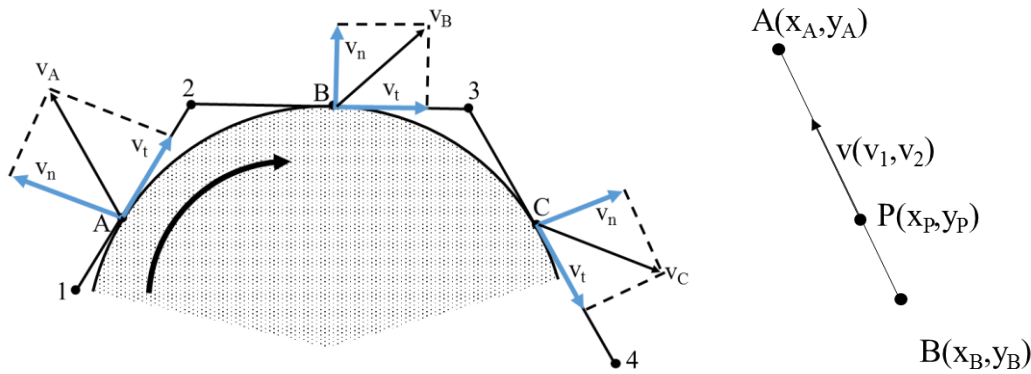


Figure 5.6: Contact velocity components a) Nodes in contact to the mould with the velocity components.

b) Sliding component in a single mould component.

5.2.4 Updating Boundary Conditions

In this section the update of boundary conditions will be briefly discussed.

- Mechanical contact boundary conditions

During the glass container production in gob loading stage it is allowed that the glass nodes slips along the mould. This can be a good approximation due to the high gob initial velocity due to the falling and low viscosity. This stage time is also very small and the cooling effect almost does not affect viscosity. In others stages the boundary conditions are redefined as sticking conditions as the node of the finite element mesh touches the mould. Mechanically the node is then assumed to be fixed to the mould, which seems to be a good approximation due to the sudden drop of temperature and consequent large increase of viscosity [35].

The particular case of plunger up stage had to be addressed differently, sliding friction is present. In practice, the plunger is driven by a piston, which means that the movement is the result of an external force applied to the plunger.

The plunger contact with the glass can be added to the formulation by the minimization of a functional, or more precisely an energy term, associated to this contact that should include the work of the external force of the plunger, the internal resisting force associated to glass deformation and the constrain of impenetrability.

From the finite element solution point of view a new variable is added, V , which is the plunger vertical displacement, which is assumed to be a rigid body with only vertical displacement under an applied vertical force, F_v .

Then the external work is:

$$w_e = F_v \cdot V \quad 5.12$$

The internal work involved will be associated with the displacement (or velocity) variables at the contact nodes of the finite element mesh used in the glass. As the plunger will be geometrically modelled by lines that may not be parallel to the coordinate axes, so it is preferable to assign those restrain conditions (impenetrability and slide friction) in local coordinates. Therefore, for every contact node a local coordinate system, as in Figure 5.7, is assigned.

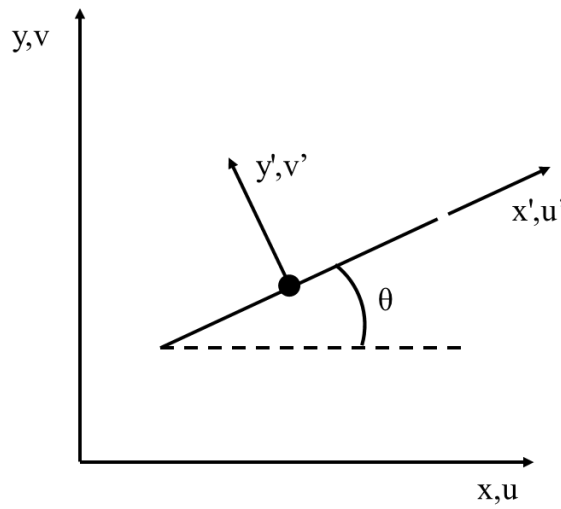


Figure 5.7: Local coordinates at each contact node between the plunger and the glass.

being,

$$\mathbf{u}_i = \begin{bmatrix} u_i \\ v_i \end{bmatrix}, \quad \mathbf{u}_i' = \begin{bmatrix} u_i' \\ v_i' \end{bmatrix} \quad 5.13$$

where,

$$\mathbf{u}_i = \mathbf{R}_i \mathbf{u}_i' \quad 5.14$$

with,

$$\mathbf{R}_i = \begin{bmatrix} \cos \theta_i & -\text{sen} \theta_i \\ \text{sen} \theta_i & \cos \theta_i \end{bmatrix} \quad 5.15$$

Here, $i = 1, m$, where m is the number of points of the mesh contacting the plunger geometrical description. Please note that the number of contacting points may change with every time step.

An energy term related with the friction, may be added as:

$$w_{if} = \frac{1}{2} \varepsilon (u_i')^2 \quad 5.16$$

where ε is a friction factor, so that $f_i = \varepsilon u_i$ is the friction force at any contact point. Note that for $\varepsilon = 0$ the sliding condition is recovered, for a large value of ε the sticking condition is present.

The impenetrability constrain can be introduced in a penalized form including an energy term as:

$$w_{ip} = \frac{1}{2} \alpha (v_i - V)^2 \quad 5.17$$

where α is a penalty value imposing the impenetrability constrain.

Then, the global energy term may then be written as:

$$\begin{aligned} \Pi(V, \dots, u_i, \dots, v_i, \dots) &= \frac{1}{2} \sum_{i=1}^m \left([u_i \quad v_i - V] \begin{bmatrix} \cos \theta_i & -\sin \theta_i \\ \sin \theta_i & \cos \theta_i \end{bmatrix} \begin{bmatrix} \varepsilon \cos \theta_i & \varepsilon \sin \theta_i \\ -\alpha \sin \theta_i & \alpha \cos \theta_i \end{bmatrix} \begin{bmatrix} u_i \\ v_i - V \end{bmatrix} \right) - \\ &\quad - F_v \cdot V = \\ &= \frac{1}{2} \sum_{i=1}^m \left((\varepsilon \cos^2 \theta_i + \alpha \sin^2 \theta_i) u_i^2 + (\varepsilon \sin^2 \theta_i + \alpha \cos^2 \theta_i) (v_i - V)^2 - 2 \cos \theta_i \sin \theta_i (\varepsilon - \alpha) u_i (v_i - V) \right) - \\ &\quad - F_v \cdot V \end{aligned} \quad 5.18$$

By performing the minimization of this function the extra equation associated with plunger movement is obtained as

$$\sum_{i=1}^m (-\cos \theta_i \sin \theta_i) (\varepsilon - \alpha) u_i - (\varepsilon \sin^2 \theta_i + \alpha \cos^2 \theta_i) v_i + (\varepsilon \sin^2 \theta_i + \alpha \cos^2 \theta_i) V = F_v \quad 5.19$$

and the extra terms to be added to the global stiffness in equations associated with node i are

$$\begin{aligned} \dots + (\varepsilon \cos^2 \theta_i + \alpha \sin^2 \theta_i) u_i + (\cos \theta_i \sin \theta_i) (\varepsilon - \alpha) v_i + \dots + (-\cos \theta_i \sin \theta_i) (\varepsilon - \alpha) V &= 0 \\ \dots + (\cos \theta_i \sin \theta_i) (\varepsilon - \alpha) u_i + (\varepsilon \sin^2 \theta_i + \alpha \cos^2 \theta_i) v_i + \dots - (\varepsilon \sin^2 \theta_i + \alpha \cos^2 \theta_i) V &= 0 \end{aligned} \quad 5.20$$

- Thermal contact boundary conditions

In the case of thermomechanical contact problems the two fields - deformation and temperature – interact. These fields are coupled, since the constitutive parameters depend upon the temperature, i.e., the evolution of the thermal field is related to the deformation by viscosity.

The majority of the heat flow during contact between glass and the metal in the moulds is by conduction because the metal is opaque to radiation. The rate of cooling depends on the heat transfer coefficient and on the temperature difference between the glass and metal [36]. In general, two different types of boundary condition have to be considered Figure 5.8. The nodes that are in contact with the mould surface a conduction boundary conditions is assigned, in the other hand, the remaining surface nodes are assigned with convection/radiation boundary conditions.

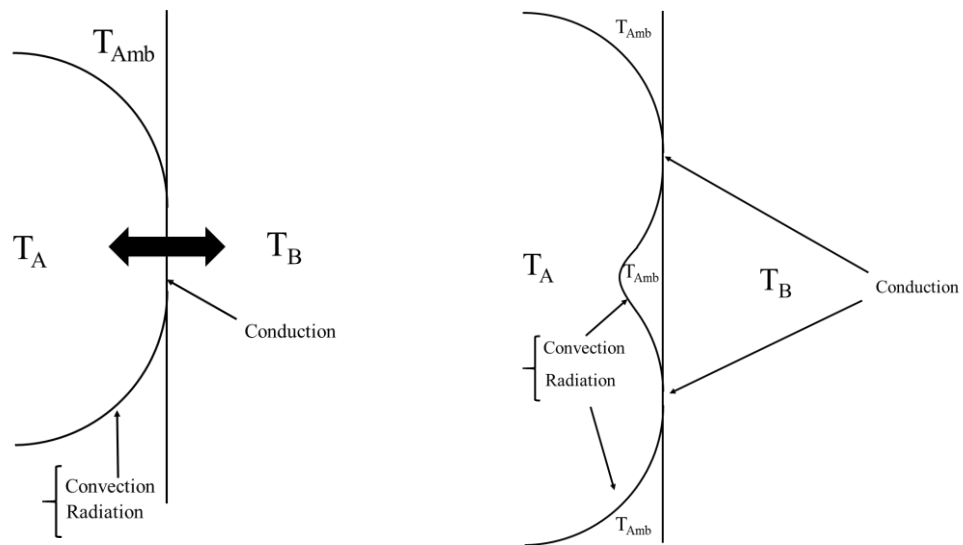


Figure 5.8: Contact between two bodies at different temperatures considering the different boundaries for each physical field.

In modelling thermal contact problems by the finite element methods some difficulties arise, Figure 5.8. First, it is impossible to model the contact at every point along the boundary. For example, in the two-dimensional case in which boundaries of individual elements are represented by straight line segments, as shown in Figure 5.9, some nodes may be in contact with the body but the segment between the nodes may not be in contact.

Also, the element type can complicate the contact between glass and mould. For example, a single element along one sides may not be touching completely the mould. Typically, in a quadratic element, along one mould element, one or two nodes may be contact the mould but another may be in contact with the air inside the mould and in these cases it have to be particularized. In Figure 5.9b) the first case has the node *T3* only in contact with the mould, the nodes *T2* and *T3* have convection/radiation boundary conditions. In the second case only two nodes contact the mould and similar analysis can be done. Then, in the third case all nodes contact the mould and the boundary conditions are the same.

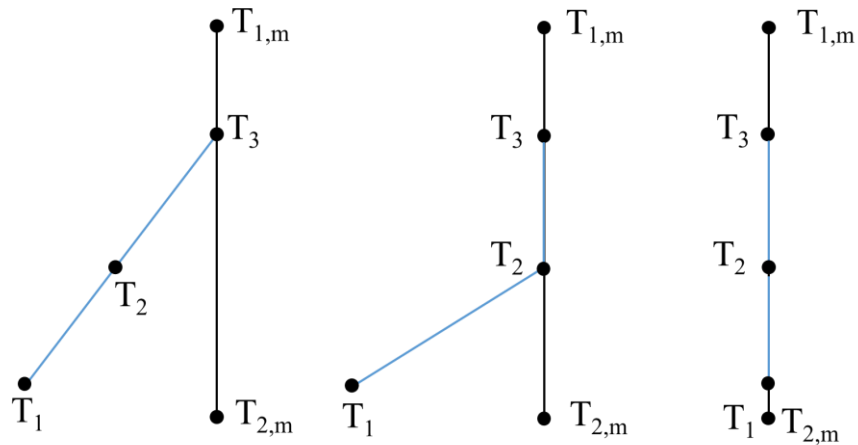


Figure 5.9: Contact between two bodies at different temperatures considering the different boundaries for each physical field.

5.3 Mesh Updating and Remeshing

Our finite element method starts with a finite element mesh generation to discretize the geometry as illustrated, for example, in Figure 5.10.

Mesh generation must be carefully done as the mesh is responsible for the accuracy of the solution computed. A special attention should be paid to the way the boundaries of the domain are approximated in order to capture the physical behaviour of the problem as accurately as possible. It means that both the number of nodes and elements must be adequate (in terms of shape, size, density, variation from region to region, etc [37]). However, mesh construction can be very expensive in terms of time.

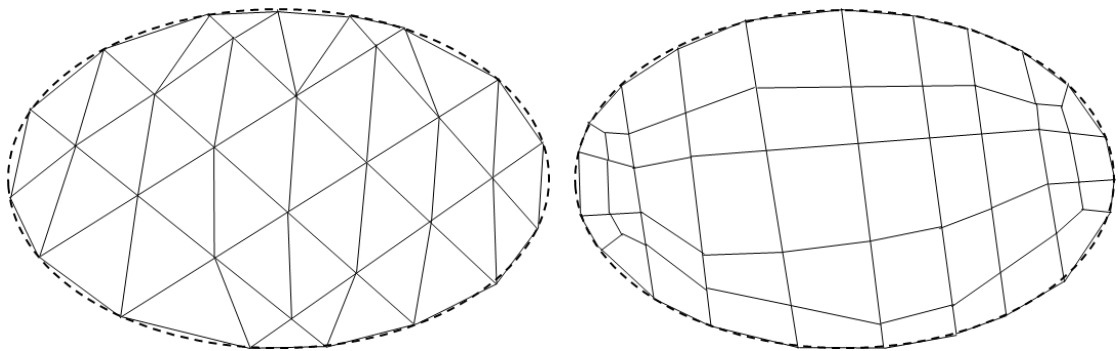


Figure 5.10: a) Example of a triangular linear mesh.

b) Example of a quadrilateral linear mesh.

The size of elements should be chosen carefully as it can influence the convergence the solution. The smaller the size of the elements the better is the accuracy of the solution but bigger the computational time [38].

5.3.1 Mesh Updating

The mesh is updated every time step, by adding to the current node coordinates the corresponding current displacements as:

$$\mathbf{x}_{t+\Delta t} = \mathbf{x}_t + \mathbf{u}_t = \mathbf{x}_t + \Delta t \mathbf{v}_t \quad 5.21$$

where $\mathbf{x}_{t+\Delta t}$ are the coordinates at time $t+\Delta t$, \mathbf{x}_t the coordinates at time t and \mathbf{v}_t the velocity at t .

At a certain stage of the simulation the mesh may be distorted and have to be redefined. Therefore, the finite element mesh should be constantly checked to detect excessive element distortion. This can be done by calculating the determinant of the Jacobian, which tends to zero. If the Jacobian becomes negative in part of the element, this implies a negative density. It may then correspond to a violation of mass conservation and continuity of the displacement field, Figure 5.11.

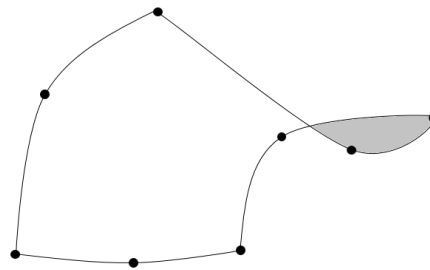


Figure 5.11: Example of an element with negative Jacobian.

Therefore, a parameter for mesh distortion is introduced. For example, for a linear quadrilateral element where full numerical integration require 4 sampling Gauss points this control parameter is:

$$DP = 4 \times \left(\frac{\min J}{area} \right) \quad 5.22$$

where $\min J$ is the minimum value of the determinant of the Jacobian at the Gauss points and *area* is the area of the element. Similar formulas are adopted for other types of elements.

If *DP* is less than a tolerance, then the element is considered unacceptably distorted and the analysis must terminate using the current mesh and a redefinition should be undertaken.

A new mesh is then created and the field variables transferred from the old to the new mesh.

A meshing tool available as open source code “*GEOMPACK*” was utilised. The mesh generator needs a boundary well defined. So, a Jacobian ratio was created to control the mesh distortion. The ratio is given by,

$$MD_{ratio} = \frac{J_n - J_{n+1}}{J_n} \quad 5.23$$

Where J_n is the Jacobian at t_n and J_{n+1} at t_{n+1} . This mesh distorted ratio gives a number between [0,1] which can be effectively done on the percentage of element distortion. When those parameters are exceeded the simulation is stopped and a new mesh is created, as will be explained in the next section. This procedure is needed to maintain the accuracy of the results. What is acceptable in one situation may be unacceptable in another [9.8].

5.3.2 Remeshing

Forming glass containers requires large material deformations, in most cases, to perform the simulation completely with the same mesh it is quite difficult, therefore, a remeshing tool is required.

The definition of the mesh should be chosen according to the element type and element size in order to find the best relation between the accuracy and the computational effort, Figure 5.12, note the example shows triangular elements but the same analogy can be done for quadrilateral elements. A refined mesh will improve the results, but it will need high investments in computer time. The accuracy of the solution depends on the element type and mesh used to represent the domain and the representation of the actual geometry. Using linear elements to represent a curved boundary is a coarse approach and mesh refinement may be needed to improve the representation of the specific geometry. A triangle can easily be decomposed into congruent subtriangles. Thus, we can easily perform a global grid refinement to halve the mesh size.

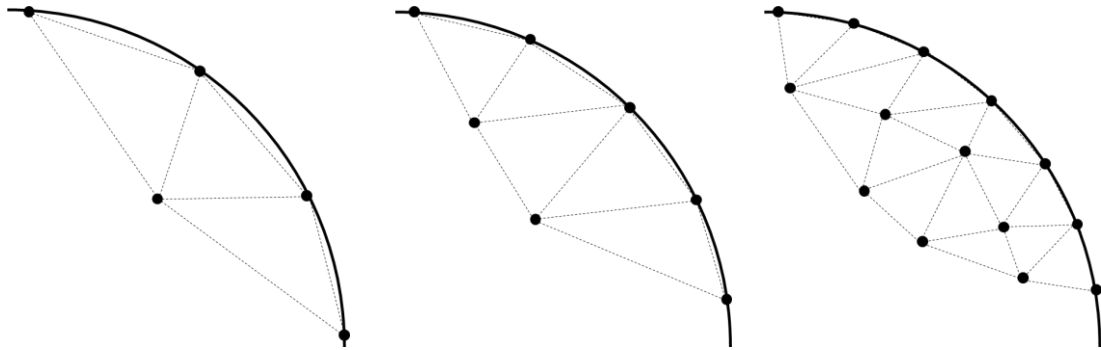


Figure 5.12: Meshing a curve with different mesh size.

If sticking boundary conditions are adopted as deformation continues elements near the boundary may become increasingly distorted diminishing the reliability of the solution. Eventually a singular matrix may become inevitable. This situation can be prevented by introducing a remeshing procedure. Remeshing is also used to prevent grid distortion, inside the domain, as the interpolation functions used are only appropriate for convex elements. The remeshing process redraws the grid and interpolates field variables from the old to the new mesh [36]. The flowchart of the remeshing technique is illustrated in Figure 5.13. Some aspects that were taken into account will be referred next.

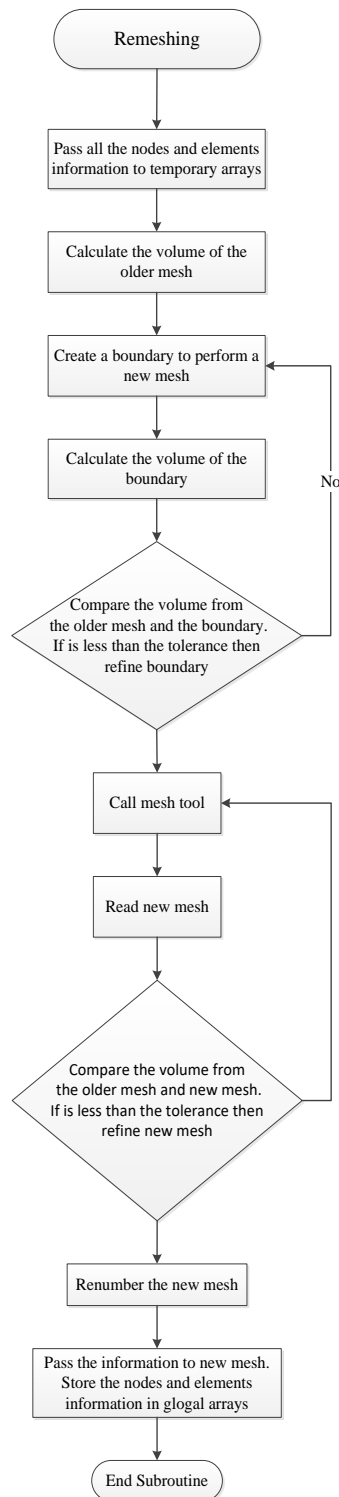


Figure 5.13: Flowchart of remeshing technique.

- Creation of the boundary through the older mesh

The data required for the remeshing stage consists of the boundary data, or more precisely, a polygonal discretization of it, input as a set of segments. The original boundary, which may be a curve, is the collection of the exterior element boundaries. The boundary uses the nodes of the older mesh to create the segments that will create the final shape of the new mesh. If the mesh required is a quadratic elements mesh, the remeshing tool will include in the middle of the segments an additional node. However, these additional nodes can lead to wrong boundary conditions if not properly dealt with. These additional nodes can also be

located such that they are interior or outside to the tool. Likewise, the refined mesh may end up with nodes that do not coincide with the boundary, Figure 5.14, note the example shows triangular elements but the same analogy can be done for quadrilateral elements. This means that these possible source of errors must be dealt with.

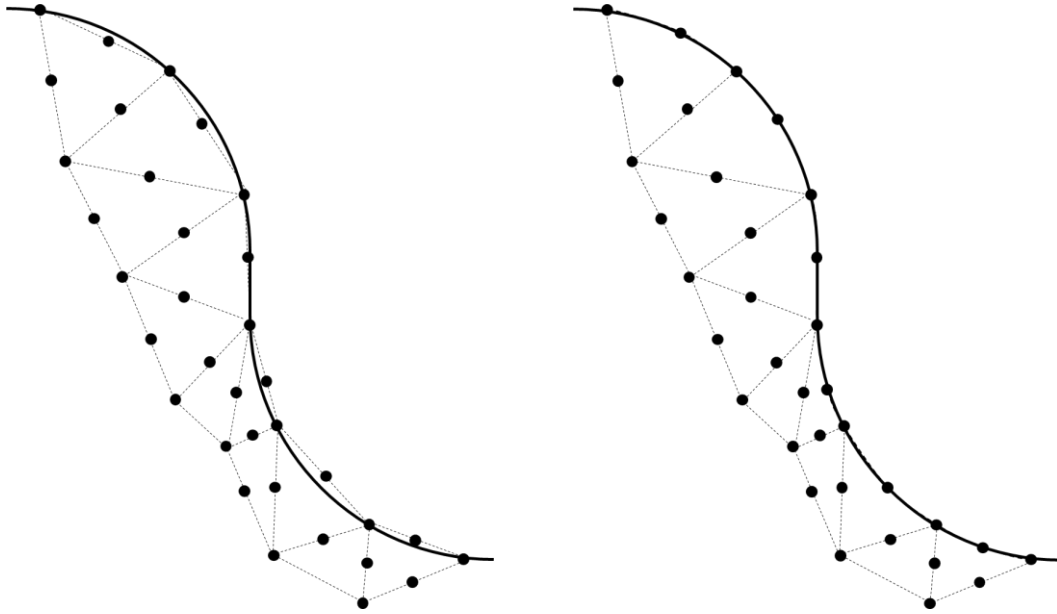


Figure 5.14: Correction of the new boundary nodes.

For a concave tool surface, we must prevent any node to penetrate into the tool domain. In order to satisfy the non-penetration condition a projection of the nodes to the tool is performed. However, errors such as material losses can become important and must be controlled.

- Volume control

The volume of the glass may increase or decrease if coarse or refined meshes are required. Then, a volume control must be implemented to maintain the glass volume constant during simulation. Two types of volume control were implemented. One control is on the boundary and other control on the new mesh.

In order to calculate the volume of material from the node boundary positions, Figure 5.15, the following algorithm is used. The boundary was parameterize by each segment as:

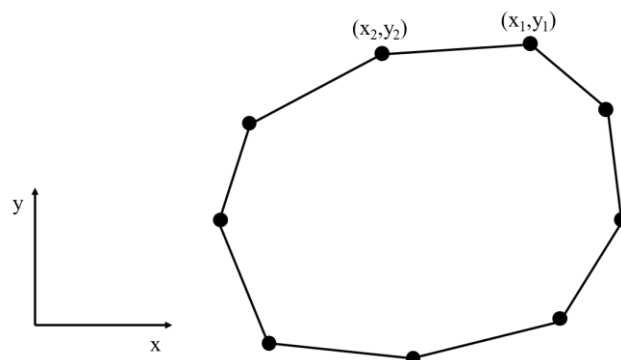


Figure 5.15: Example of a boundary segments.

$$\begin{aligned}x &= \frac{1}{2}(1-u)x_1 + \frac{1}{2}(1+u)x_2 \\y &= \frac{1}{2}(1-u)y_1 + \frac{1}{2}(1+u)y_2\end{aligned}\tag{5.24}$$

Consequently,

$$\begin{aligned}\frac{dx}{du} &= \frac{1}{2}(x_2 - x_1) \\ \frac{dy}{du} &= \frac{1}{2}(y_2 - y_1)\end{aligned}\tag{5.25}$$

Using the Green Theorem we may evaluate the total volume by a line integral along the full boundary that at each segment, takes the form

$$\frac{\pi}{2} \int_{-1}^1 \left(\frac{1}{2}(1-u)x_1 + (1+u)x_2 \right)^2 \cdot (y_2 - y_1) du\tag{5.26}$$

Simplifying,

$$\frac{\pi}{2} (y_2 - y_1) \int_{-1}^1 \left(\frac{1}{4}(1-u)^2 x_1^2 + (1-u^2)x_1x_2 + \frac{1}{4}(1+u)^2 x_2^2 \right) du\tag{5.27}$$

Resolving the integral we obtain,

$$\frac{\pi}{2} (y_2 - y_1) \left[\frac{1}{4}x_1^2u + \frac{1}{12}x_1^2u^3 + \frac{1}{2}x_1x_2u - \frac{1}{6}x_1x_2u^3 + \frac{1}{4}x_2^2u + \frac{1}{12}x_2^2u^3 \right]_{-1}^1\tag{5.28}$$

Simplifying,

$$\frac{\pi}{3} (y_2 - y_1) (x_1^2 + x_1x_2 + x_2^2)\tag{5.29}$$

The volume is the sum of the integrals on each of the n segments,

$$V_b = \sum_{i=1}^n \frac{\pi}{3} (y_2 - y_1) (x_1^2 + x_1x_2 + x_2^2)\tag{5.30}$$

To control the new mesh volume, the volume is calculated by adding the individual volumes associated with each element of the new mesh by performing a numerical integration as.

$$V_n = \sum_{i=1}^{nelem} 2\pi \sum_{j=1}^{ngaus} J_j(\xi_j) r_j w_j \quad 5.31$$

where $nelem$ is the total number of elements, $ngaus$ the number of Gauss points per element and at each Gauss point J_j is the determinant of the Jacobian, ξ_j the local coordinates, r_j the radius and w_j the weighting factors for the Gauss numerical quadrature.

These two volumes are compared with the a previous volume calculated, V_l , given a certain tolerance as

$$\begin{aligned} (V_b - V_l) &\leq |tolerance| \\ (V_n - V_l) &\leq |tolerance| \end{aligned} \quad 5.32$$

If the conditions are not satisfied a new refined mesh is created. After the mesh overcome the two conditions the program runs normally.

- Transfer of information to the new mesh

When the mesh is too distorted a new mesh is generated and field variables must be interpolated to the new mesh. This issue is crucially important to be able to pursue the simulation, after a remeshing stage and to preserve accuracy, robustness and convergence properties of the finite element solution [39].

Velocities and temperatures fields which are stored on nodes of the old mesh must be transferred to the nodes of the new mesh. This may be done by determining the spatial position of a node on the new mesh, inside a n element of the old mesh that contains it. Then, easily interpolation can be performed by using the element shape functions.

To find that element a simple algorithm is implemented as described in Figure 5.16. A node A of the new mesh is detected inside an element of the old mesh if all the third components (normal to the plane of the figure) of the three product vectors indicated are positive.

$$(\mathbf{v}_1 \times \mathbf{u}_{12})_k > 0 \wedge (\mathbf{v}_1 \times \mathbf{u}_{23})_k > 0 \wedge (\mathbf{v}_1 \times \mathbf{u}_{31})_k > 0 \quad 5.33$$

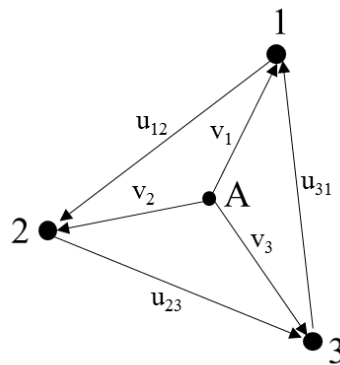


Figure 5.16: Cross product between a node that belong to a new mesh and the older element.

For other type of elements it is easy to divide in triangle and generalize the procedure.

Boundary conditions have also to be updated. In the new geometry, for practical reasons, each node of the glass is considered as being in contact with the mould when the distance between the node and the mould element is less than a very small tolerance.

This page intentionally left blank

6 Elements Validation and Testing

The glass forming simulation involves complex heat transfer processes with the material properties changing constantly with temperature and different type of non-linear boundary conditions changing throughout the forming process. The model developed should be able to deal with all these aspects and a validation of its robustness must be performed comparing the solutions obtained in real forming processes. This will be done in Chapter 8 but, prior to that, it is always helpful to run simple example tests on the code developed before embarking in more complex ones. The successful application of finite element analysis should always include an initial validation of the element to be used and its implementation in a specific computer program. Usually, the elements utilized in most problem are very well understood and tested. However, some applications can be difficult to model, and the elements used for the analysis may be more prone to numerical difficulties [40].

In our case the performance of the elements should be tested in simple thermal and thermomechanical problems, to assess their robustness. This is particularly important in glass forming problems, both from the thermal and the mechanical points of view, due to the fact that the material flow is incompressible and depends on viscosity, which is highly influenced by the temperature distribution. Thus, this requires some investigation on the behaviour of the different available elements on some specific situations that may cause some “pathological” responses.

6.1 Heat Transfer Validation

In transient heat transfer problems, for certain type of elements used in the simulation, some specific boundary conditions and geometric discretization, spurious temperature oscillations may occur particularly at initial time stages of glass forming simulations due to the small time increment presented. Our aim in this section is to understand those oscillations in temperature induced by small time increments. We want to know when those oscillations may appear and how to prevent such behaviour.

In order to validate the numerical approach to the heat transfer phenomenon the analysis was made for each one of the most common element types, i.e., Lagrangian linear triangular and quadrilateral elements and quadratic triangular and quadrilateral elements. In the first analysis not all meshes have the same element size, in order to comply the equation 5.1, but have the same number of nodes. Later the same analysis will be performed with the same element size.

The validation of the in house software was performed using analytical solutions and Abaqus software. In Figure 6.1 the meshes used with Abaqus and the inhouse software are shown. Also, the time increment was kept equal for all cases.

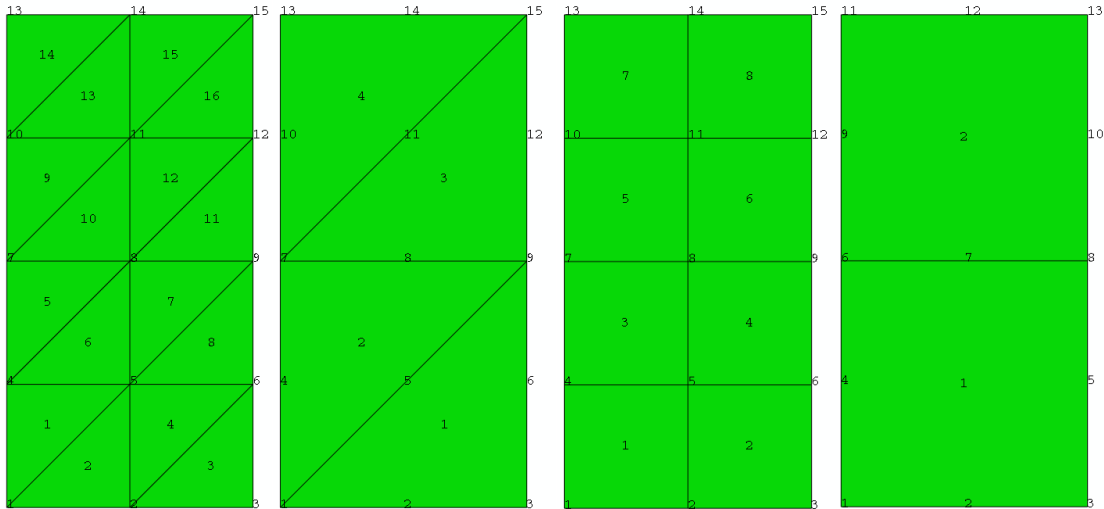


Figure 6.1: Mesh used to simulation for heat transfer validation a) linear triangle b) quadratic triangle c) linear quadrilateral d) quadratic quadrilateral.

The validation was performed creating two different boundary conditions, such as prescribing temperatures and heat fluxes. These two cases are analysed as follows.

- Prescribed temperature

The first analysis was to prescribe a boundary temperature of 500°C . A cylinder with a unitary radius and the double dimension value on the height. A material with diffusivity equal to one was used in order to simplify the analytical calculation. The initial temperature was 1000°C . The scheme can be seen in Figure 6.2.

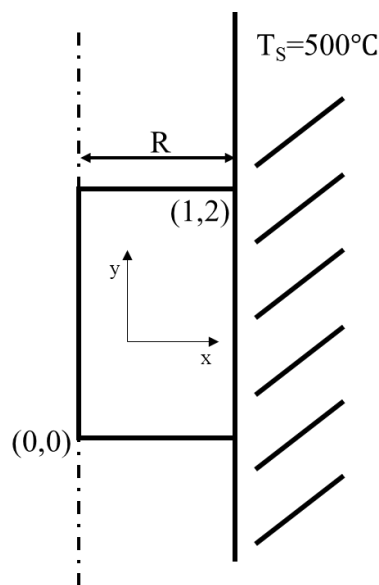


Figure 6.2: Scheme to validate the prescribed temperature at the boundary of a cylinder.

- Analytical Calculation

The analytical solution for the infinite cylinder with convection boundary condition is given by:

$$\frac{T - T_f}{T_i - T_f} = 2 \sum_{n=1}^{\infty} \frac{1}{\lambda_n} \exp(-\lambda_n^2 Fo) \frac{J_0(\lambda_n R)}{J_1(\lambda_n)} \quad 6.1$$

where T_i is the initial temperature, T_f the temperature of the outside, J_o is the Bessel function and λ_n are the values of the Taylor series which can be determined using,

$$J_0(\lambda_n) = 0 \quad 6.2$$

Fo the Fourier modulus is given by:

$$Fo = \frac{\alpha t}{R^2} \quad 6.3$$

where α is diffusivity coefficient and t is the time. The analytical solutions were obtained in [41].

The analytical solution was obtained using the equation 6.1 for a $T_f=500^\circ\text{C}$, $T_i=1000^\circ\text{C}$, $R=1\text{m}$ and $\alpha=1$. The results shown in Figure 6.3 are for initial time of 0 to 0.1 seconds with a time increment of 0.01 seconds. The low time increment was used intentionally in order to induce the spurious oscillations. Also, during the glass simulation the time increment may be very small because the contact conditions induce small time increments. The results are shown combining temperature/radius or temperature/time evolution. In the Figure 6.3, it can be seen the analytical results for the example previous explained. The results appear be consistent with the temperatures showing a quadratic evolution.

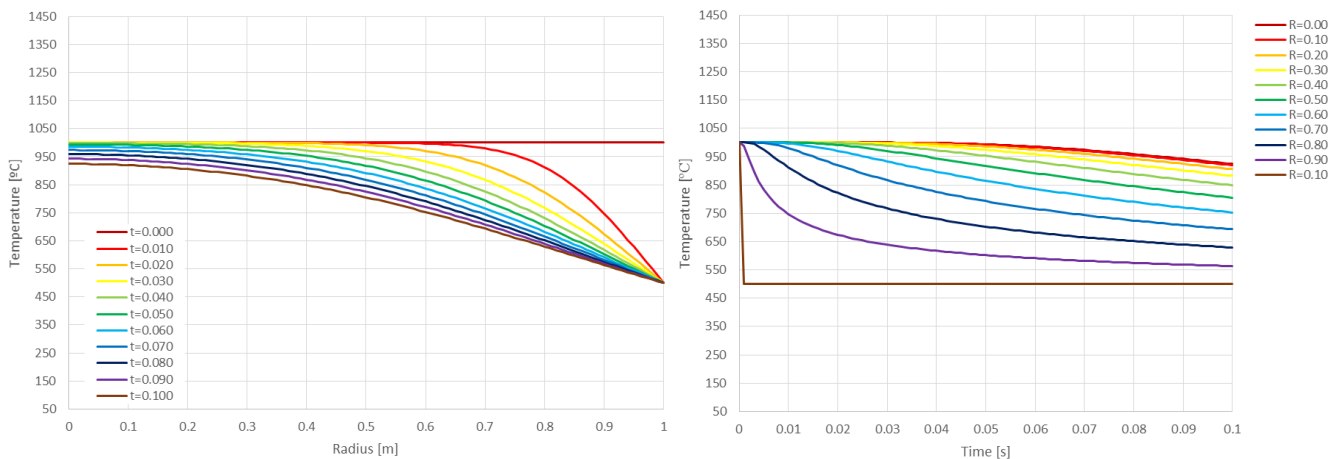


Figure 6.3: Results for the analytical equation for the prescribed boundary temperature a) Temperature/Radius b) Temperature/Time evolution.

○ Abaqus results

A model in Abaqus software was created to verify the temperature evolution with time. As discussed before the temperature evolution can have oscillations. In Figure 6.4 the results for Abaqus simulation with the different elements types are shown. The results were obtained at the following nodes of the meshes: nodes 1, 4, 7, 10, 13 for $x=0.0$, nodes 2, 5, 8, 11, 14 for $x=0.5$ and the nodes 3,6,9,12,15 for $x=1.0$. For the quadratic quadrilateral the nodes considered were 1, 4, 6, 9, 11 for $x=0.0$, 2, 7, 12 for $x=0.5$ and 3, 5, 8, 10, 13 for $x=1.0$. It can be seen that the linear elements doesn't show any kind of temperature oscillation, presenting a small deviation from the analytical solution. In other hand, the quadratic elements show a big oscillation, including nodes with higher temperatures than the initial, which is an unphysical behaviour. However, the quadratic quadrilateral elements tend to converge to the analytical solution faster than the quadratic triangular elements.

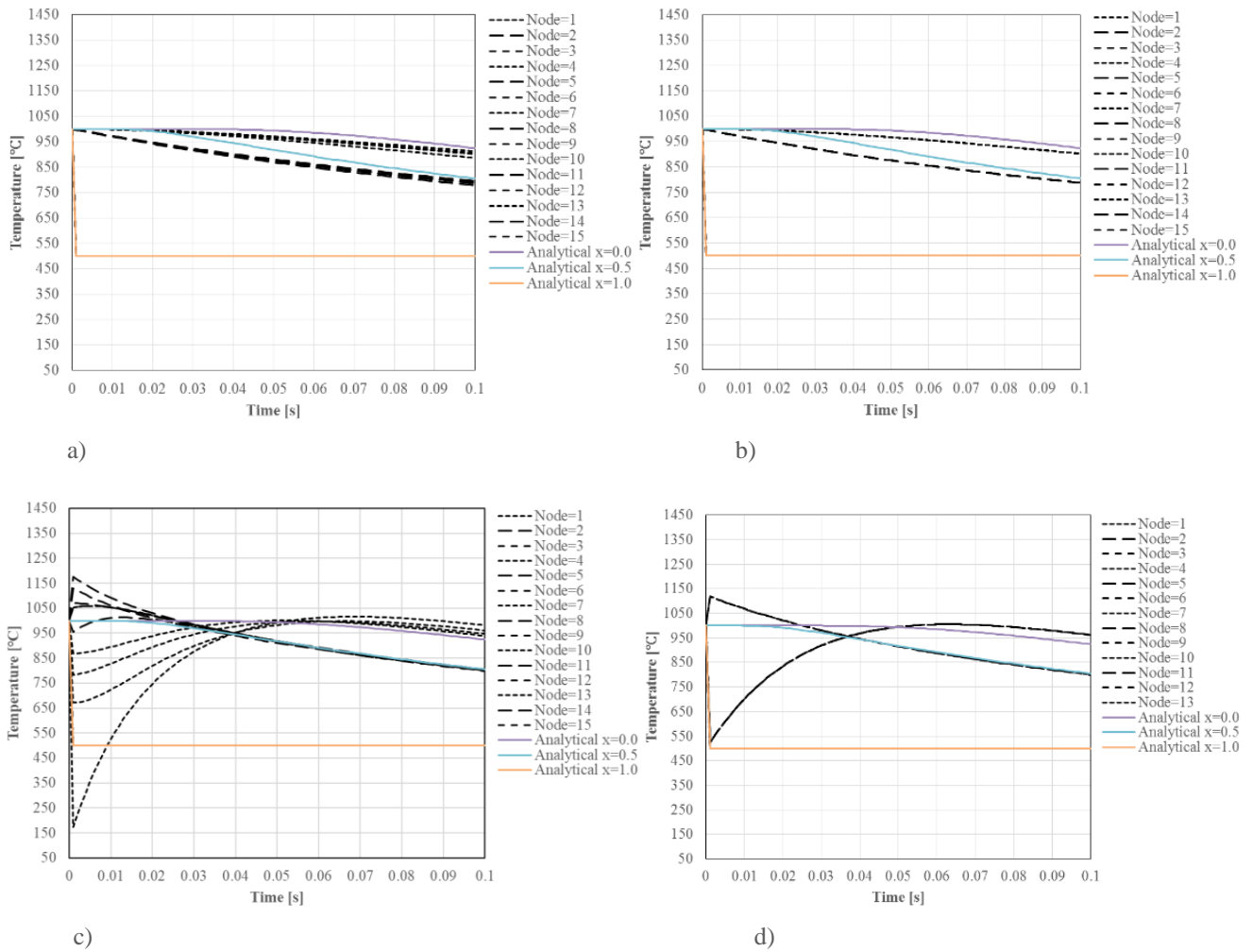


Figure 6.4: Results for Abaqus simulation for the prescribed boundary temperature a) Linear triangular elements b) Linear quadrilateral elements c) Quadratic triangular elements d) Quadratic quadrilateral elements.

o Empaktor Software

The same analysis was performed using the code developed (Empaktor software). In this case a full capacity matrix was used. Figure 6.5 shows the results for the linear triangular and quadrilateral elements as well as for the quadratic triangular and quadrilateral elements. It can be seen that the oscillations also appear in the linear elements. Nevertheless, all the situation appear to converge to the analytical solution.

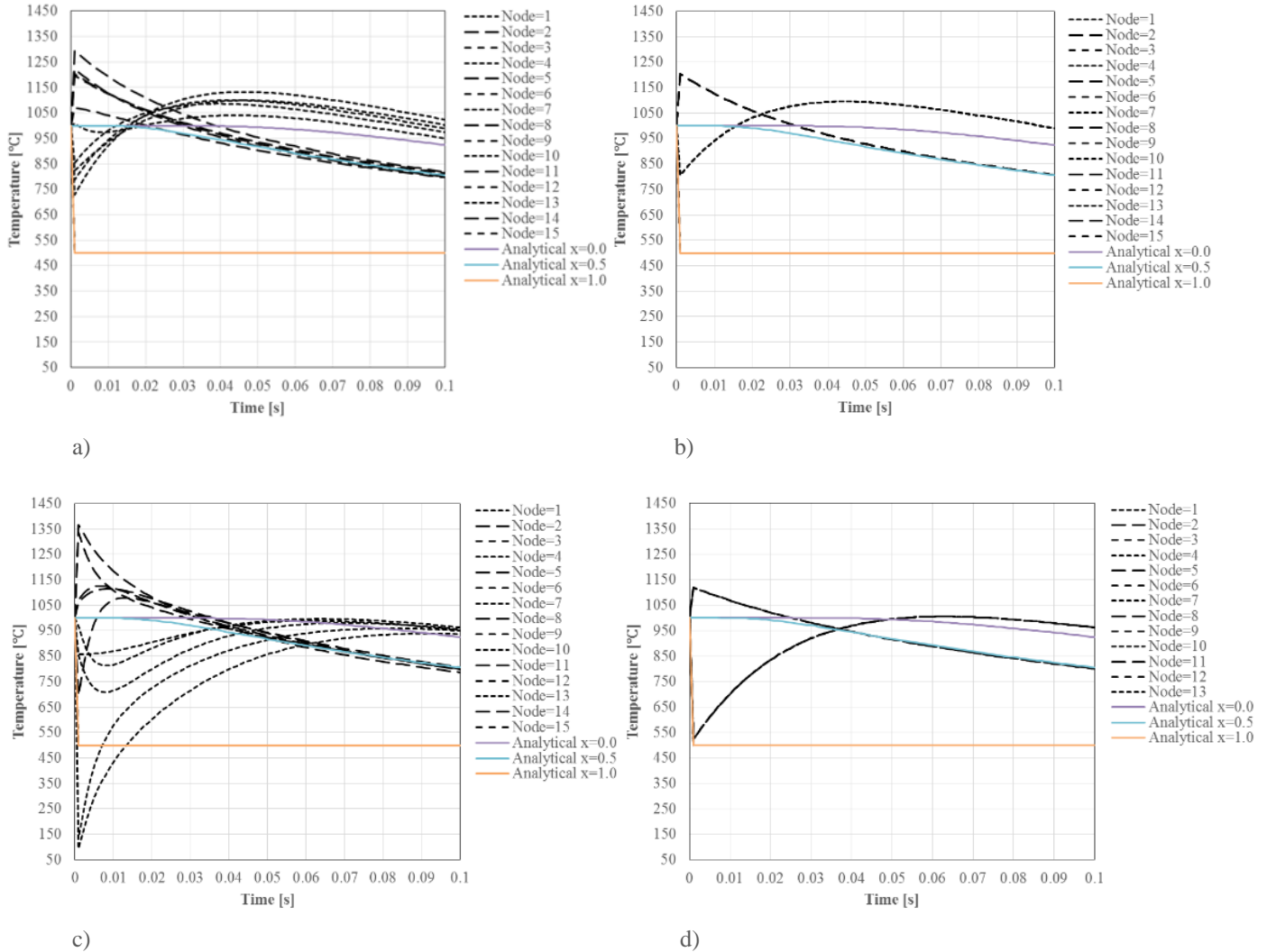


Figure 6.5: Results for Empaktor software for the prescribed boundary a) Linear triangular elements b) Linear quadrilateral elements c) Quadratic triangular elements d) Quadratic quadrilateral elements.

Inasmuch as we want to avoid the temperature oscillations, to use a full capacity matrix seems not to be advisable. Therefore, two different ways of building a lumped capacity matrix were tested. The first one is to force the non-diagonal values to be zero. The results of this case are presented in Figure 6.6. As it can be seen the temperature oscillations in the linear elements disappear but the temperatures are smaller than that analytical solution. The quadratic element present higher temperatures than the initial temperature, a situation that should be avoided. The second case is to weight the diagonal capacity matrix with the non-diagonal values, such as the diagonal values are given by:

$$C_{ii} = \frac{\sum_{i=1, j=1}^n C_{ij} + \sum_{i=1}^n C_{ii}}{\sum_{i=1}^n C_{ii}}, \quad C_{ij} = 0, \quad \text{for } i \neq j \quad 6.4$$

being n the number of nodes of the element. The results for this case are presented in Figure 6.7. A lowest deviation from the analytical solution is obtained. However, the quadratic elements still present unphysical heating.

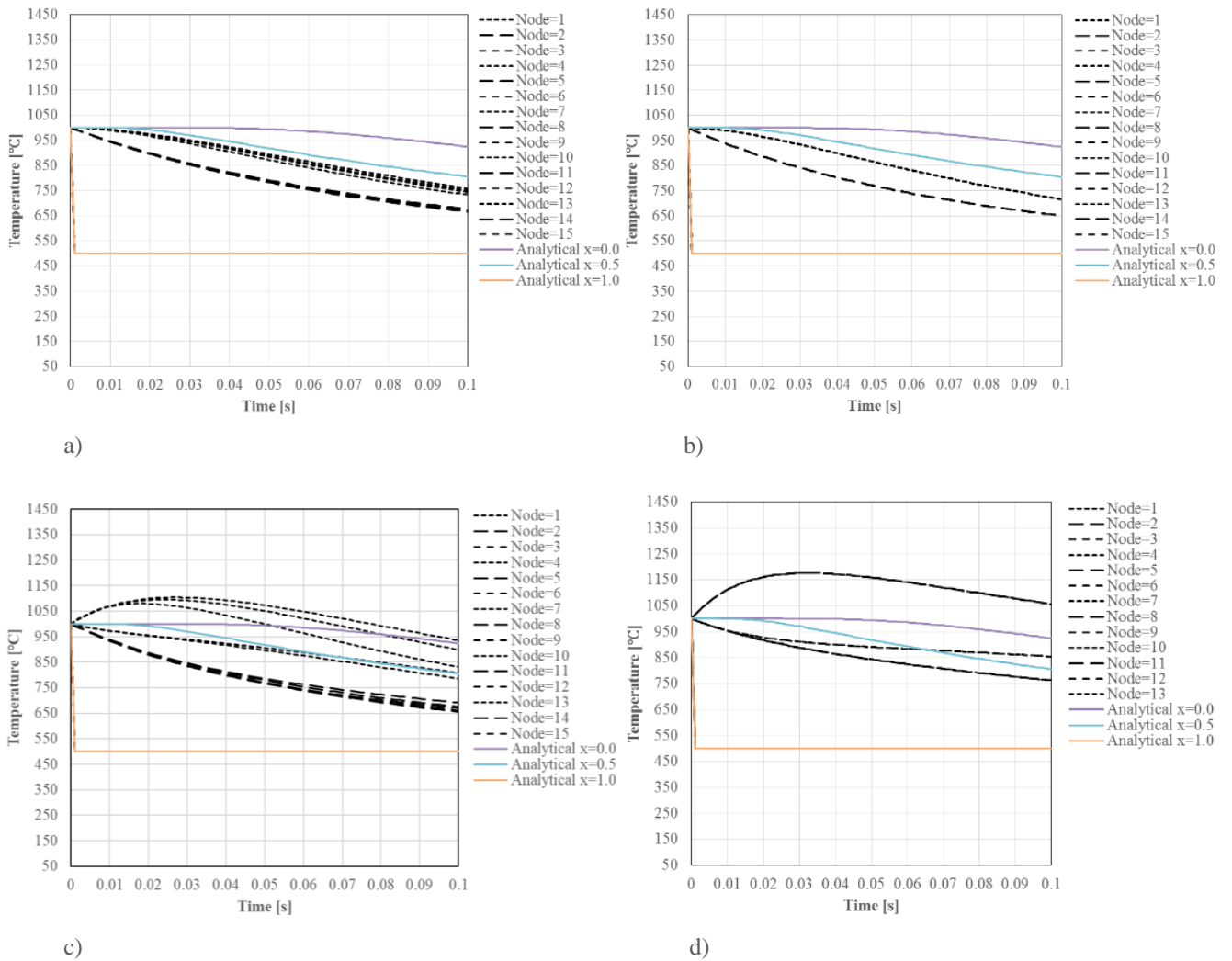


Figure 6.6: Results for Empaktor software for the prescribed boundary temperature using only the diagonal values for the capacity matrix
 a) Linear triangular elements b) Linear quadrilateral elements c) Quadratic triangular elements d) Quadratic quadrilateral elements.

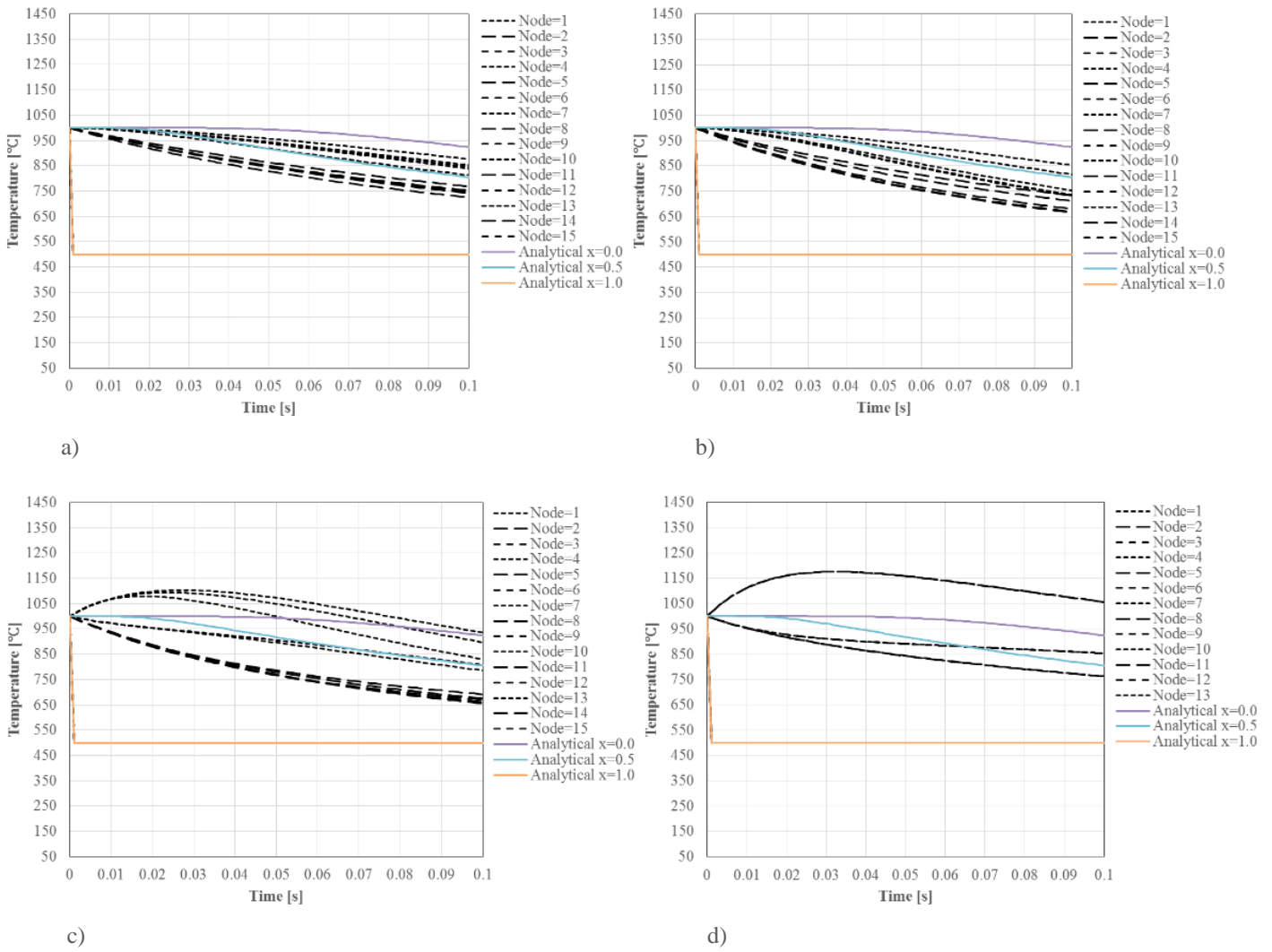


Figure 6.7: Results for Empaktor software for the prescribed boundary temperature using a pondered capacity matrix a) Linear triangular elements b) Linear quadrilateral elements c) Quadratic triangular elements d) Quadratic quadrilateral elements.

- Prescribed Flux

Here a prescribed flux was considered as the boundary conditions. The scheme of the analysis is presented in Figure 6.8.

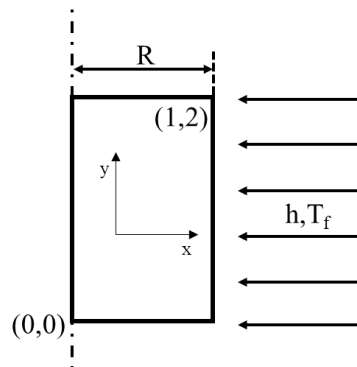


Figure 6.8: Scheme to validate the prescribed flux at the boundary cylinder.

- Analytical Calculation

The analytical solution for the infinite cylinder with convection boundary conditions is given by:

$$\frac{T - T_f}{T_i - T_f} = 2 \sum_{n=1}^{\infty} \frac{Bi J_0(\lambda_n R) \exp(-\lambda_n^2 Fo)}{(\lambda_n^2 + Bi^2) J_0(\lambda_n)} \quad 6.5$$

T_i is the initial temperature, T_f the temperature of the outside fluid, h the convection coefficient and λ_n the values of the Taylor series which can be determined using,

$$\lambda_n J_1(\lambda_n) + Bi J_0(\lambda_n) = 0 \quad 6.6$$

being Bi the Biot modulus that is given by:

$$Bi = \frac{hR}{k} \quad 6.7$$

R is radius of the cylinder, Fo is the Fourier modulus given by:

$$Fo = \frac{\alpha t}{R^2} \quad 6.8$$

where α is diffusivity coefficient and t the time.

To solve the analytical equation the following data was considered $T_f=500^\circ\text{C}$, $T_i=1000^\circ\text{C}$, $R=1\text{cm}$, $\alpha=1$ and $h=1 \text{ Wm}^{-2}\text{K}^{-1}$. The results shown in Figure 6.9 are from the initial time up to 0.1 seconds with an increment of 0.01 seconds. The results are shown in Figure 6.9 for temperature versus time and another for temperature versus radius.

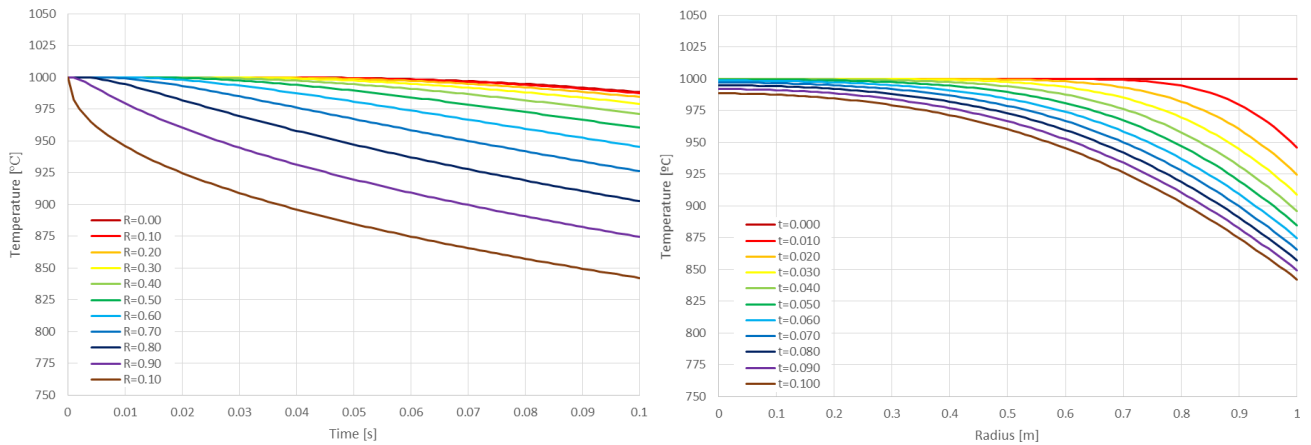


Figure 6.9: Results for the analytical equation for the prescribed boundary flux a) Temperature/Time b) Temperature/Radius evolution.

o Abaqus results

As in the previous case an Abaqus simulation with prescribed flux at the cylinder boundary was performed. In Figure 6.10 the results for Abaqus simulation with the different elements types are shown. Again the linear elements have a good correlation in relation to the analytical solution and the quadratic elements present the biggest deviation including heating.

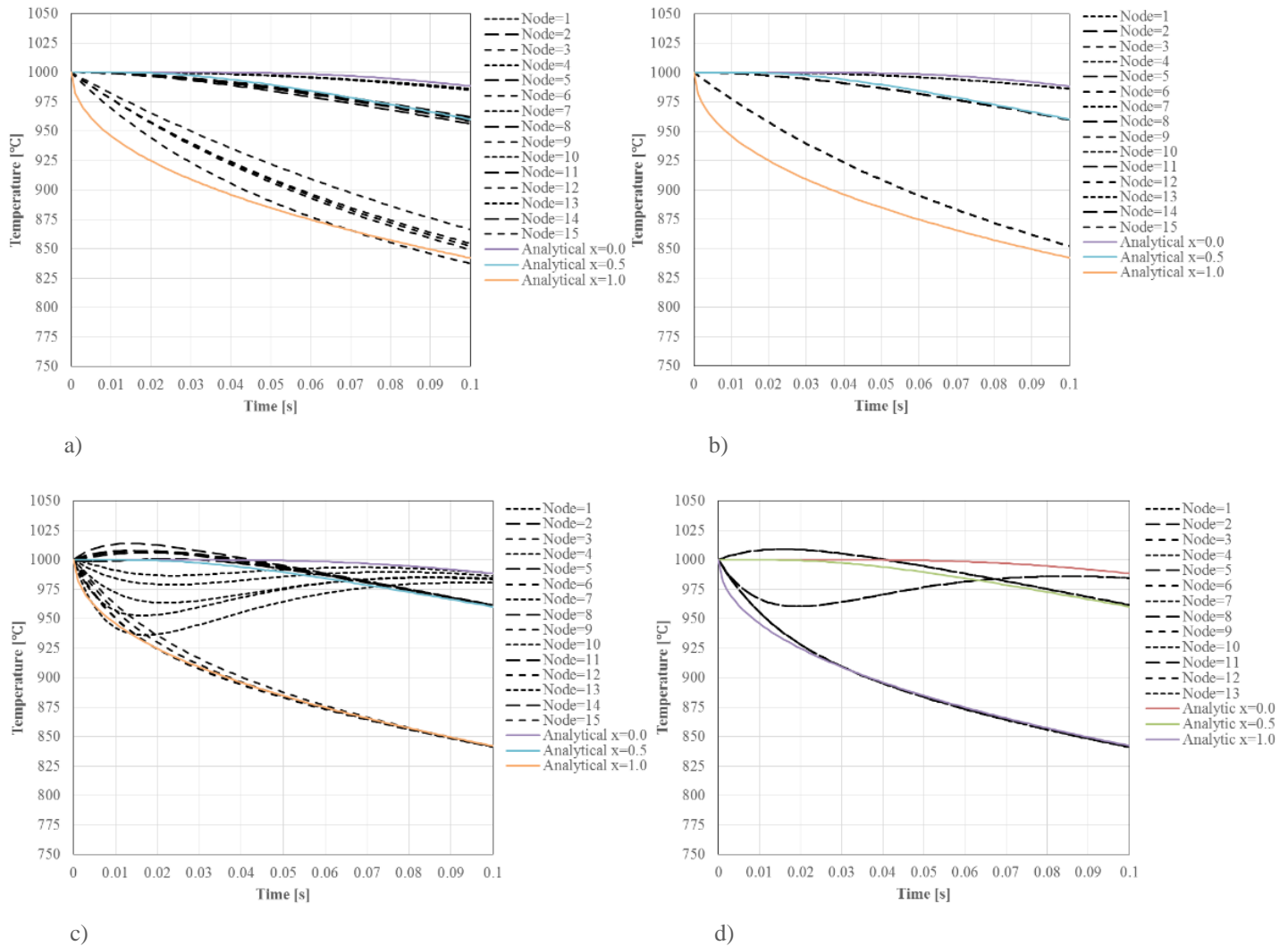


Figure 6.10: Results for Abaqus simulation for the prescribed flux a) Linear triangular elements b) Linear quadrilateral elements c) Quadratic triangular elements d) Quadratic quadrilateral elements.

o Empaktor Software

The same analysis was performed using the Empaktor software. Again three different cases the capacity matrix were tested, a full capacity matrix, a lumped capacity matrix with zero non-diagonal values, and lumped capacity matrix with non-diagonal pondered values. In Figure 6.11, Figure 6.12 and Figure 6.13 the three different studies are presented, respectively.

In the first case, the results show temperature oscillations in all the elements, however, they seems to converge to the analytical solutions. The second case, the linear elements present a higher cooling than expected and the quadratic elements present heating. In the third case, the linear elements present a good agreement with the analytical solution but the quadratic elements presents unexpected heating.

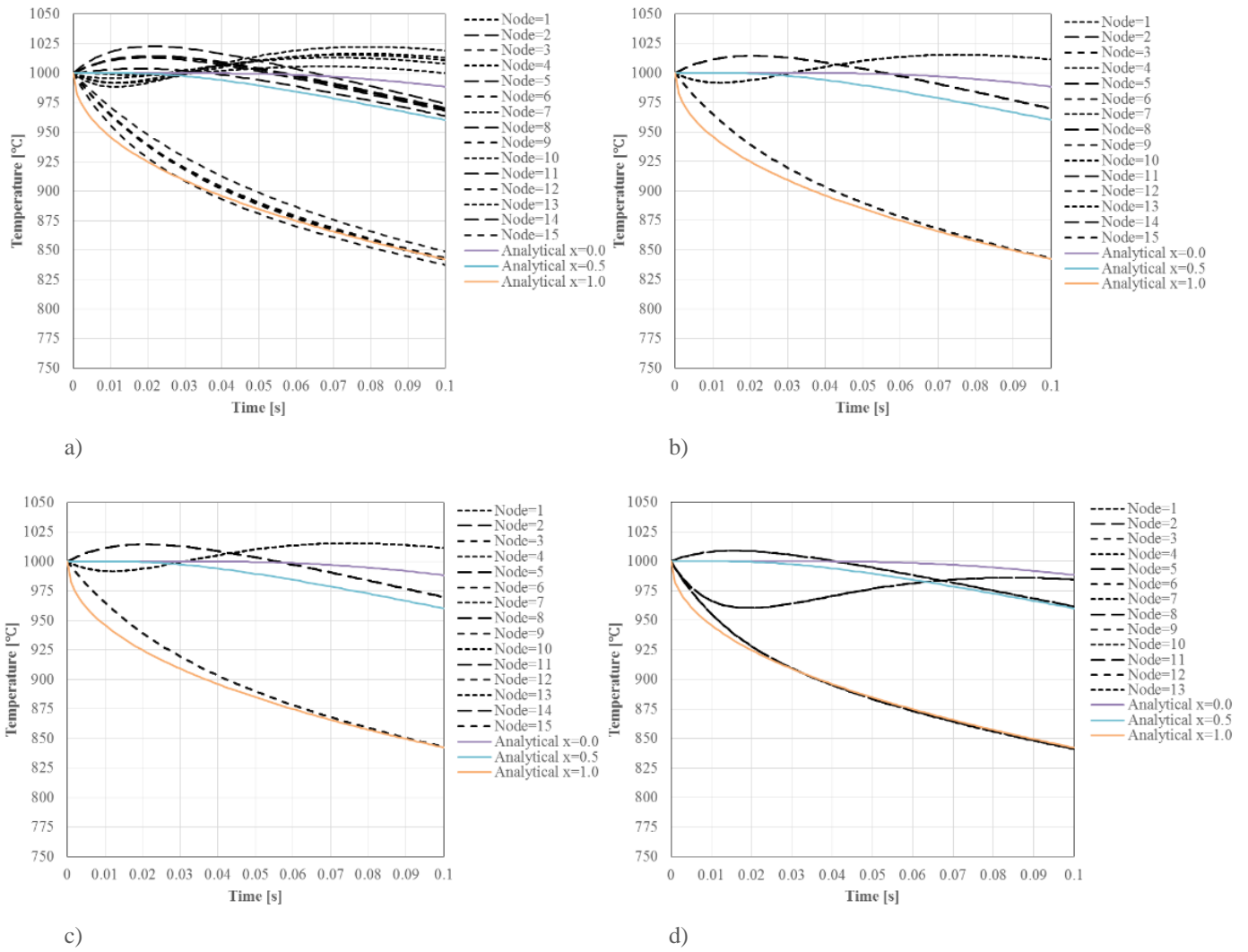


Figure 6.11: Results for Empaktor software for the prescribed Flux a) Linear triangular elements b) Linear quadrilateral elements c) Quadratic triangular elements d) Quadratic quadrilateral elements.

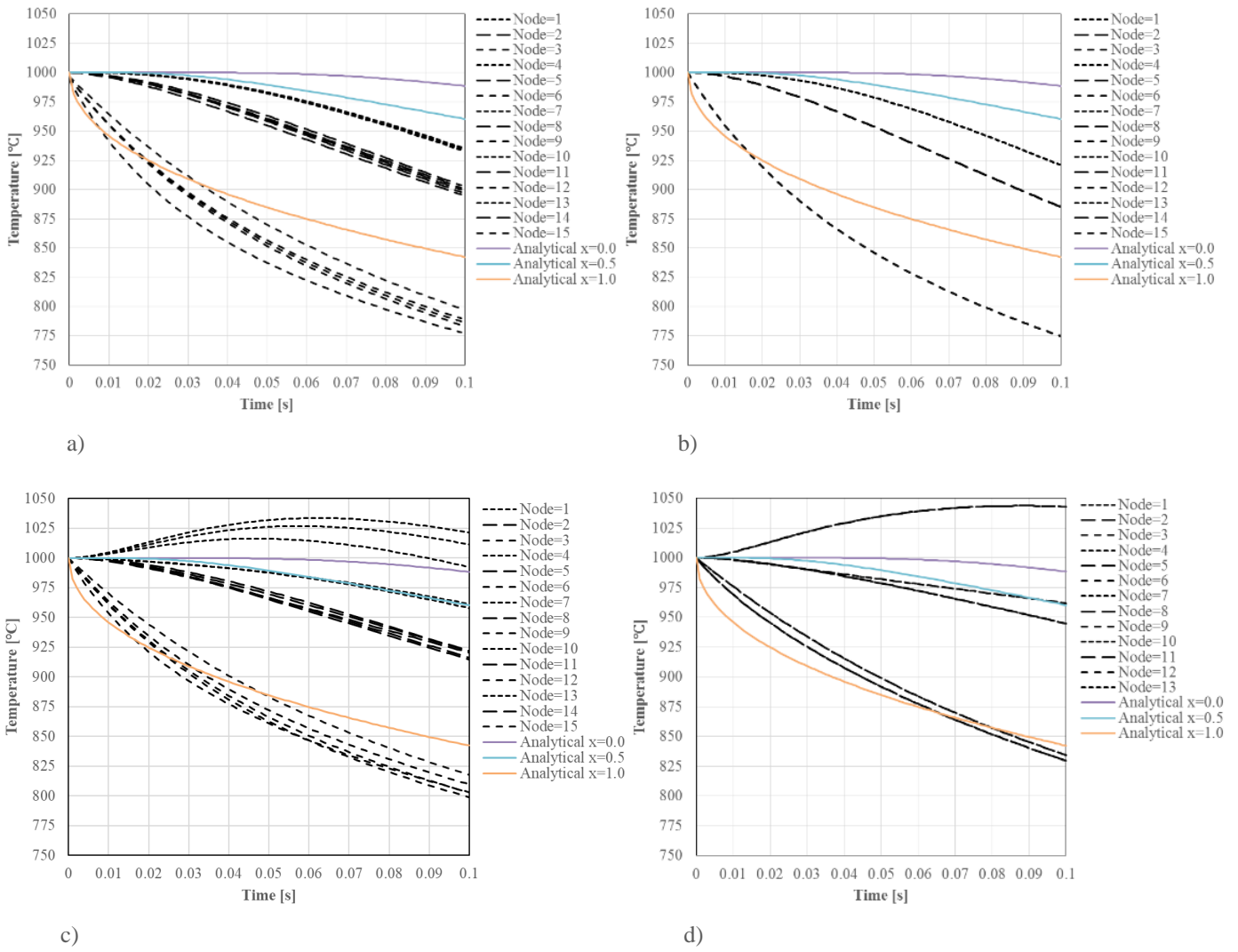


Figure 6.12: Results for Empaktor software for the prescribed flux using only the diagonal values for the capacity matrix a) Linear triangular elements b) Linear quadrilateral elements c) Quadratic triangular elements d) Quadratic quadrilateral elements.

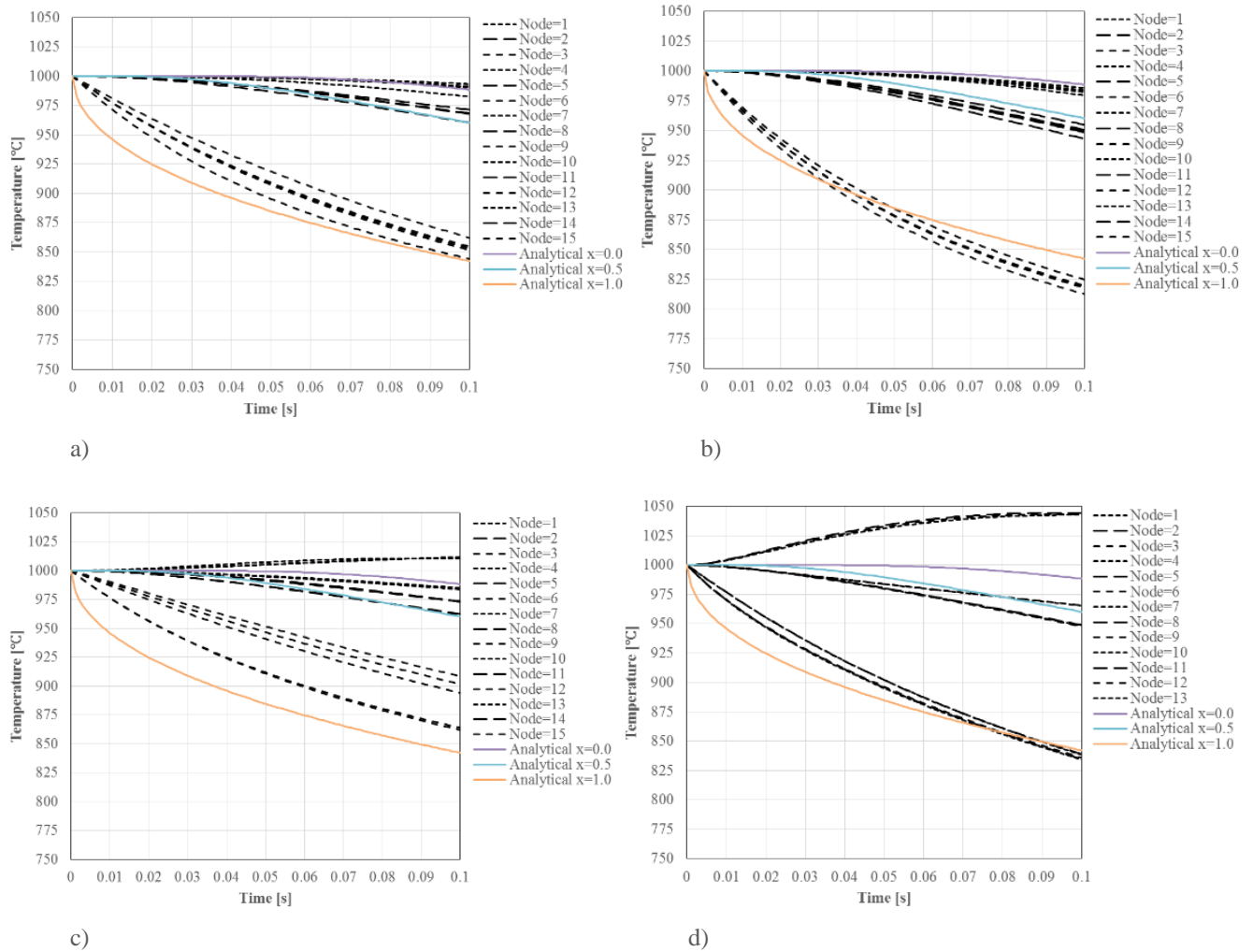


Figure 6.13: Results for Empaktor software for the prescribed flux using a pondered capacity matrix a) Linear triangular elements b) Linear quadrilateral elements c) Quadratic triangular elements d) Quadratic triangular elements.

It may be concluded that the linear elements using a lumped capacity matrix with non-diagonal values equal to zero present the better agreement to the analytical solution. Therefore, this procedure will be adopted for heat transfer with this type of elements.

In the previous test, as shown in Figure 6.1, quadratic and linear element meshes had the same number of nodes but different element sizes. Next we will use elements with the same sizes as in Figure 6.14.

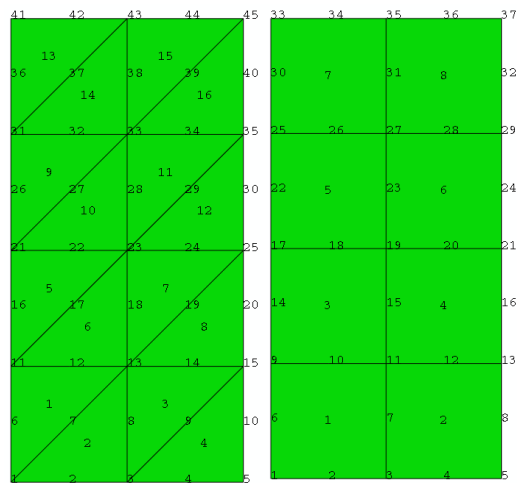


Figure 6.14: Mesh used for heat transfer validation for quadratic triangular and quadratic quadrilateral.

In Figure 6.15 the results for boundary prescribed temperature are shown. A full capacity matrix was used for Empaktor software. Although the results present temperature oscillations they are not so significant in relation to the results using the mesh of the Figure 6.14. Moreover, the results converge faster to the analytical solutions. This results agree with the equation 5.2.

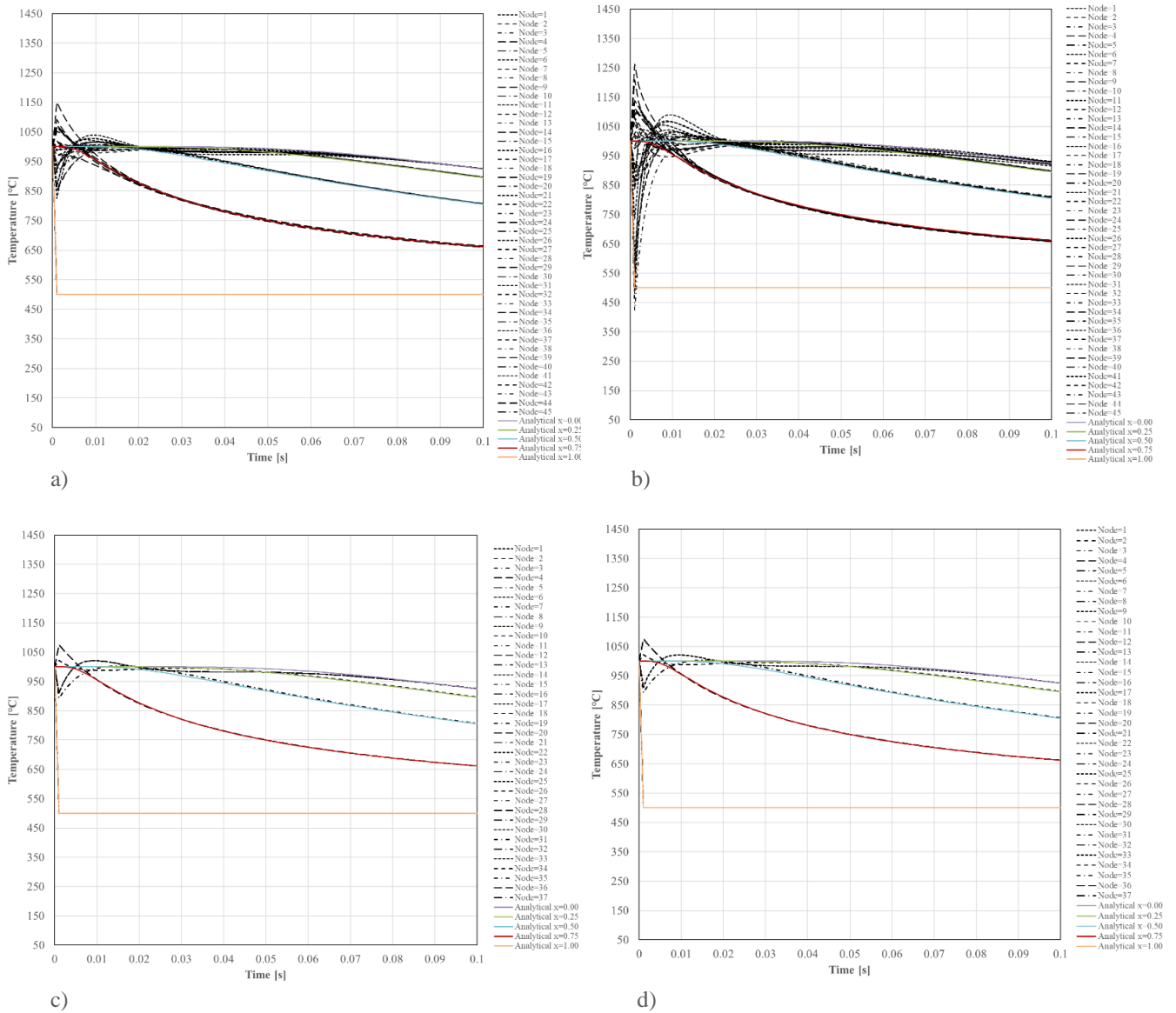


Figure 6.15: Results for prescribed temperatures a) Quadratic triangular elements in Abaqus b) Quadratic triangular elements Empaktor software c) Quadratic quadrilateral elements in Abaqus d) Quadratic quadrilateral elements Empaktor software.

Figure 6.16 present the results for the mesh of the Figure 6.14 performing the example with prescribed flux of the analogous conclusions can be drawn, i.e. the temperature oscillations are reduced when a finer mesh is used.

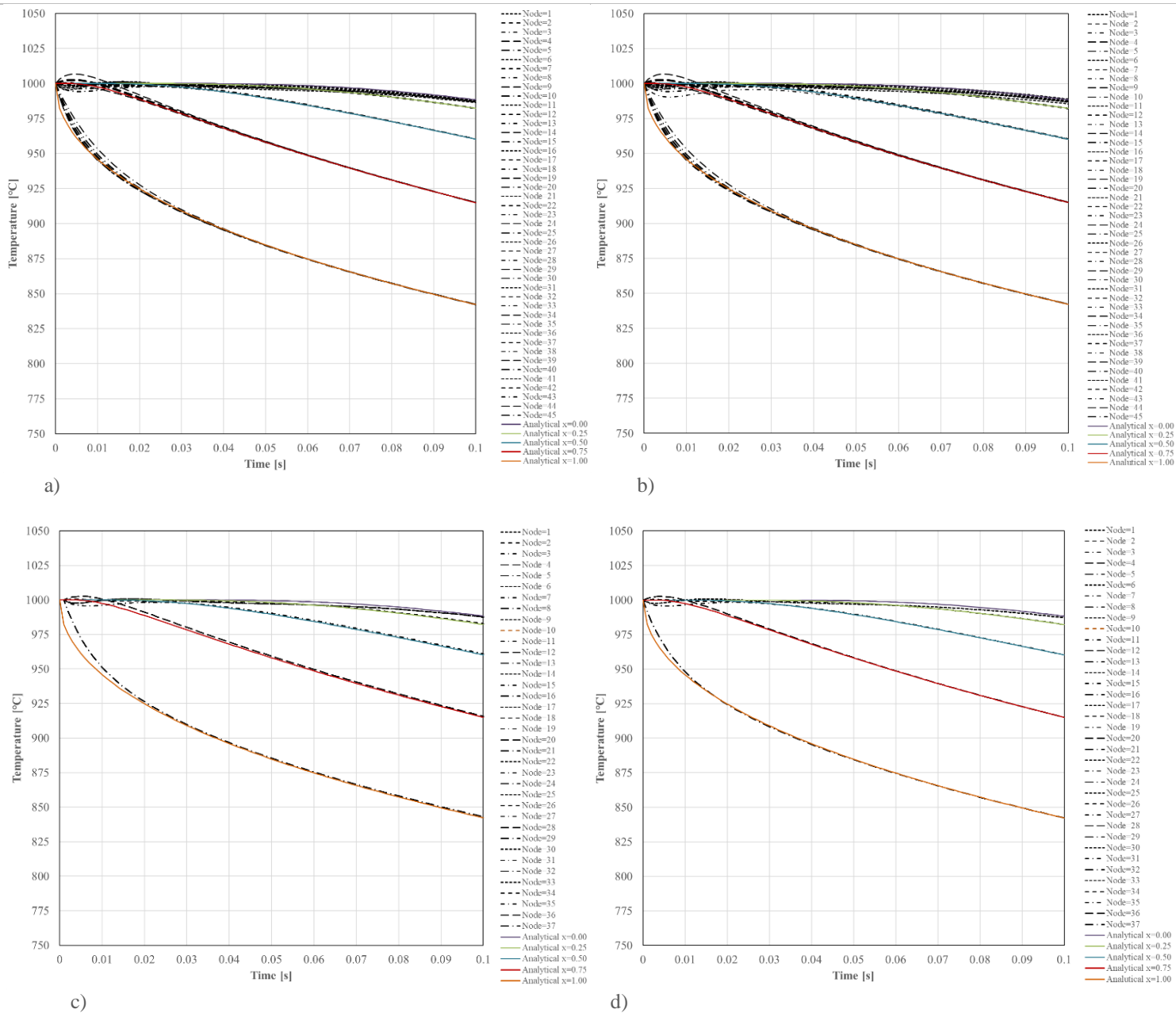


Figure 6.16: Results for prescribed flux temperatures a) Quadratic triangular elements in Abaqus b) Quadratic triangular elements Empaktor software c) Quadratic quadrilateral elements in Abaqus d) Quadratic quadrilateral elements Empaktor software.

6.2 Mechanical Validation

Here we intend to validate certain aspects related to the modelling of the mechanical behaviour of the developed program. It is not an easy task to use commercial softwares for that purpose, as the constitutive law used, with a high dependence on temperature and viscosity cannot usually be found implemented. One important aspect has to do with incompressibility of the material flow, which is a source of numerical problems in the finite element solutions. So, this restricted validation will concentrate on the ability of the elements to deal with that problem, by avoid locking, and a simple reproduction of the process performed. The ability of the elements to represent glass flow with no locking was done determining the quantity and the quality of the displacement modes associated with the incompressibility constrain. Then, a simple pressing test was performed in order to verify the displacements of each element type.

- Displacement Modes

Referring back to the previous chapter and the underlying approximation of the space of incompressible modes we have seen that it is associated to the solution obtained by a mixed formulation having displacements (velocities) and pressure as main variables:

$$\begin{bmatrix} \mathbf{K} & \mathbf{Q} \\ \mathbf{Q}^T & 0 \end{bmatrix} \begin{bmatrix} \bar{\mathbf{v}} \\ p \end{bmatrix} = \begin{bmatrix} \mathbf{f} \\ 0 \end{bmatrix} \quad 6.9$$

In which the incompressible constraint is represented by the second set of equations:

$$\mathbf{Q}^T \bar{\mathbf{v}} = \mathbf{0} \quad 6.10$$

The solution $\bar{\mathbf{v}}$ should then lie in the subspace of incompressible deformations, which represents the null space of \mathbf{Q}^T . However, the finite dimensional approximation space may not reproduce all the possible solutions. As discussed in the section 5.1.3, locking occurs when, for a given set of boundary conditions, the expected solution does not belong to the subspace solutions. In this case the solution is the trivial one to equation 4.22, i.e., $\bar{\mathbf{v}} = \mathbf{0}$. Different elements will yield different approximations to that subspace, therefore, different abilities to reproduce these type of situations.

Establishing the incompressible constraint at the integration points (Gauss points, *ngauss*).

$$\varepsilon_{kk} = \left[\frac{\partial N_i}{\partial \xi} \quad \frac{\partial N_i}{\partial \eta} \right]_{i=1, nodes} u_j = 0, \quad j=1, \text{ngauss} \quad (2D)$$

$$\varepsilon_{kk} = \left[\frac{\partial N_i}{\partial \xi} + \frac{N_i}{r_j} \quad \frac{\partial N_i}{\partial \eta} \right]_{i=1, nodes} u_j = 0, \quad j=1, \text{ngauss} \quad (\text{axisymmetric}) \quad 6.11$$

the basis modes, for each type of elements can be obtained. This is illustrated next.

- Linear Axisymmetric Triangle Element

In Figure 6.17 the deformation modes for the axisymmetric linear triangle are presented, for one point Gauss integration. Five modes are obtained but it is clear that the modes obtained shows spurious deformation patterns. Some of the deformation modes have movement through the axisymmetric axis, which is unphysical.

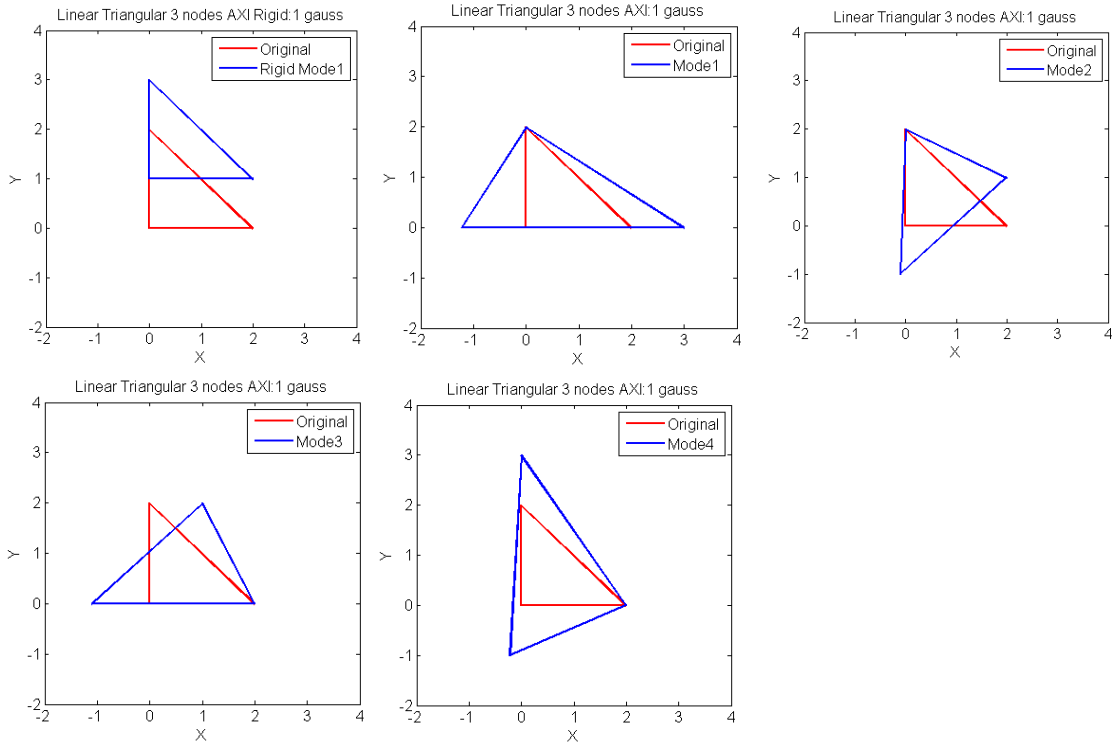


Figure 6.17: Axisymmetric deformation modes for the linear triangular element using 1 Gauss point.

In order to remove these spurious deformation modes, the solution was chosen so that the modes would be orthogonal to them and also to the rigid body mode, shown in Figure 6.18. In practical terms, the orthogonalization procedure intends to prevent these modes, as it is done in practice by imposing boundary conditions and by restricting the horizontal movement of the nodes which are in the axisymmetric axis.

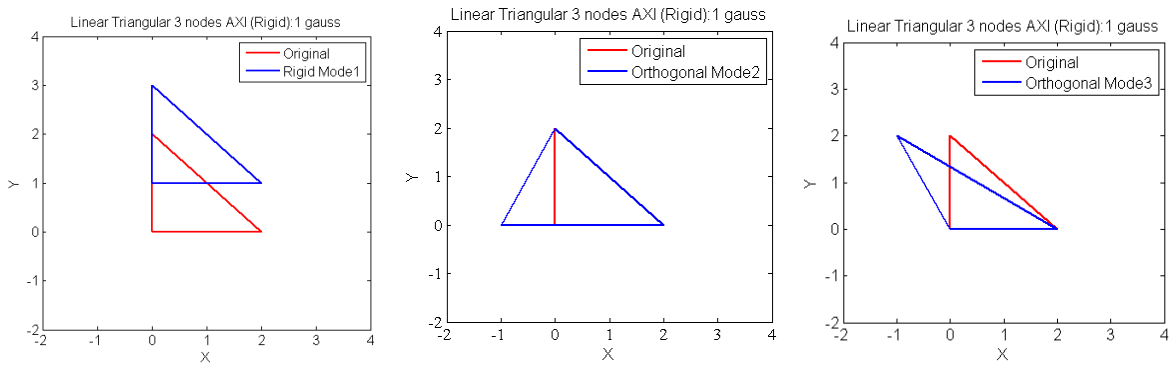


Figure 6.18: Orthogonalizing deformation modes for the linear triangular element using 1 Gauss point.

The Figure 6.19 shows the resulting deformation modes. Thus, two deformation modes were obtained.

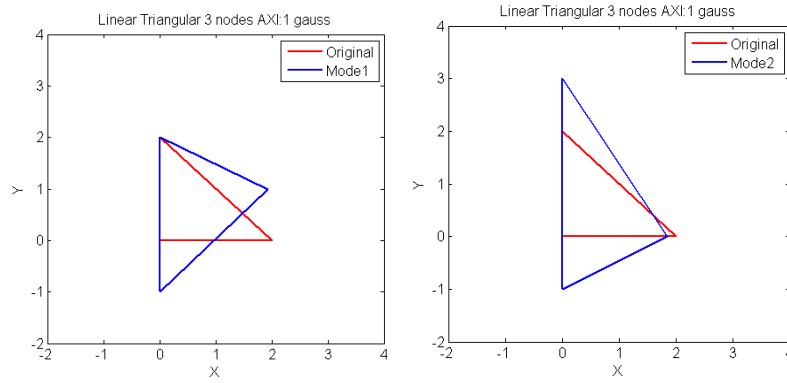


Figure 6.19: Axisymmetric deformation modes for the linear triangular element using 1 Gauss point.

The deformation modes for three and seven Gauss points are presented in Figure 6.20 and Figure 6.21 respectively. They coincide and only two modes, apart from the rigid body motion one, are obtained. No spurious modes are present. In this case, only one rigid mode was included.

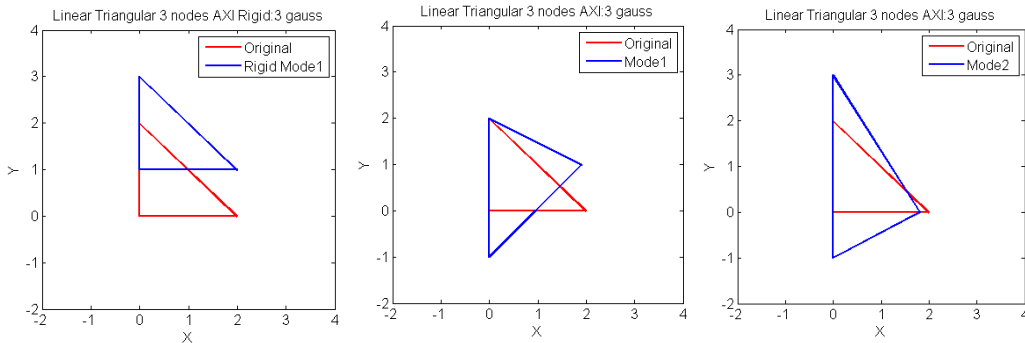


Figure 6.20: Axisymmetric deformation modes for the linear triangular element using 3 Gauss point.

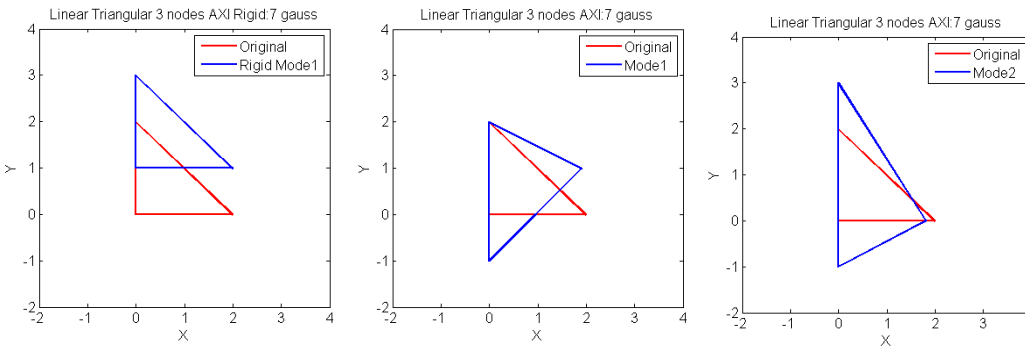


Figure 6.21: Axisymmetric deformation modes for the linear triangular element using 7 Gauss point.

o MINI Axisymmetric Triangle Element

The MINI linear triangle axisymmetric element, using only one Gauss point depicts a larger basis of deformation modes, as presented in Figure 6.22. It means that is better “equipped” to deal with incompressibility. Nevertheless one of the modes, mode 5, is clearly not satisfying the incompressibility condition and is, therefore, a spurious mode.

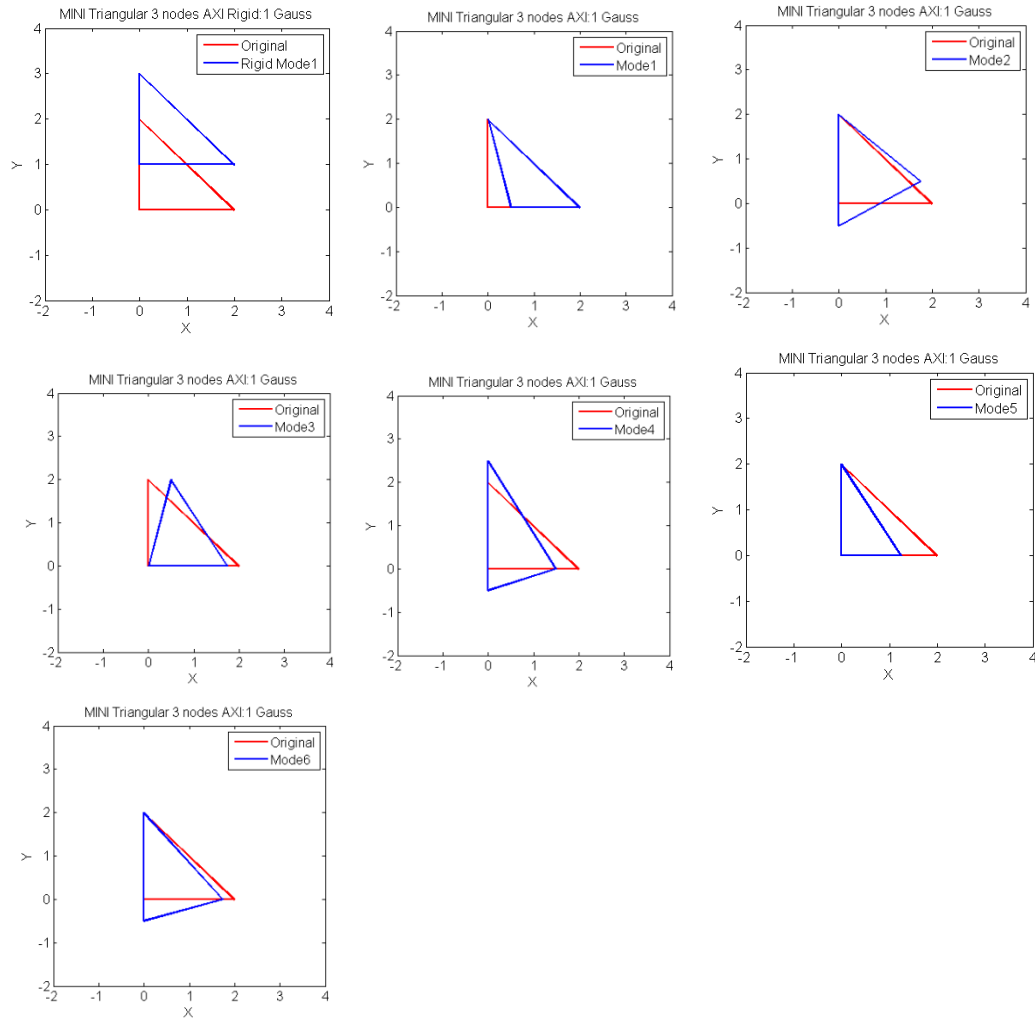


Figure 6.22: Axisymmetric deformation modes for the MINI linear triangular element using one Gauss point.

As in the case of the linear axisymmetric triangle element additional deformation modes are used, Figure 6.23, to prevent spurious and rigid body modes, by the same orthogonalization procedure.

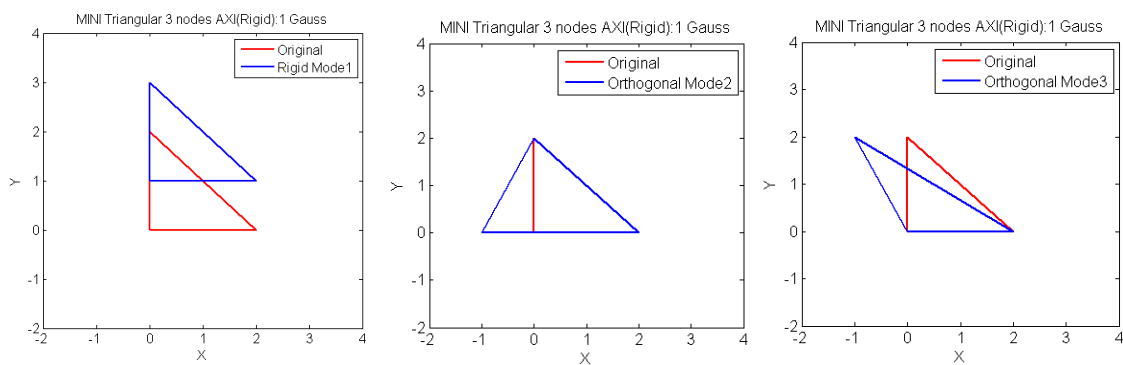


Figure 6.23: Orthogonalizing deformation modes for the MINI linear triangular element using 1 Gauss point.

The Figure 6.24 shows the resulting deformation modes. Four deformation modes were obtained.

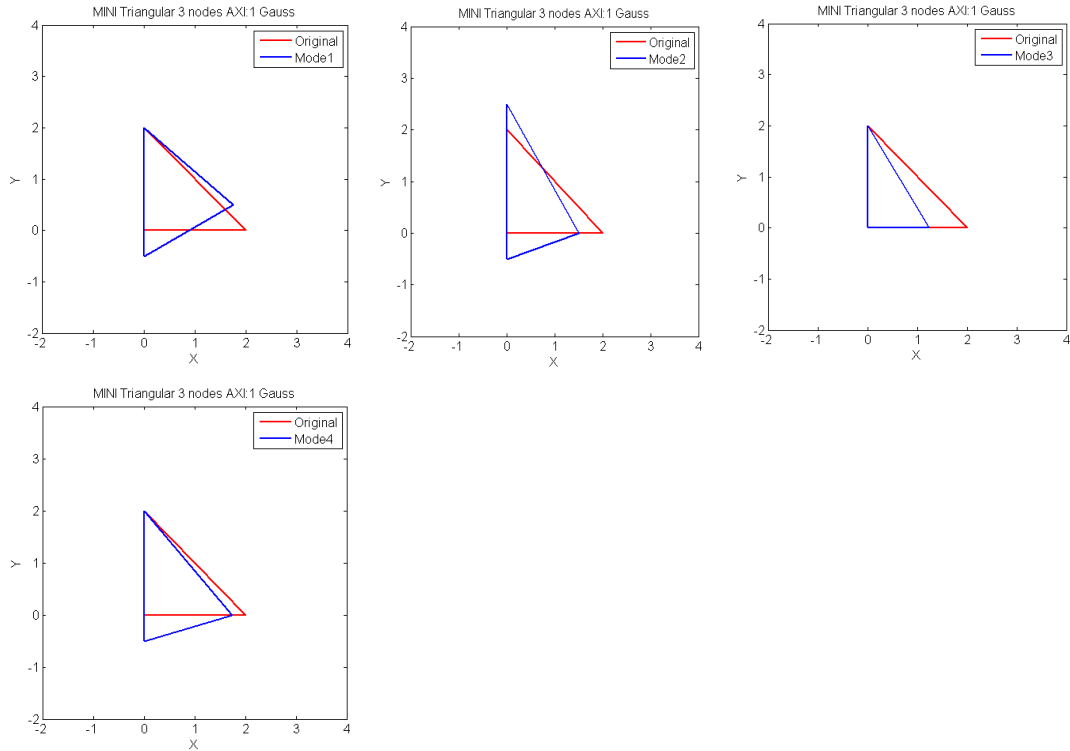


Figure 6.24: Axisymmetric deformation modes for the MINI linear triangular element using one Gauss point.

The MINI linear triangular element with three Gauss points, Figure 6.25, presents also a spurious mode, which is removed if seven Gauss points are used, Figure 6.27, but the results are then the same as for the linear triangular element.

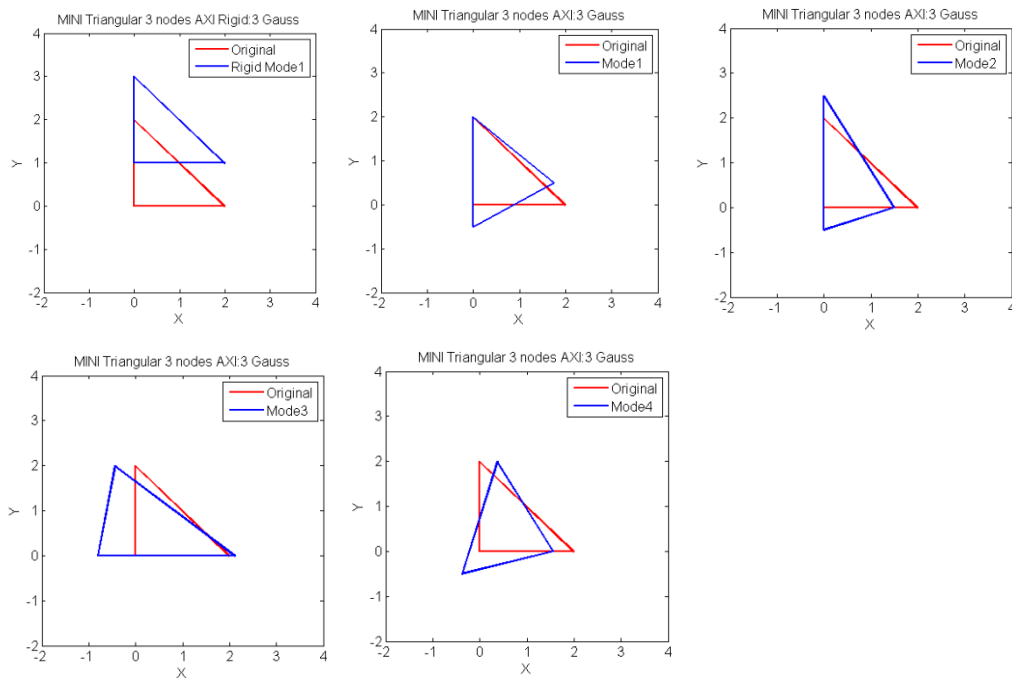


Figure 6.25: Axisymmetric deformation modes for the MINI linear triangular element using three Gauss point.

If the previous procedure is orthogonalised, the solution against the spurious modes and rigid body modes is performed, the result obtained is illustrated in Figure 6.26. These two deformation modes are the same when calculation is made with seven Gauss points.

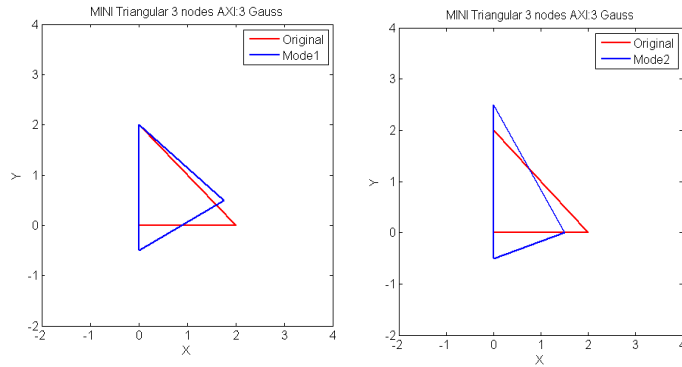


Figure 6.26: Axisymmetric deformation modes for the MINI linear triangular element using three Gauss point.

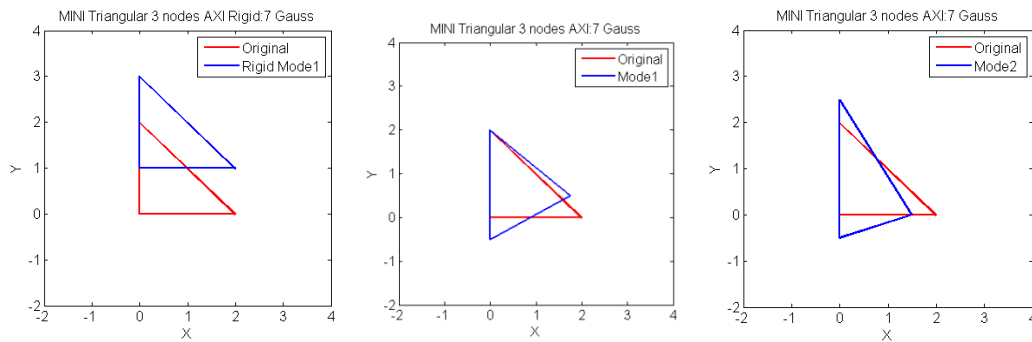
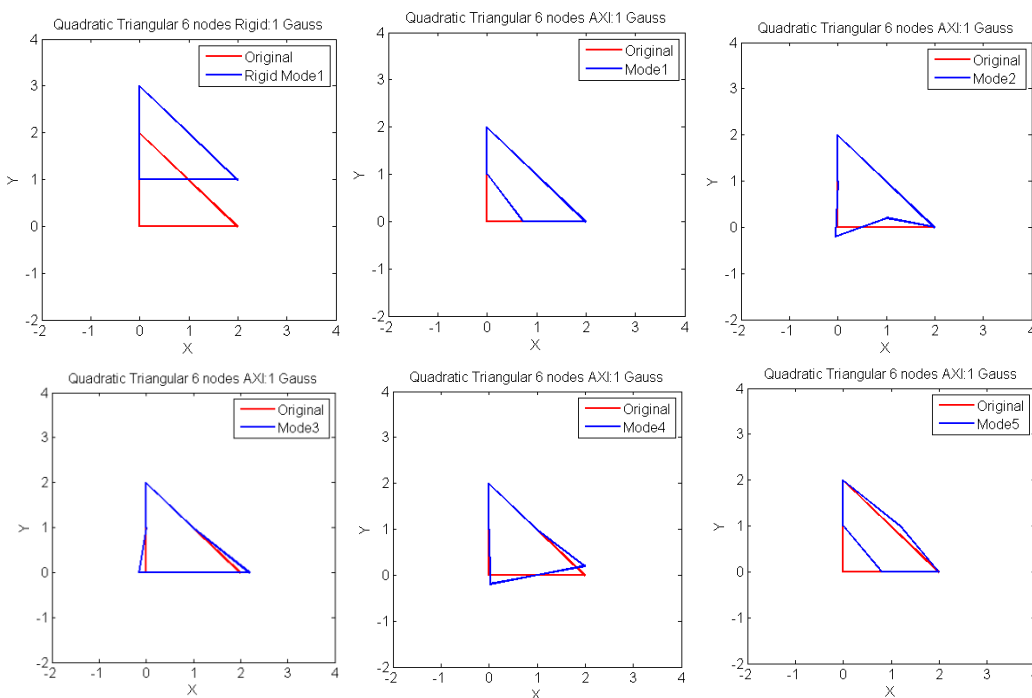


Figure 6.27: Axisymmetric deformation modes for the MINI linear triangular element using seven Gauss point.

○ Quadratic Axisymmetric Triangle Element

In Figure 6.28 the quadratic axisymmetric triangle deformation modes, using one Gauss point are presented. As expected some spurious modes are observed.



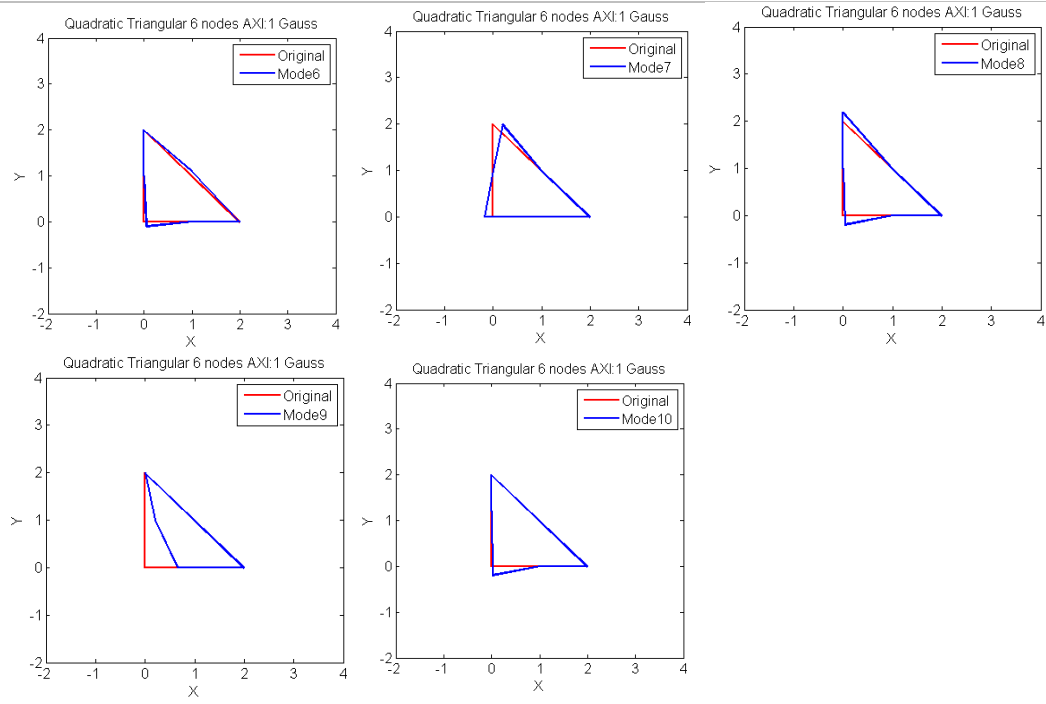


Figure 6.28: Axisymmetric deformation modes for the quadratic triangular element using one Gauss point.

Orthogonalizing the solution against the modes of Figure 6.29 the seven resulting deformation modes are shown in Figure 6.30.

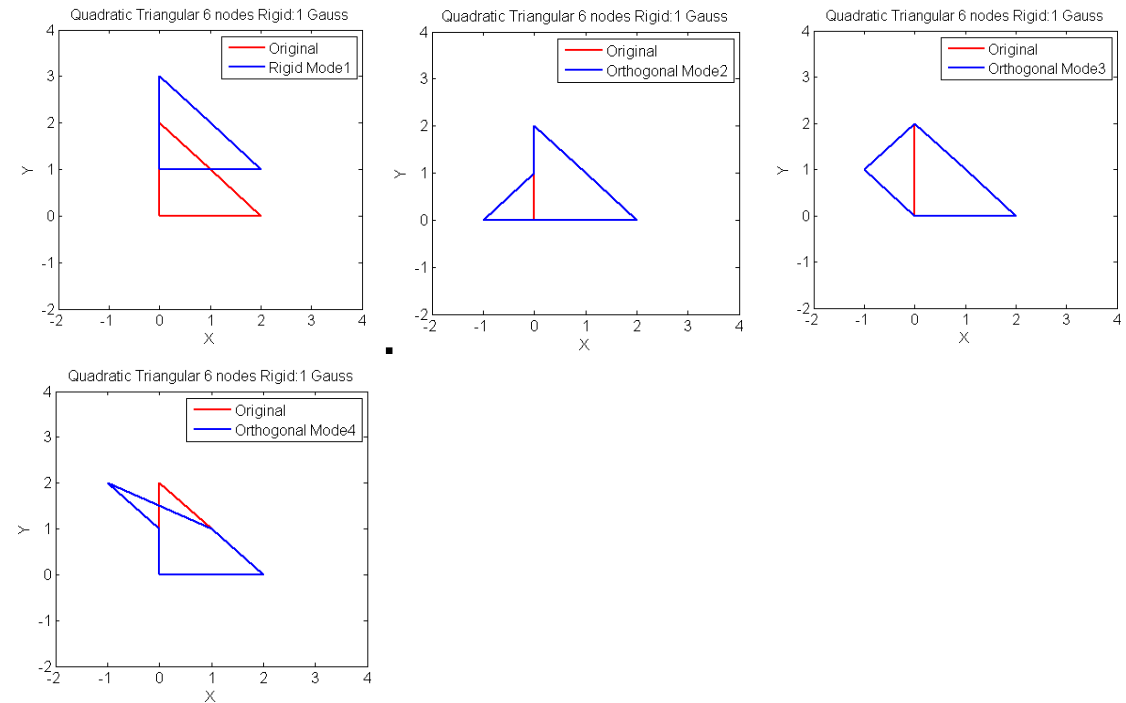


Figure 6.29: Orthogonalizing deformation modes for the quadratic triangular element using one Gauss point.

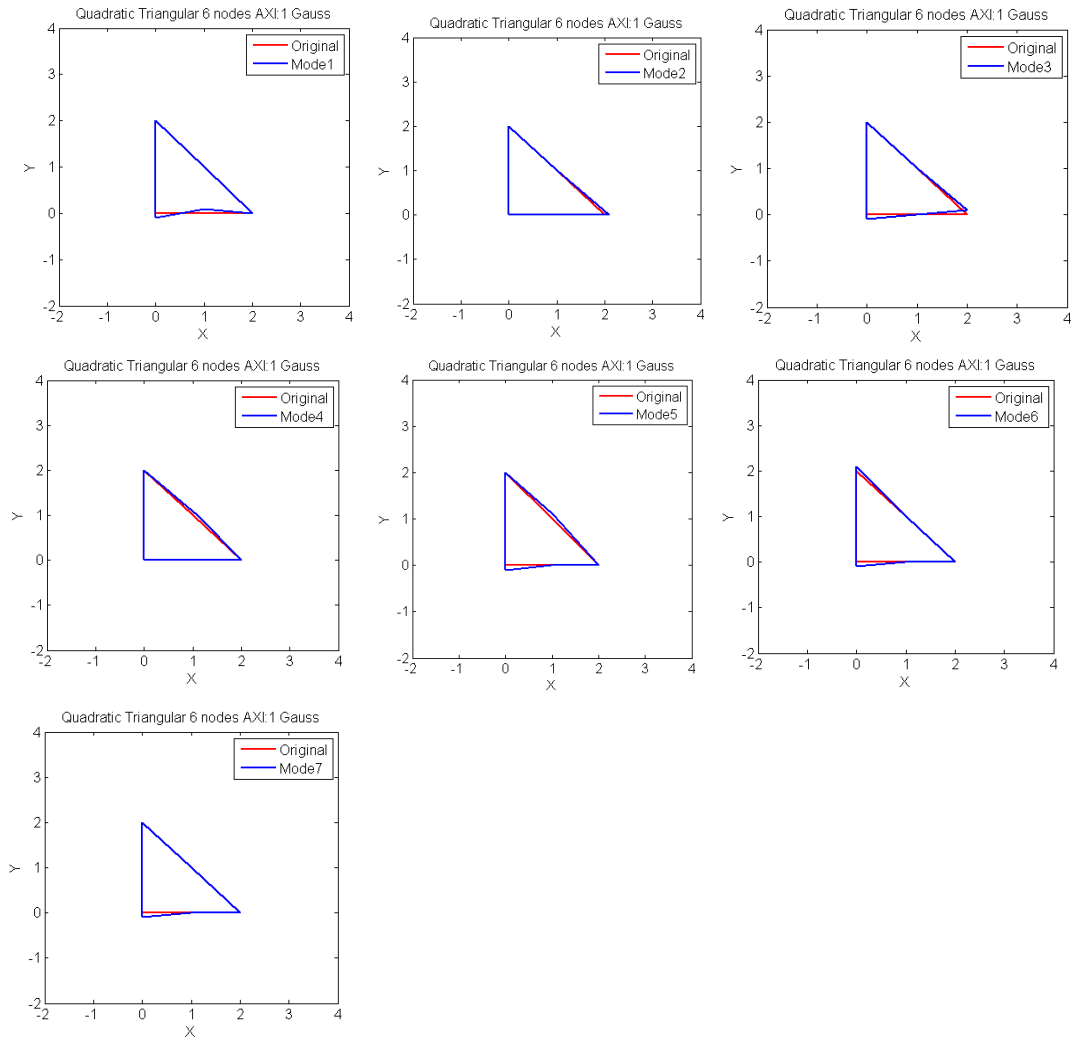


Figure 6.30: Axisymmetric deformation modes for the quadratic triangular element using one Gauss point.

The quadratic axisymmetric triangle with three Gauss points still presents some spurious modes, Figure 6.31. They are eliminated when seven Gauss points are used but the basis dimension is reduced, Figure 6.33.

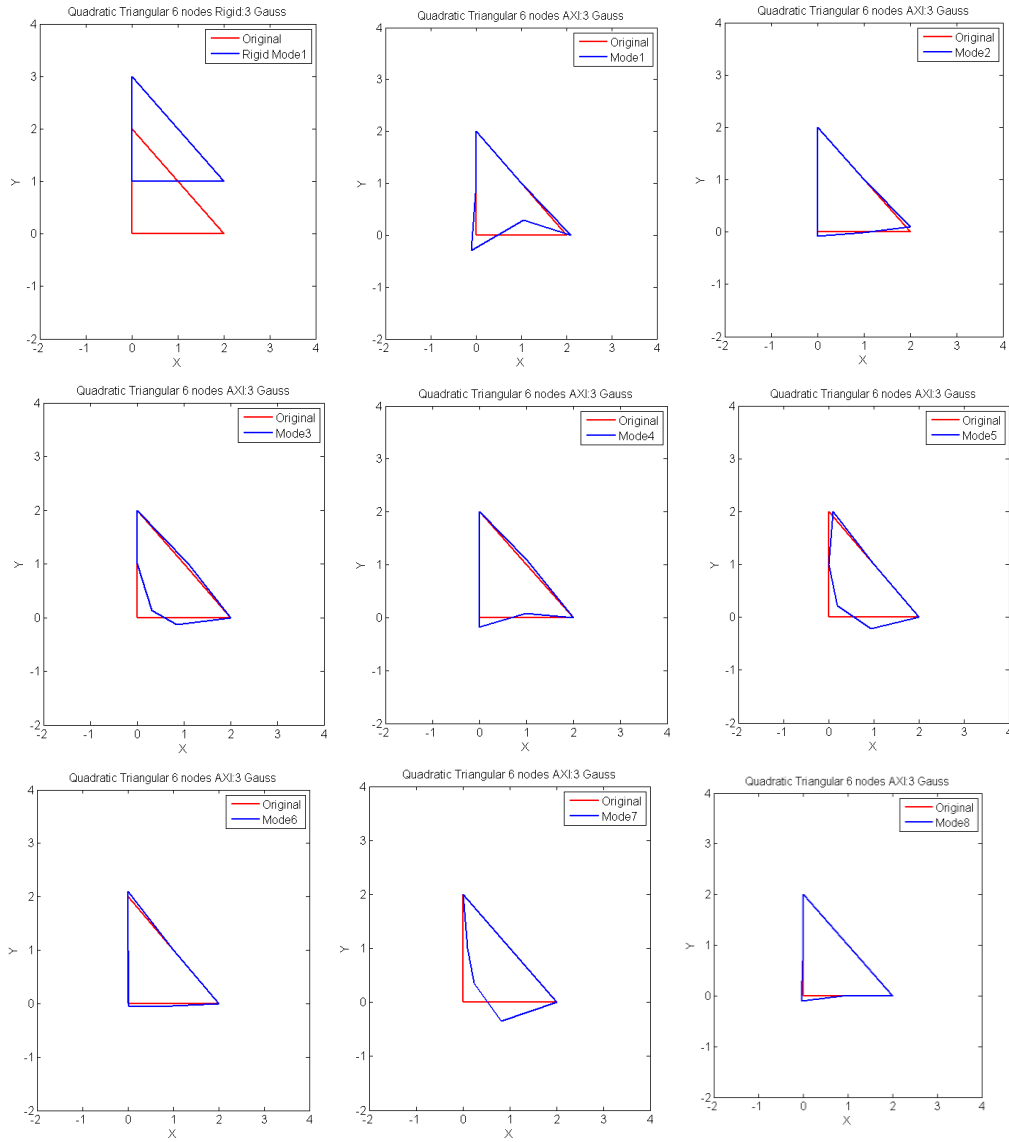


Figure 6.31: Axisymmetric deformation modes for the quadratic triangular element using three Gauss point.

The Figure 6.32 shows the resulting deformation modes. These modes were calculated taking in account the rigid motion calculated in Figure 6.29. Thus, it were obtained five deformation modes without movement throughout the axisymmetric axis. The obtained modes are the same modes calculated for the seven Gauss points.

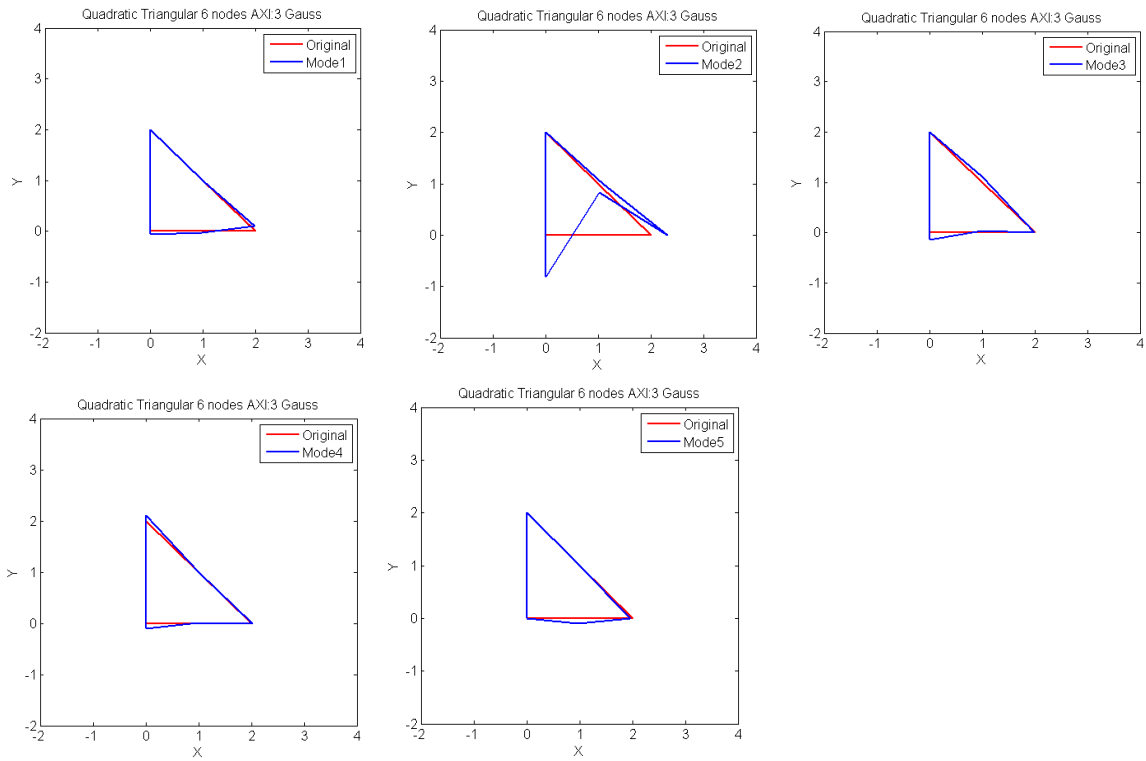


Figure 6.32: Axisymmetric deformation modes for the quadratic triangular element using three Gauss point.

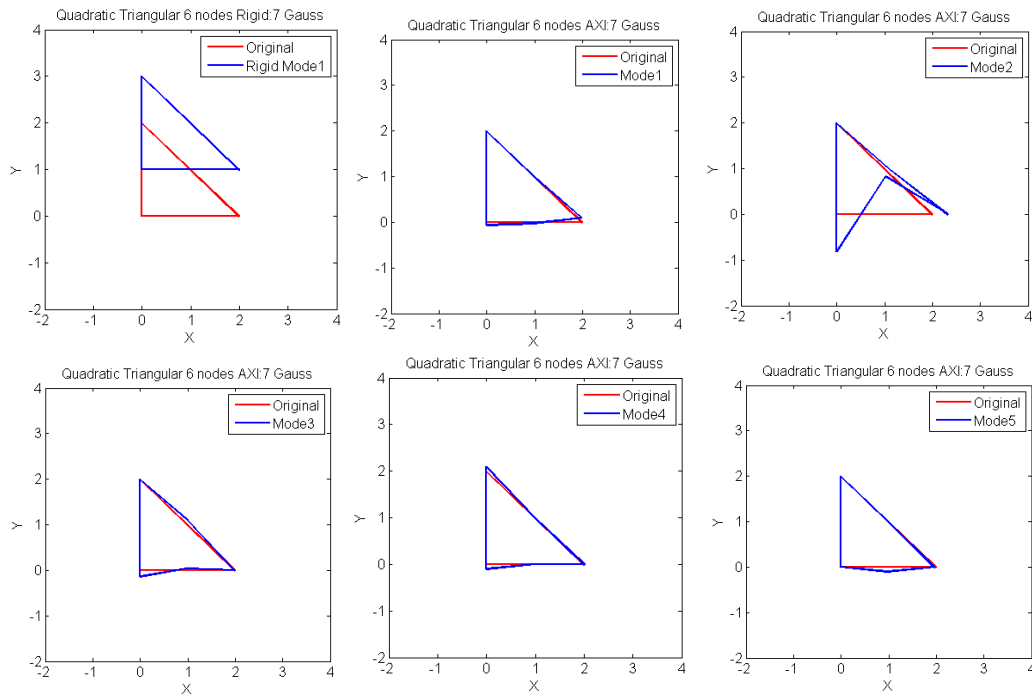


Figure 6.33 Axisymmetric deformation modes for the quadratic triangular element using seven Gauss point.

The Figure 6.34 shows the resulting deformation modes after orthogonalization to the rigid body mode.

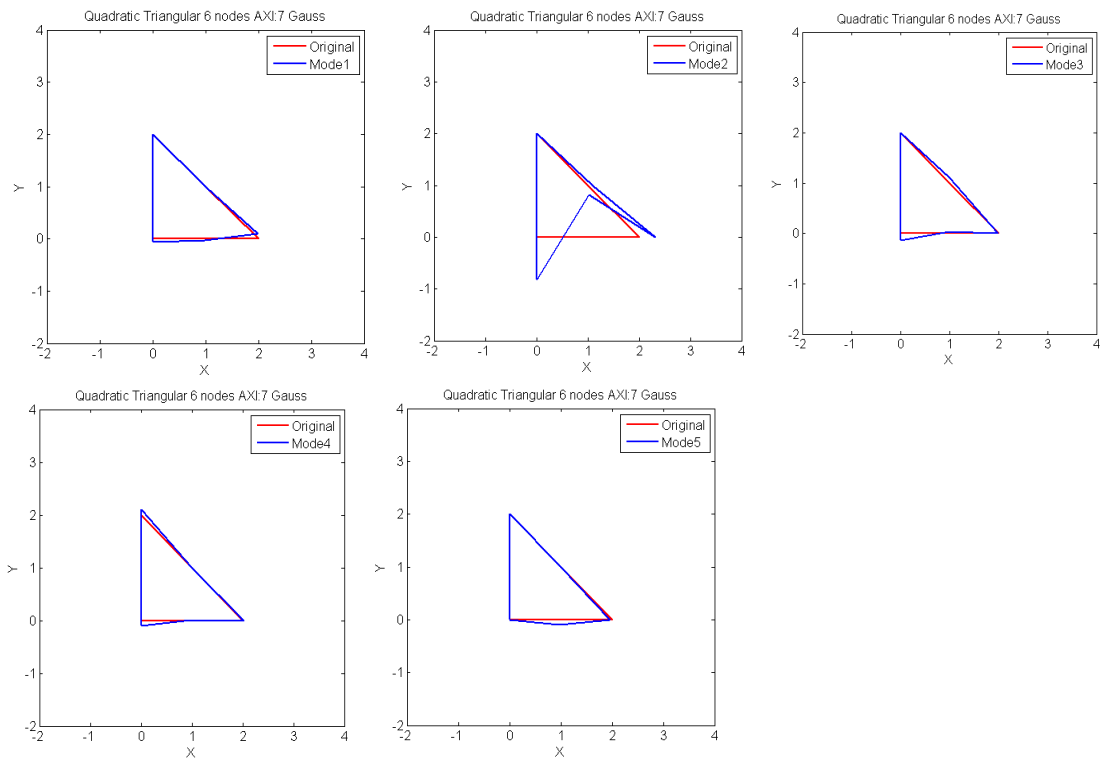


Figure 6.34 Axisymmetric deformation modes for the quadratic triangular element using seven Gauss point.

○ Linear Axisymmetric Quadrilateral Element

In Figure 6.35 the deformation modes for this element using one Gauss point are shown.

The number of deformation modes is reduced if the number of Gauss points are 2x2, Figure 6.38 or 3x3, Figure 6.40 , increasing the likelihood of locking to happen.

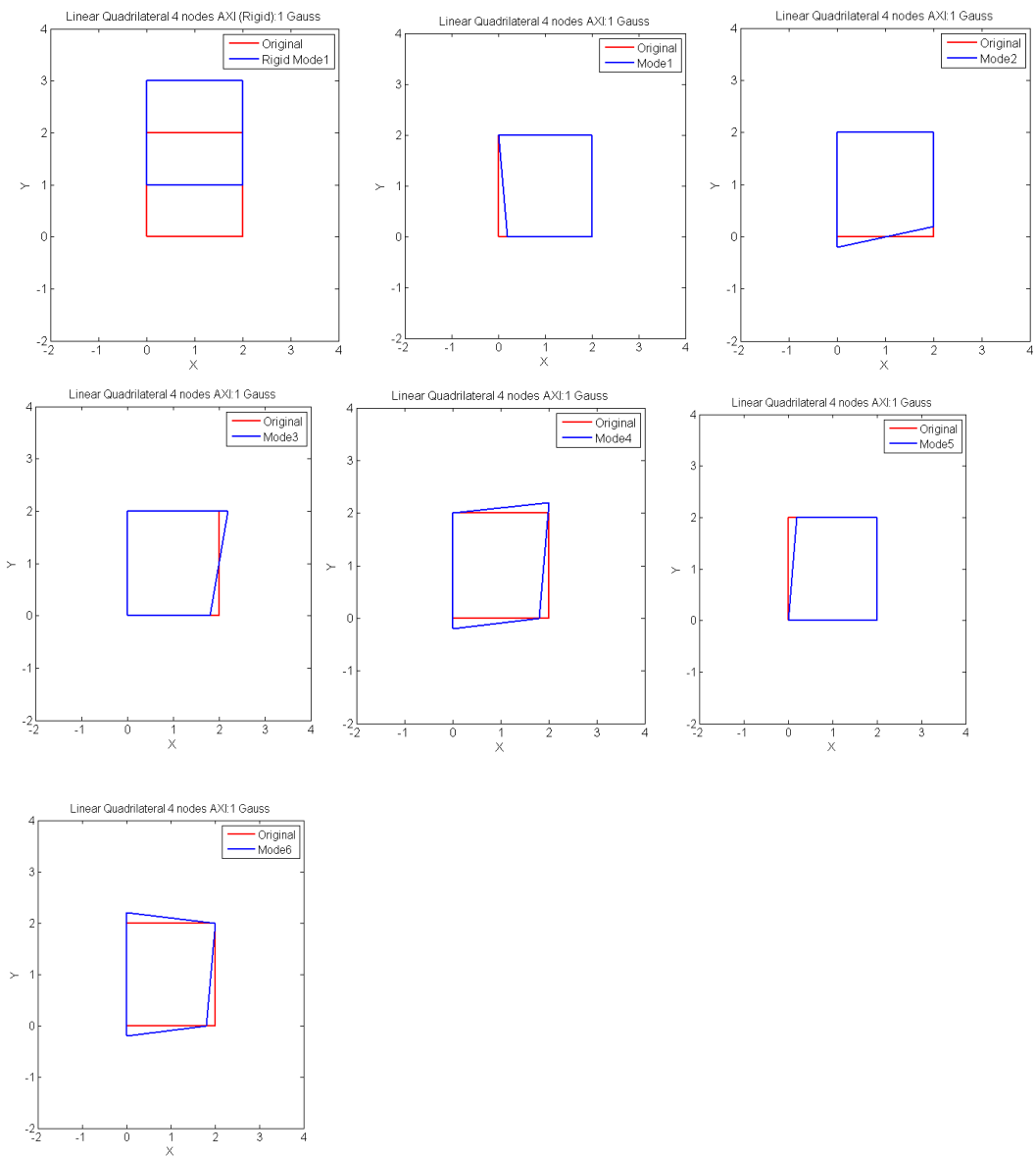


Figure 6.35: Axisymmetric displacement modes for the linear quadrilateral element using one Gauss point.

Orthogonalizing the solution against the modes represented in Figure 6.36 the four modes represented in Figure 6.37 are obtained.

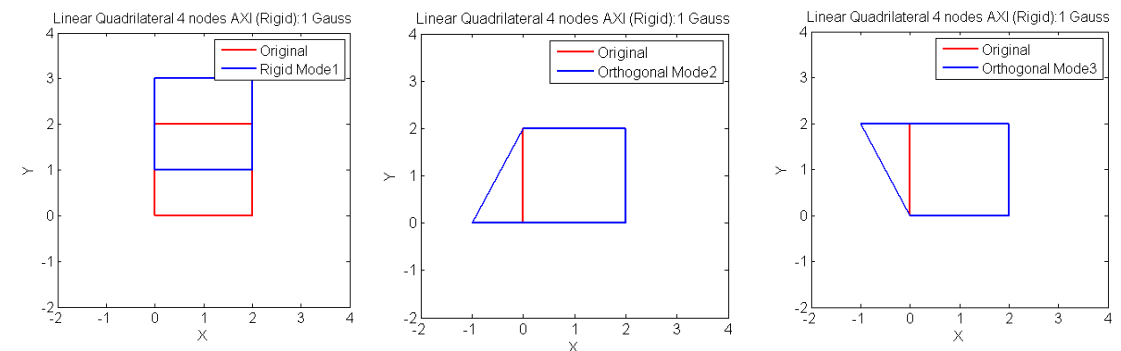


Figure 6.36: Orthogonalizing deformation modes for the linear quadrilateral element using one Gauss point.

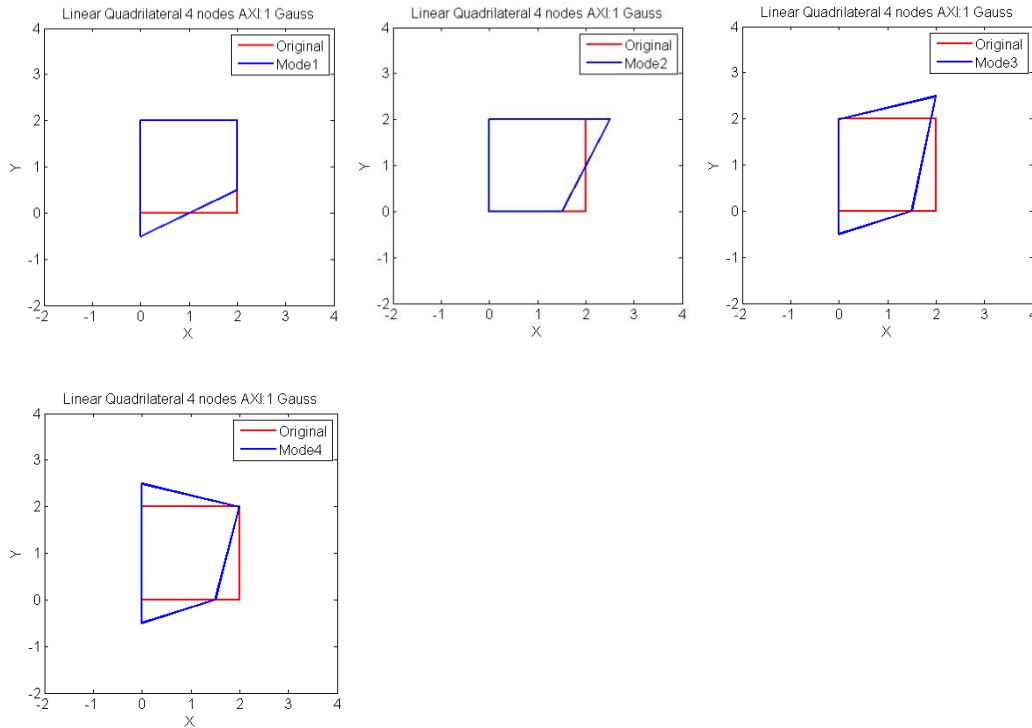


Figure 6.37: Axisymmetric deformation modes for the linear quadrilateral element using one Gauss point.

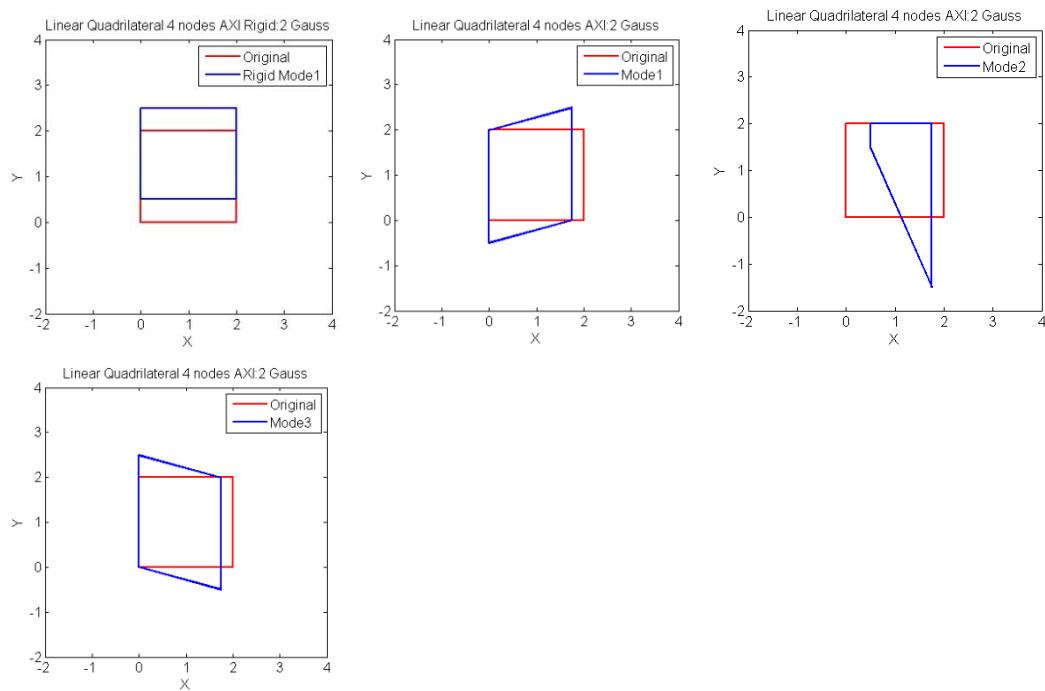


Figure 6.38: Axisymmetric deformation modes for the linear quadrilateral element using 2x2 Gauss point.

If the same type orthogonalization is performed only one mode is obtained, Figure 6.39.

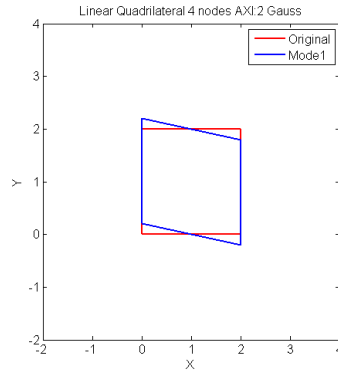


Figure 6.39: Axisymmetric deformation modes for the linear quadrilateral element using 2x2 Gauss point.

Figure 6.40 shows the deformation modes for the 3x3 Gauss points. In this case only two deformation modes, apart from the rigid body mode, were obtained. With the orthogonalization procedure only one mode is obtained, Figure 6.41.

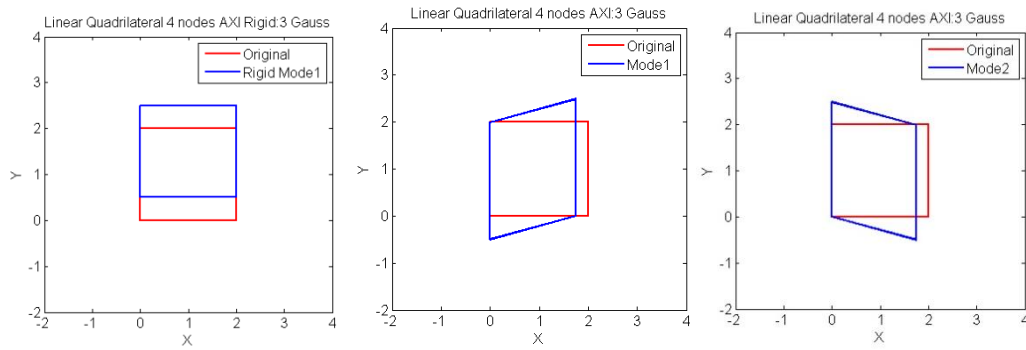


Figure 6.40: Axisymmetric deformation modes for the linear quadrilateral element using 3x3 Gauss point.

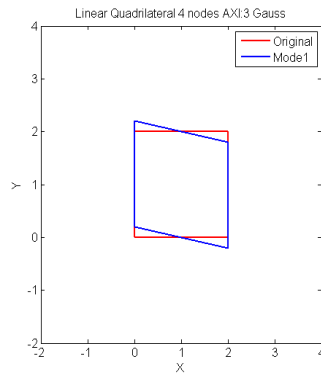
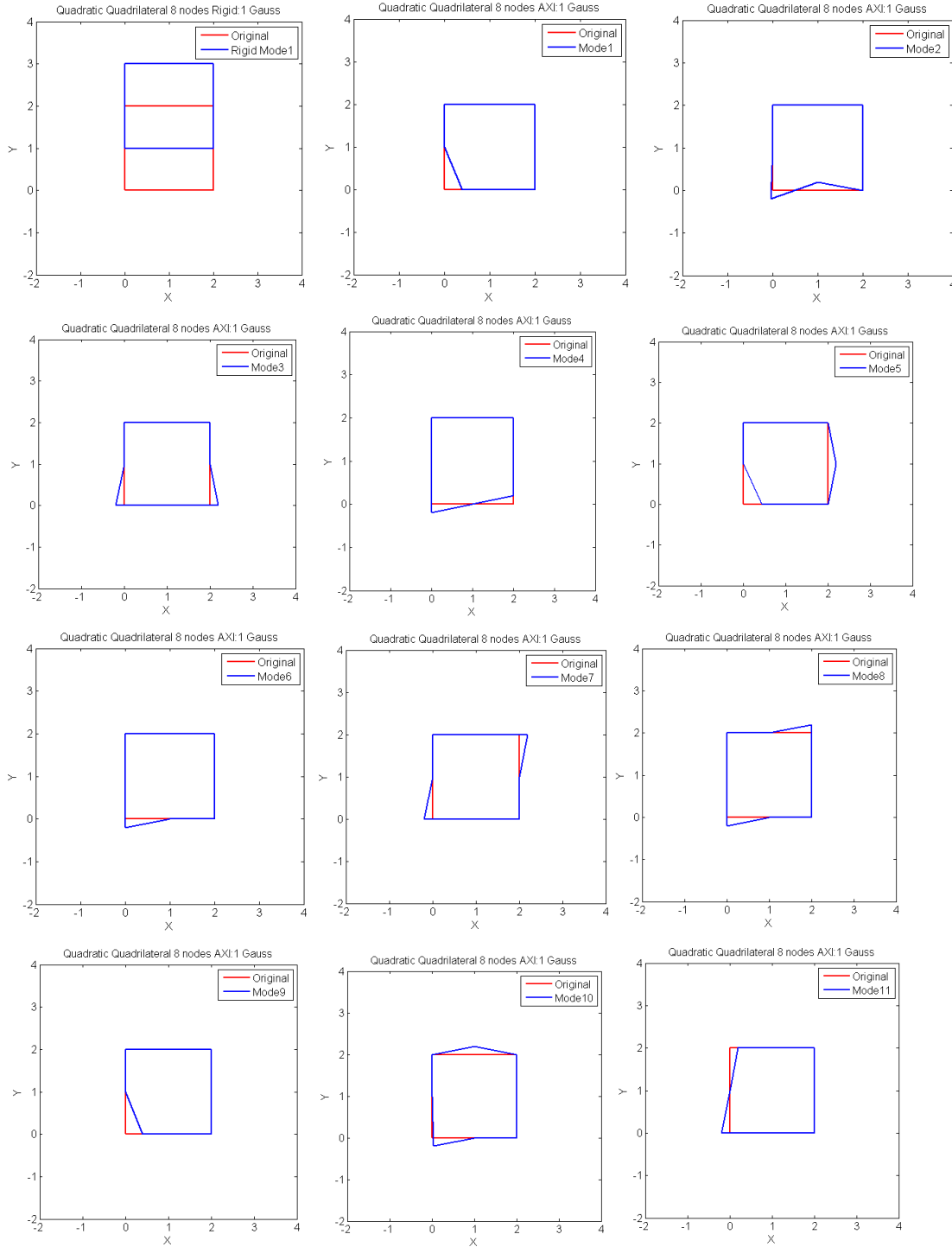


Figure 6.41: Axisymmetric deformation modes for the linear quadrilateral element using 3x3 Gauss point.

○ Quadratic Axisymmetric Quadrilateral Element

In Figure 6.42 the deformation modes for quadratic axisymmetric quadrilateral element using one Gauss point are shown. As it can be seen many spurious modes are present. This number is reduced with a 2x2 integration rule, but still some spurious modes are present, Figure 6.45.



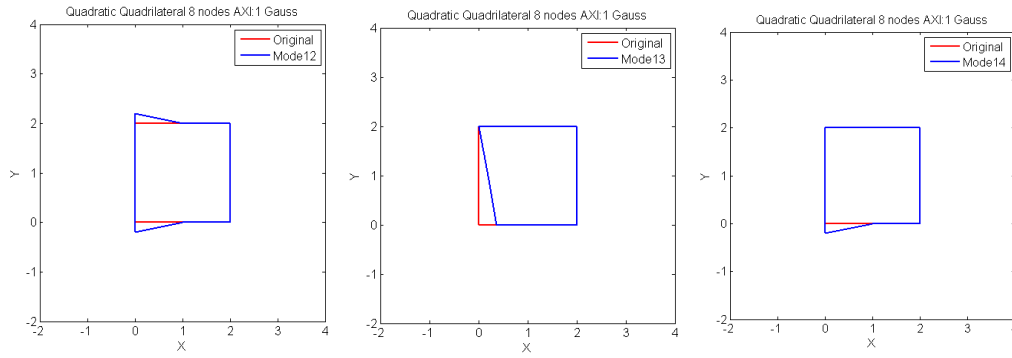


Figure 6.42: Axisymmetric deformation modes for the quadratic quadrilateral element for one Gauss point

The deformation modes were orthogonalized against the modes in Figure 6.43.

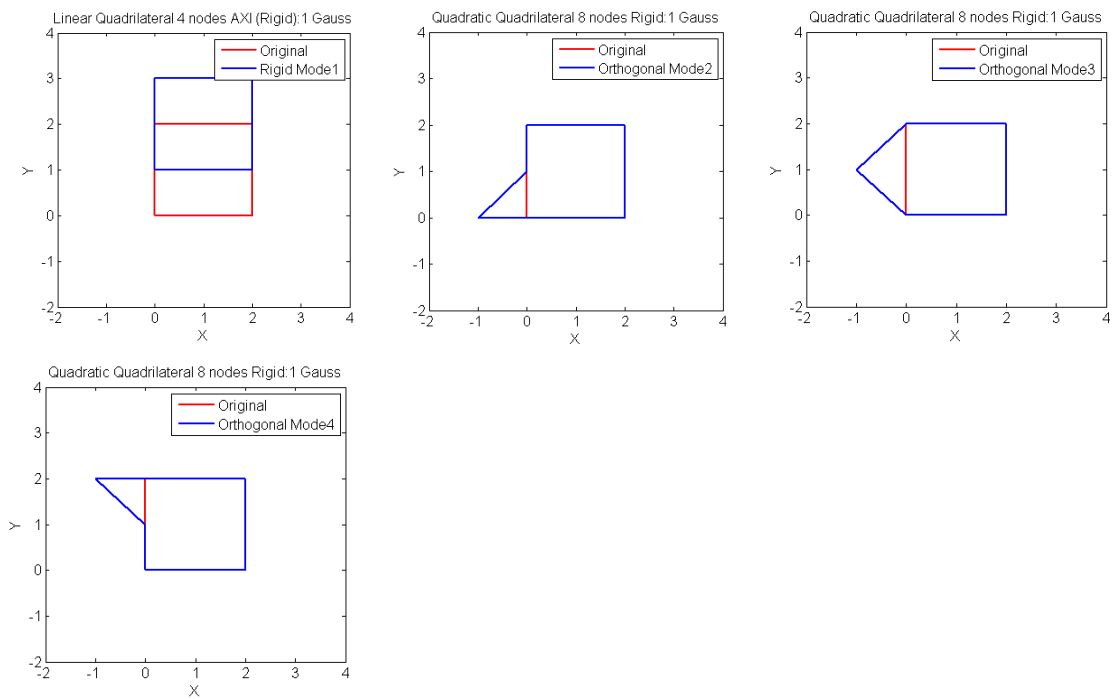


Figure 6.43: Orthogonalizing deformation modes for the quadratic quadrilateral element using one Gauss point.

The Figure 6.44 shows the resulting deformation modes.

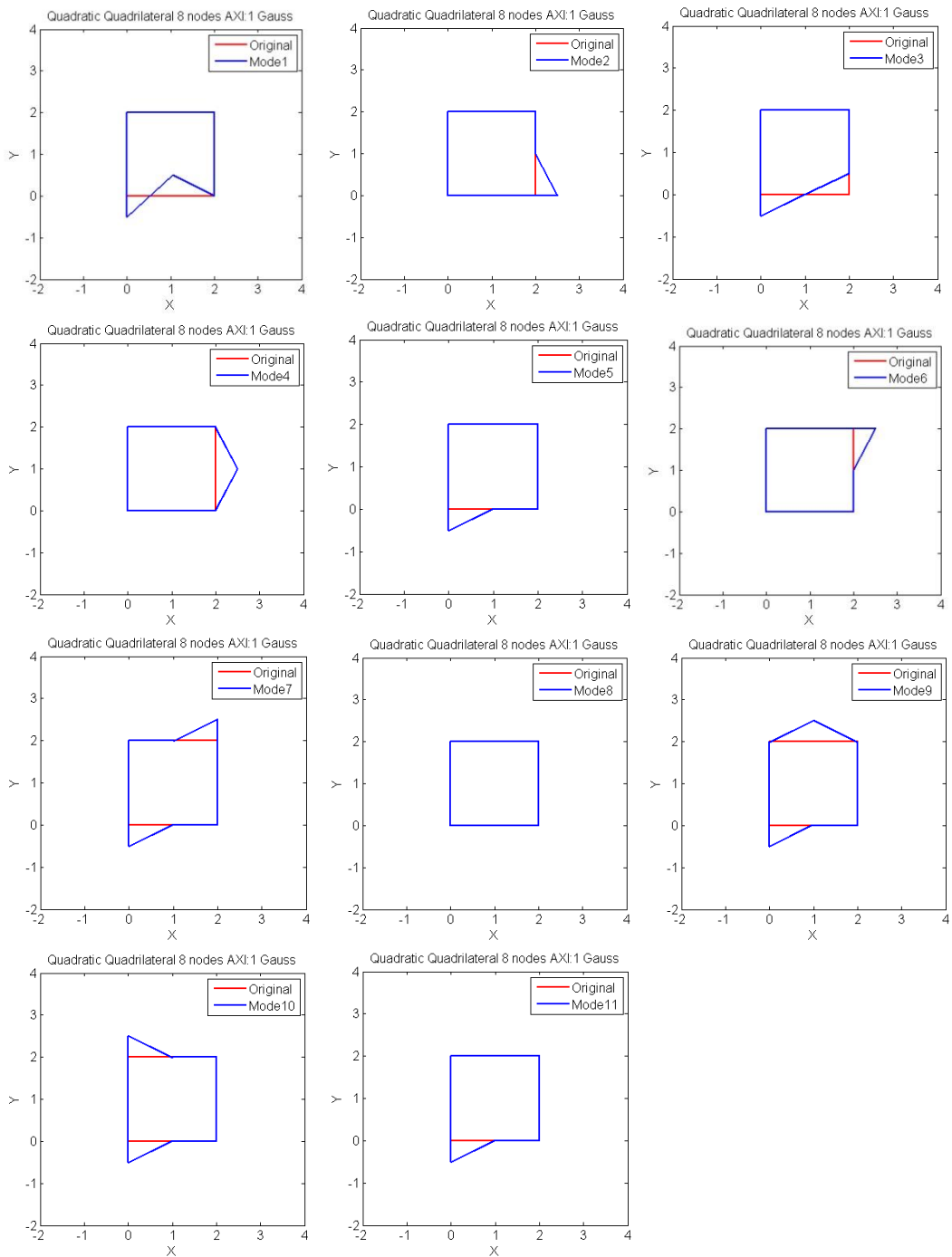
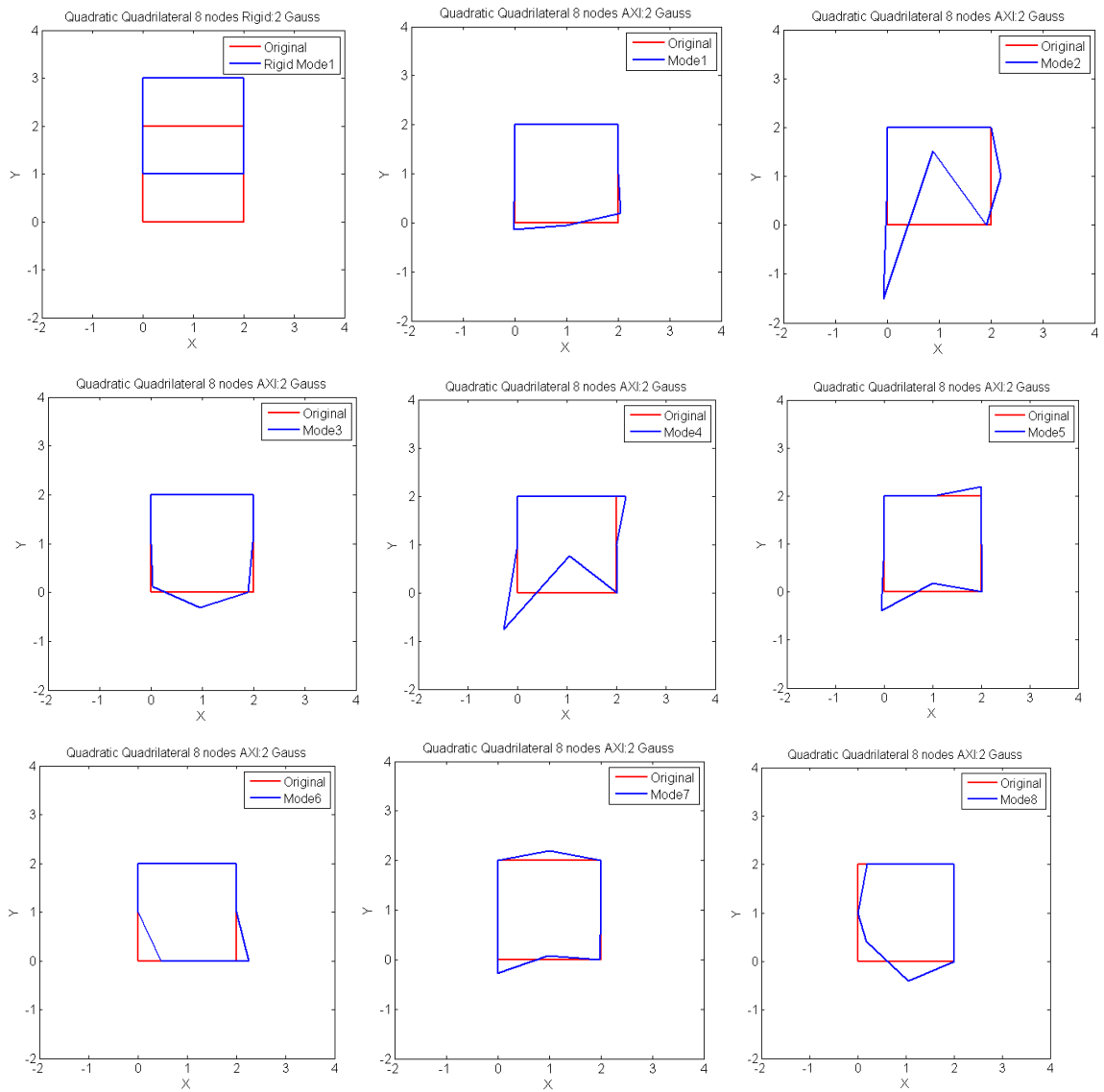


Figure 6.44: Axisymmetric deformation modes for the quadratic quadrilateral element using one Gauss point.



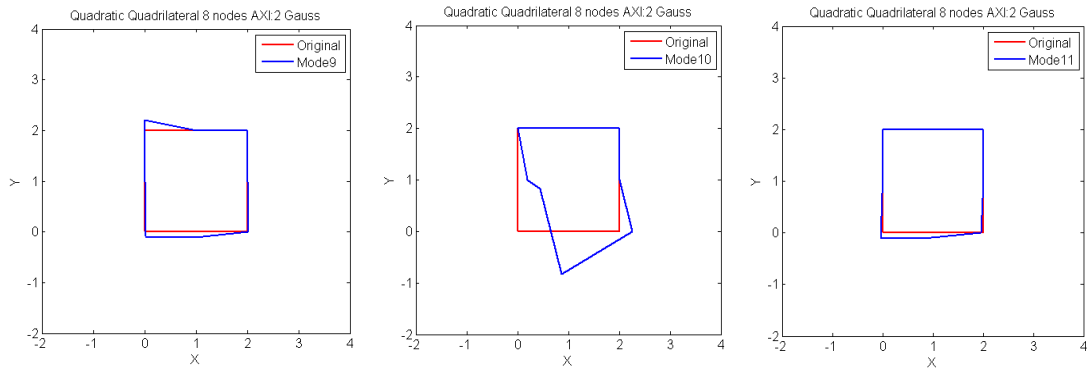


Figure 6.45: Axisymmetric deformation modes for the quadratic quadrilateral element for 2x2 Gauss point.

The Figure 6.46 shows the resulting deformation modes after the orthogonalization procedure as in the previous cases.

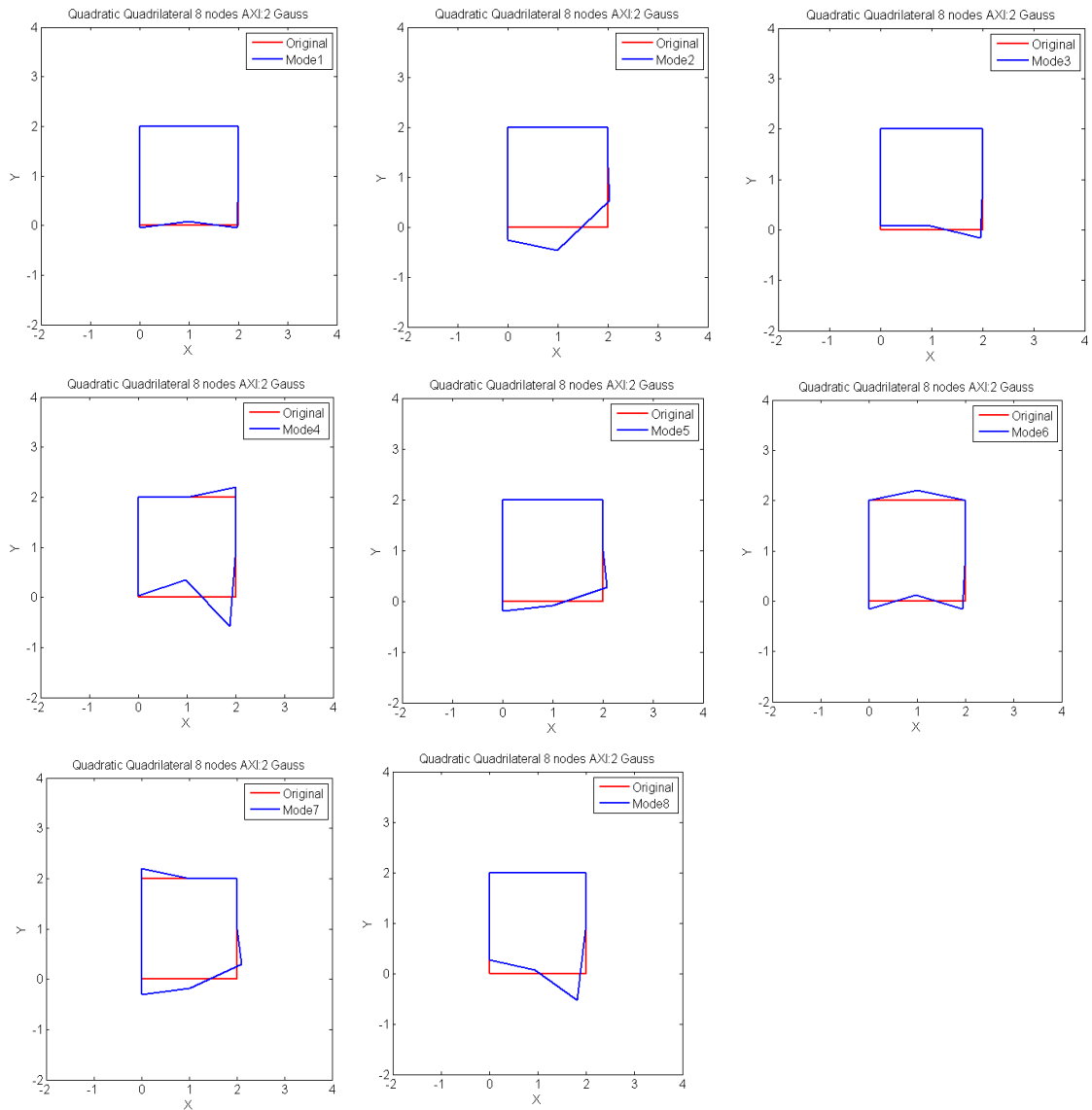


Figure 6.46: Axisymmetric deformation modes for the quadratic quadrilateral element for 2x2 Gauss point.

Figure 6.47 show the deformation modes for the 3x3 Gauss points. In this case seven deformation modes were obtained. If rigid deformation modes are not include only six deformation modes should be considered, Figure 6.48.

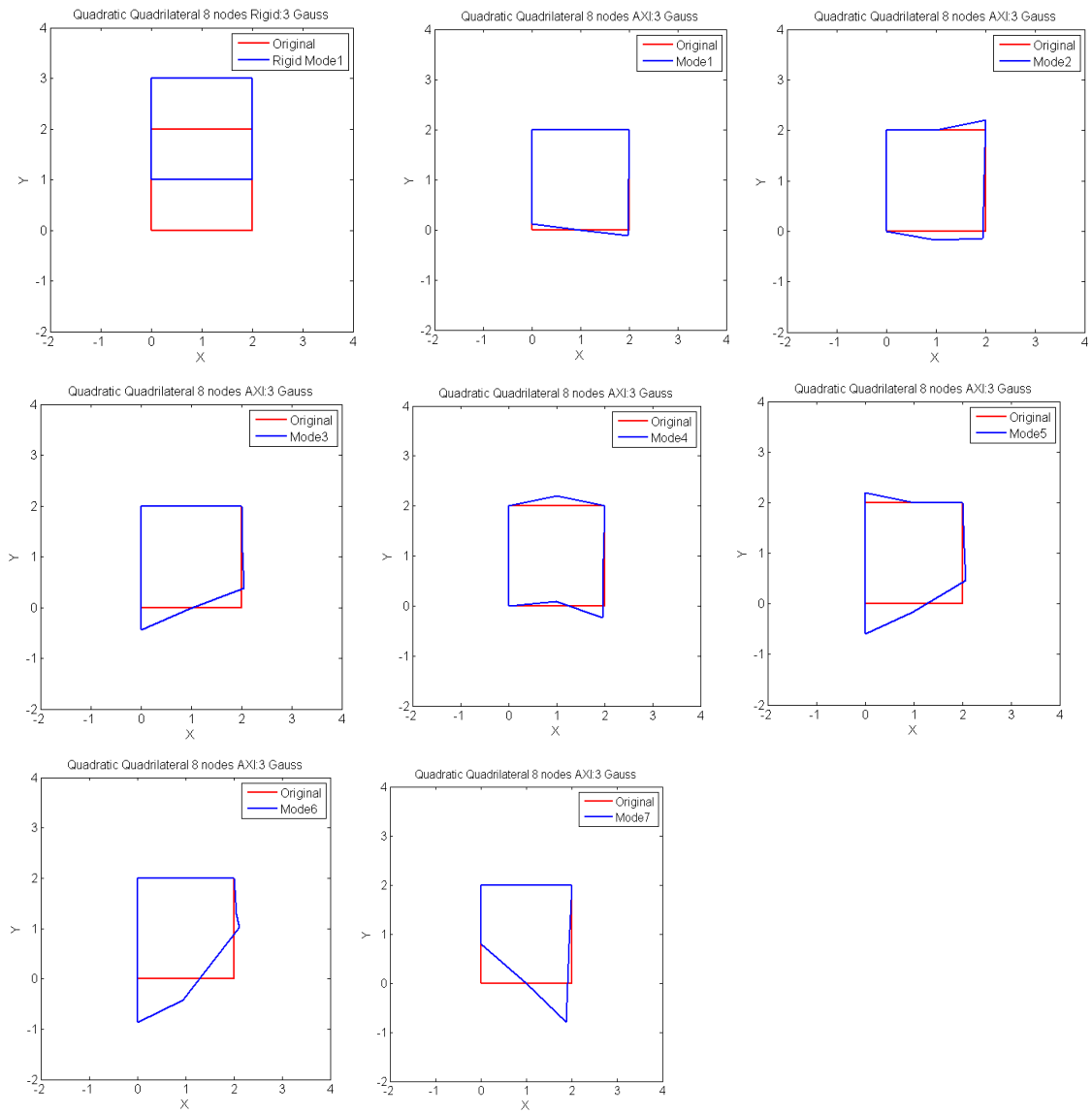


Figure 6.47: Axisymmetric deformation modes for the quadratic quadrilateral element for 3x3 Gauss point.

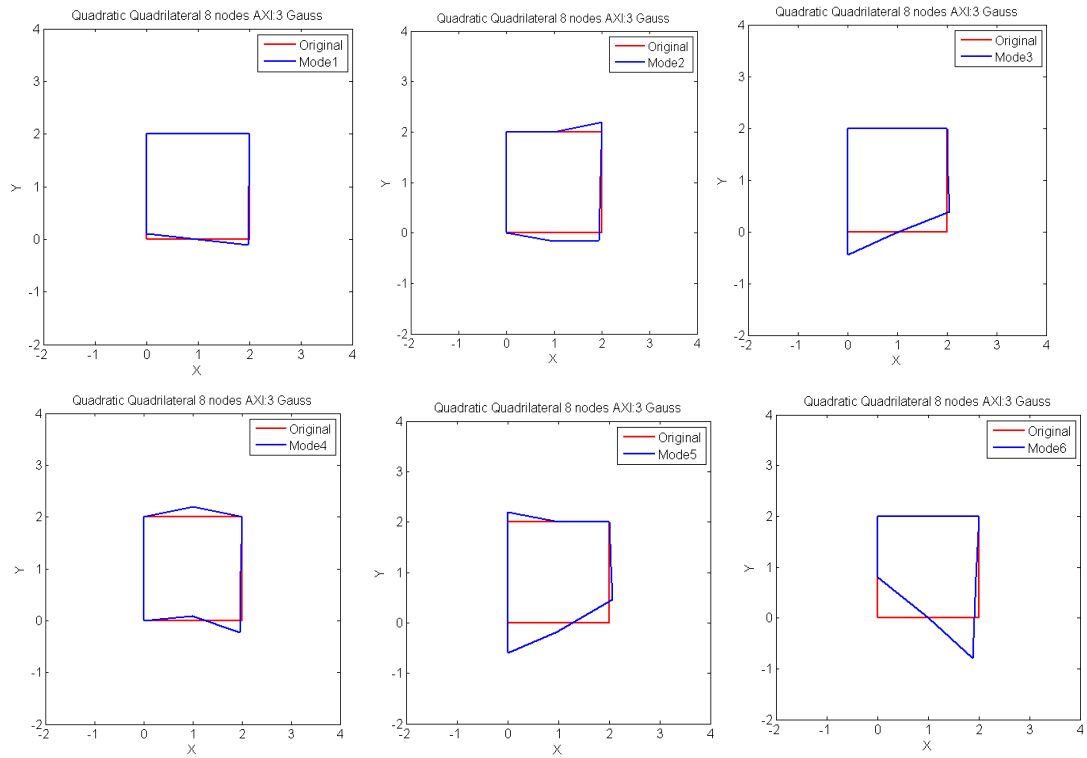


Figure 6.48: Axisymmetric deformation modes for the quadratic quadrilateral element for 3x3 Gauss point.

The Figure 6.49 show the deformation modes for the 4x4 Gauss points. In this this case six deformation modes were obtained, including the rigid body mode.

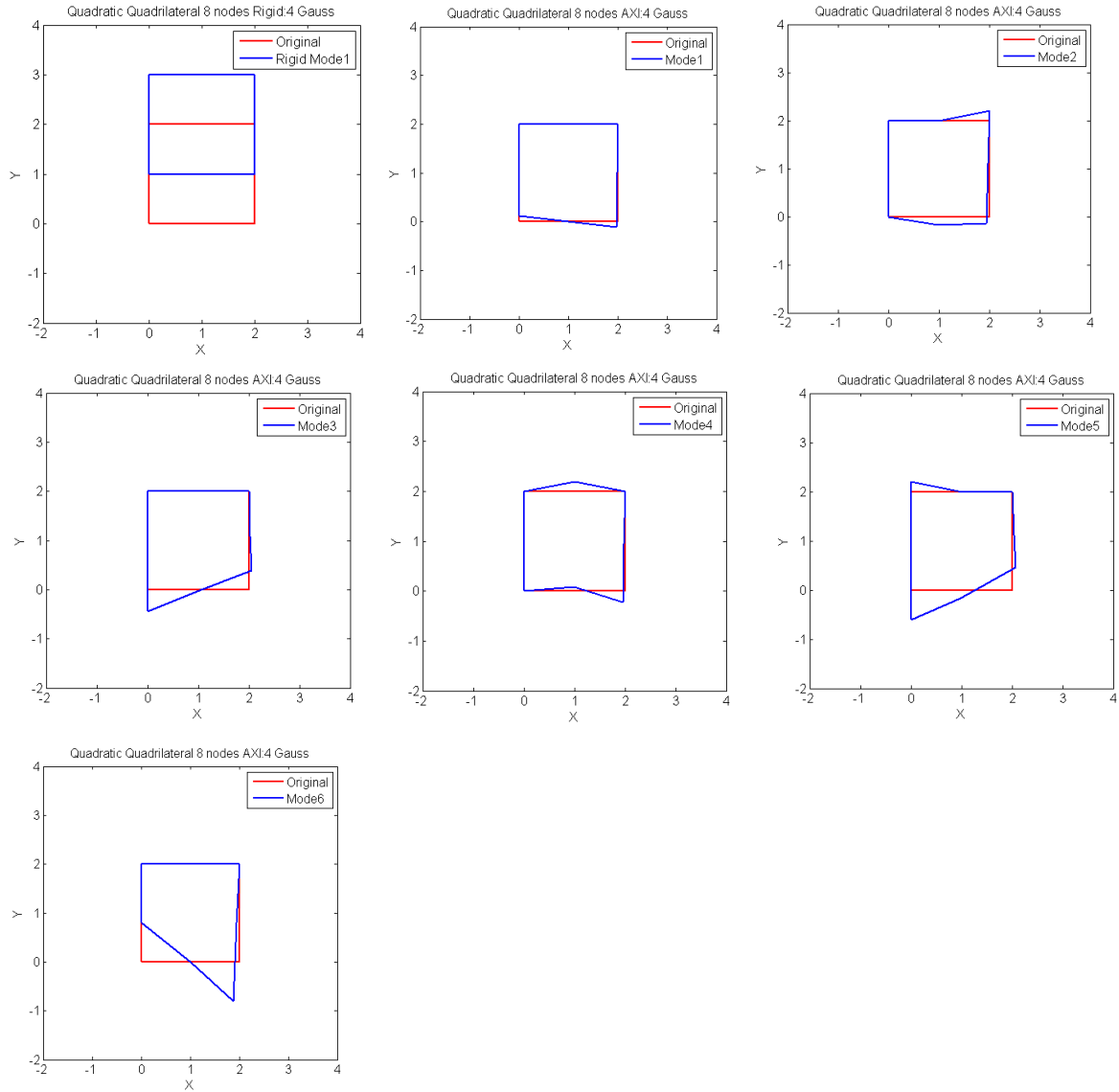


Figure 6.49: Axisymmetric deformation modes for the quadratic quadrilateral element for 4x4 Gauss point.

- **Plunger Compression Test**

In this section a simple compression model was tested. A rectangular domain was considered. The material within the rectangle can only flow out through the right side. Furthermore, on top and on the bottom sides, stick conditions are prescribed, whereas the left side represents the symmetry-axis. The scheme of the testing is presented in Figure 6.50. Structured meshes of triangular and quadrilateral elements were constructed by partitioning the domain into different elements, Figure 6.51. The height of the domain is equal to 10cm.

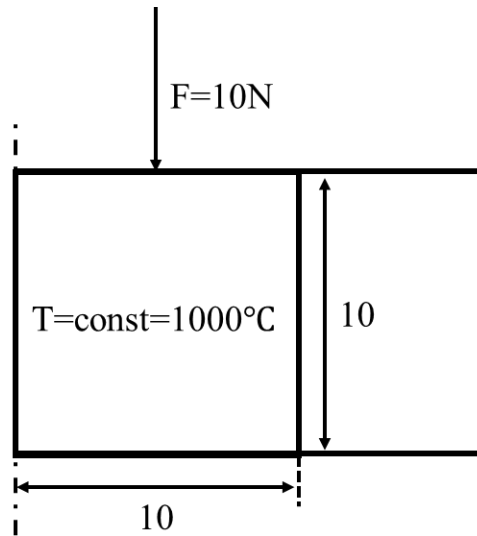


Figure 6.50: Scheme for the compression test.

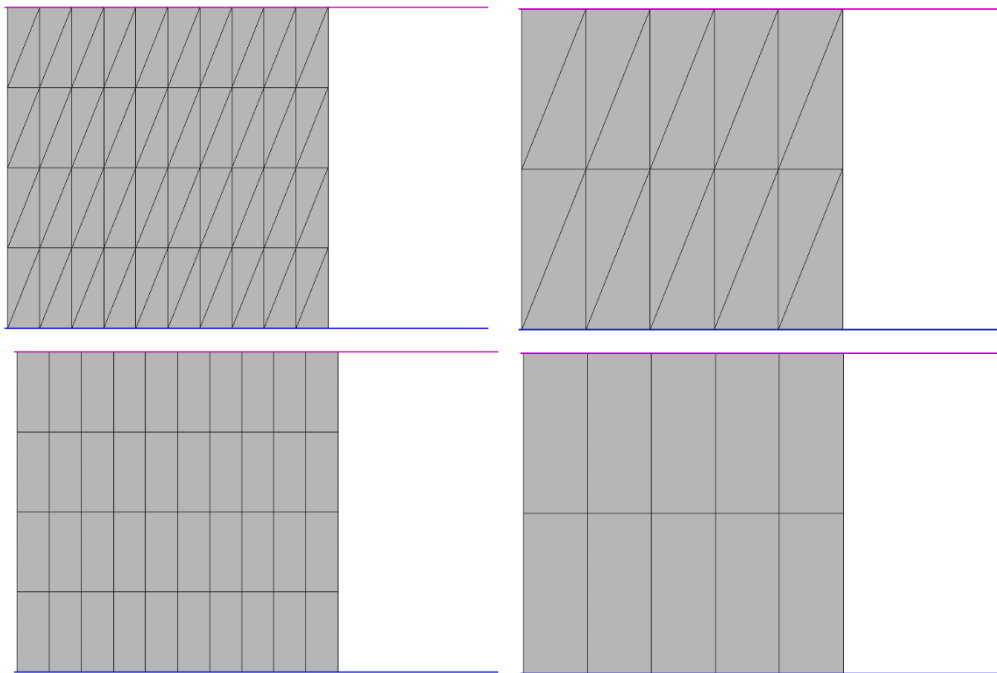


Figure 6.51: Mesh used for compression test a) Linear triangular elements b) Quadratic triangular elements c) linear quadrilateral elements d) Quadratic quadrilateral elements.

The results of the compression test with displacement/time are presented in Figure 6.52. The selective reduce integrations cases are referred as RI. It can be seen that the linear elements show a locking behaviour if full integration is used and that it can be prevented resorting to selective reduce integration. Quadratic elements do not show locking evidence.

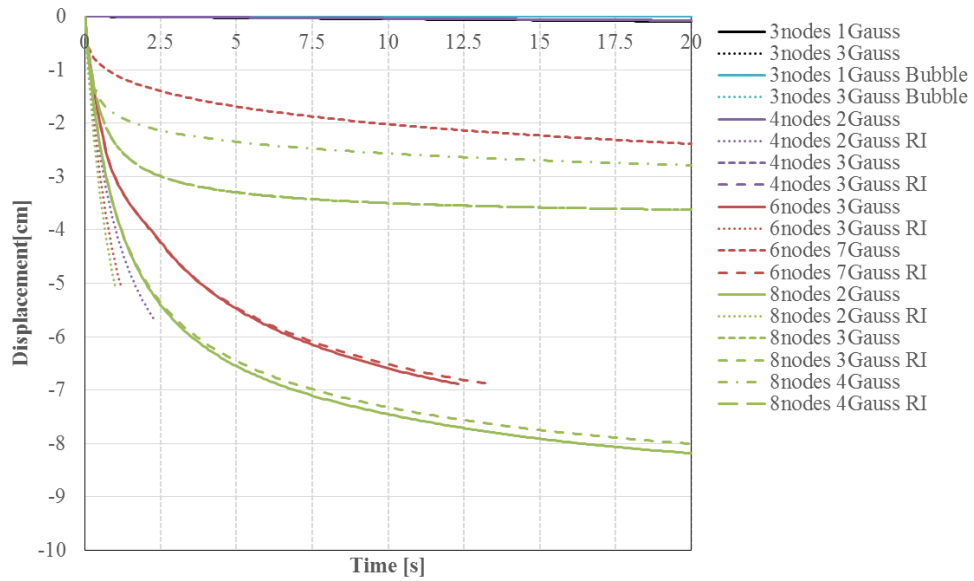


Figure 6.52: Displacement results for the compression test for the different elements type.

- Pressure Compression Test

An important case, not reported anywhere, as far as we know, must be taken when dealing with these axisymmetric selective reduced integrated elements when pressure loads are applied, especially near the symmetry axis.

The problem is illustrated in the following example, representing a cylinder of an incompressible material (glass at high temperature) with an applied pressure. An axisymmetric linear quadrilateral element is used, as in Figure 6.53. Any movement should be prevented due to the imposed boundary conditions and to the fact that the material is incompressible. However, if the correct full integration is used along the boundary where the pressure is applied, two different nodal force values will be obtained: a bigger value for the outer node and a smaller value for the inner node. This may activate the deformation mode, as in Figure 6.54a), that exists in the underlying subspace of incompressible modes associated to this element, which is not physically acceptable. To alleviate this problem a simple solution is to evaluate the nodal forces using also a reduced integration technique for integrate the loads and recover the physical solution, as shown in Figure 6.54b).

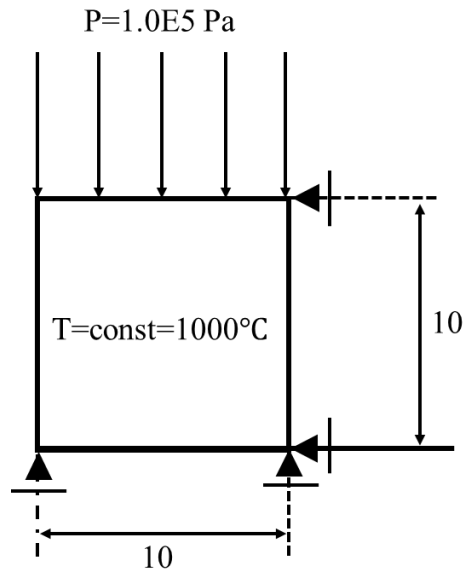


Figure 6.53: Scheme to validate the prescribed temperature at the boundary cylinder.

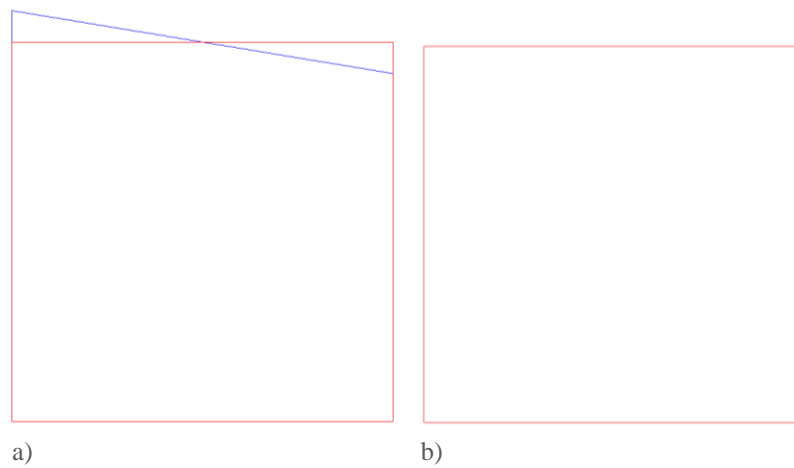


Figure 6.54: a) Pressure teste for one linear quadrilateral element using two Gauss points to integrate the force b) using one Gauss point to integrate the force.

After the thermal and mechanical analyses performed, the linear quadrilateral element with selective reduced integration (one Gauss point) for the incompressibility term was mostly adopted, as it was considered the most balanced element, both in controlling artificial inner heating effects as well as the possible locking effects associated with the incompressible law of glass at high temperatures.

CHAPTER 7

7 Computer Program

The finite element method has become an essential analysis tool in many industries as a result of the increase in computer power and the breakthrough in numerical computation technologies. The method has increased in both reputation and performance with the development of user-friendly pre and postprocessing software. Effective use of the method was enhanced with the introduction of low cost computer graphics systems that brought both the possibility of visually displaying both the model and the computed results [42].

The requirement for a software environment to provide an integrated computational tool to support engineering design and manufacture is ever growing at the industry level. A key component of an integrated environment is the use of computational engineering to assist and support solutions for complex design [42]. In a software package the analysis must be accompanied by preprocessor and postprocessor tools [43].

In this direction a preprocessing and postprocessing which was developed to support the present work is described here.

7.1 Software environment

In order to design the software environment several technical requirements have been considered. These requirements are as follows: graphic engine, data structure, input and output phases.

7.1.1 Graphic Engine

The graphical software packages include slices (sectioning), hidden lines, present or removed, views from various directions, windowing, zoom, and perspectives. The graphic engine is developed by a set of graphical features. Geometry and results in this work have been drawn and visualized using customized GID software.

7.1.2 Preprocessor

In finite element preprocessing, the geometric model are the basis for defining a finite element mesh. The main objective of the geometric model is to display geometry objects. This allows an interaction control

over details, such as point of view, appearance of surfaces and lines, etc. The software used should handle any number of objects and control over them [42].

The finite element preprocessing defines the types of meshing algorithms that can be used, the type of elements that can be selected the resulting mesh density, the quality of the mesh and the feasibility of creating a finite element mesh. The geometric model can be used to associate the mesh with the physical attributes such as material properties, element properties, boundary conditions and loads. When the mesh is modified these attributes are assigned to the geometry and remain constant. This implies that a direct correspondence between the geometry and the mesh must be maintained. As soon as the geometry model is correctly defined it can be discretized to create finite elements that contains the appropriate type of elements required for the specific analysis. This process is known as mesh generation [42].

In Figure 7.1 a view of the preprocessor menu and appearance is depicted. The title bar indicates the name of the model database. The menu bar contains all the available menus; the menus give access to all the functionality in the product. Different menus appear in the menu bar depending on which module you selected from the context bar. The toolbar provides quick access to items that are also available in the menus. The Model Tree provides you with a graphical overview of your model and the objects that it contains, such as parts, materials, steps, loads, and output requests. The toolbox area displays tools in the toolbox that are appropriate for that module. The toolbox allows quick access of the module functions that are also available from the menu bar. Viewports are windows to displays your model. The command line interface is used to make an action when a task is applied.

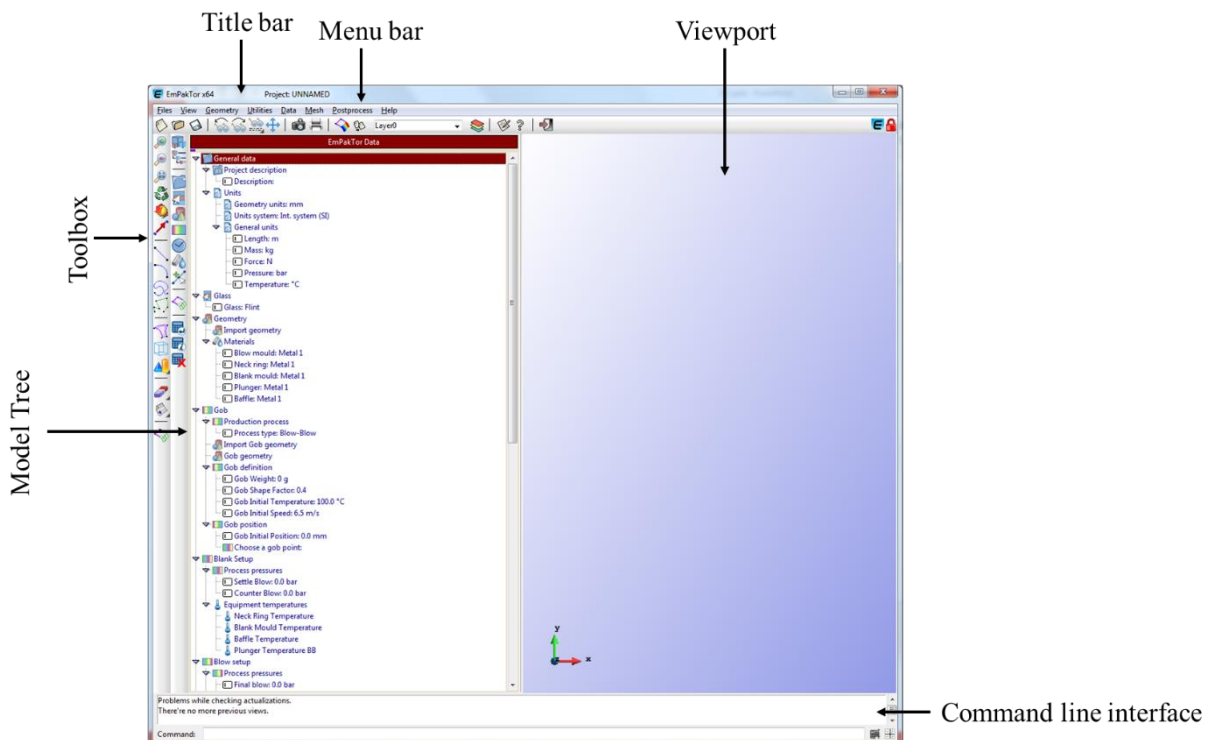


Figure 7.1: Layout of the preprocessor.

The preprocessor is used to define the element types, material properties, initial conditions, gob shape, the mould shape, machining parameters, process parameters. The boundary conditions and loads are calculated automatically by the software, Figure 7.2. The geometries of the moulds are essential as an input for the simulation.

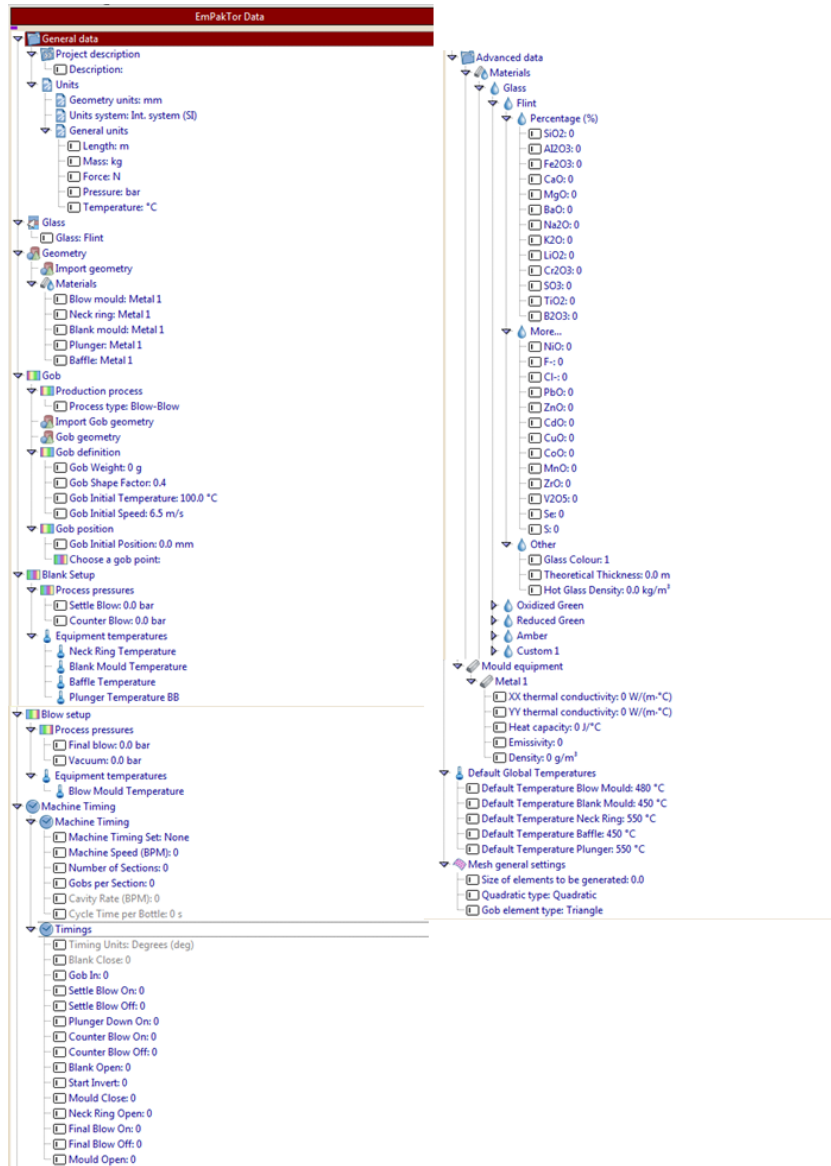


Figure 7.2: Option to model the simulation.

7.1.3 Postprocessor

Postprocessing is designed into two distinct categories; graphical postprocessing and postprocessing text files, both forms are extremely useful in interpreting the results of finite element analysis. The combined option makes the finite element analysis more productive. The graphical postprocessing allows to quickly assess the behaviour of the model. The postprocessing text files provides detailed numerical data necessary to fully understand the results of finite element analysis [42].

The software developed produces lists and tables of many types of results that are normally displayed on the screen. However, it is possible to save the results to a file to be later analysed or included in a report.

The general postprocessor is used to review results over the entire model. Using the postprocessor contour displays the results to review and interpret the results. It is able to display temperatures and displacements contours. In Figure 7.3 and Figure 7.4 it can be seen the overview of the postprocessor software. Also, the software is able to create a movie of the simulation. At the end of the simulation a thickness distribution is generated, Figure 7.5.

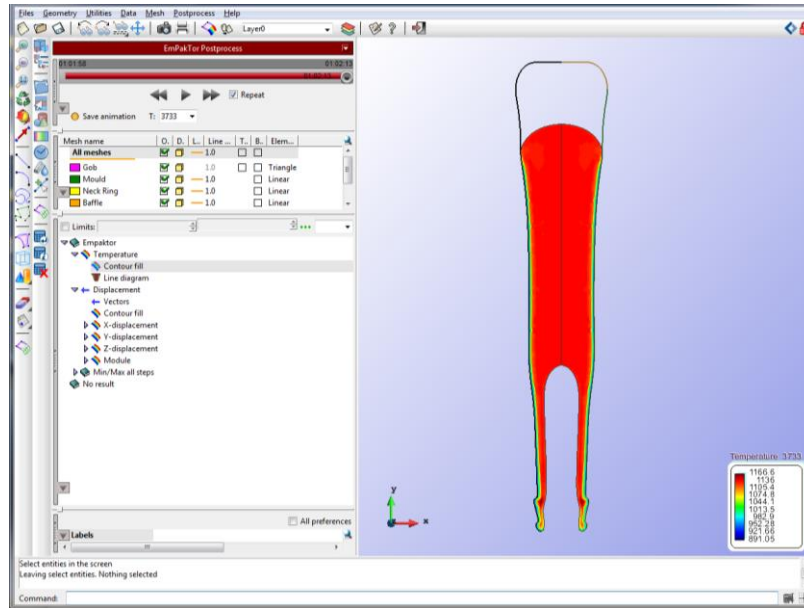


Figure 7.3: Software postprocessor overview.

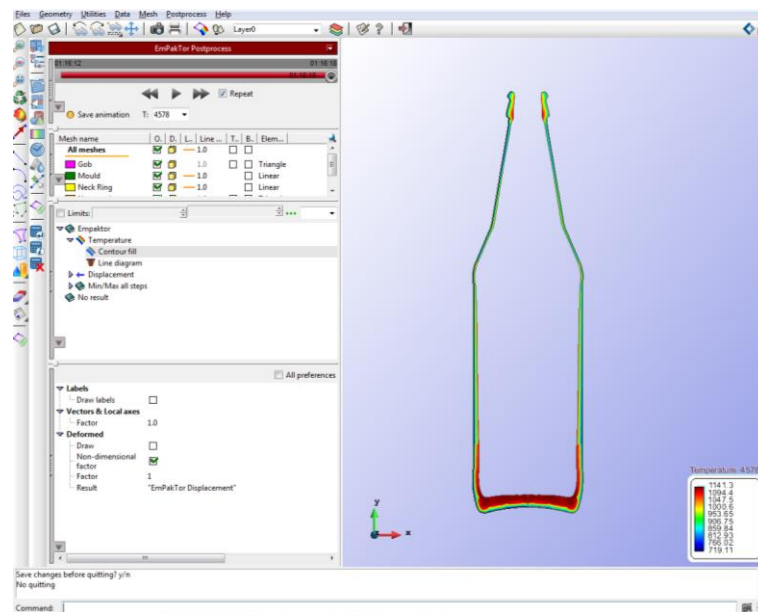


Figure 7.4: Software postprocessor.

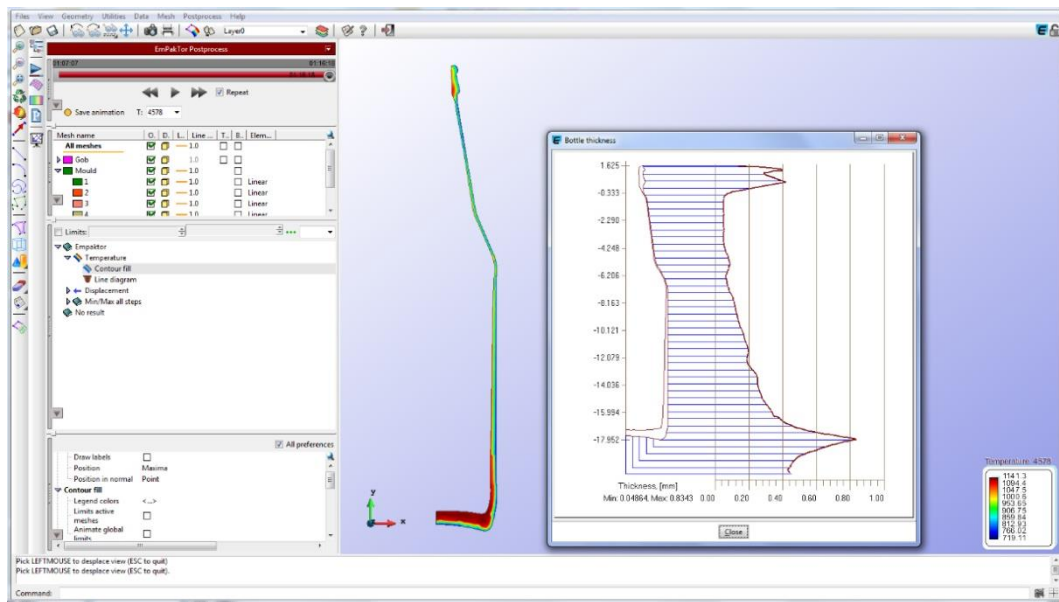


Figure 7.5: Software postprocessor thickness distribution.

7.2 Software Core

The software is composed by two main executable files. These two executable files perform different tasks. Meshing and remeshing, that must be performed periodically due to high deformation present in the glass forming is deal automatically by an executable file, the *preflow* file. The second executable file, called *flow*, performs the finite element calculation.

Figure 7.6 show the layout of the software. When the user creates a model and runs the simulation, the preprocessor interface creates a file (*.epk) that contains the user model. Then the model is loaded by the *preflow* which reads the data creates the first mesh. When *preflow* is ready, it passes the first calculation input for *flow*. At that point the calculation is done. When the mesh is too distorted *flow* writes the results and an update file and transfers the data to *preflow* to deal it. At this point a cycle is performed at the point the simulations ends.

The programing language used to write the software was FORTRAN

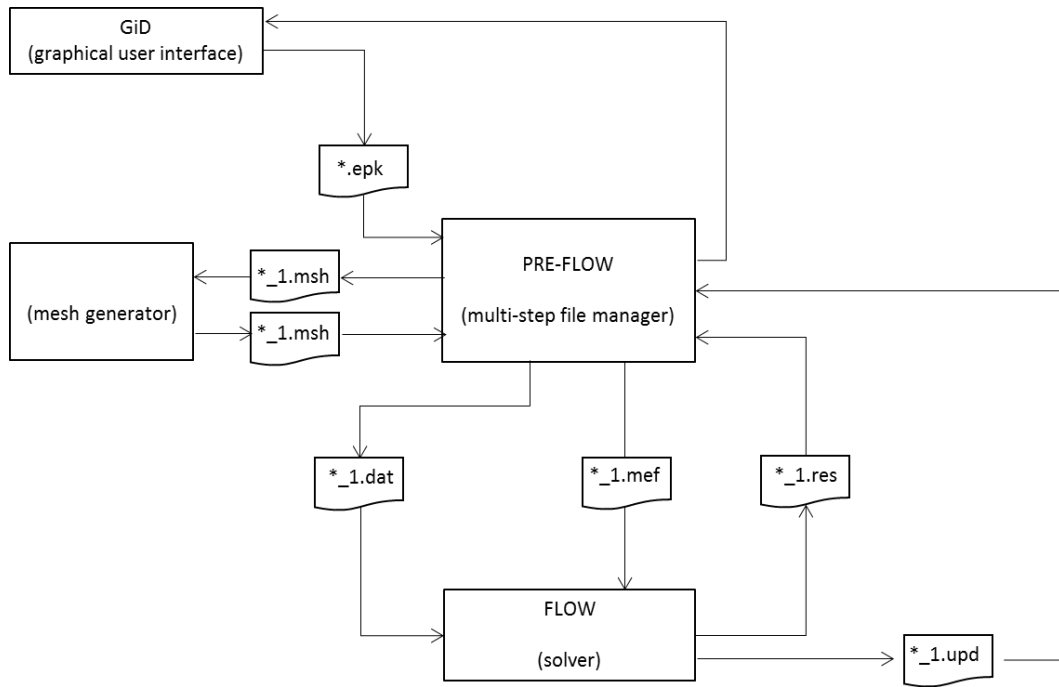


Figure 7.6: Software core diagram.

7.3 Computer Program Files

Software allows a "check run" that stops of solving global equations or even generating them. The check run applies automatic data checks and may also estimate storage requirements and solution time that will be required by the actual analysis.

When a simulation starts texts (ASCII) files are created. This files are needed to share information between the software and the remeshing tool and also gives information to the user (result, warning, error, debugging files, etc). The software have a restart function that restart the simulation from a desirable process stage and a file is also created. The Table 4 presents the files generated by the software.

Type of file	File extension	Description
Input model data	*.dat	Finite element model data
Input simulation file	*.mef	Input file for several solutions during the simulation
Result File	*.res	Result file for several solutions during the simulation
Warning File	*.war	Save warnings during simulation
Error File	*.err	Save the error description
Restart File	*.res	Restart the simulation from a previous stage
Remeshing File	*.msh	File containing a mesh from a remeshing tool
Update File	*.upd	File containing data at the end of the simulation
Mesh Information	*.post.msh	File contain mesh coordinates and connectivity
Information file	*.info	Information data during the simulation
Logging file	*.log	Information registry during the simulation

Table 7.1: Files created during the simulation.

7.3.1 Input File

The input file developed contains all information about the problem to be analysed such as control information (type of analysis, etc.), material properties, mesh (element types, nodal coordinates, connectivities), applied force and heat flux data, boundary conditions (e.g., prescribed flux, displacement restrictions), initial conditions and the parameters of the solver as well as various control parameters required in the finite element analysis. The result is an input file which is used then by the computational program, Figure 7.7.

```

general_data
!Title
!IPROC (1->BB; 2->PB)
!UNITS (1->Metrics; 2->Imperial)
!Number of Nodes
!Number of Elements
!Element size (m)
!Geometry unit
bb_sample_1
1
1
1677
836
5.0
mm
end general_data
nodes
!NodeID X-coord (m) Y-coord (m)
1 0.00912 0.01853
2 0.00912 0.01853
3 0.00912 0.018105
(...)
end nodes
elements
!ElementID PartID MatID NNodes Node1 Node2 ~ No
!Gob
!Plunger
540 2 6 3 2 4 3
541 2 6 3 103 100 102
542 2 6 3 100 97 99
(...)
!Blank mould
559 3 6 3 1092 1085 1088
560 3 6 3 1085 1079 1082
561 3 6 3 1079 1073 1076
(...)
!Baffle
781 5 6 3 1152 1150 1151
782 5 6 3 1150 1148 1149
783 5 6 3 1148 1146 1147
(...)
!Blow mould
1 6 6 3 1596 1594 1595
2 6 6 3 114 118 116
3 6 6 3 118 122 120
(...)
end elements

materials_props_glass
!MaterialID Colour Thickness Hot Glass Density
!Composition (26 values)
1 1 0.0025 2430
71.742 1.771 0.051 10.198 2.402 0.015
12.841 0.578 0.001 0.001 0.316
0.023 0 0.001 0.008 0.027
0.009 0.003 0 0 0
0.012 0 0 0.002 0
end materials_props_glass
materials_props_mould
!MaterialID XX_thermal_conductivity YY_thermal_conductivity Heat_capacity Emissivity
2 0 0 0 0 0
end materials_props_mould
bc_temperature
!NodeID Temperature (°C)
!Plunger
2 -550
3 -550
4 -550
(...)
!Blank Mould
113 -450
115 -450
117 -450
(...)
!Neck
1 -550
5 -550
8 -550
(...)
!Blow Mould
114 -480
116 -480
118 -480
(...)
end bc_temperature

```

```

process_conditions
!Gob Weight (Kg)
!Gob Shape Factor
!Initial Gob Temperature (°C)
!Initial Gob Velocity (m/s)
!Settle Blow Pressure (Pa)
!Counter Blow Pressure (Pa)
!Final Blow Pressure (Pa)
!Vacuum (Pa)
0.400
0.4
1135
6.5
250000
250000
250000
-150000
end process_conditions

machine_timings
!Machine Speed (BPM)
!Number of Sections
!Gobs per Section
!Cavity Rate
!Cycle Time per Bottle (s)
!Timing Units
!Blank Close
!Gob In
!Settle Blow On
!Settle Blow Off
!Plunger Down On
!Counter Blow On
!Counter Blow Off
!Blank Open
!Start Invert
!Mould Close
!Neck Ring Open
!Final Blow On
!Final Blow Off
!Mould Open
360
10
3
12
5
deg
0
22
55
78
83
108
215
225
265
305
325
40
160
165
end machine_timings

```

Figure 7.7: Input file example. (Cont.)

7.3.2 Result File

After running the program successfully, a second file (output file) which contains the simulation results is generated. Furthermore, a file (postscript file) is also generated so that the user can view the contour plots graphically. The program also produces an output file that is intended to be an input file for a postprocessor. The contents and structure of this file are shown in Figure 7.8.

```

GiD Post Results File 1.0
Result "Temperature" "FLOW" 0 Scalar OnNodes
Values
  1 0.1000000E+04
  2 0.1000000E+04
  3 0.1000000E+04
(...)
End Values
Result "Displacement" "FLOW" 0 Vector OnNodes
ComponentNames "X-Displacement", "Y-Displacement", "Z-Displacement"
Values
  1 0.0000000E+00 0.0000000E+00 0.0000000E+00
  2 0.0000000E+00 0.0000000E+00 0.0000000E+00
  3 0.0000000E+00 0.0000000E+00 0.0000000E+00
(...)
End Values

```

Figure 7.8: Example of the results file.

7.3.3 Warning File

Listing of all warning messages

7.3.4 Error File

The error file list all error messages that can occur during the simulation. This file is generated during the simulation. The error encountered may stop the simulation. The file contains the complete database at the time of its creation.

7.3.5 Restart File

During a solution a restart file is saved containing the current solution data in a file. A restart file is always created when a process stage is successful completed. When the restart file is called the finite element analysis is restarted from the position where the restart file was created.

7.3.6 Remeshing Files

The remeshing files are a set of files necessary to perform the remeshing. These set of files are the input files from the remeshing tool and the output. The input data are the boundary consisting of the coordinates, connectivity and parameter from the remeshing tool. The output is a file containing the new mesh.

7.3.7 Update File

The update file includes the information that connects the solver and a data management file. This information is mostly on the actual displacements and temperatures at the end of each calculation, Figure 7.9.

```
100      1      0
1.0000000000000000
15
1  0.3581762498844077E-01  0.6799206898570276E+00  0.0000000000000000E+00  0.0000000000000000E+00  0.0000000000000000E+00  0.0000000000000000E+00  0.9999999999999999E+03  0.
2  0.2148845085200541E+00  0.6799015874537453E+00  0.0000000000000000E+00  0.0000000000000000E+00  0.0000000000000000E+00  0.0000000000000000E+00  0.9999999999999999E+03  0.
3  0.39399500855430413E+00  0.6798977111396756E+00  0.0000000000000000E+00  0.0000000000000000E+00  0.0000000000000000E+00  0.0000000000000000E+00  0.9999999999999999E+03  0.
(...)
```

Figure 7.9: Example of the update file.

7.3.8 List File

The list file is created in order to write the information during a simulation. The file is helpful for debugging while performing the calculation or even when an error was encountered. Figure 7.10 shows an example. It can be seen that besides the simulation data the file contains the convergence ranges for each step and other numerical information, errors, etc.

Chapter 7 Computer Program

```

HEAT CONDUCTION ONLY - F

NPOIN = 15   NELEM = 16   NNODE = 3   NMATS = 1   NGAUH = 3
NGAUC = 3   NTYPE = 1   ITOUT = 0   NALGO = 1   NSHEM = 3
LSTEP = 1   NCCORR = 0   ISTAT = 0   NMPOI = 0   NMELE = 0
IFSLIP = 0   GOBLOAD = 0

ELEMEN  PROPERTY
1 1 1 1 5 4
2 1 1 1 2 5
3 1 1 2 3 6
(...)
      NODE  X-COORD  Y-COORD      NODE  X-COORD  Y-COORD
      1  1.000000  -10.000000      9  11.000000  0.000000
      2  6.000000  -10.000000     10  1.000000  5.000000
      3  11.000000 -10.000000     11  6.000000  5.000000
(...)

HEAT TRANSFER PROPERTIES (erg/cm3/ C-erg/cm/s/ C)
0 NO. OF THERMAL VARIABLES PER ELEMENT = 3

THERMAL ELEMENT PROPERTIES :
0 MATERIAL  X-CONDUCTIVITY  Y-CONDUCTIVITY  HEAT CAPACITY  HEAT-GEN.RATE
1 0.100452E+06  0.100452E+06  0.278001E+08  0.000000E+00
NLIN.PAR. AX= 0.000000E+00 AY= 0.000000E+00 AC= 0.000000E+00

0 HTC AIR      HTC PLUNGER  HTC BLANK MOULD  HTC NECK RING  HTC BAFFLE  HTC BLOW MOULD  HTC BLOW MOULD
100000.00  100000.00  1000000.00  1000000.00  1000000.00  1000000.00  1000000.00

0 TEMPERATURE (C)  DENSITY (G/CM3)  VISCOSITY (LOG(u))  SPECIFIC HEAT (ERG/CM2.K)  THERMAL CONDUCTIVITY (ERG/CM.K)  ALTERNATIVE VISCOSITY
340.00  2.451954  68.468598  20423480.504702  557060.003281  53.817610
350.00  2.450421  59.261083  20637064.190412  614739.990234  47.636399
400.00  2.442757  35.565226  21704982.618963  675199.985504  29.993389
(...)

PRESCRIBED INITIAL TEMPERATURES :
KIPIE = 0  NUSIT = 15

      NODE  TEMPERATURE
      1  1000.00000
      2  1000.00000
      3  1000.00000

BOUNDARY CONDITIONS :
0 NO. OF BOUNDARY POINTS-TYPE (A) = 0
0
NO. OF NODAL APPLIED "LOADS" = 0
NGAUF = 3  NVFIX = 1  NINTG = 1  LOUP = 0

      NODE  CODE  PRESCRIBED VALUES
      7  0  0.00000  0.00000

      1  AVALU 1.5220E+00  BVALU 4.3500E+03  THICK 1.0000E+00  DENSE 2.5000E+00  PENIC 1.0000E+08  TZERO 2.2600E+02

      DTIME = 0.01000  TTIME = 0.000000THEND = 1.00000  NCHAN = 2
STEP NUMBERS WHERE THE PRESSURE CHANGES:
1 2
PRESSURE FACTORS :
0.00000 50.00000
0 CONVERGENCE TOLERANCE = 0.01000  MAX.NO. OF TIME STEPS = 9999  FREQ.OUTP.PAR.= 1
0 TOLIT = 0.01000000  MTERM = 20

*** ISTEP = 1***
0 ITERATION NO.= 1  ICHEK = 0  RATIT = 0.000000E+00  RTLOD = 0.192143E-13

TOTAL TIME = 0.100000E-01
0 POINT = 1  MAX.THERMAL RATE = 0.000000E+00  POINT = 1  MIN.THERMAL RATE = 0.000000E+00

.....

INTERNAL PRESSURE & GRAVITY LOADING

IFLOD = 0  IGRAV = 0  IEDGE = 1
0 NO. OF LOADED EDGES = 4
0 LIST OF LOADED EDGES AND APPLIED LOADS
1
1 1 4
-10000.000  0.000  -10000.000  0.000
5
4 7
-10000.000  0.000  -10000.000  0.000
(...)

*** ITERATION NUMBER (FL) 1 ***
CONV. CODE= 0  MAX.DIVER. = 0.000E+00  VELO. RATIO= NaN

*** ISTEP = 2***
0 ITERATION NO.= 1  ICHEK = 0  RATIT = 0.000000E+00  RTLOD = 0.130991E-13

```

Figure 7.10: Example of the list file.

CHAPTER 8

8 Glass Containers Simulation Cases

In this chapter real forming operations were modelled, using, real values for the various physical parameters.

Two different forming processes of glass containers were used, namely blow/blow and press/blow processes. Five different cases of blow/blow process and eight in press/blow processes were performed. Each case and the respective description is shown in the Table 8.1.

Process	Case	Description
	Case 1	Kingfisher650ml
	Case 2	Bacardi
	Case 3	Ardagh750ml
	Case 4	Senzo750ml
	Case 5	Wine bottle750ml
	Case 1	NNPB
	Case 2	Ambev343ml
	Case 3	Malta7oz
	Case 4	Parkam
	Case 5	Sgbeer
	Case 6	Gallipot
	Case 7	Fruitz
	Case 8	President650ml

Table 8.1: Simulation cases for the blow/blow and press/blow process.

Usually to choose the process to produce a glass bottle or other container several indicators have to be accounted for. One of the indicators is the size of the container. For a small container in size the narrow neck press/blow process (NNPB) is the advisable. On other hand, blow/blow processes are a preferable choice for big containers, Figure 8.1.

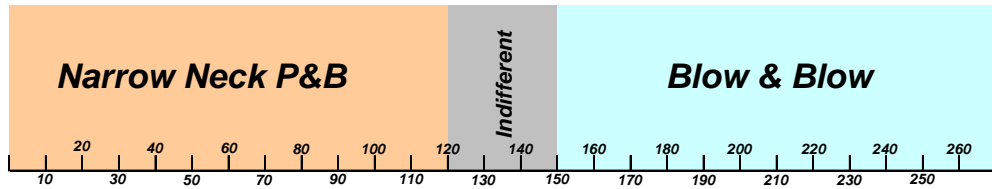


Figure 8.1: Process selection for container height (cm).

To start the simulations a gob has to be created. As discussed in the section 3.4.1 the gob can have different shapes. These shapes can be drawn at the graphical interface. However, the gob is usually very similar to a cylindrical shape, thus, the software can create the gob using the mass of glass and some parameters to define the shape of the cylinder, Figure 8.2.

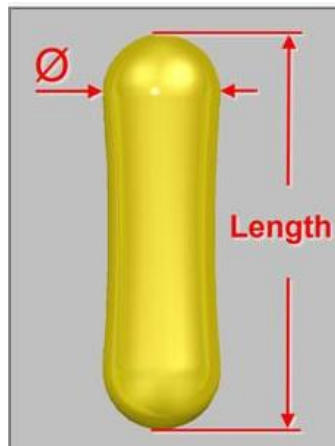


Figure 8.2: Gob shape calculation.

The diameter of the cylinder is calculated by,

$$\phi(mm) = 10 \left(\frac{Weight(g) \times Gobshapefactor}{\pi} \right)^{\frac{1}{3}} - 25.4 \left(\frac{5}{16} \right) \quad 8.1$$

and the length,

$$Lenght(mm) = \phi + \frac{\left(\left(\frac{Weight(mm)}{Density(g / mm^3)} \right) - \left(\frac{\pi \cdot \phi^3}{6} \right) \right)}{\frac{\pi \times \phi^2}{4}} \quad 8.2$$

The several simulations reported were performed using the parameters of the Table 8.2. . These parameters may be given or altered by the user. Those parameters comprise the gob definition, the process air pressures, the equipment temperatures, the machine timings and the material parameters.

		Case 1	Case 2	Case 3	Case 4	Case 5
Gob Definition	Gob Weight [Kg]	0.415	0.450	0.400		0.580
	Gob Shape Factor	0.4	0.4	0.4	0.4	0.4
	Gob Initial Temp [°C]	1135	1070	1150	1132	1140
	Gob Initial Speed [m/s]	6.5	6.5	6.5	6.5	6.5
	Gob Initial Position [mm]	6.5	6.5	6.5	6.5	6.5
Process Pressures [bar]	Settle Blow	2.5	2.8	2.8	2.5	2.4
	Counter Blow	2.5	2.5	2.5	2.5	2.2
	Final Blow	2.5	2.0	2.0	2.00	1.2
	Vacuum	0.5	0.6	0.6	0.00	0.5
Equipment Temperatures [°C]	NeckRing	550	550	420	450	420
	Blank Mould	450	450	470	450	465
	Baffle	450	450	450	450	450
	Plunger	550	450	550	550	500
	Blow Mould	480	450	480	480	480
Machining Timming	Machine Speed [BPM]	360	120	136	22	170
	Number of Sections	10	8	8	6	12
	Gobs per Section	3	2	2	1	2
	Cavity Rate	12.0	7.5	8.5	3.7	7.1
	Cycle Time per Bottle [s]	5.00	8.00	7.06	16.36	8.47
Material	Glass Color	Flint	Flint	Flint	Flint	Flint
	Theoretical Thickness [mm]	1.0	2.5	2.5	5.0	3.5
	Hot Glass Density [Kg/m3]	2730	2450	2430	2430	2430

		Case 1	Case 2	Case 3	Case 4	Case 5	Case 6	Case 7	Case 8
Gob Definition	Gob Weight [Kg]	0.170	0.180	0.136	0.152	0.189	0.285	0.200	0.200
	Gob Shape Factor	0.6	0.6	0.6	0.6	0.55	0.6	0.7	0.6
	Gob Initial Temp [°C]	1170	1170	1162	1185	1190	1153	1151	1139
	Gob Initial Speed [m/s]	6.5	6.5	7.0	6.5	6.5	6.5	6.5	6.5
	Gob Initial Position	-10	-10	-10	-10	-10	-10	-10	-10
Process Pressures	Final Blow [bar]	2.5	2.0	1.5	2.4	1	2.5	2.5	2.5
	Vacuum [bar]	0.5	0.5	0.5	0.5	0.0	0.5	0.0	0.5
	Plunger Force [N]	400	400	400	400	350	900	900	900
Equipment Temperatures [°C]	NeckRing	550	420	450	410	420	550	400	400
	Blank Mould	450	450	470	450	470	450	460	450
	Baffle	450	450	450	410	450	450	460	450
	Plunger	500	550	500	410	550	550	450	480
	Blow Mould	450	480	480	475	480	480	480	480
Machining Timming	Machine Speed [BPM]	450	326	375	576	288	203	195	142
	Number of Sections	12	10	10	16	12	8	8	8
	Gobs per Section	3	3	3	3	2	2	2	2
	Cavity Rate	12.5	10.9	12.5	12.0	12.0	12.7	12.19	8.87
	Cycle Time per Bottle [s]	4.80	5.52	4.80	5.00	5.00	4.73	4.92	6.76
Material	Glass Color	Flint	Flint	Flint	Flint	Flint	Flint	Oxidized Green	Amber
	Theoretical Thickness [mm]	1.0	1.0	2.5	1.0	2.0	1.0	1	2.5
	Hot Glass Density [Kg/m3]	2430	2430	2430	2500	2430	2430	2387	2430

Table 8.2: Simulation variables for blow/blow (left) and press/blow (right) processes.

In Table 8.3 and Table 8.4 the machine timing is shown for the cases of the blow/blow process and press/blow process. The machine timing is measured in degrees as it is usual in the shop floor. Such measure can be difficult to understand but, the machine timing may be converted into seconds so that it can be used in the simulation. The cycle time is calculated as:

$$\text{Cycle Time [s]} = \text{Number sections} \times \frac{\text{Gob per Section} \times 60}{\text{Machine Speed [BPM]}} \quad 8.3$$

thus, the machine timing is converted to seconds as

$$\text{Machining Timing [s]} = \frac{\text{Machining Timing [deg]} \times \text{Cycle Time [s]}}{360} \quad 8.4$$

Chapter 8 Glass Containers Simulation Cases

Machine Timings				
#	Name	Deg	Initial Time [s]	End Time [s]
1	Blank Close	0	0.000	0.306
2	Gob In	22	0.306	0.764
3	Settle Blow on	55	0.764	1.083
4	Settle Blow off	78	1.083	1.153
5	Plunger Down On	83	1.153	1.500
6	Counter Blow On	108	1.500	2.986
7	Counter Blow Off	215	2.986	3.264
8	Blank Open	235	3.264	3.958
9	Start Invert	285	3.958	4.514
10	Mould Close	325	4.514	4.792
11	Neck Ring Open	345	4.792	5.833
12	Final Blow On	60	5.833	7.222
13	Final Blow Off	160	7.222	7.292
14	Mould Open	165	7.292	

Case 1

Machine Timings				
#	Name	Deg	Initial Time [s]	End Time [s]
1	Blank Close	0	0.000	0.294
2	Gob In	15	0.294	0.490
3	Settle Blow on	25	0.490	0.784
4	Settle Blow off	40	0.784	1.627
5	Plunger Down On	83	1.627	1.863
6	Counter Blow On	95	1.863	3.627
7	Counter Blow Off	185	3.627	3.824
8	Blank Open	195	3.824	4.706
9	Start Invert	240	4.706	5.490
10	Mould Close	280	5.490	5.980
11	Neck Ring Open	305	5.980	7.843
12	Final Blow On	40	7.843	10.196
13	Final Blow Off	160	10.196	10.294
14	Mould Open	165	10.294	

Case 3

Machine Timings				
#	Name	Deg	Initial Time [s]	End Time [s]
1	Blank Close	0	0.000	0.863
2	Gob In	30	0.588	1.381
3	Settle Blow on	48	0.941	2.245
4	Settle Blow off	78	1.529	2.360
5	Plunger Down On	82	1.608	3.281
6	Counter Blow On	114	2.235	5.899
7	Counter Blow Off	205	4.020	6.158
8	Blank Open	214	4.196	7.482
9	Start Invert	260	5.098	8.346
10	Mould Close	290	5.686	9.439
11	Neck Ring Open	328	6.431	1.727
12	Final Blow On	60	8.235	6.417
13	Final Blow Off	223	11.431	7.108
14	Mould Open	247	11.902	10.360

Case 5

Machine Timings				
#	Name	Deg	Initial Time [s]	End Time [s]
1	Blank Close	0	0.000	0.111
2	Gob In	5	0.111	1.667
3	Settle Blow on	75	1.667	2.667
4	Settle Blow off	120	2.667	2.778
5	Plunger Down On	125	2.778	2.889
6	Counter Blow On	130	2.889	4.444
7	Counter Blow Off	200	4.444	5.000
8	Blank Open	225	5.000	5.889
9	Start Invert	265	5.889	7.667
10	Mould Close	345	7.667	7.889
11	Neck Ring Open	355	7.889	8.022
12	Final Blow On	1	8.022	8.067
13	Final Blow Off	3	8.067	11.667
14	Mould Open	165	11.667	16.000

Case 2

Machine Timings				
#	Name	Deg	Initial Time [s]	End Time [s]
1	Blank Close	0	0.000	0.144
2	Gob In	5	0.144	1.007
3	Settle Blow on	35	1.007	1.439
4	Settle Blow off	50	1.439	1.583
5	Plunger Down On	55	1.583	2.590
6	Counter Blow On	90	2.590	4.748
7	Counter Blow Off	165	4.748	5.468
8	Blank Open	190	5.468	6.475
9	Start Invert	225	6.475	7.338
10	Mould Close	255	7.338	7.770
11	Neck Ring Open	270	7.770	9.209
12	Final Blow On	-40	9.209	14.101
13	Final Blow Off	130	14.101	14.245
14	Mould Open	135	14.245	20.720

Case 4

Table 8.3: Machining timing for the blow/blow cases being respectively the case 1, case 2, case 3, case 4 and case 5.

Chapter 8 Glass Containers Simulation Cases

Machine Timings				
#	Name	Deg	Initial Time [s]	End Time
1	Blank Close	0	0.000	0.467
2	Gob In	35	0.467	0.533
3	Baffle On	40	0.533	0.000
4	Remove Plug	0	0.000	0.800
5	Plunger Up	60	0.800	2.000
6	Plunger Down	150	2.000	2.067
7	Blank Open	155	2.067	2.733
8	Start Invert	205	2.733	3.760
9	Mould Close	282	3.760	4.027
10	Neck Ring Open	302	4.027	1.000
11	Final Blow On	75	5.800	7.267
12	Final Blow Off	185	7.267	7.400
13	Mould Open	195	7.400	9.600

Case 1

Machine Timings				
#	Name	Deg	Initial Time [s]	End Time
1	Blank Close	0	0.000	0.067
2	Gob In	5	0.067	0.800
3	Baffle On	60	0.800	0.000
4	Remove Plug	0	0.000	1.147
5	Plunger Up	86	1.147	2.053
6	Plunger Down	154	2.053	2.133
7	Blank Open	160	2.133	3.160
8	Start Invert	237	3.160	3.733
9	Mould Close	280	3.733	4.133
10	Neck Ring Open	310	4.133	5.467
11	Final Blow On	50	5.467	7.467
12	Final Blow Off	200	7.467	7.600
13	Mould Open	210	7.600	9.600

Case 3

Machine Timings				
#	Name	Deg	Initial Time [s]	End Time
1	Blank Close	0	0.000	0.069
2	Gob In	5	0.069	0.625
3	Baffle On	45	0.625	0.000
4	Remove Plug	0	0.000	0.972
5	Plunger Up	70	0.972	2.222
6	Plunger Down	160	2.222	2.361
7	Blank Open	170	2.361	2.847
8	Start Invert	205	2.847	3.819
9	Mould Close	275	3.819	4.361
10	Neck Ring Open	314	4.361	5.694
11	Final Blow On	50	5.694	7.361
12	Final Blow Off	170	7.361	7.847
13	Mould Open	205	7.847	10.000

Case 5

Machine Timings				
#	Name	Deg	Initial Time [s]	End Time
1	Blank Close	0	0.000	0.067
2	Gob In	5	0.077	0.333
3	Baffle On	25	0.383	0.000
4	Remove Plug	0	0.000	0.747
5	Plunger Up	56	0.859	1.667
6	Plunger Down	125	1.917	1.800
7	Blank Open	135	2.070	2.467
8	Start Invert	185	2.837	3.400
9	Mould Close	255	3.910	3.840
10	Neck Ring Open	288	4.416	4.267
11	Final Blow On	-40	4.907	6.627
12	Final Blow Off	137	7.621	7.133
13	Mould Open	175	8.203	9.600

Case 2

Machine Timings				
#	Name	Deg	Initial Time [s]	End Time
1	Blank Close	0	0.000	0.236
2	Gob In	17	0.236	0.556
3	Baffle On	40	0.556	0.000
4	Remove Plug	0	0.000	0.889
5	Plunger Up	64	0.889	1.875
6	Plunger Down	135	1.875	1.944
7	Blank Open	140	1.944	2.778
8	Start Invert	200	2.778	4.194
9	Mould Close	302	4.194	4.375
10	Neck Ring Open	315	4.375	5.972
11	Final Blow On	70	5.972	7.375
12	Final Blow Off	171	7.375	7.750
13	Mould Open	198	7.750	10.000

Case 4

Machine Timings				
#	Name	Deg	Initial Time [s]	End Time
1	Blank Close	0	0.000	0.066
2	Gob In	5	0.066	0.460
3	Baffle On	35	0.460	0.000
4	Remove Plug	0	0.000	0.801
5	Plunger Up	61	0.801	1.997
6	Plunger Down	152	1.997	2.023
7	Blank Open	154	2.023	3.180
8	Start Invert	242	3.180	3.561
9	Mould Close	271	3.561	4.099
10	Neck Ring Open	312	4.099	5.584
11	Final Blow On	65	5.584	7.174
12	Final Blow Off	186	7.174	7.647
13	Mould Open	222	7.647	9.460

Case 6

Machine Timings					Machine Timings				
#	Name	Deg	Initial Time [s]	End Time	#	Name	Deg	Initial Time [s]	End Time
1	Blank Close	0	0.000	0.478	1	Blank Close	0	0.000	0.094
2	Gob In	35	0.478	0.820	2	Gob In	5	0.094	0.488
3	Baffle On	60	0.820	0.000	3	Baffle On	26	0.488	0.000
4	Remove Plug	0	0.000	0.957	4	Remove Plug	0	0.000	1.127
5	Plunger Up	70	0.957	2.050	5	Plunger Up	60	1.127	3.098
6	Plunger Down	150	2.050	2.296	6	Plunger Down	165	3.098	3.192
7	Blank Open	168	2.296	2.870	7	Blank Open	170	3.192	3.943
8	Start Invert	210	2.870	3.485	8	Start Invert	210	3.943	4.788
9	Mould Close	255	3.485	4.032	9	Mould Close	255	4.788	5.539
10	Neck Ring Open	295	4.032	5.057	10	Neck Ring Open	295	5.539	6.854
11	Final Blow On	10	5.057	7.175	11	Final Blow On	5	6.854	9.858
12	Final Blow Off	165	7.175	7.653	12	Final Blow Off	165	9.858	10.516
13	Mould Open	200	7.653	9.840	13	Mould Open	200	10.516	13.520

Case 7

Case 8

Table 8.4: Machining timing for the press/blow cases being respectively the case 1, case 2, case 3, case 4, case 5, case 6, case 7 and case 8.

The air temperature was considered fixed in every stage. However, the air temperature can vary for different stages in the process according the conditions, as shown in, Table 8.5.

Process	Stages	Air Temperature
Blow Blow	Blank Close	45
	Gob In	45
	Settle Blow on	50
	Settle Blow off	350
	Plunger Down On	450
	Counter Blow On	500
	Counter Blow Off	800
	Blank Open	60
	Start Invert	40
	Mould Close	60
	Neck Ring Open	200
	Final Blow On	250
	Final Blow Off	300
	Mould Open	150
	Press Blow	Blank Close
Gob In		45
Baffle On		300
Remove Plug		350
Plunger Up		500
Plunger Down		800
Blank Open		60
Start Invert		40
Mould Close		60
Neck Ring Open		200
Final Blow On		250
Final Blow Off		300
Mould Open		150

Table 8.5: Air temperature considered in the different stages.

The chemical compositions of the glass for the different cases are presented in the Table 8.6. The material properties, needed for the simulation, are calculated using the chemical properties. The material properties vary with the temperature, as illustrated in the Table 8.7 and Table 8.8 for blow/blow process and press/blow process.

Chapter 8 Glass Containers Simulation Cases

Material Percentage [%]	Case 1	Case 2	Case 3	Case 4	Case 5
SiO2	71.742	71.953	72.490	72.490	71.060
Al2O3	1.771	1.343	1.310	1.310	1.900
Fe2O3	0.051	0.067	0.051	0.051	0.470
CaO	10.198	11.250	7.470	7.470	11.000
MgO	2.402	2.123	4.480	4.000	2.000
BaO	0.015	0.050	0.017	0.017	0.000
Na2O	12.841	12.430	13.240	13.240	12.210
K2O	0.578	0.527	0.710	0.710	0.690
LiO2	0.001	0.000	0.000	0.000	0.000
Cr2O3	0.001	0.003	0.002	0.002	0.270
SO3	0.316	0.131	0.182	0.182	0.000
TiO2	0.023	0.000	0.028	0.028	0.000
B2O3	0.000	0.000	0.000	0.000	0.000
NiO	0.001	0.000	0.000	0.000	0.000
F	0.008	0.000	0.000	0.000	0.000
Cl	0.027	0.000	0.000	0.000	0.000
PbO	0.009	0.012	0.002	0.002	0.000
ZnO	0.003	0.000	0.000	0.000	0.000
CdO	0.000	0.000	0.000	0.000	0.000
CuO	0.000	0.000	0.000	0.000	0.000
CoO	0.000	0.000	0.000	0.000	0.000
MnO	0.012	0.000	0.000	0.000	0.000
ZrO	0.000	0.000	0.000	0.000	0.000
V2O5	0.000	0.000	0.000	0.000	0.000
Se	0.002	0.000	0.000	0.000	0.000
S	0.000	0.000	0.000	0.000	0.000

Material Percentage [%]	Case 1	Case 2	Case 3	Case 4	Case 5	Case 6	Case 7	Case 8
SiO2	71.742	72.000	71.200	70.110	71.06	72.120	71.635	71.634
Al2O3	1.771	1.450	2.000	1.900	1.90	1.400	1.675	1.675
Fe2O3	0.051	0.280	0.500	0.225	0.47	0.075	0.357	0.357
CaO	10.198	10.900	11.000	10.400	11.00	11.000	10.890	10.890
MgO	2.402	0.800	2.000	0.000	2.00	1.950	0.258	0.258
BaO	0.015	0.020	0.000	13.750	0.00	0.000	0.100	0.100
Na2O	12.841	13.900	12.000	0.050	12.21	12.090	14.400	14.400
K2O	0.578	0.340	1.000	0.000	0.69	0.710	0.670	0.670
LiO2	0.001	0.055	0.000	0.180	0.00	0.000	0.000	0.000
Cr2O3	0.001	0.013	0.250	0.040	0.27	0.004	0.006	0.006
SO3	0.316	0.050	0.050	0.000	0.00	0.000	0.070	0.070
TiO2	0.023	0.035	0.000	0.000	0.00	0.000	0.000	0.000
B2O3	0.000	0.000	0.000	0.000	0.00	0.000	0.000	0.000
NiO	0.001	0.000	0.000	0.000	0.00	0.000	0.000	0.000
F	0.008	0.000	0.000	0.000	0.00	0.000	0.000	0.000
Cl	0.027	0.000	0.000	0.000	0.00	0.000	0.000	0.000
PbO	0.009	0.000	0.000	0.000	0.00	0.000	0.000	0.000
ZnO	0.003	0.000	0.000	0.000	0.00	0.000	0.000	0.000
CdO	0.000	0.000	0.000	0.000	0.00	0.000	0.000	0.000
CuO	0.000	0.000	0.000	0.000	0.00	0.000	0.000	0.000
CoO	0.000	0.000	0.000	0.000	0.00	0.000	0.000	0.000
MnO	0.012	0.000	0.000	0.000	0.00	0.000	0.000	0.000
ZrO	0.000	0.000	0.000	0.000	0.00	0.000	0.010	0.010
V2O5	0.000	0.000	0.000	0.000	0.00	0.000	0.000	0.000
Se	0.002	0.000	0.000	0.000	0.00	0.000	0.000	0.000
S	0.000	0.000	0.000	0.000	0.00	0.000	0.000	0.000

Table 8.6: Material chemical composition for different simulations cases in blow/blow and press/blow processes.

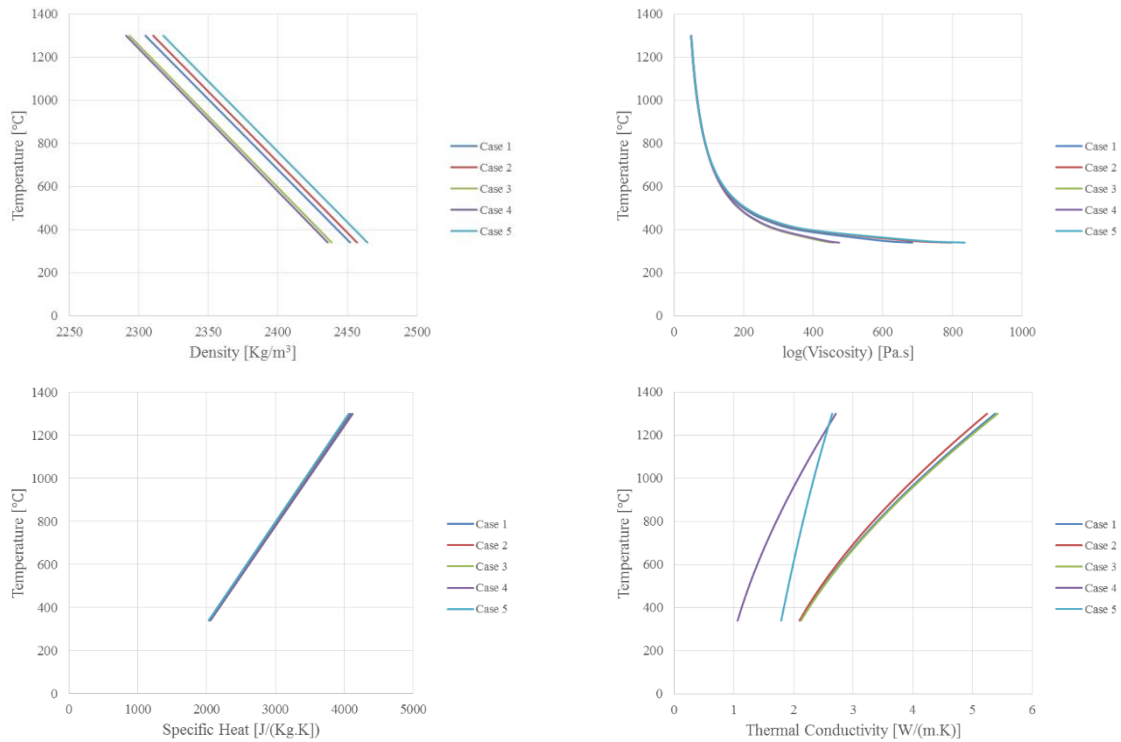


Table 8.7: Material behaviour for different simulations cases in blow/blow process.

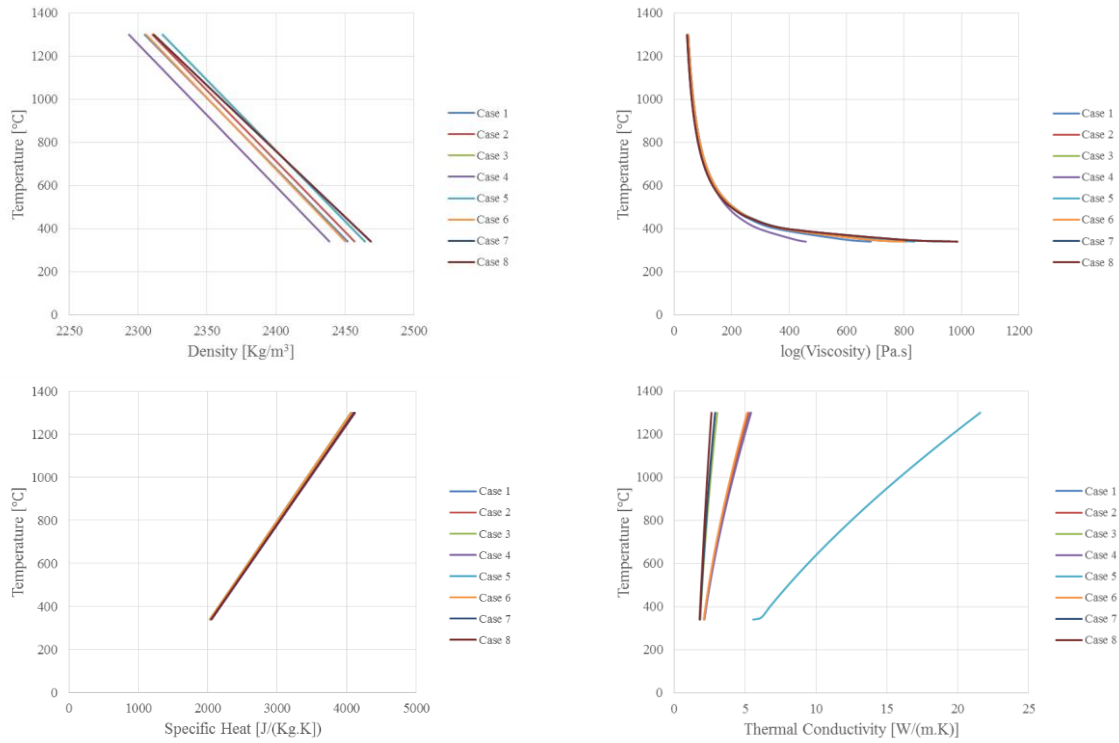


Table 8.8: Material behaviour for different simulations cases in press/blow process.

8.1 Blow/Blow Process

In this chapter complete simulations of blow/blow process are presented, for the cases referred in the previous chapter. The results are shown at all stages.

8.1.1 Gob Loading

The gob loading is the first stage of the blow/blow process. At the beginning the gob falls from the feeder to the interior of the moulds. At this stage it was admitted that the glass can slip along the moulds edges in order to reproduce the possible slipping effect resulting from the initial velocity.

For case 1 the shape and temperature contour of the glass are plotted in Figure 8.3. Since the blank mould has a narrowing zone and the gob diameter is higher than the diameter of the blank near the necking, the first contact between the glass and the mould is in the blank mould wall. Note that the initial time does not correspond to the initial machine time in the Table 8.3, this is due to the fact that the time that the gob spends due to the gob falling from the feeder until the mould contact. Then, the glass slips, by gravity, along the blank mould until it reaches the plunger. Once the glass contacts the plunger, the necking begins to form. In addition, it can be seen that at the end of this stage the glass container neck is almost filled. Also, in Figure 8.4 it can be seen at the boundary temperature of the glass. It can be seen that the glass that is in contact with the mould is cooling faster than the glass that is cooling to the air.

For case 2 the shape and temperature contours of the glass are plotted in Figure 8.5. Also, the first contact between the glass and the mould was in the blank mould wall. Again the glass slips along the blank mould until reaching the plunger. When the glass contacts the plunger, the necking begins to form. As the necking of this container is very narrow the bottle neck is not completely filled at this stage. In Figure 8.6 the boundary temperature for the case 2 is presented. Similarly, the glass cools faster near to the mould than to the air. Additionally, in Figure 8.7 it can be seen the displacement values, while the glass slips around the edge of the blank mould. The results shows clearly that when the blank mould becomes narrower the

glass tends to slow down. Also, the Figure 8.8 and Figure 8.9 shows in detail the beginning of the neckring filling, where the glass flows into the neckring due gravity force until finishing the stage.

For case 3 the shape and temperature contours of the glass are plotted in Figure 8.10. Similar results in the previous cases are observed. In Figure 8.11 the boundary temperatures for the case 3 are presented. For Case 4 the shape and temperature contours of the glass are plotted in Figure 8.12. This bottle is very geometric different from the last examples, however, similar results were obtained. In the boundary temperatures for the case 4 are presented, Figure 8.13. It can be observed that due to this stage is longer than in the previous cases the glass presents a more evident cooling. For case 5 the shape and temperature contour of the glass are plotted in Figure 8.14. The result are quite similar to the last ones. Figure 8.15 the boundary temperatures for the case 5 are presented.

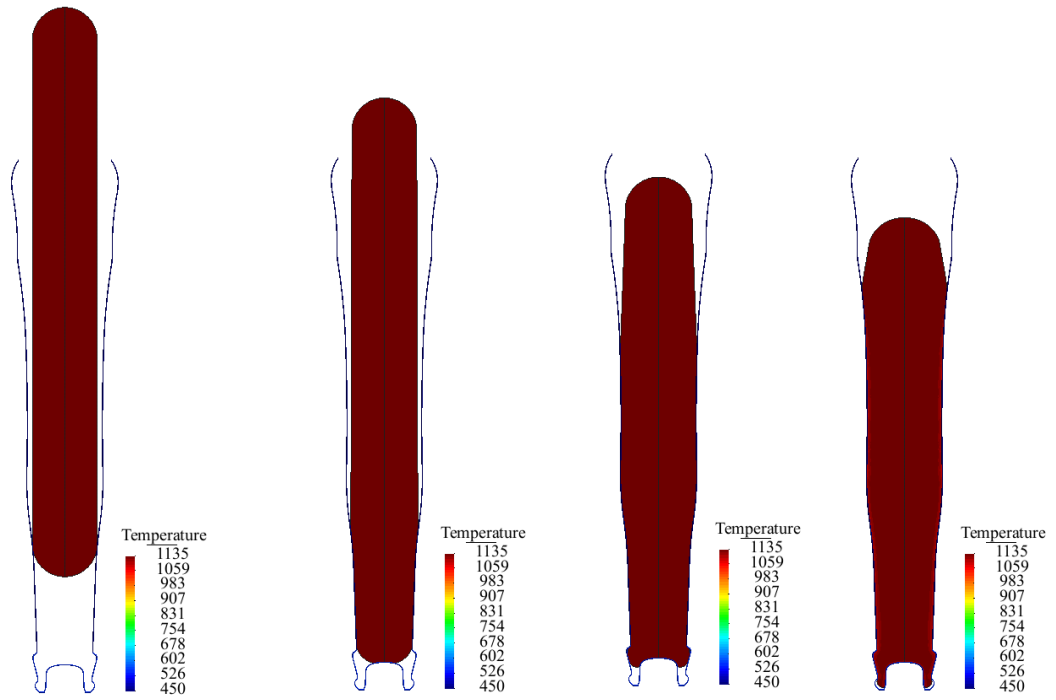


Figure 8.3: Temperature distribution in gob loading for the case 1 for 0.334s, 0.342s, 0.427s and 0.763s.

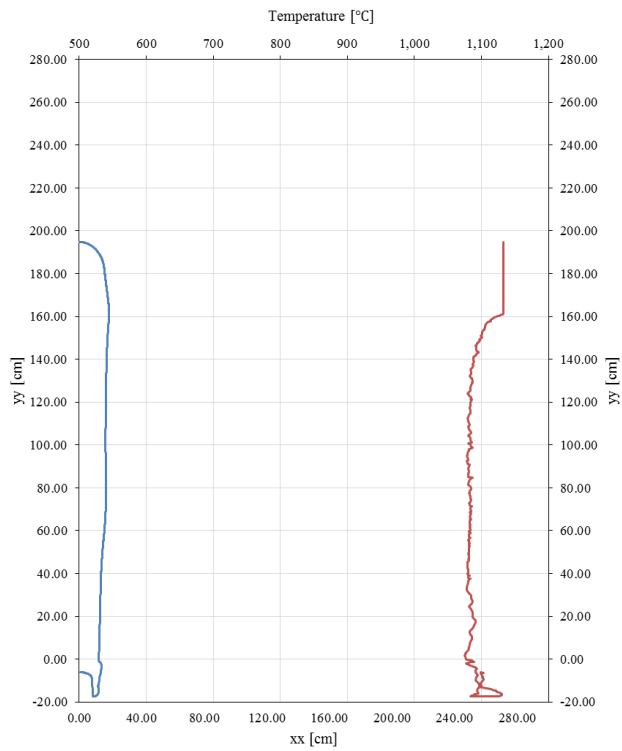


Figure 8.4: Boundary temperature for gob loading stage for case 1.

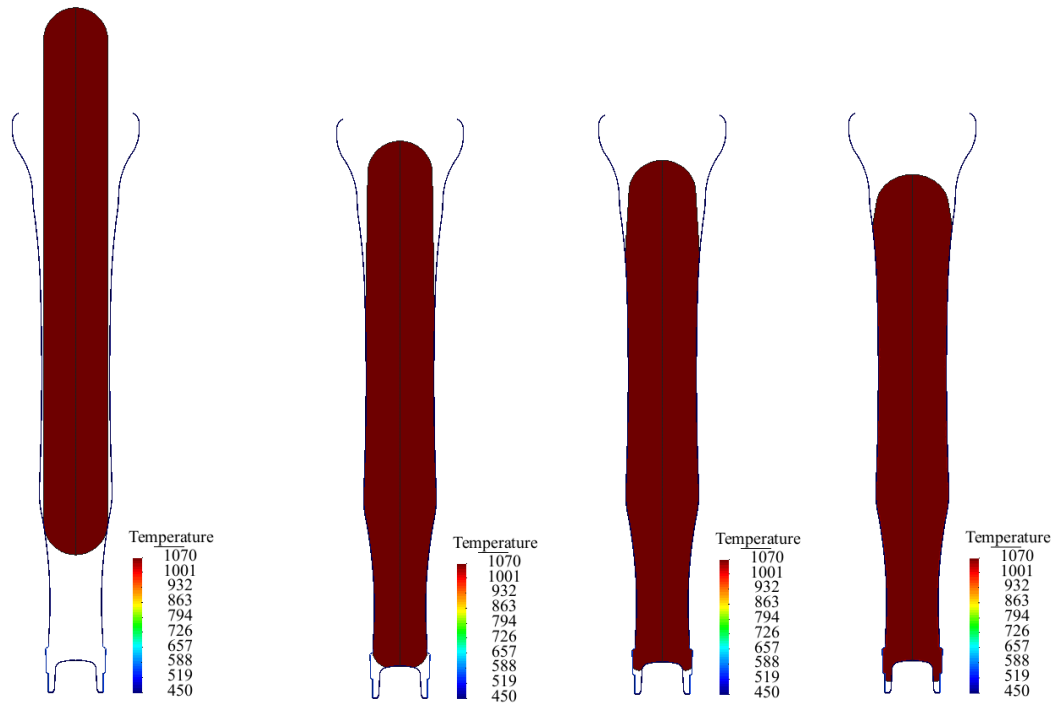


Figure 8.5: Temperature distribution in gob loading for case 2 for 0.365s, 0.382s, 0.429s and 0.555s.

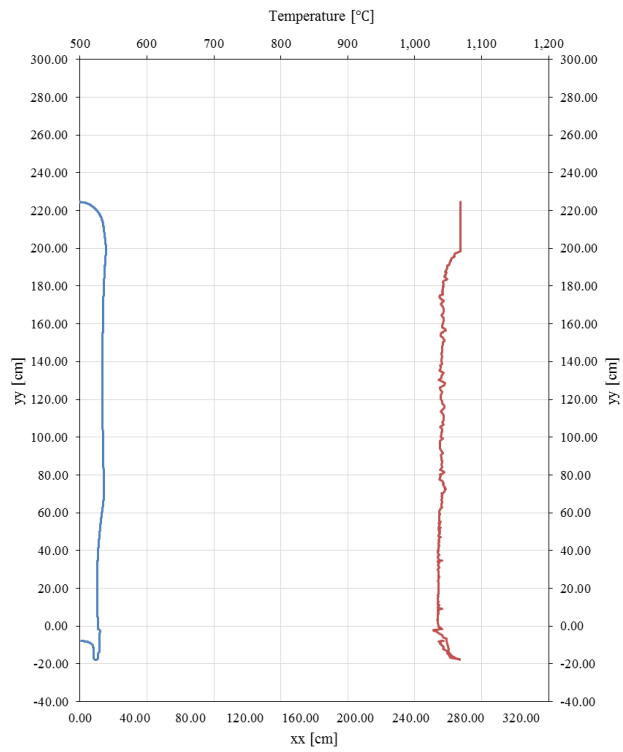


Figure 8.6: Boundary temperature for gob loading stage for case 2.

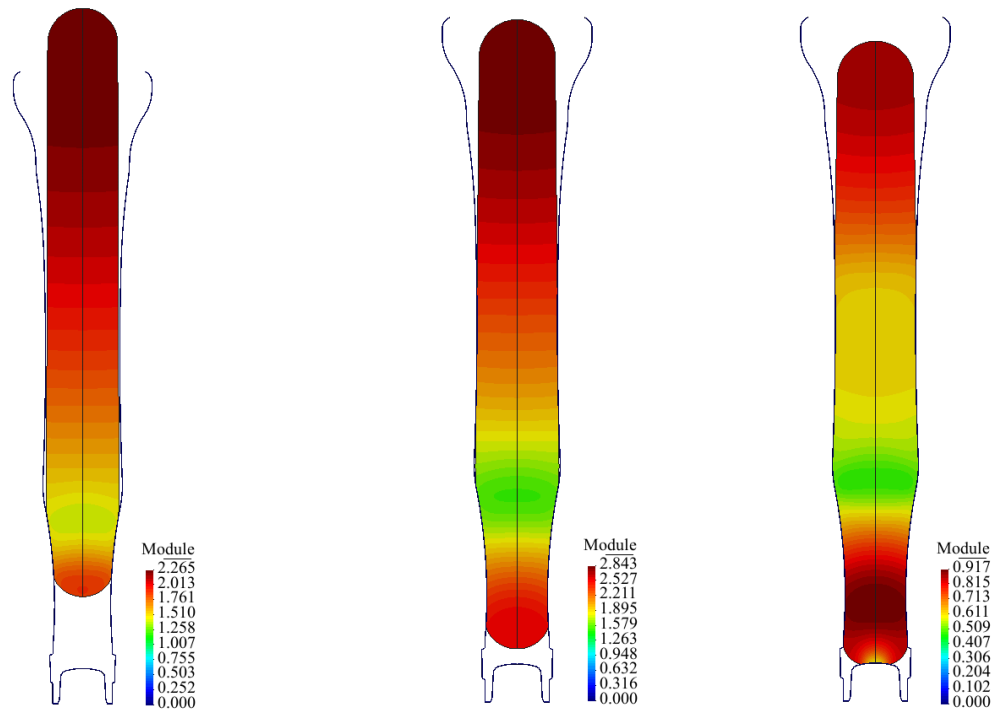


Figure 8.7: Displacement module in gob loading for case 2 for 0.368s, 0.375s and 0.381s.

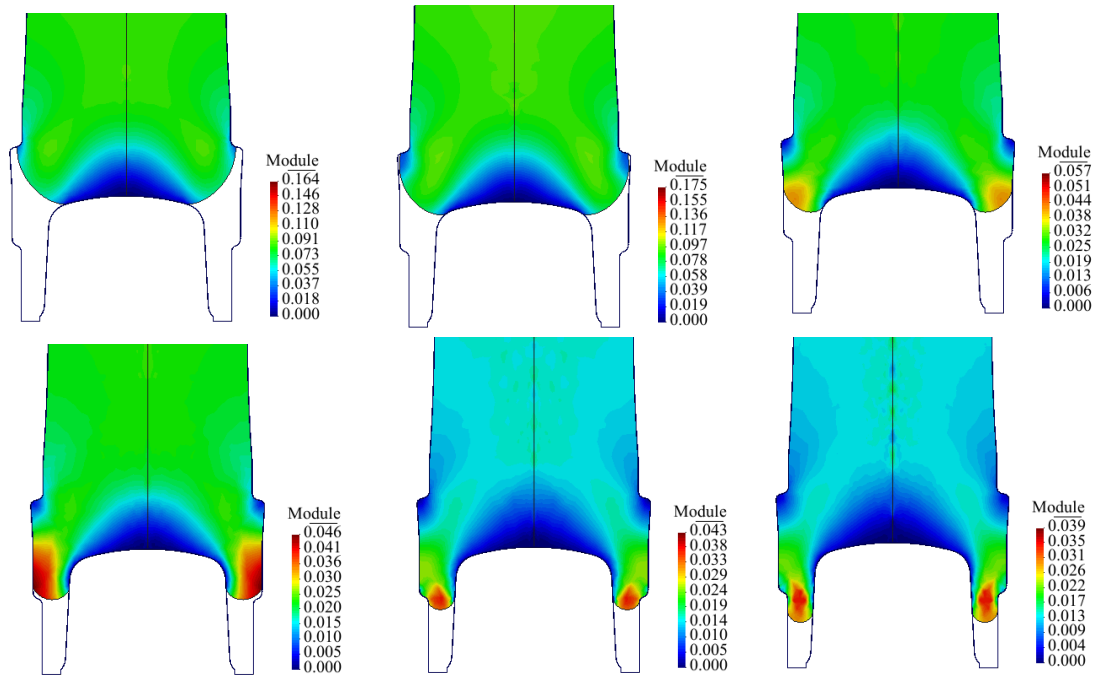


Figure 8.8: Displacement module with the neckring detail in gob loading for case 2 for 0.3877s, 0.3973s 0.4165s.

0.4558s

0.4842s

0.5414s

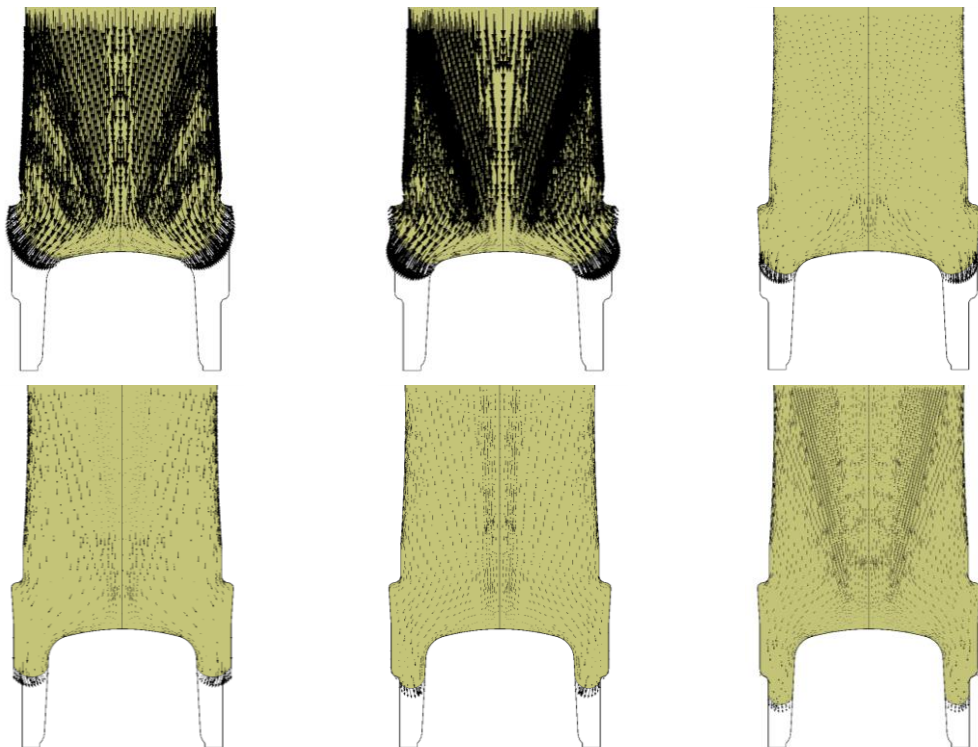


Figure 8.9: Displacement vector with neck ring detail in gob loading for case 2 for 0.3877s, 0.3973s 0.4165s

0.4558s

0.4842s

0.5414s

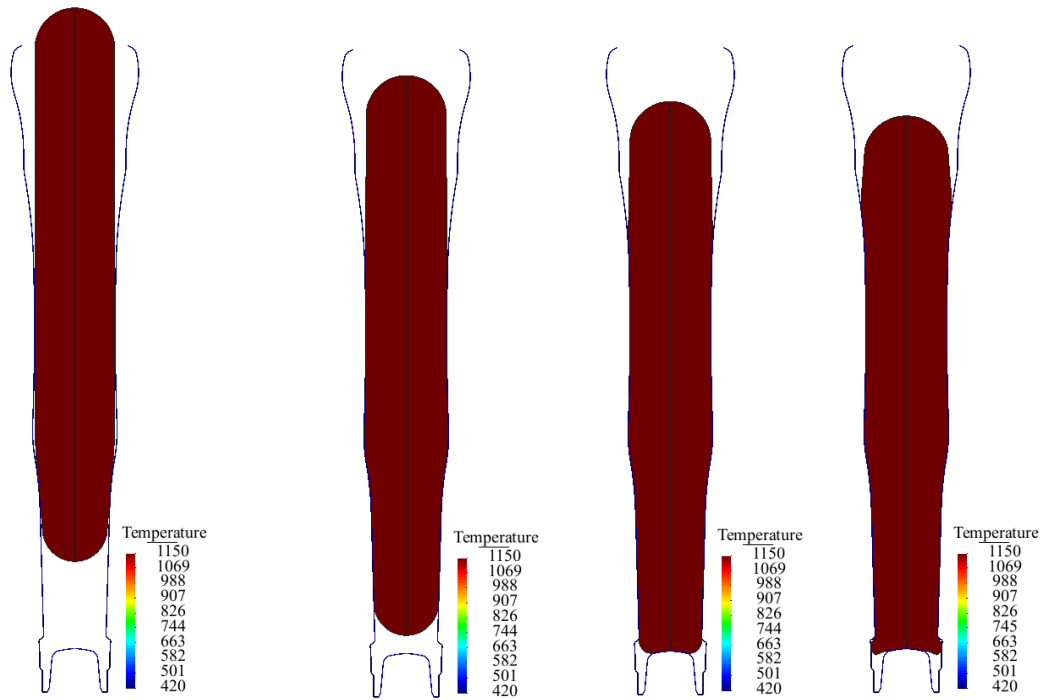


Figure 8.10: Temperature distribution in gob loading for case 3 0.326s, 0.335s, 0.369s and 0.490s.

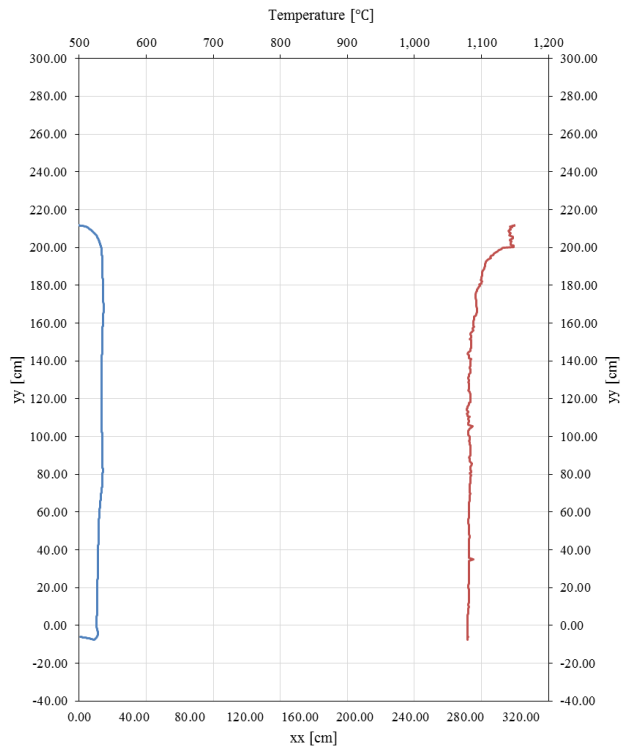


Figure 8.11: Boundary temperature for gob loading stage for case 3.

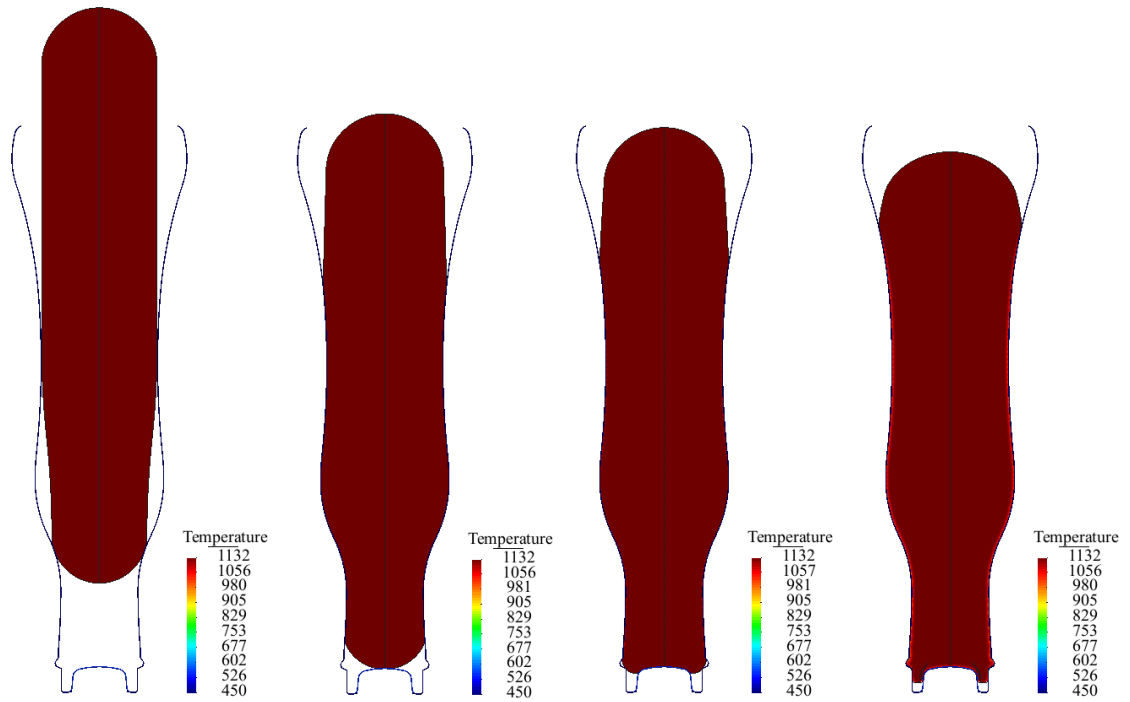


Figure 8.12: Temperature distribution in gob loading for case 4 for 0.255s, 0.310s, 0.373s and 0.772s.

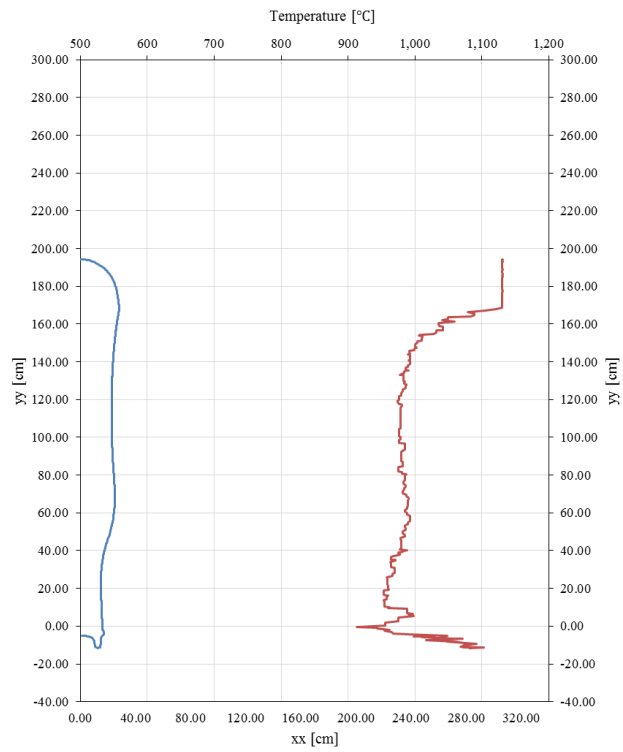


Figure 8.13: Boundary temperature for gob loading stage for case 4.

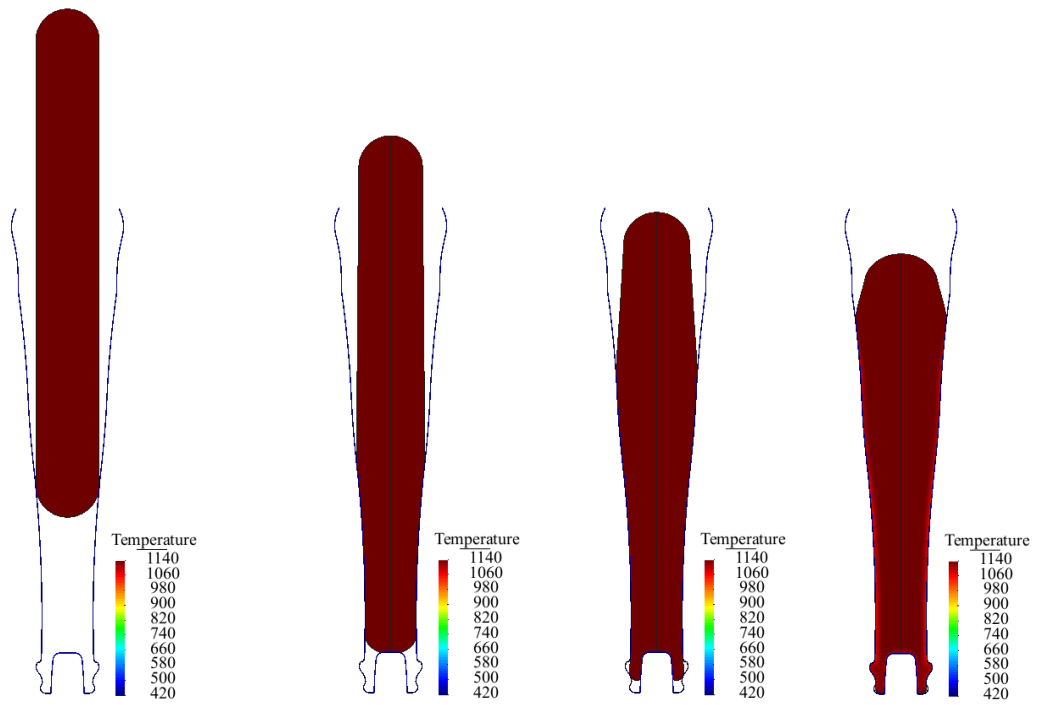


Figure 8.14: Temperature distribution in gob loading for case 5 for 0.731s, 0.745s, 0.819s and 1.129s.

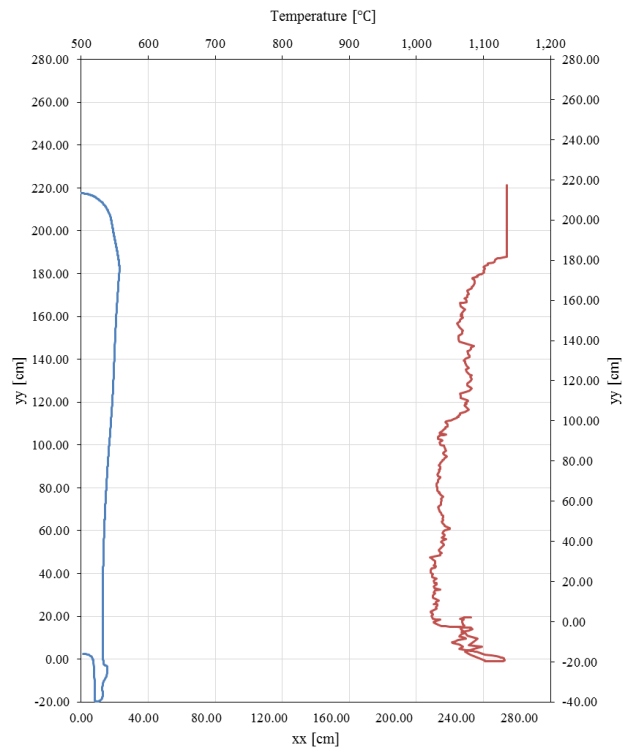


Figure 8.15: Boundary temperature for gob loading stage for case 5.

8.1.2 Settle Blow

The settle blow is the stage that follows the gob loading. In order to fill completely the neckring a top pressure is applied.

For case 1 the shape and temperature contours of the glass are plotted in Figure 8.16. In this stage a pressure is applied to force the glass to fill completely the neckring zone, it can be seen that in the end of the stage the neckring is completely filled. In addition, it can be noted that the top of the gob, due to the air pressure, becomes slightly flattened. In Figure 8.17 it can be seen that the glass in contact to the moulds cools faster. Also inside the neckring and near to the corner it can be seen that the temperature drops faster relatively to the zone where there is more glass.

For case 2 the shape and temperature contours of the glass are plotted in Figure 8.18. The filling of the neckring is more evident, as well as the flattening of the top of the gob. Also, in Figure 8.19 it can be seen that the temperature along the glass in contact with the mould is constant. However, the temperature near the neckring varies significantly in the zones near to the neckring corner. In addition, in Figure 8.20 and Figure 8.21 the displacement value (meaning its norm) and the displacement vector are shown in order to, in detail, show the filling movement of the neckring.

For case 3 the shape and temperature contours of the glass are plotted in Figure 8.22. The results for this case are very similar with the case 2. In Figure 8.23 the boundary temperatures are represented and the pattern is analogous to what is verified in case 2.

For case 4 the shape and temperature contours of the glass are plotted in Figure 8.24. The longer cooling effect in the glass in contact with the mould is more visible here. In Figure 8.25 representing the boundary temperature.

For case 5 the shape and temperature contours of the glass are plotted in Figure 8.26 and the boundary temperature in Figure 8.27. Again, similar comments to the previous one apply here.

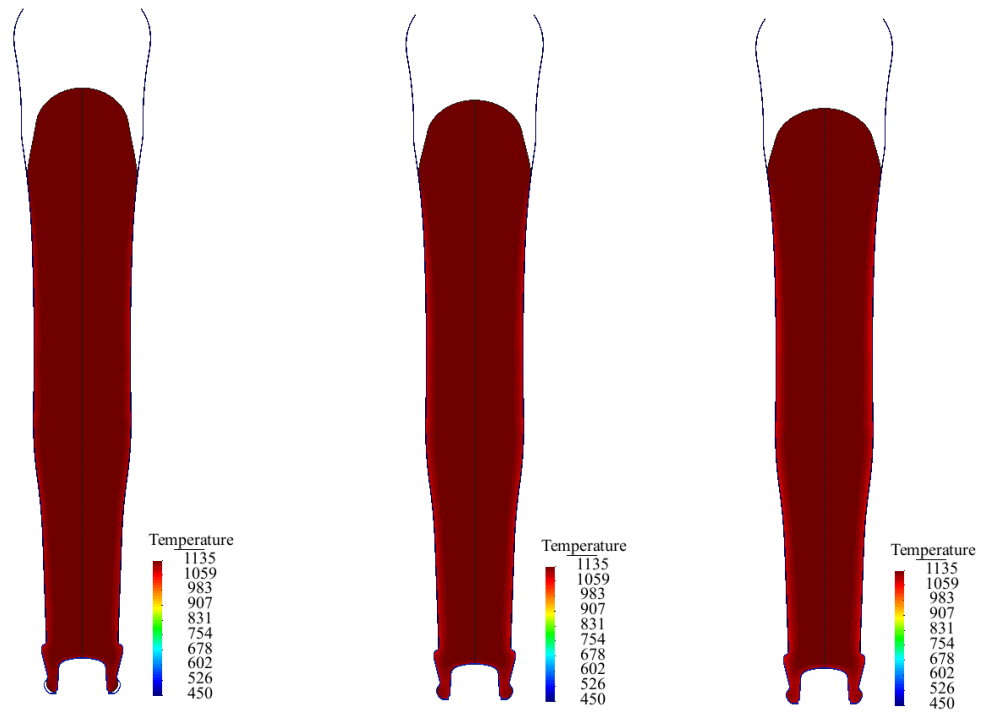


Figure 8.16: Temperature distribution in settle blow for the case 1 for 0.796s, 0.934s and 1.083s

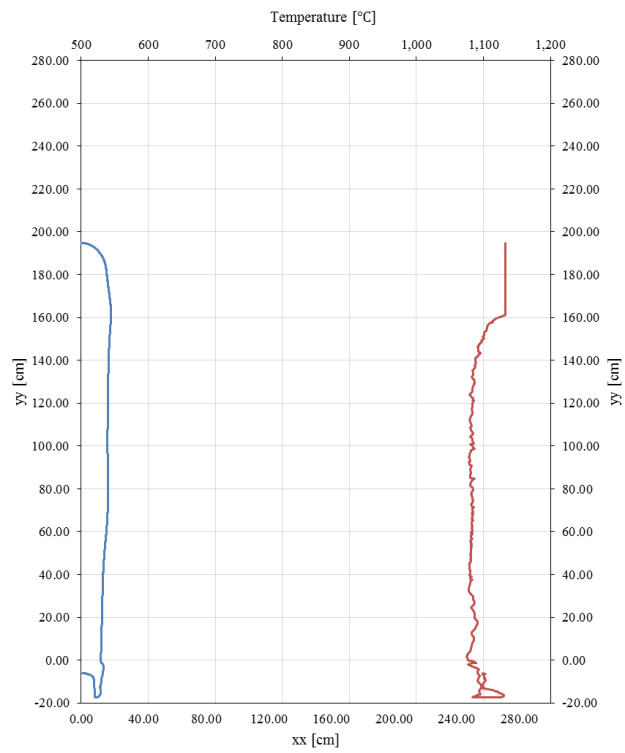


Figure 8.17: Boundary temperature for settle blow stage for case 1.

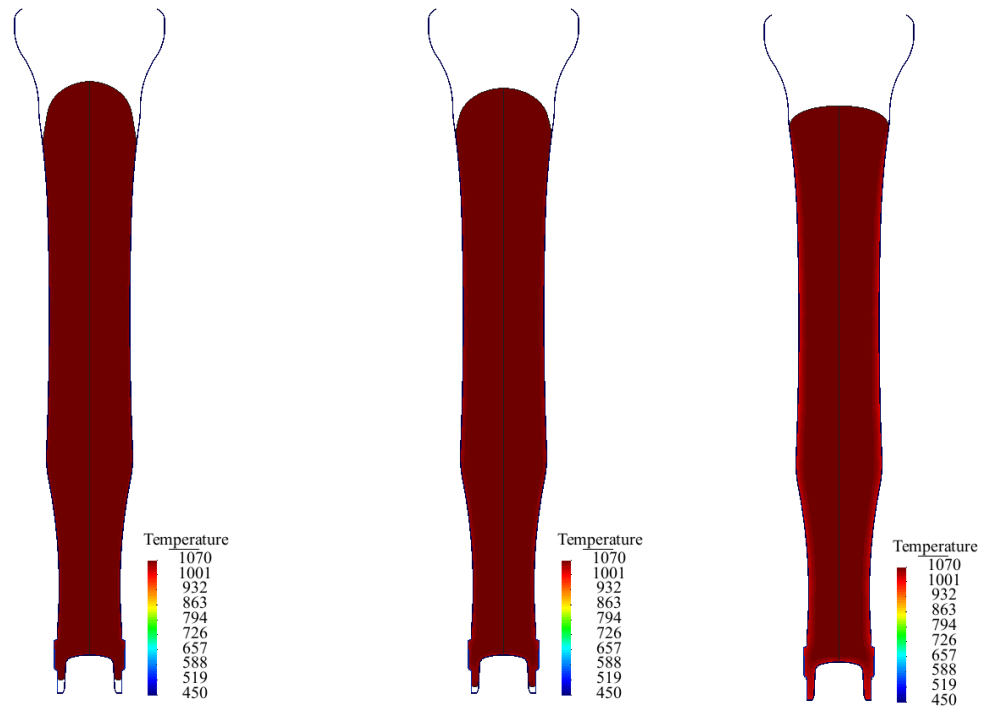


Figure 8.18: Temperature distribution in settle blow for the case 2 for 0.555s, 0.666s and 1.333s.

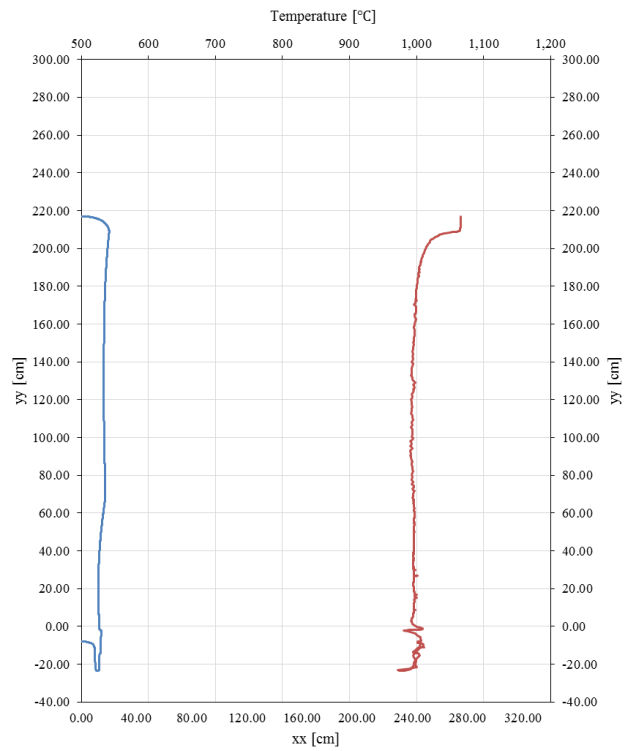


Figure 8.19: Boundary temperature for settle blow stage for case 2.

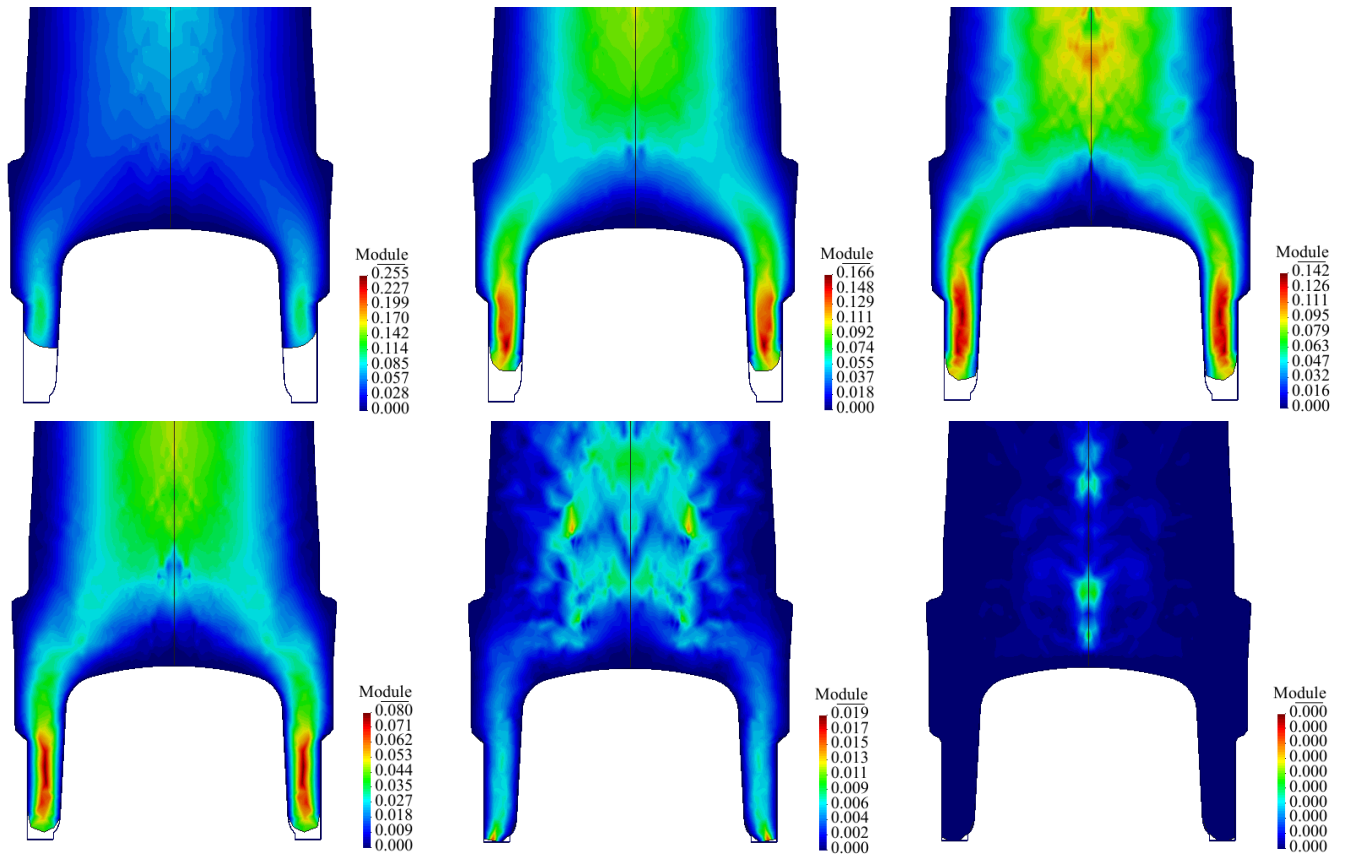


Figure 8.20: Displacement module with the necking detail in gob loading for case 2 for 0.555s, 0.744s 0.850s.

1.005s

1.154s

1.333s

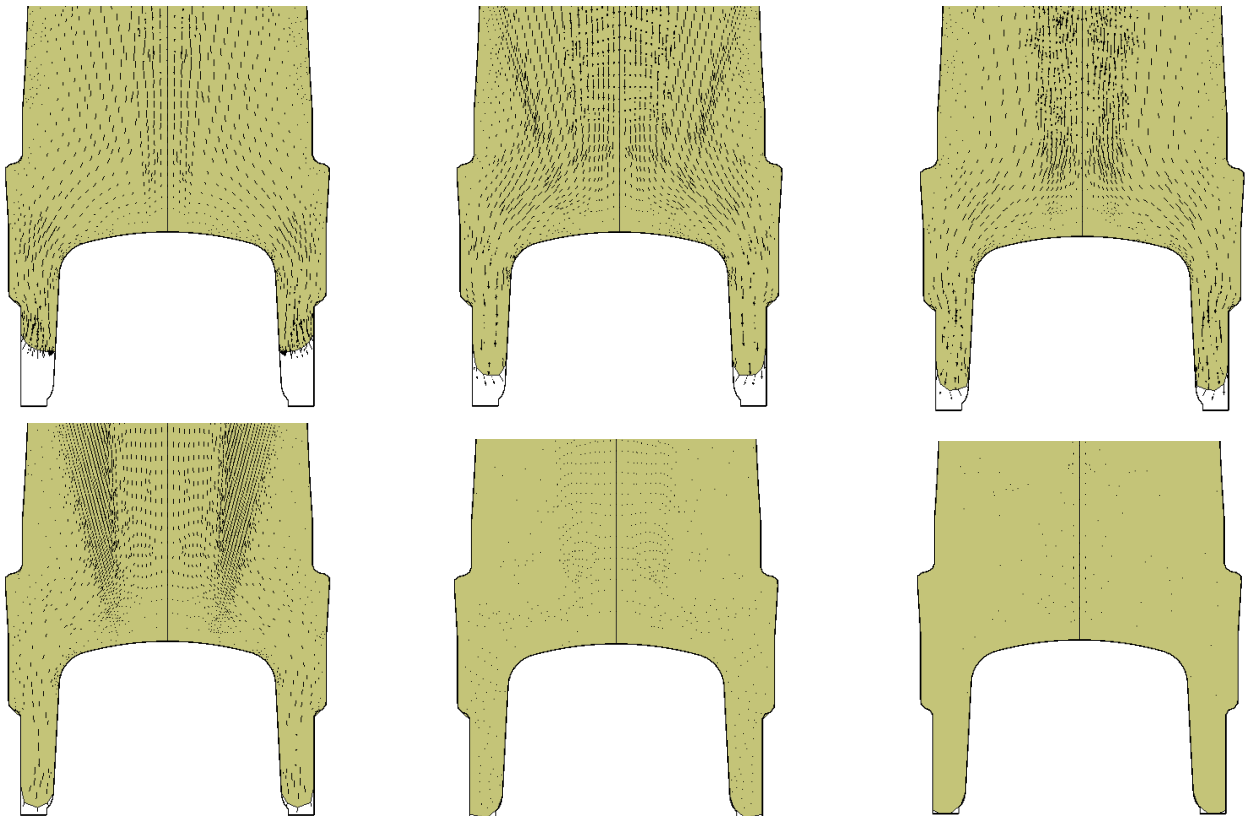


Figure 8.21: Displacement vector with the necking detail in gob loading for case 2 for 0.555s, 0.744s 0.850s.

1.005s

1.154s

1.333s

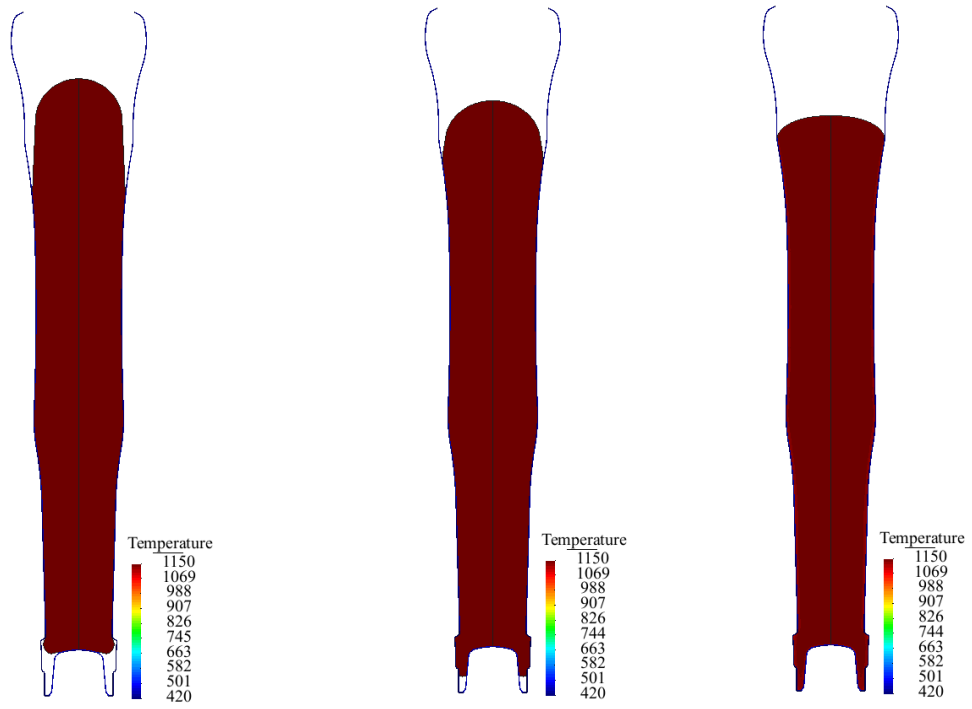


Figure 8.22: Temperature distribution in settle blow for the case 3 for 0.500s, 0.543s and 0.784s.

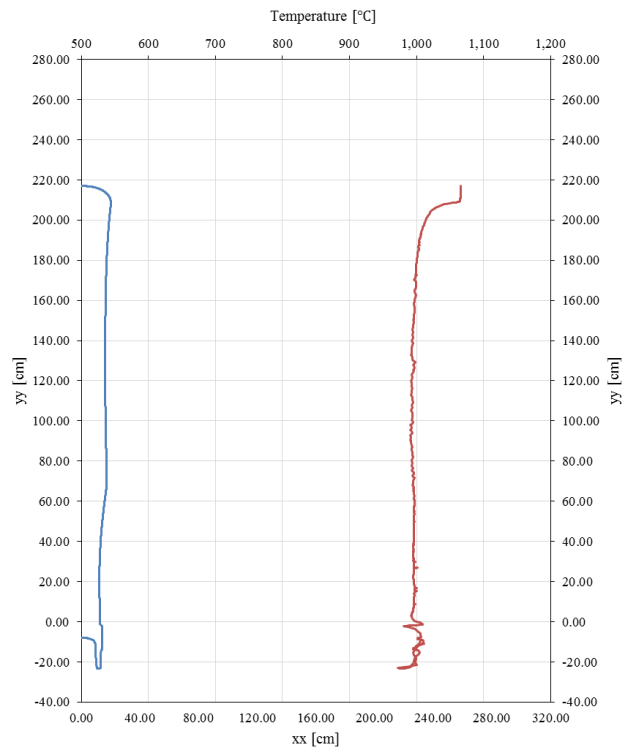


Figure 8.23: Boundary temperature for settle blow stage for case 3.

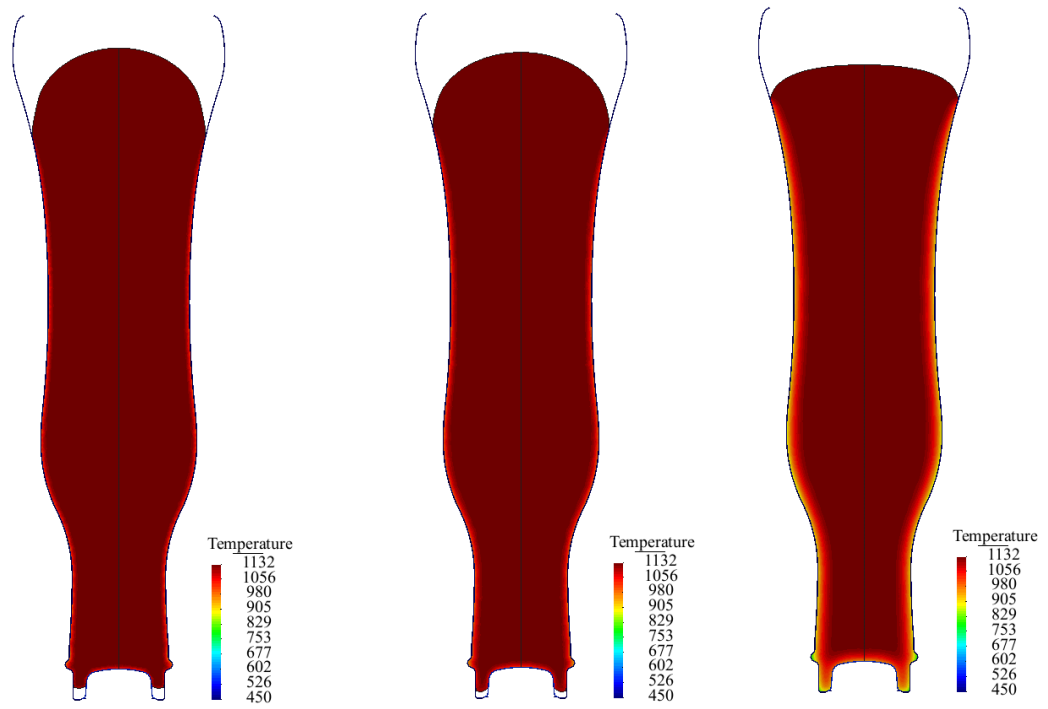


Figure 8.24: Temperature distribution in settle blow for the case 4 for 0.772s, 0.951s and 2.272s.

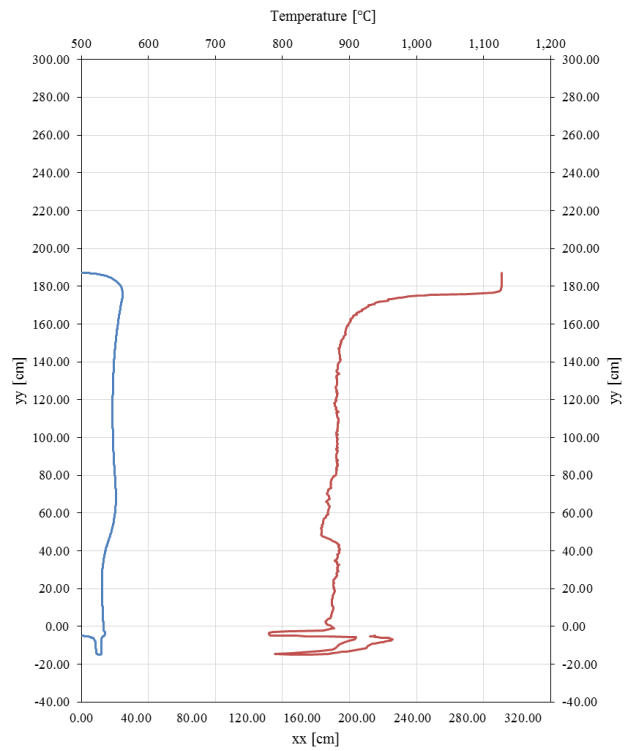


Figure 8.25: Boundary temperature for settle blow stage for case 4.

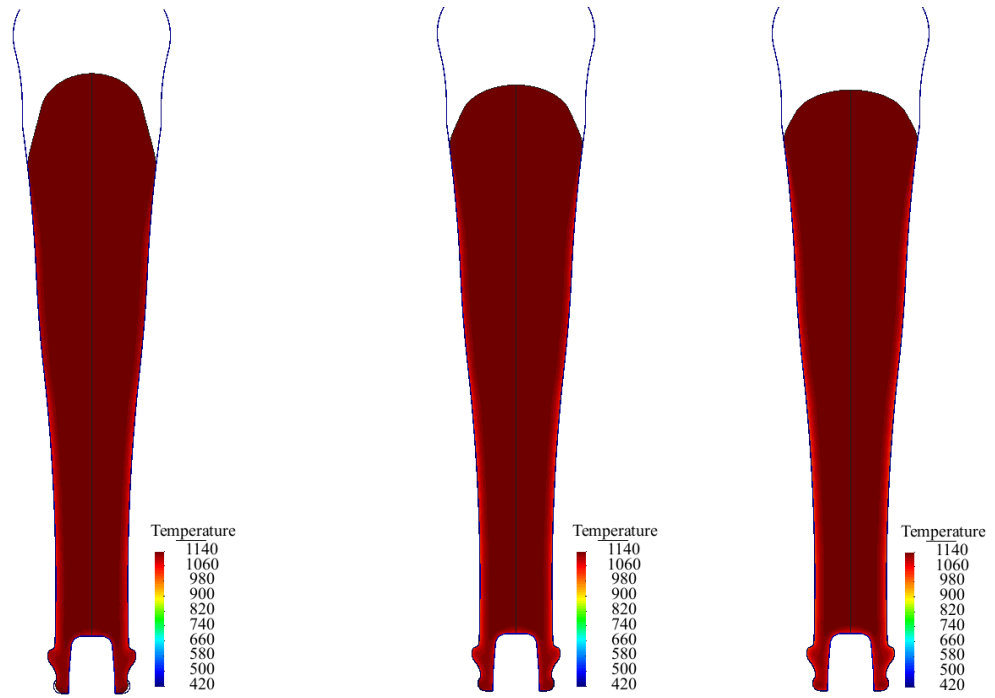


Figure 8.26: Temperature distribution in settle blow for the case 5 for 1.129s, 1.424s and 1.835s.

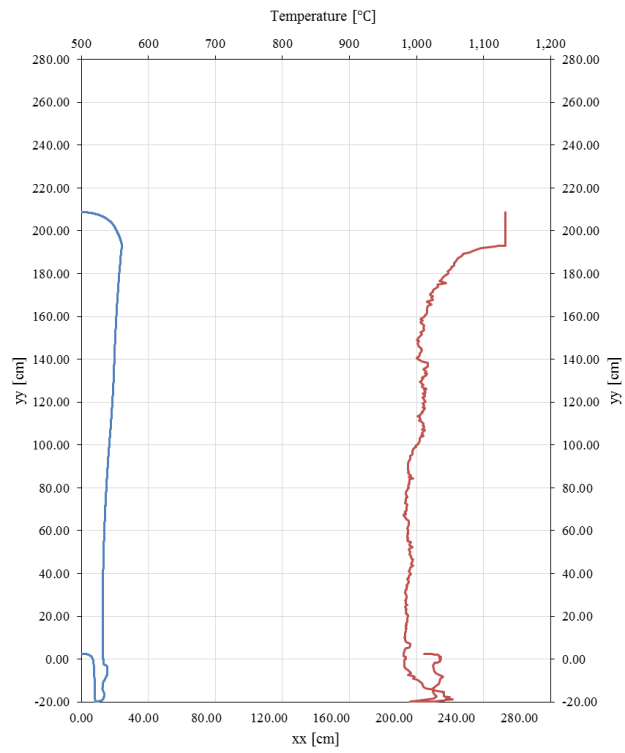


Figure 8.27: Boundary temperature for settle blow stage for case 5.

8.1.3 Corkage Reheat

After the settle blow stage the plunger is removed to allow the corkage to reheat in the plunger area, i.e. in the glass nearby the plunger, therefore, to “soften” this zone just before the counter blow pressure is applied. The baffle tool is also set in the top of the blank mould. The results from this stage are shown in Figure 8.28 for all the cases. That effect is more evident in case 4.

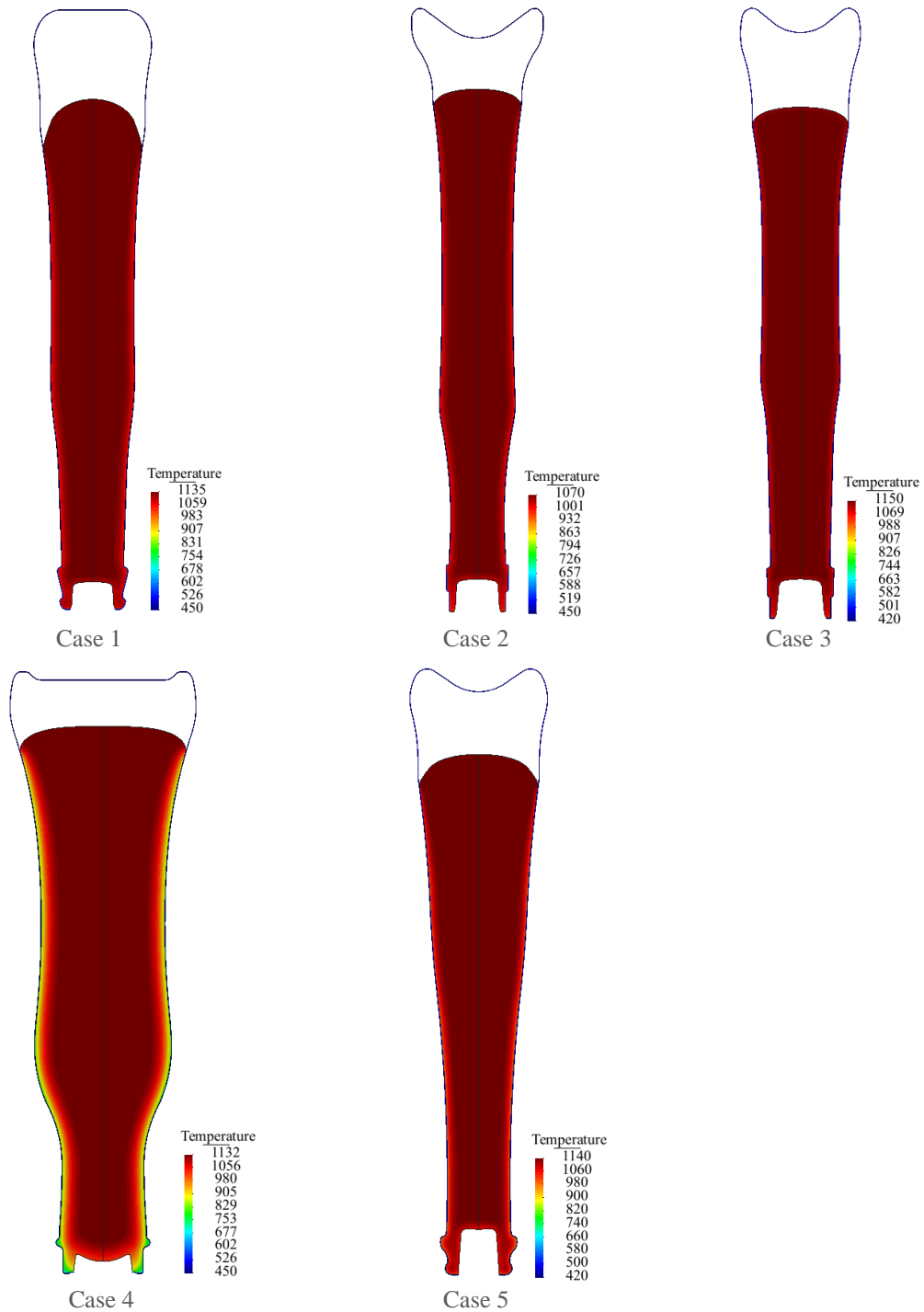


Figure 8.28: Temperature distribution in corkage reheat for the case 1 in 1.500s, for the case 2 in 2.044s, for the case 3 in 1.863s, for the case 4 in 4.090s and for the case 5 in 2.682s.

8.1.4 Counter Blow

Air pressure is applied in the bottom part of the glass, pushing the glass to the baffle zone and forming the parison. The pressure used must be suited to the particular size of the bottle, that is, the larger the quantity of glass the greater the pressure.

For case 1, the shape and temperature contours of the glass are plotted in Figure 8.29. The gob starts to rip a hole in the zone where the glass has a higher temperature creating a wall against the blank mould. The thickness of the wall depends on the cooling rate between the blank moulds and the glass. During the counter blow the wall of the parison is cooling in contact with the mould. After the glass reaches the bottom of the blank mould, filling the baffle zone, the parison is completely formed. For a short time air pressure continues to push the glass against the mould with the only purpose to cool the parison. At the end of the stage the parison is formed and cooled enough to pass to other stages.

In Figure 8.30 the temperatures at the glass boundary are represented. It is clear that at the boundary that was in contact with the mould the glass is cooler than at the boundary where the air pressure was applied. The boundary zone that had contact with the mould, since the gob loading stage is cooler than the glass zone that only contacted the mould during the counter blow stage. The same happens with the boundary where the air pressure was applied. The boundary contacting the mould is around 730°C and the boundary contacting the air is around 950°C.

At the end of the stage, the glass has an almost constant wall thickness, Figure 8.30. The bottom part of the container presents a higher thickness. The cooling rate between the glass and moulds during this stage can influence the final thickness. If the glass cools more than it should the parison will have a larger wall thickness and a smaller thickness at the bottom zone and if the cooling is enough the opposite happens. So, it can be concluded that the cooling rate influences dramatically the final parison shape. Of course, also other parameters play here an important role as conductivity, capacity, mould temperatures, etc.

Additionally, in Figure 8.31 displacement contours are represented during the counter blow stage. The displacement is higher just above the counter blow pressure and while the glass is spread around the edges of the blank mould the displacement increases. When the glass hits the baffle the displacement becomes almost null when the parison is formed.

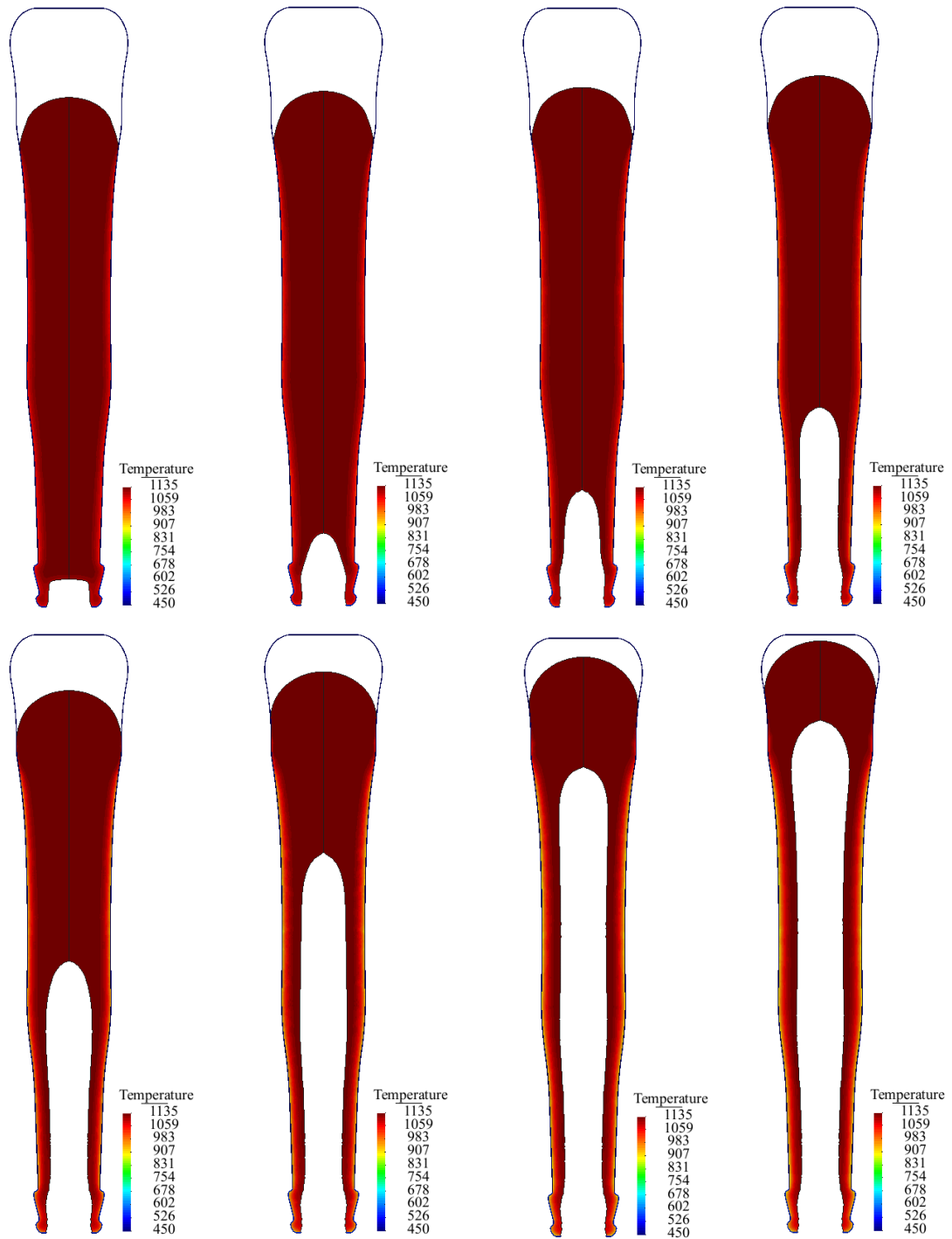
For case 2, the shape and temperature contours of the glass are plotted in Figure 8.32. Again, the air pressure pushes the material to the baffle in order to form the parison. Here the baffle has a complex shape, so the remaining material must accommodate in the baffle gaps. After the parison is formed, the exterior boundary cools in contact with the moulds and the interior boundary with the air. In Figure 8.33 it can be seen that at the parison the exterior boundary temperature is around 870°C, while the interior is around 1050°C.

In addition, the thickness at the end of the stage is presented. Also, in Figure 8.34 and Figure 8.35 it can be seen the evolution of the displacement while the counter blow stage forms the parison, as well as the detail of the displacement vector when the baffle is filled. The results are very similar to the case 1, but because the baffle has here a more complicated shape, a detail of the displacement vector is shown to illustrate the filling of the edges of the baffle.

For case 3, the shape and temperature contours of the glass are plotted in Figure 8.36. In this case the behaviour is very similar to the case 3. In Figure 8.37 the boundary temperatures are represented. The exterior parison wall ends this stage with around 770°C, while the interior with around 1100°C. It also can be noted that the necking zone has the lower temperatures, as it is a thin zone and has more area in contact with the mould.

For case 4, the shape and temperature contours of the glass are plotted in Figure 8.38. The cooling between glass and moulds are more evident due to the high stage time. Air pressure pushes the hot glass to the baffle. When the parison is formed the glass cools around the exterior boundary at a higher rate than in the interior. Figure 8.39 the boundary temperatures are represented.

For case 5, the shape and temperature contours of the glass are plotted in Figure 8.40. Quite similar results were obtained when comparing to the previous examples. In Figure 8.41 the boundary temperatures are represented. The exterior boundary ends the stage with around 650°C and in the bottom zone around 720°C. In the interior of the parison temperature is around 1100°C.



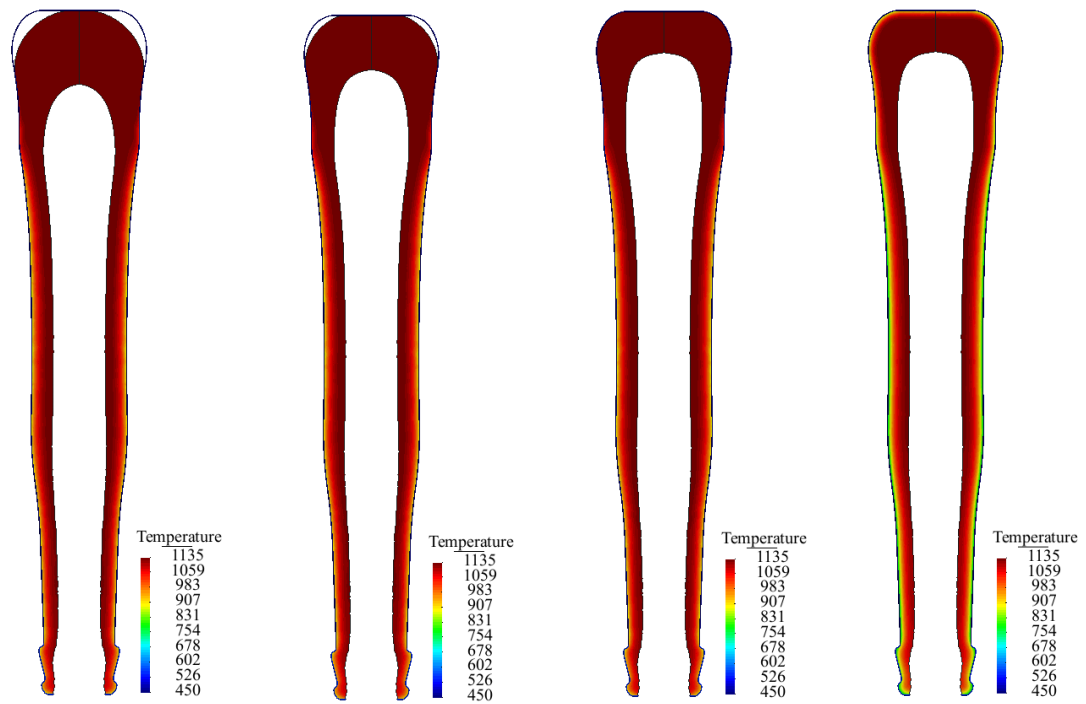


Figure 8.29: Temperature distribution in counter blow for the case 1 for 1.500s, 1.538s, 1.570s, 1.622s,

1.664s	1.705s	1.722s	1.727s
1.729s	1.731s	1.733s	2.986s

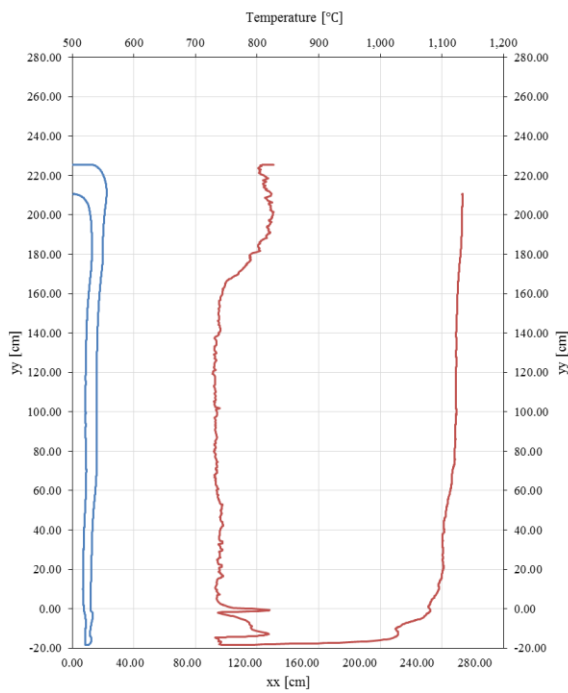
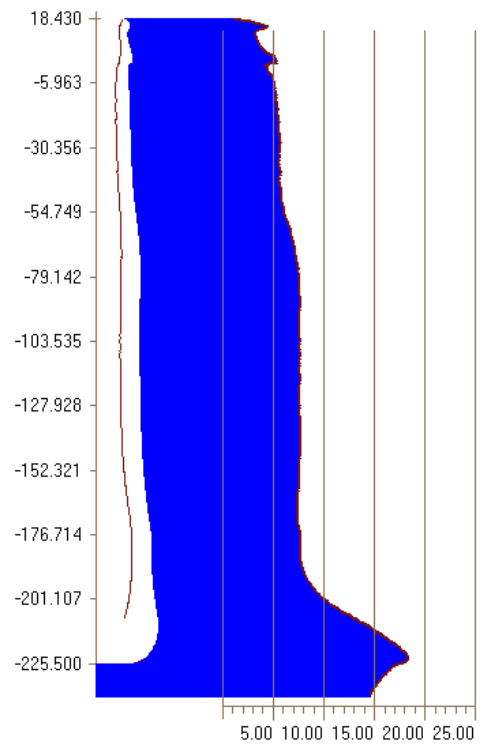
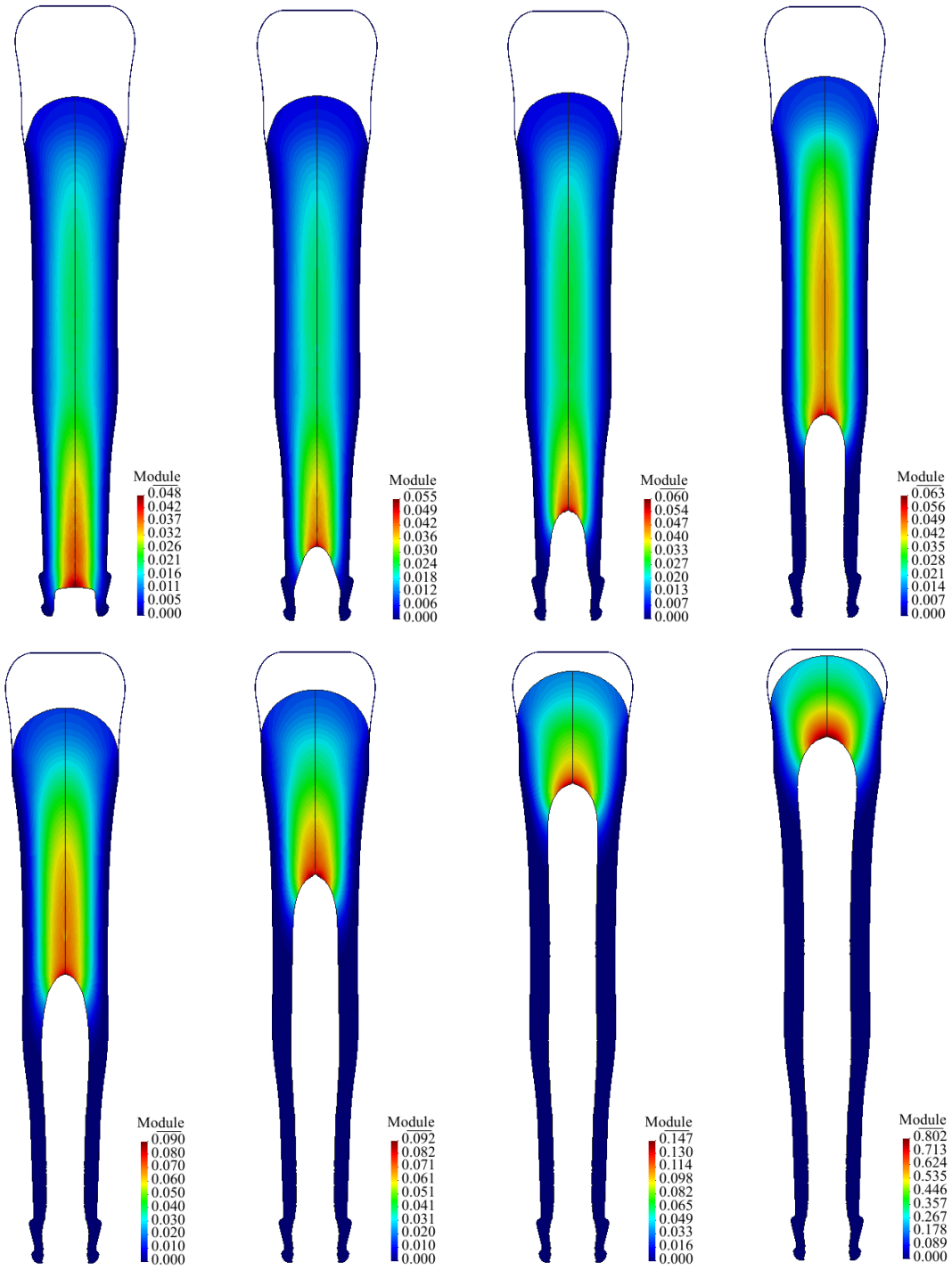


Figure 8.30: Simulation temperature of the boundary for counter blow stage for case 1.



Simulation thickness (mm) in counter blow stage for case 1.



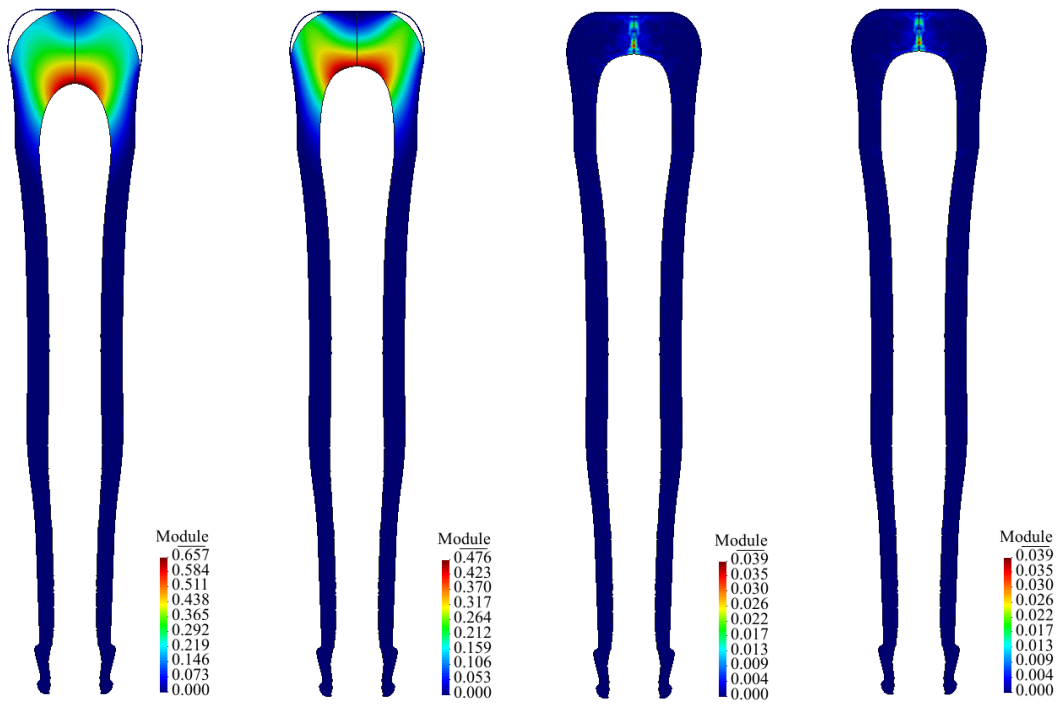
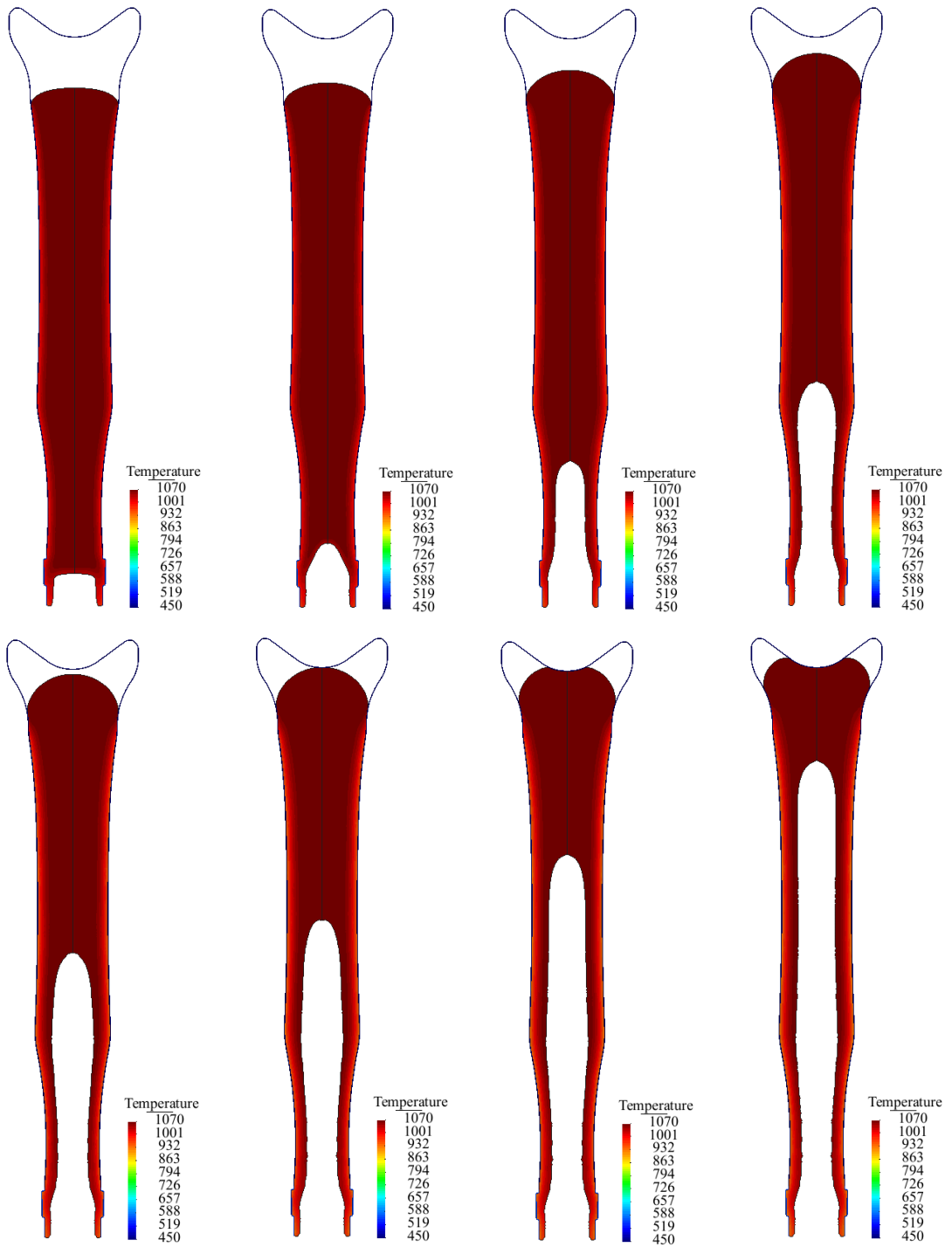


Figure 8.31: Displacement module in counter blow for the case 1 for 1.500s, 1.538s, 1.570s, 1.622s,

1.664s	1.705s	1.722s	1.727s
1.729s	1.731s	1.733s	2.986s



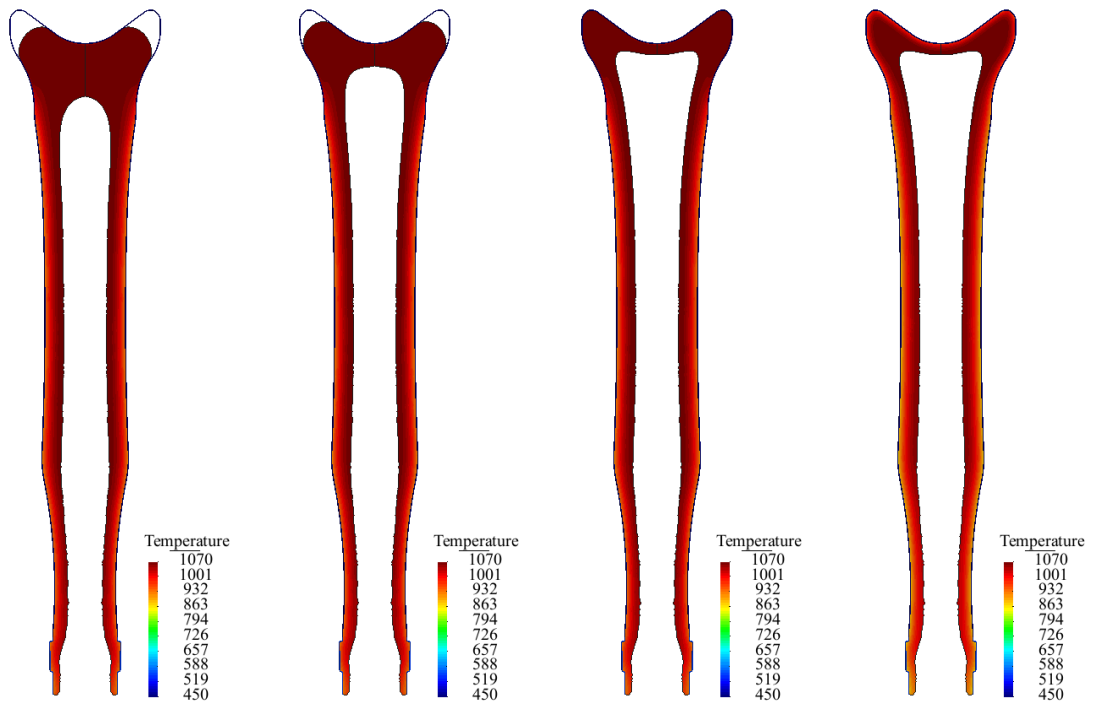


Figure 8.32: Temperature distribution in counter blow for the case 2 for 2.044s, 2.161s, 2.376s, 2.571s,

2.711s	2.769s	2.865s	2.939s
2.962s	2.974s	2.991s	4.777s

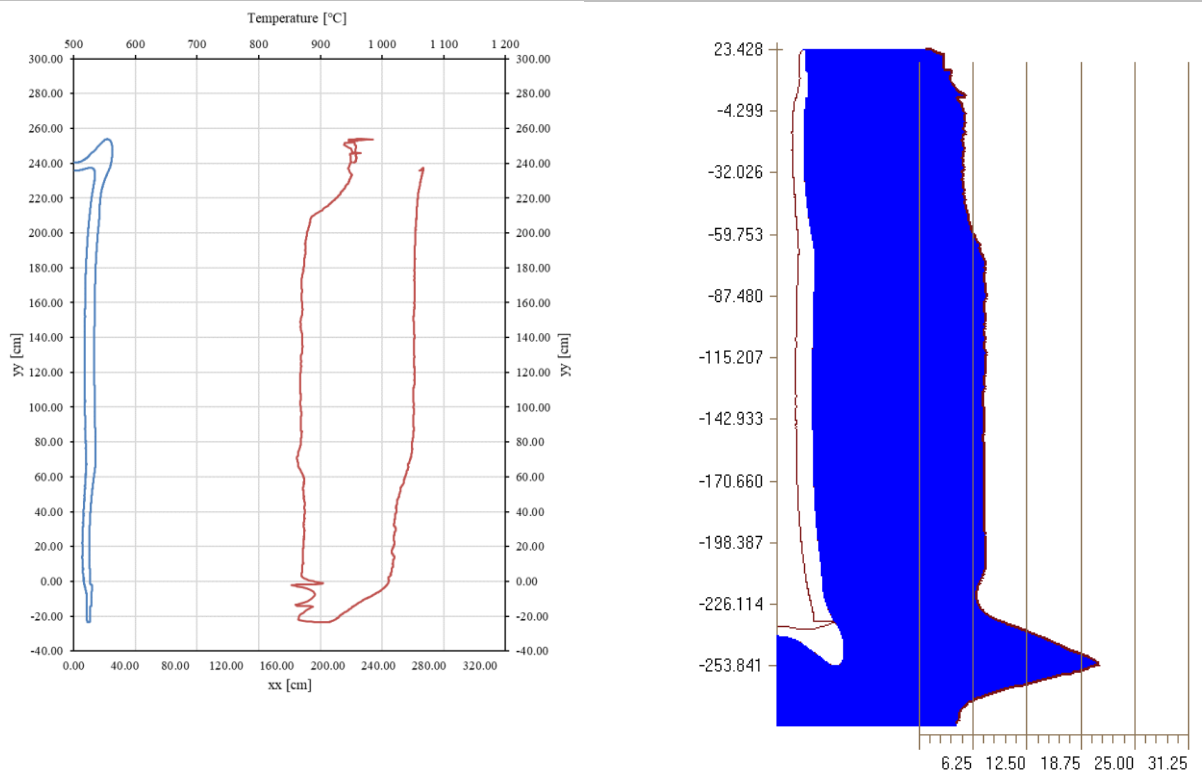
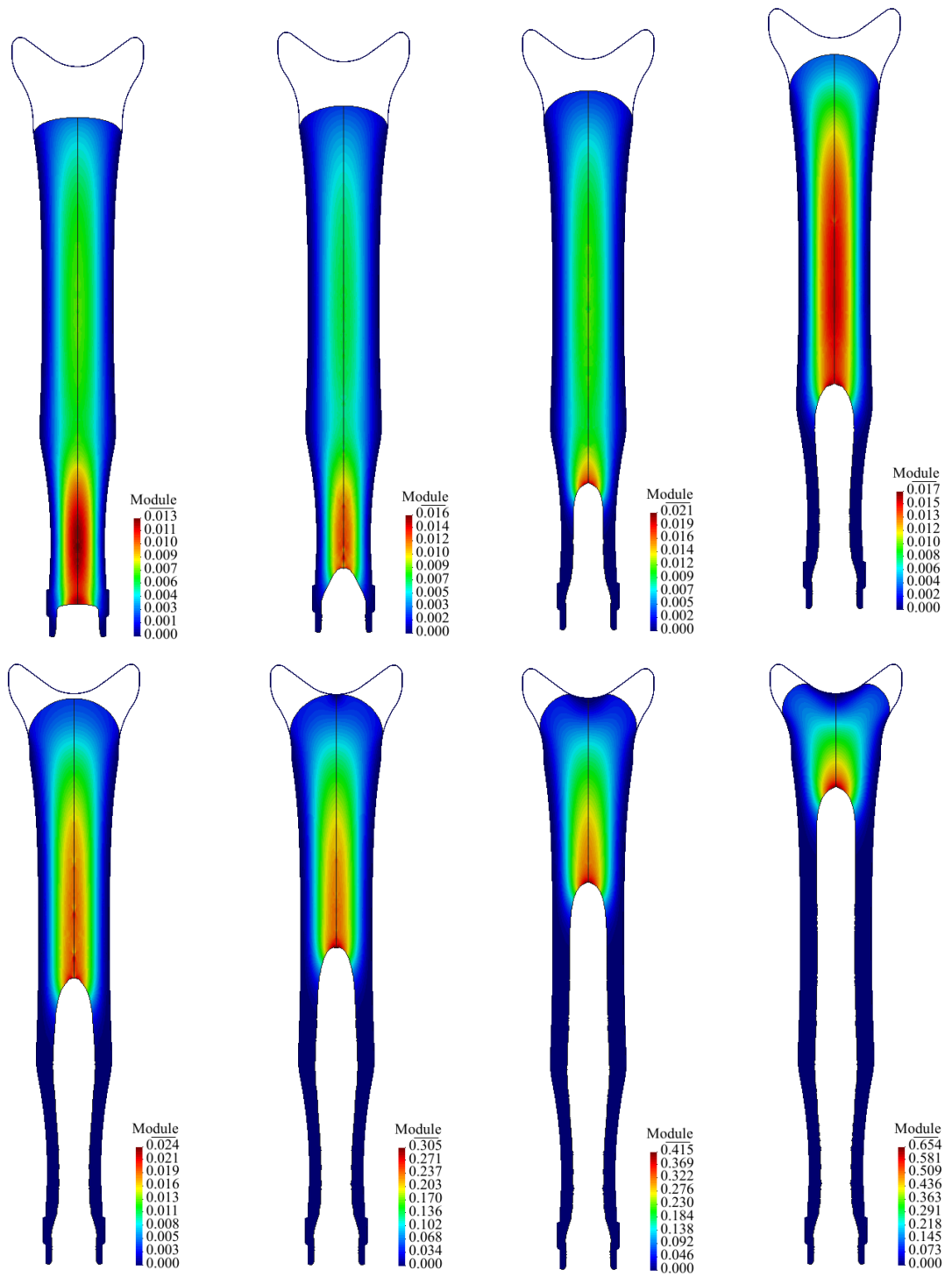


Figure 8.33: Boundary temperature for counter blow stage for case 2.

Thickness in counter blow stage for case 2.



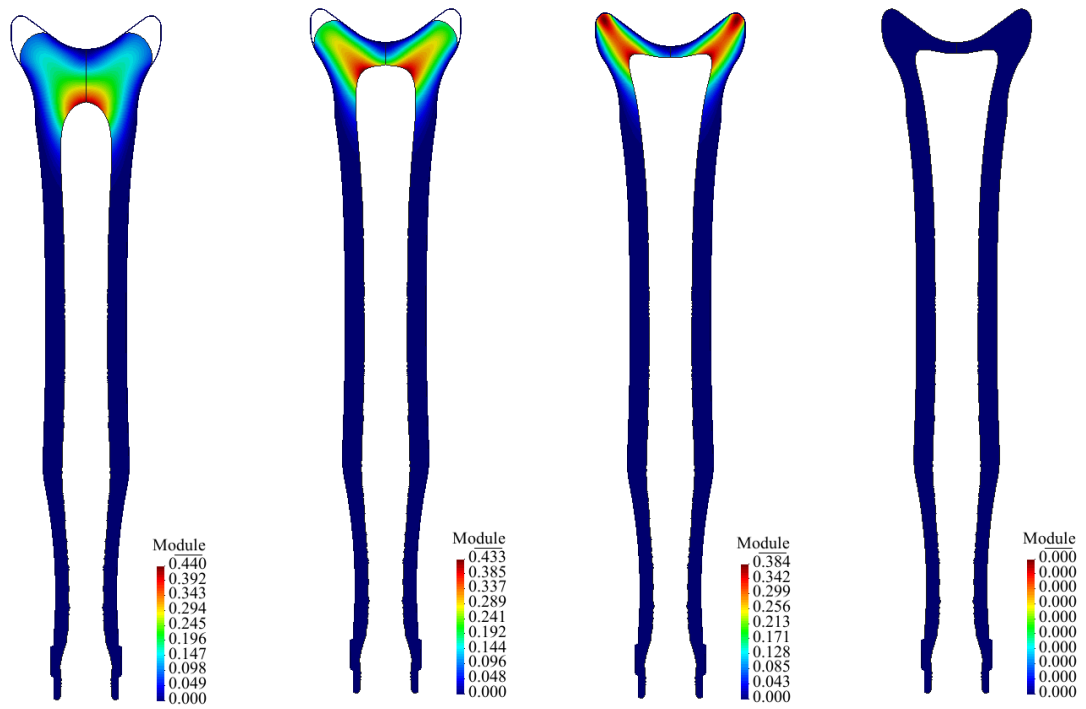


Figure 8.34: Displacement module in counter blow for the case 2 for 2.044s, 2.161s, 2.376s, 2.571s,

2.711s	2.769s	2.865s	2.939s
2.962s	2.974s	2.991s	4.777s

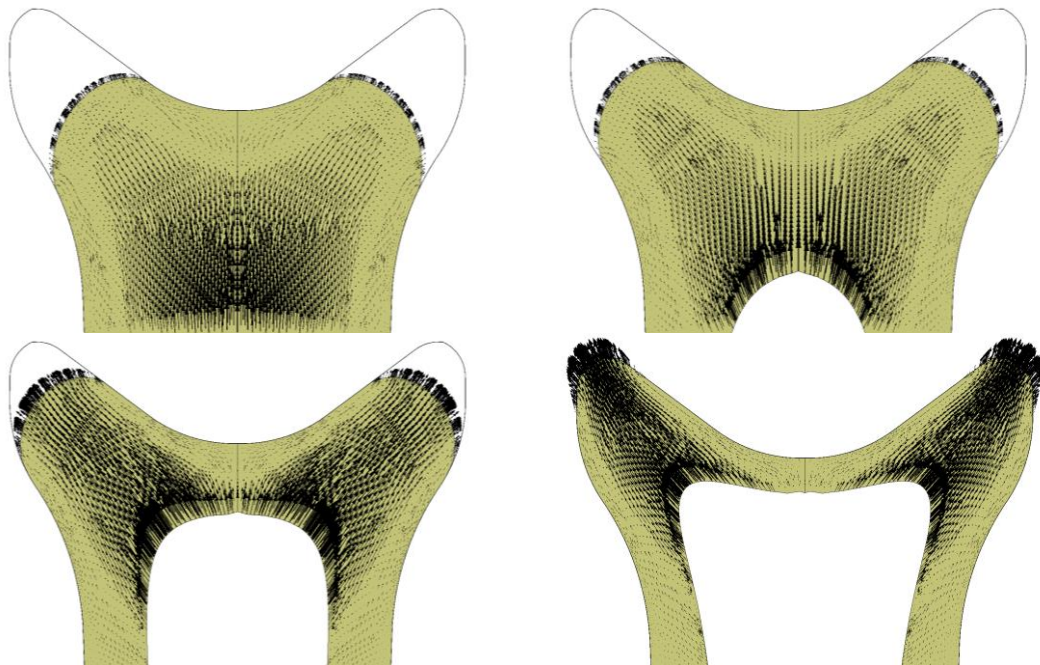
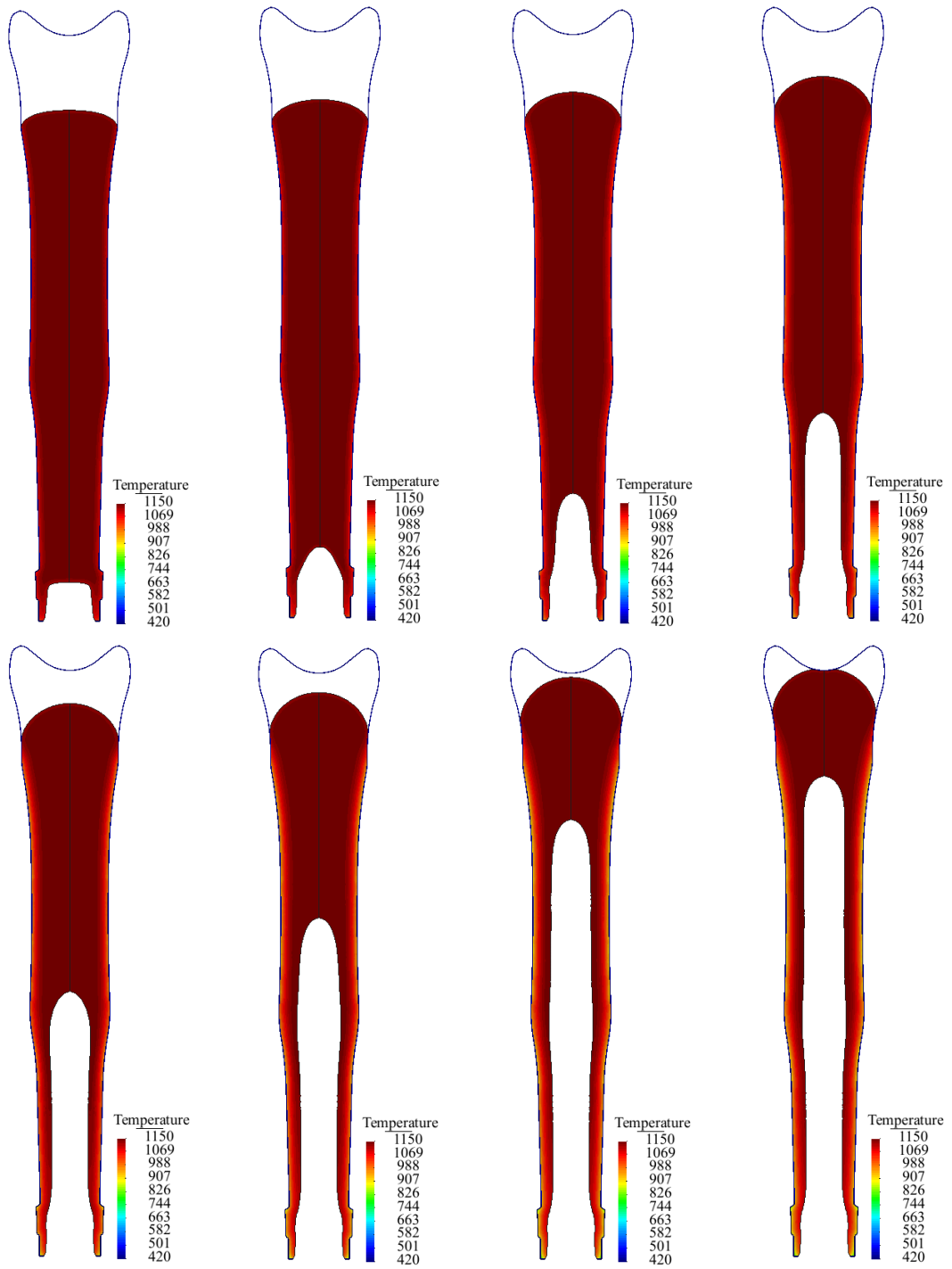


Figure 8.35: Displacement vectors with the baffle detail in counter blow for the case 2 for 2.939s, 2.962s, 2.974s and 2.991s.



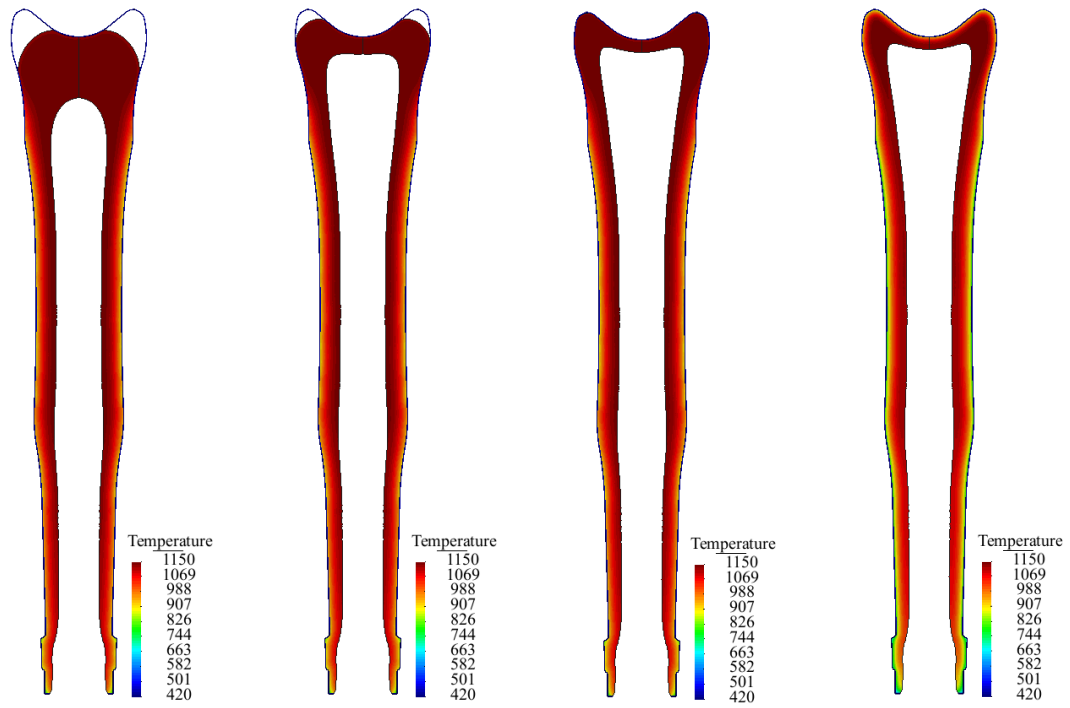


Figure 8.36: Temperature distribution in counter blow for the case 3 for 1.863s, 1.891s, 1.938s, 1.994s,

2.036s	2.081s	2.116s	2.124s
2.130s	2.134s	2.139s	3.627s

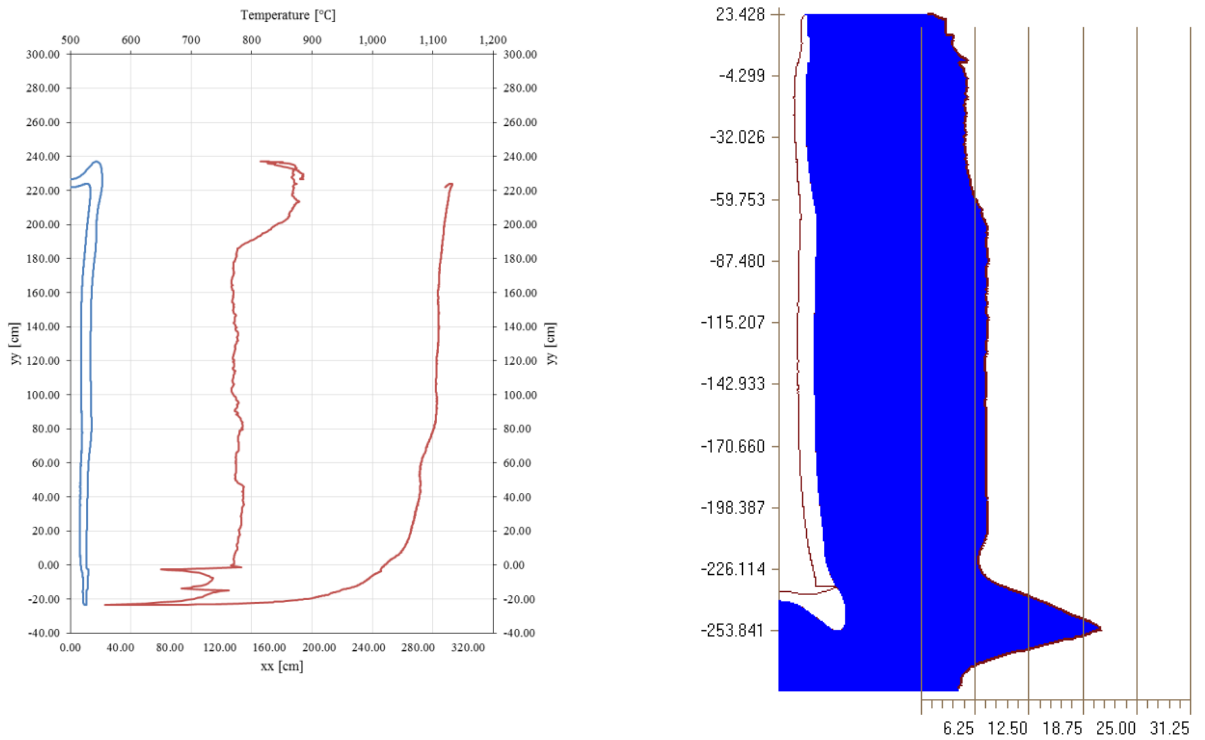
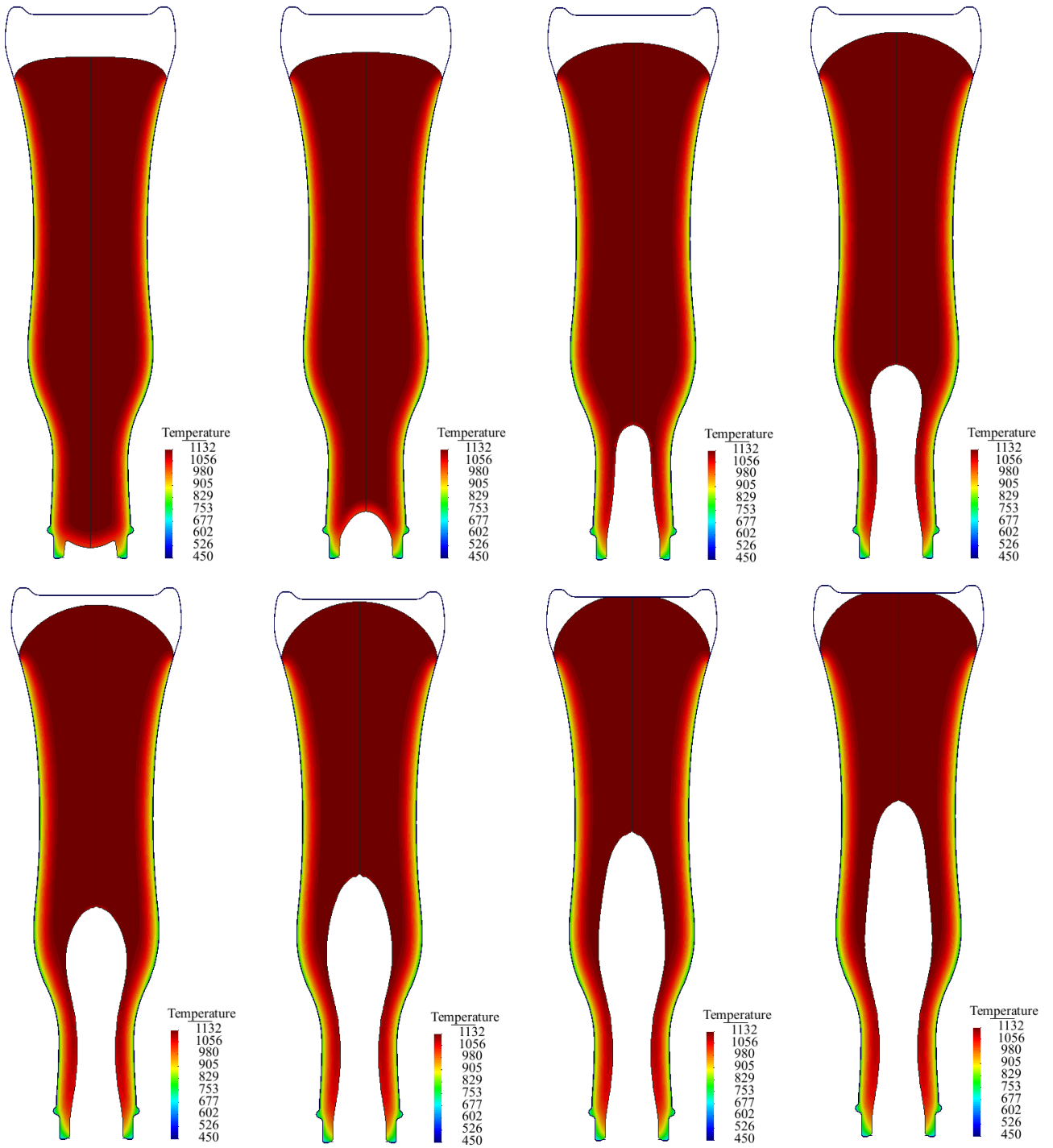


Figure 8.37: Boundary temperature for counter blow stage for case 3.

Thickness (mm) in counter blow stage for case 3.



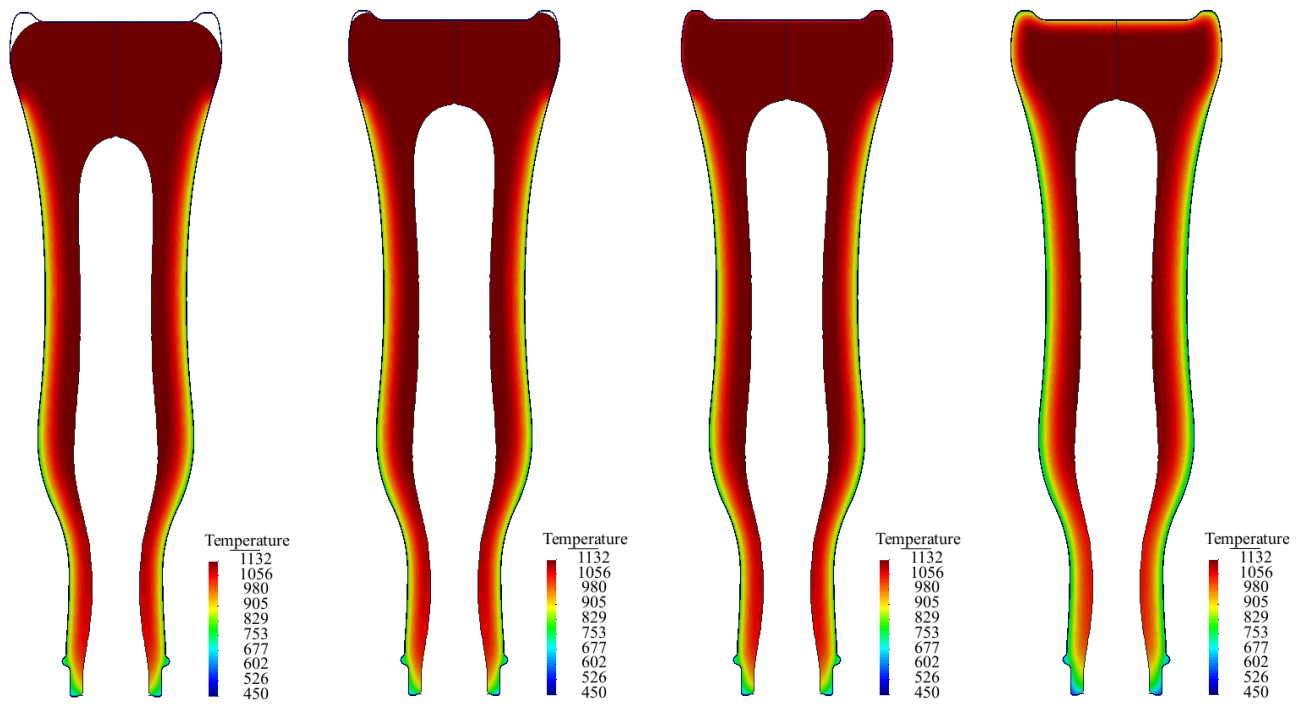


Figure 8.38: Temperature distribution in counter blow for the case 4 for 4.090s, 4.126s, 4.190s, 4.218s,

4.237s	4.253s	4.268s	4.276s
4.298s	4.303s	4.580s	7.499s

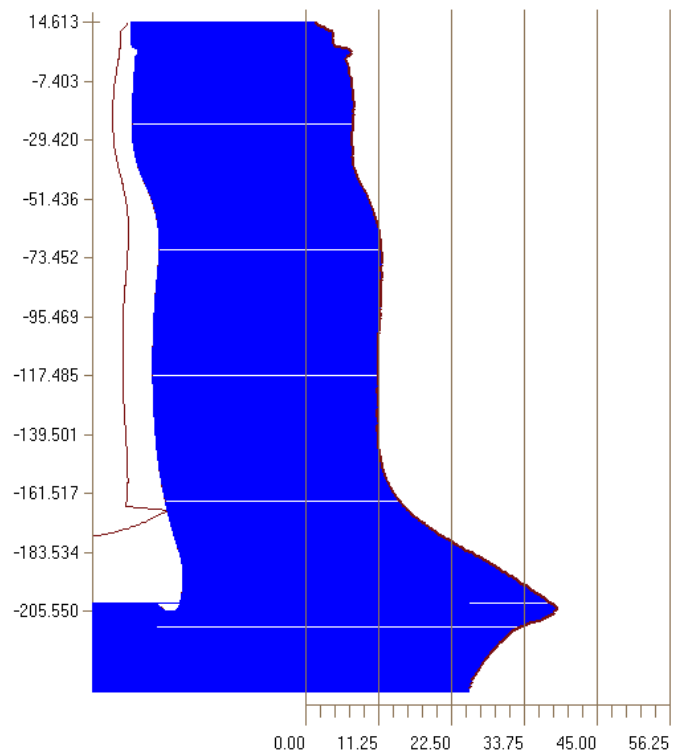
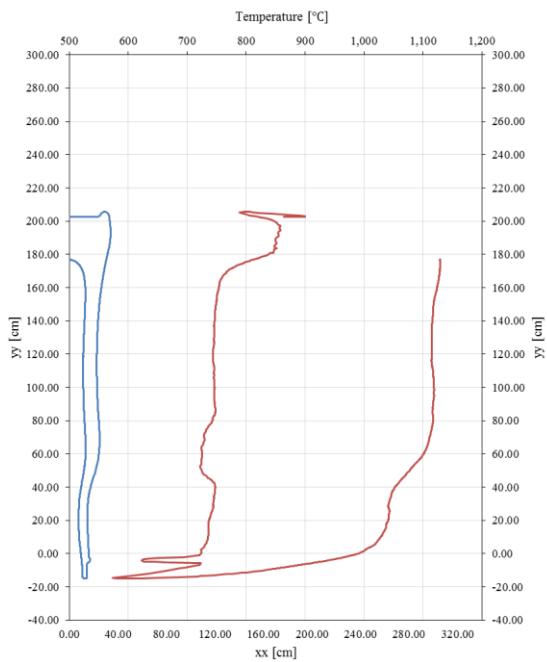
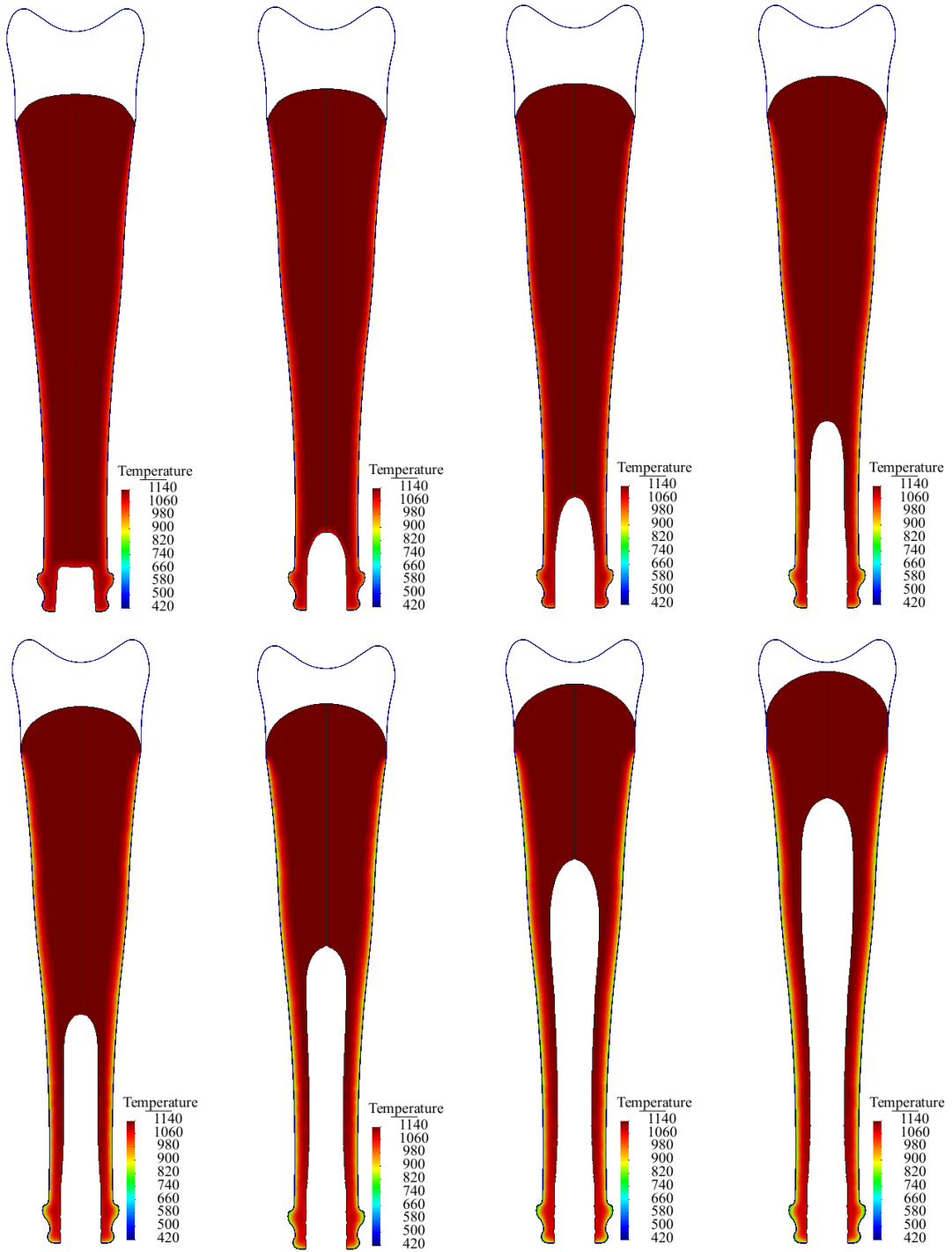


Figure 8.39: Boundary temperature for counter blow stage for case 4.

Thickness (mm) in counter blow stage for case 4.



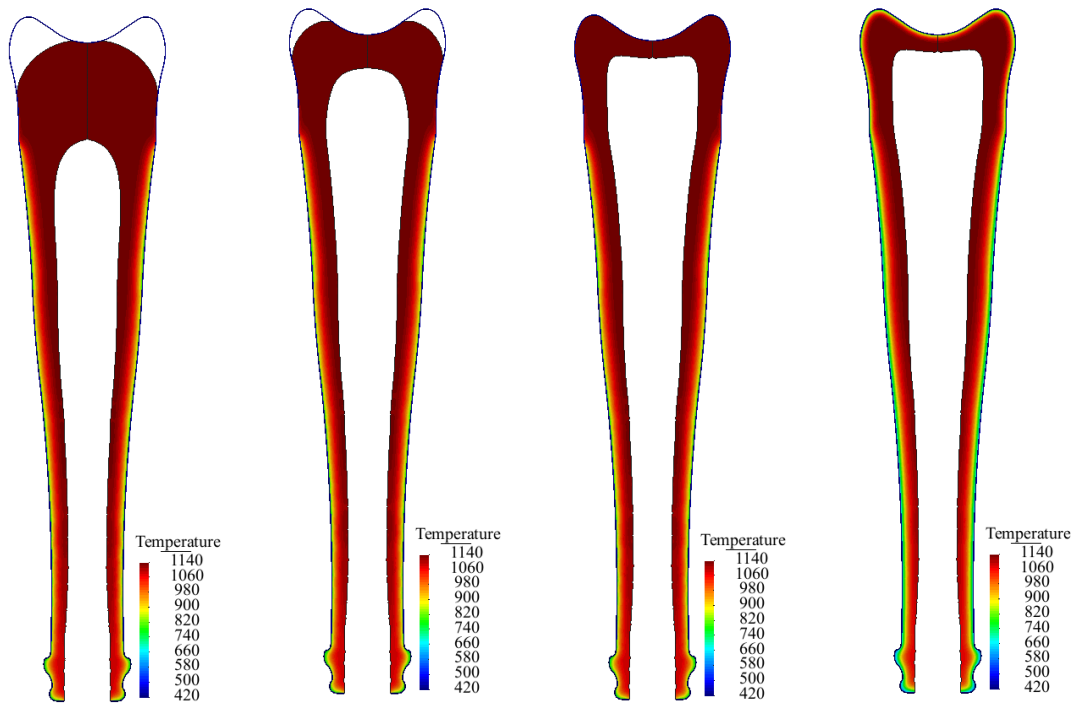


Figure 8.40: Temperature distribution in counter blow for the case 5 for 2.682s, 2.723s, 2.758s, 2.822s,

2.847s	2.879s	2.905s	2.918s
2.925s	2.931s	2.939s	4.823s

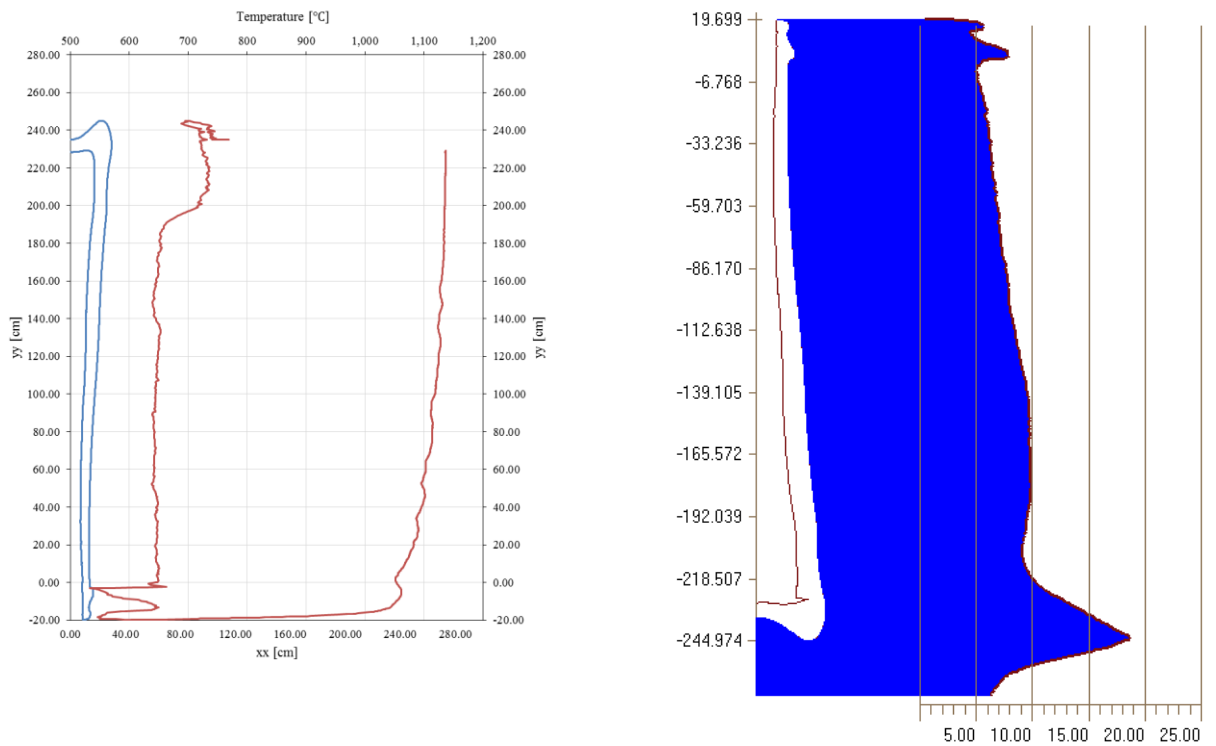


Figure 8.41: Boundary temperature for counter blow stage for case 5.

Thickness (mm) in counter blow stage for case 5.

8.1.5 Reheat

A reheat stage follows, which is essential for obtaining the right temperature distribution to initiate the next stage. Excessive or insufficient heating may cause too thin or too thick walls at the run down stage that follows. The results from the stage can be seen in Figure 8.42.

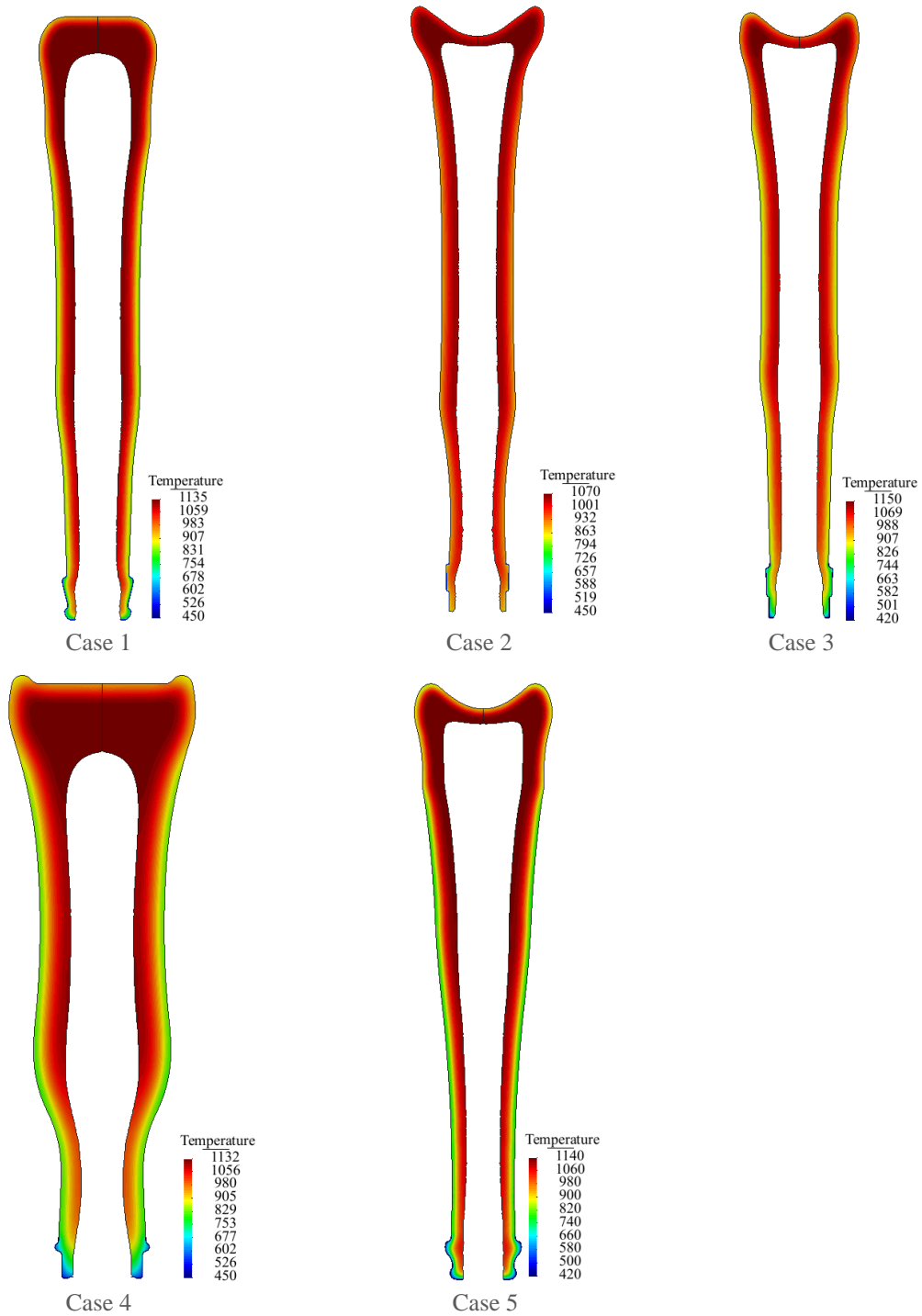


Figure 8.42: Temperature distribution in reheat for the case 1 in 3.958s, for the case 2 in 5.622s, for the case 3 in 4.705s, for the case 4 in 10.227s and for the case 5 in 6.117s.

8.1.6 Invert

Before inverting the parison the blank mould is opened and reheating is allowed. While the parison is moved to the blow mould reheating of the parison is allowed, and heat is transferred from the hotter zones (inside) to the colder ones (outside). Stretching and cooling of the parison can be helped by the use of overhead cooling over the blow mould. The results from this stage can be seen in Figure 8.43. It is clear that the temperature at the exterior boundary of the parison increases due to the temperature equalization. Heat from the inside part travels to the outside to equalize the parison temperature. In Figure 8.44 the boundary temperatures at the end of the invert stage are presented.

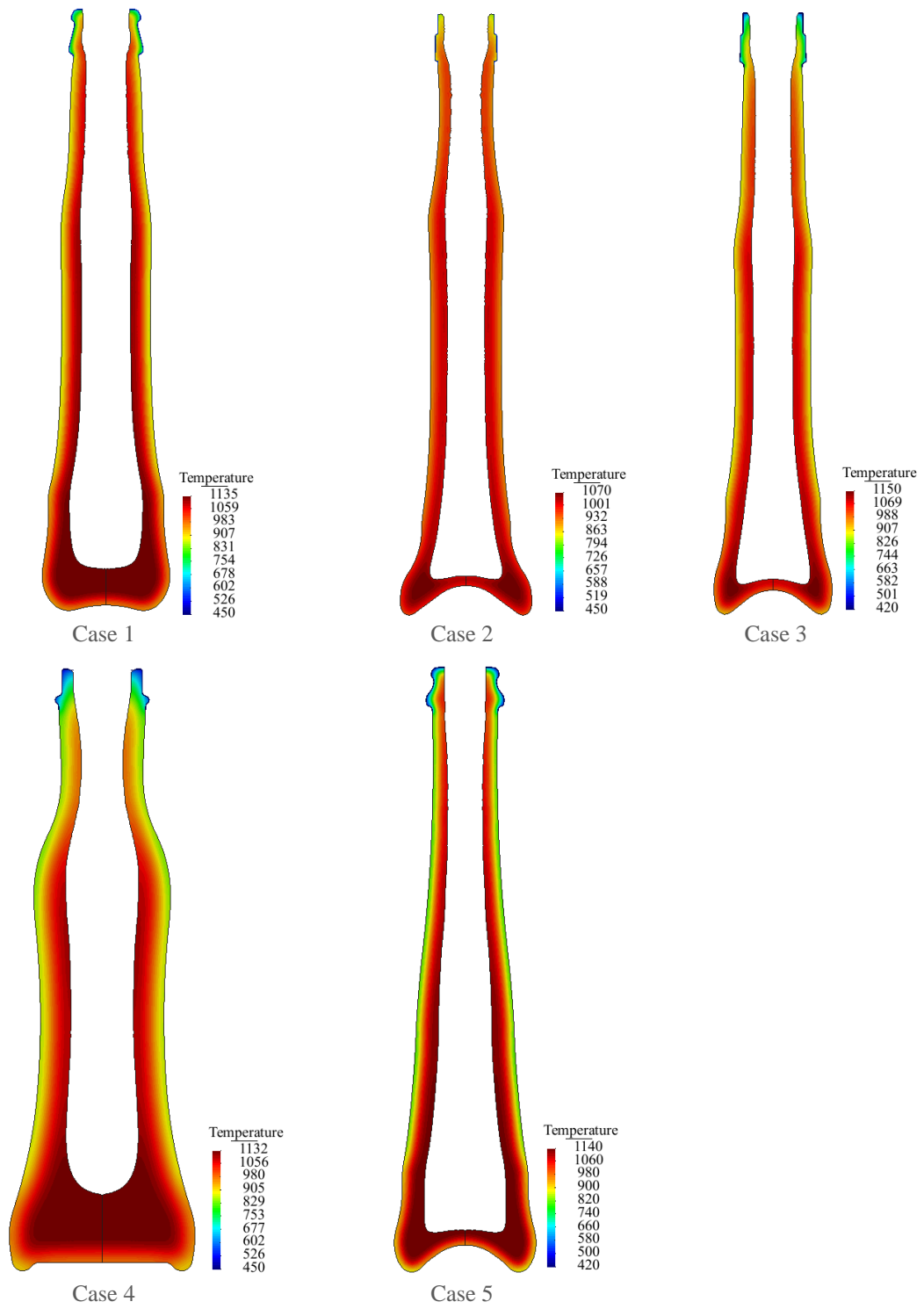
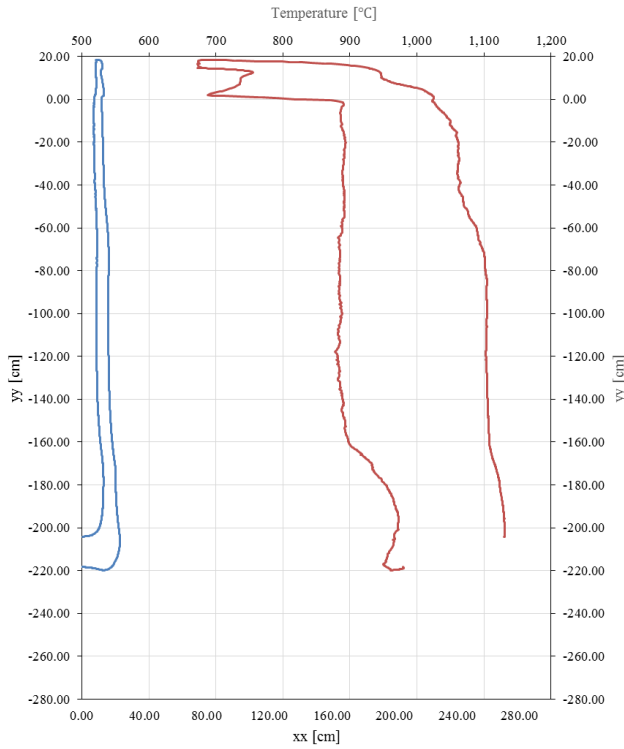
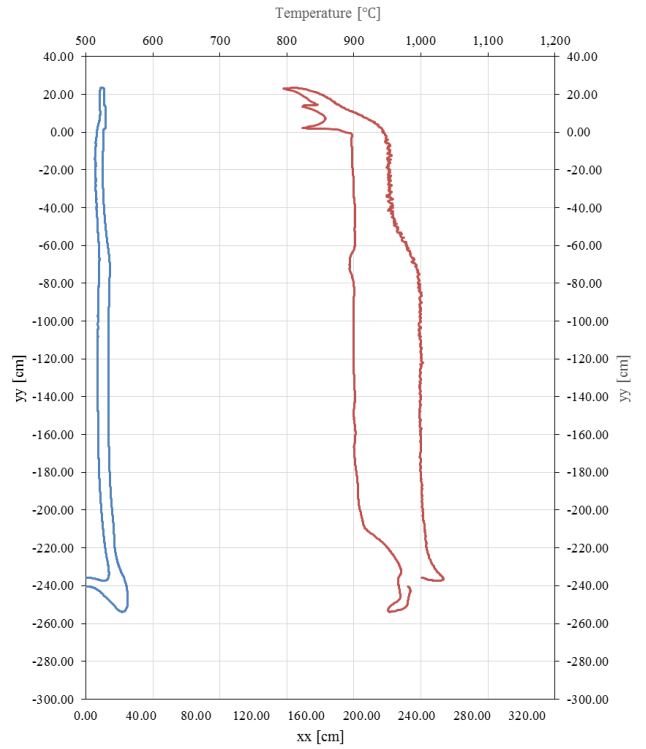


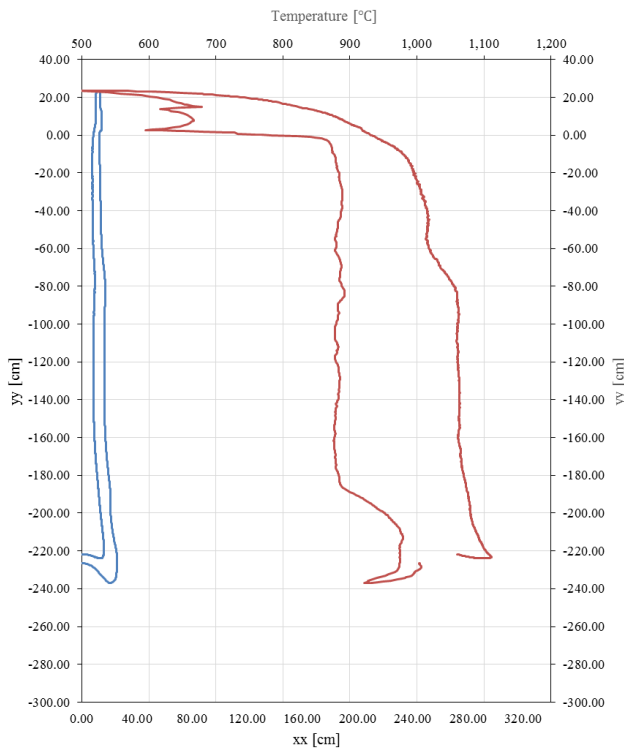
Figure 8.43: Temperature distribution in invert for the case 1 in 4.514s , for the case 2 in 6.666s, for the case 3 in 5.490s, for the case 4 in 11.590s and for the case 5 in 6.823s.



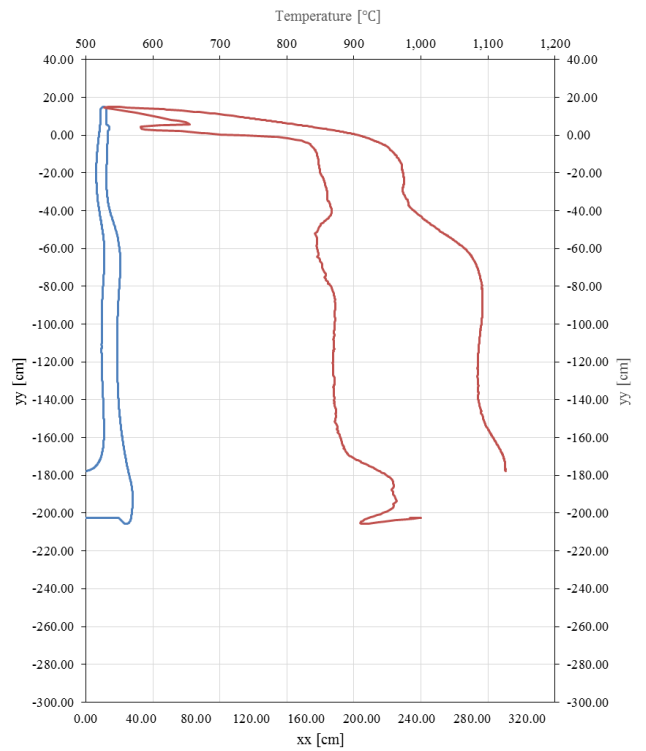
Case 1



Case 2



Case 3



Case 4

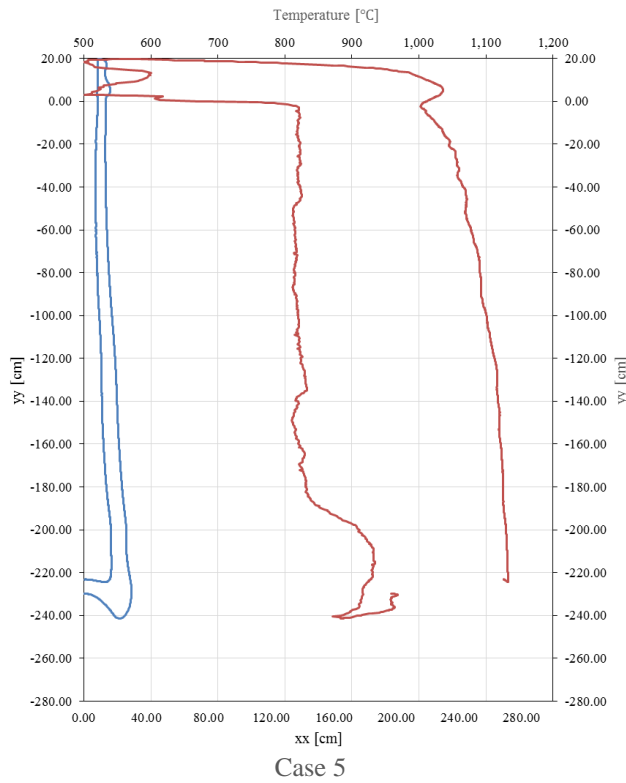


Figure 8.44: Boundary temperature for invert stage for case 1, case 2, case 3, case 4 and case 5.

8.1.7 Rundown

For case 1 the shape and temperature contour of the glass are plotted in Figure 8.45. The glass falls due to gravity until it reaches the bottom of the blow mould cooling until the end of the stage. In Figure 8.46 the boundary temperature can be seen, where is clear that the neckring continues to lose heat. The exterior boundary of the parison is around 920°C while the interior 1090°C. In addition, the bottom zone has a higher temperature due to the fact that it has a greater mass of glass.

For case 2 the shape and temperature contours of the glass are plotted in Figure 8.47. Again, the glass falls until the bottom of parison completely accommodates the bottom of the blow mould. The exterior boundary is around 900°C while the interior is around 970°C and in the bottom zone of the parison lower temperatures are visible, as shown in Figure 8.48. Additionally, in Figure 8.49 it can be seen the displacement field. While the glass does not hit the bottom of the blow mould, the highest displacement is located at the bottom zone of the parison. This effect is due to the fact that parison has more mass at the bottom zone. When the glass parison reaches the blow moulds then the higher displacements are located at the middle wall of the parison.

Very similar results are presented for case 3, case 4 and case 5. The respective shape and temperature contours of the glass are plotted in Figure 8.50, Figure 8.52 and Figure 8.54. The boundary temperatures are presented in Figure 8.51, Figure 8.53 and Figure 8.55.

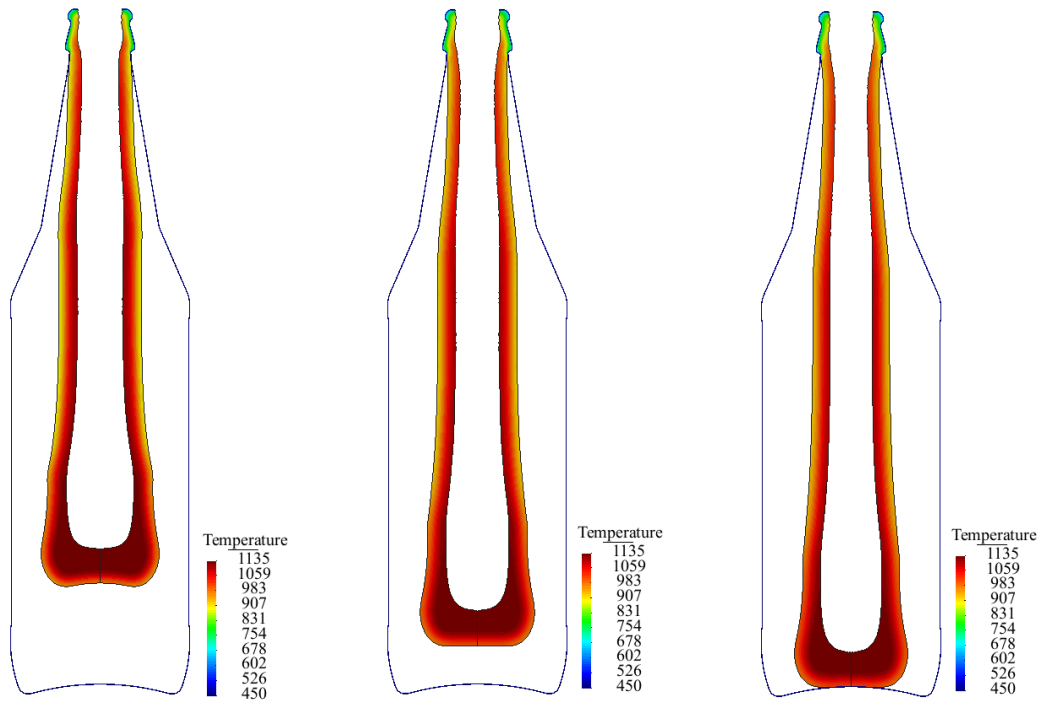


Figure 8.45: Temperature distribution in rundown for the case 1 in 4.514s, 5.201s, 5.833s.

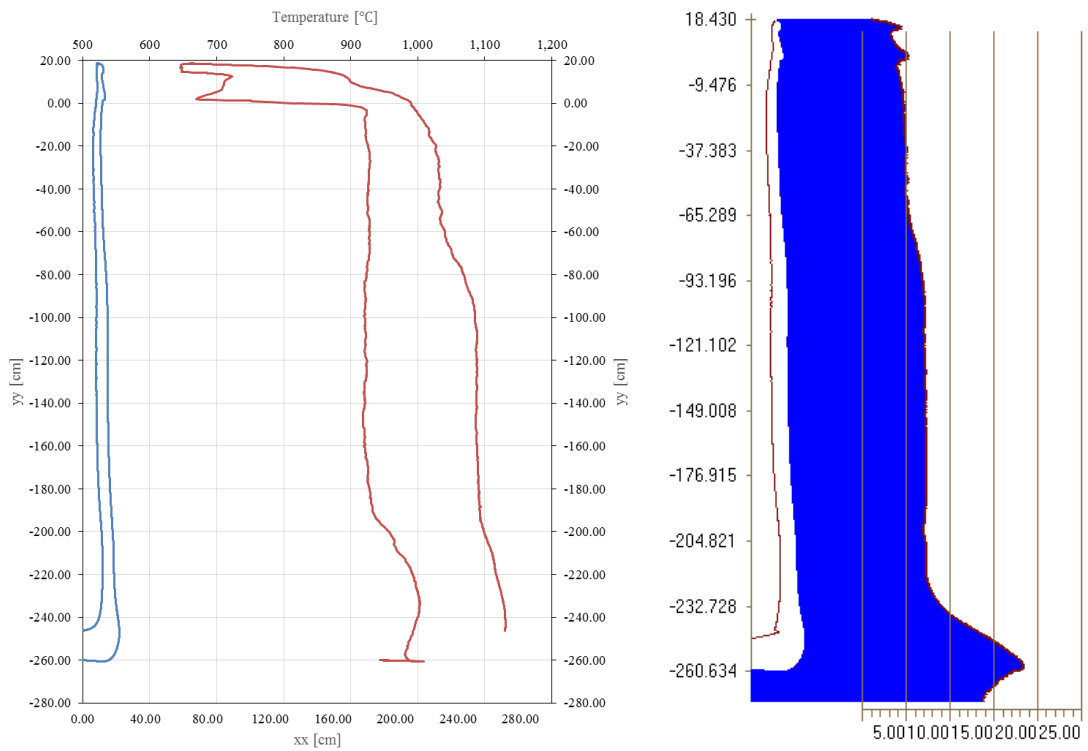


Figure 8.46: Boundary temperature in rundown for case 1.

Thickness (mm) in rundown stage for case 1.

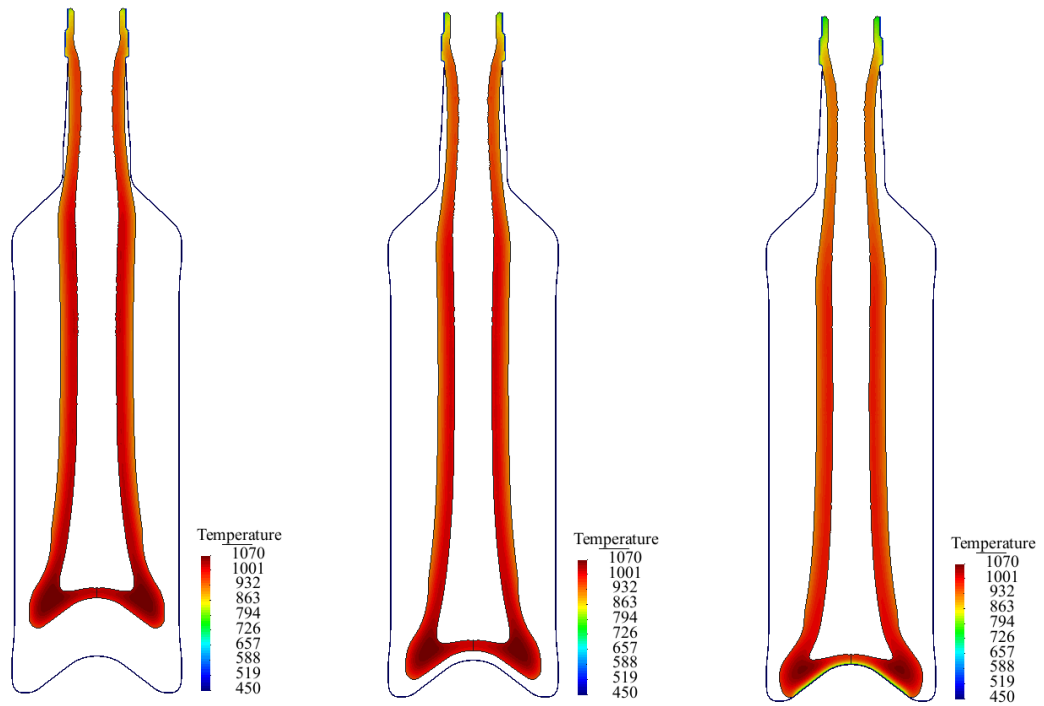


Figure 8.47: Temperature distribution in rundown for the case 2 in 6.666s, 7.222s and 9.111s.

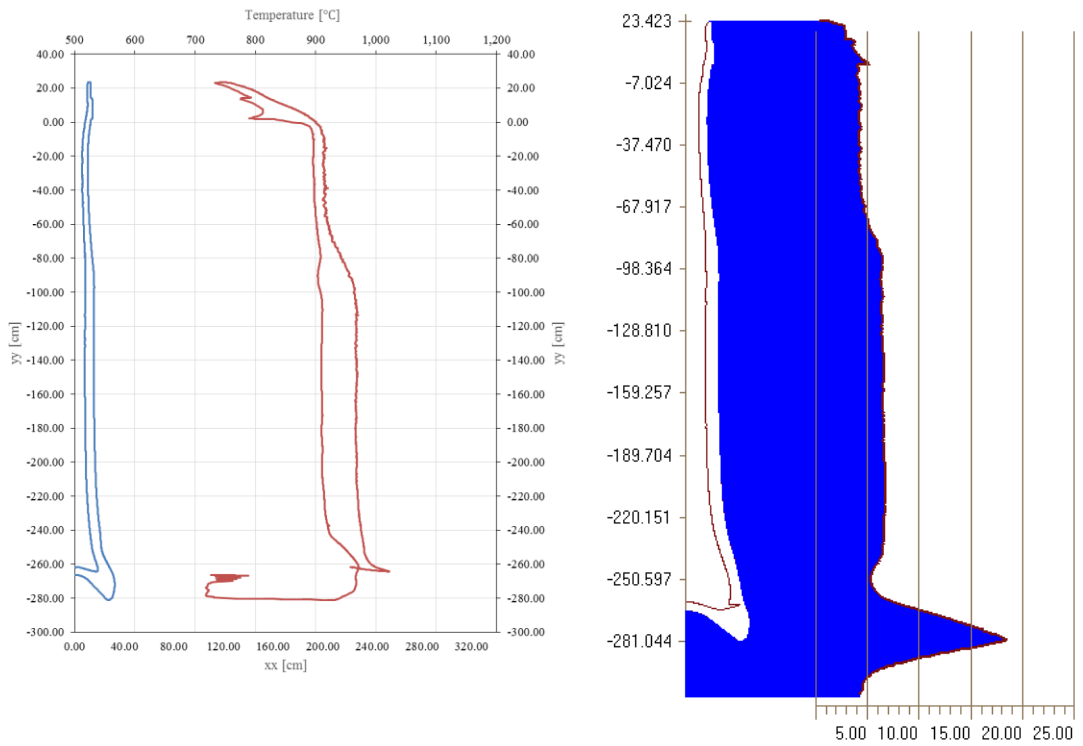


Figure 8.48: Boundary temperature in rundown for case 2.

Thickness (mm) in rundown stage for case 2.

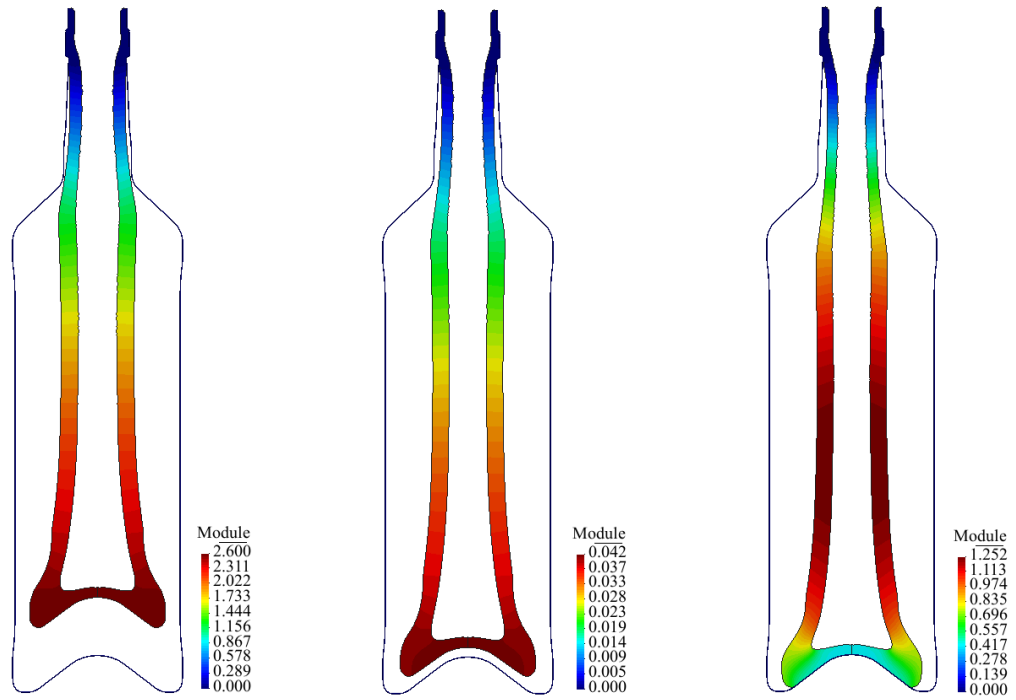


Figure 8.49: Displacement module in rundown for the case 2 in 6.666s, 7.222s and 9.111s.

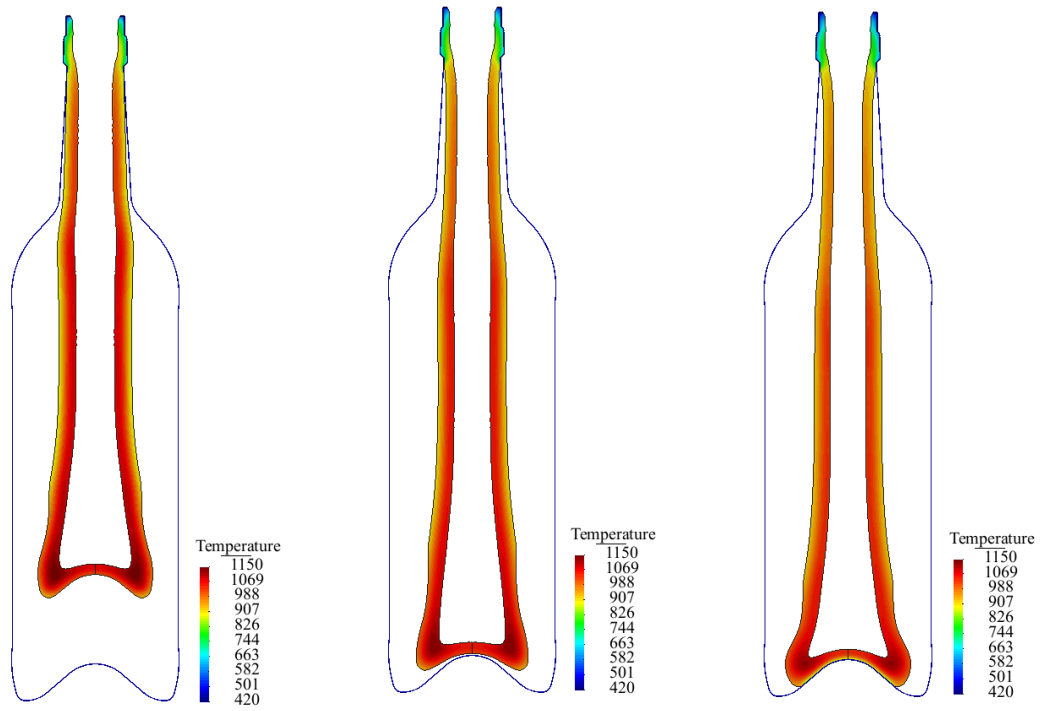


Figure 8.50: Temperature distribution in rundown for the case 3 in 5.490s, 6.590s and 7.843s.

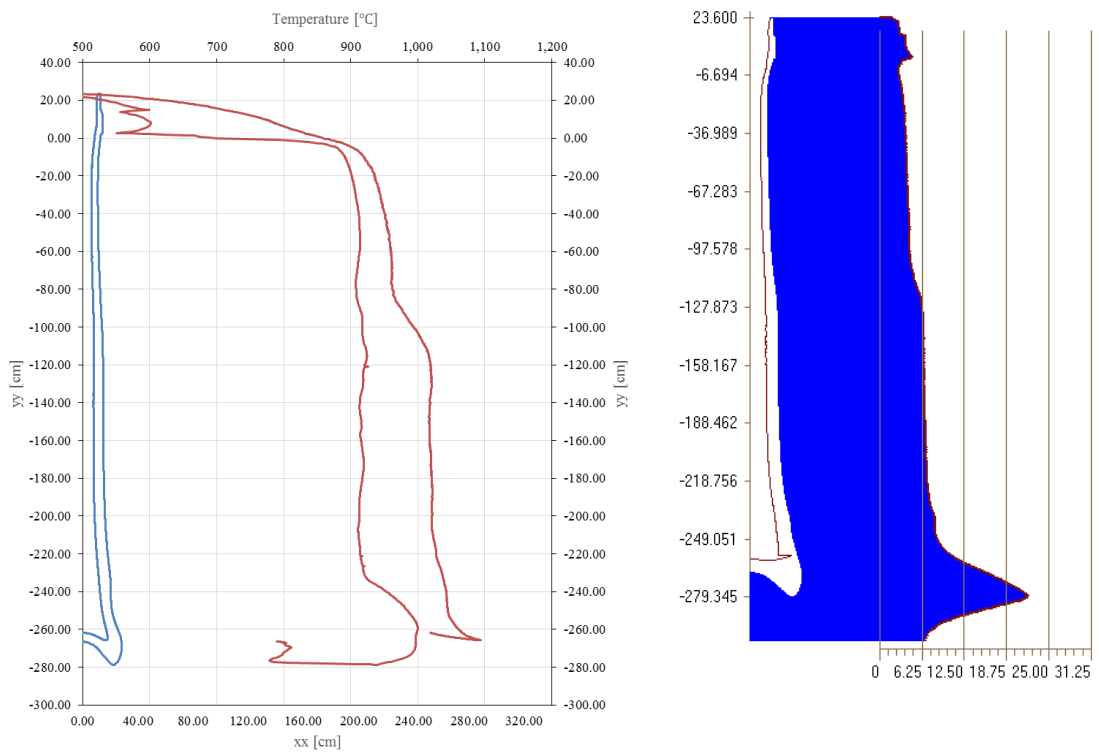


Figure 8.51: Boundary temperature in rundown for case 3.

Thickness (mm) in rundown stage for case 3.

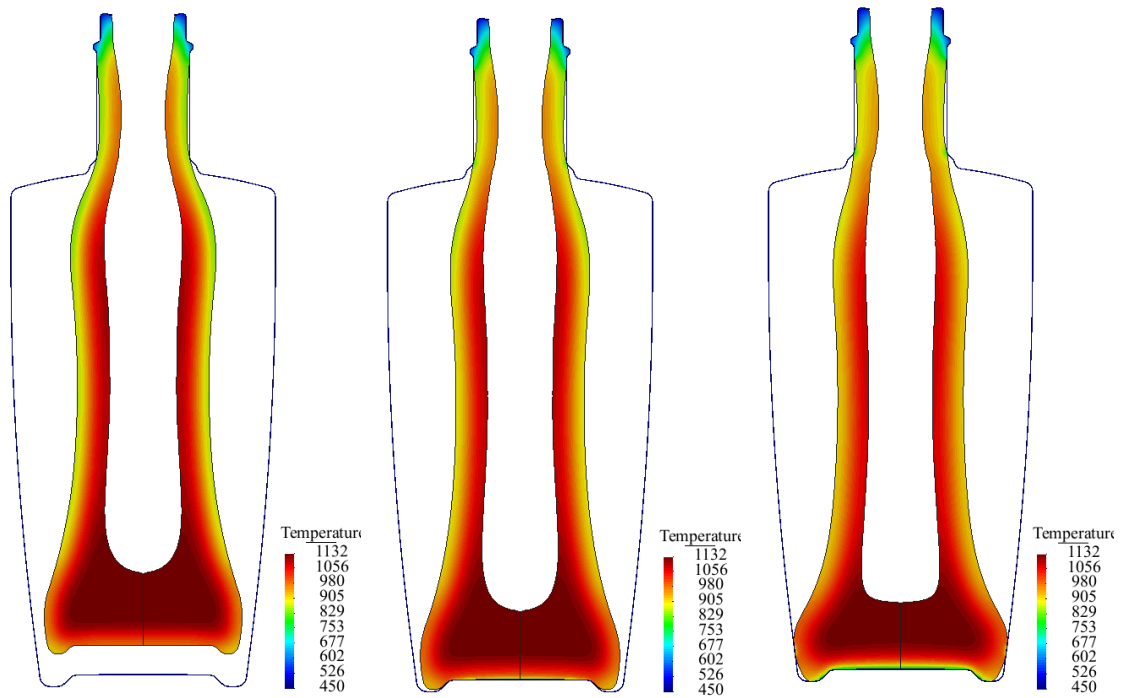


Figure 8.52: Temperature distribution in rundown for the case 4 in 11.590s, 12.898s, 14.545s.

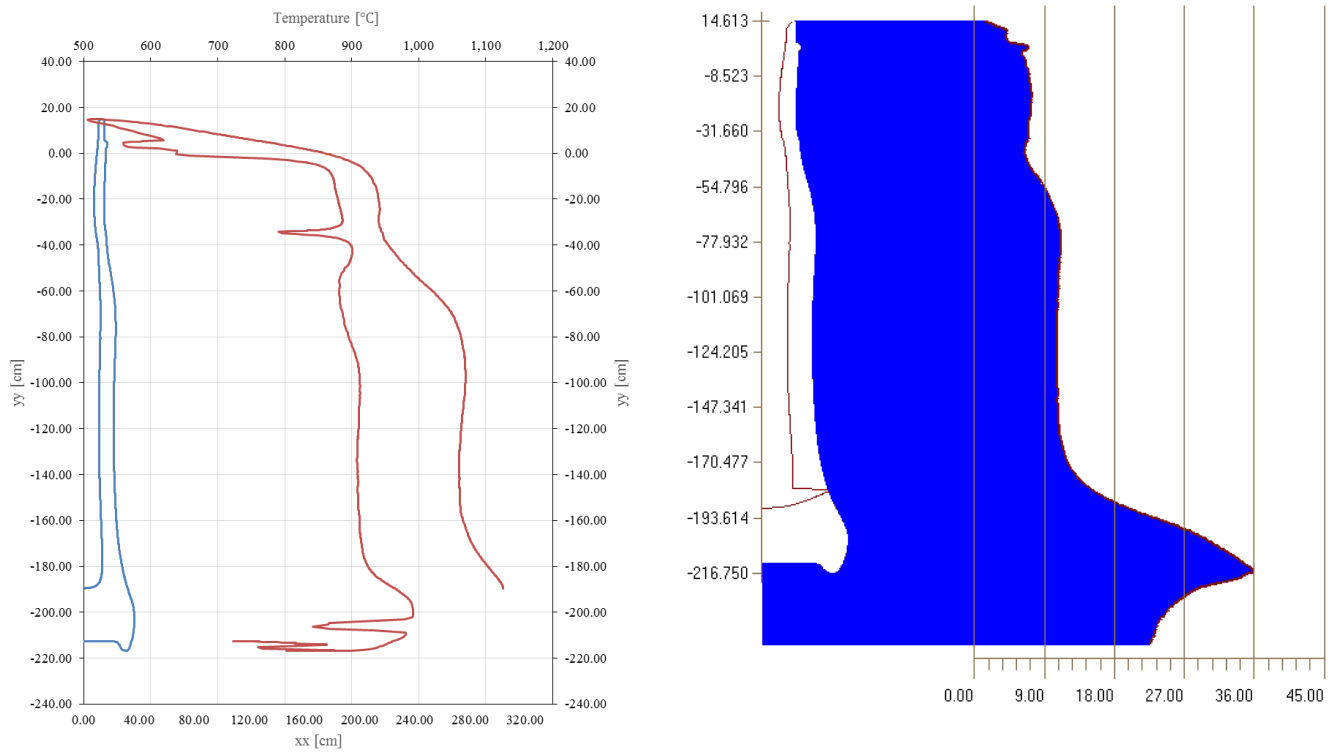


Figure 8.53: Boundary temperature in rundown for case 4.

Thickness (mm) in rundown stage for case 4.

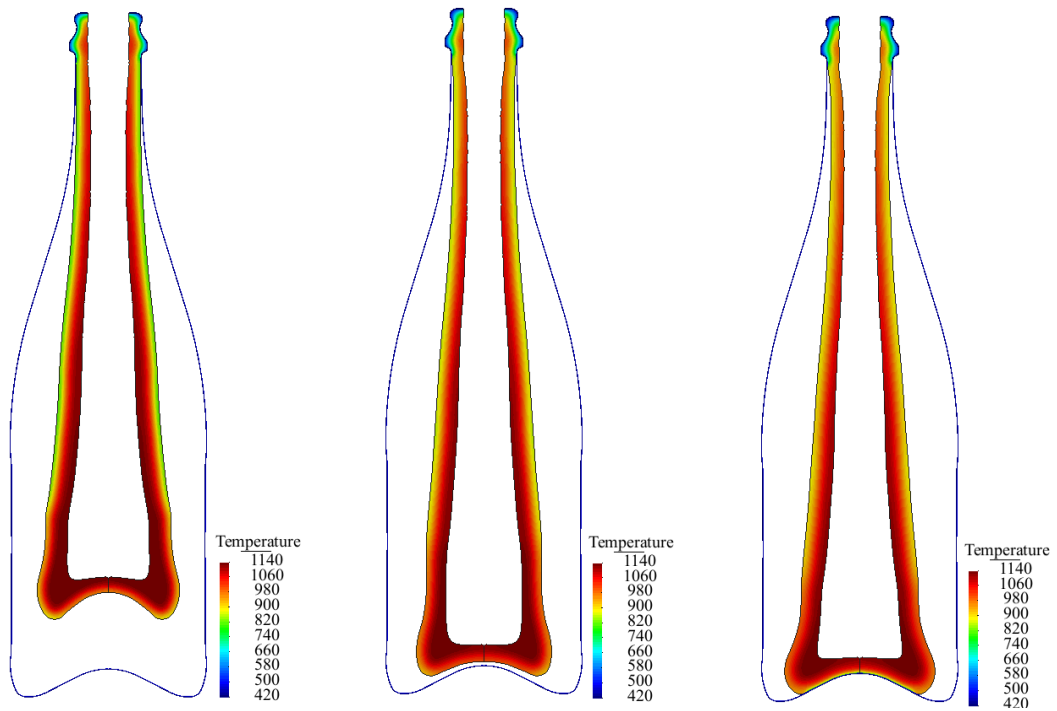


Figure 8.54: Temperature distribution in rundown for the case 5 in 6.823s, 8.527s and 9.882s.

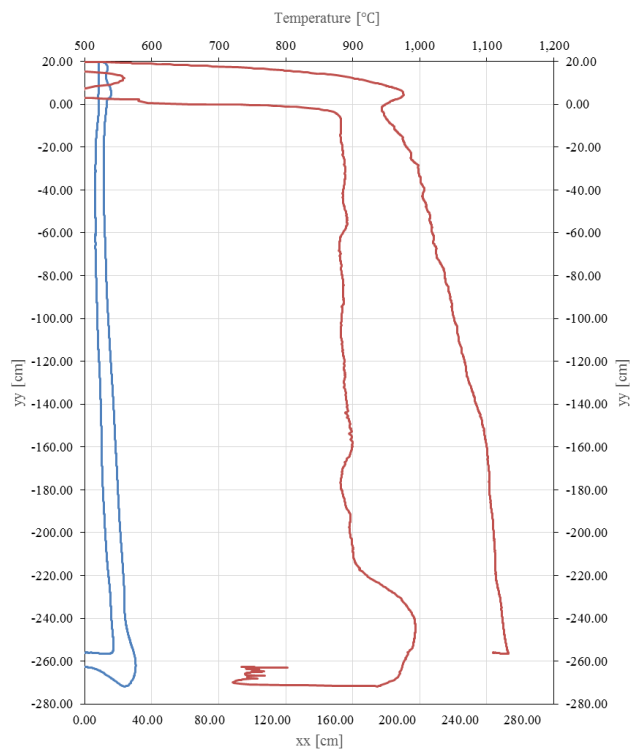
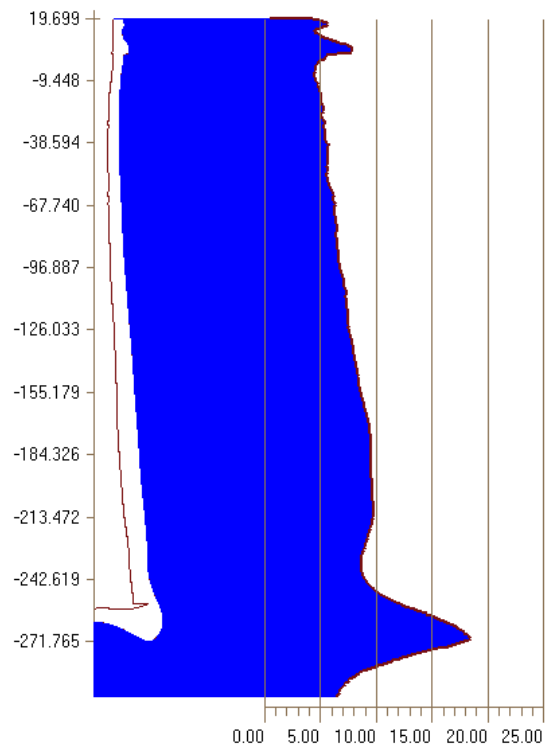


Figure 8.55: Boundary temperature in rundown for case 5.



Thickness (mm) in rundown stage for case 5.

8.1.8 Final Blow

Vacuum is applied to the blow mould cavity to form the finished bottle, and the final blow air is also used in helping to form the shape of the bottle. Circulating air through the internal cooling blow head arm, when the blow head is on top of the mould, causes the internal temperature of the bottle to be reduced. Vacuum and final blow time should be the maximum to form the bottle before being removed from the blow mould.

For case 1 the shape and temperature contours of the glass are plotted in Figure 8.56. As it can be seen the air pressure forces the glass to contact the mould. Hotter and thinner zones have higher velocities moving to the boundaries, therefore, the “correct” temperature distribution is required for an even thickness distribution to be obtained. When the final shape of the glass container is completely formed the glass cools against the mould.

For the case 2, case 3, case 4, case 5 the temperatures contour of the glass are plotted in Figure 8.57, Figure 8.59, Figure 8.60, Figure 8.61. Despite the fact that the shape of the containers are different the behaviour with the final blow is quite similar.

The displacement field for the case 2 is shown in Figure 8.58. At the beginning the higher displacements are located in the zone that has higher temperature, forcing the glass to hit the blow mould wall. Then the glass wall gets progressively into contact with the mould, ending with the contact at the container shoulder.

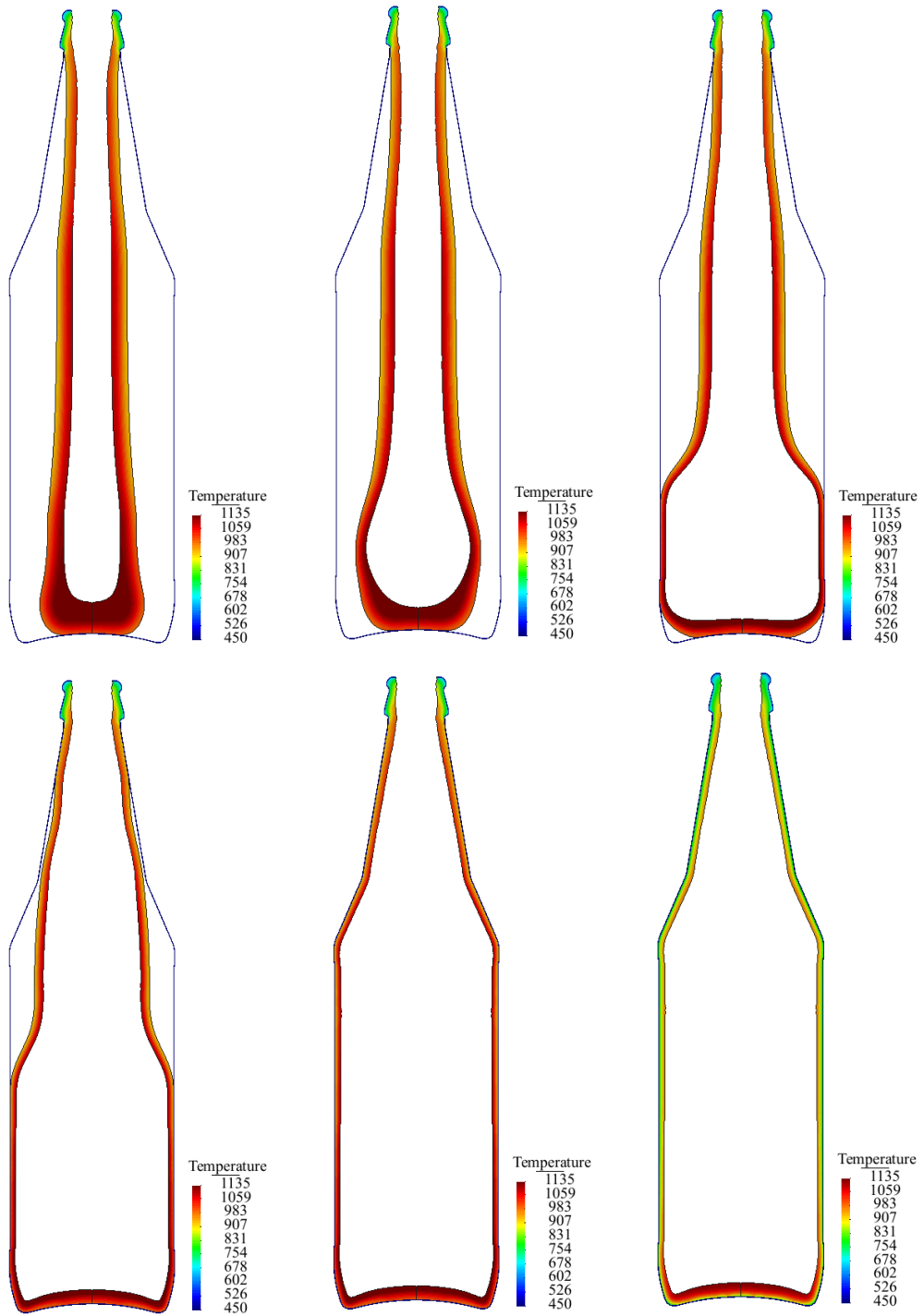


Figure 8.56: Temperature distribution in final blow for the case 1 in 5.555s, 5.556s, 5.558s,

5.561s

5.570s

7.222s

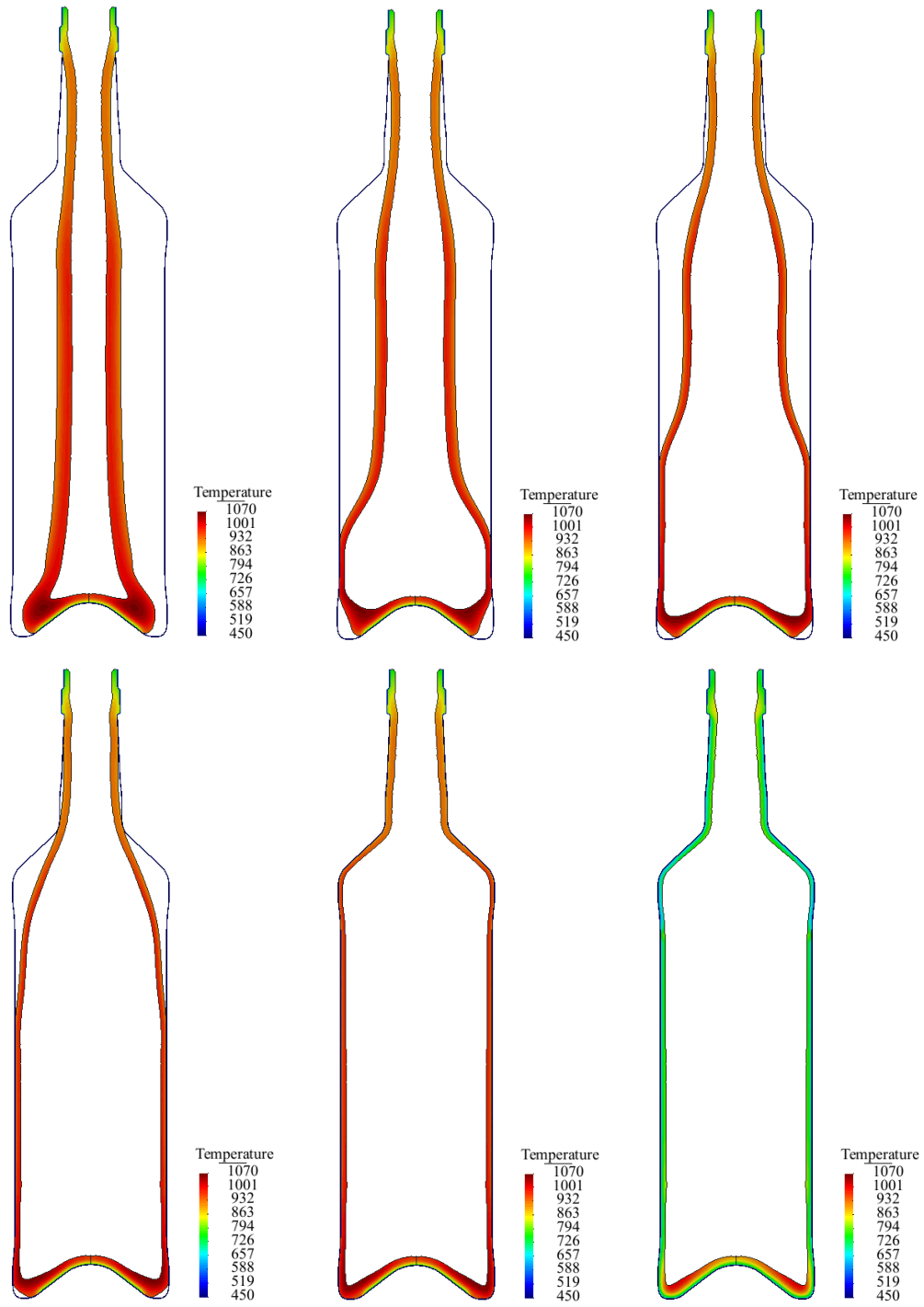


Figure 8.57: Temperature distribution in final blow for the case 2 in 9.111s, 9.125s, 9.133s,

9.139s

9.188s

12.333s

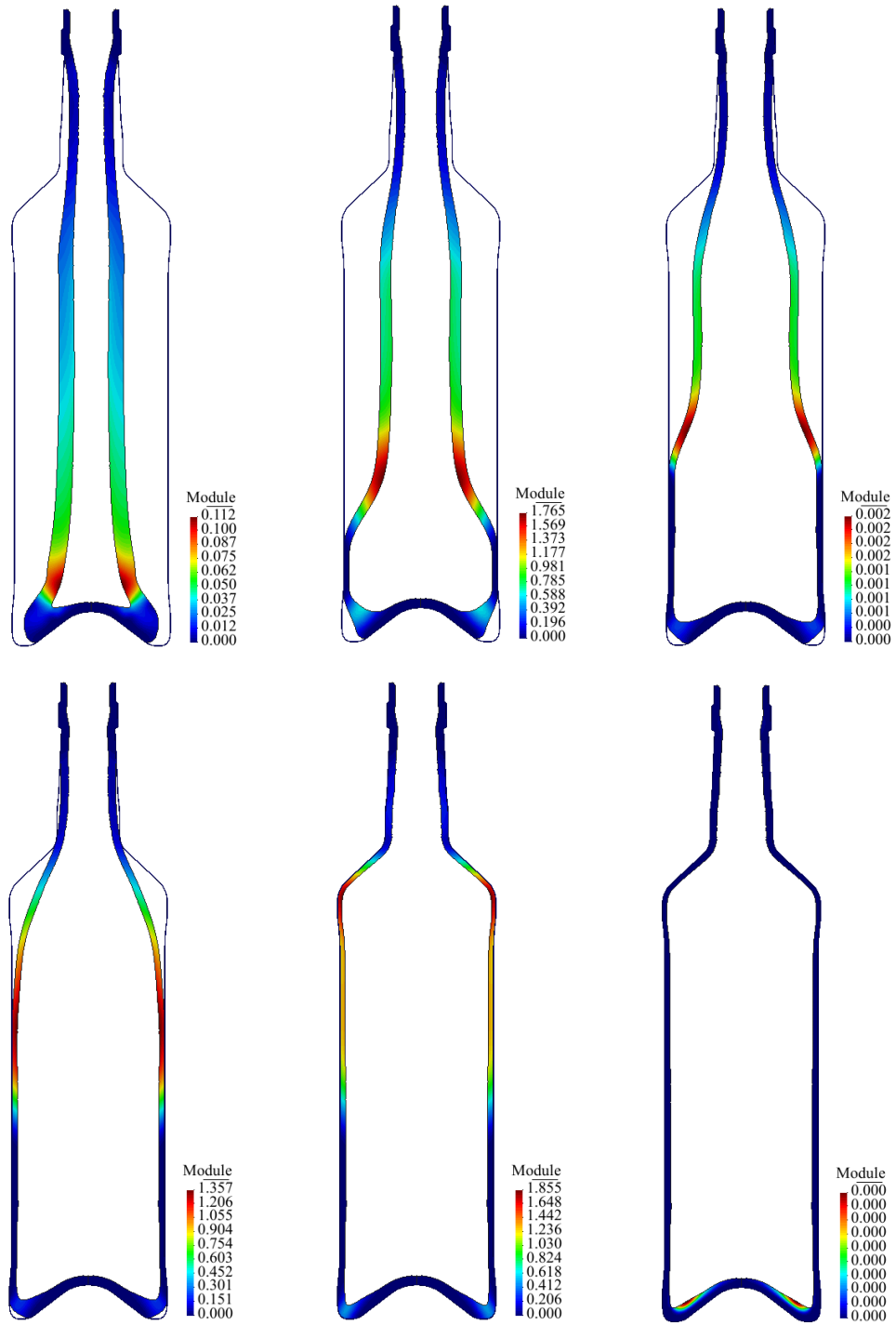


Figure 8.58: Displacement module in final blow for the case 2 in 9.111s, 9.125s, 9.133s,

9.139s

9.188s

12.333s

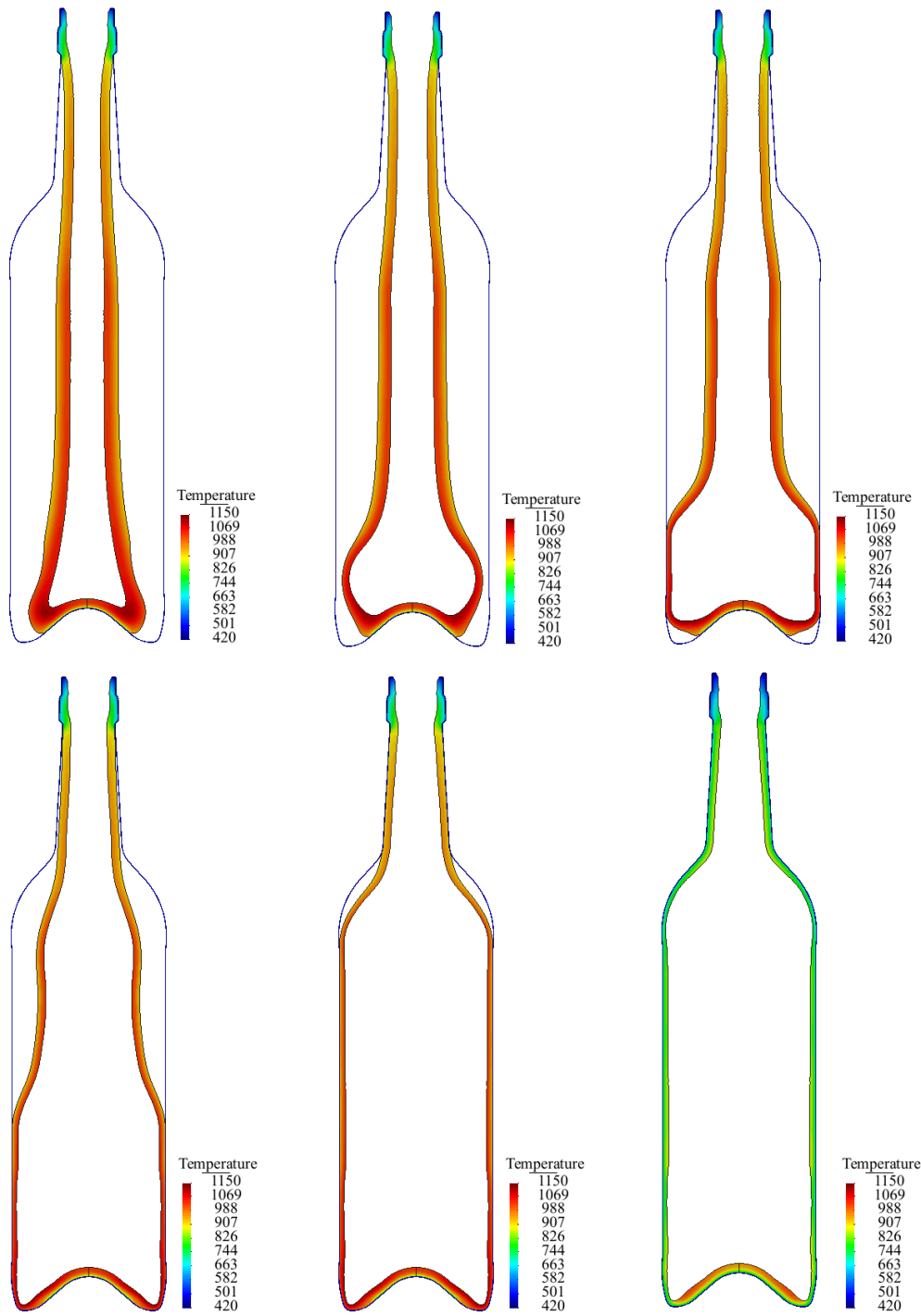


Figure 8.59: Temperature distribution in final blow for the case 3 in 7.843s, 7.846s, 7.848s,

7.853s

7.857s

10.196s

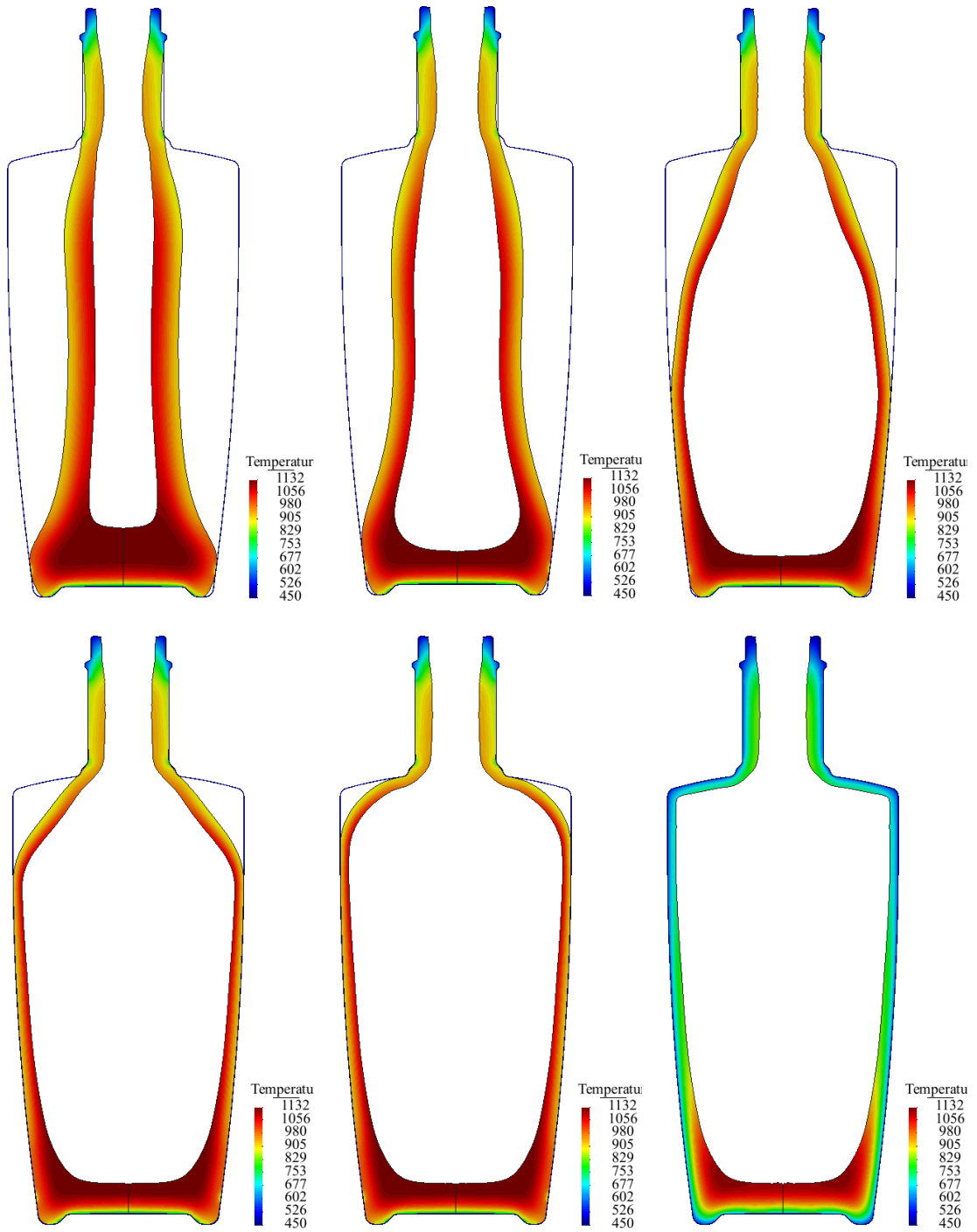


Figure 8.60: Temperature distribution in final blow for the case 4 in 14.545s, 14.552s, 14.563s,

14.569s

14.576s

22.272s

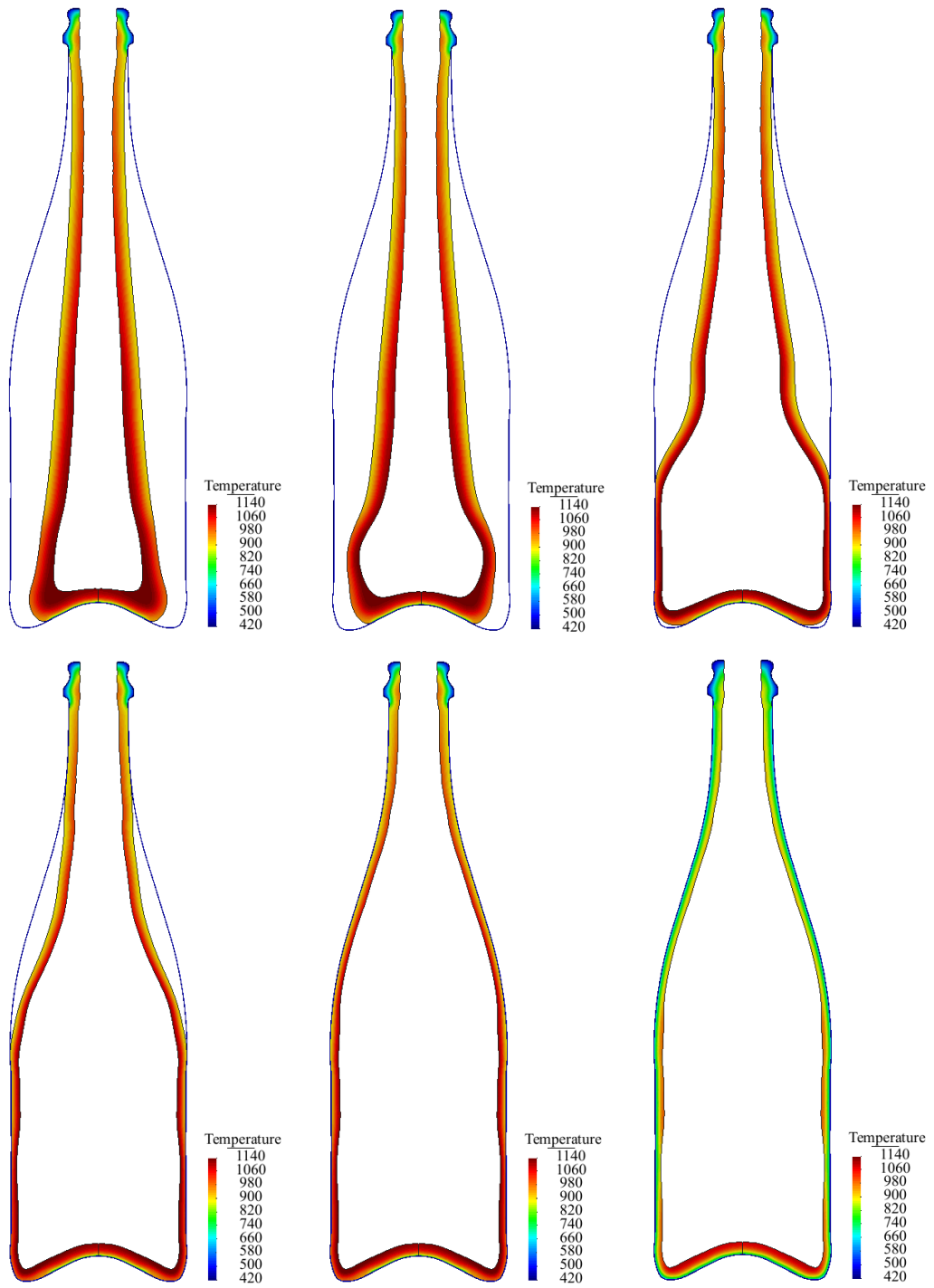


Figure 8.61: Temperature distribution in rundown for the case 5 in 9.882s, 9.884s, 9.892s,

9.902s

9.916s

13.717s

8.1.9 Mould Open

Mould open is the last stage the process, in which basically, the blank opens allowing the glass cooling to the ambient air, however, the simulation at this stage is considered thermomechanical to be possible some defects. The results are presented in Figure 8.62. It can be noted that the exterior temperature are around 600°C as it can be seen in Figure 8.63. It can be seen that in the container there are zones where temperatures are lower. This effect is caused by the thickness difference, thin zones cool faster and thick zones cool slower. This is clearly seen in the bottom on the container which is always thicker than the wall.

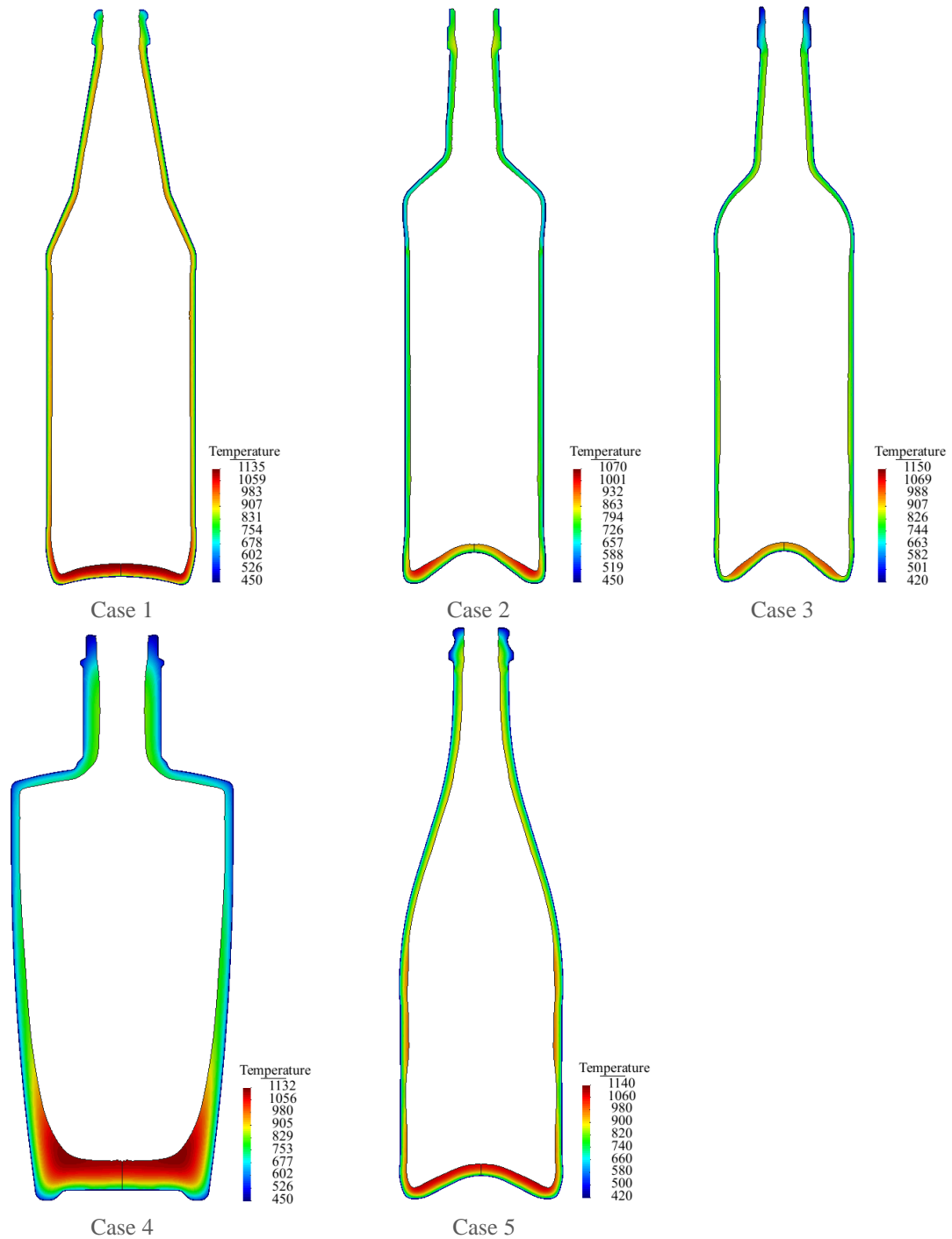
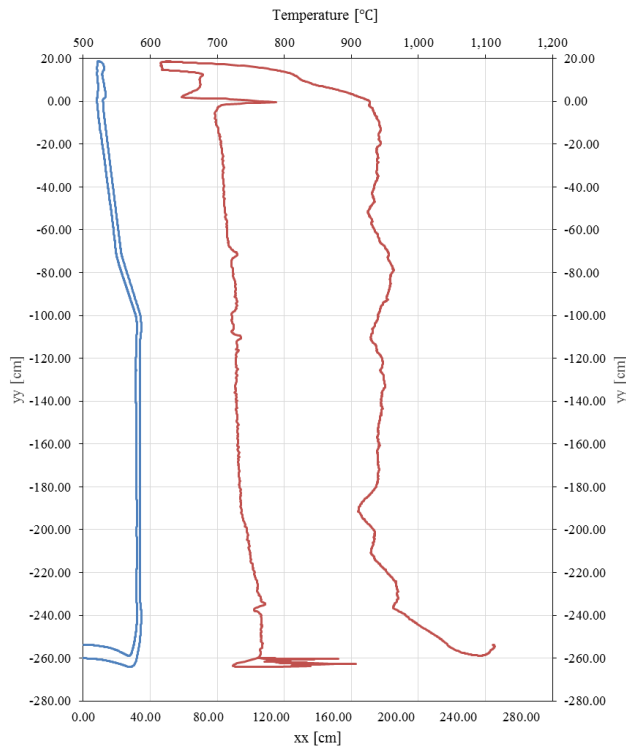
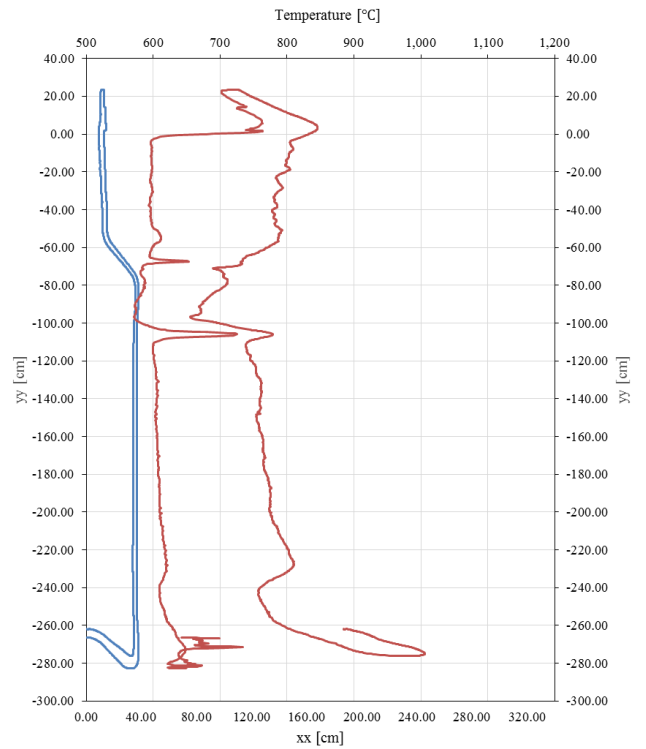


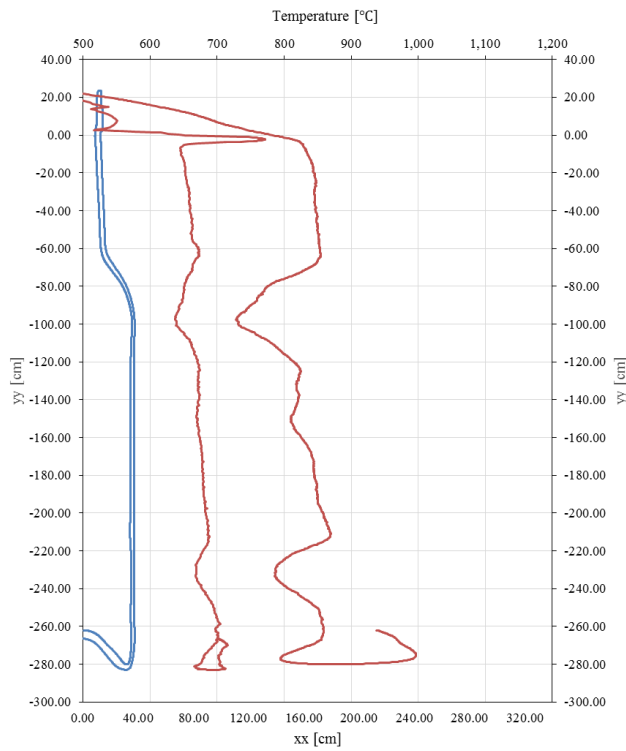
Figure 8.62: Temperature distribution in mould open for the case 1 in 7.292s, for the case 2 in 12.555s, for the case 3 in 10.294s, for the case 4 in 22.500s and for the case 5 in 14.282s.



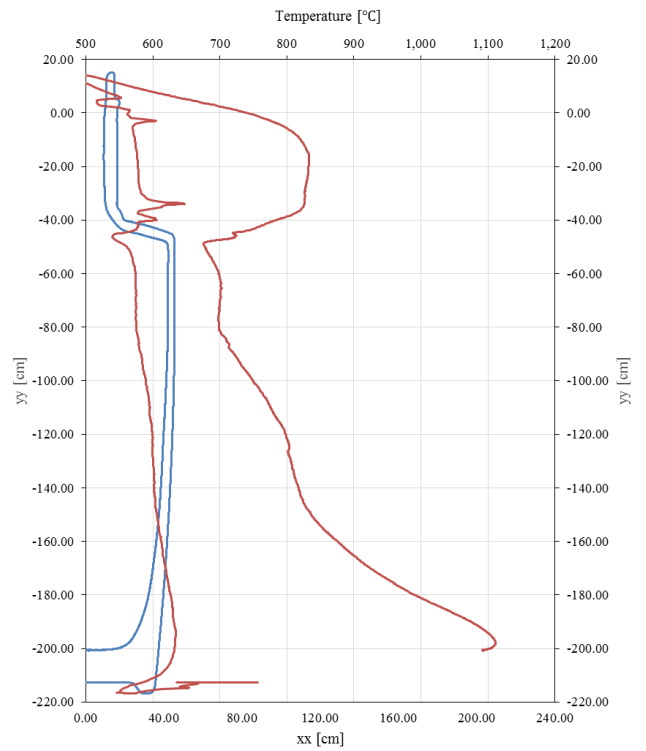
Case 1



Case 2



Case 3



Case 4

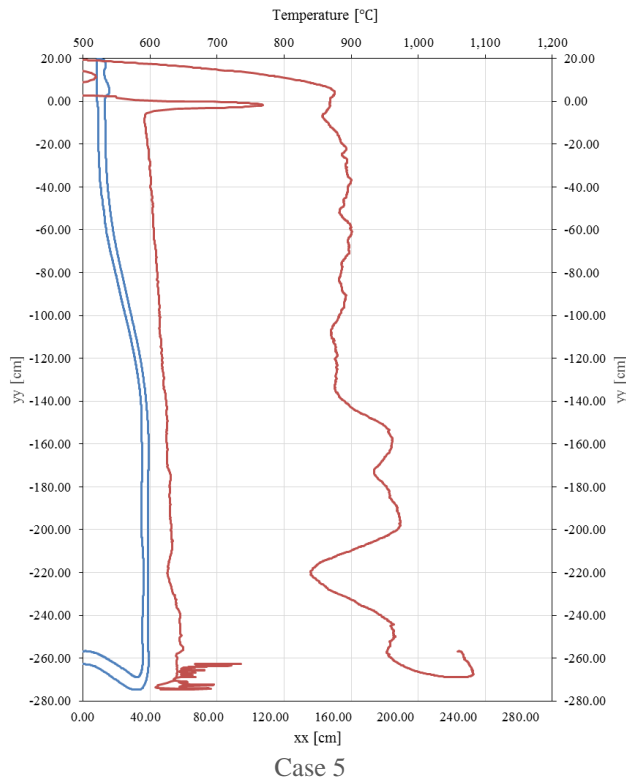


Figure 8.63: Final boundary temperature for case 1, case 2, case 3, case 4 and case 5.

8.1.10 Bottle Thickness

Next, the thickness distribution for the processes of blow/blow examples are presented.

- Case 1

In Figure 8.64 the thickness distribution for the case 1 is shown. The wall of the container has some variance, showing a decrease of the thickness in the shoulder. Also, at the end of the wall the glass container has a slender profile due to the fact that is the zone where the final blow pressure deform the glass firstly. Additionally, the bottom zone of the container has a higher thickness.

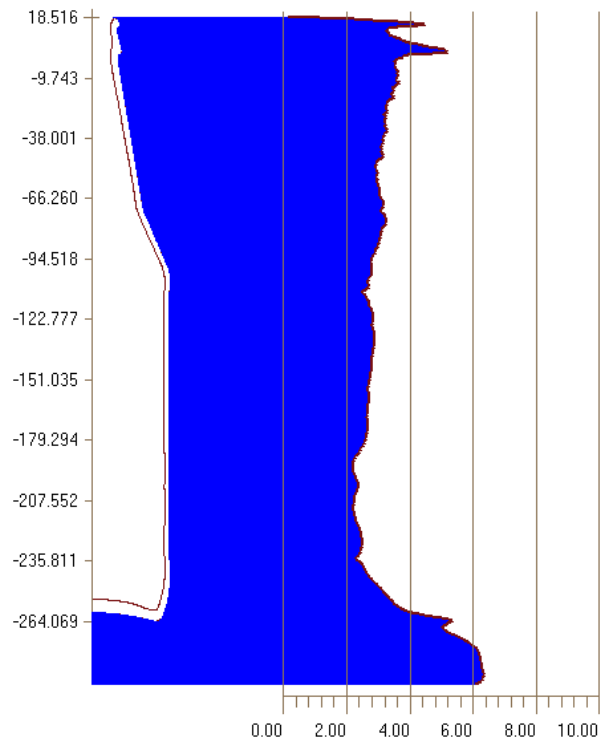


Figure 8.64: Bottle thickness (mm) distribution in case 1.

- Case 2

Figure 8.65 shows the thickness distribution for the case 2. The neck wall has a decreasing thickness, ending at the container shoulder. Then the thickness distribution slowly gets an increasing thickness until reaching the bottom zone of the wall, where it is thinner. The bottom part of the container has a higher thickness, which is decreasing to the centre of the container.

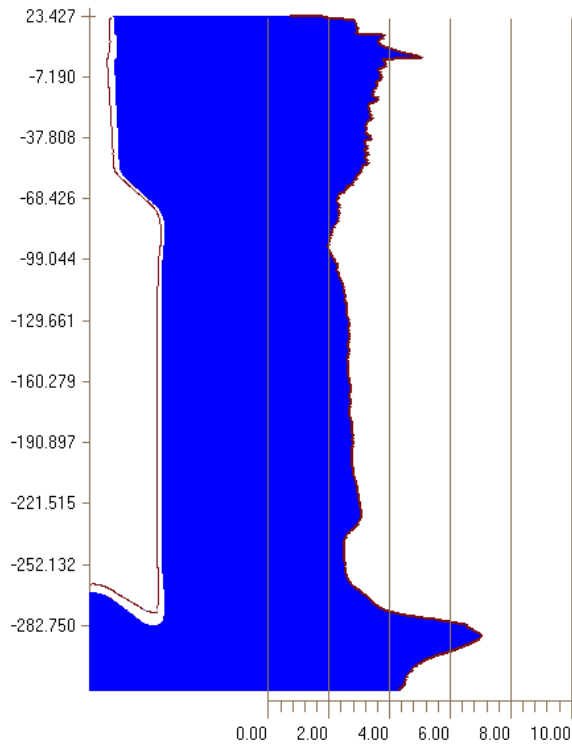


Figure 8.65: Bottle thickness (mm) distribution in case 2.

- Case 3

Figure 8.66 shows the thickness distribution for the case 3. As in the case 2 the container has a decreasing thickness profile in the neck wall until it reaches the container shoulder. Then, the bottle wall has an increasing profile thickness until the bottom part. Then, as in the previous results, the glass wall has a smaller thickness, finishing at the bottom zone with a larger thickness.

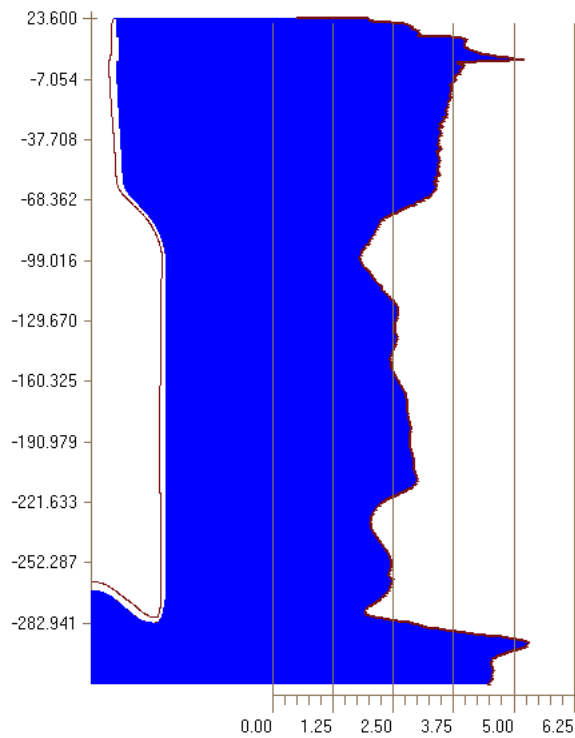


Figure 8.66 Bottle thickness (mm) distribution in case 3.

- Case 4

Figure 8.67 presents the case 4 final shape, as well as, the experimental glass bottle. As it can be seen the profile obtained with the simulation is quite similar to the experimental. The bottom zone has a large thickness while in the shoulder a thinner profile is observed. The neck wall has an almost constant thickness. In Figure 8.68 the simulation thickness profile is presented. Considering the comparison to the experimental bottle, it can be seen that the results are similar.

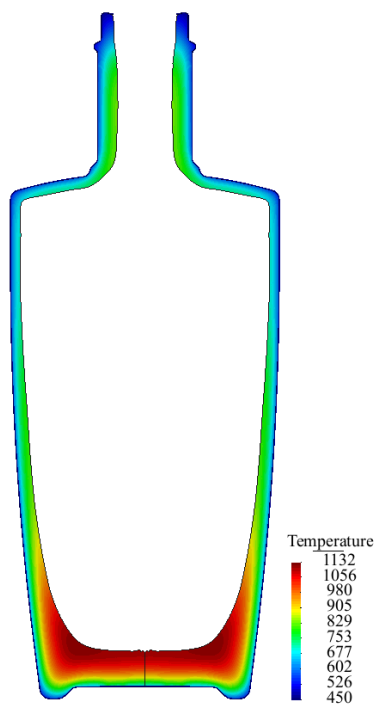


Figure 8.67: Final bottle shape for the case 4.



Experimental bottle thickness for the case 4.

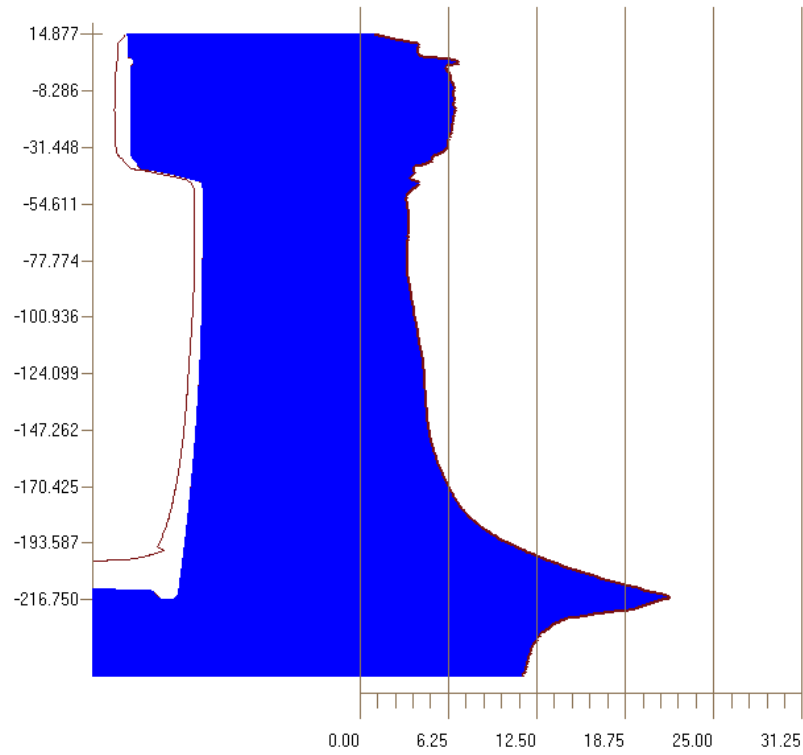


Figure 8.68: Bottle thickness (mm) distribution in case 4.

- Case 5

Figure 8.69 shows the results for the case 5. This container presents a very similar behaviour comparing with the previous cases, thinner zones located at the shoulder and at the bottom of wall and a thicker zone located at the bottom zone.

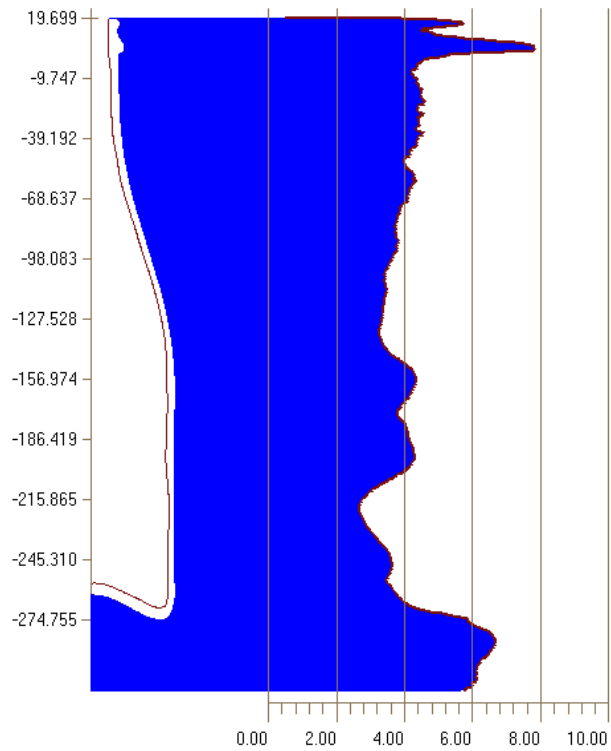


Figure 8.69: Bottle thickness (mm) distribution in case 5.

8.2 Press/Blow Process

In the press/blow process a glass gob is dropped down into a mould. Once the gob is inside the blank mould, the baffle closes and the plunger moves up. When the plunger is at its highest position, the ring closes itself around the plunger, so that the mould plunger tool is closed below. Finally, when the plunger is lowered, the ring is decoupled from the blank mould and the glass preform is carried by means of a robotic arm to the blow mould. In the blow stage the parison is usually first left to sag due to gravity for a short period. Then pressurized air blows inside to force the glass in a mould shape. It is important to know the right shape of the preform beforehand for an appropriate distribution of glass over the mould wall.

During the parison forming a large amount of heat is removed from the glass and the temperature distribution in the glass changes. Due to the temperature dependence of the viscosity the glass flow depends on the initial temperature of the gob and the subsequent steps of heat transfer in the glass, blank mould and plunger. Any disturbance in heat transfer during parison forming can result in an uneven glass distribution, circumferentially as well as axially.

The input parameters for simulations consist of the parison geometries, i.e. the mould and the plunger descriptions, the initial position of the plunger, the initial position of the computational (glass) domain, and a number of parameters characterizing the properties of glass as were used previously.

8.2.1 Gob Loading

In the gob loading stage, glass is dropped directly against the plunger and starts to cool. This stage is similar to the blow/blow process.

For case 1 the shape and temperature contours of the glass are plotted in Figure 8.70. After falling from the feeder the gob contacts the plunger and only a little accommodation in the gap between the plunger and the neckring. In this stage, the gob must be under baffle so that the baffle doesn't hit the gob while is closing. In Figure 8.71 the boundary temperatures are represented.

For case 2, case 3, case 4, case 5, case 6, case 7 and case 8 the shape and temperature contour of the glass are plotted in Figure 8.72, Figure 8.74, Figure 8.76, Figure 8.80, Figure 8.82, Figure 8.84 and Figure 8.86, in which a similar behaviour for all cases is depicted.

Also, Figure 8.73, Figure 8.75, Figure 8.77, Figure 8.81, Figure 8.83, Figure 8.85 and Figure 8.87 present the boundary temperatures for the cases 2 to 8. A very similar pattern of the temperature at the boundary is evident. Except for the case 6, since then there is no contact with the mould, the gob only contact the plunger.

The displacement contours for the case 4 are presented in Figure 8.78 as well the displacement vectors in Figure 8.80. It quite evident the gravity force the glass to flow inside the neckring.

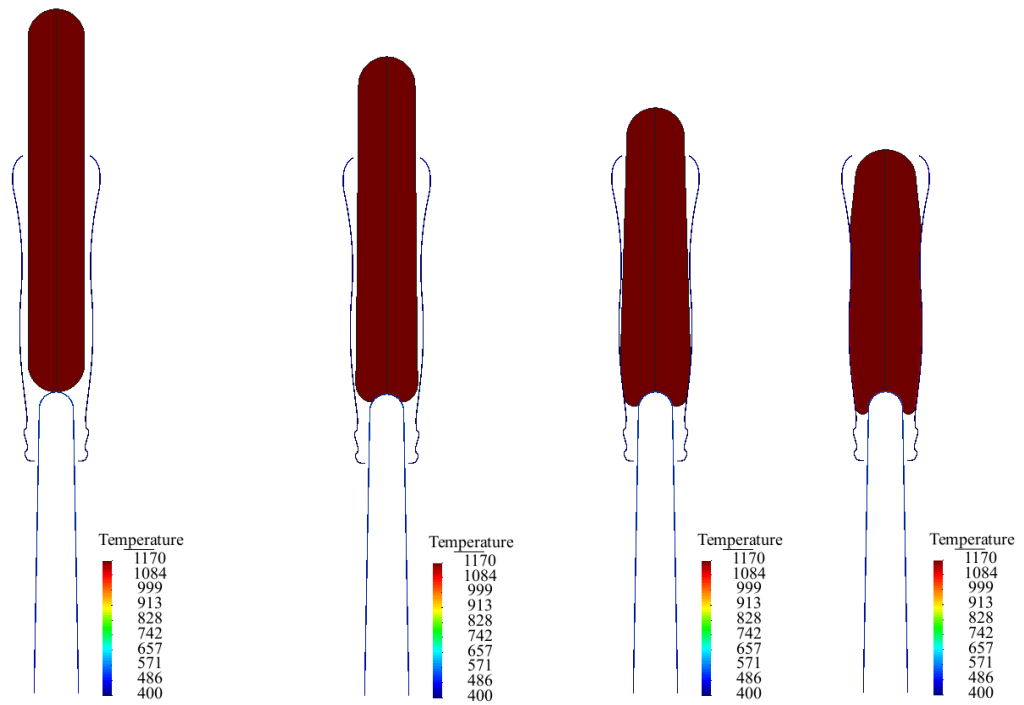


Figure 8.70: Temperature distribution in gob loading for the case 1 in 0.175s, 0.199s, 0.252s and 0.466s.

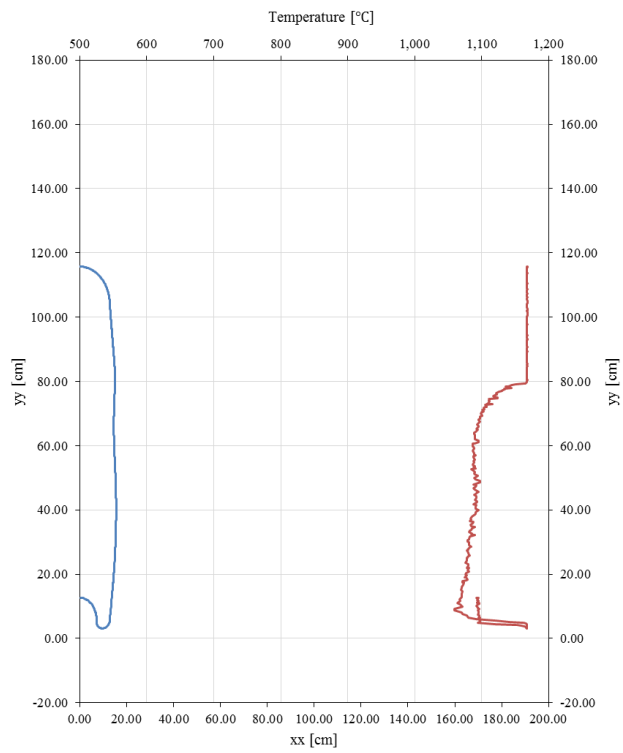


Figure 8.71: Boundary temperature for gob loading stage for case 1.

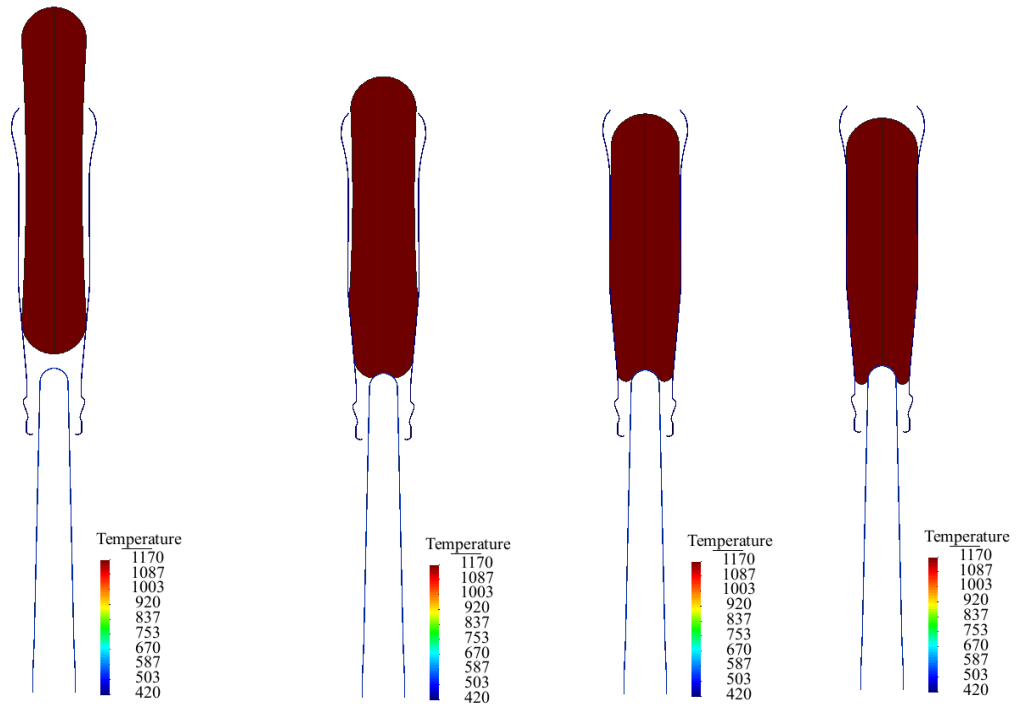


Figure 8.72: Temperature distribution in gob loading for the case 2 in 0.096s, 0.140s, 0.238s, 0.383s.

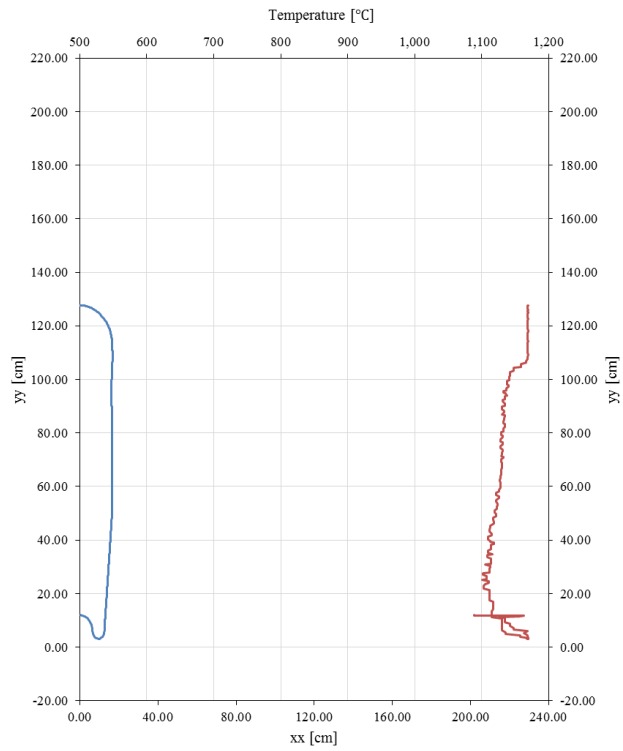


Figure 8.73: Boundary temperature for gob loading stage for case 2.

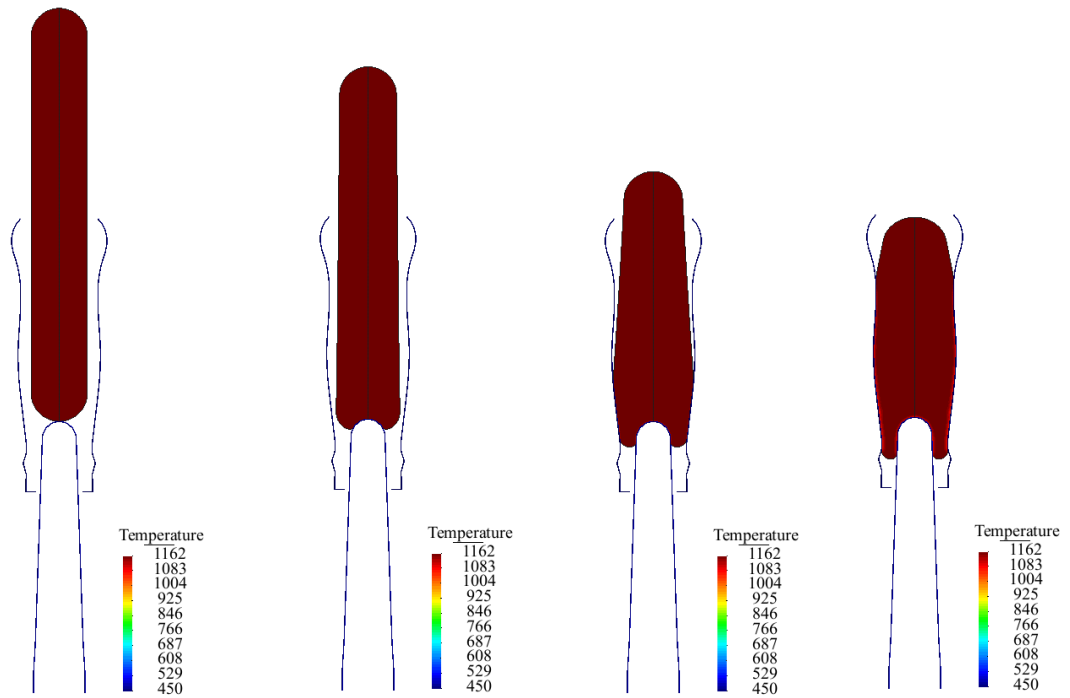


Figure 8.74: Temperature distribution in gob loading for the case 3 in 0.078s, 0.115s, 0.275s, 0.800s.

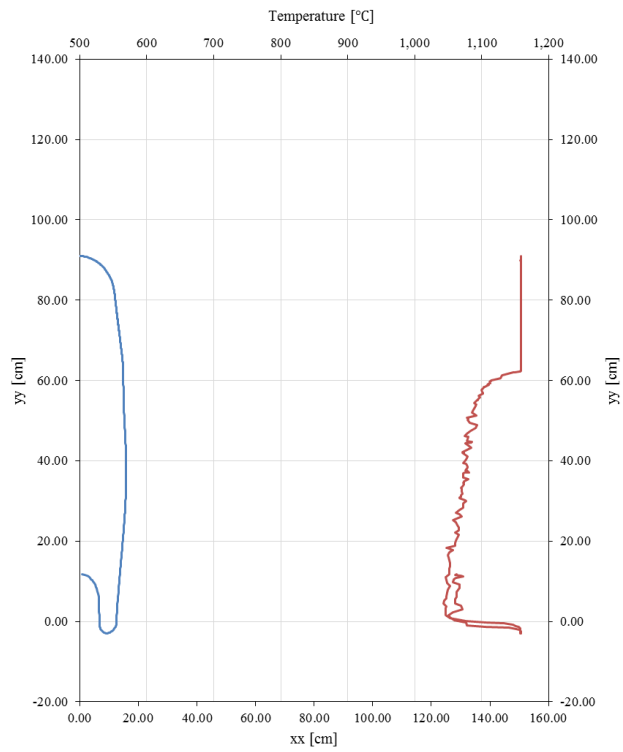


Figure 8.75: Boundary temperature for gob loading stage for case 3.

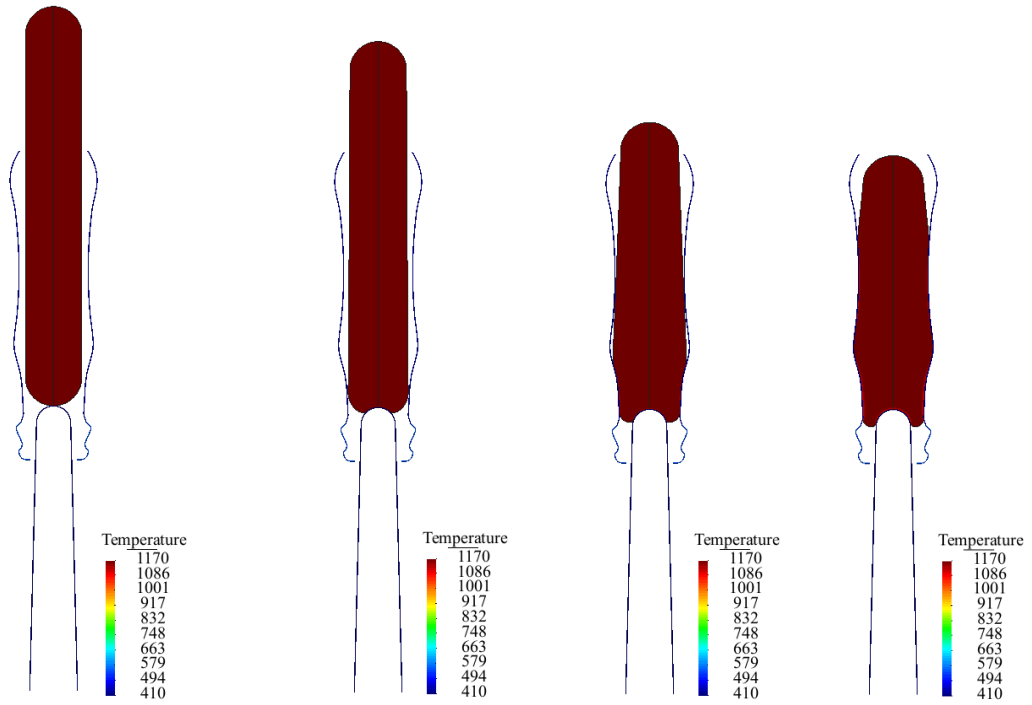


Figure 8.76: Temperature distribution in gob loading for the case 4 in 0.251s, 0.266s, 0.355s, 0.555s.

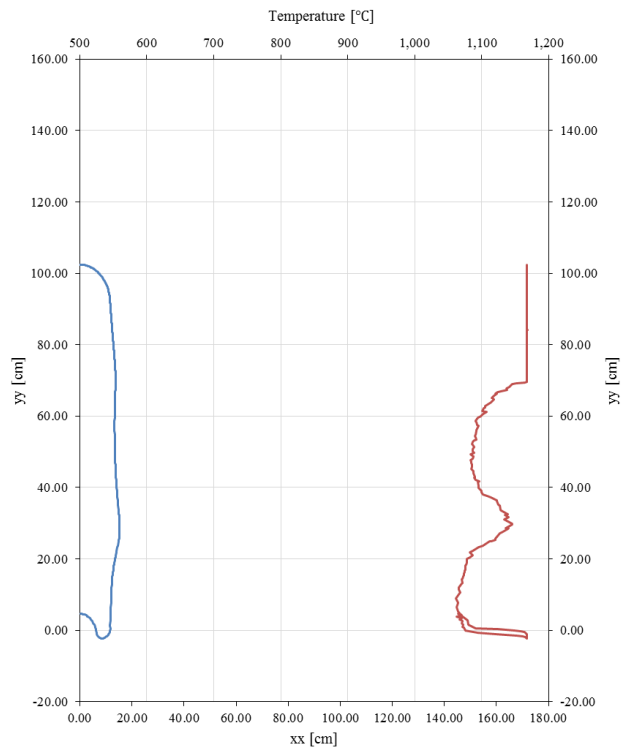


Figure 8.77: Boundary temperature for gob loading stage for case 4.

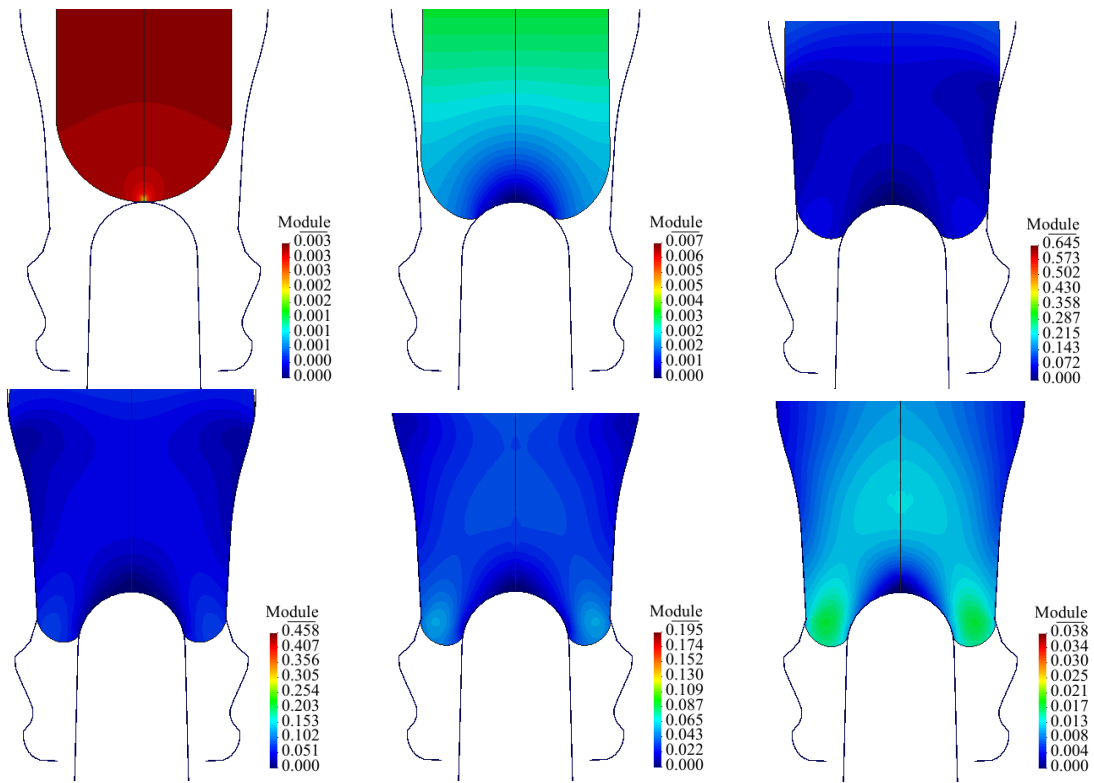


Figure 8.78: Displacement module in gob loading for the case 4 in 0.2513s, 0.2667s, 0.3213s

0.4797s

0.5349s

0.5555s

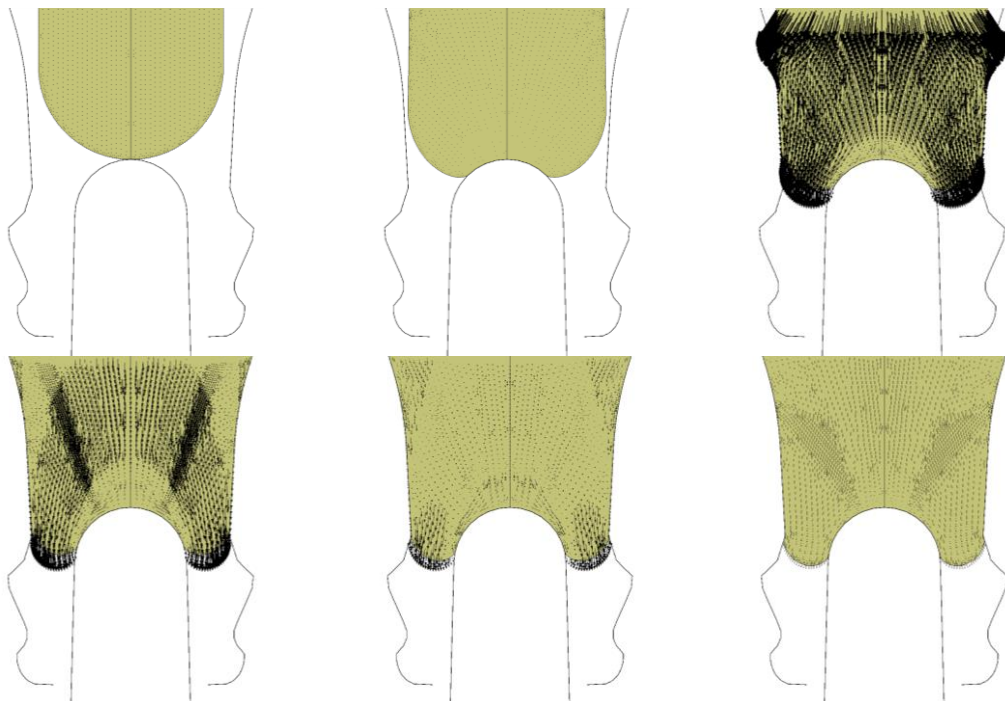


Figure 8.79: Displacement vector in gob loading for the case 4 in 0.2513s, 0.2667s, 0.3213s

0.4797s

0.5349s

0.5555s

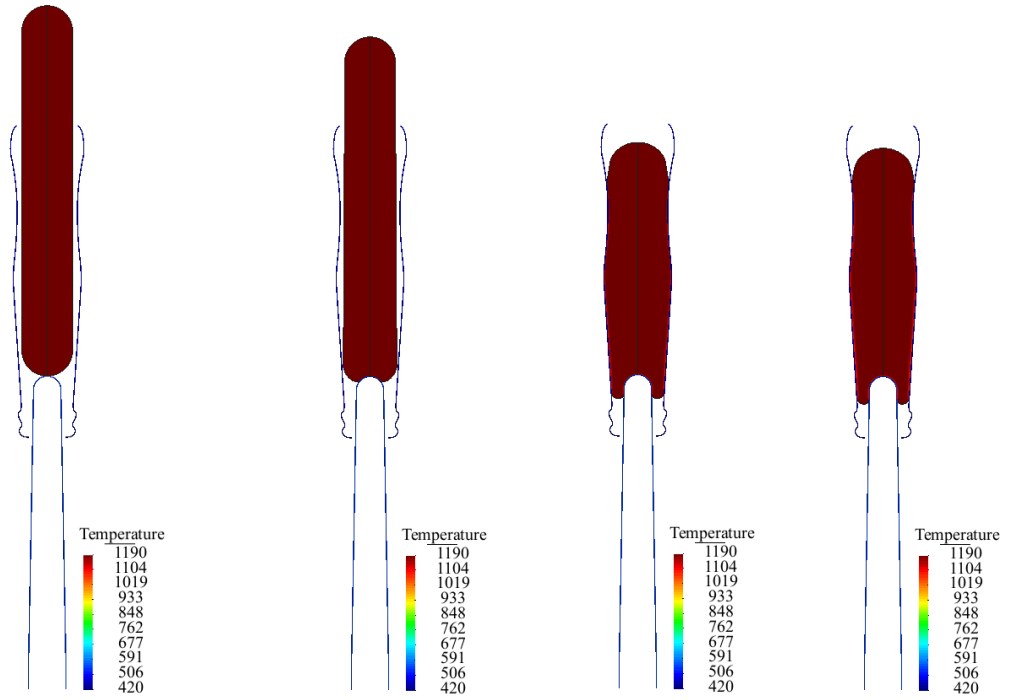


Figure 8.80: Temperature distribution in gob loading for the case 5 in 0.088s, 0.107s, 0.421s, 0.625s.

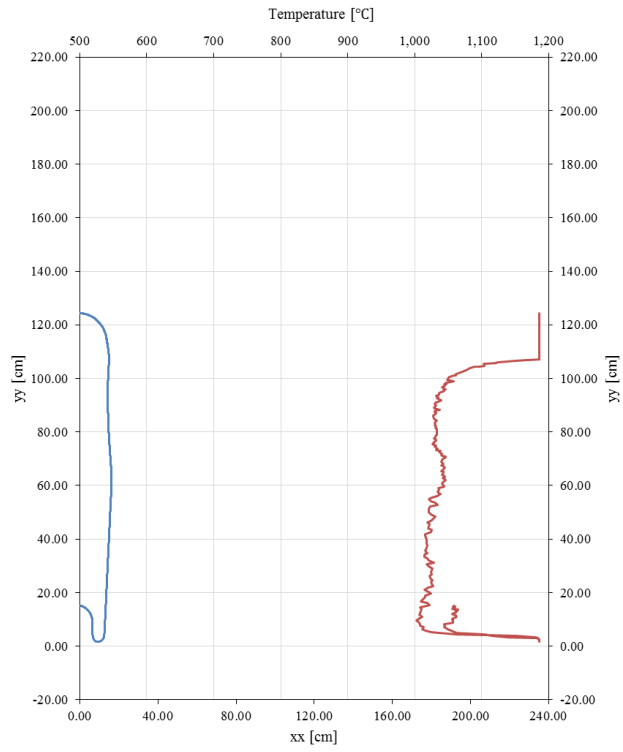


Figure 8.81: Boundary temperature for gob loading stage for case 5.

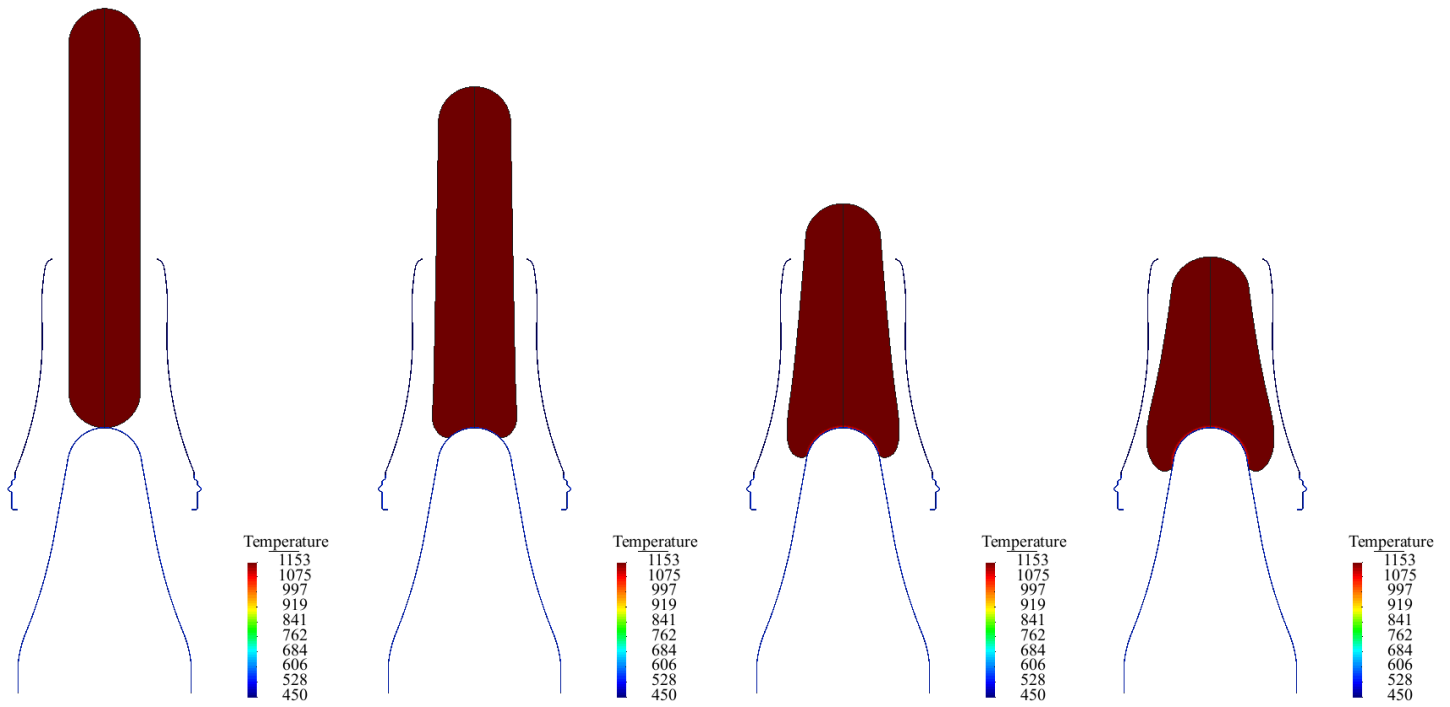


Figure 8.82: Temperature distribution in gob loading for the case 6 in 0.076s, 0.128s, 0.303s and 0.460s.

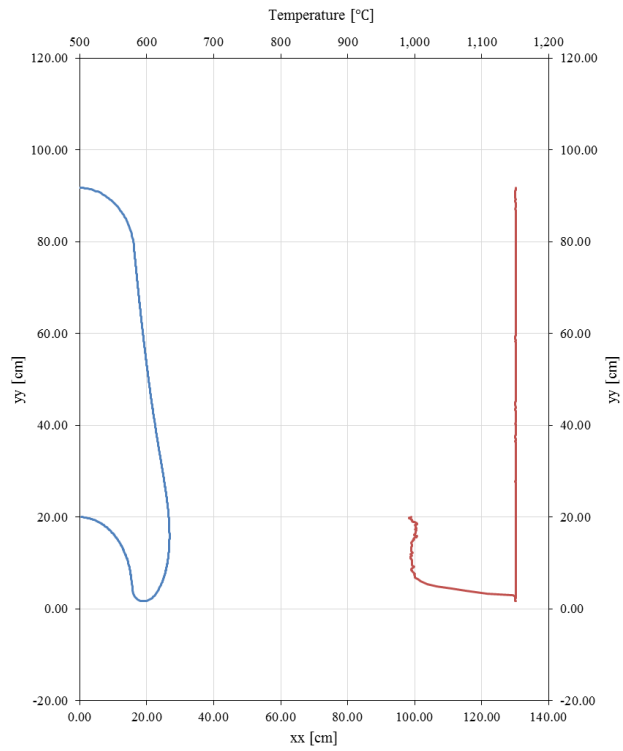


Figure 8.83 Boundary temperature for gob loading stage for case 6.

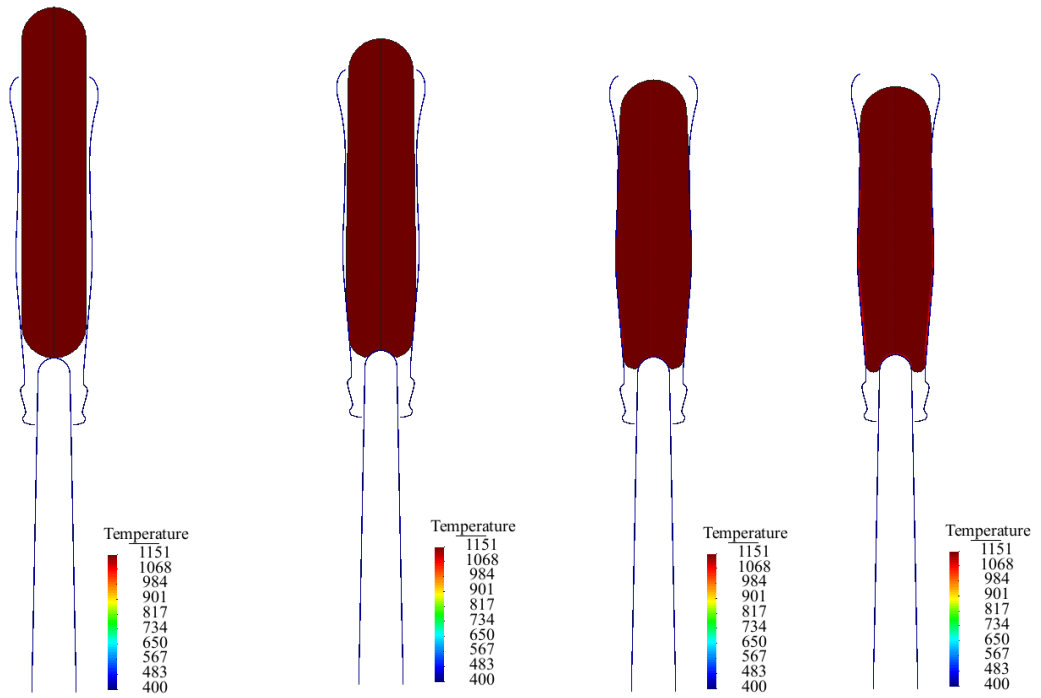


Figure 8.84: Temperature distribution in gob loading for the case 7 in 0.497s, 0.531s, 0.635s, 0.820s.

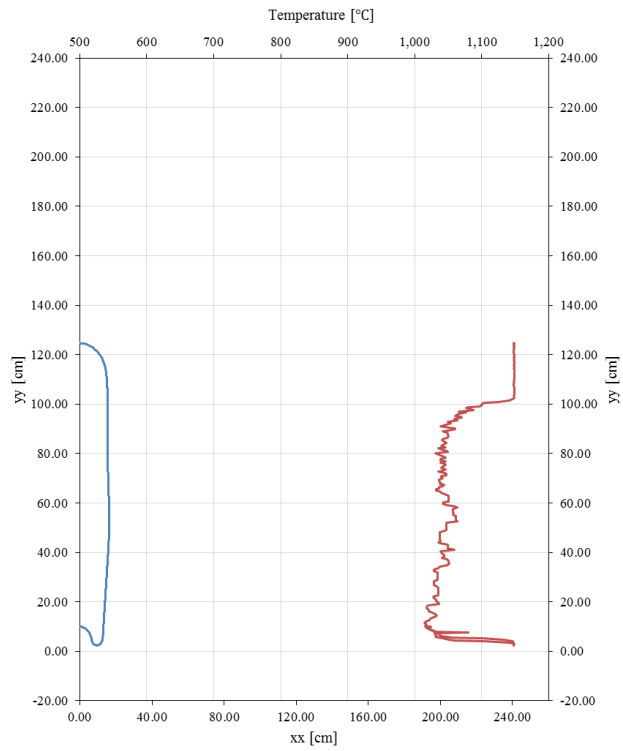


Figure 8.85: Boundary temperature for gob loading stage for case 7.

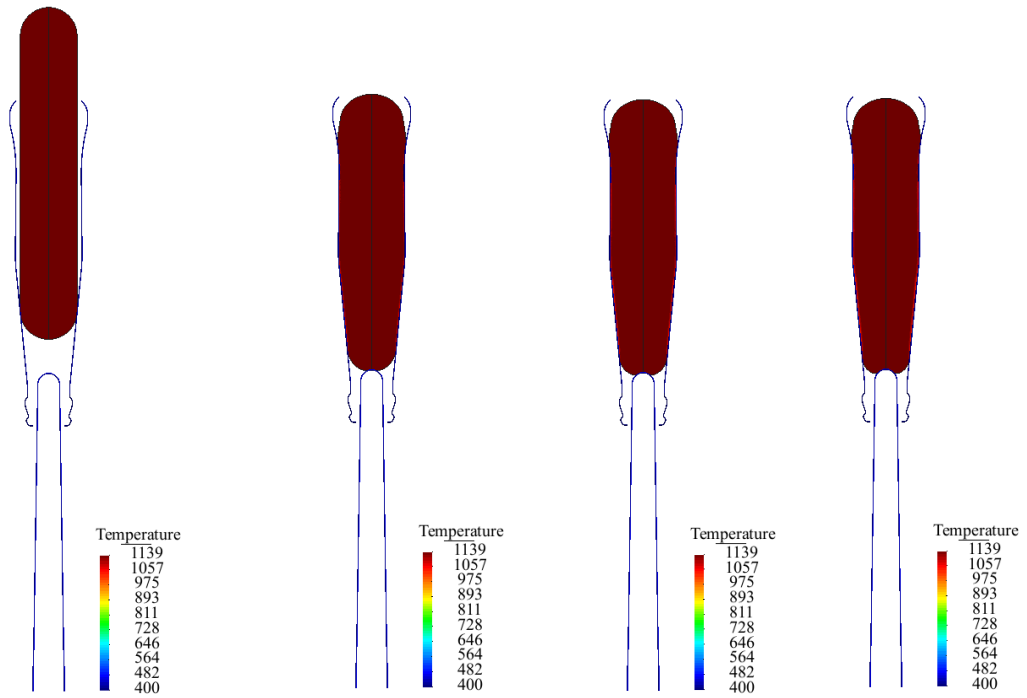


Figure 8.86: Temperature distribution in gob loading for the case 8 in 0.095s, 0.548s, 0.609s, 0.676s.

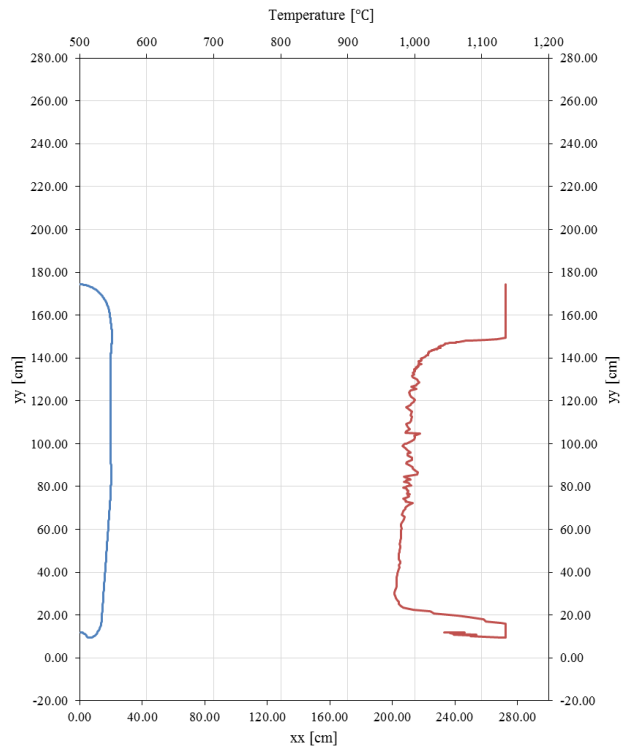


Figure 8.87: Boundary temperature for gob loading stage for case 8.

8.2.2 Baffle On

The baffle is positioned on top of the blank mould allowing the plunger to move towards the baffle with a prescribed force. While the tool is being positioned in the top of the blank mould the glass continues to cool. In Figure 8.88 all the press/blow cases in baffle on stage are presented.

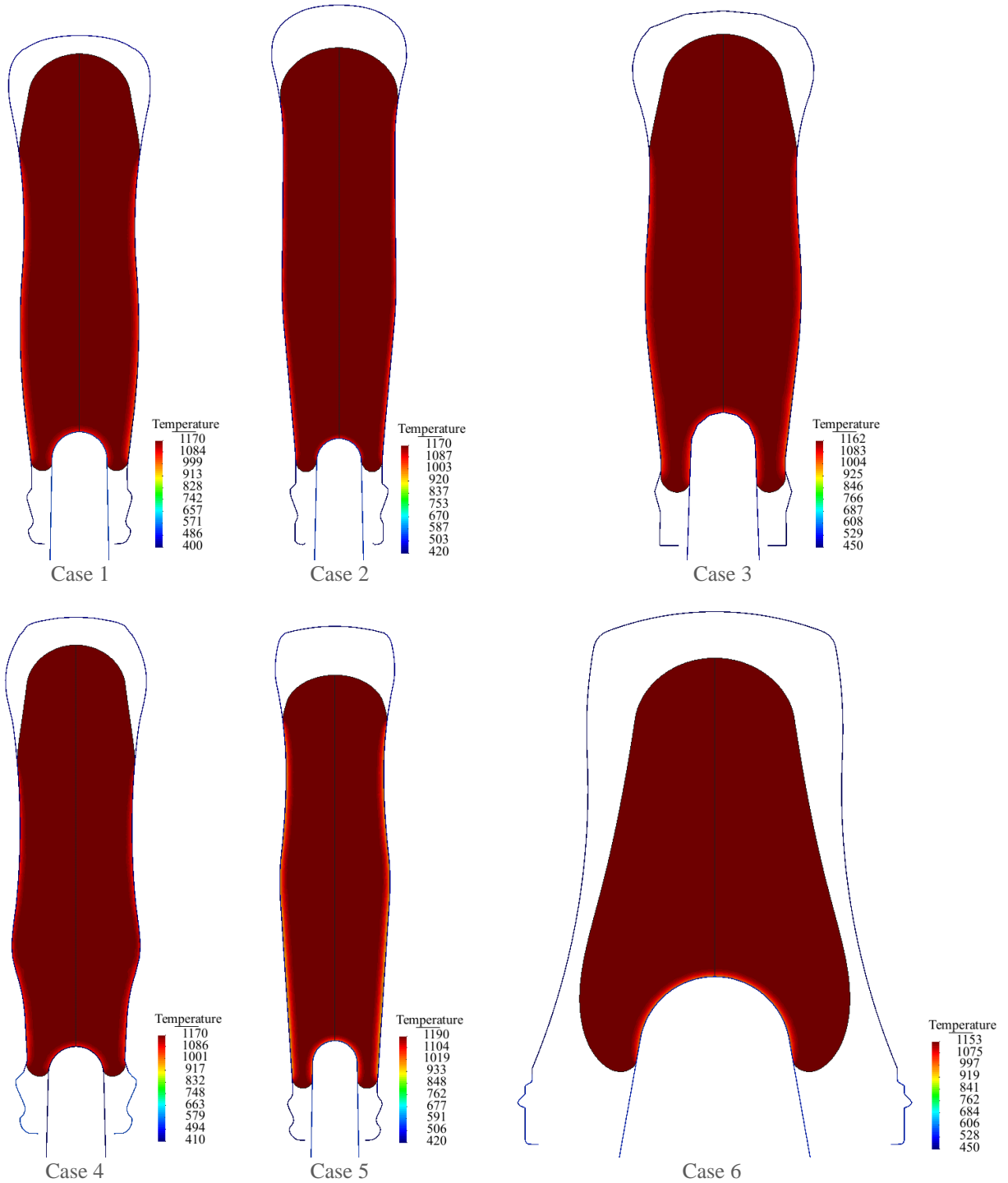




Figure 8.88: Temperature distribution in baffle on for the case 1 in 0.800s, for the case 2 in 0.859s, for the case 3 in 1.147s, for the case 4 in 0.889s, for the case 5 in 0.972s, for the case 6 in 0.801s, for the case 7 in 0.957s and for the case 8 in 1.126s.

8.2.3 Plunger Up

In this section the results of plunger up stages are plotted to observe how they behave. In the beginning of this process the gob is already above the plunger and ready for the plunger movement. In practice, the plunger is pushed by a piston. This means that the flow velocity is the result of an external force applied to the plunger. The plunger moves upwards, forcing the glass to fill in the space between the mould and the plunger. At a certain point the glass hits the bottom of the mould (the baffle part) and gets closer to the neckring part. At this point the pressure in glass increases. In the last instants the glass is obliged to move and fill the neckring. Here, a bad misalignment may create finish defects.

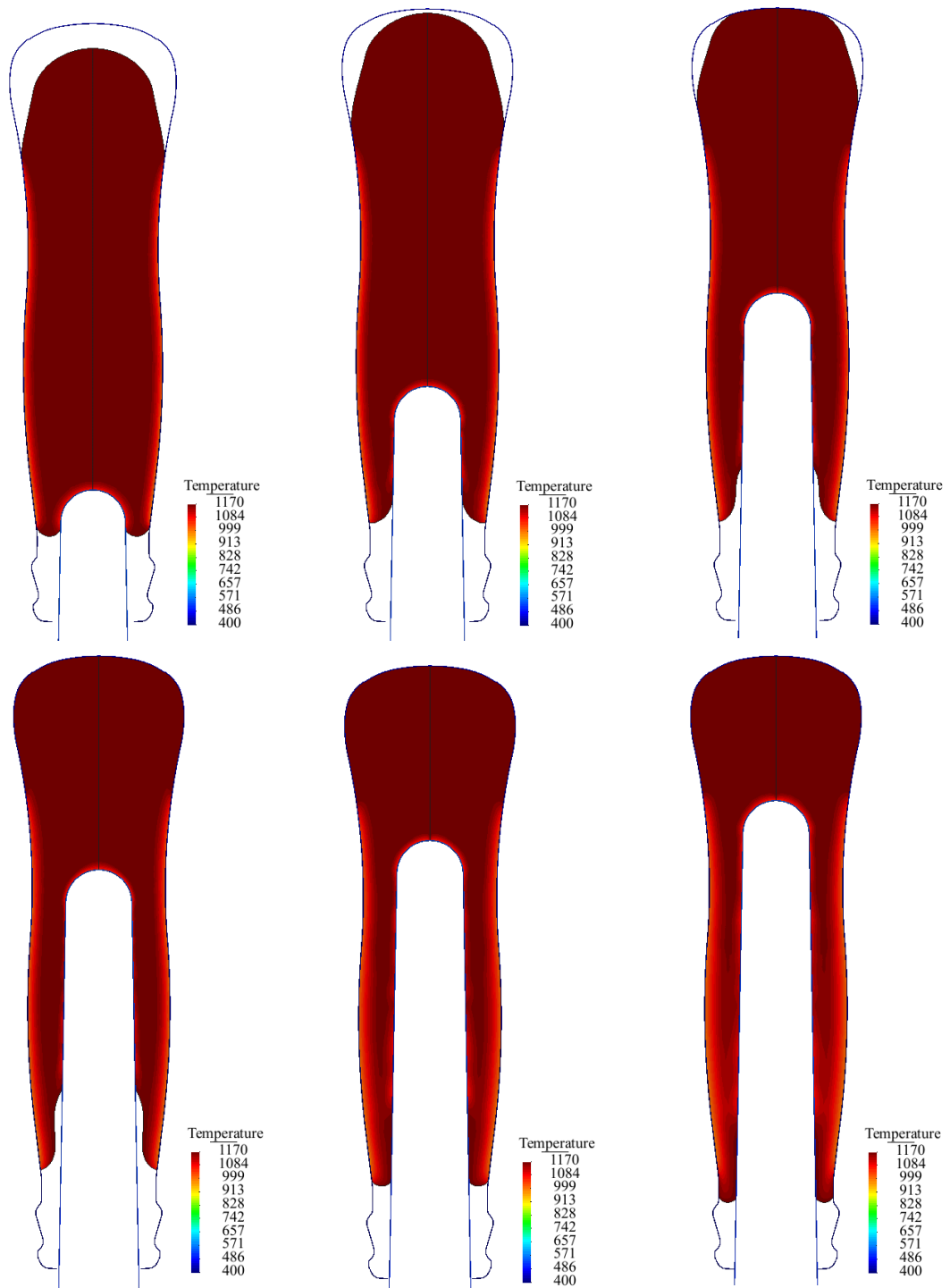
For case 1 the shape and temperature contours of the glass are plotted in Figure 8.89. While the plunger moves up the nodes that are in contact with the plunger are allowed to slip on the mould with a friction coefficient, but in the other hand the nodes that are in contact with the rest of the moulds are maintained fixed. This assumption is justified by practical observations. When the glass hits the baffle zone the glass starts to spread and fills all the remaining space. Then glass flows down from the top of the parison to completely fill the neckring area. Next, heat transfer from the moulds to the glass takes place.

In Figure 8.90 the boundary temperatures are represented. The inner and outer boundary have similar temperatures as in this stage the two tools “remove” more “evenly” the heat from the glass from the two sides of the parison. The results also show that the neckring has a higher temperature since it was the last zone be formed. Additionally, the thickness distribution at the end of the plunger up stage is presented.

For cases 2 to 8 the shape and temperature contours of the glass are plotted in Figure 8.91, Figure 8.93, Figure 8.95, Figure 8.99, Figure 8.101, Figure 8.103 and Figure 8.105. A very similar behaviour for all cases was observed. The boundary temperatures from the remaining cases are presented in Figure 8.92, Figure 8.94, Figure 8.96, Figure 8.100, Figure 8.102, Figure 8.104 and Figure 8.106.

The displacement contours during the plunger up are shown in Figure 8.97. It can be seen that at the beginning of the stage the maximum displacement is near the plunger and when the neckring is completely

filled the displacement is almost null. Also in Figure 8.98 the displacement vector is presented when the baffle and the neckring is being filled with the glass.



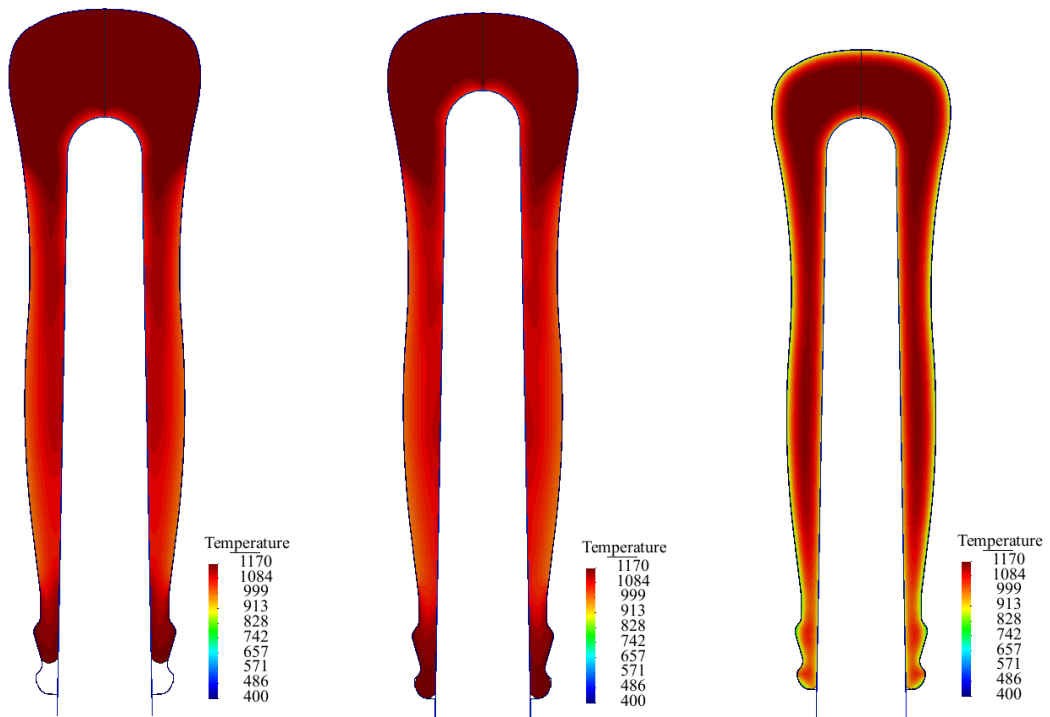


Figure 8.89: Temperature distribution in plunger up for the case 1 in 0.8000s, 0.8002s, 0.8003s

0.8005s	0.8011s	0.8018s
0.8035s	0.8050s	2.0000s

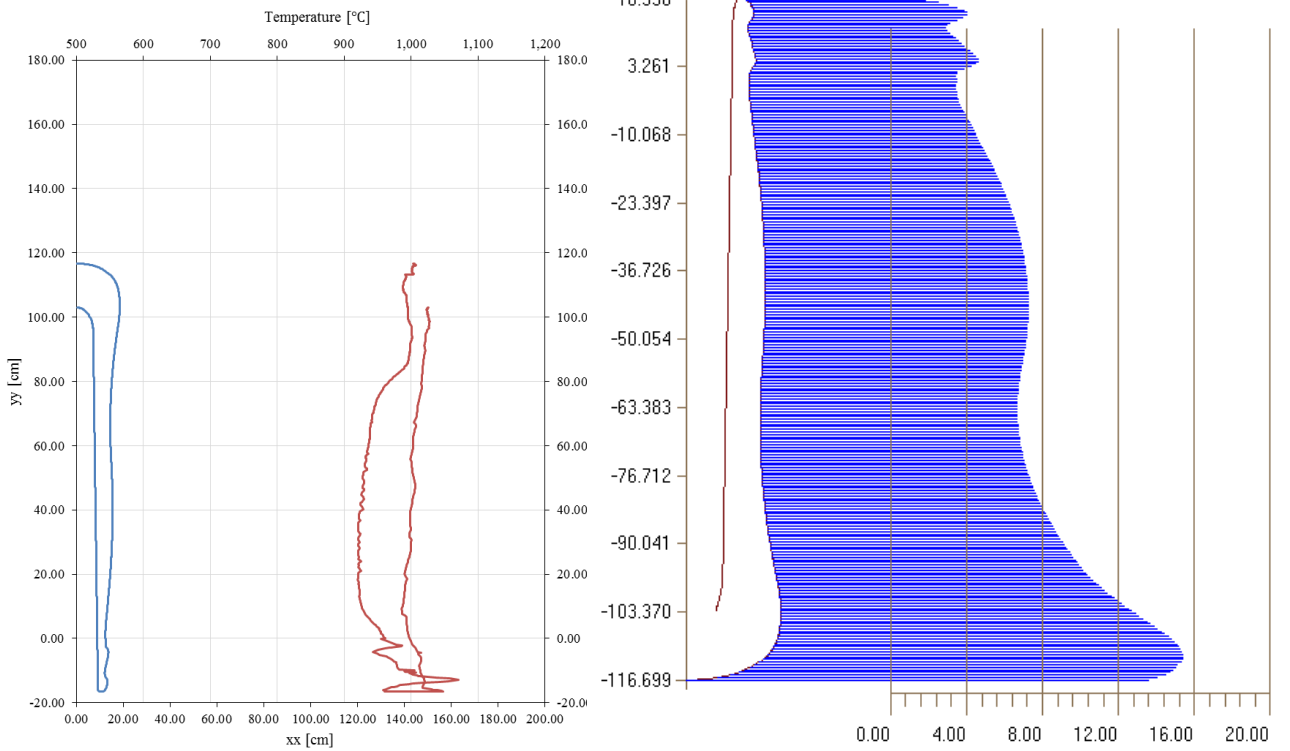
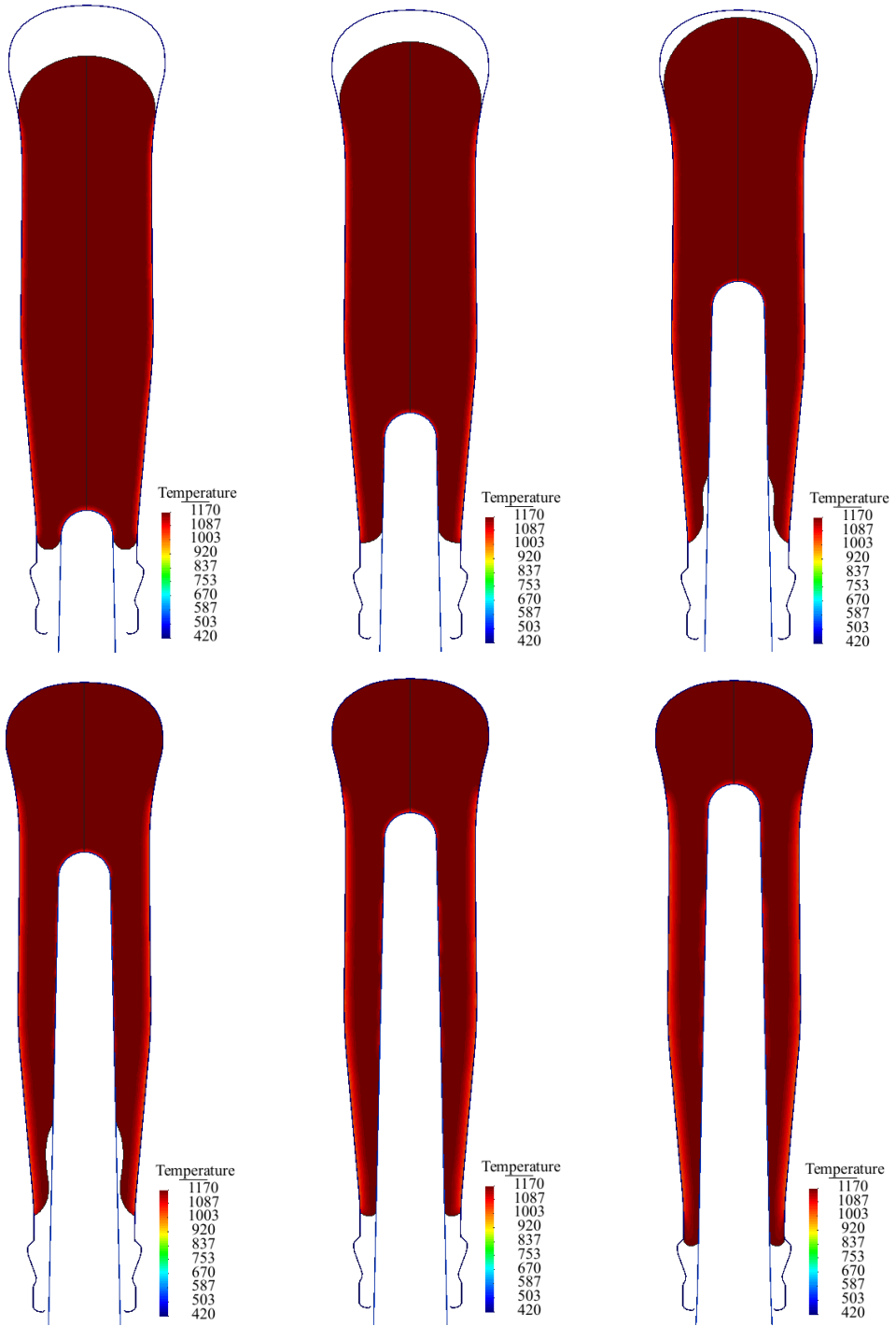


Figure 8.90: Boundary temperature in plunger up for case 1.

Thickness (mm) in plunger up stage for case 1.



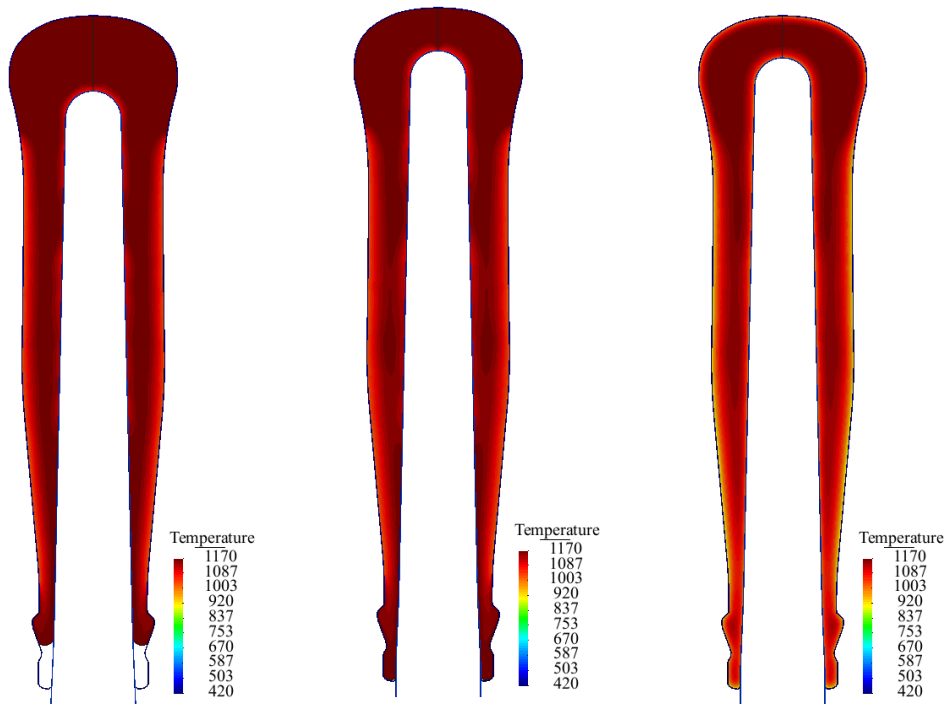


Figure 8.91: Temperature distribution in plunger up for the case 2 in 0.8588s, 0.8590s, 0.8592s

0.8594s	0.8599s	0.8606s
0.8616s	0.8630s	1.9171s

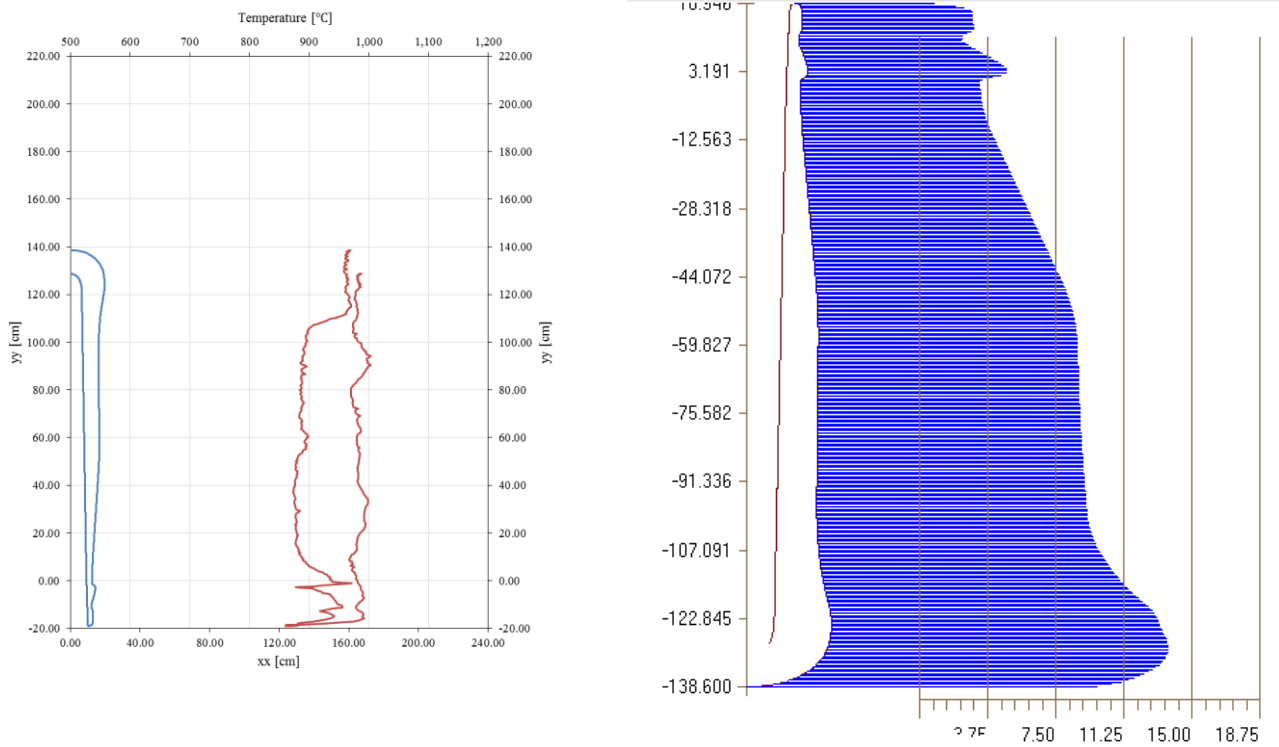
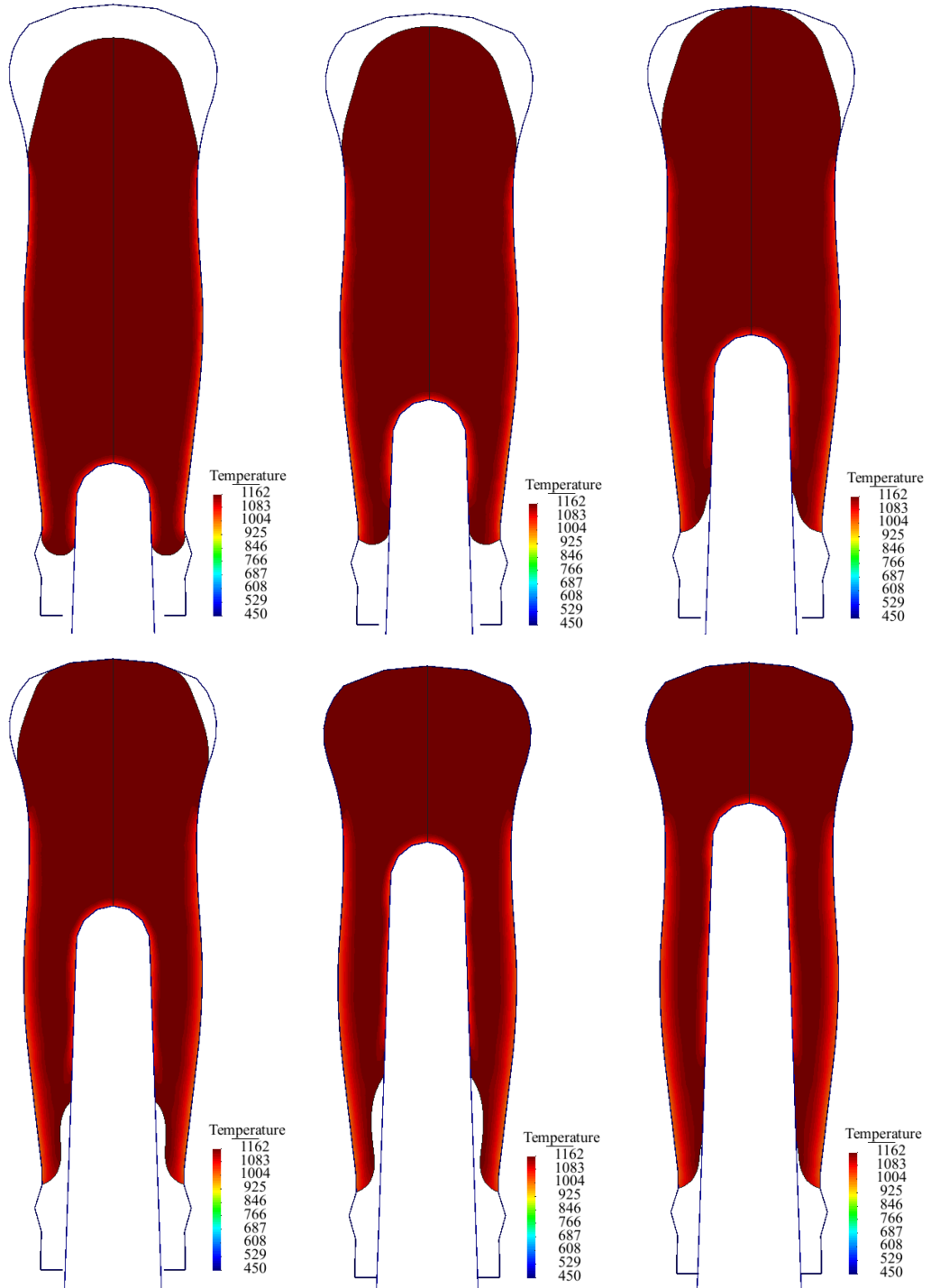


Figure 8.92 Boundary temperature for plunger up stage for case 2.

Thickness (mm) in plunger up stage for case 2.



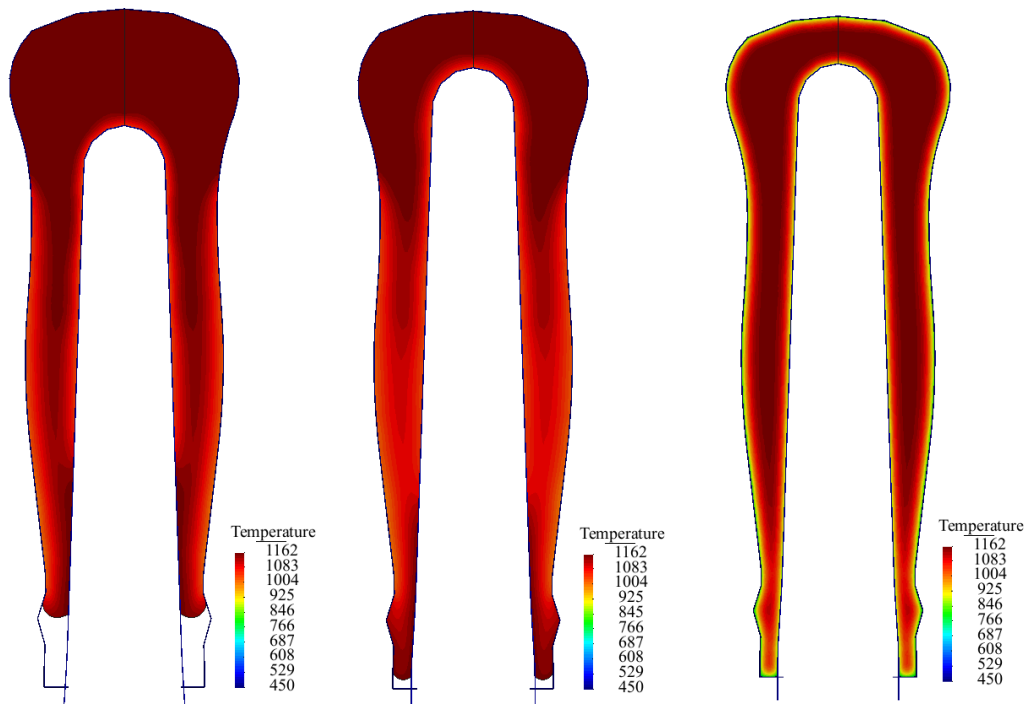


Figure 8.93: Temperature distribution in plunger up for the case 3 in 1.1466s, 1.1468s, 1.1469s

1.1470s	1.1472s	1.1475s
1.1482s	1.1500s	2.0533s

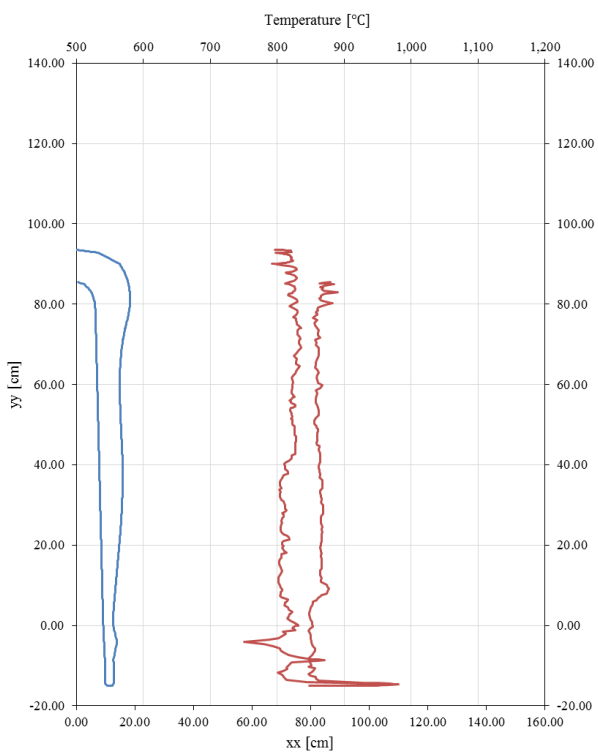
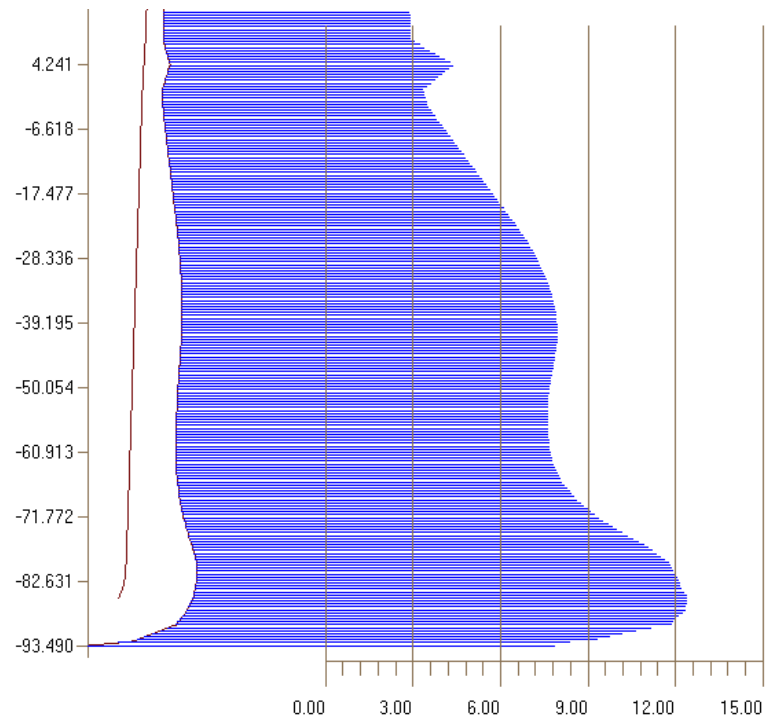
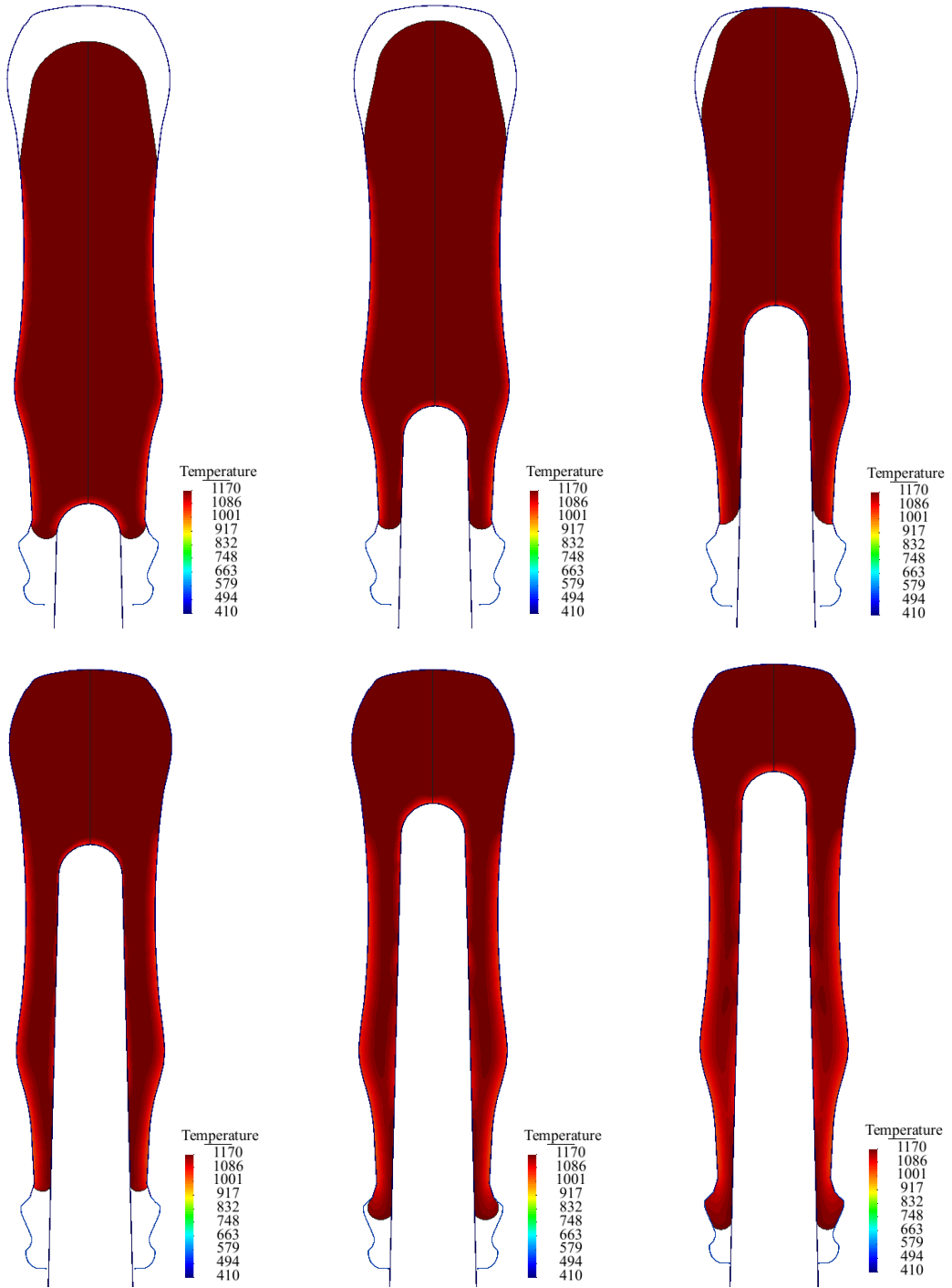


Figure 8.94 Boundary temperature for plunger up stage for case 3.



Thickness (mm) in plunger up stage for case 3.



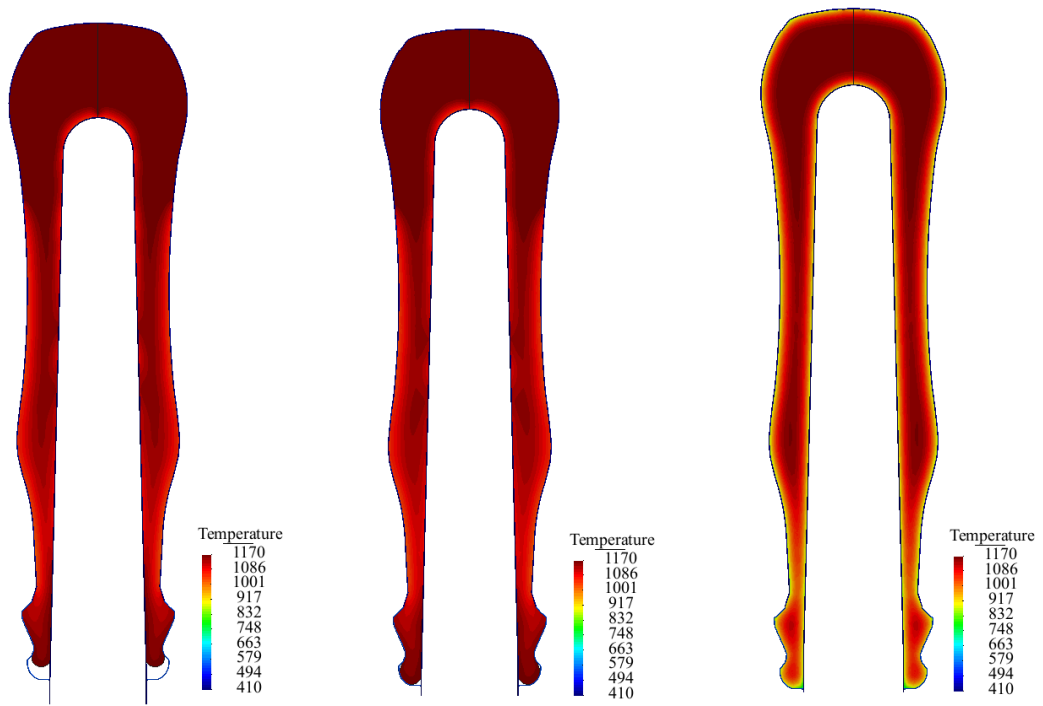


Figure 8.95: Temperature distribution in plunger up for the case 4 in 0.8888s, 0.8890s, 0.8891s

0.8896s	0.8907s	0.8915s
0.8925s	0.8931s	1.8750s

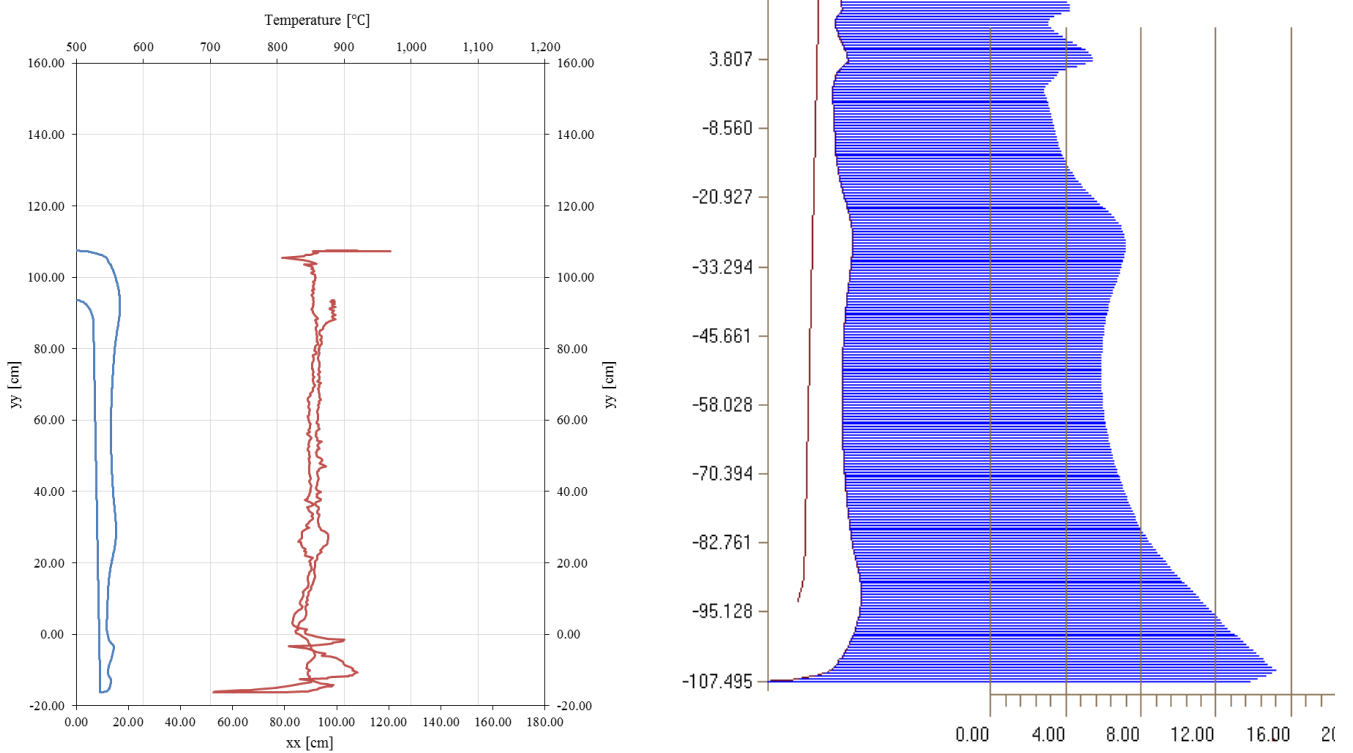
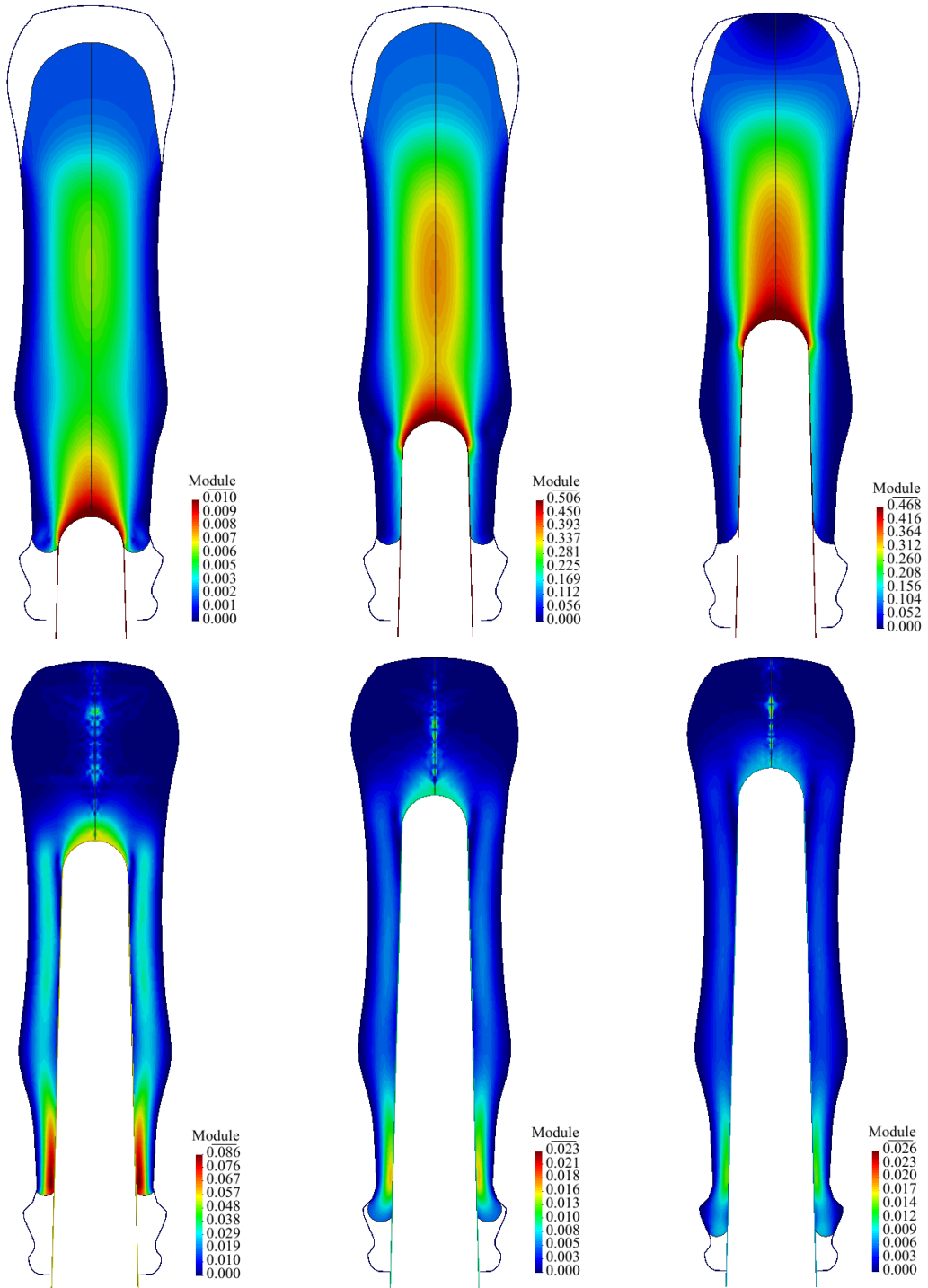


Figure 8.96 Boundary temperature for gob loading stage for case 4.

Thickness (mm) in plunger up stage for case 4.



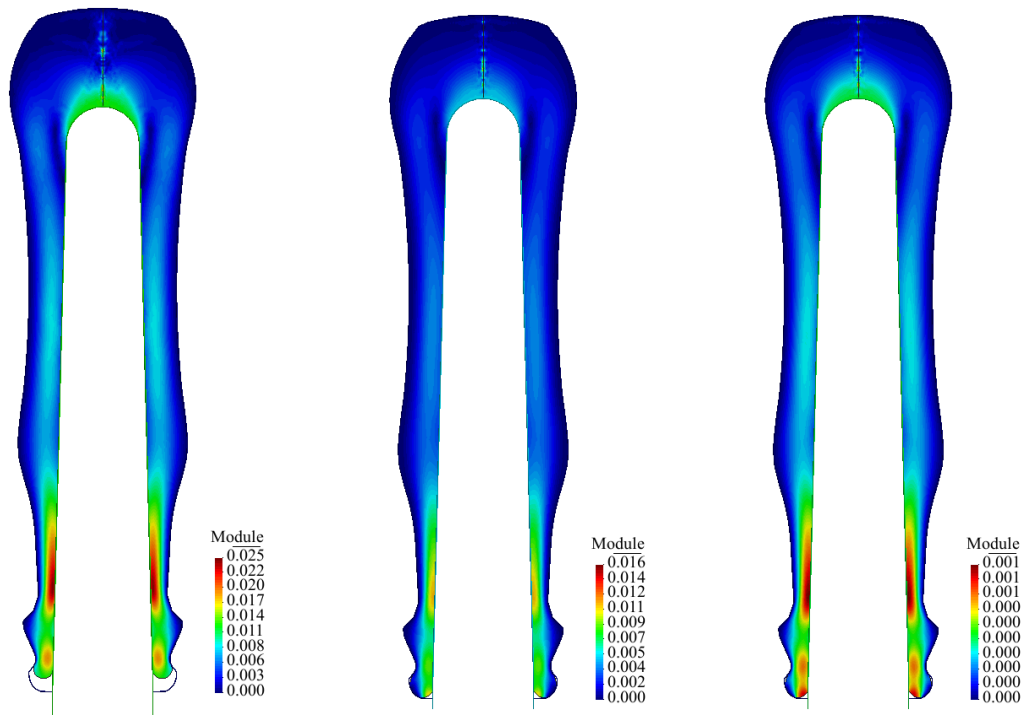


Figure 8.97: Displacement module in plunger up for the case 4 in 0.8888s, 0.8890s, 0.8891s

0.8896s	0.8907s	0.8915s
0.8925s	0.8931s	1.8750s

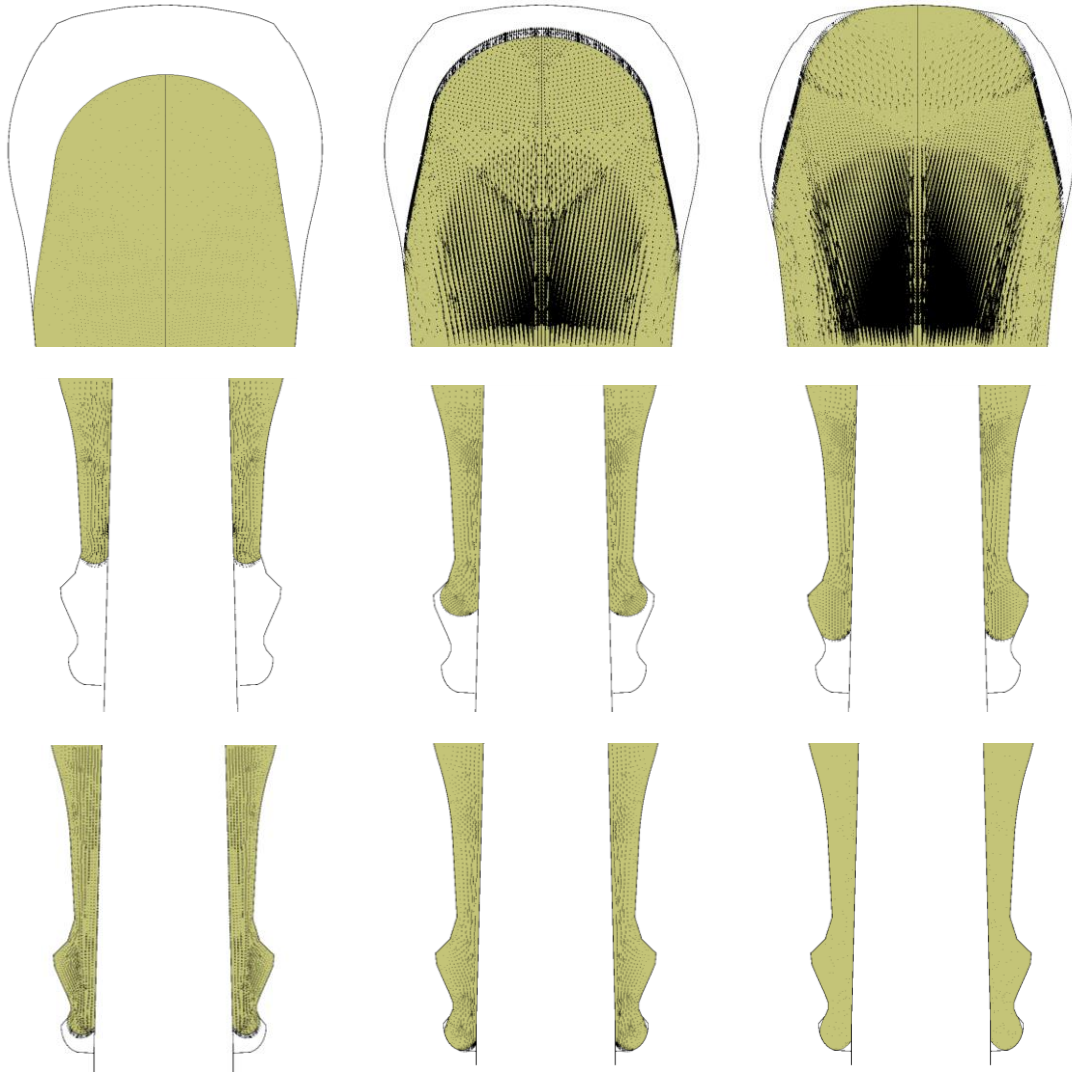
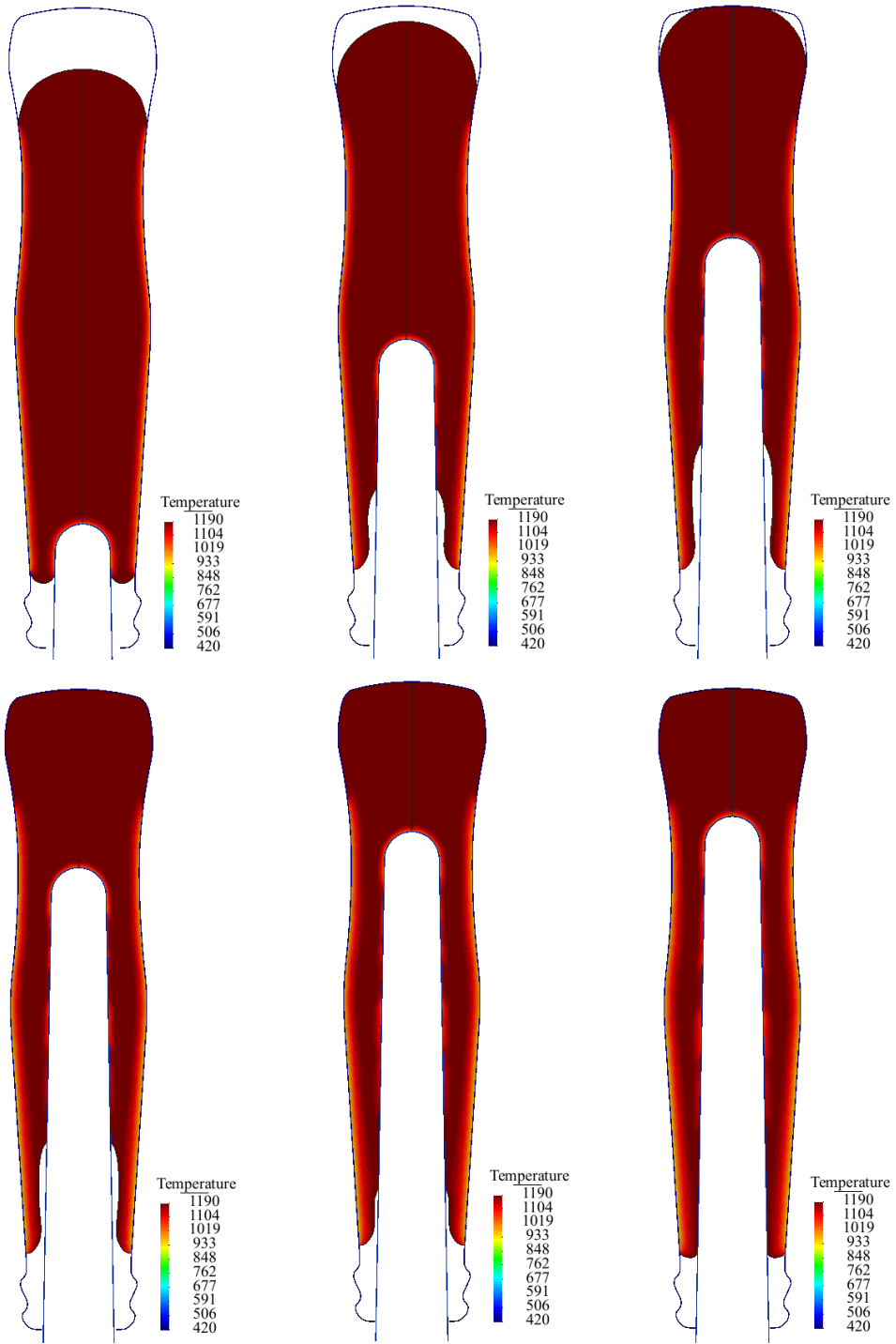


Figure 8.98: Displacement vectors in plunger up for the case 4 in 0.8888s, 0.8890s, 0.8891s

0.8896s	0.8907s	0.8915s
0.8925s	0.8931s	1.8750s



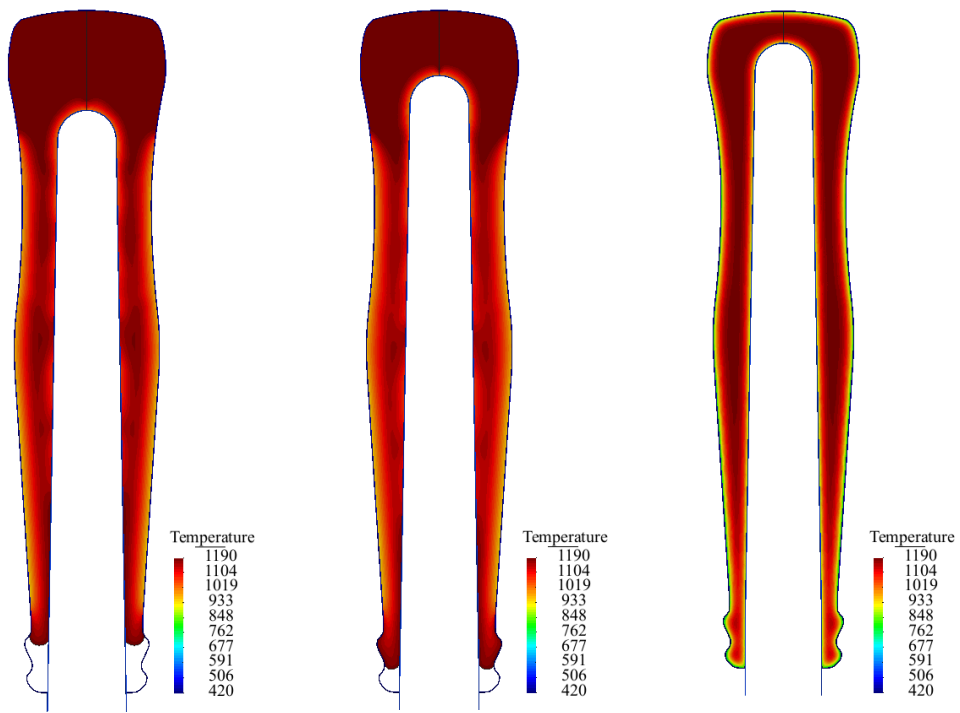


Figure 8.99: Temperature distribution in plunger up for the case 5 in 0.9722s, 0.9727s, 0.9729s

0.9733s	0.9737s	0.9744s
0.9759s	0.9777s	2.2222s

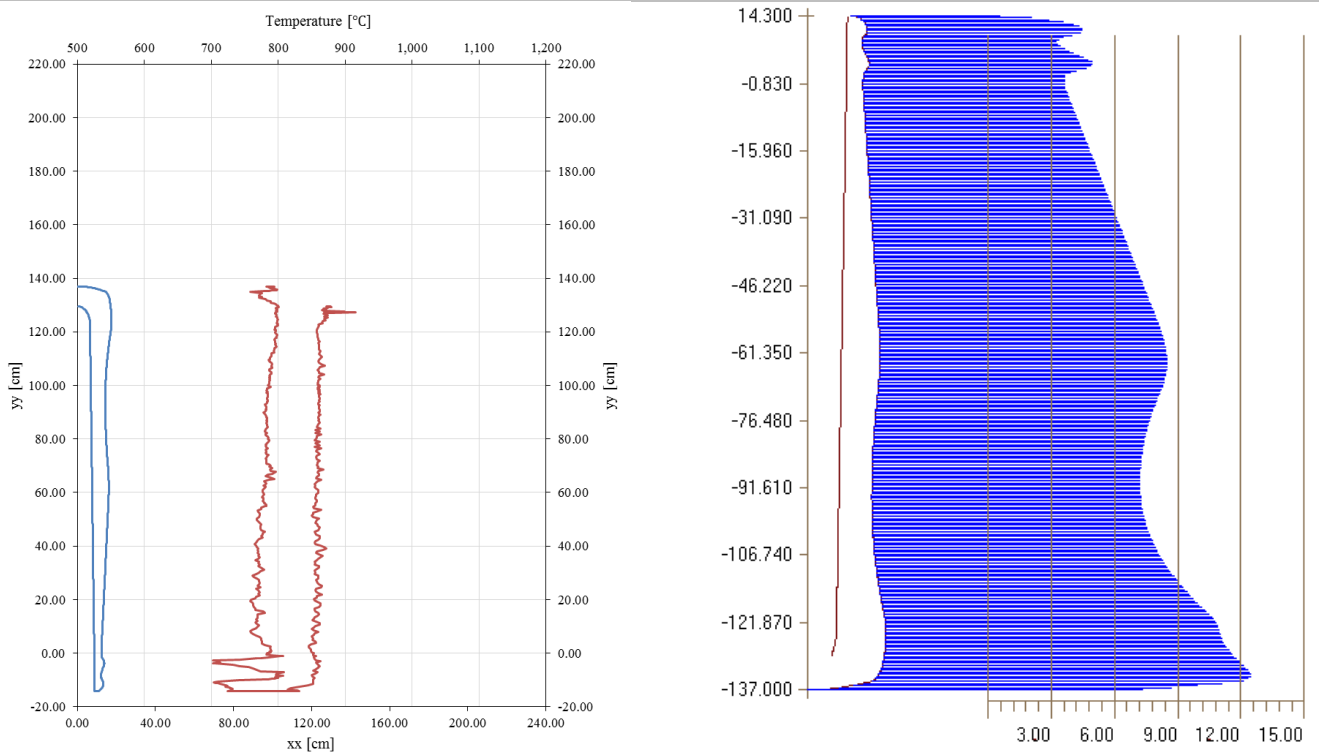


Figure 8.100 Boundary temperature for plunger up stage for case 5.

Thickness (mm) in plunger up stage for case 5.

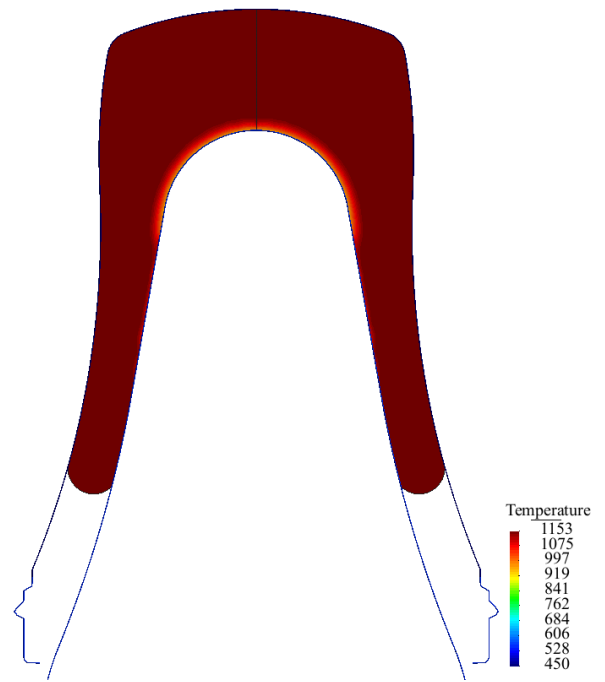
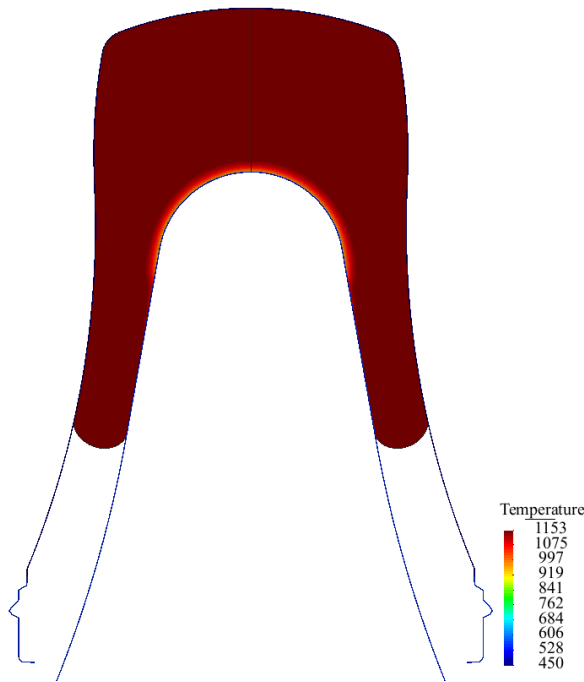
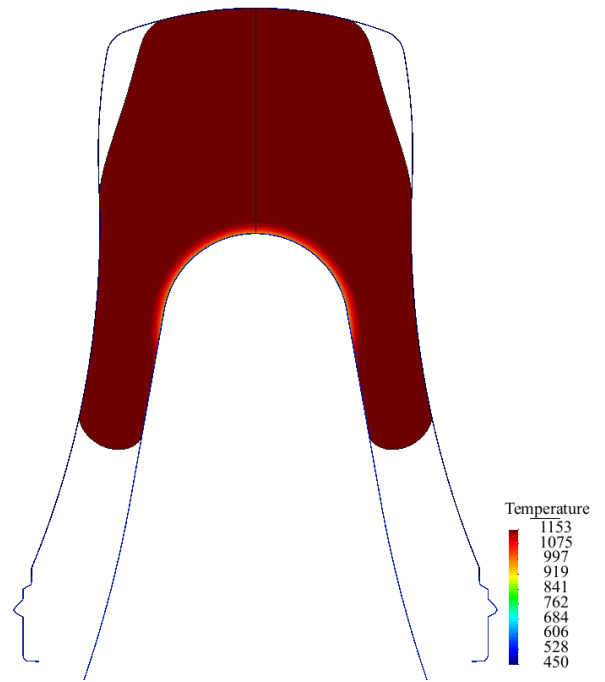
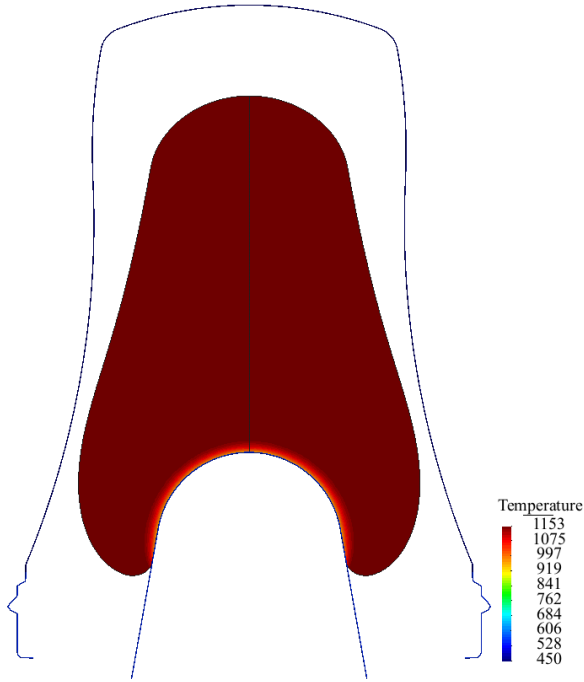




Figure 8.101: Temperature distribution in plunger up for the case 6 in 0.8013s, 0.8014s

0.8015s	0.8020s
0.8030s	0.8050s
0.8067s	1.9967s

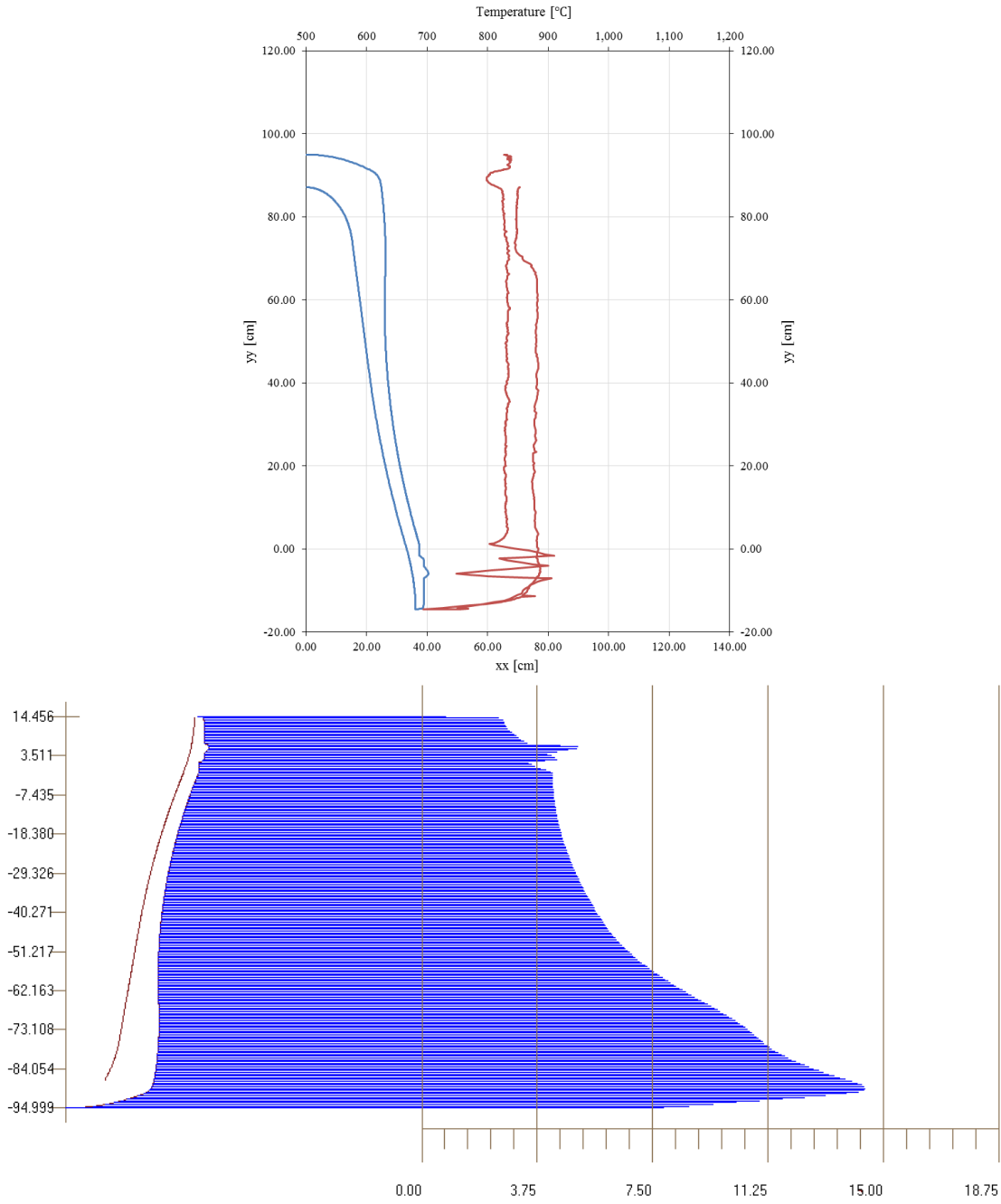
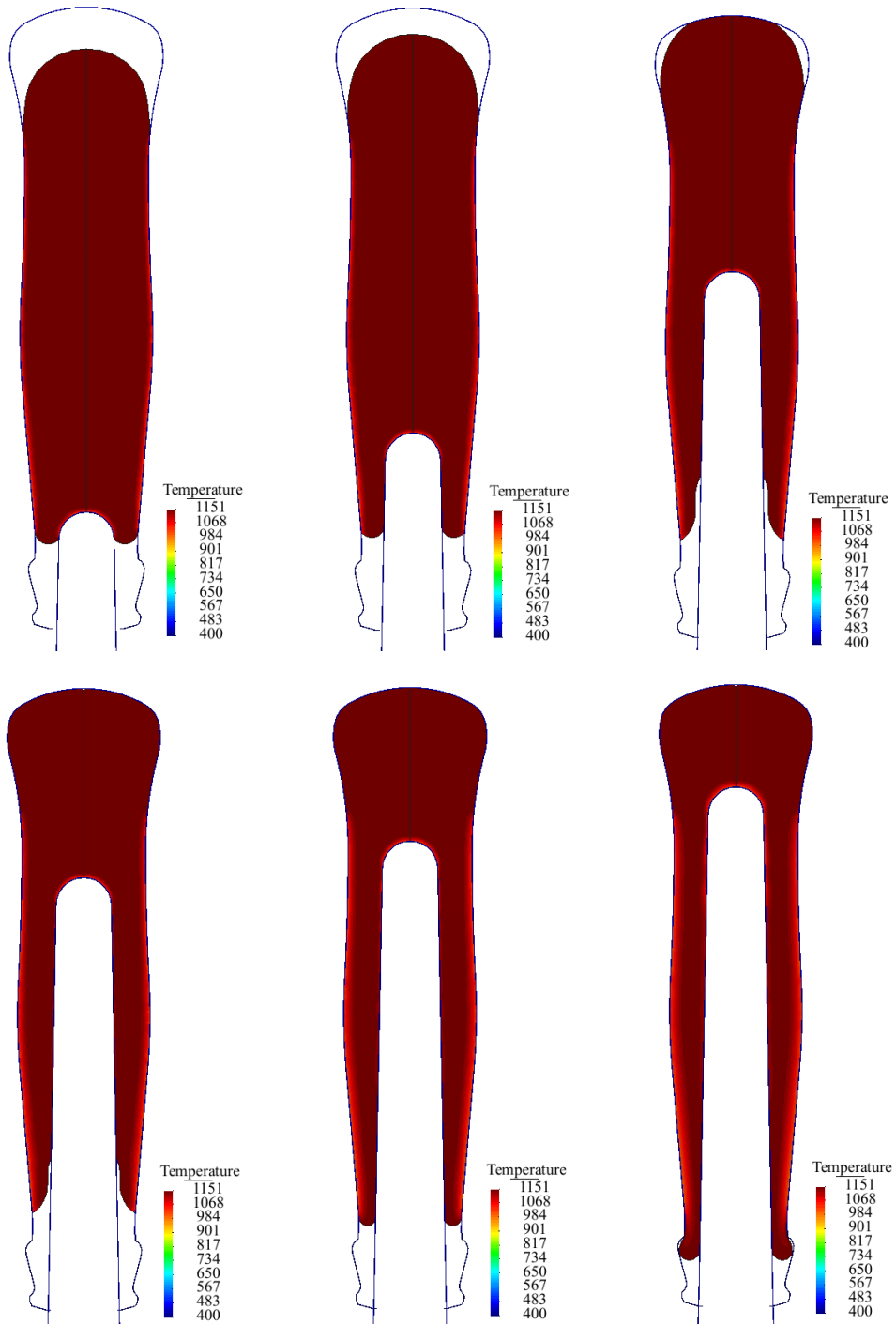


Figure 8.102: Boundary temperature in plunger up for case 6 and the thickness (mm) in plunger up stage for case 6.



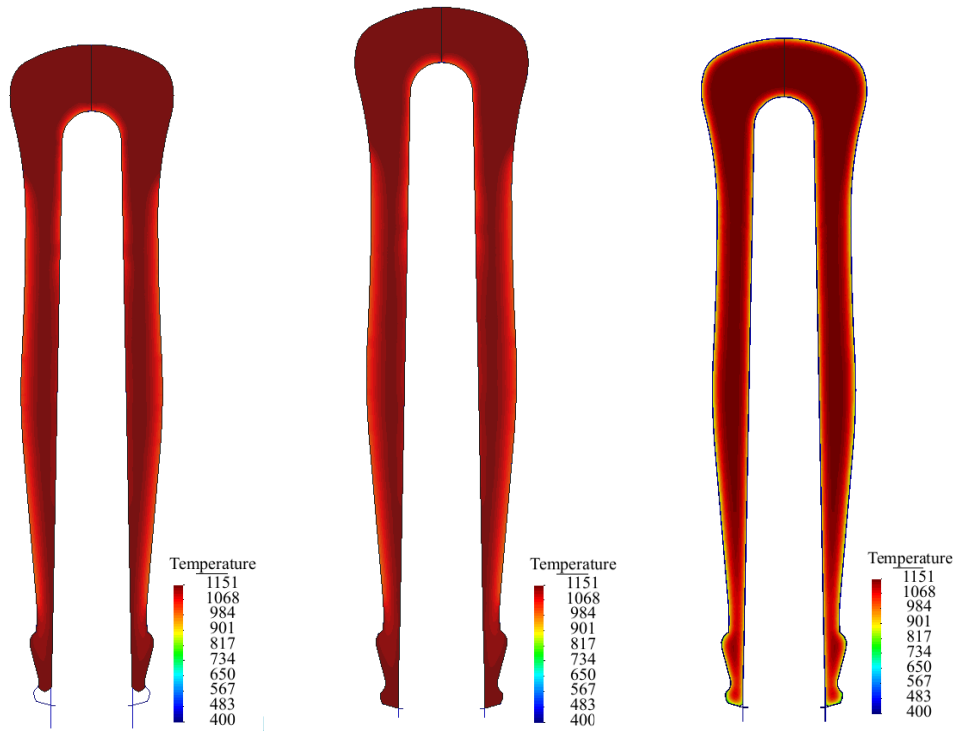


Figure 8.103: Temperature distribution in plunger up for the case 7 in 0.9572s, 0.9575s, 0.9580s

0.9587s	0.9597s	0.9623s
0.9651s	0.9666s	2.0512s

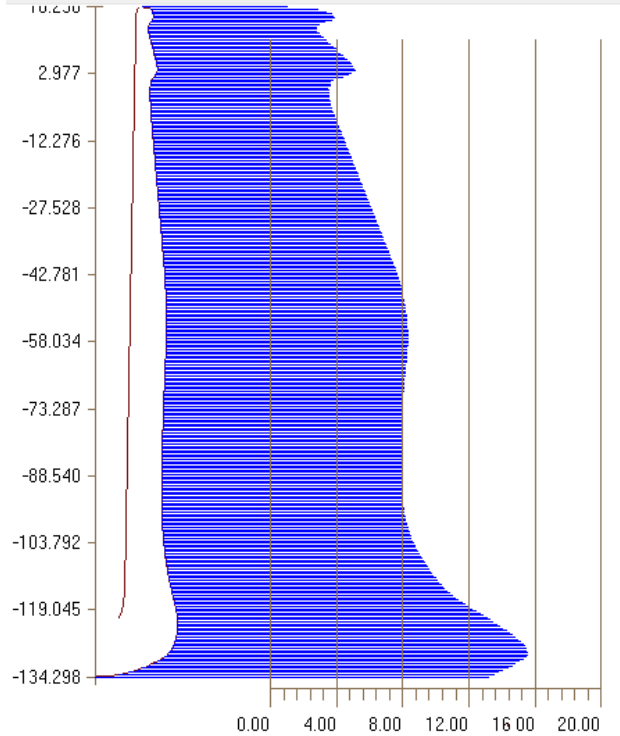
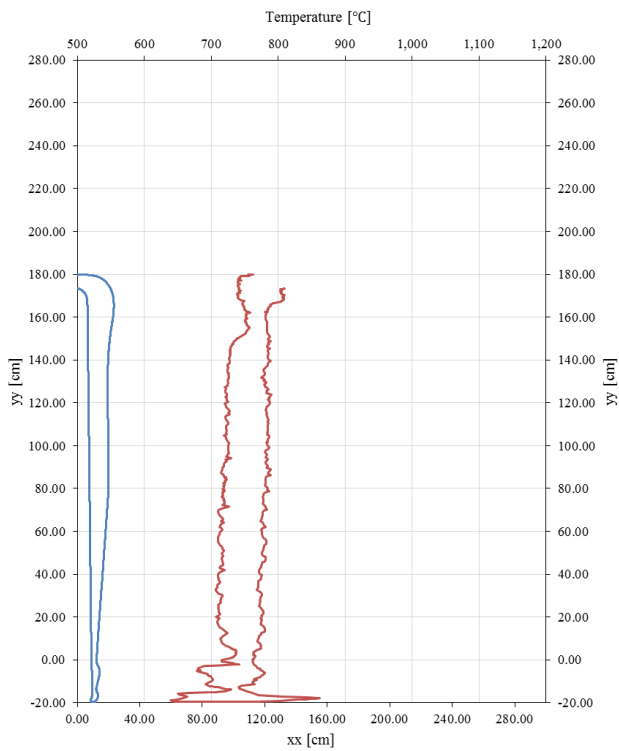
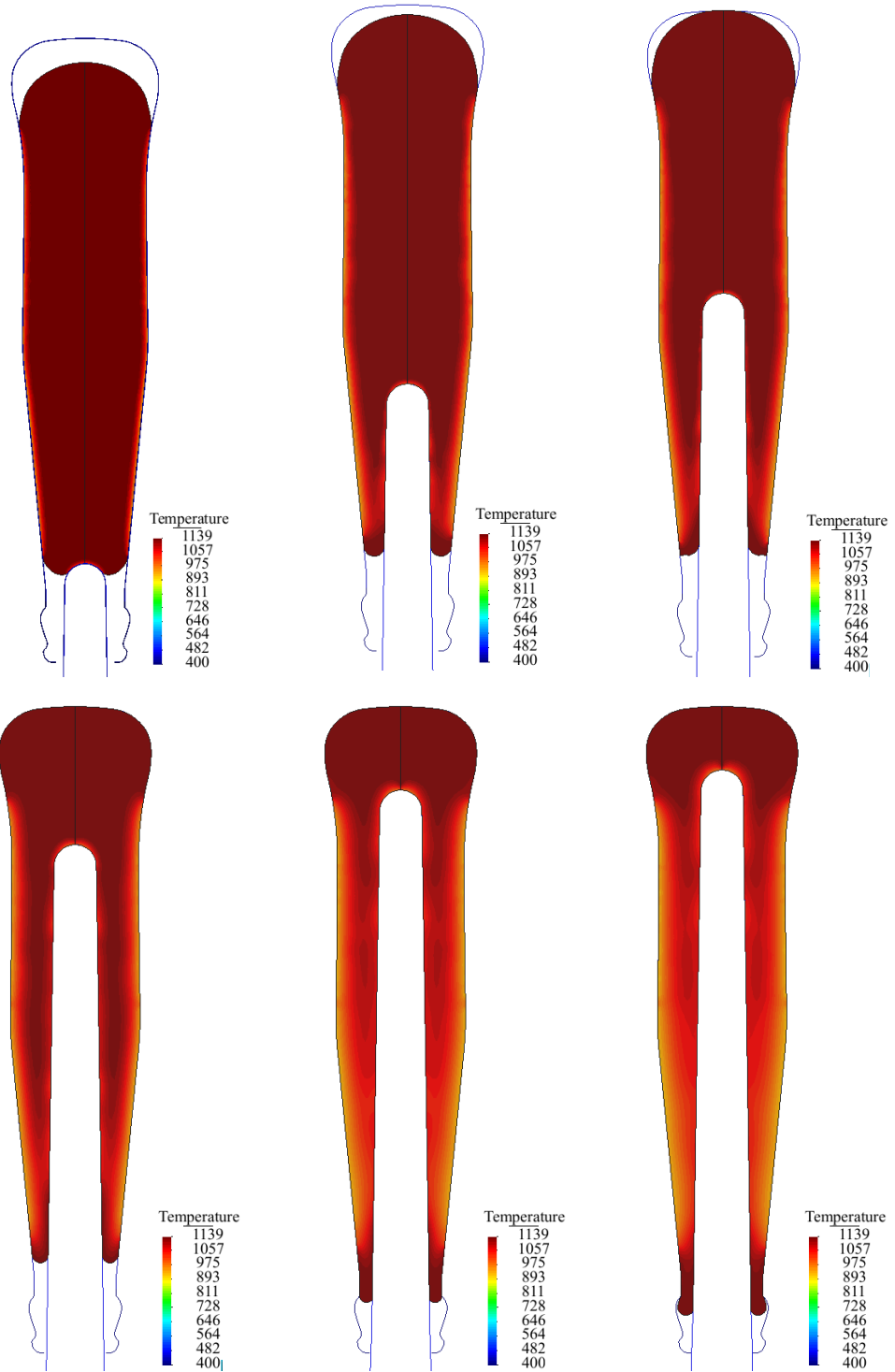


Figure 8.104 Boundary temperature for plunger up stage for case 7.

Thickness (mm) in plunger up stage for case 7.



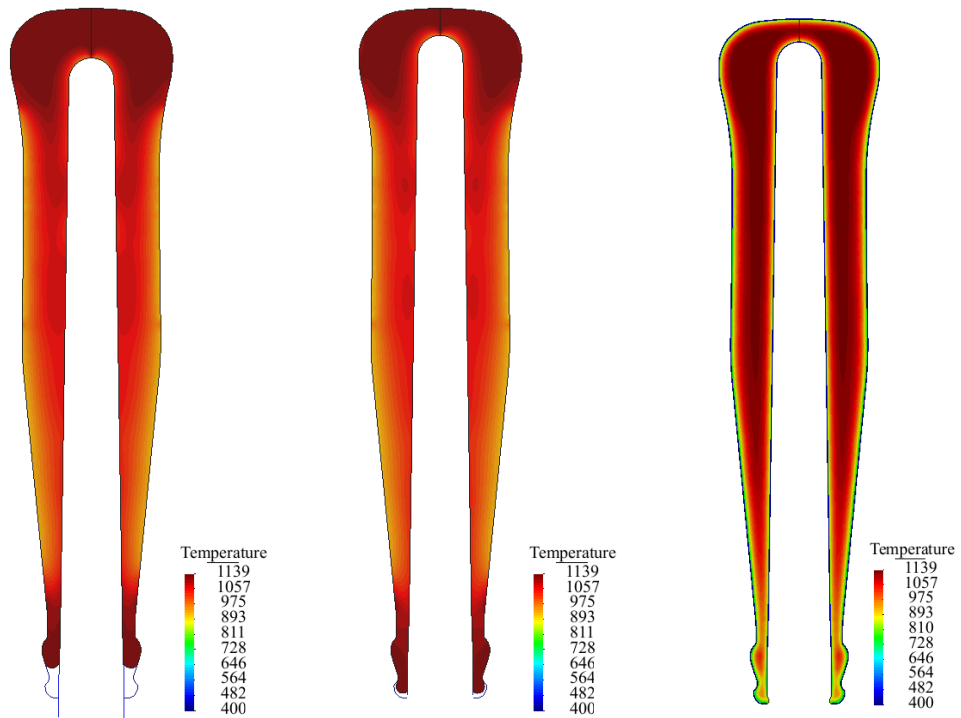


Figure 8.105: Temperature distribution in plunger up for the case 8 in 1.1267s, 1.1272s, 1.1277s

1.1298s	1.1332s	1.1351s
1.1370s	1.1400s	3.098s

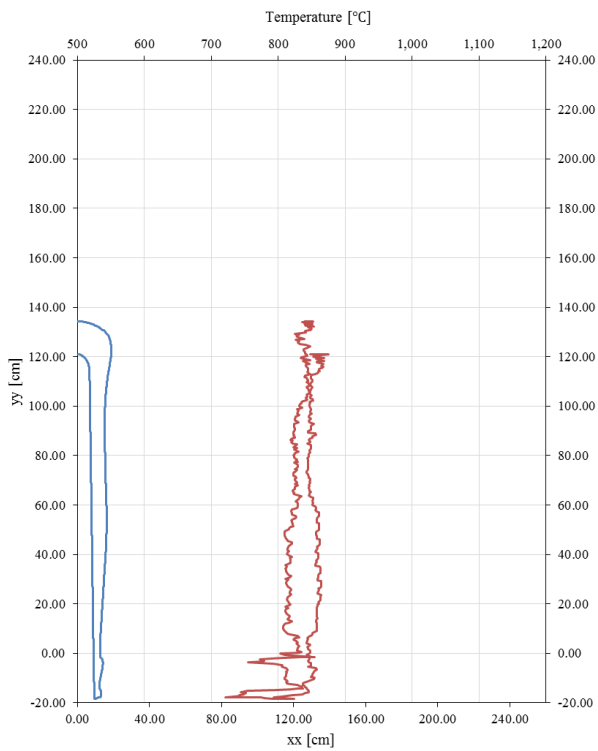
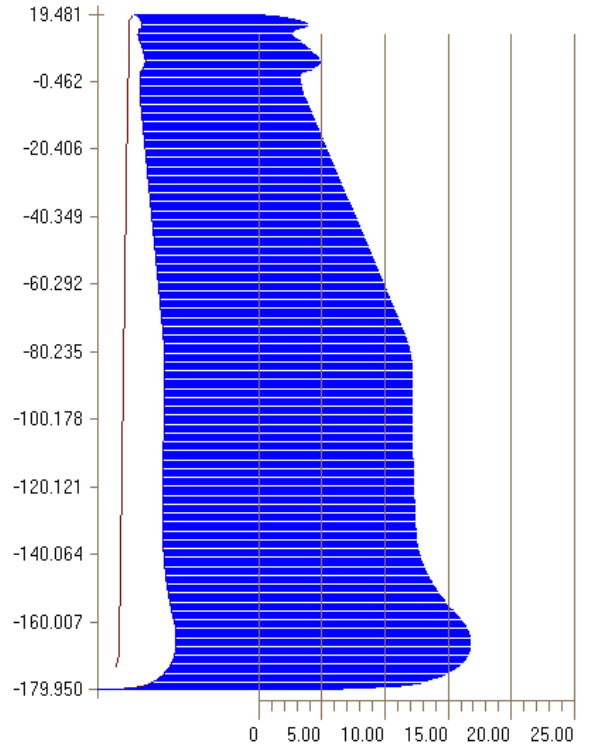


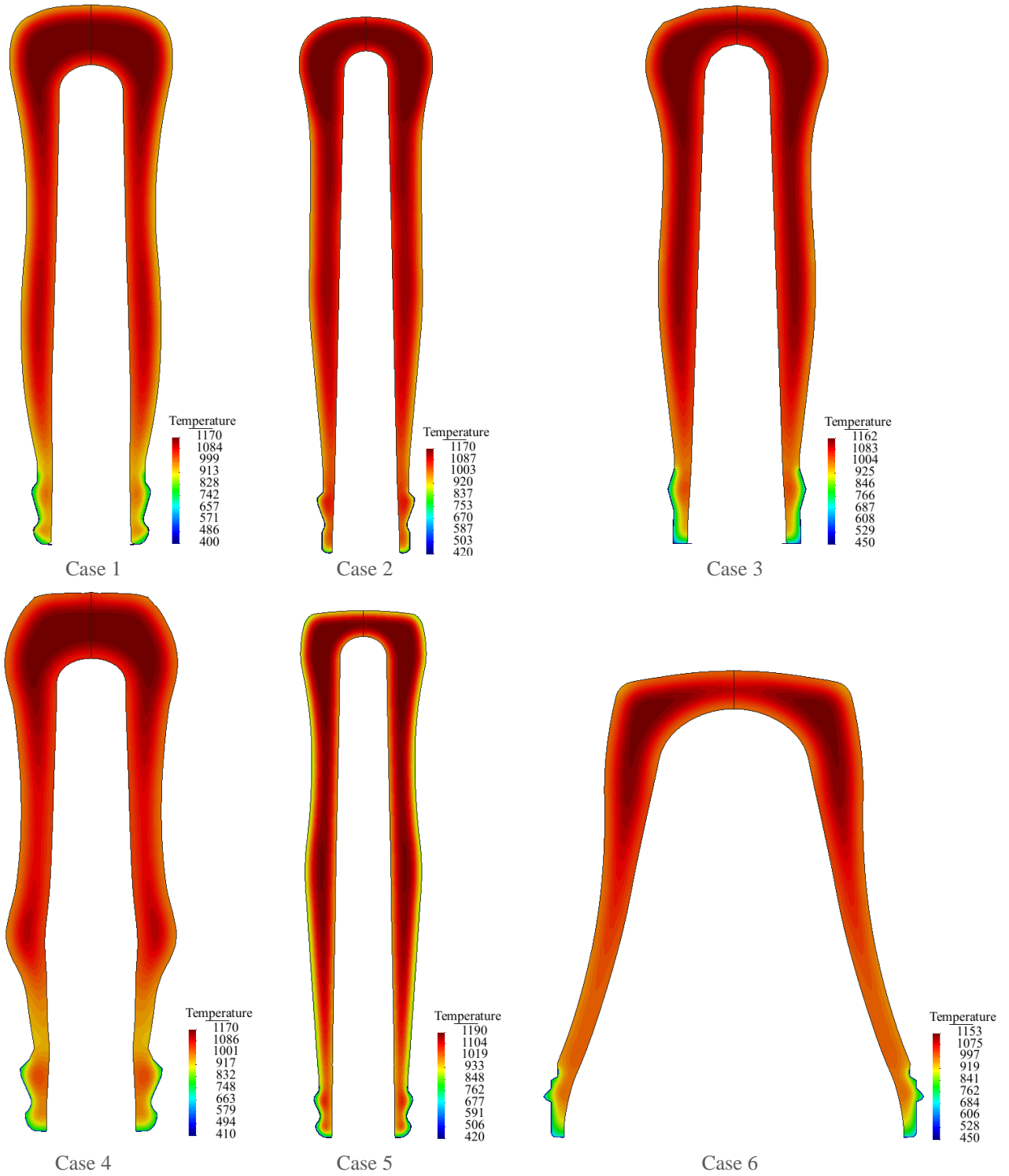
Figure 8.106 Boundary temperature for plunger up stage for case 8.



Thickness (mm) in plunger up stage for case 8.

8.2.4 Reheat

After the plunger down stage the baffle is removed and the blank mould opens to allow the parison to reheat, i.e. heat is transferred from hotter zones to the cooler zones. This effect will eliminate skin conditions before the invert stage. The reheat stage is equivalent to the one in the blow/blow process. The results from the reheat stage can be seen in Figure 8.107. The lowest temperature is verified at the wall parison. This temperature effect is due to the heat transfer from the glass to moulds during the gob loading and the baffle on.



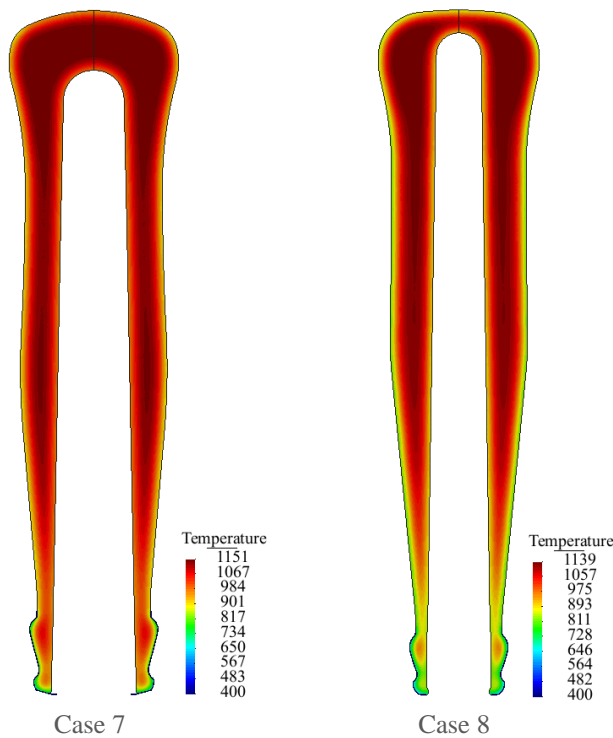


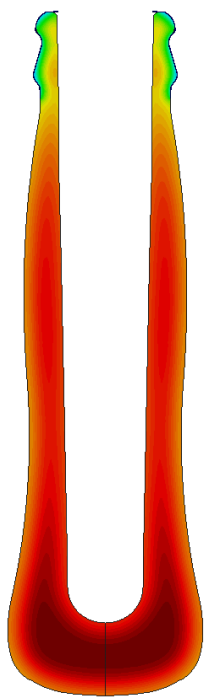
Figure 8.107: Temperature distribution in reheat for the case 1 in 2.733s, for the case 2 in 2.837s, for the case 3 in 3.160s, for the case 4 in 2.777s, for the case 5 in 2.847s, for the case 6 in 3.178s, for the case 7 in 2.871s and for the case 8 in 3.943s.

8.2.5 Invert

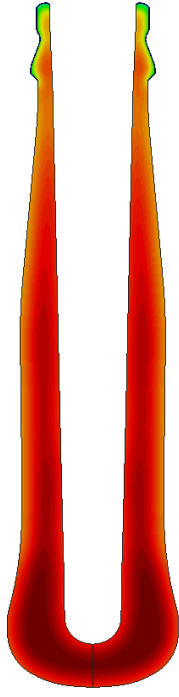
During the time to change tools, i.e. while blank mould and blow mould are swapped, the parison is always reheating. When invert stage starts, speed must be regulated to the size and temperature of the parison, as centrifugal forces will oscillate the parison, pushing the glass mass to the bottom of the parison and affecting the mass distribution. This is the period of time between the end of the parison transfer and the start of the final blow. During this time the parison continues to reheat and gravity stretches the parison while holding it in the blow mould. The inertia forces involved in this stage was not considered.

Time is also an important factor influencing the invert stage, as an excessive time can create a sag in the parison and this effect must be counterbalanced. Also, overhead cooling can happen causing a deficient rundown and even preventing the parison to fall. A short time, in other hand, may cause the opposite effect, an excessive stretching in the necking area that may produce a very thin wall glass during the rundown. Thus, the time of the invert stage should be in according the desired final shape.

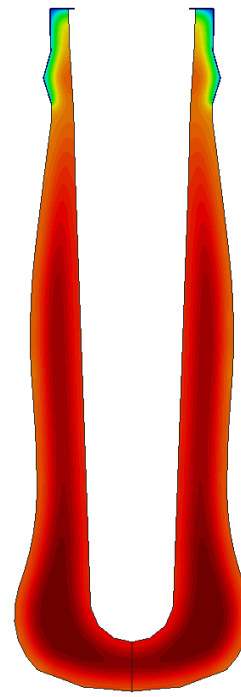
The results from the invert stage are presented in Figure 8.108. It is clearly noted that the bottom zone of the parison has more mass, therefore, a higher temperature than the parison wall and neckring. Additionally, the boundary temperature are shown in Figure 8.109. The coolest zones are located at the neckring while the hottest zones are at the bottom zone of the parison.



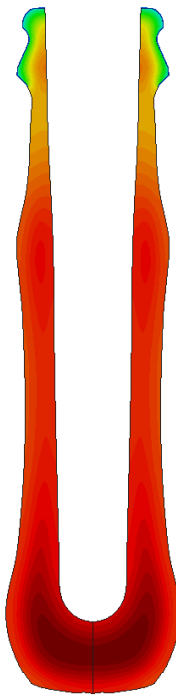
Case 1



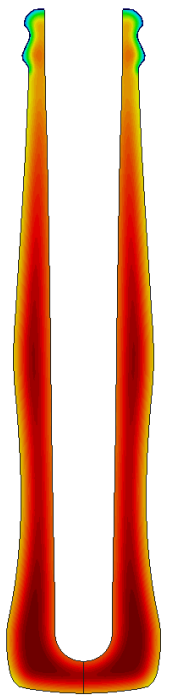
Case 2



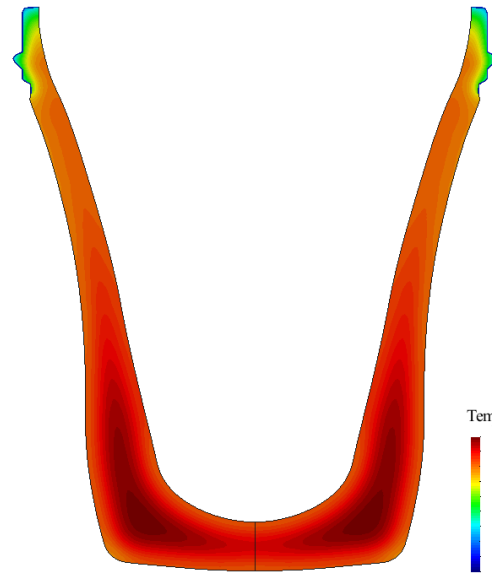
Case 3



Case 4



Case 5



Case 6

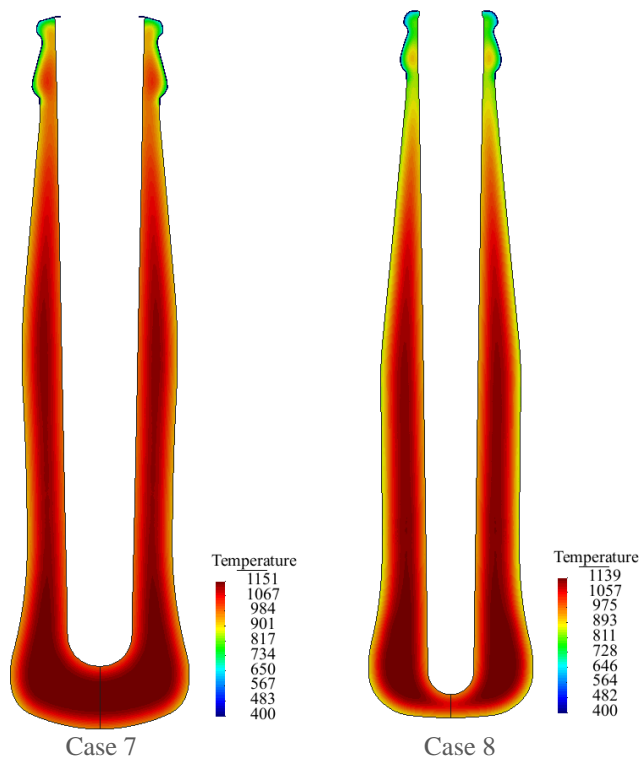
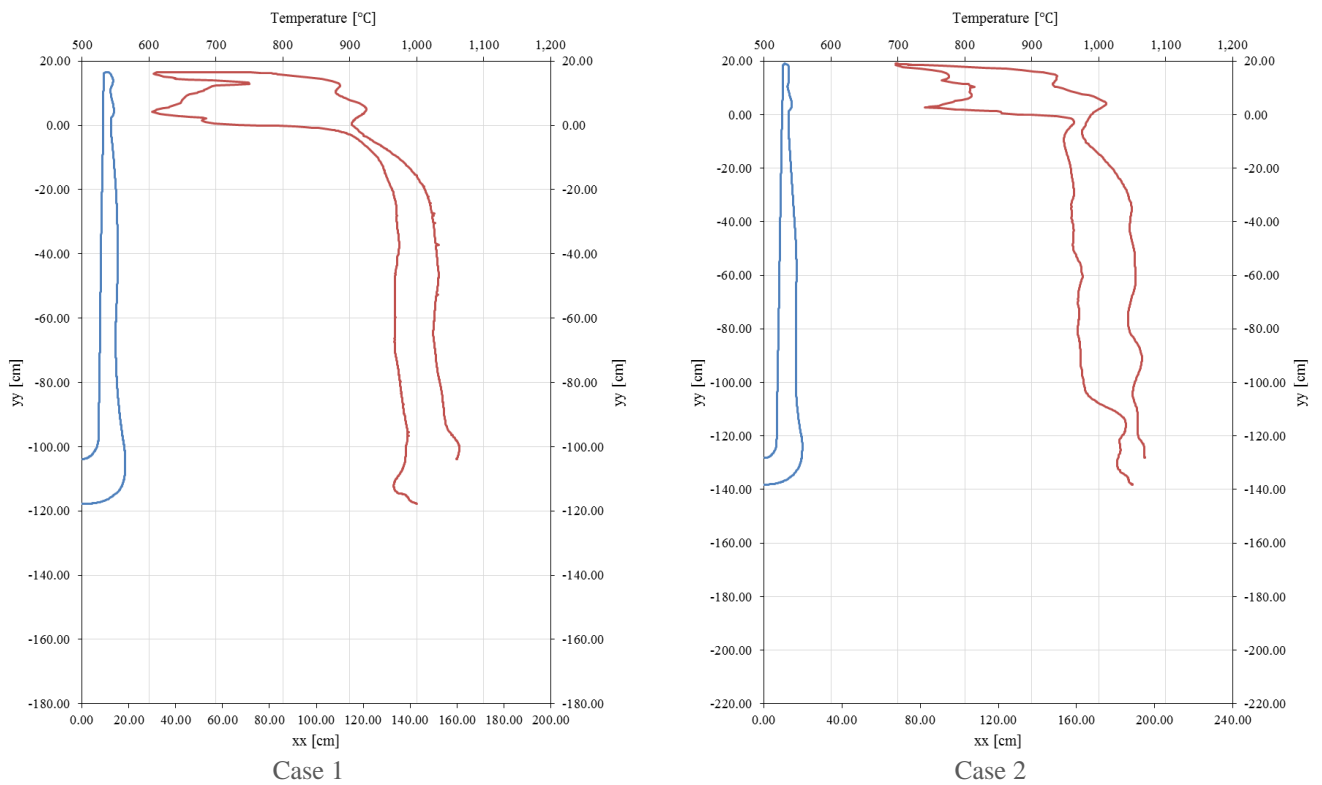
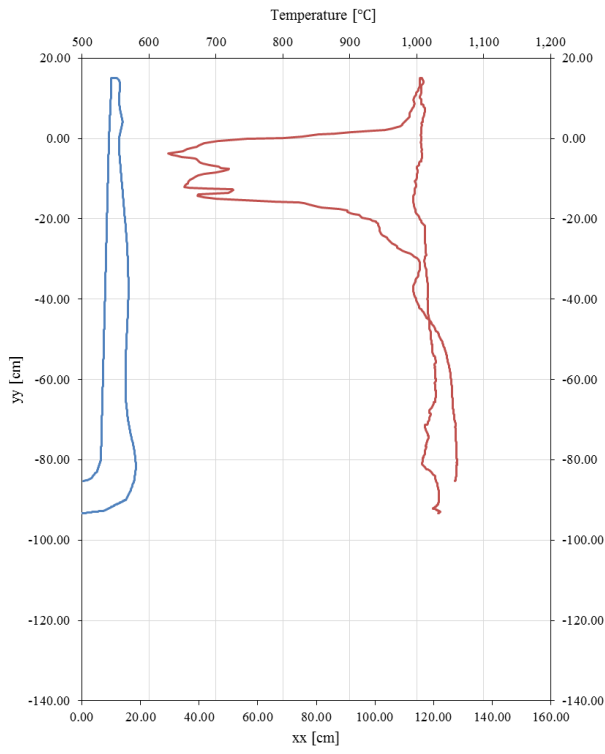
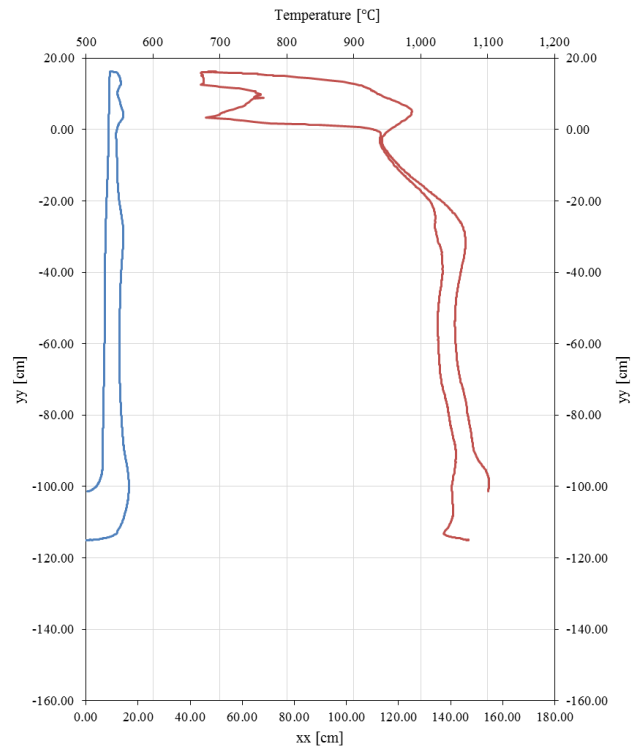


Figure 8.108: Temperature distribution in invert for the case 1 in 3.760s, for the case 2 in 3.910s, for the case 3 in 3.733s, for the case 4 in 4.194s, for the case 5 in 3.819s and for the case 6 in 3.561s, for the case 7 in 3.487s and for the case 8 in 4.788s.

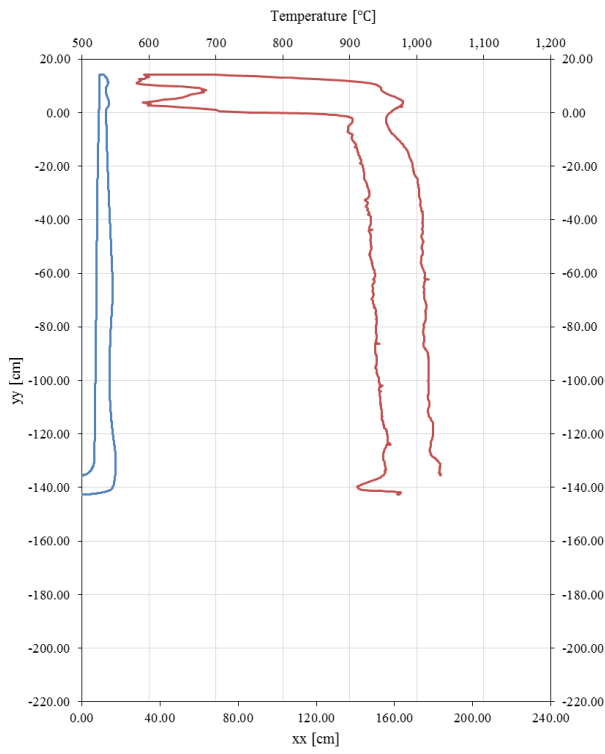




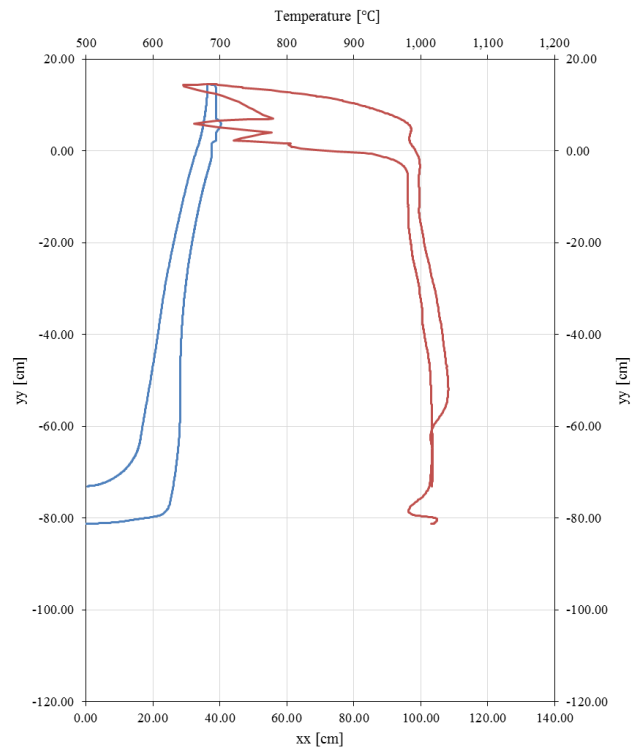
Case 3



Case 4



Case 5



Case 6

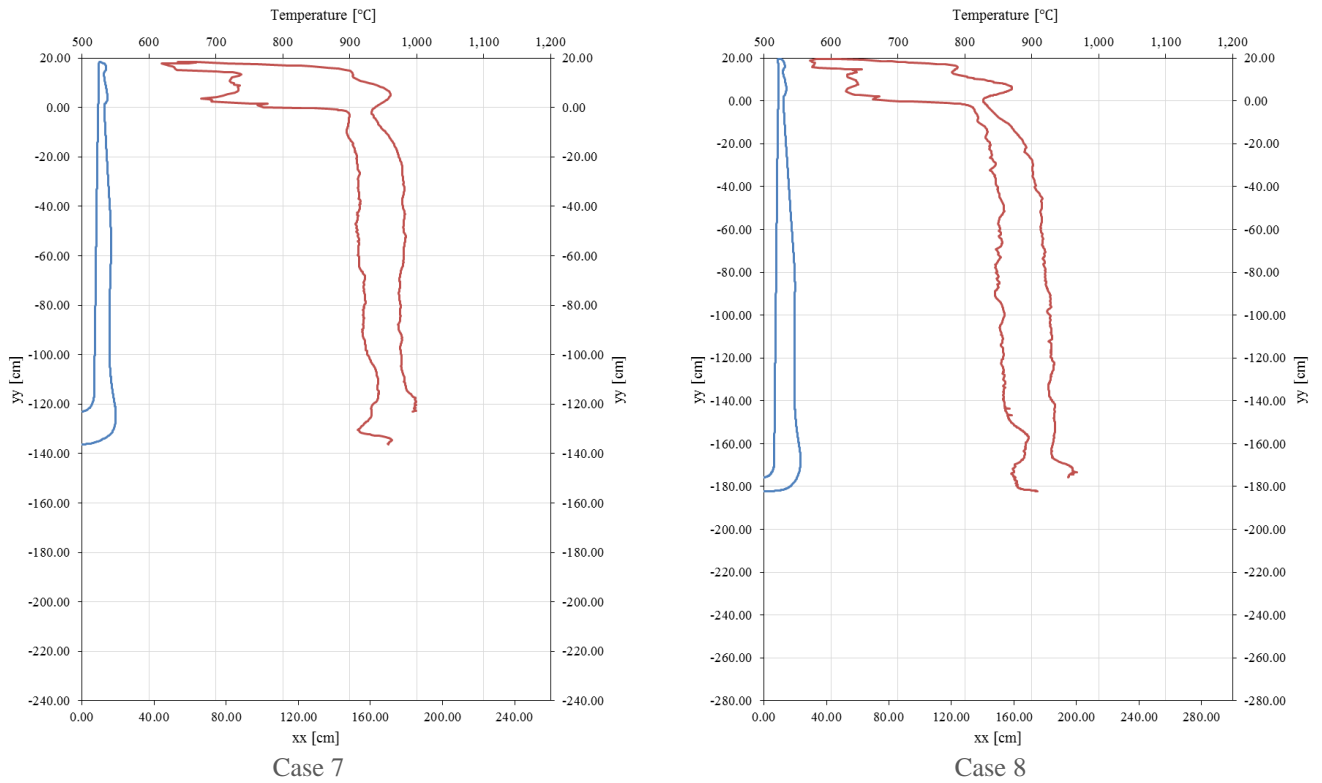


Figure 8.109: Boundary temperature for invert stage for case 1, case 2, case 3, case 4, case 5, case 6, case 7 and case 8.

8.2.6 Rundown

At the rundown stage glass stretches due to gravity until it reaches the shape to start the final blow. Figure 8.110 shows the result for the case 1. The glass parison starts to fall due to gravity until it reaches the blow mould. The boundary temperatures as well the thickness are presented in Figure 8.112. The results show that the parison wall has an increase of temperature, while the bottom zone of the parison has a large drop on the temperature due to the contact to the blow mould.

Figure 8.112, Figure 8.114, Figure 8.116, Figure 8.119, Figure 8.121, Figure 8.123 and Figure 8.125 present the results for the cases 2 to 8. A quite similar behaviour is depicted for all those cases. The boundary temperatures and the parison thickness is presented in Figure 8.113, Figure 8.115, Figure 8.117, Figure 8.120, Figure 8.122, Figure 8.124 and Figure 8.126 The results also show a very similar behaviour.

Additionally, the displacement contours for the case 4 can be seen in Figure 8.118. In the beginning the higher displacements are located at the bottom zone of the parison. When the parison hits the blow moulds the higher displacements are located in the middle of the parison.

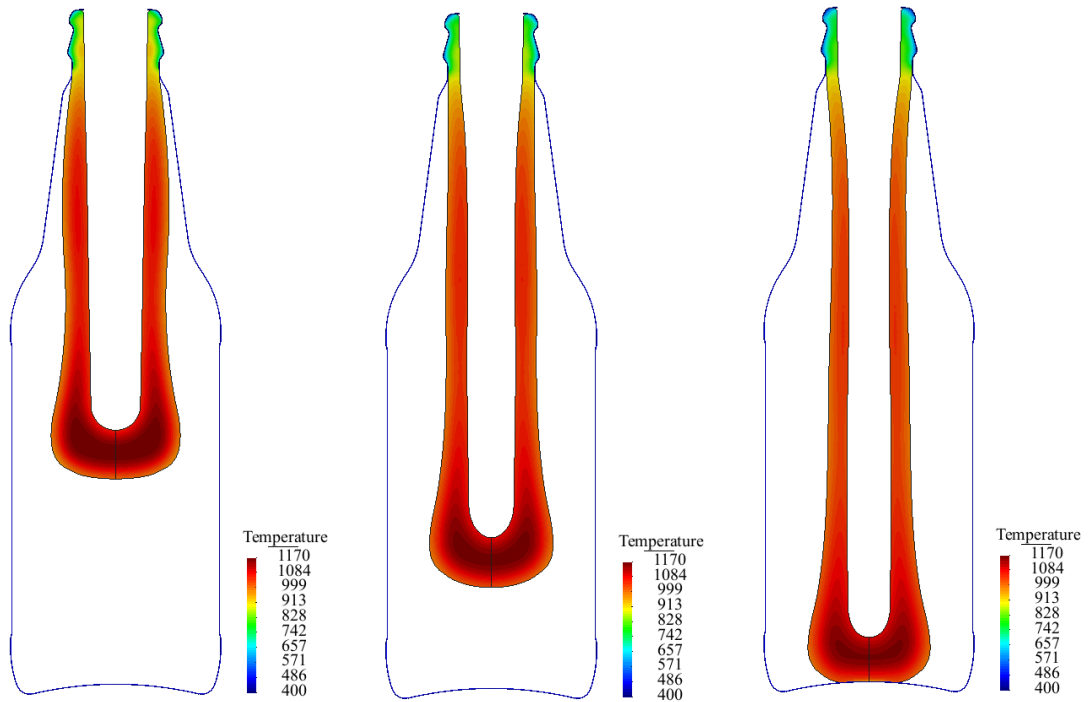


Figure 8.110: Temperature distribution in rundown for the case 1 in 3.760s, 5.026s and 5.800s.

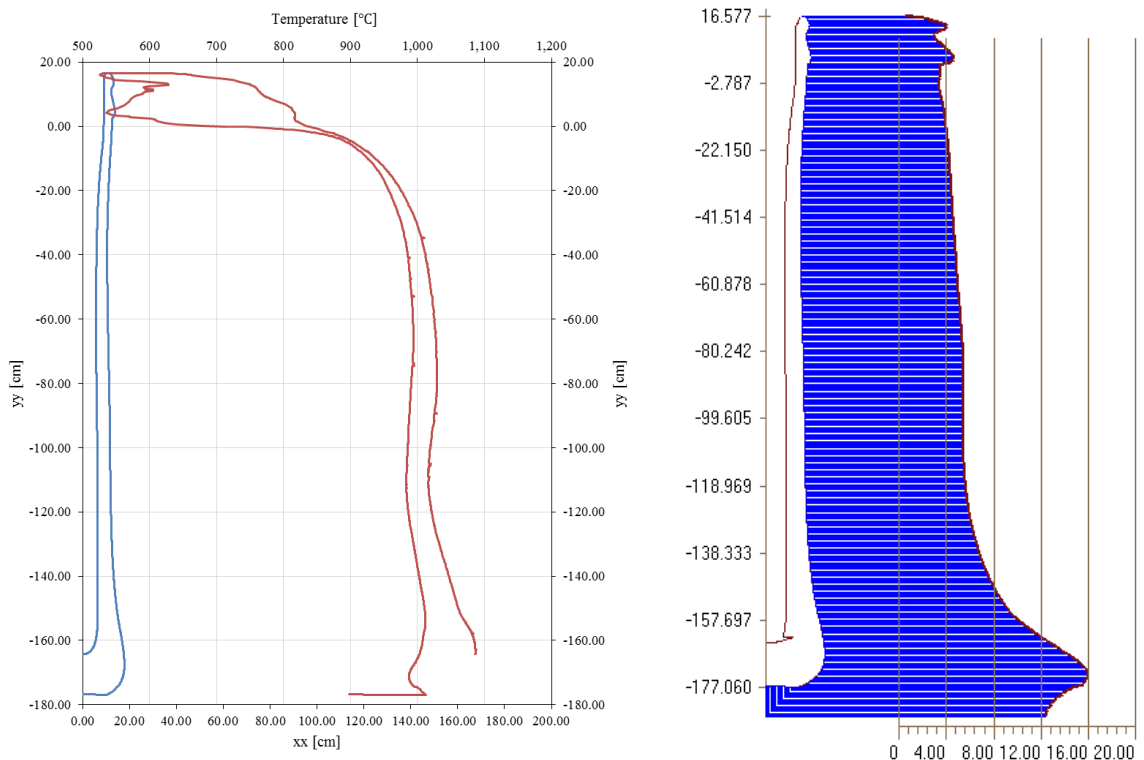


Figure 8.111 Boundary temperature for run down stage for case 1

Thickness (mm) in run down stage for case 1.

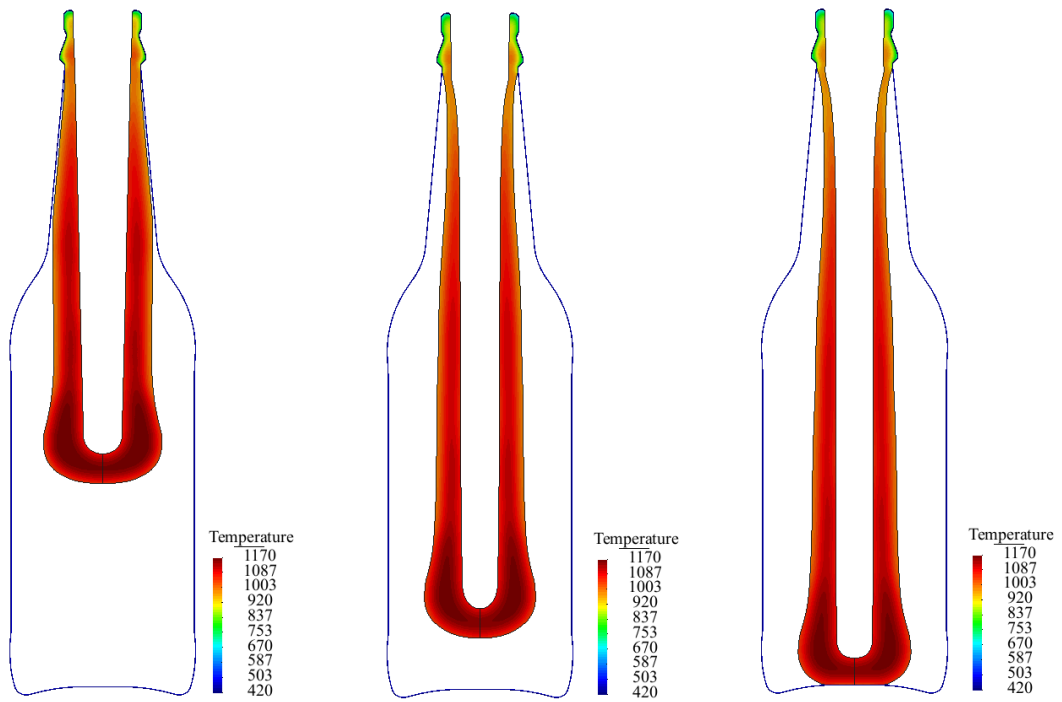


Figure 8.112: Temperature distribution in rundown for the case 2 in 3.910s, 4.627s and 4.907s.

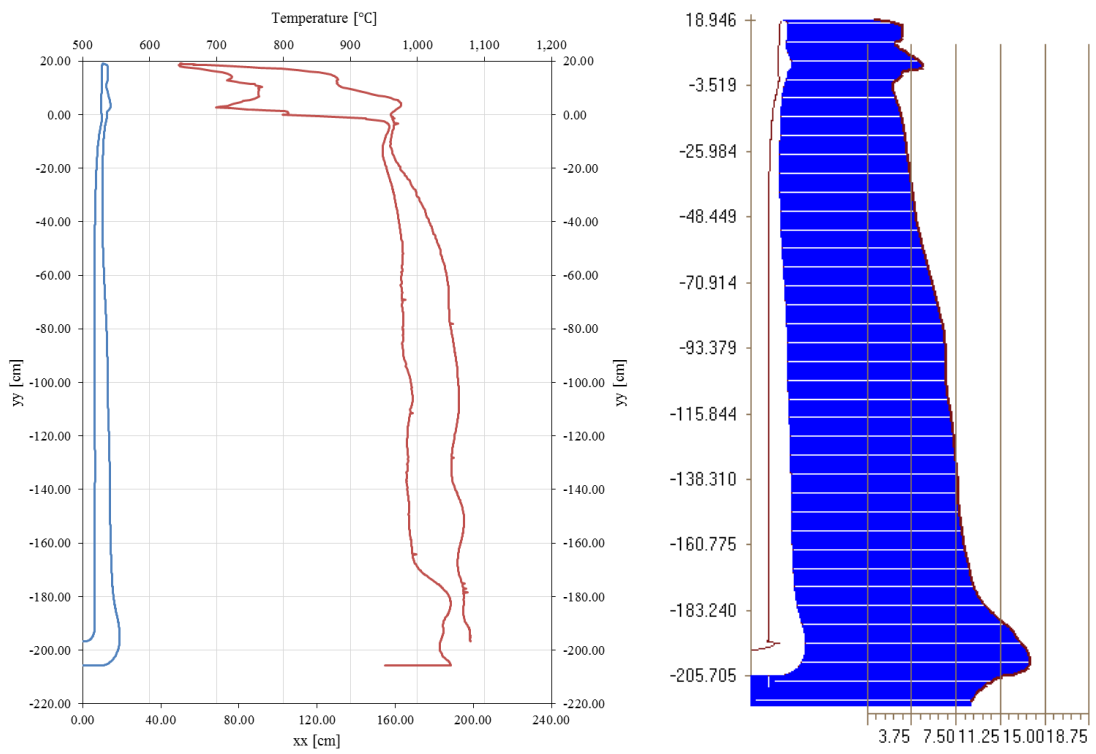


Figure 8.113: Boundary temperature in rundown for case 2.

Thickness (mm) in rundown stage for case 2.

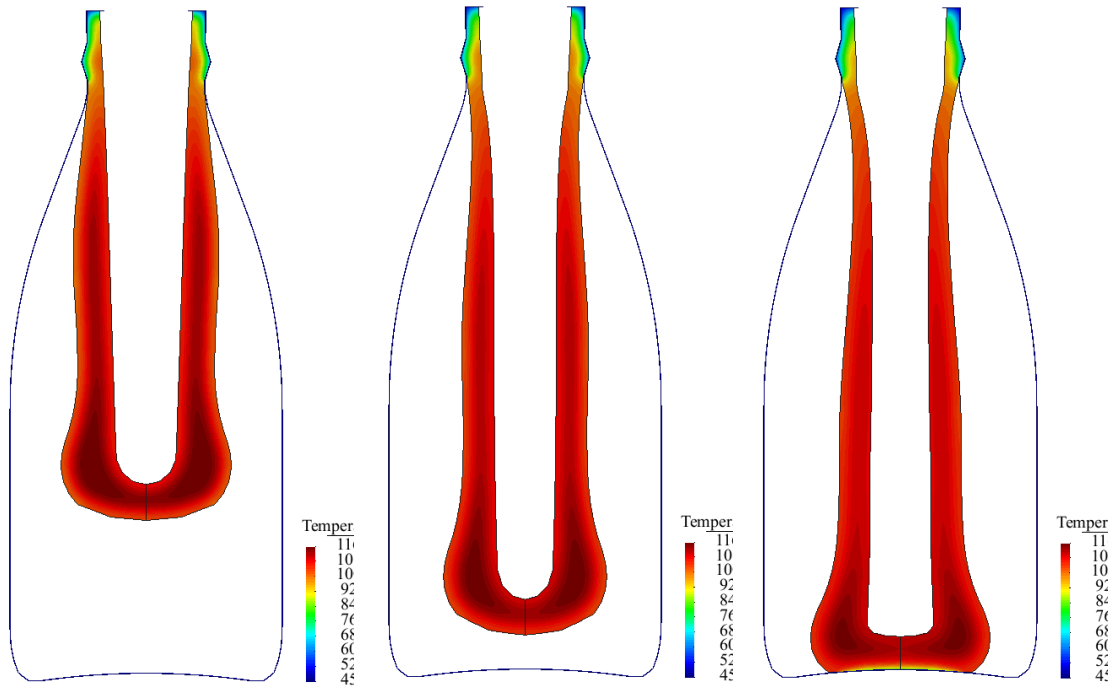


Figure 8.114: Temperature distribution in rundown for the case 3 in 3.733s, 4.543s and 5.467s.

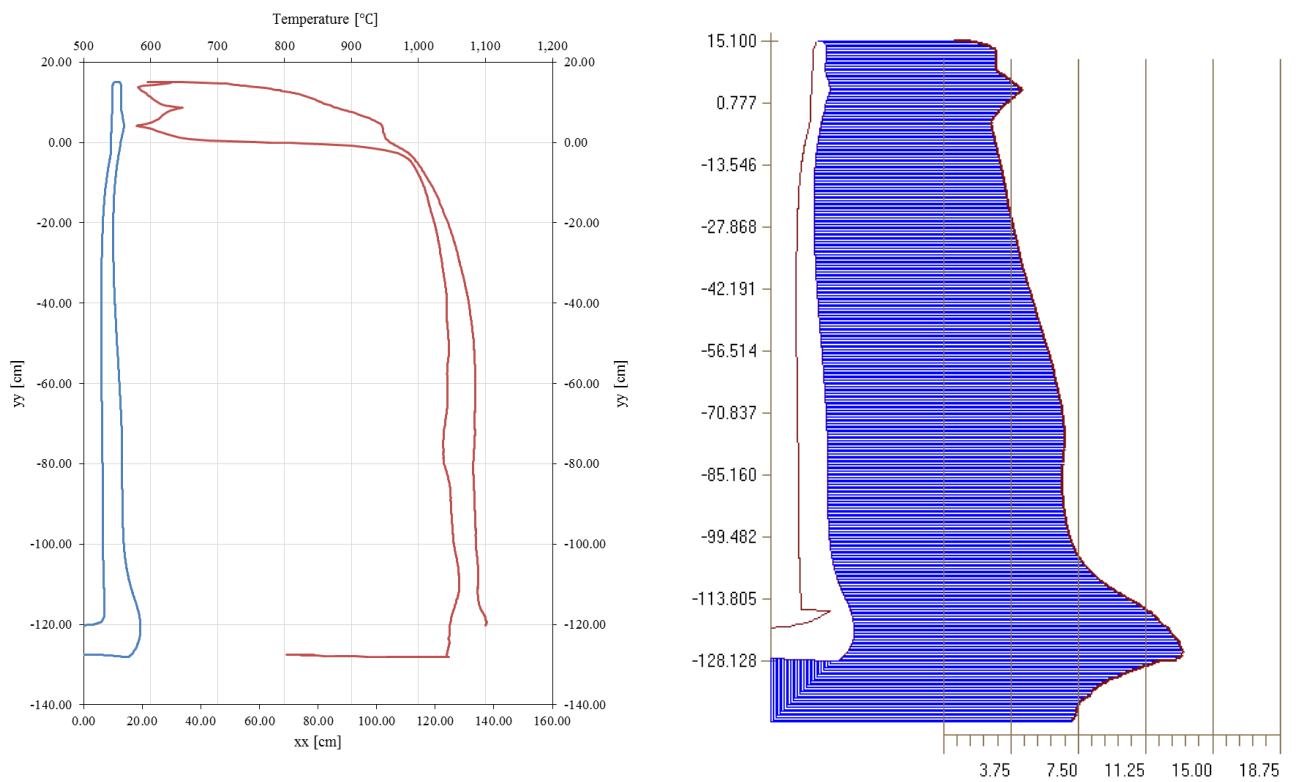


Figure 8.115: Boundary temperature in rundown for case 3.

Thickness (mm) in rundown stage for case 3.

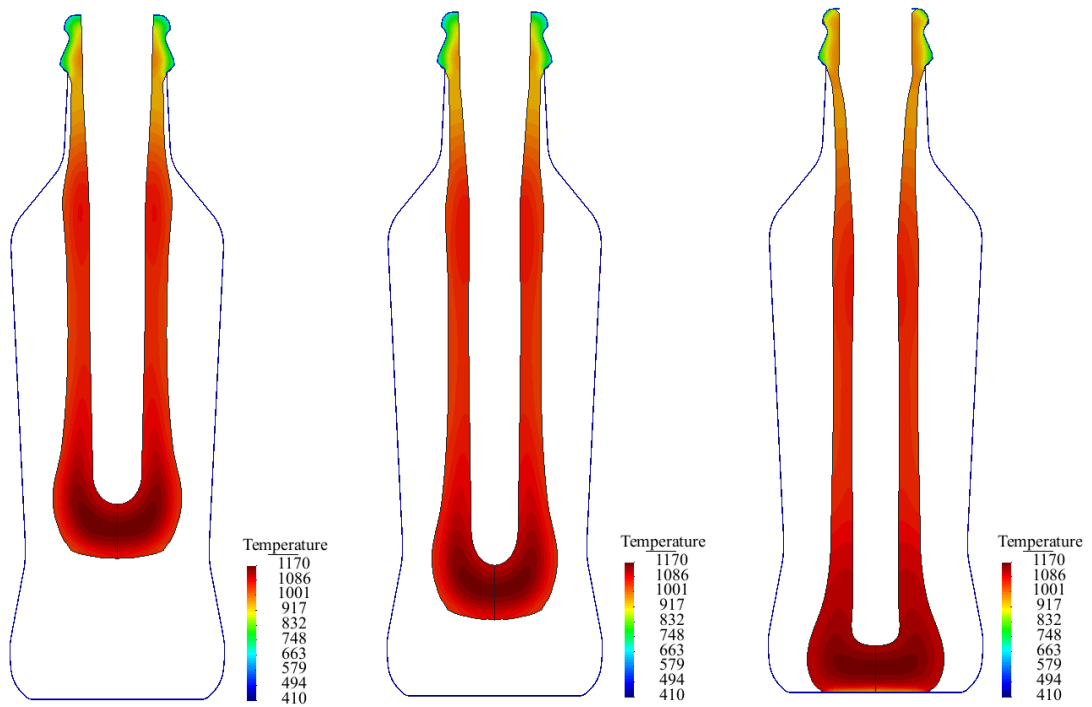


Figure 8.116: Temperature distribution in rundown for the case 4 in 4.194s, 4.974s and 5.972s.

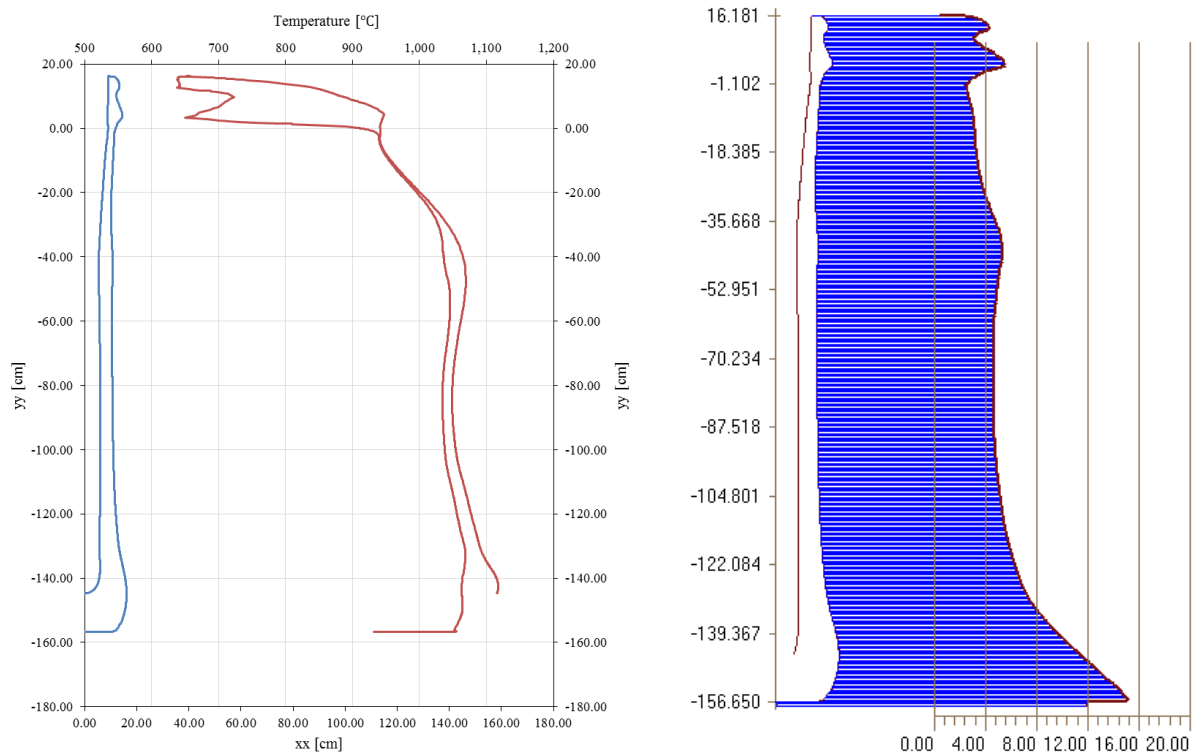


Figure 8.117: Boundary temperature in rundown for case 4.

Thickness (mm) in rundown stage for case 4.

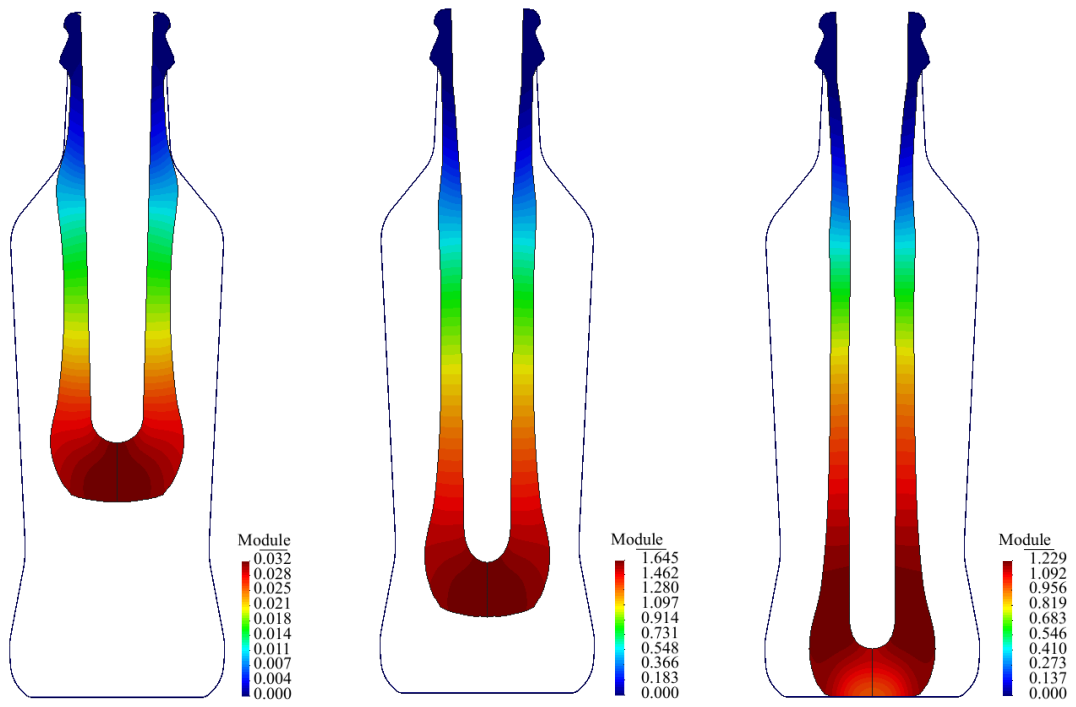


Figure 8.118: Displacement module in rundown for the case 4 in 4.194s, 4.974s and 5.972s.

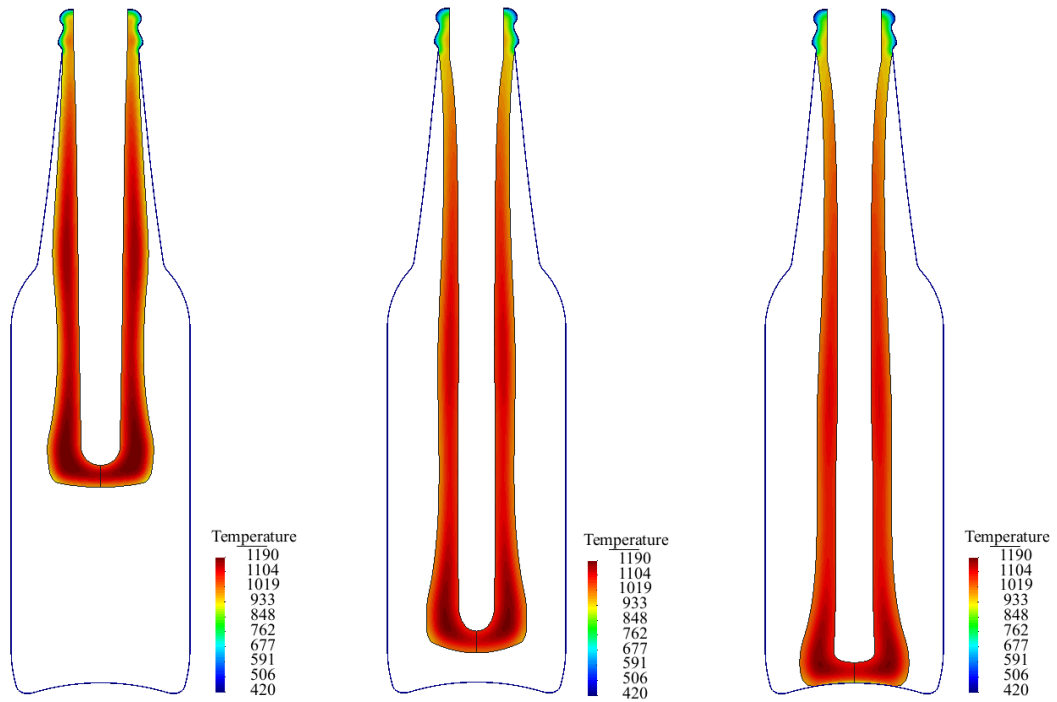


Figure 8.119: Temperature distribution in rundown for the case 5 in 3.819s, 5.131s and 5.694s.

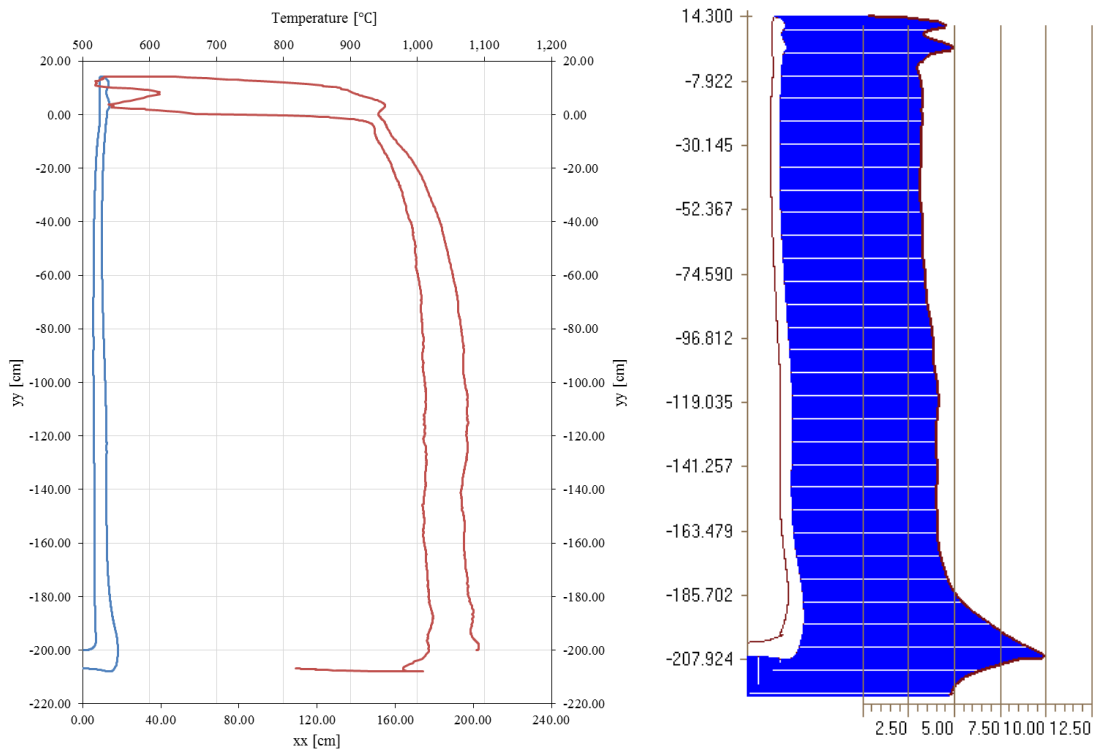


Figure 8.120: Boundary temperature in rundown for case 5.

Thickness (mm) in run down stage for case 5.

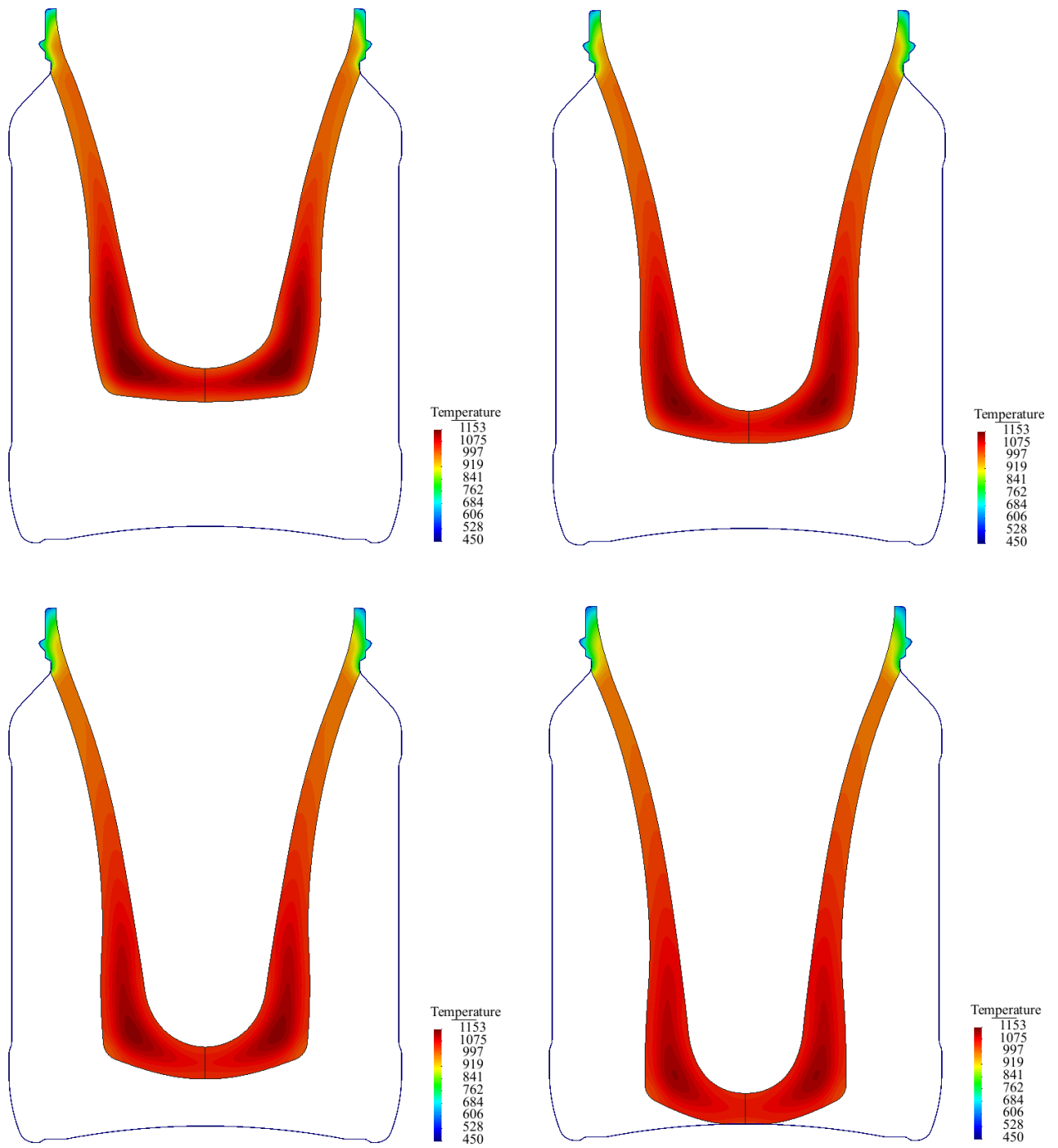


Figure 8.121: Temperature distribution in rundown for the case 6 in 3.561s, 4.298s

4.898s

5.584s

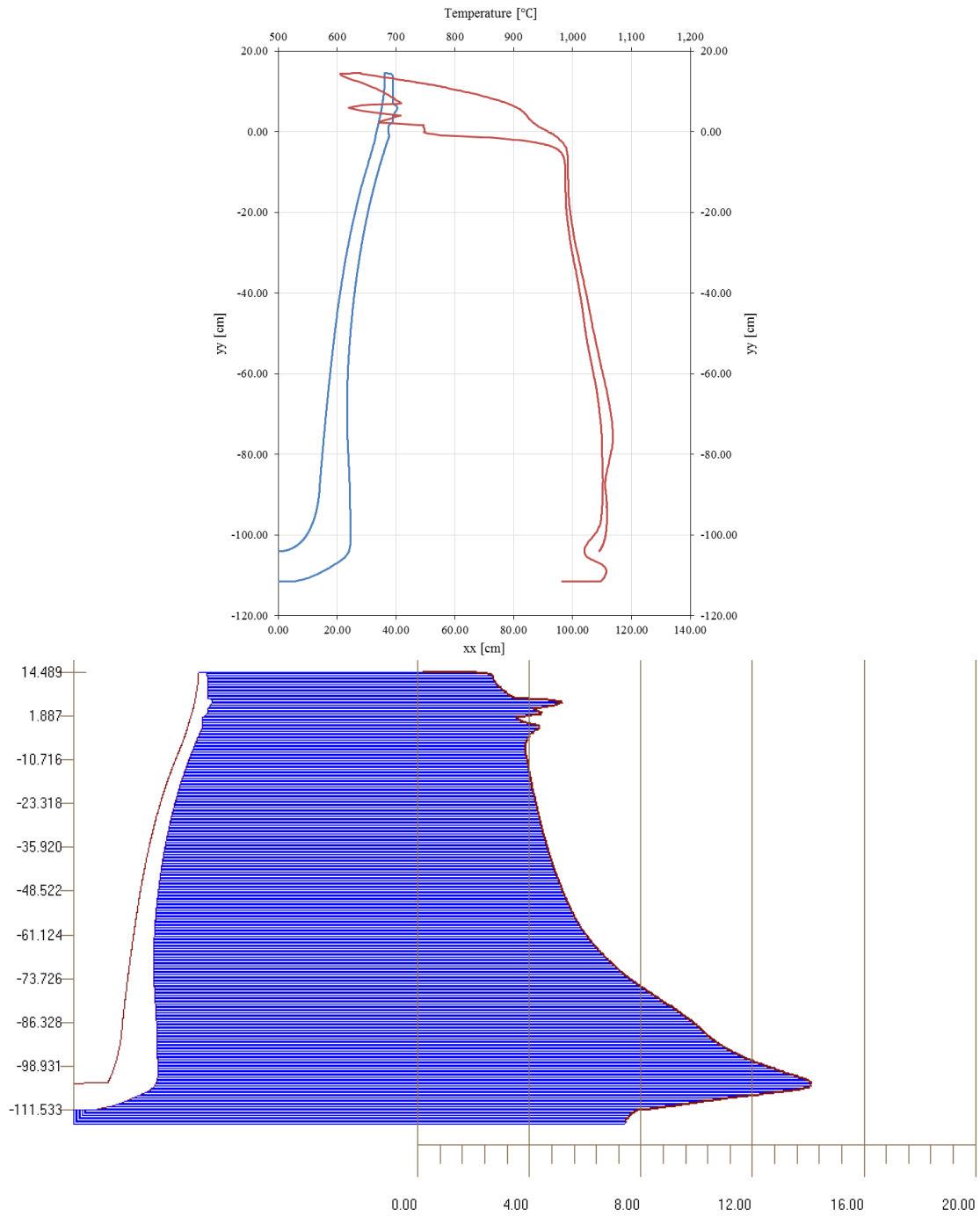


Figure 8.122: Boundary temperature in rundown for case 6 and the thickness (mm) in run down stage for case 6.

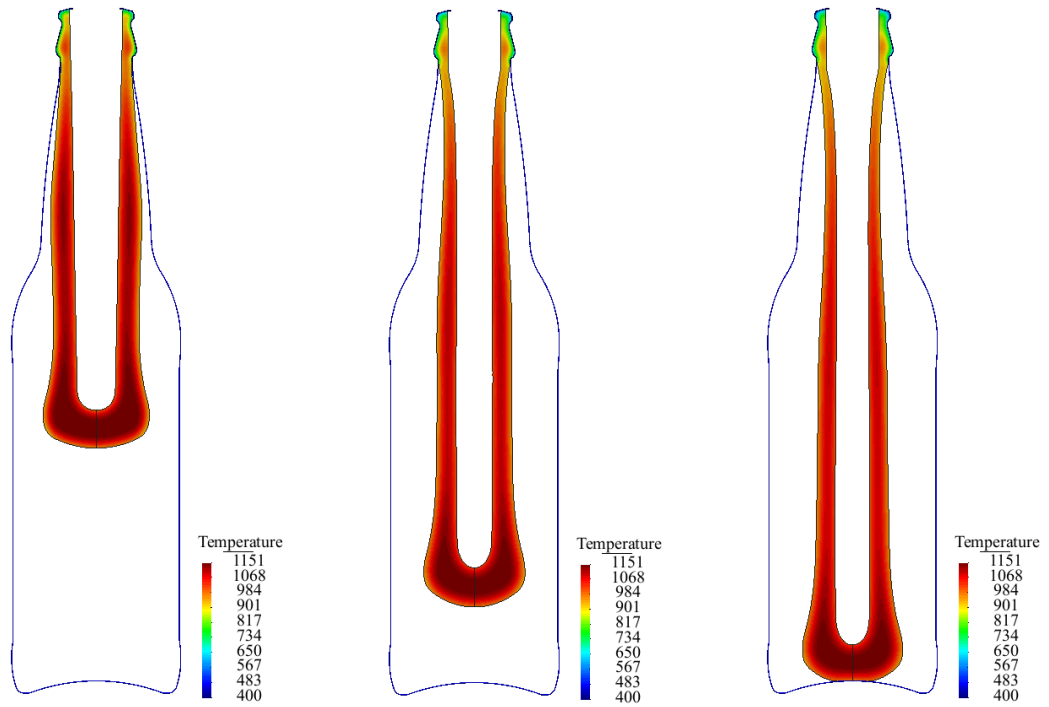


Figure 8.123: Temperature distribution in rundown for the case 7 in 3.487s, 4.664s and 5.059s.

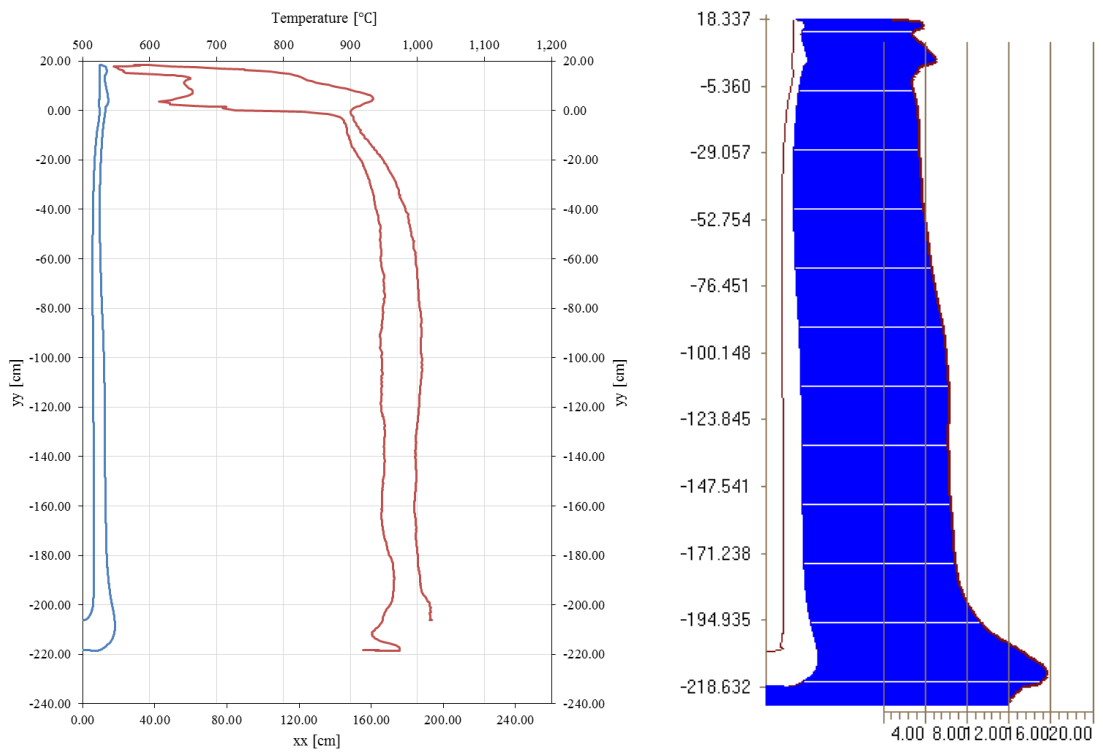


Figure 8.124: Boundary temperature in rundown for case 7.

Thickness (mm) in run down stage for case 7.

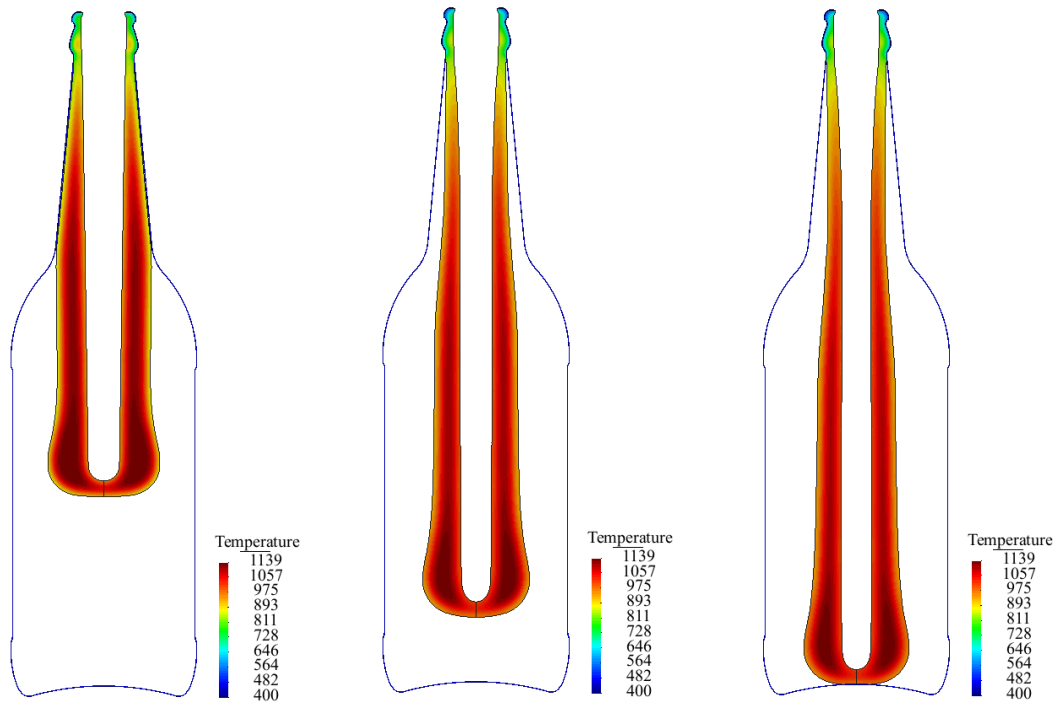


Figure 8.125: Temperature distribution in rundown for the case 8 in 4.788s, 6.459s and 6.854s.

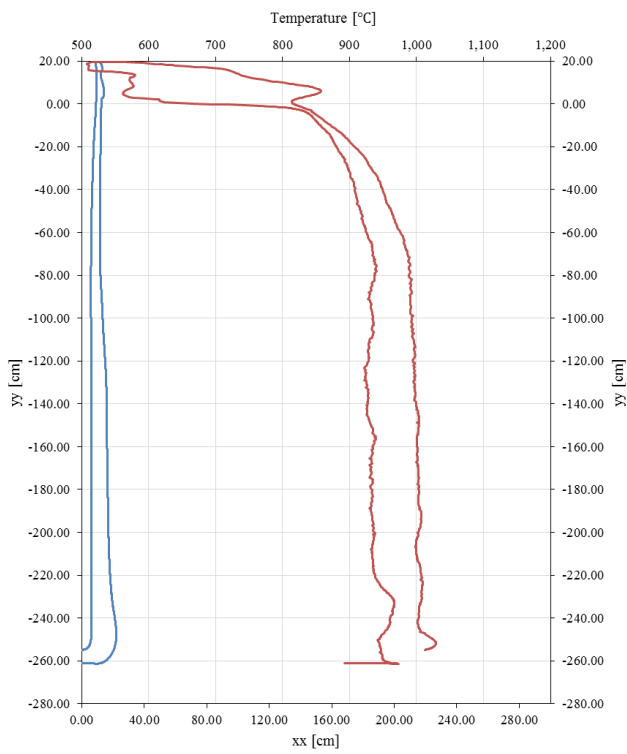
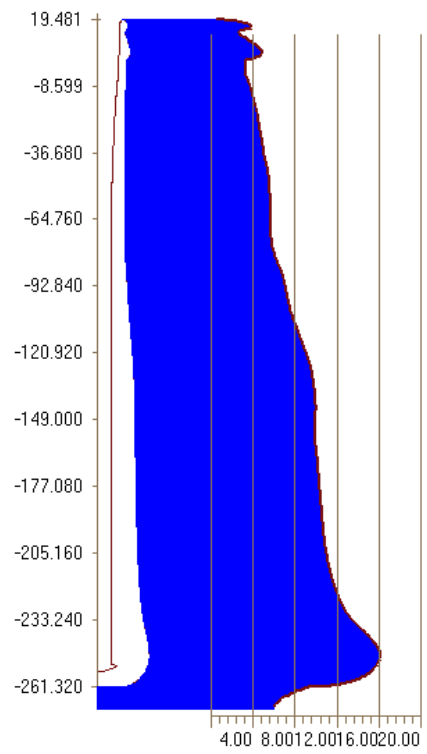


Figure 8.126: Boundary temperature in rundown for case 8.



Thickness (mm) in run down stage for case 8.

8.2.7 Final Blow

Insufflated pressurize air forces the parison to finalize the container shape. Additionally, vacuum is also applied from the blow mould, not only to give stability when the parison walls is forced to stick to the blow mould, but also to reduce the internal pressure. After the vacuum and the final blow pressure the final product should have no geometric imperfections.

The temperature distribution is presented in Figure 8.127 for case 1. The air pressure forces the glass to touch the blow mould. When all the glass is in contact with the mould heat transfer between the glass and moulds occurs along all its length.

In Figure 8.128, Figure 8.129, Figure 8.130, Figure 8.131, Figure 8.132, Figure 8.133, Figure 8.134 and Figure 8.135 present the temperature distribution for the cases 2 to 8. Note that the neckring and the shoulder are cooler than the other zones, as expected.

Additionally, Figure 8.131 shows the displacement contours during the final blow stage. The results show that the highest displacement is located at the end of the parison wall and then “travels” to the container shoulder. After all the glass boundary is in contact with the mould no further displacement is observed.

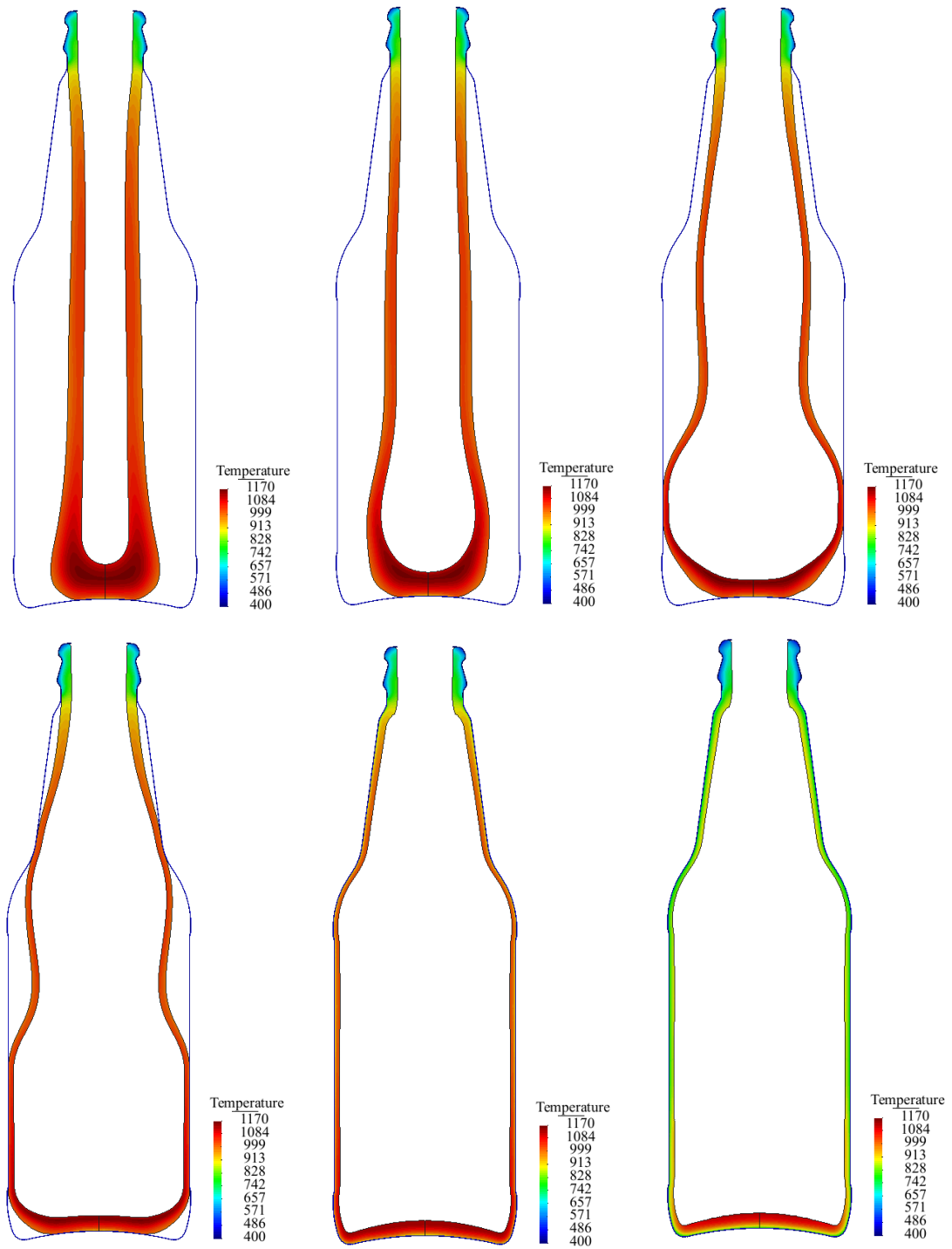


Figure 8.127: Temperature distribution in final blow for the case 1 in 5.800s, 5.803s, 5.804s

5.805s

5.833s

7.266s

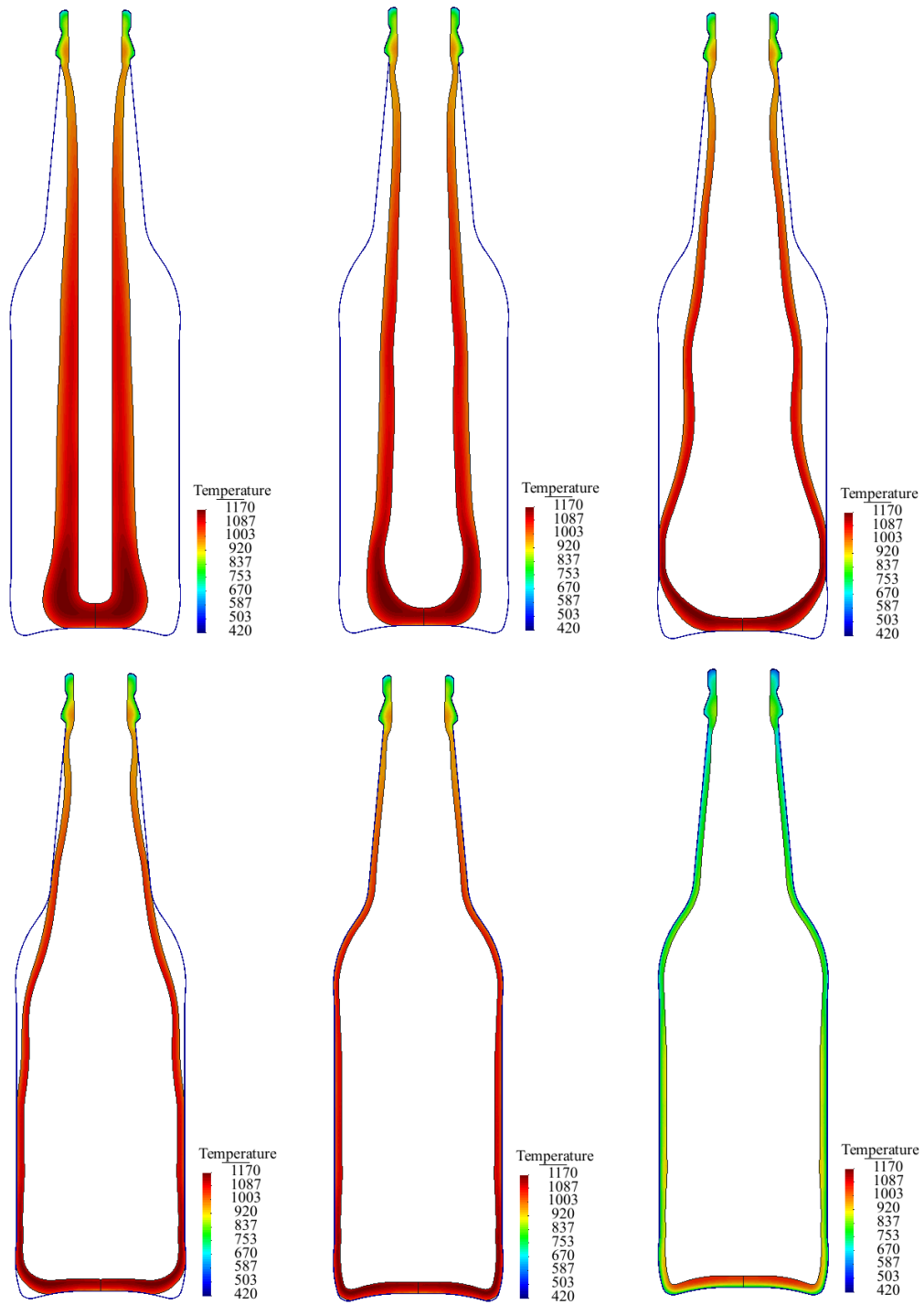


Figure 8.128: Temperature distribution in final blow for the case 2 in 4.907s, 4.909s, 4.910s

4.911s

4.912s

7.621s

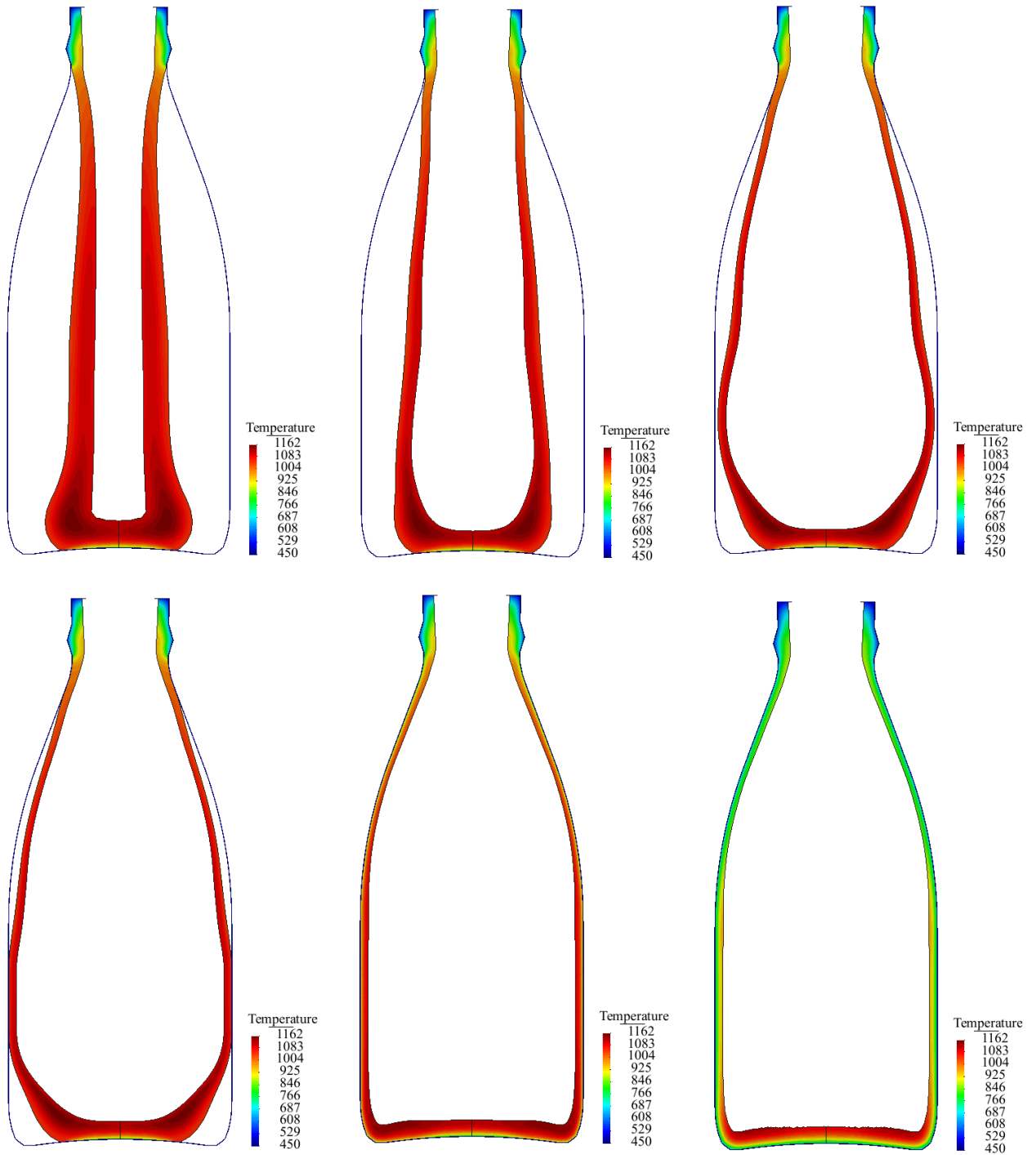


Figure 8.129: Temperature distribution in final blow for the case 3 in 5.467s, 5.469s, 5.471s

5.470s

5.479s

7.467s

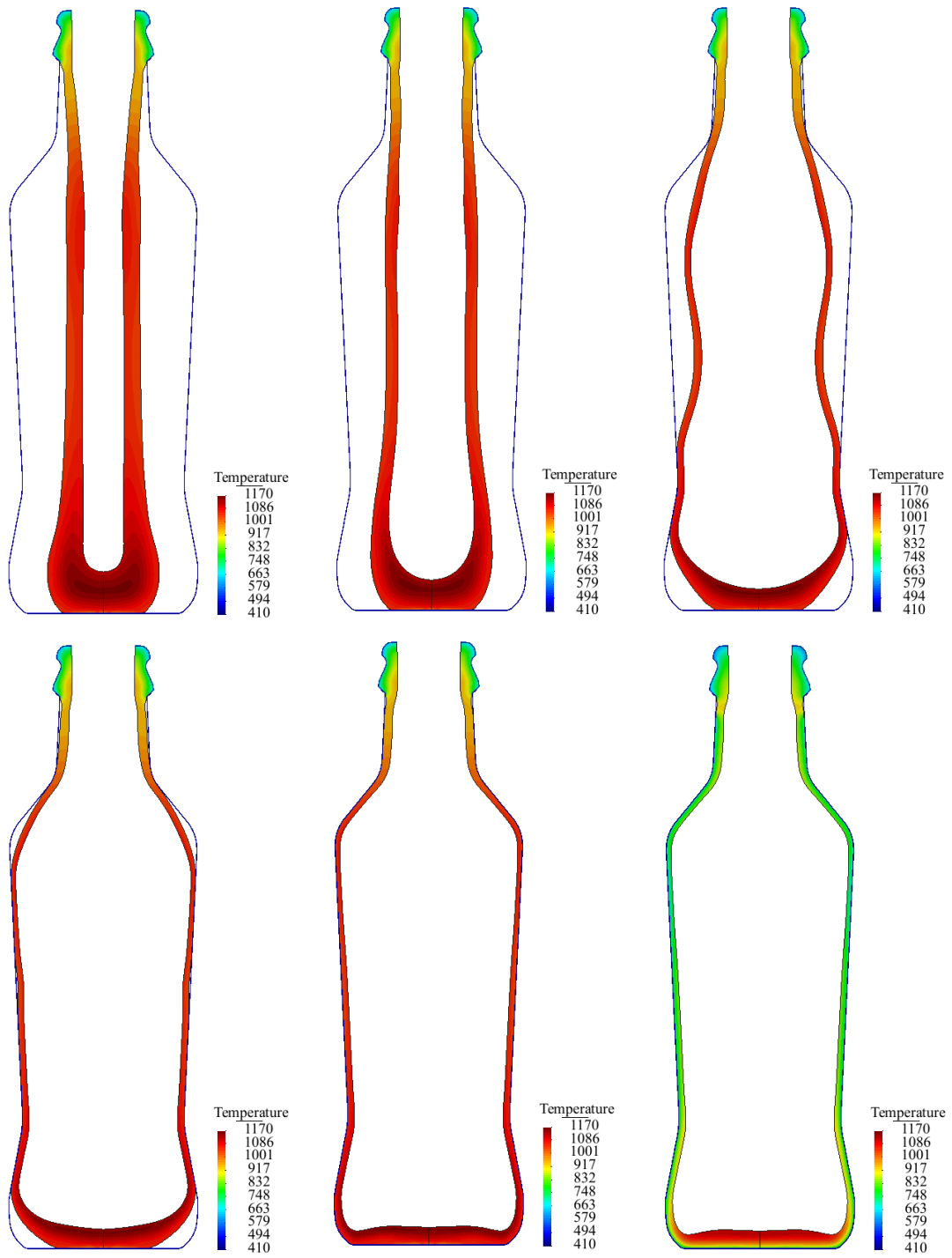


Figure 8.130: Temperature distribution in final blow for the case 4 in 5.972s, 5.418s, 5.419s

5.419s

5.420s

7.375s

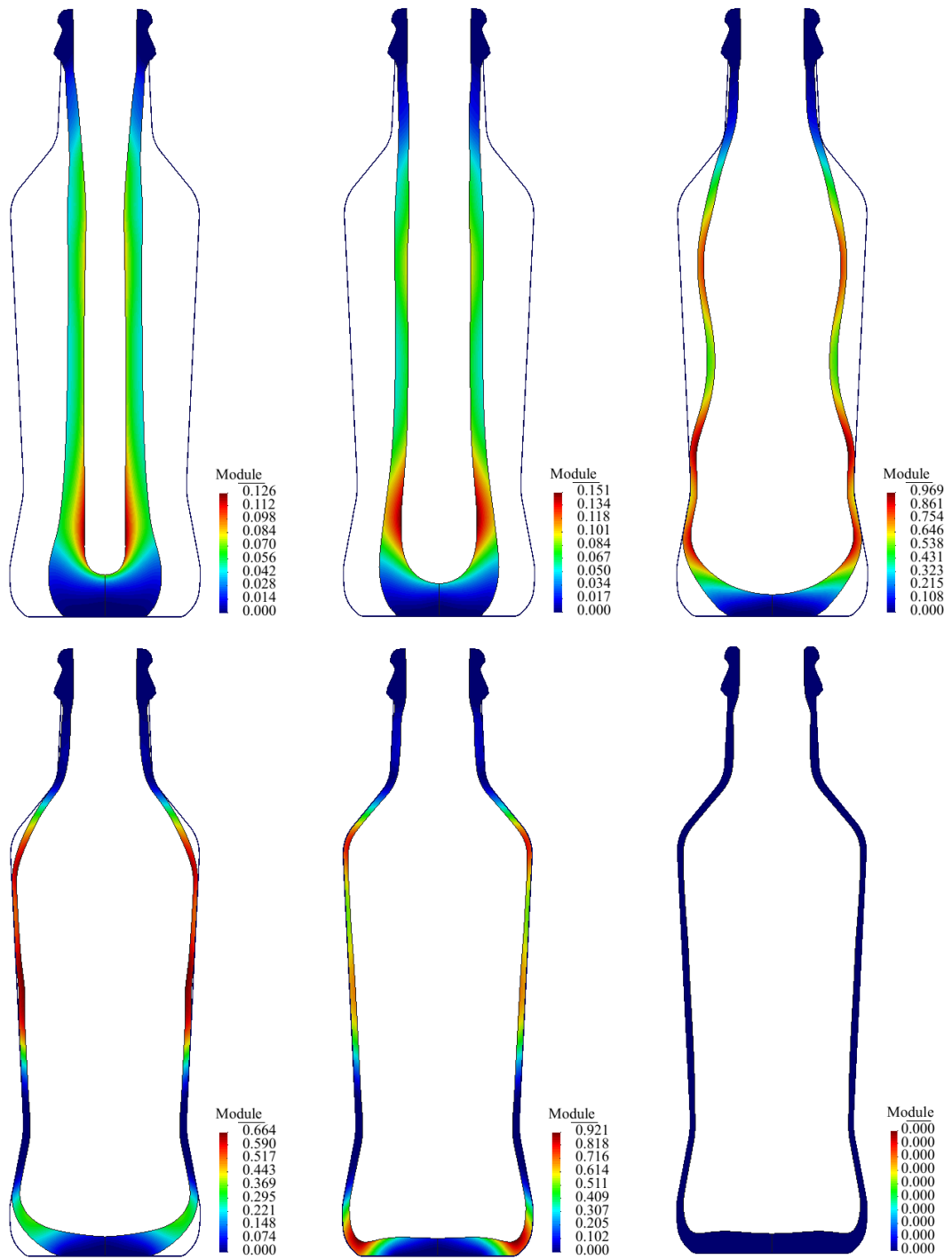


Figure 8.131: Displacement module in final blow for the case 4 in 5.972s, 5.418s, 5.419s

5.419s

5.420s

7.375s

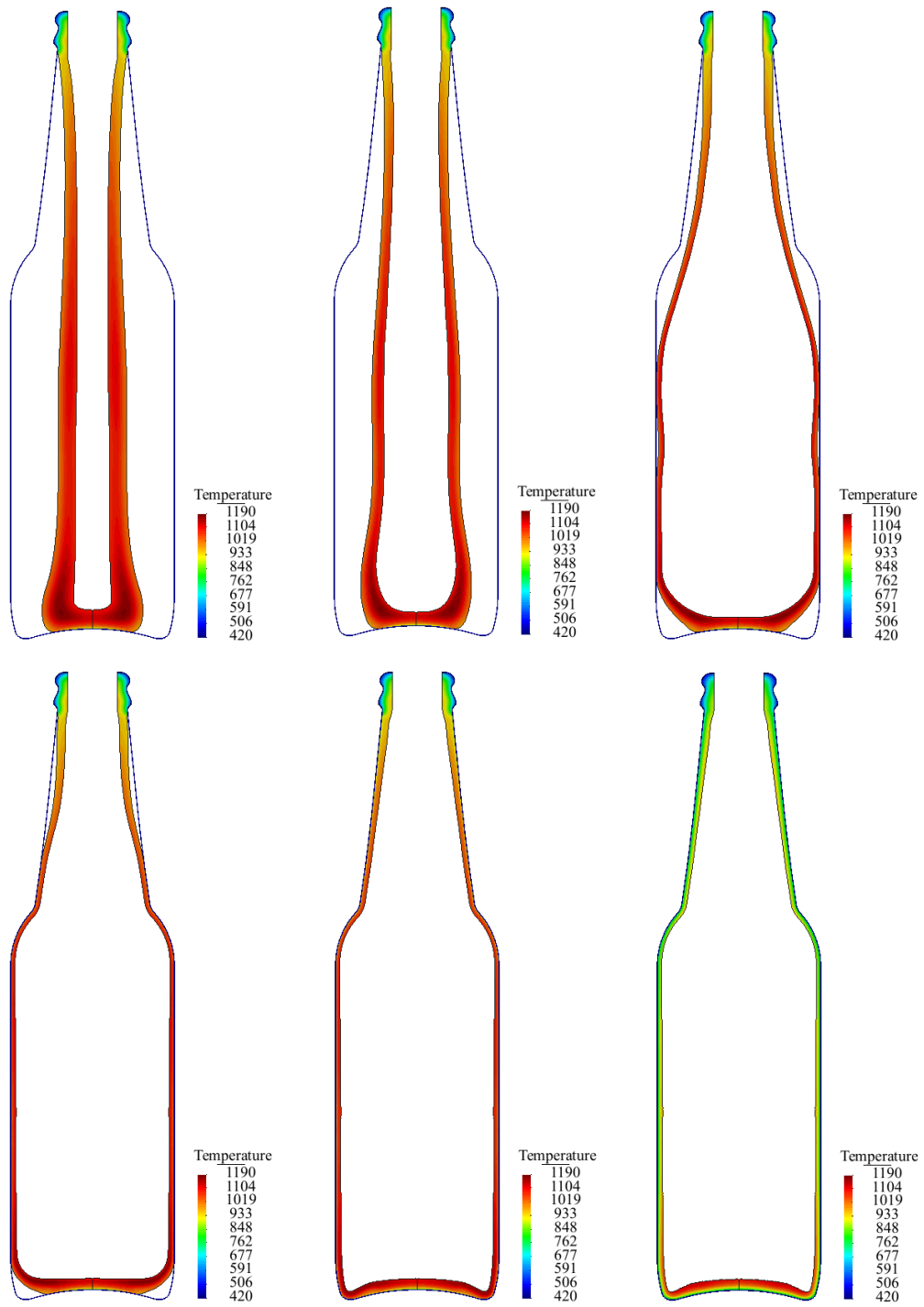


Figure 8.132: Temperature distribution in final blow for the case 5 in 5.694s, 5.700s, 5.705s

5.706s

5.909s

7.361s

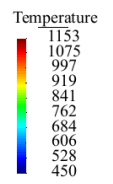
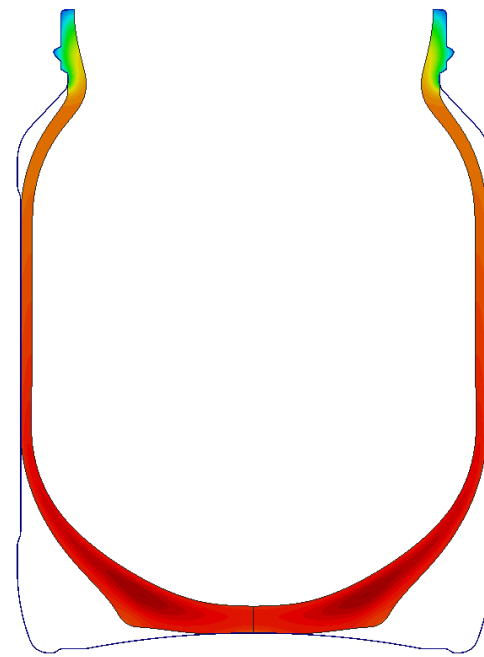
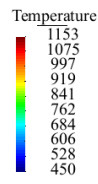
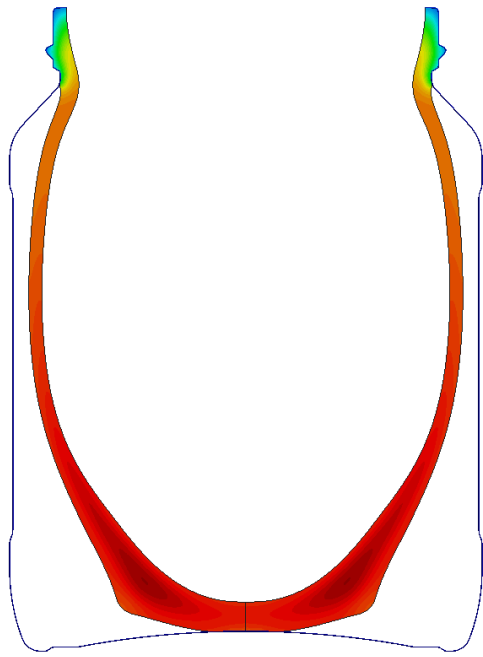
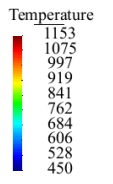
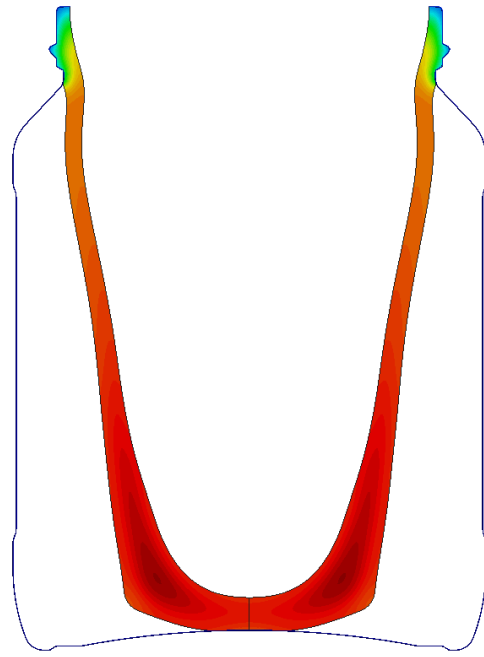
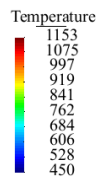
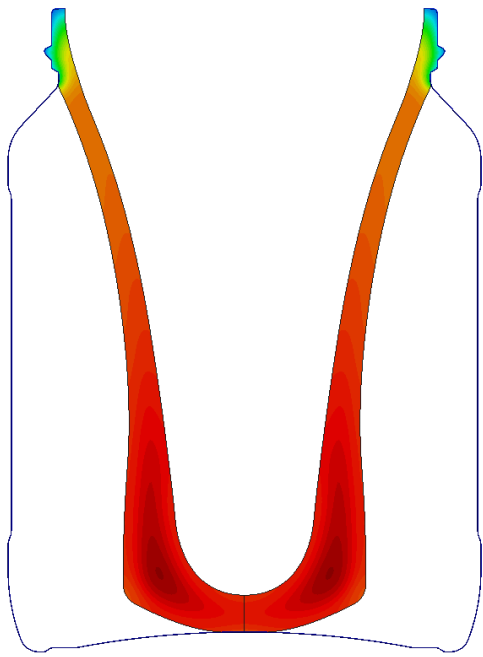




Figure 8.133: Temperature distribution in final blow for the case 6 in 5.584s 5.583s

5.584s	5.585s
5.586s	7.174s

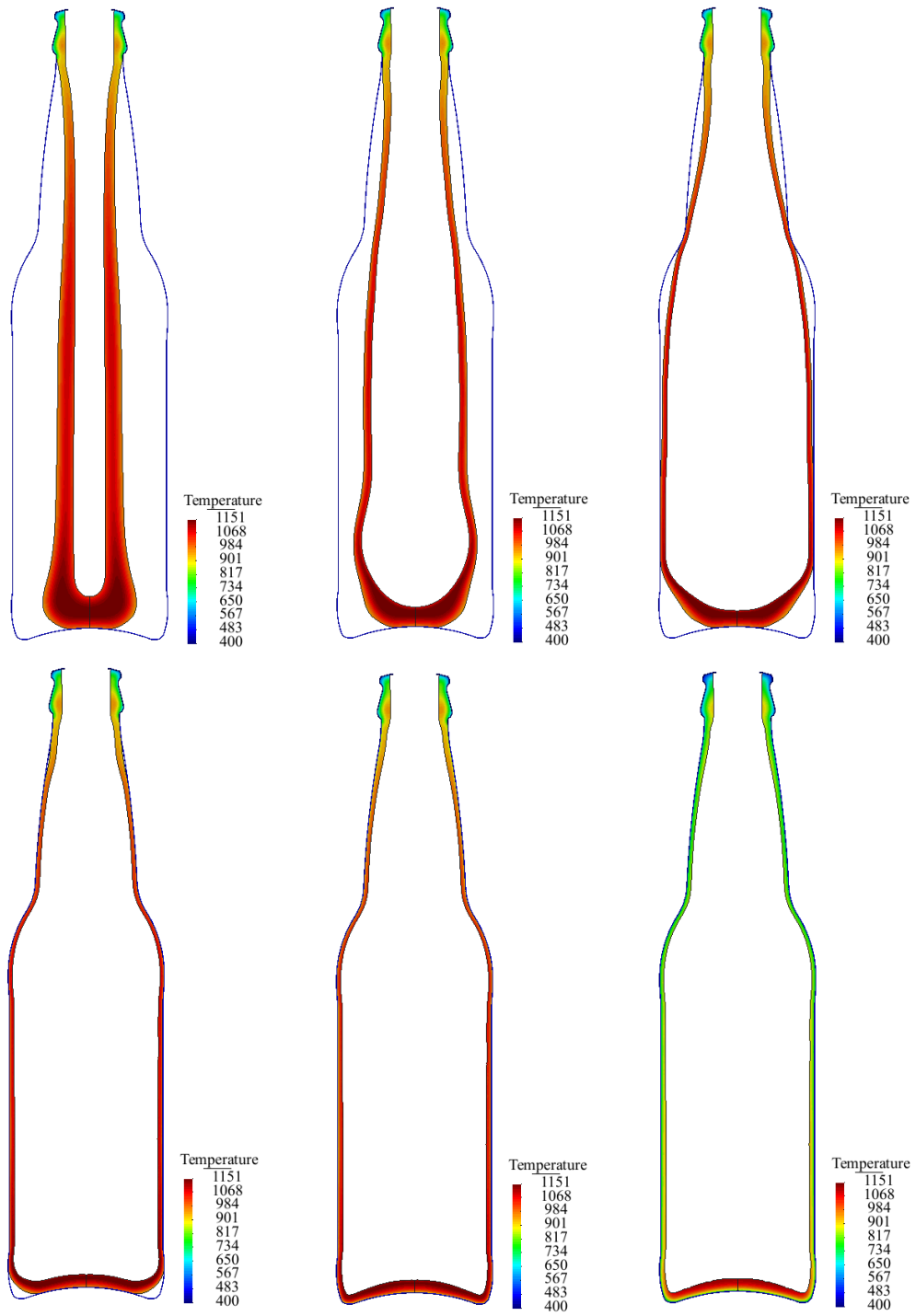


Figure 8.134: Temperature distribution in final blow for the case 7 in 5.059s, 5.065s, 5.067s

5.070s

5.080s

7.179s

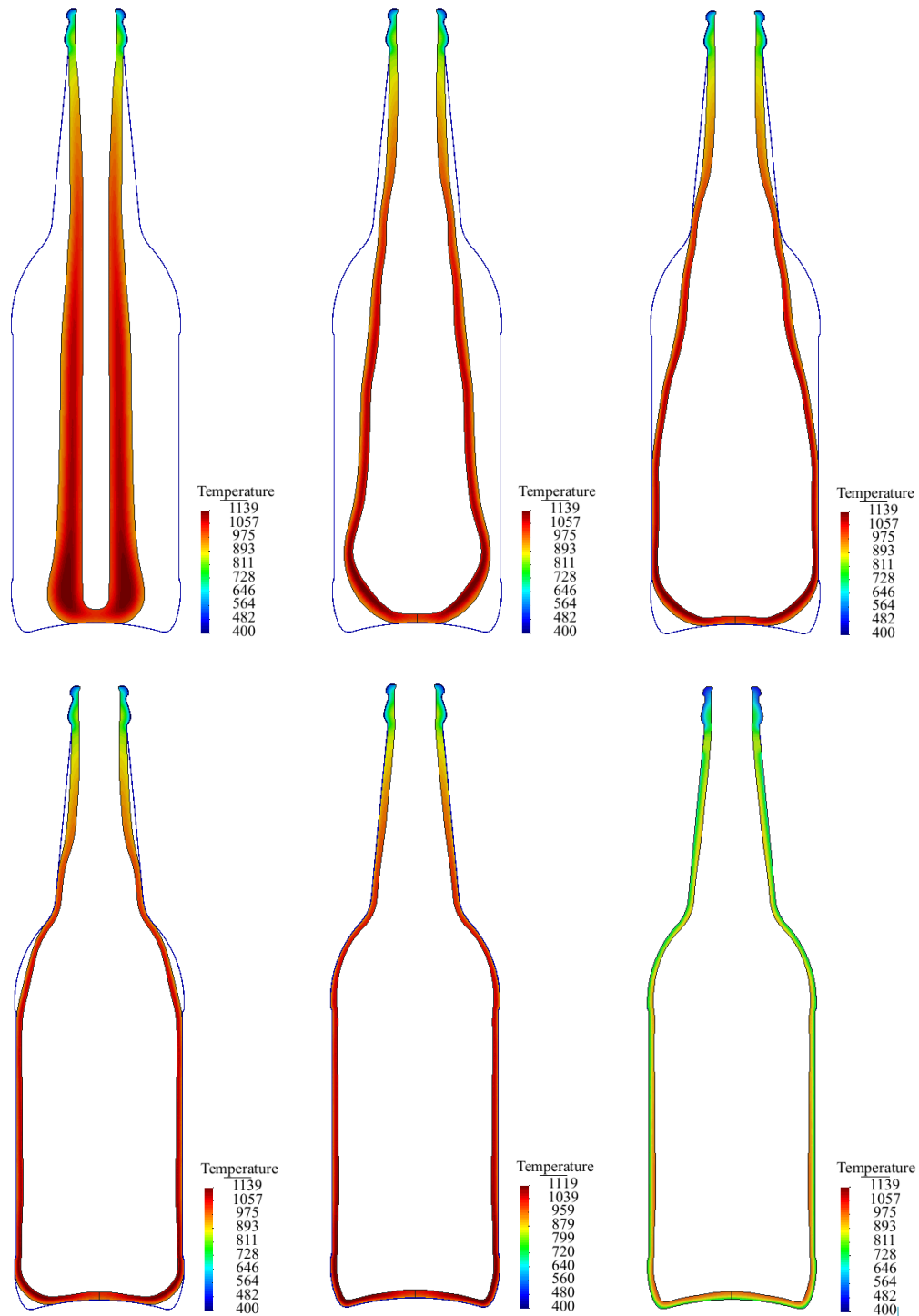


Figure 8.135: Temperature distribution in final blow for the case 8 in 6.854s, 6.860s, 6.862s

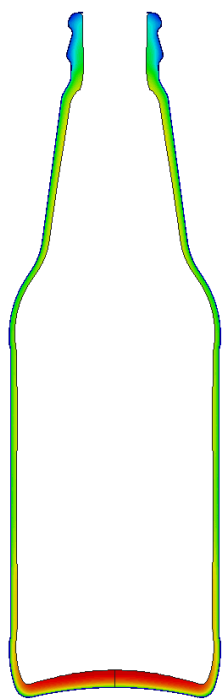
6.862s

6.871s

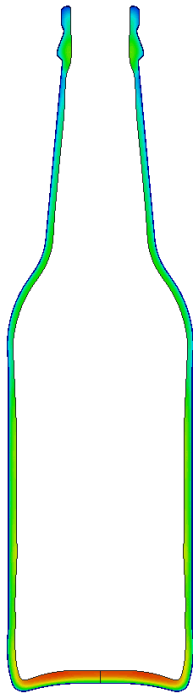
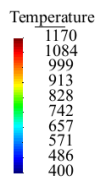
9.859s

8.2.8 Mould Open

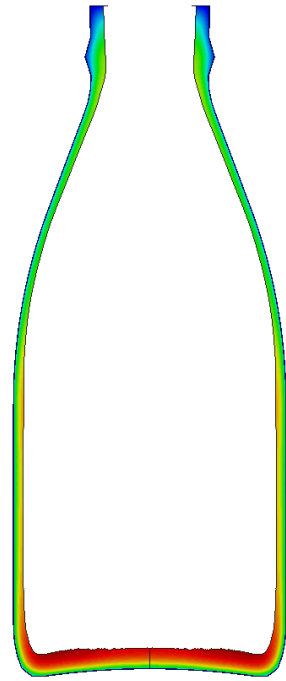
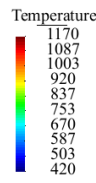
Mould open is the last stage of the press/blow process. The results can be found in Figure 8.136 for all cases. The boundary temperature at the end of the process is presented in Figure 8.137. The results show that the side that was in contact with the mould show a range of temperatures between 600°C and 700°C while in the inner side of the container temperatures are around 700°C. In addition, the inner part of the bottom zone has the highest temperatures due to the fact that largest glass mass is located in this area.



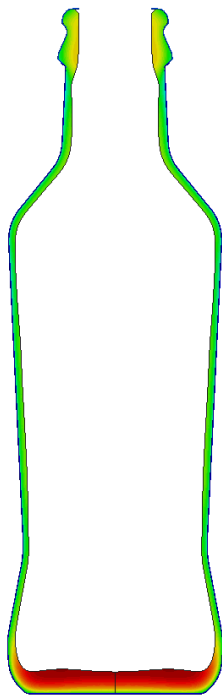
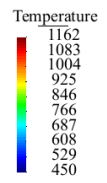
Case 1



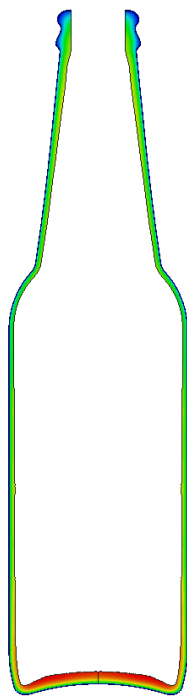
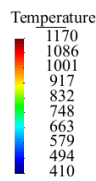
Case 2



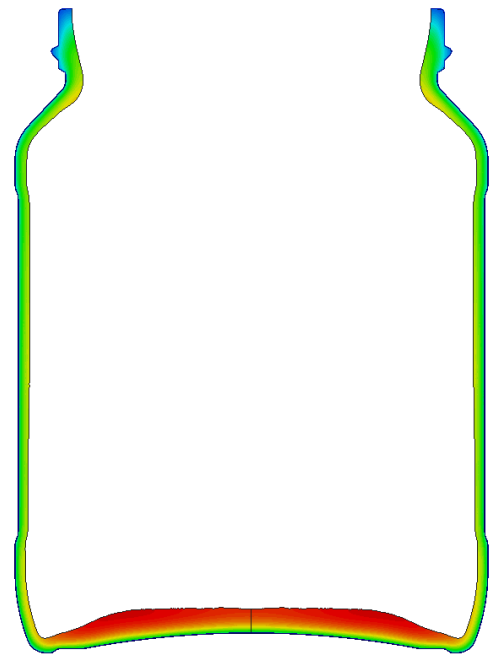
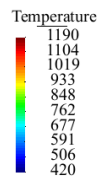
Case 3



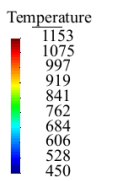
Case 4



Case 5



Case 6



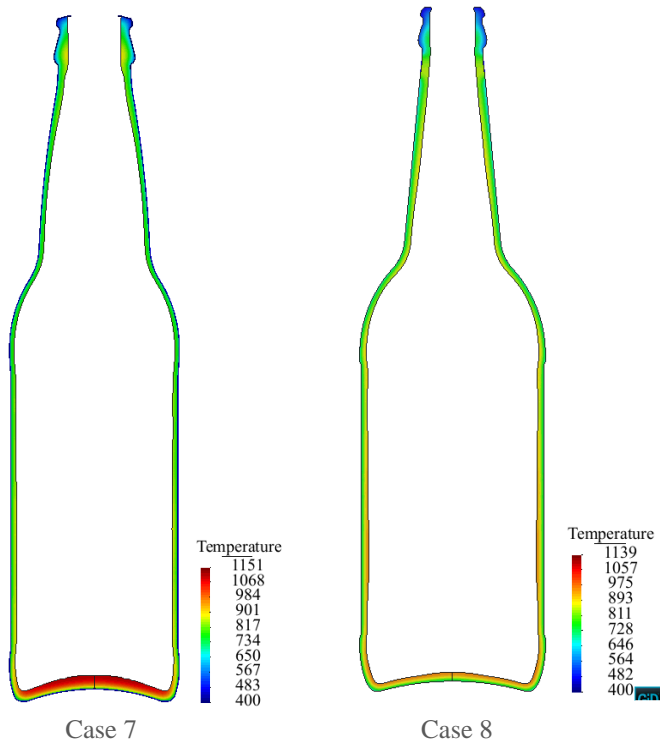
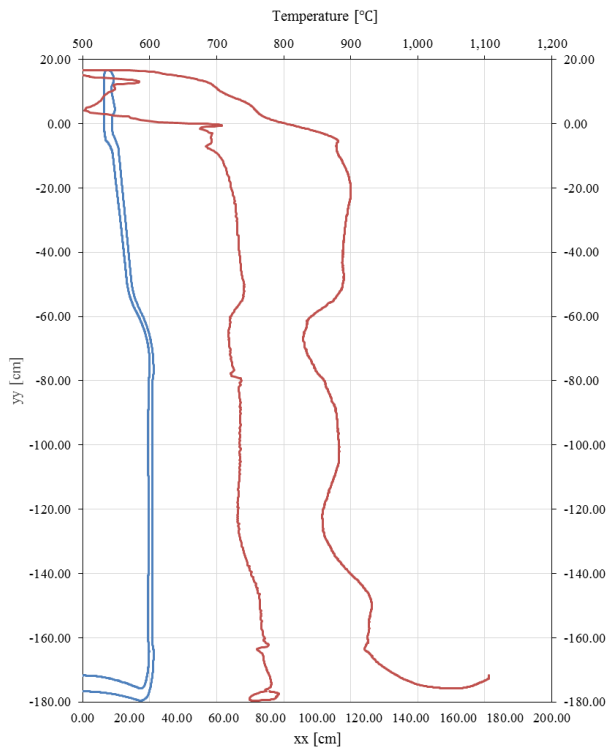
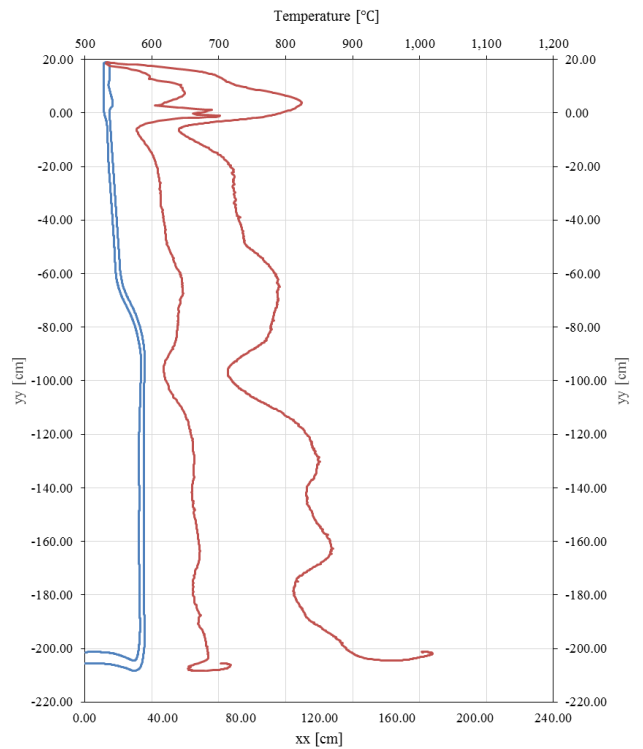


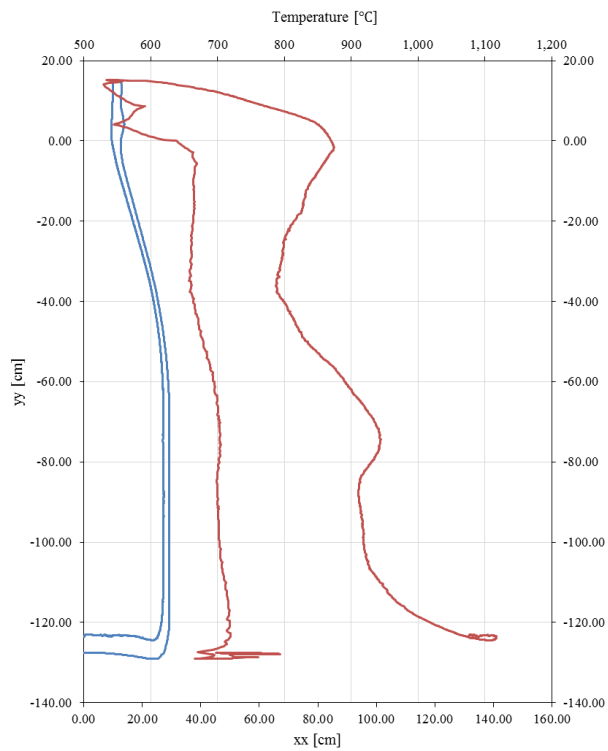
Figure 8.136: Temperature distribution in mould open for the case 1 in 7.399s, for the case 2 in 8.205s, for the case 3 in 7.600s, for the case 4 in 7.750s, for the case 5 in 7.847s, for the case 6 in for the case 7 in 7.653s and for the case 8 in 10.516s.



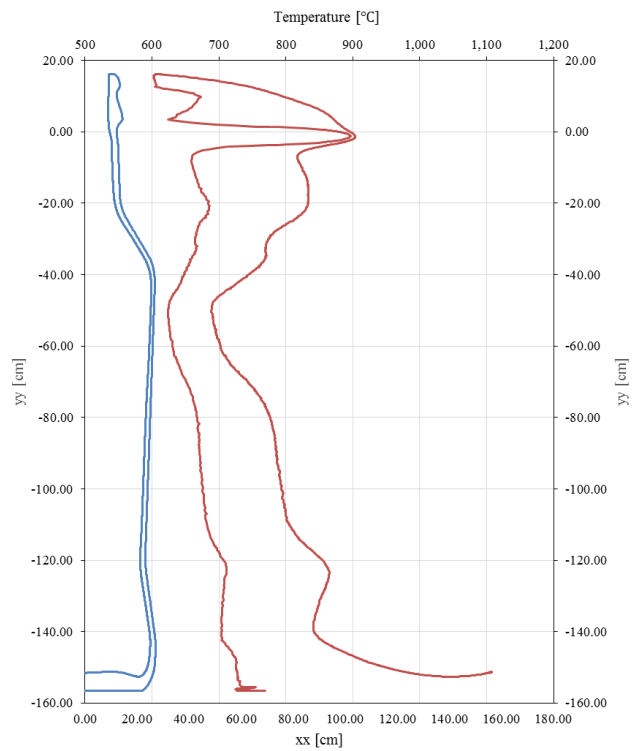
Case 1



Case 2



Case 3



Case 4

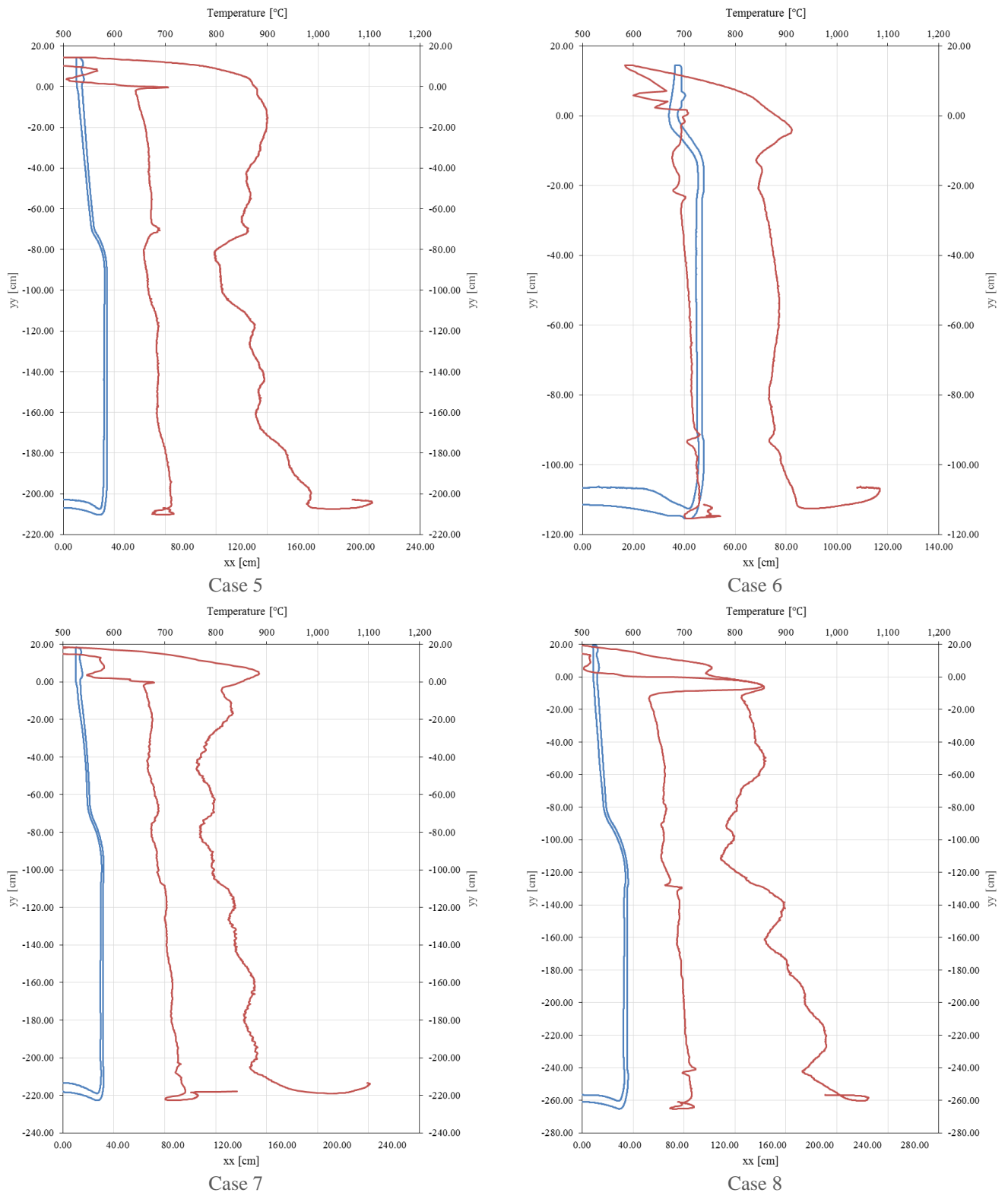


Figure 8.137: Final boundary temperature for case 1, case 2, case 3, case 4, case 5, case 6, case 7 and case 8.

8.2.9 Bottle Thickness

Next, the thickness distribution for the processes of press/blow examples are presented.

- Case 1

Figure 8.138 presents the thickness distribution for the case 1. The thinner zones are located at the end of the neckring and under the container wall.

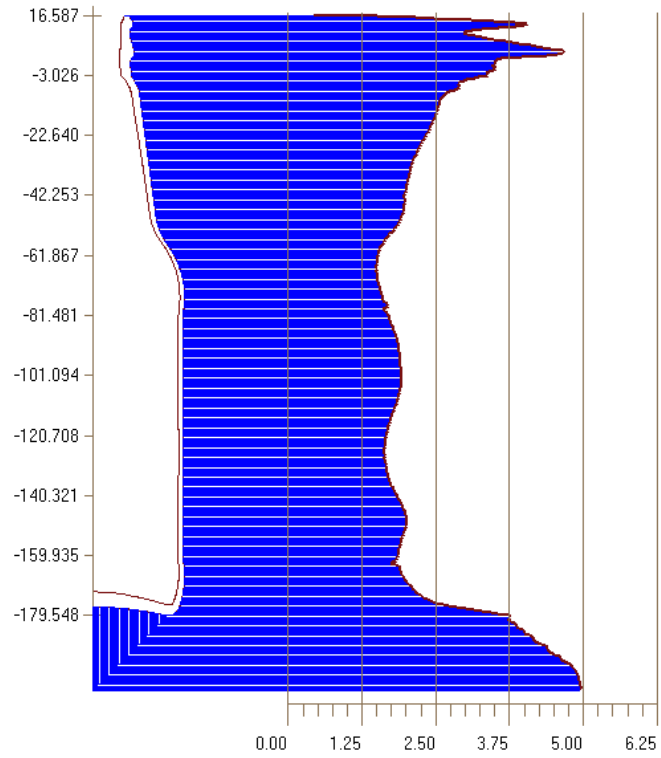


Figure 8.138: Bottle thickness (mm) distribution in case 1.

- Case 2

Figure 8.139 presents the thickness distribution for the case 2. The profile shows a thickness around 2.5 mm.

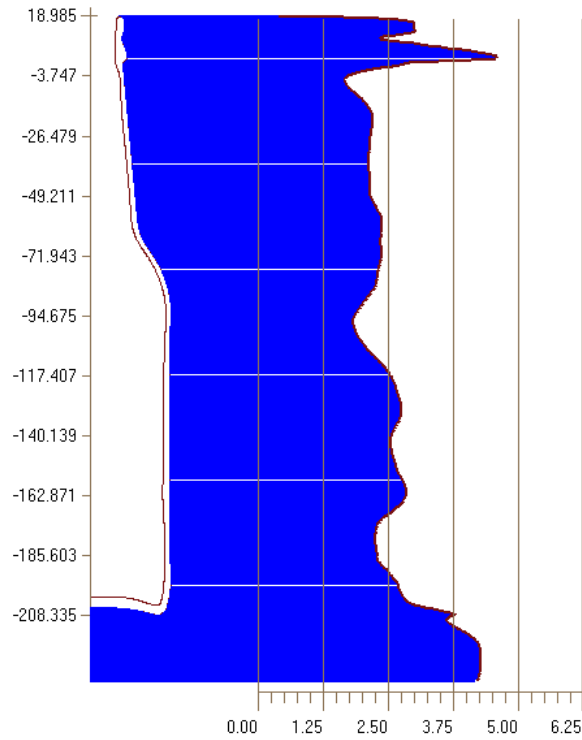


Figure 8.139: Bottle thickness (mm) distribution in case 2.

- Case 3

Figure 8.140 presents the thickness distribution for the case 3. The profile presents thicker zones at the end of the neckring and also at the wall. The experimental cut of the container is presented in Figure 8.140. The real container has an almost constant thickness along the wall. The simulation result present 1.5 mm of thickness near the shoulder while in the experimental data it was near 2.5 mm. Above the shoulder the simulation result is about 2mm. Finally, at the bottom zone the thickness obtained in the simulation is around 4.75 mm. The distribution is quite similar with the experimental results.

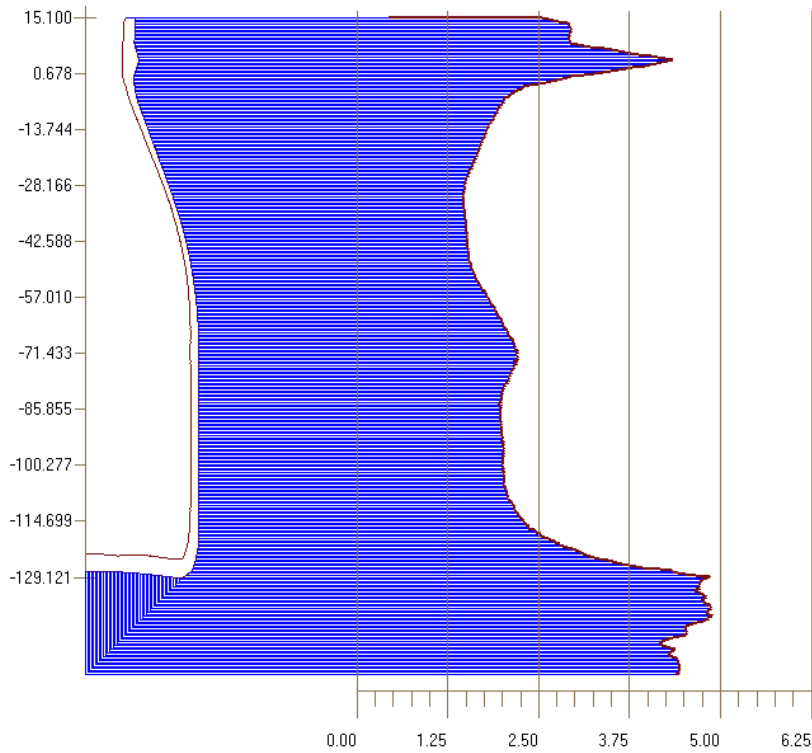


Figure 8.140: Bottle thickness (mm) distribution in case 3.



Real bottle thickness distribution in case 3.

- Case 4

Figure 8.141 presents the thickness distribution for the case 4. The container wall present a constant thickness around 1.5 mm while in the bottom is observed a thickness of 6 mm. The experimental thickness distribution is presented in Figure 8.142.

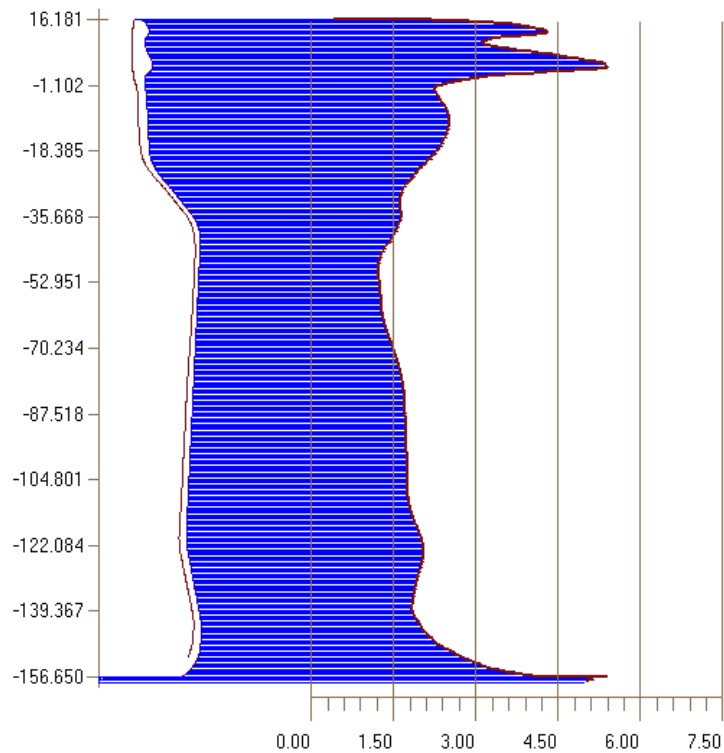


Figure 8.141: Bottle thickness (mm) distribution in case 4.

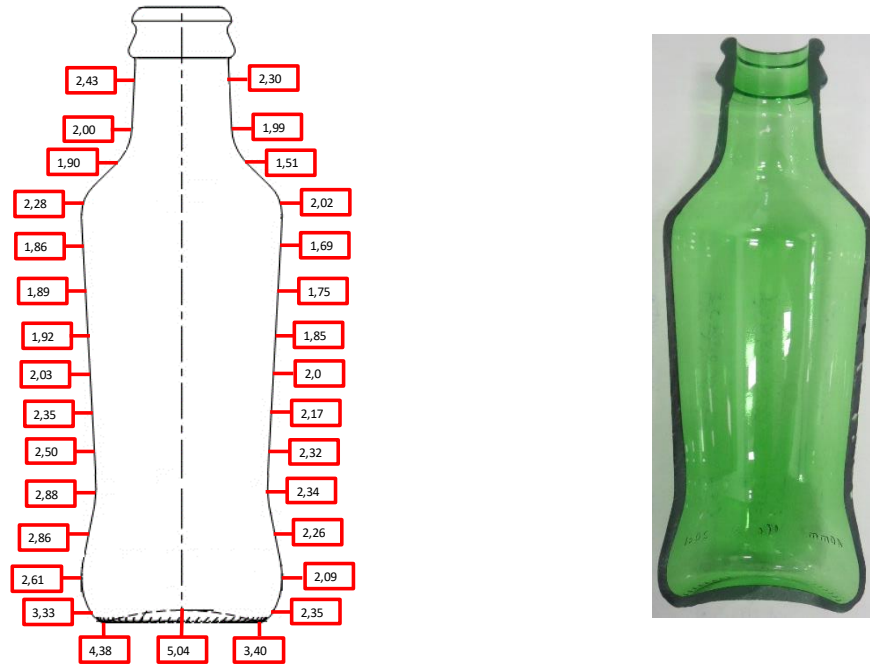


Figure 8.142: Real thickness (mm) distribution in case 4.

- Case 5

Figure 8.143 presents the thickness distribution for the case 5. Comparing the simulation with the real case a different thickness distributed was obtained, requiring a better parameter calibration.

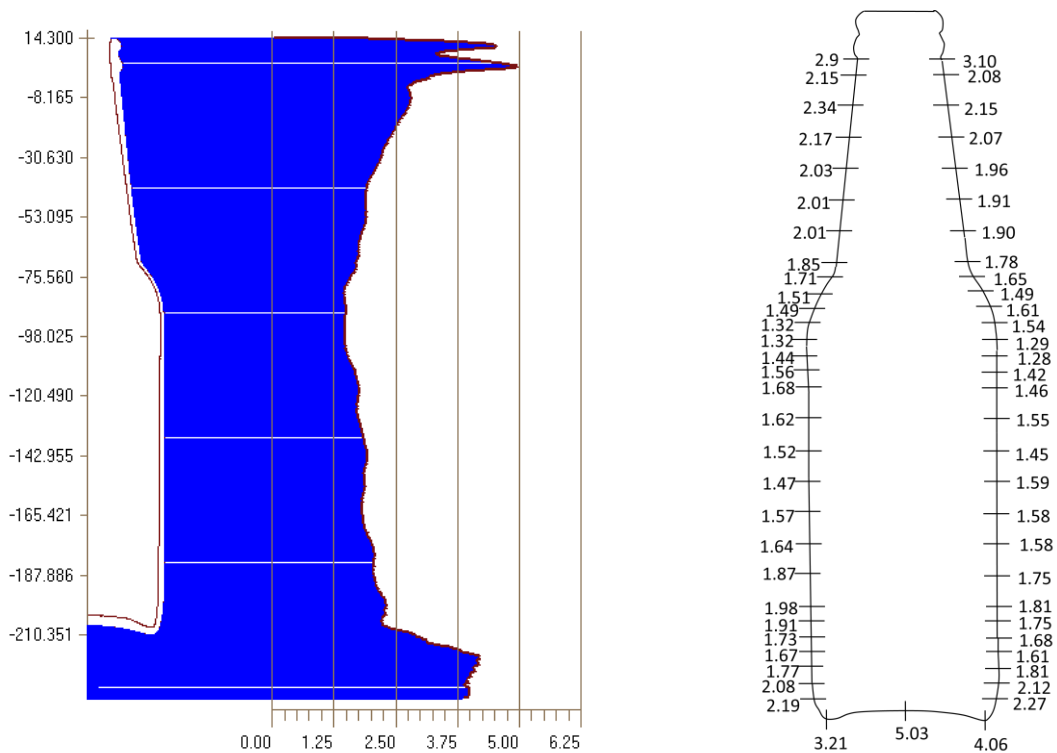


Figure 8.143: Thickness (mm) distribution in case 5.

Real thickness (mm) distribution in case 5.

- Case 6

The Figure 8.139 presents the thickness distribution for the case 6. The profile presents a thickness around 2.0 mm on the walls and 6 mm at the bottom zone.

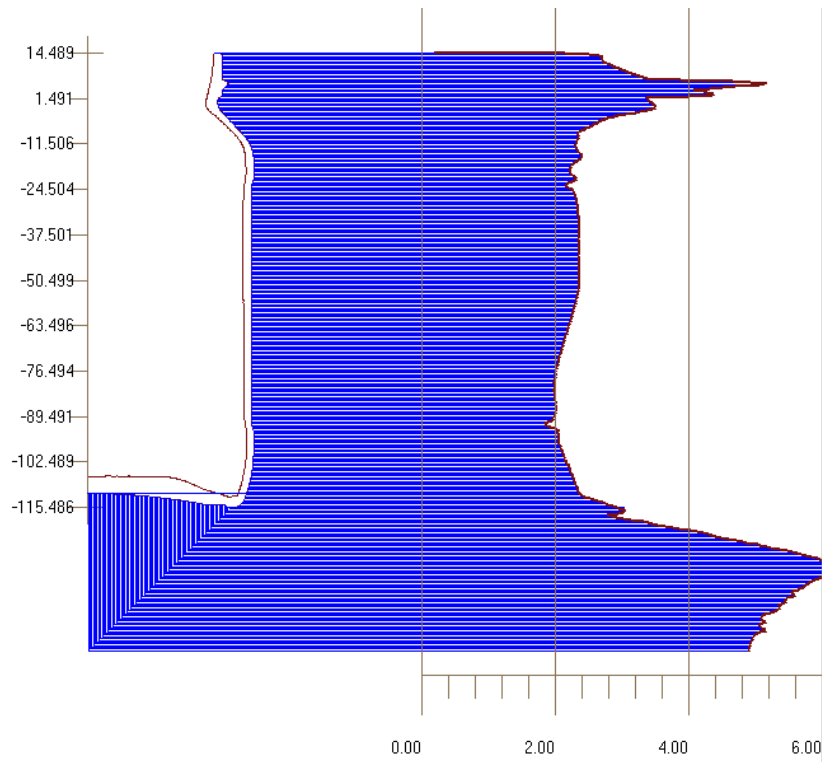
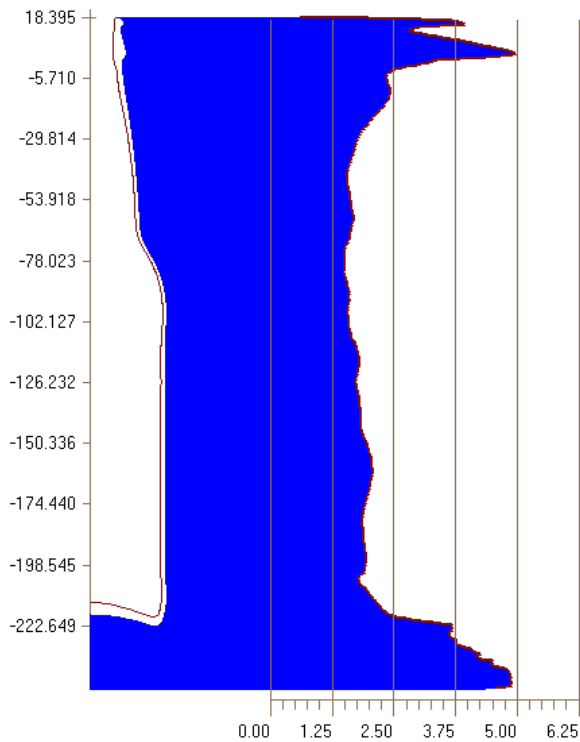


Figure 8.144: Thickness (mm) distribution in case 6.

- Case 7

The Figure 8.139 presents the thickness distribution for the case 7. The profile presents at the walls a thickness around 2.0 mm while in the bottom zone the thickness is around 6 mm. The experimental results present for the neck an average thickness of 2.14cm, in the sidewall an average of 2.32cm, in the heel a average of 1.99cm and in the bottom an average of 4.63. It can conclude that the simulation results are very close to the experimental result.



CAV.NO	Thickness																				
	NECK (Area "B")				Upper Major Diameter (Area "C")				Pinch, Mid-Panel or Sidewall (Area "D")				Heel Major Diameter(Area "E")				Minimum Bottom Overall (Area "G")			Center Bottom (Area "H")	
	Max	Min	AVG	Max 2.5	Max	Min	AVG	Max 2.5	Max	Min	AVG	Max 2.5	Max	Min	AVG	Max 2.5	Max	Min	AVG	Max 2.5	
	mm	mm	mm	mm	mm	mm	mm	mm	mm	mm	mm	mm	mm	mm	mm	mm	mm	mm	mm	mm	
Min.	2,16	1,75	1,98	1,05	2,12	1,14	1,64	1,29	2,37	1,80	2,13	1,32	2,10	1,32	1,75	1,19	4,80	3,32	4,13	1,08	4,82
Max.	2,60	2,14	2,28	1,46	2,70	1,81	2,15	2,00	2,94	2,08	2,47	1,59	2,67	1,92	2,26	1,86	5,69	4,60	4,93	1,66	5,17
Aver.	2,35	1,93	2,14	1,22	2,33	1,48	1,90	1,61	2,68	1,96	2,32	1,37	2,35	1,62	1,99	1,47	5,28	3,98	4,63	1,34	5,01
St.Dev.	0,10	0,12	0,08	0,09	0,12	0,22	0,14	0,24	0,14	0,09	0,08	0,09	0,18	0,18	0,13	0,20	0,29	0,36	0,21	0,15	0,10

Figure 8.145: Thickness (mm) distribution in case 7.

Experimental thickness distribution in case 7.

- Case 8

The Figure 8.139 presents the thickness distribution for the case 8. Again, the profile presents at the walls a thickness around 2.0 mm while in the bottom zone the thickness is around 6 mm. The thickness distribution present some fluctuation in the side wall. Thus, it is difficult to compare to the experimental data but in general the bottle shape appears to be quite similar.

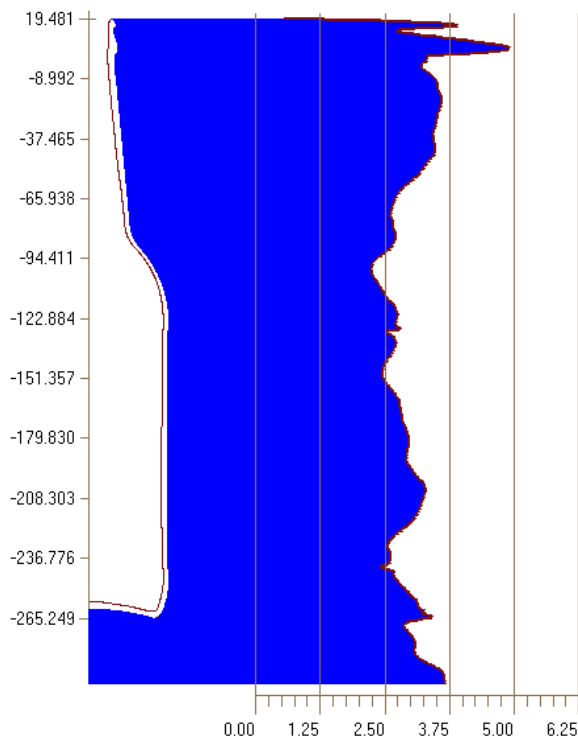
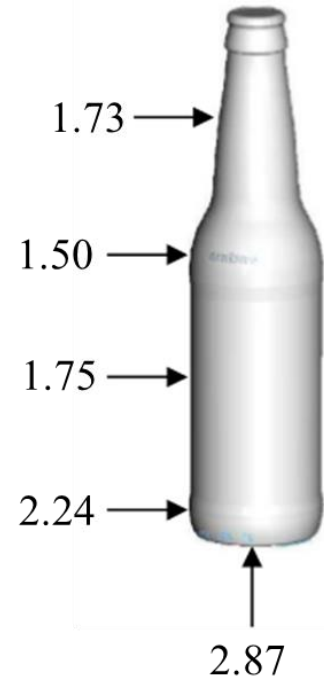


Figure 8.146: Thickness (mm) distribution in case 8.



Experimental thickness (mm) distribution in case 8.

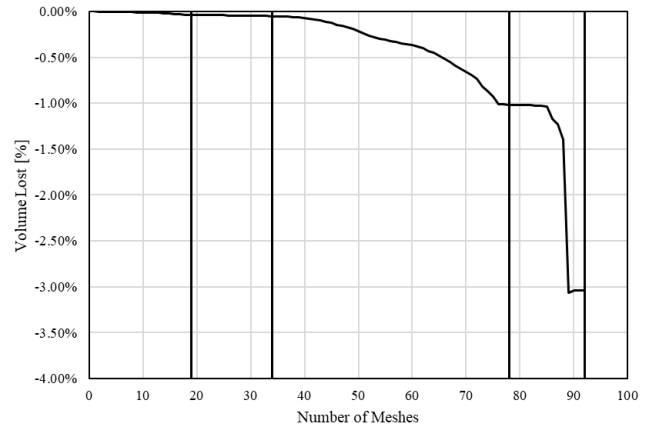
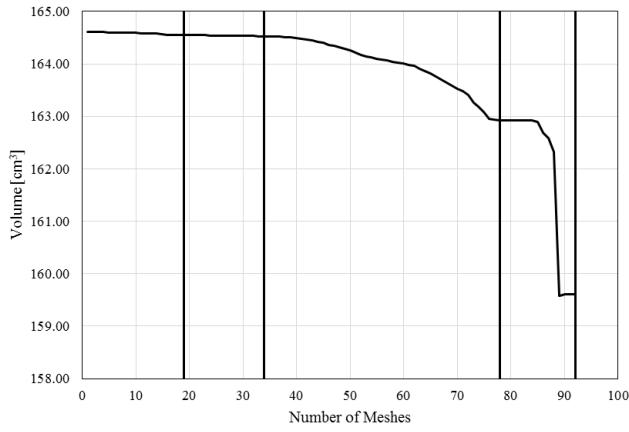
8.3 Evaluation of some numerical aspects

In this section some additional information is provided on some numerical aspects which illustrate some problems that need to be addressed in the near future in order to improve the performance of the software developed.

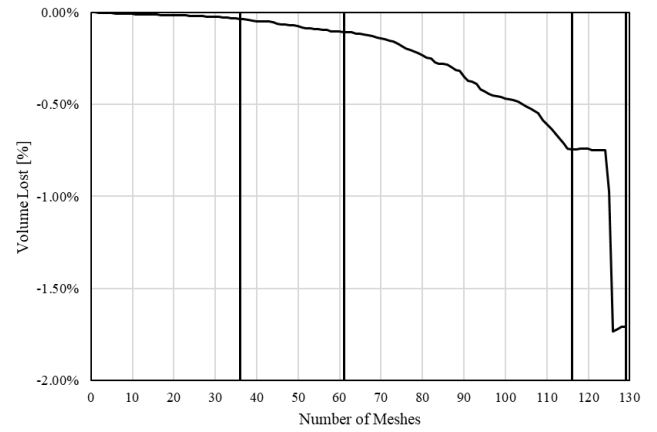
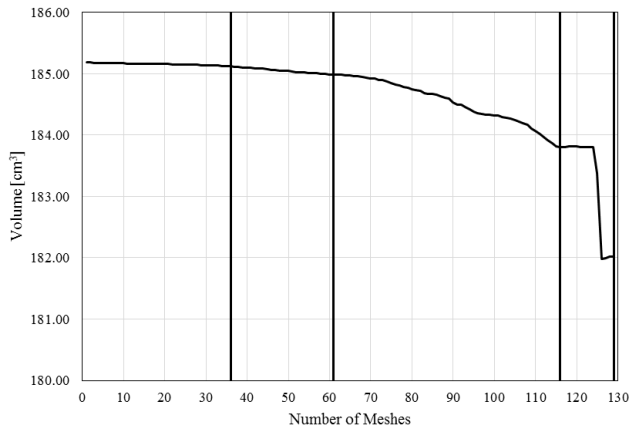
8.3.1 Volume Evolution

Since incompressibility is assumed, the glass volume should be conserved. Nevertheless, because incompressibility is imposed via a penalty method and many mesh refinements and redefinitions take part some violations are expected.

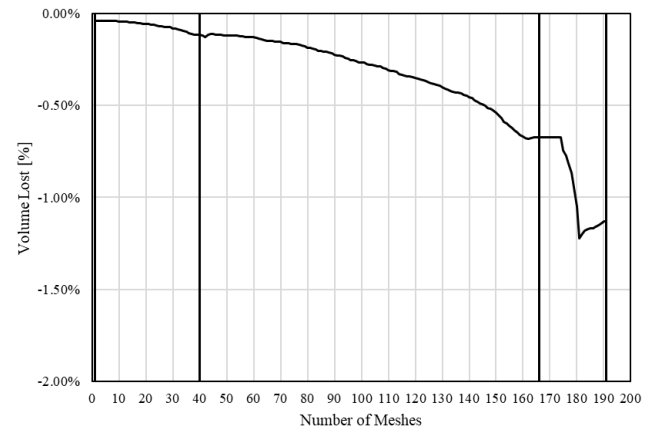
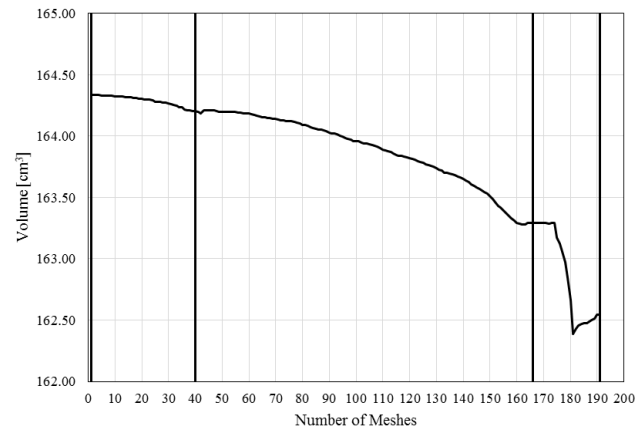
Figure 8.147 presents the volume evolution for all de cases of blow/blow process. The vertical line refer to the end of the most important stages such as gob loading, settle blow, counter flow and final blow respectively. The results show that in gob loading and settle blow the volume slightly decreases and is accentuated in the counter blow and final blow.



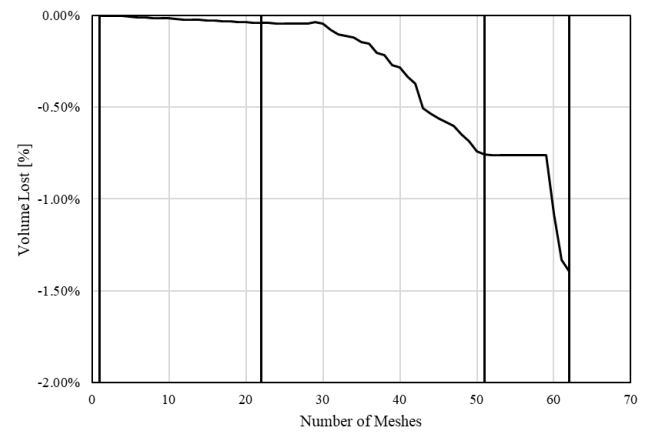
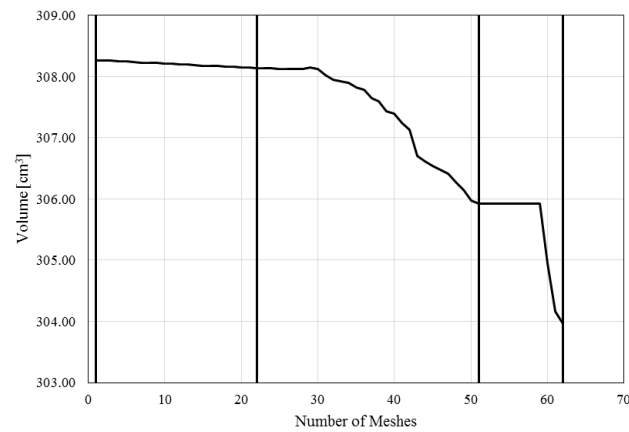
Case 1



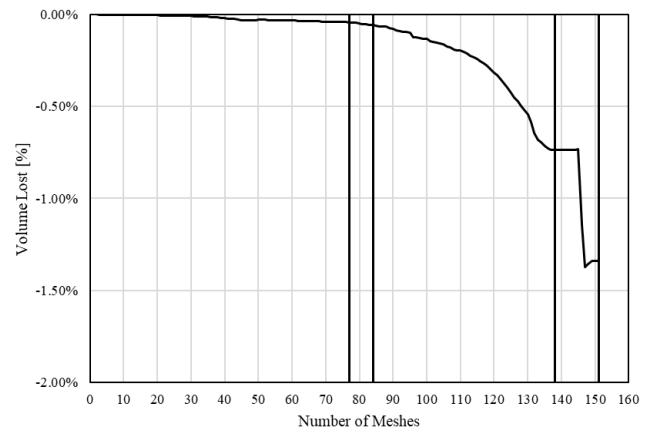
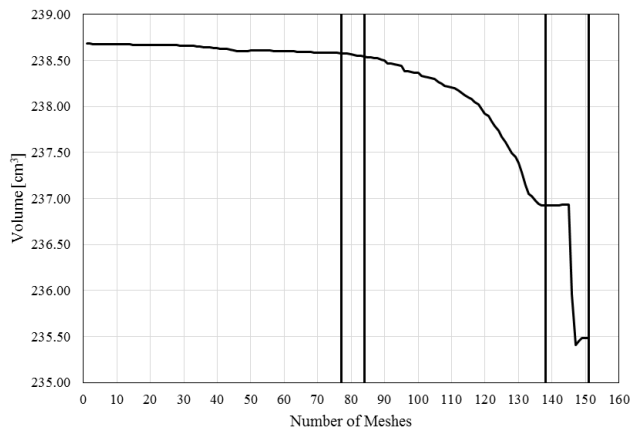
Case 2



Case 3



Case 4

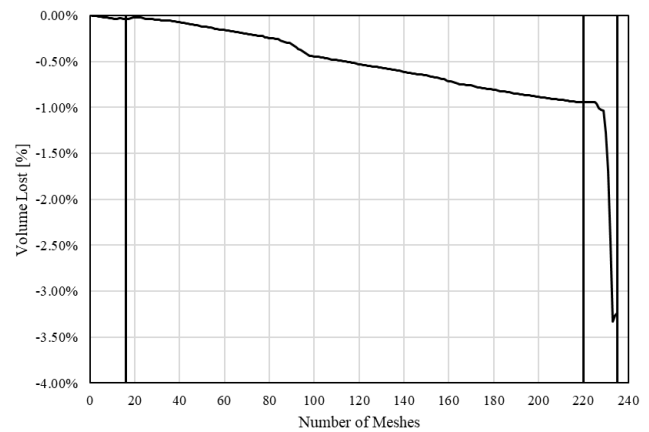
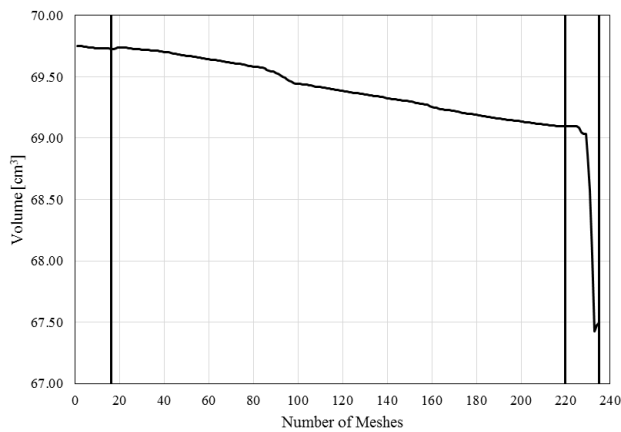


Case 5

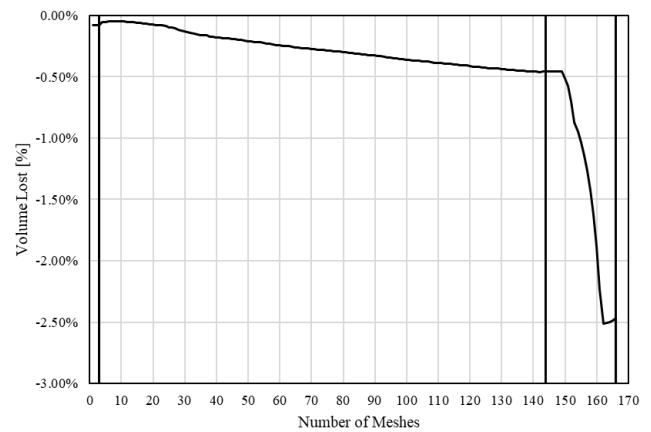
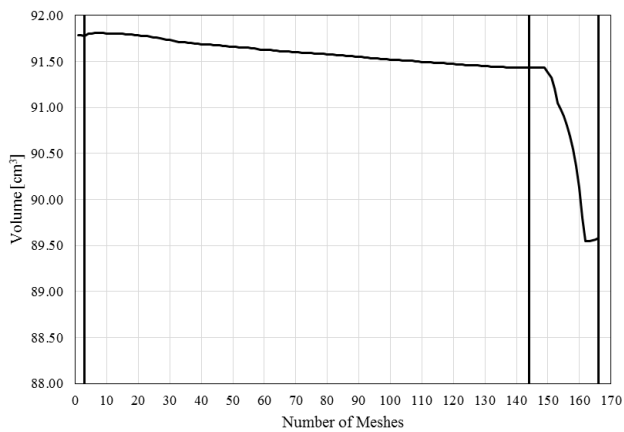
Figure 8.147: Volume evolution for blow/blow process for the case 1, case 2, case 3, case 4 and case 5.

Figure 8.148 presents the volume evolution for all the cases of press and blow process. The volume evolution starts to decrease almost uniformly during the plunger upstage having a huge drop at the final blow. However, the total volume decrease seems not be significant enough to compromise the final results.

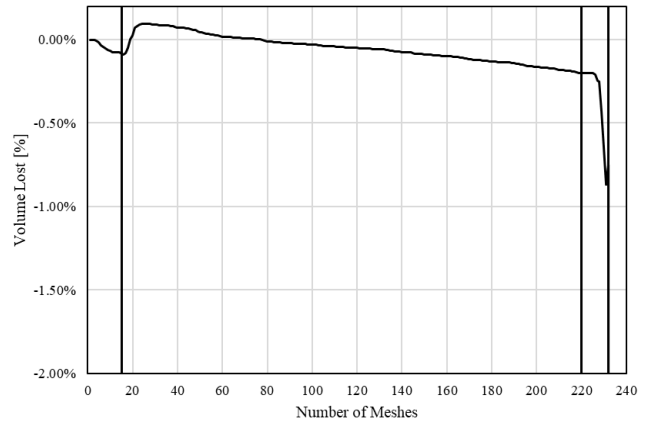
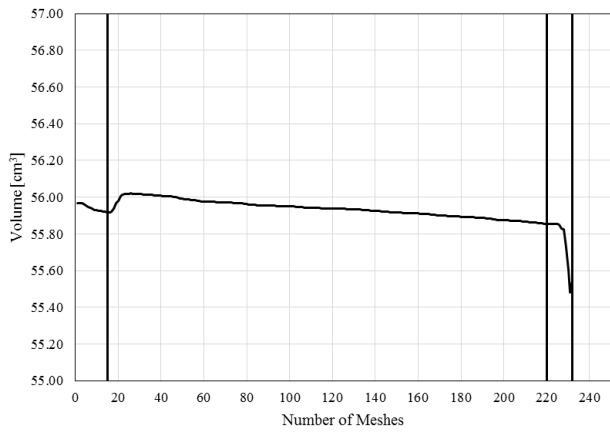
This type of evaluation can be an important tool to calibrate the penalty terms and improve the reliability of the mesh refinement tools.



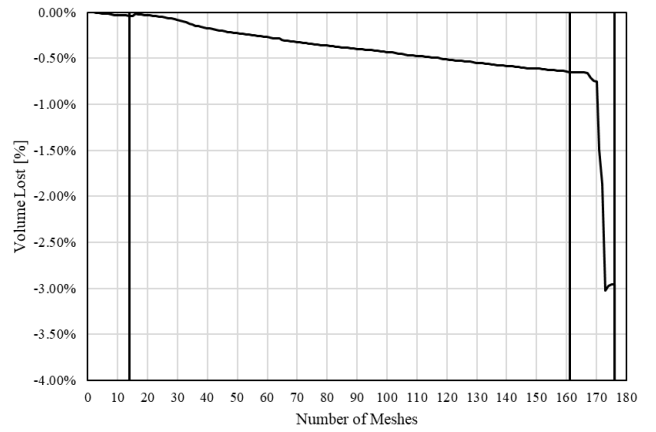
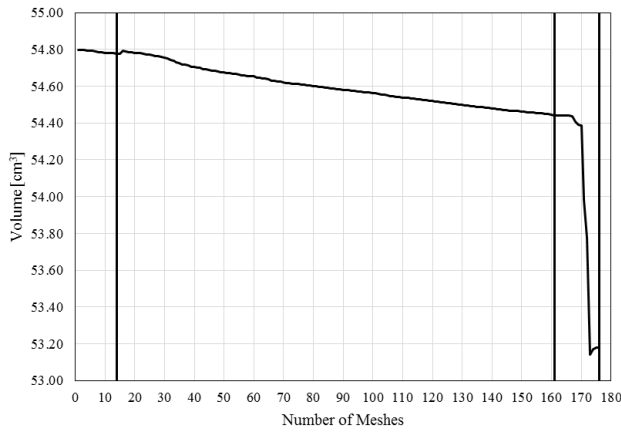
Case 1



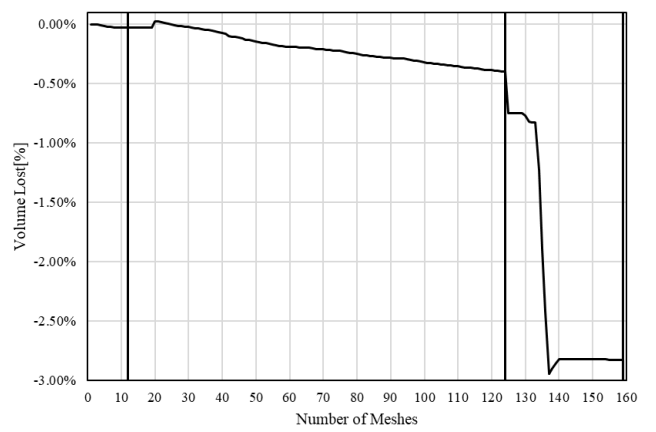
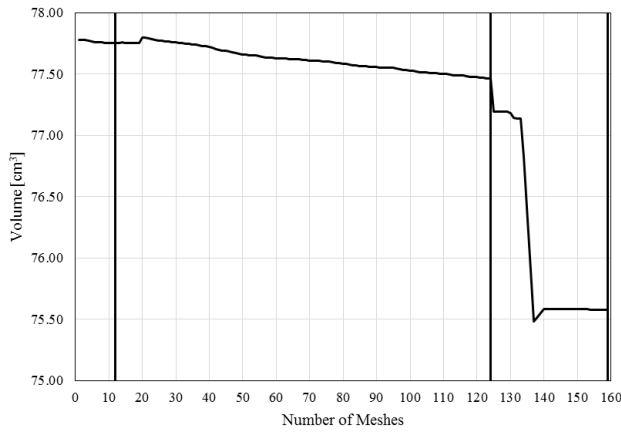
Case 2



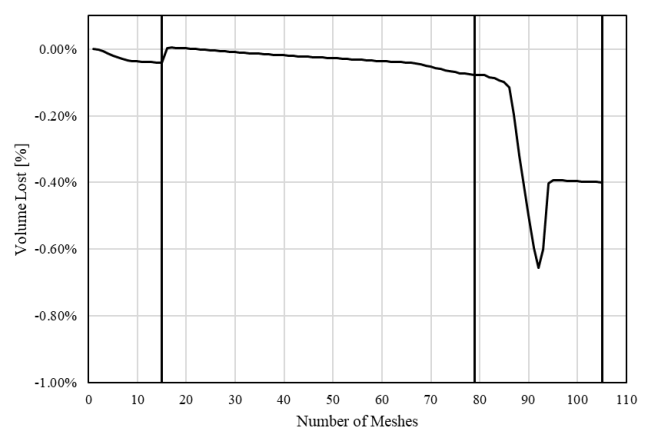
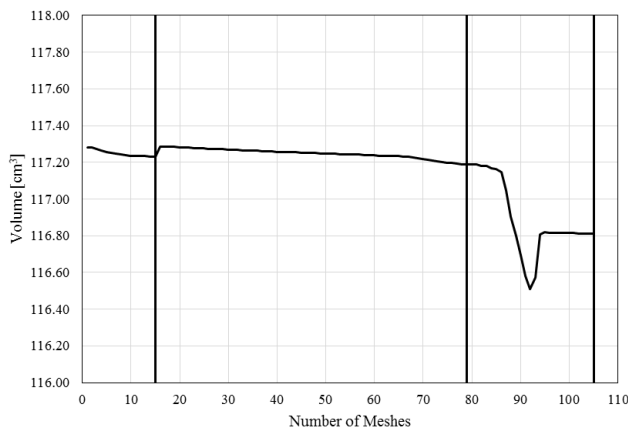
Case 3



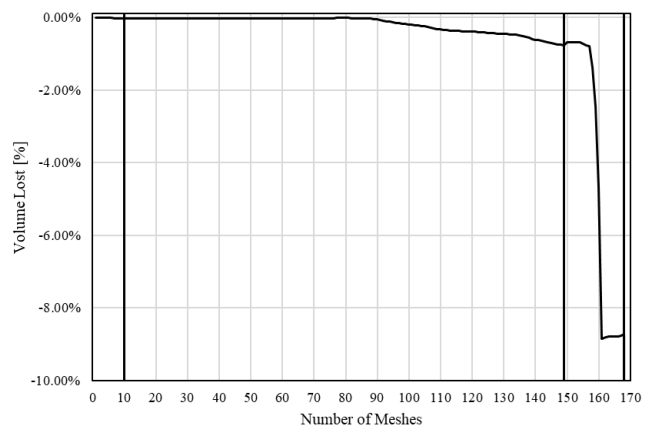
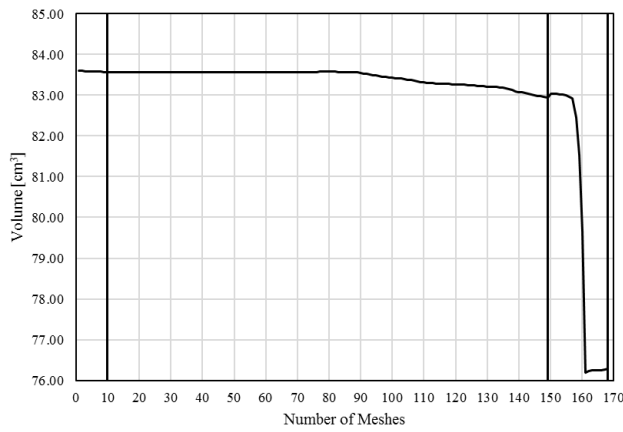
Case 4



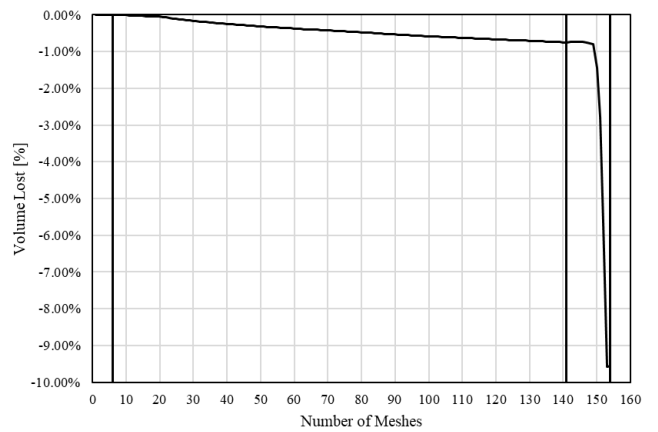
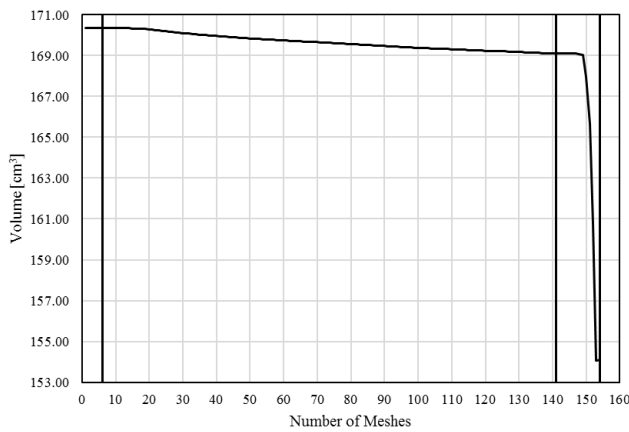
Case 5



Case 6



Case 7



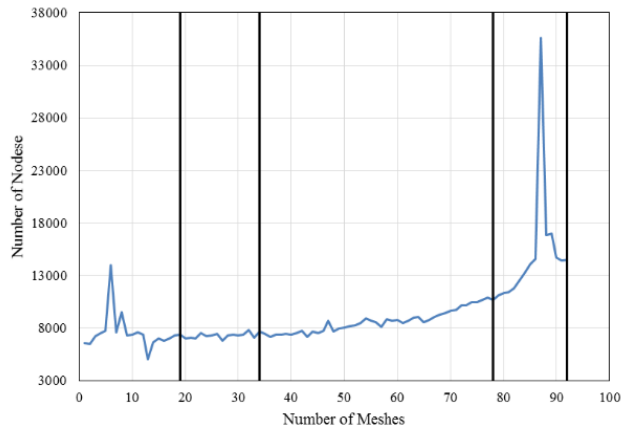
Case 8

Figure 8.148: Volume evolution for press/blow process for the case 1, case 2, case 3, case 4, case 5, case 6, case 7 and case 8.

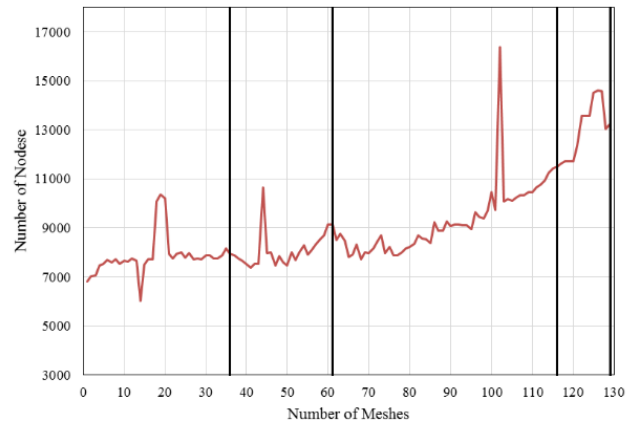
8.3.2 Evolution of the Number of Nodes

The evolution of the number of nodes, therefore, the number of degrees of freedom, was evaluated in each simulation, as this is an important indicator how it may affect the simulation time required.

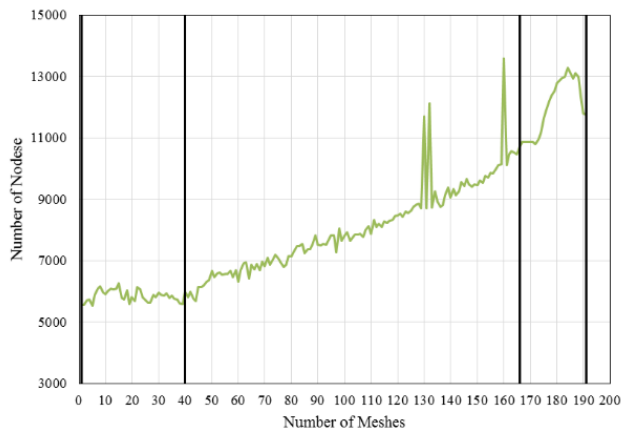
Figure 8.149 presents the evolution of the number of nodes for all de cases of blow/blow process. The vertical line means the end stages of gob loading, settle blow, counter blow and final blow respectively. The results show that in gob loading and settle blow almost a constant number of nodes is kept. As the simulation proceeds to create the parison and the final container the number of nodes increases with intermediate remeshing procedures, sometimes with some significant peaks corresponding to the remeshing in some complex shape boundary zones.



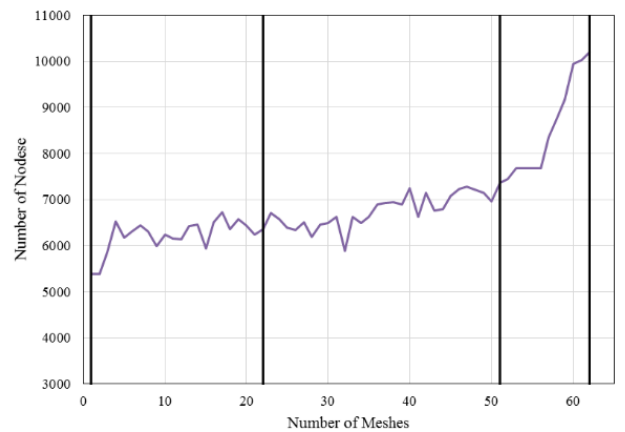
Case 1



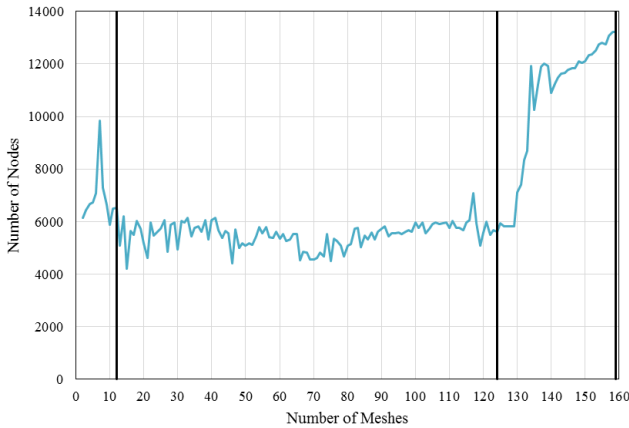
Case 2



Case 3



Case 4

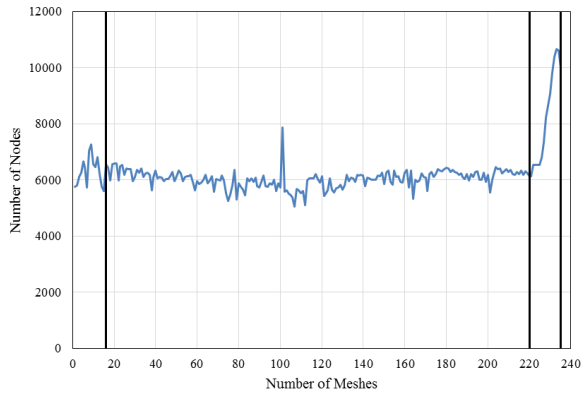


Case 5

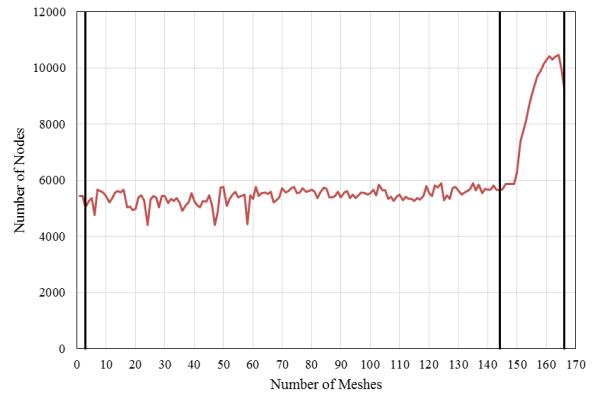
Figure 8.149: Number of nodes for the case 1, case 2, case 3 case 4 and case 5.

The Figure 8.150 presents the evolution the number of nodes for all de cases of press/blow process. The number of nodes seems to maintain almost constant until the final blow stage. In the final blow stage an increase of number of nodes is noted corresponding to some complex shapes during the final forming of the container.

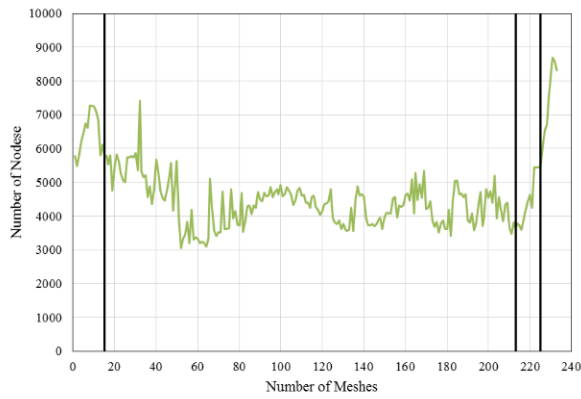
This type of evaluation can be an important to trigger the need to use better remeshing tools and solvers for the nonlinear system of equations involved.



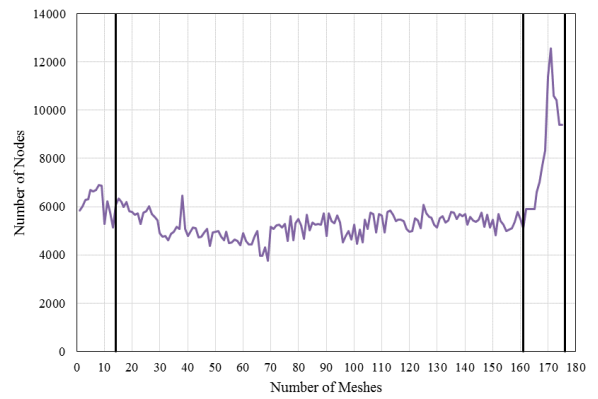
Case 1



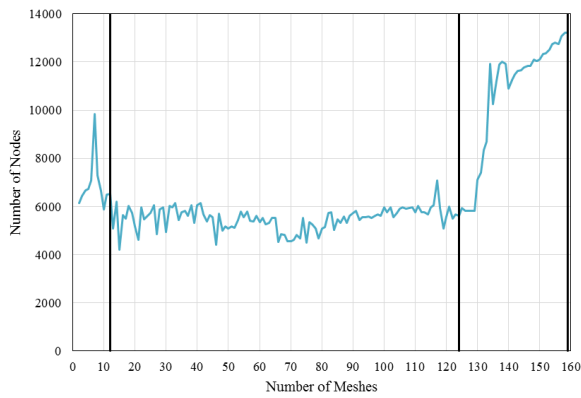
Case 2



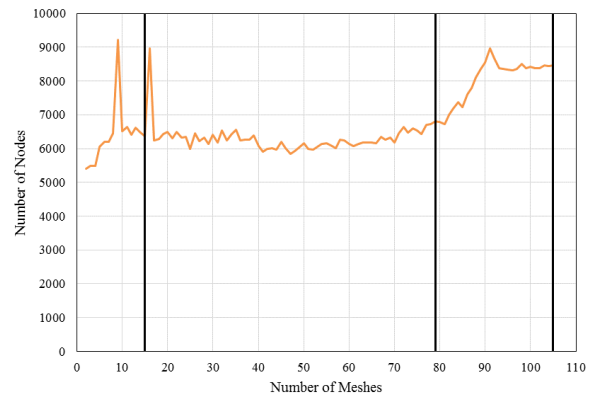
Case 3



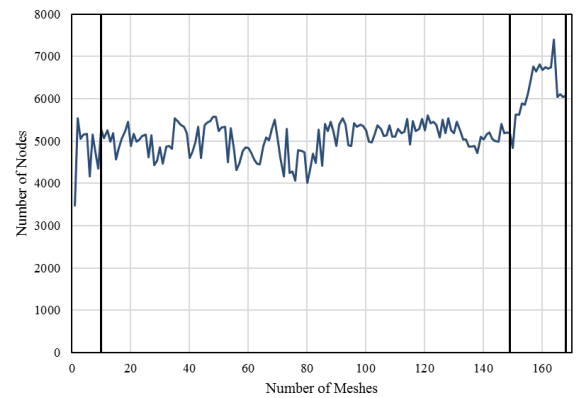
Case 4



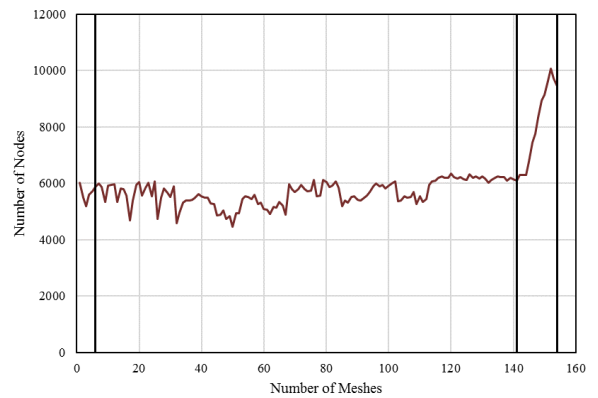
Case 5



Case 6



Case 7



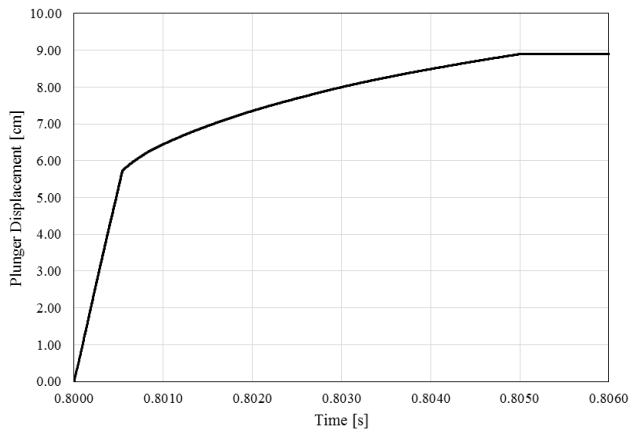
Case 8

Figure 8.150: Number of nodes for the case 1, case 2, case 3 case 4, case 5, case 6, case 7 and case 8.

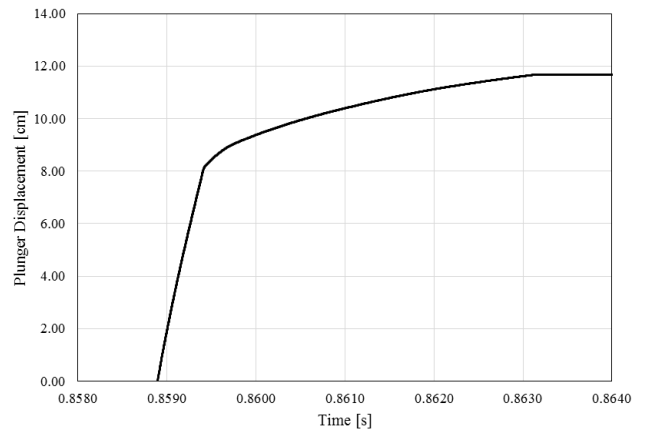
8.3.3 Plunger Displacement

The plunger displacement versus time can be an important data to validate the plunger up stage. Therefore, the plunger displacement during the simulation was registered. Figure 8.151 shows the results for the six cases. It can be noted that while the glass doesn't hit the baffle the displacement has an almost linear behaviour. Then, when the glass moves to the necking the plunger displacement rate is decreasing until zero when the necking is complexly filled.

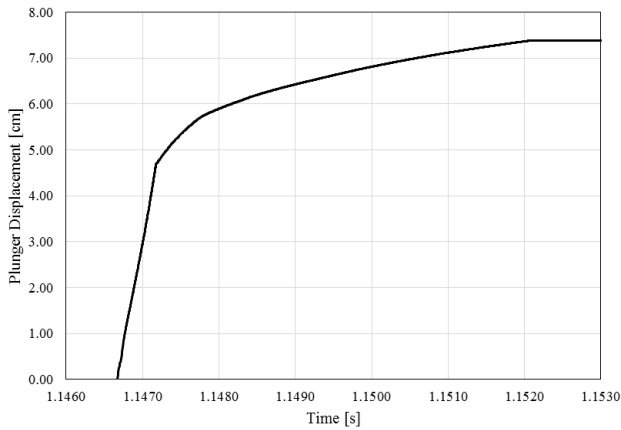
These type of curves can be used to calibrate the friction between the glass and the plunger to reproduce experimental data that may be obtained at the industrial site and later be used in the simulation. It is noteworthy that the existing software's used on glass forming simulation do not include the possibility of applying a force to a plunger, as it was developed in this work, i.e., they rely only on an imposed displacement condition, which is neither real nor acceptable from the industry point of view.



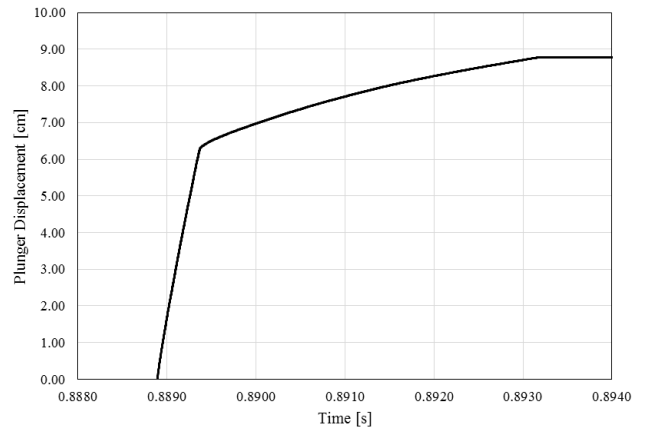
Case 1



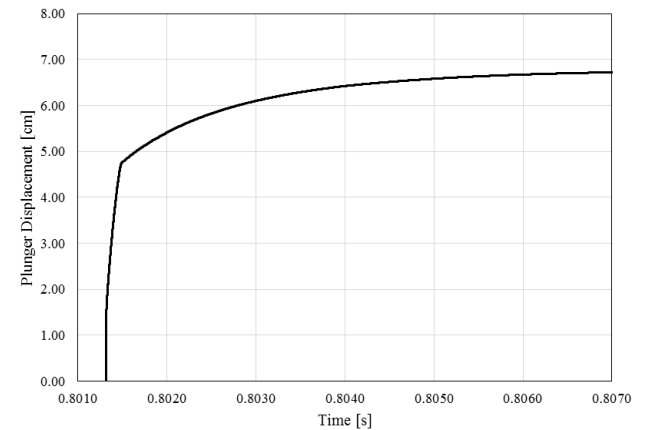
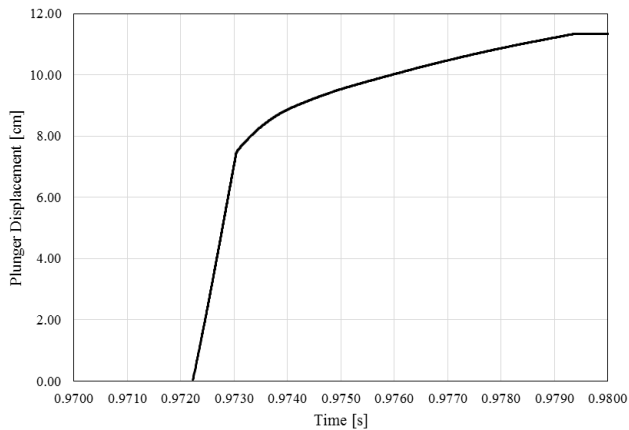
Case 2



Case 3



Case 4



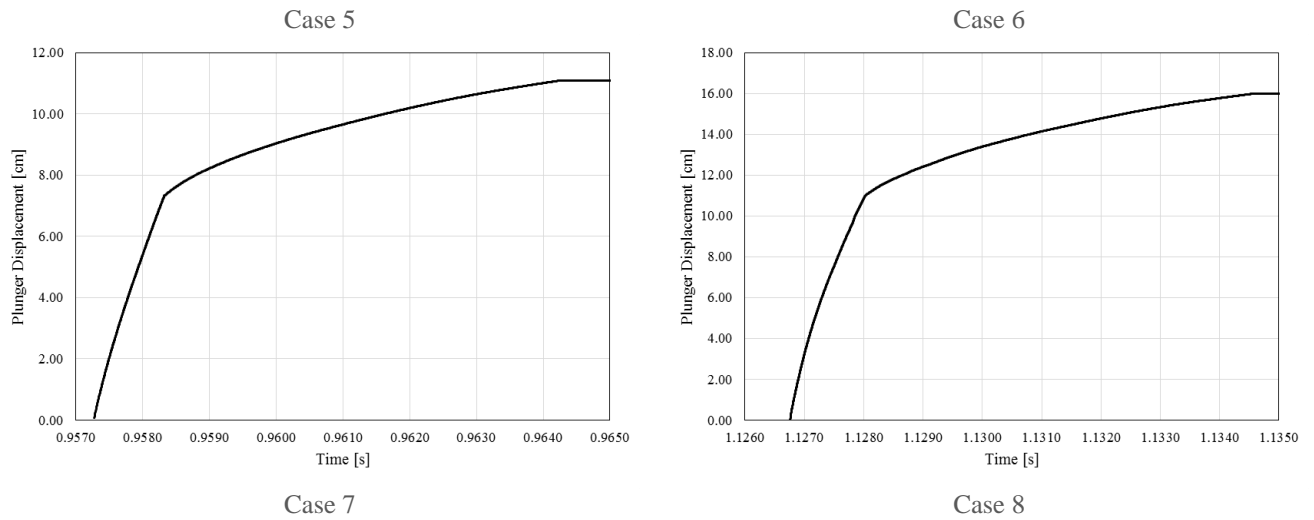
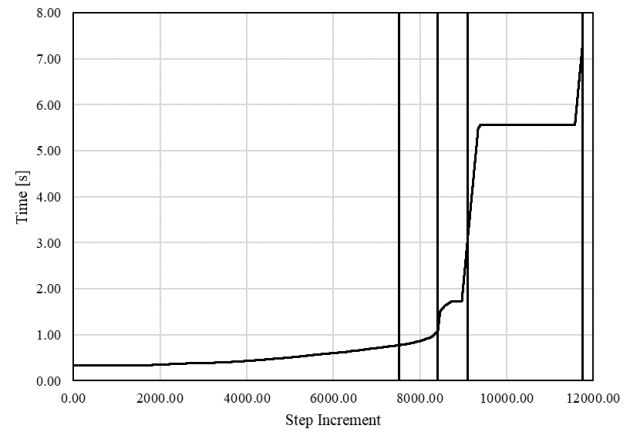
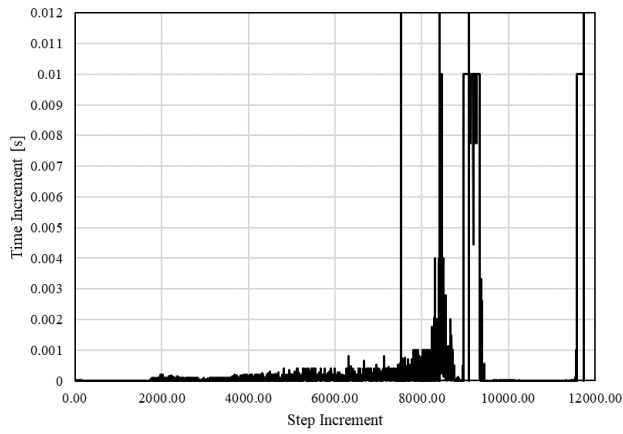


Figure 8.151: Plunger displacement for case 1, case 2, case 3, case 4, case 5, case 6, case 7 and case 8 for a slip penalty value of 1.0e04.

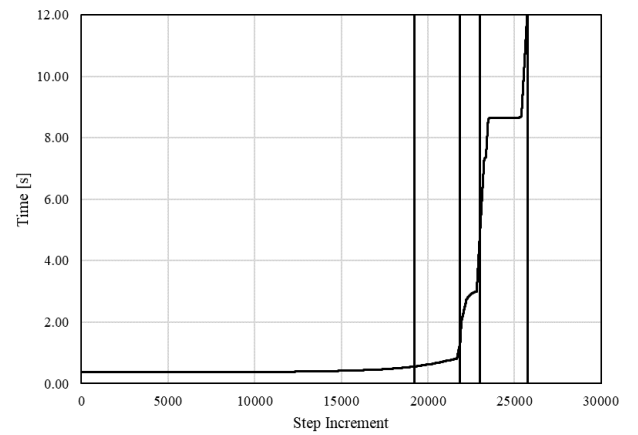
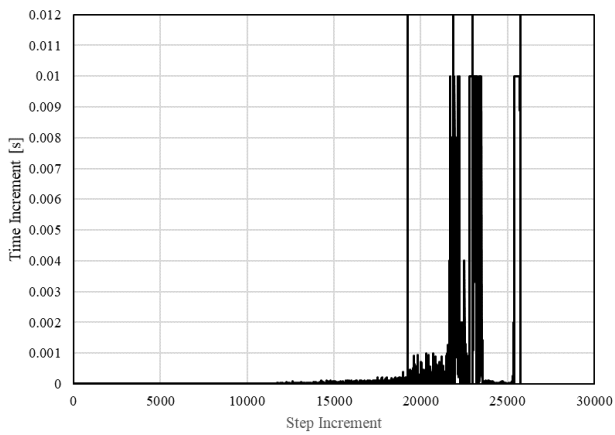
8.3.4 Time Evolution

The increment of time used throughout the simulation is highly dependent on the contact procedure.

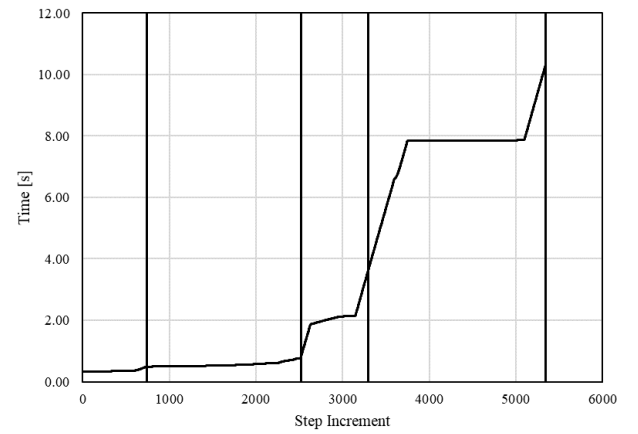
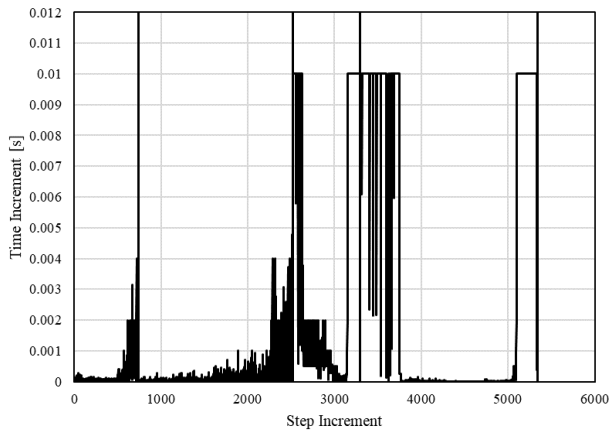
The Figure 8.152 presents the time increment and the total time per step increment for all de cases of blow/blow process. In the beginning of the blow/blow process, i.e. gob loading, a lot of contact involving slipping conditions is very much present, which greatly limits the size of the time increment. Then, when settle blow is applied higher time increments are possible as sliding is no longer present. In the corkage reheat stage time increments are be bigger, as the thermal problem is dominant. At the counter blow stage, despite the fact that low contact situations are present, small time increments are needed due to quick mesh distortions resulting from the applied pressure. In the reheat, invert and run down stages, a higher time increment is used. Finally, the final flow stage require very small time increments due to the heavy deformation that takes place. On the right side of the Figure, the time evolution shows clearly the stages that require more increments. An almost constant time evolution is seen corresponding to gob loading, settle blow, counter blow and final blow stages. The other stages are performed faster as higher time increments may be used.



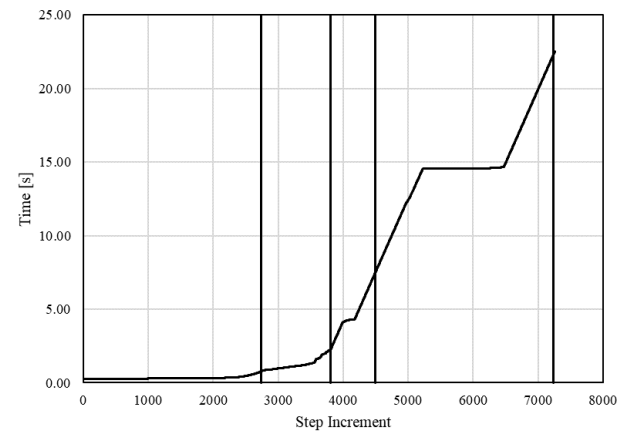
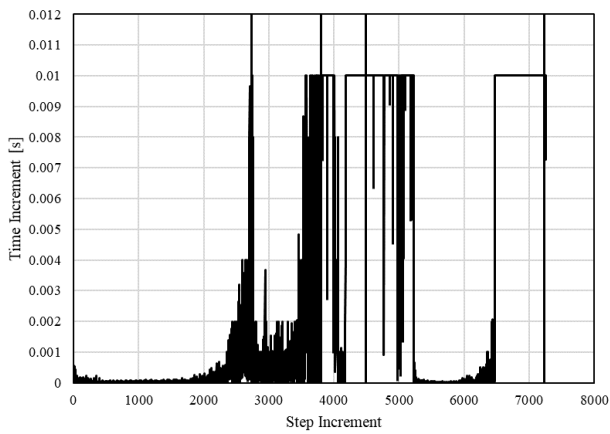
Case 1



Case 2



Case 3



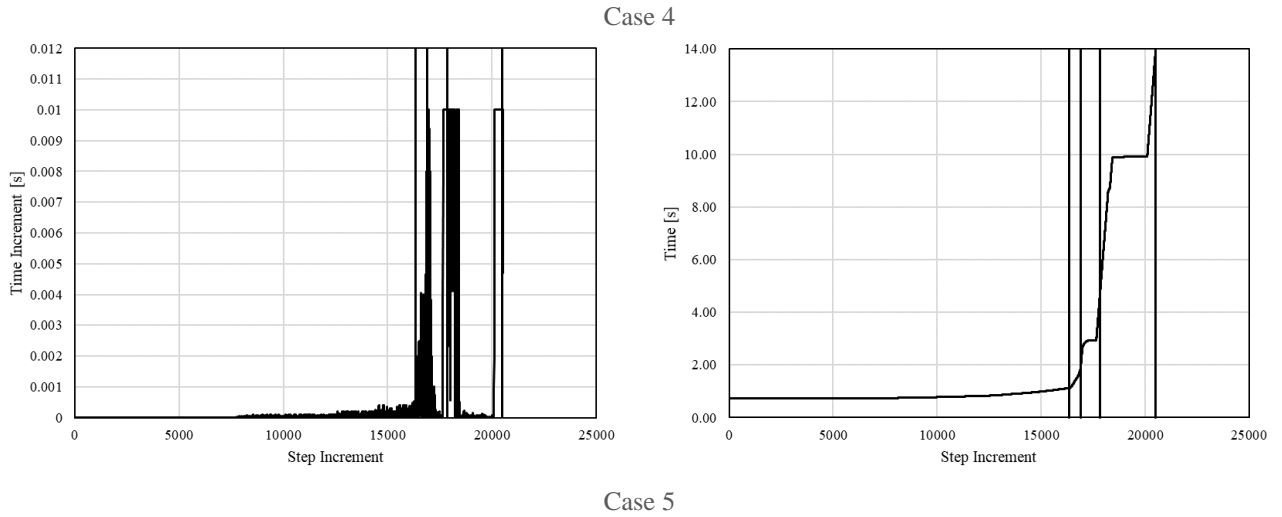
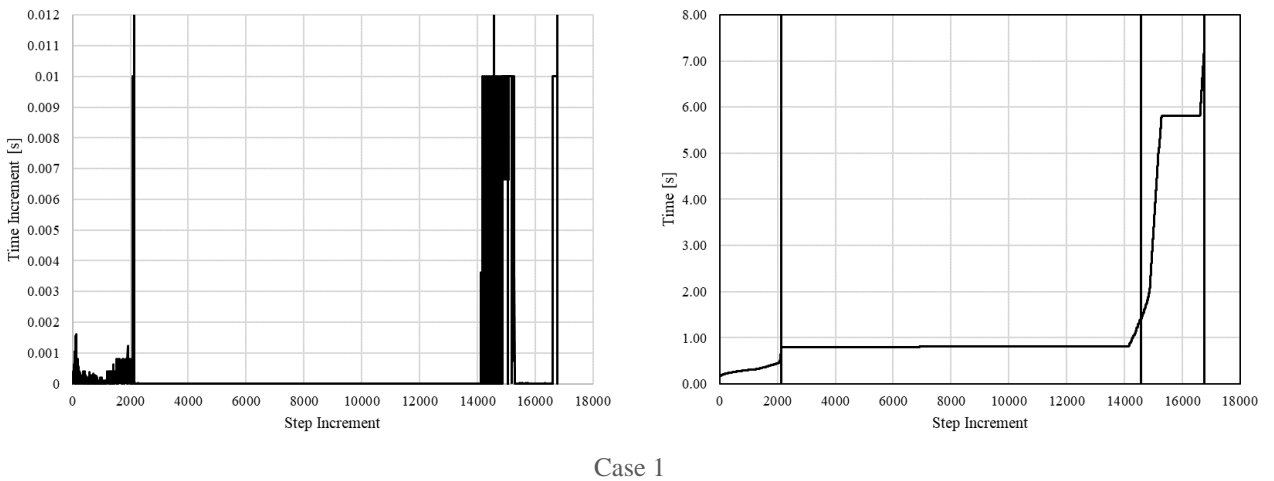
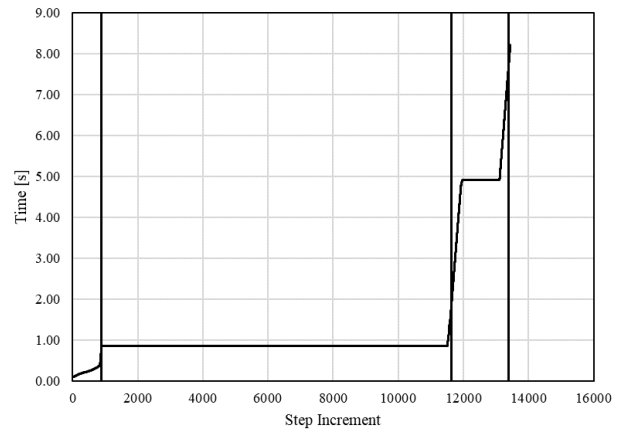
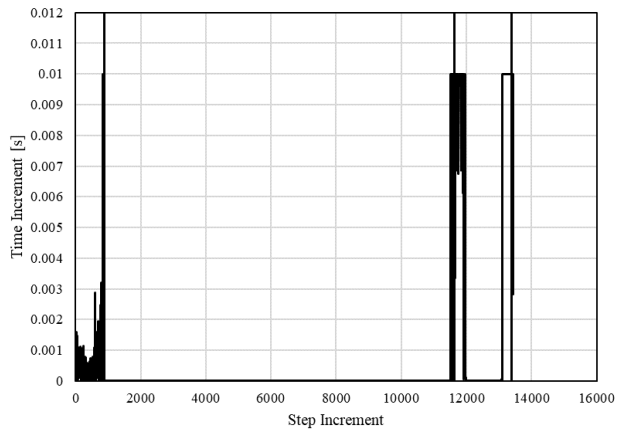


Figure 8.152: Time increment for blow/blow process for case 1, case 2, case 3, case 4 and case 5. Time evolution for blow/blow process for case 1, case 2, case 3, case 4 and case 5.

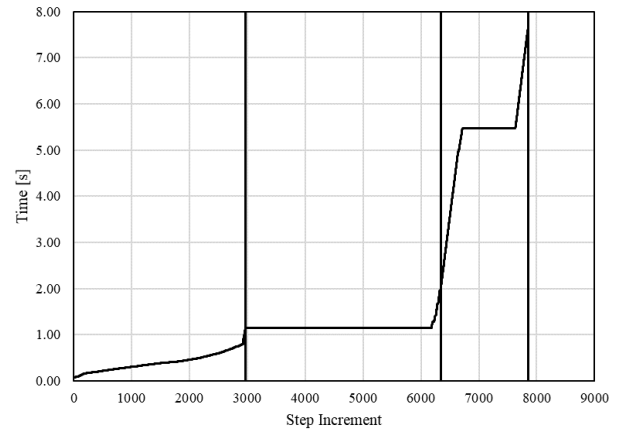
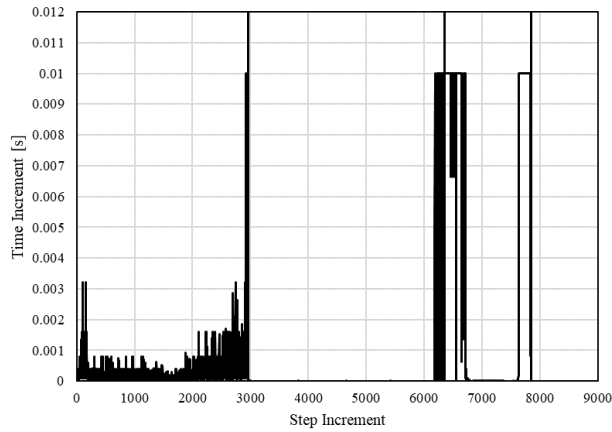
Figure 8.153 presents a similar information for all de cases of press/blow process. The results are consistent in all the cases. In the beginning gob loading stage uses small time increments that are increasing until the baffle on stage. Then in the plunger up stage the time increments are very small. This effect is due to the slipping contact condition in this stage. In the following stages time increments are higher until the final blow. With the contact to the blow mould time increments decrease again.

This type of evaluation of the time increment size used in each stage can be an important indicator in future developments to optimise the contact algorithms, therefore, diminish the computing time.

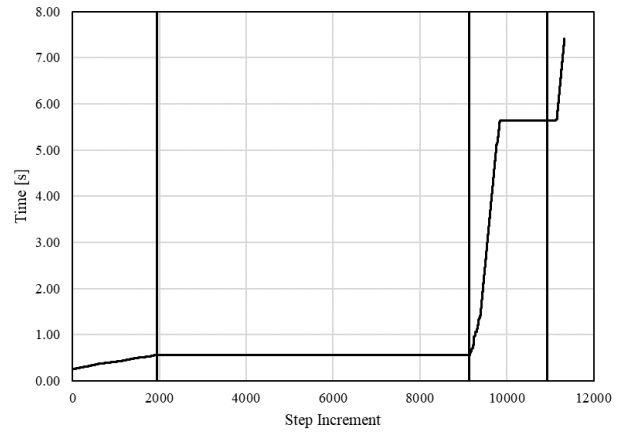
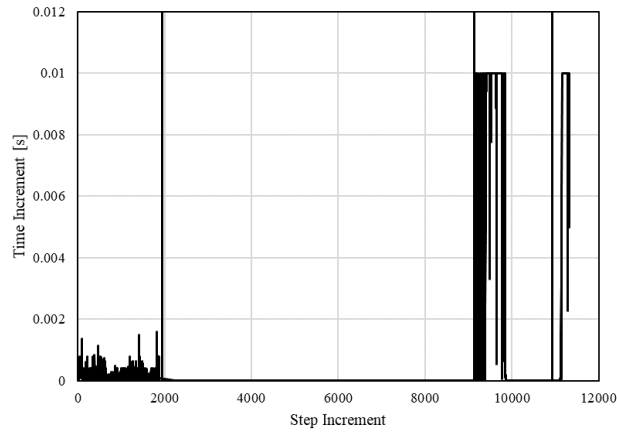




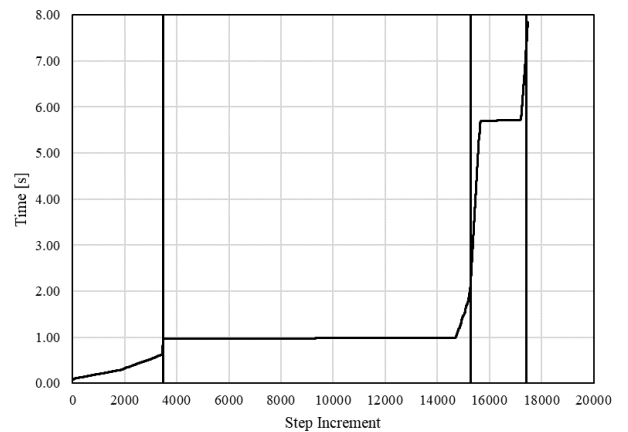
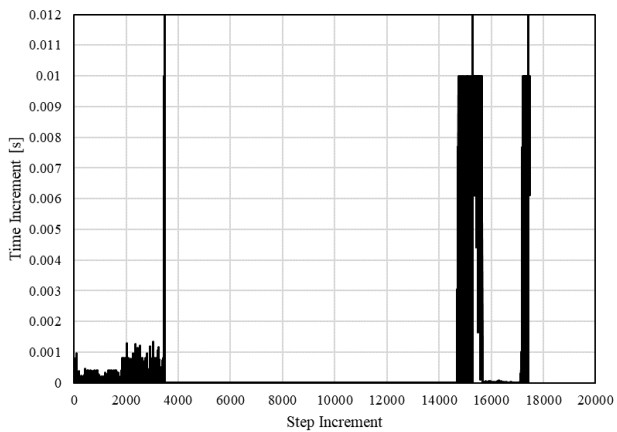
Case 2



Case 3



Case 4



Case 5

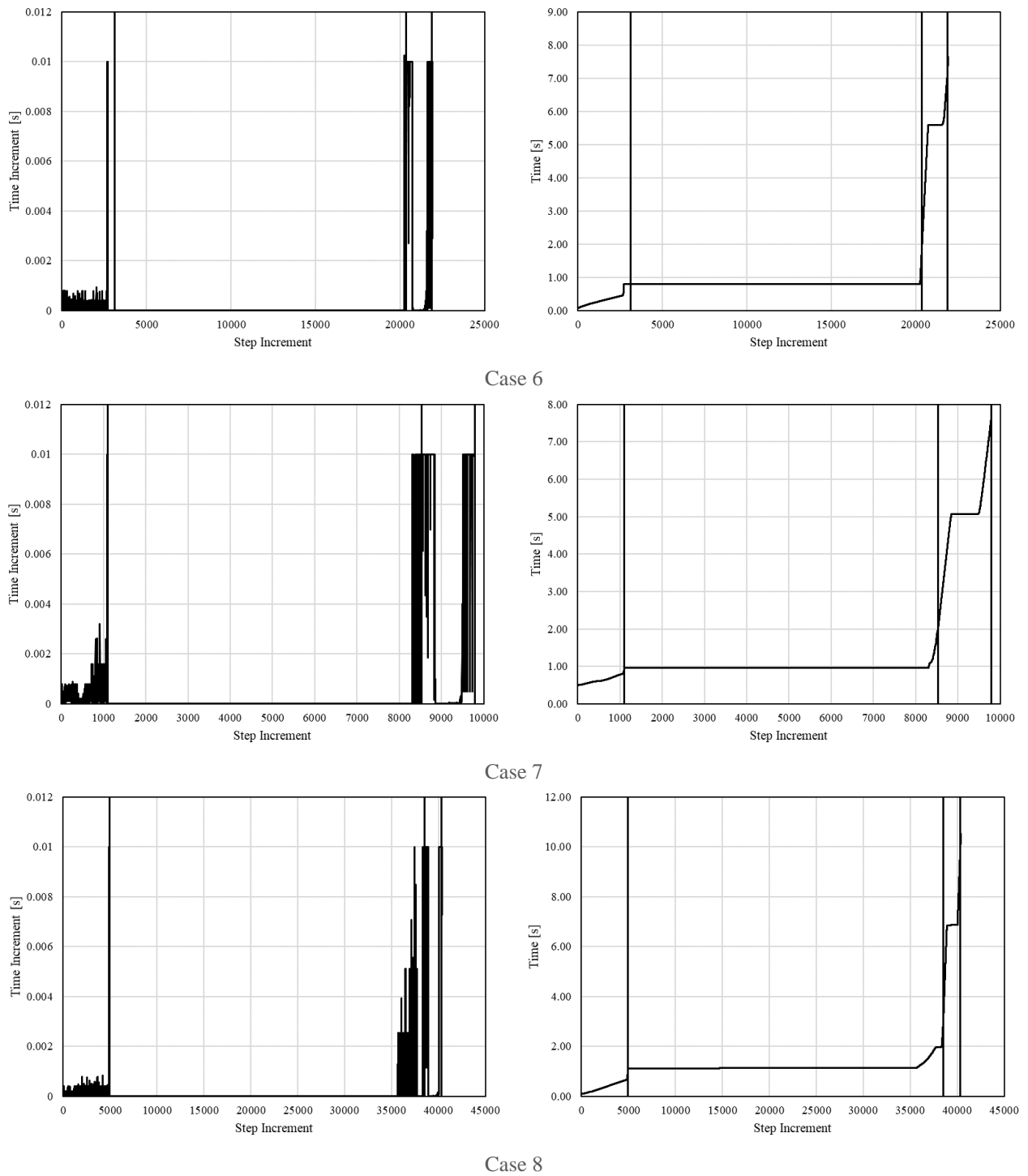


Figure 8.153: Time increment for blow/blow process for case 1, case 2, case 3, case 4, case 5, case 6, case 7 and case 8.

Time evolution for blow/blow process for case 1, case 2, case 3, case 4, case 5, case 6, case 7 and case 8.

Together with the previous improvement proposals and with parameter calibration, which is now possible at industrial ambient, the developed software is a strong basis product in the direction of obtaining a practical decision support system in the design, production and quality control of glass containers.

CHAPTER 9

9 Conclusions and Future Work

A development of numerical software for forming of glass containers has been performed. Several different glass containers have been simulated for the two typical blow/blow and press/blow processes.

The main goal was to perform automatically all the process stages without user handling. The software is able to efficiently choose the timestep, boundary conditions, loads, remeshing parameters and to transfer all information to a new mesh, as well as all to perform the simulation successfully. The software is capable to compute and visualise the container shape, the thickness of the final product as well as the temperatures and displacement that the glass and mould undergo during the process. Contact algorithms accounting for sticking and slipping conditions were implemented.

A mesh updating and a remeshing scheme for linear and quadratic triangles and quadrilaterals finite elements was included.

Various types of equation solvers were implemented, such as the MKL Library and a Lapack solver. For this type of problem the skyline solver presented more efficiency. In addition, the software was developed having in mind computation resources optimization. The examples presented ran with less than 20Mb of RAM memory.

Quadratic elements were in some cases unsatisfactory to model temperature in transient analysis, giving some non reliable physical results. Solution relied on finer meshes with consequent increase in computational time. As glass viscosity is dramatically dependent on temperature the element choice was an important decision. Linear quadrilateral elements was chosen as they depicted the most balanced performance, taking into account thermal response, incompressibility control and contact handling.

The software development requirement had various initial milestones to be reached, that were attained successfully such as:

- i. Different element types were implemented, the software is able to run with linear and quadratic triangles and quadrilateral elements.
- ii. Thermal and mechanical contact were implemented with all the inherent features.
- iii. Remeshing techniques were included for all element types.
- iv. Automatic mesh distortion detection and remeshing triggering.

- v. Automatic boundary conditions definition after remeshing, with no user intervention required
- vi. Automatic data transfer from older to new meshes after the remeshing stage.
- vii. Implementation of triangle and quadrilateral elements meshing tools
- viii. Implementation of renumbering techniques
- ix. Implementation of plunger movement driven by force or velocity
- x. Integration of a complete friction formulation.
- xi. Several equation solver implemented.
- xii. Optimization of the computer resources, such as the RAM usage.
- xiii. Automated job creation.
- xiv. Implementation thermal and mechanical processes in the several stages and its automatic execution.
- xv. Easy process stages configuration (active tools, gravity direction, etc.)
- xvi. Material properties code integration
- xvii. Integration of a preprocessor with the solver
- xviii. Inclusion of an intelligent file management.
- xix. Definition of strategy for output files and postprocessing
- xx. Error detection checks
- xxi. Restart option (continue analysis) after each calculated stage
- xxii. Implementation of the possible of different system units (Imperial, SI, cgs, etc)
- xxiii. Intermediate validation of numerical results performed.

Several cases tests were performed. The results showed the reliability and robustness of the developed computational tool.

When starts a Ph.D. thesis and even more when the work is related to software development, improvement and researching, is a continuous task that will never end. It is expectable that new challenges and developments in the glass container simulations domain appears. Considering some perspectives concerning the continuity of the present work and further developments for future research some proposals may be outlined.

- i. Further improvement of the computational efficiency, robustness, rigor and reliability.
- ii. Testing of different industrial cases and for different materials.
- iii. Enhancing the developed models, aiming at the description of more features, such as taking into account more complex models for heat radiation or the inclusion of inertia effects.
- iv. Introduction of a selfcontact algorithm.
- v. Investigation on the influence of the moulds in the heat transfer problem
- vi. Generalizing the software for full 3D forming processes.

The actual state of the software has a good perspective to simulate accurately the glass container forming process from the initial stage to final shape container. It would be decisive to test some more real cases to enhance its performance. Since glass forming processes have stages that are clearly separated, experimental data from the individual stages can be very useful for a multistage validation of the software.

As the mechanical behaviour of glass depends highly on viscosity, validation of heat transfer coefficients, lubrication and cooling moulds parameters are critical. Also, friction between glass and moulds is very important to understand the nature of an appropriated friction law. A parallel experimental work to provide an accurate indication of the physical parameters involved is needed.

Although some work has done in the mesh size effect, a mesh sensitivity study in order to obtain converged results is still necessary. Presently, a new full mesh is always created when a critical distortion value is exceeded. This distortion can be in a certain zone or just in one element. The mesh creation could be improved in a way that the remeshing would be only on the distorted zone in order to reduce the computing time.

Incremental time is very much influenced by contact. Thus, improving the contact algorithm is mandatory.

The evolution of the design can lead to develop non axisymmetric glass containers opening the software to others potentialities such as the extension from axisymmetric to three dimensional. Thus, the possibility the software to perform 3D simulation are quite interesting. This can involve a huge expansion in the number of variables, increasing the computer time as well as the storage space. Remeshing and visualization of the results would also be challenging tasks.

Additionally, other modules could be added to the software of the glass container process related to the mould design, melting optimization, quality control, etc. Mould design module could include the cooling pipes design, material, shape, etc. In relation to quality control a structural module to inspect admissible pressures and loads could be included, i.e., to possibility to evaluate the integrity of the final containers subjected to vertical, lateral, combined loads and internal pressure.

Actually, the software is already almost capable to perform a full simulation with the discretised moulds. However, the results were not included here as is still an ongoing development. This will be a decisive tool to test and optimize different mould cooling systems such as the axial or radial cooling or the use of different materials in some zones in the mould.

10 References

1. Bourhis, E.L., *Glass: Mechanics and Technology*. 2014: Wiley.
2. Rao, K.J., *Structural Chemistry of Glasses*. 2002: Elsevier.
3. Shelby, J.E., *Introduction to Glass Science and Technology*. 2005: Royal Society of Chemistry.
4. Ropp, R.C., *Handbook of Glass Fractography*. 2008: AuthorHouse.
5. Groot, J.A.W.M., C.G. Giannopapa, and R.M.M. Mattheij, *Numerical Shape Optimization in Industrial Glass Blowing*. *Journal of Pressure Vessel Technology*, 2014. **136**(6): p. 061301-061301.
6. Warude, A., *Analysis of glass mold to enhance rate of heat transfer*. 2004.
7. Groot, J., C. Giannopapa, and R. Mattheij, *Development of a numerical optimization method for blowing glass parison shapes*. *Journal of Manufacturing Science and Engineering*, 2011. **133**(1): p. 011010.
8. Kaipio, J. and E. Somersalo, *Statistical and Computational Inverse Problems*. 2006: Springer New York.
9. Siedow, N., *Radiative Heat Transfer and Applications for Glass Production Processes II*, in *Mathematical Models in the Manufacturing of Glass: C.I.M.E. Summer School, Montecatini Terme, Italy 2008*, A. Fasano, Editor. 2011, Springer Berlin Heidelberg: Berlin, Heidelberg. p. 135-171.
10. Louzguine-Luzgin, D.V., L.V. Louzguina-Luzgina, and H. Fecht, *On limitations of the viscosity versus temperature plot for glass-forming substances*. *Materials Letters*, 2016. **182**: p. 355-358.
11. César de Sá, J., *Numerical modelling of glass forming processes*. *Engineering Computations*, 1986. **3**(4): p. 266-275.
12. Empakglass, *GLASS CONTAINER TECHNOLOGY TRAINING*. 2013. p. 609.
13. Green, D.J., *An Introduction to the Mechanical Properties of Ceramics*. 1998: Cambridge University Press.
14. Mallick, K.K. and U.o.W.D.o. Physics, *Strengthening of Container Glasses and Related Compositions*. 2013.
15. Ojovan, M.I. and W.E. Lee, *Viscosity of network liquids within Doremus approach*. *Journal of applied physics*, 2004. **95**(7): p. 3803-3810.
16. Rouxel, T., *Thermodynamics of viscous flow and elasticity of glass forming liquids in the glass transition range*. *The Journal of chemical physics*, 2011. **135**(18): p. 184501.
17. *Modernisation of batch plant for efficient operations*, in *Glass International*. 2010.
18. Institute, G.P. *Glass Furnace Operations*.
19. Sorg, *Glass Melting Technology*.
20. McMinn, J., *Forehearth of the future: The forehearth plays no role in chemical conditioning or refining of the glass nor does it contribute to the removal of bubble or seeds from the glass*, in *Glass Forming*.
21. BH-F, *Gob Shaping and Adjustments: Operation Manual*. 1995.
22. Duga, R.J., et al., *Electronic glass feeder plunger operating mechanism*. 1985, Google Patents.
23. Davey, R.G. and D.E. Schupbach, *Molten glass gob delivery system*. 1988, Google Patents.
24. Sarwar, M. and A. Armitage, *Tooling requirements for glass container production for the narrow neck press and blow process*. *Journal of Materials Processing Technology*, 2003. **139**(1): p. 160-163.
25. Snyder, H.M., *Cold-end coatings in glass container manufacture*. *American Ceramics Society Bulletin*, 1990. **69**(11): p. 1831-1833.
26. van Wijk, E., et al., *GLASS COATING: THE KEY TO GLASS PRODUCTION*. Sterling Publications Ltd, 1995., 1995: p. 125-128.
27. Lindner, G.H. and R.W. Barkalow, *Coating hood with air flow guide for minimizing deposition of coating compound on finish of containers*. 1987, Google Patents.
28. Mikelic, A., et al., *Mathematical Models in the Manufacturing of Glass*. 2011, Springer.
29. Glass, B., *General Information on the Packaging of Glass Containers for their Safe Transport and Delivery to the Customer*. British Glass Publication, 1998. **TEC 11**.
30. Bathe, K.J., *Finite Element Procedures*. 2006: Prentice Hall.

31. Farina, A., et al., *Mathematical Models in the Manufacturing of Glass: C.I.M.E. Summer School, Montecatini Terme, Italy 2008*. 2010: Springer Berlin Heidelberg.
32. Hutton, *Fundamentals Of Finite Element Analysis*. 2005: McGraw-Hill Education (India) Pvt Limited.
33. Hibbitt, K. and Sorensen, *ABAQUS: Theory Manual*. 1997: Hibbitt, Karlsson & Sorensen.
34. Yastrebov, V.A., *Numerical Methods in Contact Mechanics*. 2013: Wiley.
35. César de Sá, J., et al., *A computational model for glass container forming processes*. 1999.
36. Humphreys, C.E., *Mathematical modelling of glass flow during a pressing operation*. 1991.
37. George, P., *Automatic mesh generation and finite element computation*. Handbook of numerical analysis, 1996. **4**: p. 69-190.
38. Rao, S.S., *The Finite Element Method in Engineering*. 2011: Elsevier Science.
39. Perić, D., M. Dutko, and D. Owen, *Aspects of adaptive strategies for large deformation problems at finite inelastic strains*. Studies in Applied Mechanics, 1998. **47**: p. 349-363.
40. Akin, J.E., *Finite Element Analysis with Error Estimators: An Introduction to the FEM and Adaptive Error Analysis for Engineering Students*. 2005: Elsevier Science.
41. VanSant, J.H. and L.L.N. Laboratory, *Conduction Heat Transfer Solutions*. 1983: Lawrence Livermore National Laboratory.
42. Khoei, A., *Computational Plasticity in Powder Forming Processes*. 2010: Elsevier Science.
43. Cook, R.D., *Finite element modeling for stress analysis*. 1995: Wiley.



Faculdade de Engenharia da Universidade do Porto
Rua Dr. Roberto Frias, s/n 4200-465 Porto PORTUGAL
ww.fe.up.pt